

UNIVERSITA' DELLA CALABRIA
Dottorato di Ricerca in Biochimica Cellulare
ed Attività dei Farmaci in Oncologia.

Il giorno 27 Ottobre 2014 alle ore 11.30 si è riunito, per via telematica, il Collegio dei Docenti del Dottorato di Ricerca in Biochimica Cellulare ed Attività dei Farmaci in Oncologia per discutere il seguente ordine del giorno.

1. Valutazione relazioni fine anno dottorandi XXVIII ciclo.

OMISSIS

Punto 1 all'ordine del giorno: Valutazione relazioni fine anno dottorandi XXVIII ciclo.

Sono pervenute le relazioni di fine anno dei Dottorandi del XXVIII ciclo. Tra queste anche le relazioni dei dottorandi con borsa FSE nell'ambito del Polo di Innovazione Regionale delle "Tecnologie della Salute". Come ogni anno il Collegio dei Docenti è chiamato ad esprimere il proprio parere sul lavoro svolto dai dottorandi.

Il presidente chiede al Collegio dei Docenti di esprimere un giudizio sulle relazioni presentate dai Dottorandi con borsa FSE.

OMISSIS

Con borsa d'Ateneo

Dott. Fiorillo Marco.

Durante il dottorato di Ricerca in "Biochimica Cellulare ed attività dei Farmaci in Oncologia" (XXVIII ciclo) l'attività scientifica del Dr. Marco Fiorillo è stata rivolta allo studio di due flavonoidi, statino-simili, (brutieridina e melitidina) estratte dal bergamotto (*Citrus bergamia*), ma presenti anche in altre specie del genere *Citrus*. Come molecola di riferimento è stata considerata la statina commerciale più prescritta nell'uomo, la simvastatina.

Durante i primi due anni il Dr. Fiorillo ha effettuato la valutazione, "in vivo", dell'attività ipocolesterolemica e ipolipidemica delle frazioni oggetto di studio. In primo luogo è stato ottenuto un modello animale ipercolesterolemico, in seguito al trattamento degli animali (ratti) con una dieta opportuna. Successivamente, sul modello ottenuto è stato monitorato il metabolismo del colesterolo, mediante la valutazione del livello di espressione dei geni codificanti l'enzima HMGR ed il recettore delle LDL, sia a livello di trascritto che a livello proteico. Attraverso lo studio condotto dal Dr. Fiorillo è stato dimostrato che le due molecole estratte dal bergamotto, brutieridina e melitidina, sono dotate di attività ipocolesterolemica, dovuta all'azione inibitoria esercitata nei confronti dell'enzima HMGR. L'interesse scientifico, nel terzo anno di dottorato, è stato quello di valutare, "in vitro", l'aspetto anti-proliferativo ed antinfiammatorio dei due flavonoidi studiati. Il contributo scientifico del Dr. Marco Fiorillo è dimostrato dai lavori pubblicati su riviste internazionali la cui rilevanza scientifica della collocazione editoriale è di ottimo livello e dalla partecipazione a diversi congressi Nazionali e Internazionali. Durante i tre anni di dottorato, ha dimostrato entusiasmo, notevole attitudine alla ricerca e spirito critico nella elaborazione e nella interpretazione dei risultati sperimentali; ha acquisito buona padronanza delle metodologie utilizzate che si evince dalla capacità di svolgere attività di ricerca in grande autonomia e con senso di responsabilità.

Il Dr. Fiorillo ha svolto regolarmente le attività di studio e di ricerca previste per il terzo anno di corso; inoltre, l'esperienza maturata durante i tre anni di dottorato è stata accresciuta da un periodo di formazione svolto presso il laboratorio diretto dal Dr. Michael Lisanti presso il Breakthrough Breast Cancer Research Unit, University of Manchester (da Febbraio 2014 ad oggi). Pertanto si esprime parere estremamente positivo sull'attività scientifica svolta dal Dr. Marco Fiorillo.

Il Collegio dei docenti valutato il contenuto della relazione di fine anno del Dott. Marco Fiorillo esprime parere favorevole alla partecipazione all'esame finale del corso di Dottorato.

OMISSIS

Rende, 27.10.2015

**Il Coordinatore
Prof. Diego Sisci**



UNIVERSITÀ DELLA CALABRIA



Dipartimento di Farmacia e Scienze della Salute e della Nutrizione

Dottorato di Ricerca in

Biochimica Cellulare e Attività dei Farmaci in Oncologia

CICLO XXVIII

**New natural statin-like compounds with
anticholesterolemic and antiproliferative
properties: “in vitro and in vivo studies”**

Settore Scientifico Disciplinare BIO/10

Coordinatore:

Ch.mo Prof. Diego SISI

Supervisore/Tutor:

Ch.ma Prof.ssa Anna Rita CAPPELLO

Dottorando: Dott. Marco FIORILLO

Abstract

Il rischio di malattia coronaria è aumentato negli individui che mostrano elevata concentrazione di colesterolo nelle lipoproteine plasmatiche a bassa densità (LDL). È stato dimostrato che l'inibizione del 3-idrossi-3-metilglutaril-CoA reduttasi (HMGR), enzima che catalizza la conversione di HMG-CoA in mevalonato (MVA), tappa limitante la velocità di biosintesi del colesterolo, è l'approccio più efficace per la diminuzione plasmatica di LDL e la riduzione del tasso di eventi cardiovascolari. Come parte di un meccanismo compensatorio, alla deplezione di colesterolo nel fegato, dovuto all'inibizione dell'enzima HMGR, segue l'aumento della produzione di recettori per le LDL e il successivo smaltimento di LDL dalla circolazione sistemica. Gli inibitori di HMGR rappresentano la classe di farmaci più efficaci e maneggevoli per la riduzione della concentrazione di LDL. Sebbene le statine siano gli inibitori di HMGR più largamente prescritti, sono associate a spiacevoli effetti collaterali quali severa miopatia e perdita della memoria statino-associata. In questo contesto l'identificazione di nuovi composti statino-simili, che agiscono come inibitori di HMGR, risulta utile per superare le limitazioni già descritte. È stato dimostrato che alcuni composti naturali, che si ritrovano nella nostra dieta, hanno proprietà terapeutiche e farmacologiche. In particolare studi condotti in seguito a somministrazione cronica di succo di alcune specie di *Citrus* hanno confermato che questa strategia influenza positivamente i livelli plasmatici dei lipidi e può essere associata alla riduzione del rischio di malattia coronarica. Durante questo lavoro di tesi, l'attenzione è stata rivolta allo studio di due flavonoidi, statino-simili, (brutieridina e melitidina) estratte dal bergamotto (*Citrus bergamia*), ma presenti anche in altre specie del genere *Citrus*. Come molecola di riferimento è stata considerata la statina commerciale più prescritta nell'uomo, la simvastatina. Gli esperimenti sono stati condotti utilizzando una frazione arricchita delle due molecole (EF) ed una purificata (BMF), al 99%. I composti testati, sono stati isolati e caratterizzati in maniera esaustiva, mediante spettrometria di massa e risonanza magnetica, dal gruppo di ricerca del Prof. G. Sindona (Dip.to di Chimica, Università della Calabria). In particolare, si è valutata "in vivo", l'attività ipocolesterolemica e ipolipidemica delle frazioni oggetto di studio. In primo luogo è stato ottenuto un modello animale ipercolesterolemico, in seguito al trattamento degli animali (ratti) con una dieta opportuna. Successivamente, sul modello ottenuto è stato monitorato il metabolismo del colesterolo, mediante la valutazione del livello di espressione dei geni codificanti l'enzima HMGR ed il recettore delle LDL, sia a livello di trascritto che a livello proteico. Il metabolismo dei trigliceridi, invece, è stato monitorato valutando il livello di trascritto e di proteina del gene che codifica per il principale enzima della sintesi degli acidi grassi e quindi dei trigliceridi, il gene FASN. Inoltre sono stati valutati i livelli di colesterolo e di trigliceridi nel fegato e nel sangue ed è stata determinata sia l'attività di HMGR che quella di due

enzimi coinvolti nella lipogenesi, in quanto responsabili della produzione di NADPH, utilizzato per la sintesi degli acidi grassi e del colesterolo, enzima malico e isocitrato deidrogenasi. I risultati ottenuti hanno evidenziato, nei ratti trattati con BMF, una riduzione dei livelli di colesterolo e dei trigliceridi, sia a livello epatico che sierico, tale decremento è risultato essere ancora più evidente nei ratti trattati con EF, rispetto ai controlli ipercolesterolemici. Dalla valutazione dei livelli di trascrizione di due principali proteine coinvolte nel metabolismo del colesterolo, HMGR ed LDLR e dell'enzima principale della biosintesi degli acidi grassi, FASN, è emerso chiaramente che il comportamento di BMF è simile a quello della simvastatina, uno dei farmaci ipocolesterolemici più utilizzati. Infine, dalla valutazione dell'attività degli enzimi HMGR, isocitrato deidrogenasi citoplasmatica ed enzima malico, negli epatociti degli animali trattati con le due frazioni rispetto a quella evidenziata negli epatociti dei ratti controllo, è stata riscontrata un'inibizione, anche in questo caso, paragonabile a quella osservata per i ratti trattati con simvastatina. Attraverso lo studio condotto è stato dimostrato che le due molecole estratte dal bergamotto, brutieridina e melitidina, sono dotate di attività ipocolesterolemica, dovuta all'azione inibitoria esercitata nei confronti dell'enzima HMGR. L'interesse scientifico inoltre, è stato quello di valutare "in vitro", l'aspetto anti-proliferativo ed antinfiammatorio dei due flavonoidi studiati. Infatti, in letteratura è riportato che le statine sintetiche riducono la proliferazione di un'ampia varietà di tipi cellulari, "in vitro", inducendo l'arresto del ciclo cellulare nella fase G1. Questa sperimentazione è stata condotta su cellule di carcinoma mammario umano, MCF7, utilizzando la frazione purificata (BMF) e comparando i risultati con quelli ottenuti dopo trattamento di cellule della stessa linea con simvastatina (profarmaco precedentemente utilizzato per gli studi "in vivo") e pravastina. Il lavoro svolto ha previsto, in primo luogo, la creazione di una linea tumorale, stabile, che fosse in grado di over-esprimere il gene HMGCR (MCF-7-HMGCR), utilizzando un metodo di trasfezione virale; successivamente è stata valutata l'attività proliferativa delle cellule tumorali (MCF-7); delle cellule tumorali trasfettate con il gene HMGCR (MCF-7-HMGCR) e di quelle epiteliali non tumorali (fibroblasti hTERT-BJ1), dopo trattamento con BMF, pravastatina e simvastatina. I risultati ottenuti hanno dimostrato che alte concentrazioni di BMF svolgono un'azione antiproliferativa meno elevata di quella riscontrata con concentrazioni più basse di simvastatina. Tuttavia è doveroso sottolineare che mentre BMF e pravastatina non inibiscono la proliferazione cellulare, nelle cellule non tumorali, la simvastatina è risultata essere tossica anche a basse concentrazioni. Mediante analisi con XFe96 Seahorse Analyzersi è effettuata la valutazione metabolica delle linee cellulari MCF-7, MCF-7-HMGCR, hTERT-BJ1. I risultati ottenuti hanno evidenziato un'aumentata respirazione mitocondriale (OCR) nella linea MCF-7-HMGCR rispetto alla MCF-7; nessuna differenza in termini di funzione glicolitica (ECAR) è stata, invece, riscontrata tra le due linee cellulari. Inoltre,

la respirazione mitocondriale, in cellule MCF-7-HMGCR, dopo trattamento con BMF, ha evidenziato una riduzione della produzione di ATP e una diminuzione della respirazione massima e della capacità respiratoria cellulare. Infine, le analisi OCR su cellule hTERT-BJ1 dopo trattamento con BMF, pravastatina e simvastatina hanno sottolineato una riduzione della respirazione mitocondriale minima, nelle cellule trattate con pravastatina; tale riduzione è risultata essere più marcata nelle cellule trattate con simvastatina. Nessuna differenza è stata, invece, riscontrata nelle cellule trattate con BMF. Questi risultati hanno confermato una leggera tossicità nelle cellule hTERT-BJ1 trattate con pravastatina ed una marcata tossicità in quelle trattate con simvastatina, a differenza delle cellule trattate con BMF. Inoltre, l'indagine effettuata su diversi pathways, implicati nella proliferazione cellulare e nell'infiammazione, ha evidenziato un potenziale effetto antinfiammatorio e antiossidante di BMF, come sottolineato da un aumento della risposta antiossidante e di quella immunitaria regolate dall'interferone I, da una diminuzione della risposta infiammatoria mediata dall'interferone-gamma e da una down-regolazione della via infiammatoria regolata dal gene STAT3, in cellule MCF-7, trattate con BMF. Il trattamento con BMF ha determinato, inoltre, la down-regolazione di due pathways coinvolti nella proliferazione tumorale e nella formazione di CSCs (cancer stem cells), regolati da Notch e Wnt. Questi risultati hanno portato ad indagare su un'eventuale coinvolgimento di BMF, nella formazione di *mammospheres* e a dimostrare, dopo trattamento con BMF, un decremento nella efficienza di formazione di *mammospheres*, dose dipendente, più marcato nelle cellule che over-esprimono l'enzima HMGCR. Successivamente, è stata riscontrata, per BMF, la capacità di ridurre lo stress ossidativo, la formazione di radicali liberi e la successiva risposta pro-infiammatoria, come evidenziato dalla diminuzione dell'espressione delle citochine pro-infiammatorie, regolata dal complesso proteico NF-kB e dalla diminuzione dell'espressione dei fattori inducibili l'ipossia, regolata dal gene HIF, riscontrate in cellule hTERT-BJ1, trasfettare con il gene *reporter* Nf-KB e HIF e trattate con BMF. Infine è stato valutato l'effetto antinfiammatorio ed antiossidante della frazione purificata di brutieridina e melitidina; dai risultati ottenuti è stato possibile evincere una riduzione dei fattori di stimolazione, coinvolti nella formazione dei granulociti e dei macrofagi, in cellule MCF-7 trattate con pravastatina ed, in egual misura, in quelle trattate con BMF. Anche la produzione di IL-8, in cellule trattate con BMF, ha mostrato un decremento, di poco inferiore a quello riscontrato in cellule trattate con pravastatina. Infine la riduzione di *cancer stem cells* (CSC) è stata valutata tramite l'impiego di un marker specifico (ALDH) che ha permesso di isolare la popolazione ALDEFLUOR-positiva relativa alla popolazione staminale, in cellule MCF7. Dopo trattamento con BMF e pravastatina, è emersa una netta diminuzione della popolazione ALDEFLUOR-positiva, nella linea cellulare MCF7. Pertanto, l'aggiunta di colesterolo (prodotto

della biosintesi del mevalonato) al mezzo cellulare, in presenza di BMF e/o pravastatina , non ha cambiato la percentuale di riduzione della popolazione di CSCs. Al contrario l'aggiunta di mevalonato al mezzo di coltura, ha riportato sia il numero di *mammospheres* che la percentuale della popolazione di CSCs ai valori del controllo. Questi risultati hanno permesso di indicare la BMF come un composto con scarsa tossicità e capace di prevenire la crescita tumorale, l'espansione tumorale mediata da fattori pro-infiammatori e la formazione di CSCs. L'impiego della BMF in concomitanza ai canonici chemioterapici, potrebbe migliorare l'effetto degli stessi e diventare un nuovo *target drug* nella terapia *add-on*.

Index

Chapter 1

<i>Introduction</i>	pag. 1
<i>Materials and Methods</i>	pag. 7
<i>Results</i>	pag. 16
<i>Discussion</i>	pag. 38
<i>References</i>	pag. 42

Chapter 2

<i>Introduction</i>	pag. 49
<i>Materials and Methods</i>	pag. 53
<i>Results</i>	pag. 65
<i>Discussion</i>	pag. 94
<i>References</i>	pag. 97

CHAPTER 1

INTRODUCTION

Cholesterol is a molecule of primary importance in animals, including humans, but is not required in the diet because hepatocytes can synthesize it starting from acetyl-CoA. The 3-hydroxy-3-methylglutaryl-CoA reductase (HMGR) is the rate-limiting enzyme in endogenous cholesterol biosynthesis and catalyzes the conversion of HMG-CoA into mevalonate [1]. Inhibition of HMGR has proven to be one of the most effective approaches for lowering plasma LDL and reducing cardiovascular event rates [2]. As part of a compensatory mechanism due to cholesterol depletion in the liver, inhibition of HMGR leads to an increased synthesis of itself and low-density lipoprotein receptors (LDLR); this latter process allows a subsequent clearance of LDL from systemic circulation [3], lowering the risk of atherosclerosis and coronary heart diseases [4 ,5]. The risk for this disease is increased in patients with elevated serum concentrations of low-density lipoproteins cholesterol (LDL), total cholesterol (TC) and triglycerides (TG) [6-9]. Several meta-analysis studies showed that statin therapy can reduce the 5-year incidence of cardiovascular diseases, by about one fifth per mmol/L reduction in LDL cholesterol [10-12]. It is well-known that statins are able to inhibit HMGR activity. Statin administration is one of the most widely used approaches to lower serum LDL level and to reduce cardiovascular event rates [13-15], they are pretty safe, well tolerated and highly efficient, nevertheless cardiovascular disease remains the main cause of mortality in westernized countries. Moreover, many patients, especially those

with the dyslipidemia associated with metabolic syndrome, are unable to reach their lipid treatment goals on statins alone [6]. Furthermore, patients might be statin-intolerant and experience significant side-effects [7], hence the importance of finding new drugs acting as statins. Some natural compounds found in the human diet have been shown to possess therapeutic and pharmacologic properties, in particular, the daily consumption of citrus fruit juice has been shown to positively influence plasma lipid levels and reduce the risk of coronary heart disease [16, 17]. Hypolipidaemic effects can be correlated to several components of citrus juice, such as flavonoids (naringin and hesperidin), pectins, and ascorbic acid, which have a high antioxidant potential and interfere with cholesterol metabolism [18-20]. Plant flavonoids are a large group of very different compounds sharing the common feature of phenolic moieties [21]. The presence of a relatively large number of flavonoids is the result of many different possible combinations among polyhydroxylated aglycones and a limited number of mono- and disaccharides. The most commonly found sugars are hexoses, such as glucose, galactose and rhamnose or pentoses such as arabinose and xylose. They are, with a few notable exceptions, plant metabolites deriving from the shikimate pathway and the phenylpropanoid metabolism [22]. In recent years, flavonoids have attracted tremendous attention due to the protection that they provide against some types of cardiovascular diseases [23]. As a consequence, many studies have been directed to the characterization of the flavonoid fractions and to the isolation of the most representative flavonoids present in the most common *Citrus* species, as well as of flavonoids present

in many local species such as *C. bergamia* Risso [24, 25]. The classes of flavonoids present in *C. bergamia* Risso fractions are flavanones and flavones. Flavanones are present as flavanone-O-glycosides, recently, flavanones diglycosides carrying the 3-hydroxy-3-methylglutaric acid (HMG) moiety have also been detected [26, 27]. Flavones are present as flavone-O-glycosides, flavone-C-glycosides or polymethoxyflavones Bergamot, the common name of the fruit *Citrus bergamia* Risso, belongs to the family Rutaceae, subfamily Esperidea, and is widespread in the Mediterranean area for centuries. The botanical and geographical origins are still uncertain; probably bergamot is native of Calabria, deriving by mutations of other citrus species, or even arrived *in loco* from Berga (hence the name of bergamot) otherwise from Antilles, Greece and Canary Islands. Afterwards, the terpene-rich essential oil, extracted from the peel of the pear-shaped fruit, and its volatile fraction have been largely employed in the cosmetic and perfumery products. Bergamot and its derivatives have also been used in calabrian folk medicine as fever palliative, antiseptic, anthelmintic, wound healing, anti-inflammatory and hypocholesterolaemic agent [28, 29]. To date, bergamot essences are used in the food industry for the preparation of teas, jams, sherbet and other commodities, but also for the domestic preparation of liquors, ice creams and pastries by the calabrian confectionery industry (www.rc.camcom.gov.it). Bergamot juice has been considered, for a long time, a secondary and waste by-product of the essential oil extraction and, because of its organoleptic properties and its bitter taste, did not reach the popularity of other citrus

juices but was used to fortify fruit juice instead of synthetic [30]. Later on, the discovery of the abundance and variety of bioactive compounds in the juice (e.g. naringin, neoeriocitrin, and neohesperidin), led to the development of several nutraceuticals (capsules, pills or soluble granular powders) in the global market [31]. Furthermore, other flavonoids, such as rhoifolin, neodiosmin, and some chrysoeriol derivatives, have been found in smaller amounts [32-34] and different tissues of the fruit produce the flavonoids diosmin and poncirin [35]. In particular, naringin seems to be active on atherosclerosis, as demonstrated by animal studies [36], neoeriocitrin is believed to strongly inhibit LDL oxidation [37] whereas, HMG-flavonoids could be able to inhibit HMGR [26]. These observations have provided the rationale to investigate the protective hypolipidemic effect of bergamot extracts in animal models and in human patients. Miceli *et al.* [38] demonstrated that daily administration of bergamot juice to hypercholesterolemic rats caused a significant reduction in TC, TG and LDL levels, an increase in serum HDL levels and a protective effect on hepatic parenchyma. In addition, fecal output of total bile acids and neutral sterols was enhanced in the bergamot juice treated group in comparison with the hyperlipidemic group. These results are in agree with previous studies, which hypothesized that pectins and flavonoids were able to lower serum cholesterol levels by modulating hepatic HMG-CoA concentration. It could be noted that in this study, the potential side-effect due to bergamottin presence in bergamot juice was not investigated. Bergamot juice is rich in bergamottin (ranging from 18 to 61 mg/L) [39, 40], a furanocoumarin compound that

inhibits cytochrome P450 3A4 enzyme activity, significantly increasing the oral bioavailability of several drugs metabolized primarily by this cytochrome [37, 41]. This problem was overcome by Mollace *et al.* [28], that analyzed the hypolipidemic effect of a defurocoumarinized bergamot-derived polyphenolic fraction supplemented with ascorbic acid on animal models of diet-induced hyperlipidemia and in patients suffering from metabolic syndrome [28]. They found that oral administration of this fraction both in animal and in patients, caused a significant reduction of TC, TG and glycemia with a concomitant increase of HDL levels. Recent prospective studies, led on patients with hyperlipidemia demonstrated that administration of a defurocoumarinized bergamot-derived polyphenolic fraction was able to reduce TC level. In the same conditions, rosuvastatin administration (10 mg/die) caused a similar reduction of TC content. Their association produced a considerable enhancement of rosuvastatin hypolipidemic effect, normalizing the serum lipid profile [42]. The authors suggested that the observed hypolipidemic effect could be mainly due to the presence in bergamot-derived polyphenolic fraction of melitidin, brutieridin and HMG-neoeriocitrin. This hypothesis was investigated by our research group [27], in a hypercholesterolemic rat model, by measuring the effects on lipid profile of administration of HMG-flavanones enriched fraction (62% of brutieridin, 14% of melitidin and 15% of HMG-neoeriocitrin), extracted from bergamot fruit, in comparison with simvastatin. HMGR, LDLR and FASN transcription levels and their correlated protein amounts were evaluated. In this study, simvastatin and HMG-flavanones enriched fraction singularly administrated

reduced levels of TC, TG, VLDL and LDL, whereas an increase in HDL content was observed exclusively in rats treated by HMG-flavanones enriched fraction [27]. Furthermore, according to previously published data, HMGR, LDLR and FAS transcription levels were found up-regulated. An increased amount of their corresponding proteins was detected [43]. Genotoxicity and toxicity were not observed by testing HMG-flavanones enriched fraction in vitro. Our hypothesis was that HMGR inhibition leads to a reduction of endogenous cholesterol level which, in turn, is responsible of HMGR and LDLR transcriptional up-regulation, as well of the higher LDLR exposure within the hepatocytes membrane, through a compensatory mechanism based on SREBPs pathway. We undertook a detailed analysis of dry extract from bergamot peel fruit. The main aim of the present work was to investigate the effects of HMG-flavanones pure fraction (70% of brutieridin and 30% of melitidin), extracted from bergamot fruit, on the total lipid profile of hypercholesterolemic rats, in comparison with simvastatin. HMGR, LDLR and FASN transcription levels and their correlated protein amounts and activities were evaluated.

MATERIALS AND METHODS

Preparation of Brutieridin and Melitidin Fraction (BMF).

Bergamot fruit was collected in December 2012 and then stored at -20° C. 7 kg of fruits were squeezed to obtain the juice (2000 mL) which was filtered and passed through a 10 g C₁₈ cartridge (Supelco, USA) in 50 mL aliquots. The loaded stationary phase was initially washed with water (2 x 50 mL) to remove the sugars and water soluble fraction, and then eluted with 50 mL of methanol to collect the flavonoid fraction. Each aliquot passed through the resin provided ca. 80 mg raw flavonoid fraction, for a total amount of 3.2 g. The polyphenolic fraction coming from the SPE step was loaded onto a glass column (46 x 2.6 cm) from Buchi (USA) packed with 100 g of C₁₈ 80-60 mesh (Sigma-Aldrich, USA) and connected to a Perkin Elmer 200 LC binary pump. H₂O (solvent A) and CH₃OH (solvent B) at the flow rate of 1.5 mL/min were used as elution solvents at the following gradient steps: isocratic at 100% A for 40 min.; linear gradient from 100% A to 70% A in 60 min.; isocratic at 70% A for 60 min.; linear gradient from 70% A to 40% A in 60 min.; isocratic at 40% A for 60 min.; linear gradient from 40% A to 0% A in 10 min.; washing of the column at 0% A for 60 min. The initial water elution was discarded and the collected fractions starting from min 40 (20 mL each) were monitored by HPLC/UV-MS using a Fractionlynx semi-preparative HPLC system (Waters Corp., Milford, MA, USA) The system was composed by an autosampler/collector Waters 2767 Sample Manager, a 600E pump working in analytical mode, a 486 UV detector and a ZMD mass spectrometer equipped with an ESI source working in negative

ionization mode. The HPLC separation was achieved using a 250 × 4.6 mm, 5 μm reversed phase C₁₈ Luna-Phenomenex column at a flow rate of 1 mL/min. The run time was 70 min and the mobile phase was composed by 0.1% formic acid in water (solvent A) and methanol (solvent B). The chromatographic run (70 min) consisted of the following steps: isocratic at 80% A for 7 min; linear gradient from 80% A to 40% A in 33 min; isocratic at 40% A for 5 min; linear gradient from 40% A to 20% A in 5 min; isocratic at 20% A for 7 min; linear gradient from 20% A to 80% A in 5 min; equilibration of the column for 8 min. The UV detector was set at 280 nm. The MS condition were the following: capillary voltage -3.15 kV, cone voltage -3 V, extractor -2 V, RF lens -0.34 V, source block and desolvation temperature 120, 250 °C respectively, ion energy 0.5 V, LM resolution 14.5, HM resolution 15.0 and multiplier 650 V. The nebuliser gas was set to 650 L/h. The fractions coming from the MPLC separation and containing respectively compound brutieridin and melitidin were evaporated under reduced pressure, lyophilized and submitted to the purification step using the Fractionlynx system working in semipreparative mode at the same experimental condition reported above except for the use of the column that was a 250 × 10 mm C₁₈ Luna from Phenomenex (Torrance, CA) and for the chromatographic run (30 min) that consisted in a isocratic at 55% A. The flow rate was set to 4.7 mL/min, and the fractions were collected every 30 seconds, while the injected sample volume was 1 mL. The purity of HMG flavonoid was verified by HPLC/UV.

Hydrolyzed flavonoid fraction from bergamot (FF).

The polyphenolic fraction coming from the SPE step was submitted to hydrolysis experiments using saturated Na₂CO₃. The hydrolysis of the HMG moiety was monitored by HPLC/UV-MS (see above for the experimental conditions). When all the HMG signal disappeared the mixture was neutralized to pH 7 and lyophilized.

Animals and diet.

Male Wistar strain rats, weighing about 100 g each, were purchased from Charles River (Lecco, Italy). All of the animal experiment protocols followed the institutional guidelines of the Italian Ministry of Health for Animal Care (D.M. 116/1992). The animals were housed in rooms maintained at 23±1°C and 55±5% relative humidity and were allowed free access to water, a standard rodent chow diet during acclimatization. Then, they were divided, randomly, into five groups of twelve animals each:

- Group N (controls) received the regular diet for 4 weeks.
- Group H (hypercholesterolemic) received the hypercholesterolemic diet (regular diet + 2% cholesterol + 0.2% cholic acid) for 4 weeks.
- Group (H+S) received the hypercholesterolemic diet (regular diet + 2% cholesterol + 0.2% cholic acid) for 4 weeks; from the 3rd to the 4th week each rat was administered by gavage with simvastatin (20 mg/kg bw/day).

- Group (H+BMF) received the hypercholesterolemic diet (regular diet + 2% cholesterol + 0.2% cholic acid) for 4 weeks; from the 3rd to the 4th week each rat was administered by gavage with the BMF (60 mg/kg bw/day).
- Group (H+EF) received the hypercholesterolemic diet (regular diet + 2% cholesterol + 0.2% cholic acid) for 4 weeks; from the 3rd to the 4th week each rat was administered by gavage with EF, at the same amount employed with BMF.
- Group (H+FF) received the hypercholesterolemic diet (regular diet + 2% cholesterol + 0.2% cholic acid) for 4 weeks; from the 3rd to the 4th week each rat was administered by gavage with Flavonoids alone, at the same amount employed with BMF.

Regular and hypercholesterolemic diets were supplied by Charles River (Lecco, Italy). During the experiment, rats were weighed daily and the 24 h food consumption was recorded, then fasted for 24 h before experiments. At the end of the treatment, blood samples were collected respectively in EDTA-treated tubes and Silica-treated tubes for plasma and serum detection, and centrifuged at 2500 x g for 15 min; the serum was separated and stored at 20°C until analyzed. The animals were anesthetized with chloral hydrate (400 mg/kg, i.p.) and killed by perfusion through the left ventricle of the heart with 100 mL of heparinized saline (pH 7.4). The liver was excised and immediately frozen in liquid nitrogen, then stored at -80°C until required.

Biochemical valuations.

The livers were cut into small pieces, washed several times in a cold buffer (0.25 M sucrose, 3 mM EDTA, 20 mM Tris–HCl, pH 7.0), next homogenized in the same buffer and treated as described in Muci et al. [44] for TC extraction. Briefly, an aliquot of 10 mg protein sample was saponified with alcoholic KOH for 90 min at 85–90 °C. Nonsaponifiable constituents were extracted three times (5 mL each) with light petroleum (b.p. 40-60°C). The pooled extracts were then evaporated to dryness under N₂ and the residue, dissolved in 2-propanol. Total lipids were extracted from liver homogenate (10 mg protein) with chloroform/methanol (1:1 v/v) according to [45]. The levels of hepatic TG and TC were measured respectively by Triglyceride Quantification Kit ab65336 (Abcam, Toronto Canada), Total Cholesterol Assay Kits (Cell Biolabs, Inc. San Diego, USA), and HPLC analysis as described in Didonna et al. [45]. The TG, TC, HDL, LDL and VLDL levels were evaluated by direct enzymatic assays using Total Cholesterol Assay Kits Cell Biolabs, Inc. San Diego, USA), Triglyceride Quantification Kit ab65336 (Abcam, Toronto Canada) HDL and LDL/VLDL Cholesterol Assay Kit ab65390 (Abcam, Toronto Canada),, respectively according to the manufacture's instruction. Alanine transaminase (ALT), aspartate transaminase (AST), bilirubin and creatinine were measured using reagent kits from Alanine Transaminase Colorimetric Assay kit (CaymanChem, Michigan USA), Aspartate Aminotransferase Activity Assay kit (CaymanChem, Michigan USA), Bilirubin Assay kit (Abnova, Taiwan) and Creatinine Colorimetric Assay kit (CaymanChem, Michigan USA).

RNA extraction, reverse transcription and quantitative real-time polymerase chain reaction.

RNAs were extracted from liver as described by Zara et al. [46] and aliquots of 1 µg were reverse-transcribed as reported in Iacopetta et al. [47]. Quantitative real-time polymerase chain reaction (RT-PCR) was performed with the obtained complementary DNAs (cDNAs) using the Applied Biosystems StepOne™ Real-Time PCR System (Applied Biosystems, Monza, Italy). Primers based on the cDNA sequences of the genes of interest were designed using Primer Express (Applied Biosystems, Monza, Italy). In each sample of 20 µl real-time PCR reaction 10 ng of cDNA, 10 µl of the Power SYBR® PCR Master Mix (Applied Biosystems, Monza, Italy) and 0.3 µL (150 nM) of the specific primers for each genes analyzed were used. Each experiment was repeated at least 3 times. The comparative threshold cycle method was used in relative gene quantification as previously described [48], using 18S gene as the endogenous control.

Microsomal fraction extraction and Western blot analysis.

The liver homogenate, obtained as previously described, was centrifuged at 800 g for 8 min, the pellet was discarded and supernatant centrifuged for 10 min at 12,000 g. The pellet containing the mitochondrial fraction was discarded and the supernatant was first centrifuged at 20,000 g for 20 min and then at 105,000 g for 60 min to obtain the

cytosolic fraction and pelleted microsomes. The latter were re-suspended in the homogenizing medium and centrifuged again under the same conditions. Contamination of microsomal preparation by other subcellular fractions, ranging from 5 to 9%, was determined by the assay of marker enzymes as described in [49] and protein concentration was determined as in [50]. Western blot analysis was conducted as described previously [51]. Antibodies anti-HMGR (H-300), fatty acid synthase (FASN, H-300), LDL receptor (C-20), anti-calnexin (C-20), anti- α -tubulin (D-10), anti-GAPDH (FL-335) were supplied by Santa Cruz Biotechnology Inc. (Santa Cruz, CA, USA) and used following the manufacturer's instructions. Anti-calnexin, anti- α -tubulin or anti-GAPDH antibodies were used to confirm the equal loading of proteins.

HPLC analysis of total cholesterol in liver samples.

The analyses of samples were performed following a method from literature [52].

Determination of HMGR activity.

The assay was carried out via the radioisotopic method, following the production of [14 C] mevalonate from 3-[14 C]- hydroxymethylglutaryl coenzyme A (3-[14 C]-HMG-CoA; specific activity 57.0 mCi/mmol; Amersham-Pharmacia, Little Chalfont, UK); as described in Pallottini et al. [53]. Briefly, five hundred milligrams of liver were

homogenised in a phosphate buffer containing 0.1 M sucrose, 0.05 M KCl, 0.04 M KH_2PO_4 , 30 mM EDTA, pH 7.4.. The activation of the enzyme by lysosomal phosphatases during the preparative procedure can be avoided by the addition of the phosphatase inhibitor NaF. Microsomes were prepared by centrifugation of the homogenates as already reported [54], microsomes (100 μg) were incubate in presence of cofactors (20 mM glucose-6-phosphate, 20 mM NADP sodium salt, 1 IU glucose-6-phosphate dehydrogenase and 5 mM dithiotreitol). The assay, in a final volume of 200 μl , was started by the addition of 10 μl (0.088 $\mu\text{Ci}/11.7$ nmol) of 3- ^{14}C -HMG-CoA. The radioactivity of the produced ^{14}C -mevalonate, isolated by chromatography on AG1-X8 ion exchange resin (Bio-Rad Laboratories), was counted. An internal standard (3- ^3H -mevalonate, specific activity 24.0 mCi/mmol; 24.0 mCi/mmol; Amersham-Pharmacia, Little Chalfont, UK) was added to calculate the recovery.

Determination of Isocitrate dehydrogenase and Malic enzyme activities.

For lipogenic enzyme analysis, samples of liver (0.5 g) were homogenized in 5 mL of buffer (pH 7.4) containing 0.25 M sucrose, 3 mM EDTA, 20 mM Tris-HCl, pH 7.0. The cytosolic fraction was obtained as described in par. "*Microsomal fraction extraction and Western blot analysis*" and used for quantification of enzyme activities. Isocitrate dehydrogenase (IDH) activity was assayed by the method of Ochoa [55] and malic enzyme activity as described by Ochoa [56]. Enzyme activities were measured

spectrophotometrically and were expressed either as nmol NADPH produced, per minute, per mg of protein. Protein concentration was determined by the Bradford method [57].

Statistical analysis.

All data is presented as means \pm SD for the number of experiments indicated in each case. Data was analyzed by Student's t-test using the GraphPAD Prism5 software (GraphPad Software, USA). Differences were considered statistically significant at $P < 0.05$.

RESULTS

Food intake and body weight gain.

The data on food intake and body weight evidenced no significant alteration, for each group (i.e. simvastatin (H+S), or BMF (H+BMF), or EF (H+EF), or flavonoids alone (H+FF) treated rats versus control), during the experimental phase (data not shown). These observations indicate that the diet and treatments used in these studies were well tolerated in rats, given that no physical alteration, body weight loss or food intake reduction occurred over the period of study. Two groups of rats were fed a regular and hypercholesterolemic diet respectively, in order to verify the induced hypercholesterolemia.

Effect of simvastatin, BMF, EF and flavonoids on serum and hepatic lipid content.

Firstly, in order to establish whether the hypercholesterolemic rat model has been achieved, we compared the serum and hepatic lipid profile of the regular diet fed rats (group N) and the hypercholesterolemic ones (group H). The TC, TG, VLDL, LDL and HDL levels, in rat serum of H group (Fig. 2, panel A), showed a significant increase (100, 32, 53 and 82% respectively) respect to those of N group, whose values were 105.85±5.6 mg/dl for TC, 204.7±12.3 mg/dl for TG, 39.02±1.5 mg/dl for VLDL and 49,03±3.1 mg/dl for LDL. Whereas no significant variation has been found for HDL levels (in N group, the HDL value was 45.52±3.3 mg/dl). Furthermore, a strong

increase of the hepatic TC and TG levels (Fig. 2, panel B) has been observed in H group (150 and 300% respectively) compared to group N, whose values were 1.98 ± 0.9 mg/g liver for TC and 4.87 ± 0.39 mg/g liver for TG. These results confirmed that H group can be used as a hypercholesterolemic and hyperlipidemic model in the following experiments. Then, we investigated the effects triggered by BMF and simvastatin treatments on serum and hepatic TC of hypercholesterolemic rats, compared to group H. We observed a significant decrease of the serum TC that was more evident after BMF treatments (of about 40 and 55%, respectively). In rats treated with flavonoids fraction without brutieridin and melitidin (FF) was detected a less noticeable decrease (23%), compared to the hypercholesterolemic ones (Fig. 3, panel A). Moreover, the liver TC content showed a lower reduction, but with similar trends in H+S and H+BMF groups, of 25 and 45% respectively (Fig. 3, panel B). The direct correlation between an increase in the concentration of LDL in serum and the risk that the incidence of atherosclerosis and cardiovascular disease/cerebrovascular becomes higher is well known [58]. Besides, the HDL concentration has been correlated inversely with the onset of atherosclerosis associated diseases [59], whereas the data concerning the VLDL role in atherosclerotic plaque formation are still controversial [60]. For the above reason, we evaluated serum levels of LDL, HDL and VLDL. A significant reduction of VLDL and LDL was measured in H+S (25 and 30% lower, respectively), H+BMF groups (45 and 60% lower, respectively) and H+FF (55 and 25% lower, respectively) groups (Fig. 4, panels A and B, respectively). Conversely, any significant difference in the HDL

cholesterol was found in the H+S group, whereas, surprisingly, an increase of 30% was found in the H+BMF group respect to H group (Fig. 4, panel C). The increase exceeded of 15% in rats of H+FF group. Since HMGR inhibitors have been shown to contribute at reducing serum triacylglycerols, in experimental animals [61], we measured serum and hepatic TG content, in our model. The obtained results showed that, in both cases, there was a decrease in H+S, H+BMF and H+FF groups respect to H group of about 30, 40 and 60%, respectively, for serum TG (Fig. 5, panel A) and of about 25, 63 and 60%, respectively, for hepatic TG (Fig. 5, panel B).

Effect of simvastatin and HMGF administration on hepatic HMGR, LDLR and FASN mRNAs and proteins levels.

In order to further investigate the HMGF effects in H groups, we evaluated the transcriptional levels of two main proteins involved in cholesterol metabolism, i.e. HMGR and LDLR, and the expression of the main enzyme of fatty acid biosynthesis, i.e. FASN [62]. Simvastatin and BMF treatments produced a similar modulation on the gene expression of the above mentioned proteins (Fig. 6; panel A). Particularly, simvastatin administration, respect to H group, brought to an increased transcription of HMGR, LDLR and FASN genes in an extent of 1.45, 1.88 and 1.50 fold respectively. As well BMF treatment increased the expression of HMGR, LDLR and FASN genes of 1.70, 1.80 and 1.90 fold respectively. In both cases, the mRNAs increase is appreciable

respect to the untreated H group. Conversely, the FF treatment determine a significant increased transcription of LDLR and FASN genes. These data were confirmed by Western blot analyses performed on the microsomal or cytoplasmic fractions or on liver homogenate extract, considering the different sub-localization of proteins analyzed. As shown in figure 6, (panels B-D), according to RT-PCR results, both simvastatin and BMF treatments led to a clear increase of HMGR, respect to H group, whereas the FF treatment determine a significant increase of LDLR protein that was more evident for FASN protein (1.45 and 2.8 fold respectively).

HMGR activity.

As HMGR is the rate limiting enzyme in cholesterol biosynthesis, we investigated whether reduction in cholesterol content in the liver and serum in hypercholesterolemic rats, upon treatment with BMF and FF, was due to the inhibition of HMGR. The HMGR activity was analysed in the liver microsomal fraction, following the production of [¹⁴C]-mevalonate from 3-[¹⁴C]-HMG-CoA. A significant decrease in the HMGR activity was detected when hypercholesterolemic rats were treated with simvastatin and BMF (Fig.7). Administration of two compounds decreased the HMGR activity by about 50% and 55%, respectively as compared to control hypercholesterolemic rats. No differences were found in HMGR activity, in hypercholesterolemic rats treated with FF. These results clearly demonstrated that

brutieridin and melitidin (the two flavonoids in BMF) function as statin-like compounds, against HMGR.

Isocitrate dehydrogenase and malic enzyme activities.

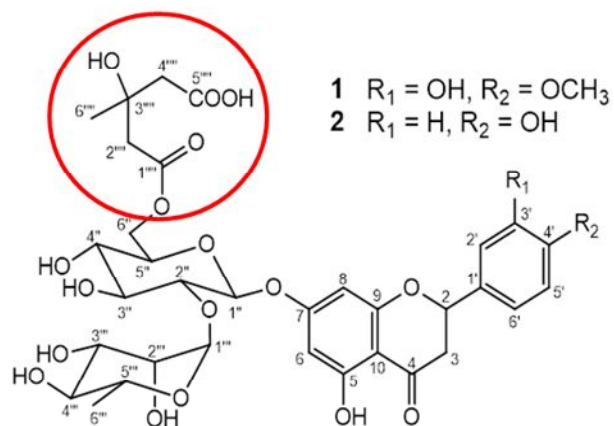
It is known that the effects of statins on fat accumulation are controversial. Therefore, to establish whether brutieridin and melitidin, were able to influence *de novo* lipogenesis, we determine the activities of isocitrate dehydrogenase (Fig. 8, panel A) and malic enzyme (Fig. 8, panel B). These enzymes are related to this pathway as responsible for the formation of reduction potential, in the form of NADPH, required for *de novo* fatty acids synthesis. The results here reported show, in our animal model, a decrease of two tested enzyme activities, in statin and BMF treated rats. With regard to isocitrate dehydrogenase enzyme, the reduction was found about 50%, both after treatment with simvastatin that BMF. The decrease in the malic enzyme activity, instead, is more marked after treatment with simvastatin compared to that observed with BMF (lower 60 and 50%, respectively). Smaller decrease was detected in activities of both enzymes, in FF treated rats (30% isocitrate dehydrogenase and 40% malic enzyme, respectively)

Influence of simvastatin, BMF and FF on rat ALT, AST, bilirubin and creatinine levels.

At last, we investigated, in our animal model, the effects triggered by simvastatin, BMF and FF, on hepatic and renal functional parameters, (e.g. ALT, AST, bilirubin and creatinine). The creatinine levels decreased in simvastatin and FF treated rats by 14% compared to those of hypercholesterolemic rats. This reduction is even more marked, reaching 25%, in BMF treated rats; this latter treatment brings the creatinine level to normal values (group N values). Conversely, no significant difference was found for serum total bilirubin in treated rats, compared to those of groups N and H (Table 1). Compared with N group, the serum ALT and AST levels of the H group rats have had a greater increase, of 83% and 54% respectively. Serum ALT and AST levels were lowered significantly in rats belonging to H+S and H+FF groups (28% and 21% respectively), when comparing them to the hypercholesterolemic rats. This reduction was greater, by 40% and 31% respectively, in rats belonging to H+BMF group (Table 1). The results obtained in the present study are in good accordance with those reported by Iseri et al. [63] who observed that daily simvastatin treatment of rats, markedly improves cisplatin-induced kidney and liver dysfunction, as confirmed by biochemical assays.

FIGURE 1.

A



B

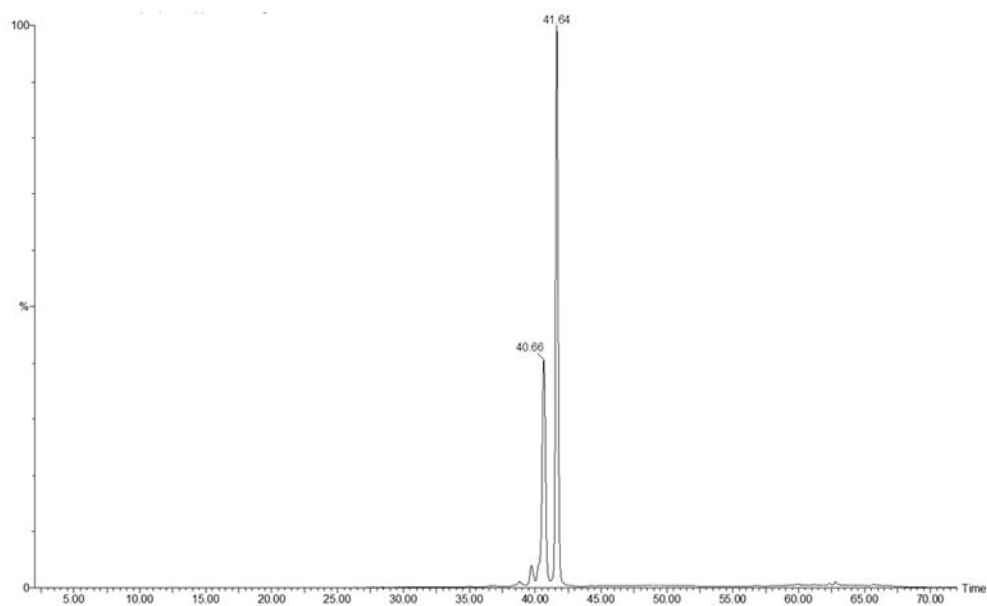


Fig. 1: HPLC/UV Chromatogram and structures of pure HMG flavonoid fraction (BMF).

Panel A: structures of brutieridin and melitidin. Panel B: structures of brutieridin and melitidin.

the revealed molecules were 75% w/w brutieridin (r.t. 41.64) and 24% w/w melitidin (r.t.

40.66).

FIGURE 2.

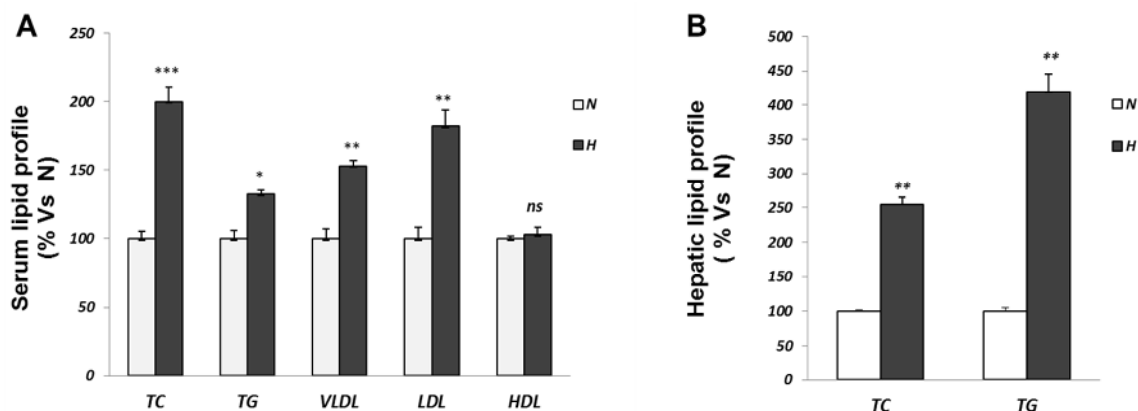


Fig. 2: Serum and hepatic lipid profile variations between normal and hypercholesterolemic rats. Normal (white bars, N) and hypercholesterolemic (grey bars, H) rats groups were fed as described in par 2.3. The total cholesterol (TC), triglycerides (TG), very low density lipoproteins (VLDL), low density lipoproteins (LDL) and high density lipoproteins (HDL) levels were measured in N and H serum (panel A, N as control). TC and TG were also measured in N and H liver (panel B, N as control). The obtained results were plotted as percentage and columns are mean \pm SD of three independent experiments performed in duplicate. *, $P = 0.01$ vs. control; **, $P < 0.01$ vs. control; ***, $P < 0.005$ vs. control; ns, nonsignificant.

FIGURE 3.

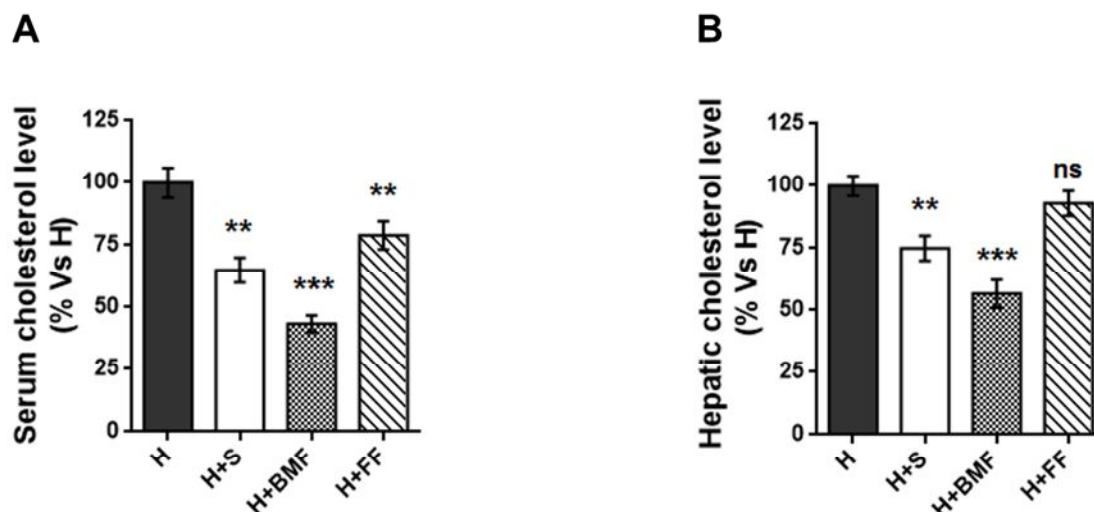


Fig. 3: Serum and hepatic total cholesterol variations between hypercholesterolemic and treated rats. Hypercholesterolemic (grey bars, H), simvastatin treated (white bars, H+S), BMF treated (checked bars, H+BMF) FF treated (striped bars, H+FF) rats groups were fed as described in par 2.3. The total cholesterol (TC) levels were measured in H, H+S, H+BMF and H+FF serum (panel A, H as control). TC was also measured in H, H+S, H+BMF and H+FF liver (panel B, H as control). The obtained results were plotted as percentage and columns are mean \pm SD of three independent experiments performed in duplicate. *, $P = 0.01$ vs. control; **, $P < 0.01$ vs. control; ***, $P < 0.005$ vs. control; ns, non significant.

FIGURE 4.

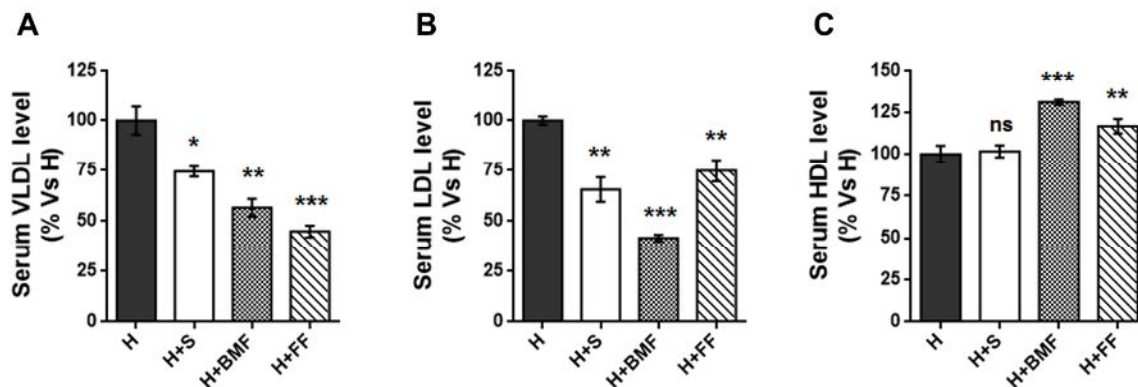


Fig. 4: Serum lipid profile variations between hypercholesterolemic and treated rats.

Hypercholesterolemic (grey bars, H), simvastatin treated (white bars, H+S), BMF treated (checked bars, H+BMF) FF treated (striped bars, H+FF) rats groups were fed as described in par 2.3. The very low density lipoproteins (VLDL), low density lipoproteins (LDL) and high density lipoproteins (HDL) levels were measured in H, H+S, H+BMF and H+FF serum (panels A, B and C, respectively, H as control). The obtained results were plotted as percentage and columns are mean \pm SD of three independent experiments performed in duplicate. *, $P = 0.01$ vs. control; **, $P < 0.01$ vs. control; ***, $P < 0.005$ vs. control; ns, non significant.

FIGURE 5.

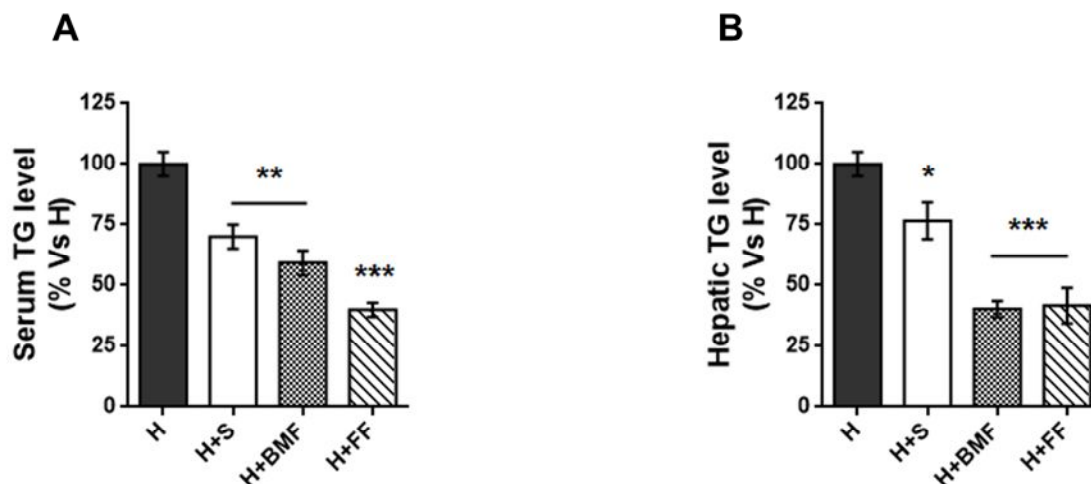


Fig. 5 :Serum and hepatic *triacylglycerols* variations between hypercholesterolemic and treated rats. Hypercholesterolemic (grey bars, H), simvastatin treated (white bars, H+S), BMF treated (checked bars, H+BMF) and FF treated (striped bars, H+FF) rats groups were fed as described in par 2.3. The *triacylglycerols* (TG) levels were measured in H, H+S, H+BMF and H+FF serum (panel A, H as control). TG were also measured in H, H+S, H+BMF and H+FF liver (panel B, H as control). The obtained results were plotted as percentage and columns are mean \pm SD of three independent experiments performed in duplicate. *, P = 0.01 vs. control; **, P < 0.01 vs. control; ***, P < 0.005 vs. control; ns, non significant.

FIGURE 6.

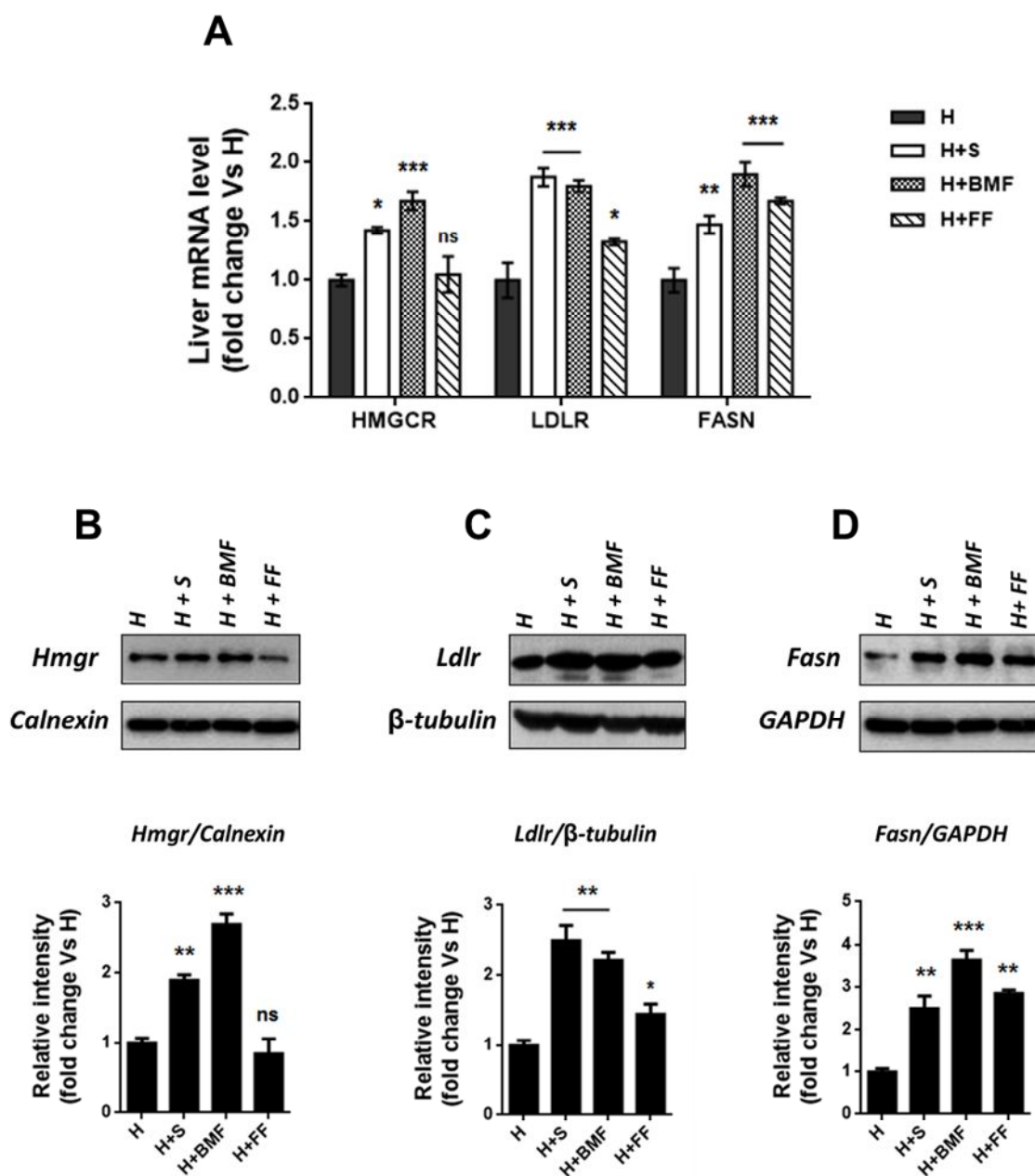


Fig. 6: Effect of simvastatin, BMF and FF on HMGR, LDLR and FASN mRNAs and proteins expression in experimental rats. Panel A: livers were isolated from hypercholesterolemic untreated rats (grey bars, H), hypercholesterolaemic treated with

simvastatin (white bars, H+S) or with BMF (checked bars, H+HMGF) or with FFF (striped bars, H+FF). The HMGR, LDLR and FASN mRNAs levels were analyzed by RT-PCR and normalized to that of 18S. The values are plotted as fold of H group and are representative of three independent experiments. *, $P < 0.01$ vs. H; **, $P < 0.01$ vs. control; ***, $P < 0.005$ vs. control. Panels B-D: protein levels of HMGR (97 kDa, panel B), LDLR (160 kDa, panel C) and FASN (270 kDa, panel D) are shown. A total of 100 μ g of microsomes or cellular liver extracts were used for Western blot analysis; Calnexin (90 kDa), α -tubulin (55 kDa) or GAPDH (37 kDa) were used as a control for equal loading and transfer. Densitometric analyses of the blots are also shown. The immunoblots are representative of three separate experiments. *, $P < 0.01$ vs. H; **, $P < 0.01$ vs. control; ***, $P < 0.005$ vs. control; ns, non significant.

FIGURE 7.

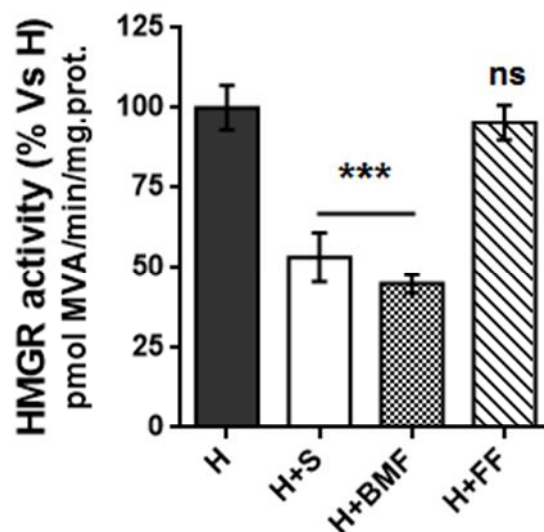


Fig. 7: Effect of simvastatin, BMF, and FF on HMGR activity, in experimental rats.

Hypercholesterolemic (grey bars, H), simvastatin treated (white bars, H+S), BMF treated (checked bars, H+BMF) FF treated (striped bars, H+FF); rats groups were fed as described in par 2.3. The enzyme activity was measured spectrophotometrically in liver from rats of different experimental groups, as described in Materials and Methods, (H as control). It was expressed as pmol mevalonate produced, per minute, per mg of protein. The obtained results were plotted as percentage vs. control (control value was 265 pmol MV/min/mg protein). The columns are mean \pm SD of three independent experiments performed in duplicate. ***, $P < 0.005$ vs. control; ns, non significant.

FIGURE 8.

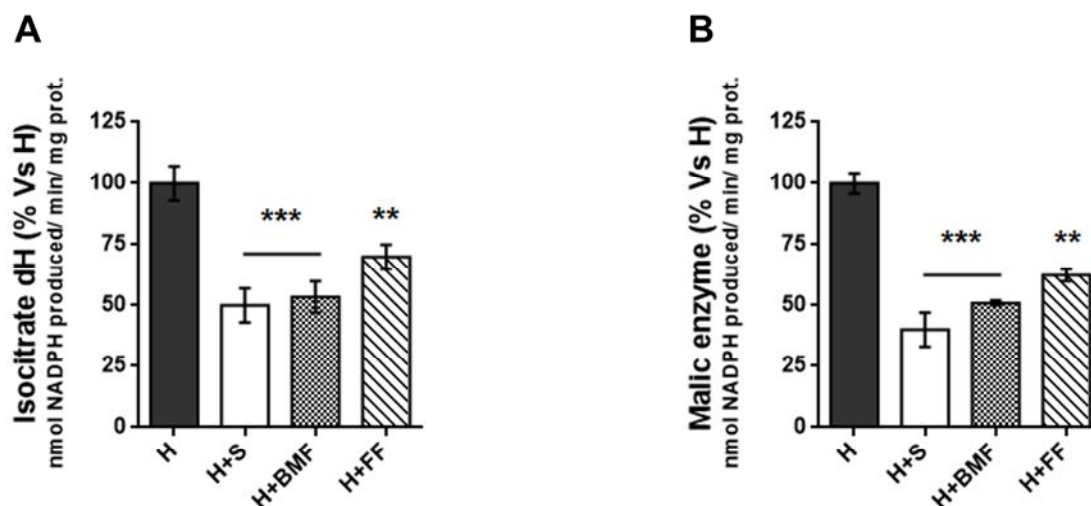


Fig. 8 Effect of simvastatin, BMF or FF and isocitrate dehydrogenase and malic enzyme activities, in experimental rats. Hypercholesterolemic (grey bars, H), simvastatin treated (white bars, H+S), BMF treated (checked bars, H+BMF) FF treated (striped bars, H+FF) rats groups were fed as described in par 2.3. The enzyme activities were measured spectrophotometrically in liver from rats of different experimental groups, as described in Materials and Methods, (H as control). They were expressed as nmol NADPH produced, per minute, per mg of protein. The obtained results were plotted as percentage vs. control (malic enzyme activity of control was 73 nmol NADPH/min/mg protein; isocitrate dehydrogenase of control was 186 nmol NADPH/min/mg protein). The columns are mean \pm SD of three independent experiments performed in duplicate. **, $P < 0.01$ vs. control; ***, $P < 0.005$ vs. control.

TABLE 1**Tab. 1: Bilirubin, creatinine ALT and AST serum levels in in experimental rats.**

GROUP	Total Bilirubin (mg/dl)	Creatinin (mg/dl)	ALT (U/L)	AST (U/L)
<i>N</i>	0.29 ± 0.05	0.52 ± 0.06	41.391 ± 2.730	102.996 ± 5.124
<i>H</i>	0.30 ± 0.04	0.69 ± 0.02	75.832 ± 3.654	157.019 ± 4.673
<i>H+S</i>	0.31 ± 0.05	0.60 ± 0.04	54.269 ± 4.002	123.998 ± 4.329
<i>H+BMF</i>	0.29 ± 0.06	0.52 ± 0.02	45.678 ± 3.423	109.375 ± 4.997
<i>H+FF</i>	0.29 ± 0.04	0.59 ± 0.03	54.269 ± 4.002	123.987 ± 5.689

ALT: alanine transferase; AST: aspartate transferase. Values are means ± SD.

DISCUSSION

The cholesterol homeostasis is subtly regulated at several levels as intestinal absorption, hepatic uptake of LDL, *de novo* synthesis and excretion. When its blood concentration raise over certain levels, the incidence of atherosclerosis and cardiovascular/cerebrovascular diseases becomes higher [64], hence it followed the need to develop many statin classes, as advanced pharmacological treatment, during the twentieth century [65]. Besides, it became pretty clear that a more correct daily diet could prevent the hypercholesterolemia, lowering the risk of the associated-diseases onset, as already reported from traditional cures employed in folk medicine [38]. Concerning this, the right habit of eating foods containing many bioactive compounds, as flavonoids, pectins, ascorbic acid [66, 20], has been shown to positively influence serum lipid levels and, most importantly, to reduce atherogenic lipoproteins. Recent studies have shown the presence of some statin-like compounds in the *Citrus bergamia* Risso [26-28], to which can be ascribed the beneficial effects exerted on human health. Starting from the latter data, in the present study we demonstrated that the two statin-like flavanones, extracted from bergamot and contained in BMF, exert a similar behaviour respect to commercial simvastatin on a model of hypercholesterolemic rats. The achievement of this model has been validated by the serum and liver lipid profile comparison of N versus H group, which has been used in the subsequent experiments in order to test BMF effects. The daily diet supplementation of H group with BMF, over the period of the study, led to a decrease of serum TC and TG, as in H+S group, but

exhibited a higher ability in decreasing LDL levels, accompanied by a significant increase in serum HDL content. The latter peculiarity represents a favourable event, given that HDL are able to picking up cholesterol from peripheral tissues or cells and carries it back to liver [67], where they are readily catabolized contributing to prevent atherosclerosis. It has been reported that elevated LDL levels and decreased HDL levels in serum represent independent risk factors for the onset of atherosclerosis associated diseases [59], whereas the data reporting the VLDL role in atherosclerotic plaque formation are still controversial [60]. In our experiments, BMF was found able to exert its beneficial actions on the LDL/HDL ratio but also to decrease VLDL serum levels, the latter event represents another very interesting feature. Then, we investigated the TC and TG hepatic levels, observing a drop of both in simvastatin treated rats hepatocytes and, in a higher extent, in BMF treated group. The TG and TC diminished availability determines the observed fall in VLDL liver secretion, required for cholesteryl ester transport to extra-hepatic districts. The effects on serum and hepatic lipid contents are strictly related to the variation of hepatic key enzymes and proteins involved in TC and TG metabolism. Particularly, we evaluated the expression level of HMGR and LDLR transcripts and proteins, as main indicators of cholesterol metabolism, together with the transcript and protein levels of FASN gene, mainly involved in TG metabolism. We found an up-regulation in HMGR and LDLR genes transcription under simvastatin treatment, according to previously published data [43] and also a significant induction of FASN gene transcription which should be included in the knowledge of simvastatin

induced effects, not yet reported. Similar results have been obtained in H+ BMF group, but in a higher extent, confirming one more time the BMF statin-like behaviour. This positive gene regulation consequently affects the proteins expression in liver indeed, in our experimental model, the increase in HMGR, LDLR and FASN gene transcription and protein translation under BMF treatment is clearly evident and justify the hypolipidemic effects observed in rat serum. The inhibition of HMGR activity detected and the induced expression of hepatic LDLR may be considered amongst the events responsible of TC and LDL decrease. As it is known, the HMGR expression and activity may change in response to the content of local cholesterol in cells and/or tissues [1]. In our model, HMGR inhibition lead to a reduction of endogenous cholesterol which, in turn, is responsible of the up-regulation of HMGR and LDLR genes transcription, as well of the higher LDLR exposure within the hepatocytes membrane, through a compensating mechanism based on sterol regulatory element-binding proteins (SREBPs) pathway [14]. It should be recalled that cholesterol depletion below a certain threshold is also responsible of FASN gene transcription increase, via SREBPs activation [14, 68], which is one of the effects we observed under both simvastatin or BMF treatments. However, the isocitrate dehydrogenase and malic enzyme activities decreased by BMF treatment. As these enzymes lead to the production of NADPH, required for *de novo* fatty acids synthesis, it can be suggested that, in our animal model, a decrease in this pathway is triggered by statins and BMF treatment. Our idea is that this reduction could be responsible for the decrease in serum and hepatic triglyceride

levels, observed in statins and BMF treated rats. Anyway, literature data on the effects of statins on fat accumulation are controversial and it seems to be influenced by on the type of statin, as well as on the metabolic status of individuals [69]. The outcomes here reported indicate that BMF could be a high potential control agent in hypercholesterolemia caused diseases, confirming one more time the ancient use of bergamot, as source of various nutraceuticals, for instance flavonoids. Indeed, in industrialized countries there has been a general trend towards the use of traditional medicines; for their pharmacological properties and, as well, for their low toxicity in animals, flavonoids have been considered as a *panacea* in several diseases treatment [70, 71]. Effectively, the two flavanones contained in BMF did not show toxicity *in vitro*, if not at very elevated concentrations, neither a potential genotoxicity [45] and does not exert negative effects on hepatic and renal functional parameters. Our results reinforce the traditional use of bergamot fruit by the calabrian population and may be useful to broaden the survey of the literature data about bergamot and its derivatives. These data establish, in a model that is highly related to humans, that inhibition exerted by BMF on HMGR is a promising nutraceutical strategy for the control of hypercholesterolemia, the main factor responsible of the increased cardiovascular diseases risk.

REFERENCES

1. Goldstein, J. L., & Brown, M. S. (1990). Regulation of the mevalonate pathway. *Nature*, 343(6257), 425-430.
2. Ross, S.D., Allen, I. E., Connelly, J. E., Korenblat, B. M., Smith, M. E., Bishop, D., et al. (1999). Clinical outcomes in statin treatment trials: a meta-analysis. *Arch Intern Med*, 159(15), 1793-1802.
3. Brown, M. S., & Goldstein, J. L. (1986). A receptor-mediated pathway for cholesterol homeostasis. *Science*, 232(4746), 34-47.
4. Balbisi, E. A. (2006). Management of hyperlipidemia: new LDL-C targets for persons at high-risk for cardiovascular events. *Med Sci Monit*, 12(2), RA34-39.
5. Miller, J. P. (1996). Hyperlipidaemia and cardiovascular disease. *Curr Opin Lipidol*, 7(1), U18-24.
6. Maxfield, F.R. Tabas, I. Role of cholesterol and lipid organization in disease. *Nature*, 2005, 438(7068), 612-621.
7. Gielen, S.; Sandri, M.; Schuler, G. Teupser, D. Risk factor management: antiatherogenic therapies. *Eur. J. Cardiovasc. Prev. Rehabil.*, 2009, 16 Suppl 2(S29-36).
8. Stamler, J.; Neaton, J.D.; Cohen, J.D.; Cutler, J.; Eberly, L.; Grandits, G.; Kuller, L.H.; Ockene, J.; Prineas, R. Group, M.R. Multiple risk factor intervention trial revisited: a new perspective based on nonfatal and fatal composite endpoints, coronary and cardiovascular, during the trial. *J. Am. Heart Assoc.*, 2012, 1(5), e003640.
9. Stamler, J. Neaton, J.D. The Multiple Risk Factor Intervention Trial (MRFIT)--importance then and now. *JAMA*, 2008, 300(11), 1343-1345.
10. Baigent, C.; Keech, A.; Kearney, P.M.; Blackwell, L.; Buck, G.; Pollicino, C.; Kirby, A.; Sourjina, T.; Peto, R.; Collins, R.; Simes, R. Cholesterol Treatment Trialists, C. Efficacy and safety of cholesterol-lowering treatment: prospective meta-analysis of data from 90,056 participants in 14 randomised trials of statins. *Lancet*, 2005, 366(9493), 1267-1278.
11. Boekholdt, S.M.; et al. Very low levels of atherogenic lipoproteins and the risk for cardiovascular events: a meta-analysis of statin trials. *J. Am. Coll. Cardiol.*, 2014, 64(5), 485-494.

12. Boekholdt, S.M.; et al. Association of LDL cholesterol, non-HDL cholesterol, and apolipoprotein B levels with risk of cardiovascular events among patients treated with statins: a meta-analysis. *JAMA*, 2012, 307(12), 1302-1309.
13. Ross, S.D.; Allen, I.E.; Connelly, J.E.; Korenblat, B.M.; Smith, M.E.; Bishop, D. Luo, D. Clinical outcomes in statin treatment trials: a meta-analysis. *Arch. Intern. Med.*, 1999, 159(15), 1793-1802.
14. Scharnagl, H.; Schinker, R.; Gierens, H.; Nauck, M.; Wieland, H. Marz, W. Effect of atorvastatin, simvastatin, and lovastatin on the metabolism of cholesterol and triacylglycerides in HepG2 cells. *Biochem. Pharmacol.*, 2001, 62(11), 1545-1555.
15. Stone, et al. American College of Cardiology/American Heart Association Task Force on Practice, G. 2013 ACC/AHA guideline on the treatment of blood cholesterol to reduce atherosclerotic cardiovascular risk in adults: a report of the American College of Cardiology/American Heart Association Task Force on Practice Guidelines. *Circulation*, 2014, 129(25 Suppl 2), S1-45.
16. Gorinstein, S., Leontowicz, H., Leontowicz, M., Krzeminski, R., Gralak, M., Martin-Belloso, O., et al. (2004). Fresh Israeli Jaffa blond (Shamouti) orange and Israeli Jaffa red Star Ruby (Sunrise) grapefruit juices affect plasma lipid metabolism and antioxidant capacity in rats fed added cholesterol. *J Agric Food Chem*, 52(15), 4853-4859.
17. Srinivasan, S., & Pani, L. (2013). Antihyperlipidemic effect of diosmin: A citrus flavonoid on lipid metabolism in experimental diabetic rats. *Journal of Functional Foods*, 5(1), 484-492.
18. Chen, Z. Y., Ma, K. Y., Liang, Y. T., Peng, C., & Zuo, Y. Y. (2011). Role and classification of cholesterol-lowering functional foods. *Journal of Functional Foods*, 3(2), 61-69.
19. Chinapongtitiwat, V., Jongaroontaprangsee, S., Chiewchan, N., & Devahastin, S. (2013). Important flavonoids and limonin in selected Thai citrus residues. *Journal of Functional Foods*, 5(3), 1151-1158.
20. Monforte, M. T., Trovato, A., Kirjavainen, S., Forestieri, A. M., Galati, E. M., & Lo Curto, R. B. (1995). Biological effects of hesperidin, a Citrus flavonoid. (note II): hypolipidemic activity on experimental hypercholesterolemia in rat. *Farmaco*, 50(9), 595-599.
21. Harborne, J.B. Williams, C.A. Advances in flavonoid research since 1992. *Phytochemistry*, 2000, 55(6), 481-504.
22. Vogt, T. Phenylpropanoid biosynthesis. *Mol. Plant*, 2010, 3(1), 2-20.

23. Benavente-Garcia, O. Castillo, J. Update on uses and properties of citrus flavonoids: new findings in anticancer, cardiovascular, and anti-inflammatory activity. *J. Agric. Food Chem.*, 2008, 56(15), 6185-6205.
24. Gattuso, G.; Barreca, D.; Gargiulli, C.; Leuzzi, U. Caristi, C. Flavonoid composition of Citrus juices. *Molecules*, 2007, 12(8), 1641-1673.
25. Nogata, Y.; Sakamoto, K.; Shiratsuchi, H.; Ishii, T.; Yano, M. Ohta, H. Flavonoid composition of fruit tissues of citrus species. *Biosci. Biotechnol. Biochem.*, 2006, 70(1), 178-192.
26. Di Donna, L.; De Luca, G.; Mazzotti, F.; Napoli, A.; Salerno, R.; Taverna, D. Sindona, G. Statin-like principles of bergamot fruit (*Citrus bergamia*): isolation of 3-hydroxymethylglutaryl flavonoid glycosides. *J. Nat. Prod.*, 2009, 72(7), 1352-1354.
27. Di Donna, L.; Iacopetta, D.; Cappello, A.R.; Gallucci, G.; Martello, E.; Fiorillo, M.; Dolce, V. Sindona, G. Hypocholesterolaemic activity of 3-hydroxy-3- methyl-glutaryl flavanones enriched fraction from bergamot fruit (*Citrus bergamia*): ‘In vivo’ studies. *J. Funct. Foods*, 2014, 7(558-568).
28. Mollace, V., Sacco, I., Janda, E., Malara, C., Ventrice, D., Colica, C., et al. (2011). Hypolipemic and hypoglycaemic activity of bergamot polyphenols: from animal models to human studies. *Fitoterapia*, 82(3), 309-316.
29. Trombetta, D., Cimino, F., Cristani, M., Mandalari, G., Saija, A., Ginestra, G., et al. (2010). In vitro protective effects of two extracts from bergamot peels on human endothelial cells exposed to tumor necrosis factor-alpha (TNF-alpha). *J Agric Food Chem*, 58(14), 8430-8436.
30. Di Donna, L., De Luca, G., Mazzotti, F., Napoli, A., Salerno, R., Taverna, D., et al. (2009). Statin-like principles of bergamot fruit (*Citrus bergamia*): isolation of 3-hydroxymethylglutaryl flavonoid glycosides. *J Nat Prod*, 72(7), 1352-1354.
31. Lo Curto, R. (2013). Use of Juice and By-products. In G. Dugo & I. Bonaccorsi (Eds.), *Citrus bergamia-Bergamot and Its Derivatives* (Vol. 51). Roca Baton, FL: CCR Press.
32. Barreca, D., Bellocco, E., Caristi, C., Leuzzi, U., & Gattuso, G. (2007). Flavonoid composition and antioxidant activity of juices from Chinotto (*Citrus x myrtifolia* Raf.) fruits at different ripening stages. *J Agric Food Chem*, 55(5), 3031-3036.

33. Dugo, P., Presti, M. L., Ohman, M., Fazio, A., Dugo, G., & Mondello, L. (2005). Determination of flavonoids in citrus juices by micro-HPLC-ESI/MS. *J Sep Sci*, 28(11), 1149-1156.
34. Gattuso, G., Caristi, C., Gargiulli, C., Bellocco, E., Toscano, G., & Leuzzi, U. (2006). Flavonoid glycosides in bergamot juice (*Citrus bergamia* Risso). *J Agric Food Chem*, 54(11), 3929-3935.
35. Nogata, Y., Sakamoto, K., Shiratsuchi, H., Ishii, T., Yano, M., & Ohta, H. (2006). Flavonoid composition of fruit tissues of citrus species. *Biosci Biotechnol Biochem*, 70(1), 178-192.
36. Choe, S.C.; Kim, H.S.; Jeong, T.S.; Bok, S.H. Park, Y.B. Naringin has an antiatherogenic effect with the inhibition of intercellular adhesion molecule-1 in hypercholesterolemic rabbits. *J. Cardiovasc. Pharmacol.*, 2001, 38(6), 947-955.
37. Yu, J.; Wang, L.; Walzem, R.L.; Miller, E.G.; Pike, L.M. Patil, B.S. Antioxidant activity of citrus limonoids, flavonoids, and coumarins. *J. Agric. Food Chem.*, 2005, 53(6), 2009-2014.
38. Miceli, N.; Mondello, M.R.; Monforte, M.T.; Sdrafkakis, V.; Dugo, P.; Crupi, M.L.; Taviano, M.F.; De Pasquale, R. Trovato, A. Hypolipidemic effects of *Citrus bergamia* Risso et Poiteau juice in rats fed a hypercholesterolemic diet. *J. Agric. Food Chem.*, 2007, 55(26), 10671-10677.
39. Gardana, C.; Nalin, F. Simonetti, P. Evaluation of flavonoids and furanocoumarins from *Citrus bergamia* (Bergamot) juice and identification of new compounds. *Molecules*, 2008, 13(9), 2220-2228.
40. Gattuso, G.; Barreca, D.; Caristi, C.; Gargiulli, C. Leuzzi, U. Distribution of flavonoids and furocoumarins in juices from cultivars of *Citrus bergamia* Risso. *J. Agric. Food Chem.*, 2007, 55(24), 9921-9927.
41. Paine, M.F.; Criss, A.B. Watkins, P.B. Two major grapefruit juice components differ in time to onset of intestinal CYP3A4 inhibition. *J. Pharmacol. Exp. Ther.*, 2005, 312(3), 1151-1160.
42. Gliozzi, M.; et al.. Bergamot polyphenolic fraction enhances rosuvastatin-induced effect on LDL-cholesterol, LOX-1 expression and protein kinase B phosphorylation in patients with hyperlipidemia. *Int. J. Cardiol.*, 2013, 170(2), 140-145.

43. Kong, W.J.; Wei, J.; Zuo, Z.Y.; Wang, Y.M.; Song, D.Q.; You, X.F.; Zhao, L.X.; Pan, H.N. Jiang, J.D. Combination of simvastatin with berberine improves the lipid-lowering efficacy. (2008), *Metabolism*, 57(8), 1029-1037.
44. Muci, M. R., Cappello, A. R., Vonghia, G., Bellitti, E., Zezza, L., & Gnoni, G. V. (1992). Change in cholesterol levels and in lipid fatty acid composition in safflower oil fed lambs. *Int J Vitam Nutr Res*, 62(4), 330-333.
45. Di Donna, L.; Iacopetta, D.; Cappello, A.R.; Gallucci, G.; Martello, E.; Fiorillo, M.; Dolce, V. Sindona, G. Hypocholesterolaemic activity of 3-hydroxy-3- methyl-glutaryl flavanones enriched fraction from bergamot fruit (Citrus bergamia): ‘‘In vivo’’ studies. *J. Funct. Foods*, 2014, 7(558-568).
46. Zara, V., Dolce, V., Capobianco, L., Ferramosca, A., Papatheodorou, P., Rassow, J., et al. (2007). Biogenesis of eel liver citrate carrier (CIC): Negative charges can substitute for positive charges in the presequence. *J Mol Biol*, 365(4), 958-967.
47. Iacopetta, D., Madeo, M., Tasco, G., Carrisi, C., Curcio, R., Martello, E., et al. (2011). A novel subfamily of mitochondrial dicarboxylate carriers from *Drosophila melanogaster*: biochemical and computational studies. *Biochim Biophys Acta*, 1807(3), 251-261.
48. Lunetti, P., Cappello, A. R., Marsano, R. M., Pierri, C. L., Carrisi, C., Martello, E., et al. (2013). Mitochondrial glutamate carriers from *Drosophila melanogaster*: biochemical, evolutionary and modeling studies. *Biochim Biophys Acta*, 1827(10), 1245-1255.
49. Caputi Jambrenghi, A., Paglialonga, G., Gnoni, A., Zanotti, F., Giannico, F., Vonghia, G., et al. (2007). Changes in lipid composition and lipogenic enzyme activities in liver of lambs fed omega-6 polyunsaturated fatty acids. *Comp Biochem Physiol B Biochem Mol Biol*, 147(3), 498-503.
50. Madeo, M., Carrisi, C., Iacopetta, D., Capobianco, L., Cappello, A. R., Bucci, C., et al. (2009). Abundant expression and purification of biologically active mitochondrial citrate carrier in baculovirus-infected insect cells. *J Bioenerg Biomembr*, 41(3), 289-297.
51. Cappello, A. R., Guido, C., Santoro, A., Santoro, M., Capobianco, L., Montanaro, D., et al. (2012). The mitochondrial citrate carrier (CIC) is present and regulates insulin secretion by human male gamete. *Endocrinology*, 153(4), 1743-1754.
52. Duncan, I. W., Culbreth, P. H., & Burtis, C. A. (1979). Determination of free, total, and esterified cholesterol by high-performance liquid chromatography. *J Chromatogr*, 162(3), 281-292.

53. Pallottini, V., Martini, C., Anna M. Bassi, AM, Romano, P., Nanni, G., Trentalance, A. (2006) *Journal of Hepatology*, 44, 368–374.
54. Bruscalupi G, Leoni S, Mangiantini MT, Spagnolo S, Trentalance A. (1985). True uncoupling between cholesterol synthesis and 3-hydroxy-3- methylglutaryl coenzyme A reductase in early stage of liver regeneration. *Cell Mol Biol*, 31, 365–368.
55. Ochoa, S. (1955). *Methods Enzymol.* 1: 699-704.
56. Ochoa, S. (1955). *Methods Enzymol.* 1: 739-753.
57. Bradford, M., M., (1976) A rapid and sensitive method for the quantitation of microgram quantities of protein utilizing the principle of protein-dye binding. *Anal Biochem*; 72, 248-254.
58. Steinberg, D. (1987). Lipoproteins and the pathogenesis of atherosclerosis. *Circulation*, 76(3), 508-514.
59. Arsenault, B. J., Rana, J. S., Stroes, E. S., Despres, J. P., Shah, P. K., Kastelein, J. J., et al. (2009). Beyond low-density lipoprotein cholesterol: respective contributions of non-high-density lipoprotein cholesterol levels, triglycerides, and the total cholesterol/high-density lipoprotein cholesterol ratio to coronary heart disease risk in apparently healthy men and women. *J Am Coll Cardiol*, 55(1), 35-41.
60. Stancu, C. S., Toma, L., & Sima, A. V. (2012). Dual role of lipoproteins in endothelial cell dysfunction in atherosclerosis. *Cell Tissue Res*, 349(2), 433-446.
61. Krause, B. R., & Newton, R. S. (1995). Lipid-lowering activity of atorvastatin and lovastatin in rodent species: triglyceride-lowering in rats correlates with efficacy in LDL animal models. *Atherosclerosis*, 117(2), 237-244.
62. Dolce, V., Cappello, A. R., Lappano, R., & Maggiolini, M. (2011). Glycerophospholipid synthesis as a novel drug target against cancer. *Curr Mol Pharmacol*, 4(3), 167-175.
63. Iseri, S., Ercan, F., Gedik, N., Yuksel, M., Alican, I. (2007), Simvastatin attenuates cisplatin-induced kidney and liver damage in rats. *Toxicology*, 230, 256–264.
64. Steinberg, D. (1987). Lipoproteins and the pathogenesis of atherosclerosis. *Circulation*, 76(3), 508-514.
65. Witztum, E. (1996). Drugs used in the treatment of hyperlipoproteinemias. *The Pharmacological Basis of Therapeutics*, 9th. McGraw-Hill, New York, 875–877.

66. Gorinstein, S., Leontowicz, H., Leontowicz, M., Krzeminski, R., Gralak, M., Delgado-Licon, E., et al. (2005). Changes in plasma lipid and antioxidant activity in rats as a result of naringin and red grapefruit supplementation. *J Agric Food Chem*, 53(8), 3223-3228.
67. deGoma, E. M., & Rader, D. J. (2011). Novel HDL-directed pharmacotherapeutic strategies. *Nat Rev Cardiol*, 8(5), 266-277.
68. Sato, R. (2010). Sterol metabolism and SREBP activation. *Arch Biochem Biophys*, 501(2), 177-181.
69. Aguirre, I., Hijona, E., Macarulla, M.T., et al. (2013) Several statins increase body and liver fat accumulation in a model of metabolic syndrome. *Journal of Physiology and Pharmacology*, 64, 3, 281-288.
70. Kurzawa-Zegota, M., Najafzadeh, M., Baumgartner, A., & Anderson, D. (2012). The protective effect of the flavonoids on food-mutagen-induced DNA damage in peripheral blood lymphocytes from colon cancer patients. *Food Chem Toxicol*, 50(2), 124-129.
71. Nijveldt, R. J., van Nood, E., van Hoorn, D. E., Boelens, P. G., van Norren, K., & van Leeuwen, P. A. (2001). Flavonoids: a review of probable mechanisms of action and potential applications. *Am J Clin Nutr*, 74(4), 418-425.

CHAPTER 2

INTRODUCTION

The past 20 years have seen significant reductions in mortality from breast cancer in all world. This reduction has been largely due to improvement in early detection and the development of more effective adjuvant therapies. Despite these exciting developments and despite administration of adjuvant therapies, many women still experience relapse, and metastatic breast cancer remains a largely incurable disease.[1] Emerging research suggests that one of the mechanisms accounting for treatment resistance is the existence of subpopulations within human breast cancers that display stem-cell properties. The cancer stem-cell hypothesis contains two separable but related components. The first, concerning the origin of cancers, holds that cancers arise in cell populations that either maintain or acquire the stem-cell property of self-renewal. The second is that resulting cancers are organized in a hierarchical fashion, in which self-renewing cancer stem cells drive the malignant process as well as generate a population of non-renewing cells that form the bulk of the tumor [2]. As only a very small percentage of cancer cells have “stem-like” and “tumor-initiating” properties, they are difficult to study and their key distinguishing features remain relatively uncharacterized, although they appears to resist both chemo-therapy and radiation. Interestingly, CSCs share many properties with normal stem cells, including immortality and resistance to stress, as well as asymmetric cell division [3, 4]. Two main therapeutic approaches have been developed for targeting cancer stem cells (CSCs) [5]. The first approach is based on targeting well known key

pathways regulating CSC survival, differentiation, and self-renewal. Several master pathways commonly involved in self-renewal of embryonic and adult stem cells are deregulated in CSCs and induce an expansion of this subpopulation. The second approach is an unbiased strategy based on the study of CSC-enriched populations using omics technologies or high-throughput screening of small molecule or RNA interference libraries. This second approach allows the identification of new pathways and networks regulating CSC biology. Recently was compared the transcriptional profiles of ALDEFLUOR-positive and ALDEFLUOR-negative cells isolated from breast cancer cell lines [6, 7]. Interestingly, CSCs share many properties with normal stem cells, including immortality and resistance to stress, as well as asymmetric cell division [8]. A particular distinguishing characteristic of CSCs is their ability to initiate tumors and to undergo anchorage-independent growth, when cultured in suspension [9]. Under these particular cell culture conditions, CSCs proliferate and form 3D-spheroid-like structures, containing CSCs and progenitor cells, which are known as “tumor-spheres” or “onco-spheres” [10, 11]. Importantly, each 3D-spheroid originates from the clonal proliferation of a single CSC, is not due to the self-aggregation of cancer cells. The CSC population is resistant to DNA-damage, and shows lower levels of ROS production, as well [12, 13]. 3D-tumor-spheres derived from breast cancer cells are also known as mammo-spheres [10, 11]. The mammospheres formed in these conditions showed an increase in CD24-/CD44+ cells and in ALDEFLUOR-positive cells and displayed high tumorigenic potential. Because the capacity to generate a colony in non-

adherent culture conditions is an intrinsic property of immature stem/progenitor cells from all molecular subtypes, the tumorsphere assay might offer the opportunity to screen the CSC regulatory mechanisms either in luminal or in basal subtypes [14, 15]. Here, was compared the proteomic profiles of cancer cells grown in adherent conditions to matched tumorsphere cultures in MCF-7 and T-47D. The enzymes of the mevalonate (MVA) metabolic pathway were overexpressed in basal/mesenchymal tumorspheres compared to cognate adherent cells. The mevalonate pathway leads to cholesterol synthesis, protein farnesylation, and protein geranylgeranylation (GG). The modulation of this metabolic pathway demonstrated that is a key factor of breast CSC maintenance [16]. Statins prevent the rate-limiting conversion of HMG-CoA to mevalonate by HMGCR, which is not only a precursor of cholesterol but is an essential metabolite in the formation of isoprenes. Isoprenes are critical compounds involved in the prenylation of numerous signaling molecules such as small G proteins [17]. Statin mediated inhibition of the prenylation process is reversible by the addition of the various isoprenes such as mevalonate, farnesyl-pyrophosphate, and geranyl-geranyl-pyrophosphate [16, 18]. Prenylation also occurs in many cellular and systemic regulatory pathways that are partly responsible for the pleiotropic effects of statins. Other pleiotropic effects may be independent of prenylation or inhibition of cholesterol production such as cell cycle arrest [19]. Towards this end, was investigated the therapeutic potential of BMF to target cancer cell growth and cancer stem cells (CSCs) formation by HMGCR blockade. Here, was showed BMF can be used to selectively

inhibit the proliferative of cancer stem cells. For this purpose, was employed the tumor-sphere assay, which functionally measures the clonal expansion of single cancer stem cells under anchorage-independent conditions. More specifically, is shown that BMF reduces the mitochondrial respiration increasing endogenous fatty acid oxidation in MCF7 cancer cell line. The BMF show a non-toxic effect on normal fibroblasts (h-tert-BJ1). Effectively BMF inhibits the adhesion cells stopping the cell cycle in G0/G1 phase and inhibits tumorspheres formation in MCF7 cell line. Mechanistically, is shown that BMF exerts its striking effects on CSCs by inhibiting several key signal transduction pathways (WNT, Notch and STAT-signalling), reducing interleukin-8 (IL-8) and granulocytes-macrophages colony stimulating factor (GM-CSF) levels in MCF7 and inhibiting hypoxia inducible factor (HIF) and Nf-K signalling pathways in h-tert.BJ1. Thus, BMF may be an effective non-toxic therapeutic strategy for the eradication of cancer stem cells, via mevalonate pathway inhibition

MATERIALS AND METHODS

Materials.

MCF7 breast cancer cell lines were purchased from the ATCC. Human immortalized fibroblasts (hTERT-BJ1) were originally purchased from Clontech, Inc. Cells were cultured in Dulbecco's modified Eagle's medium (DMEM), supplemented with 10% FBS (fetal bovine serum), 2 mM GlutaMAX, and 1% Pen-Strep (complete media) in a 37°C humidified atmosphere containing 5% CO₂, unless otherwise noted. Gibco-brand cell culture media (DMEM) was purchased from Life Technologies. Lentiviral vector for the over-expression of HMGCR was obtained commercially from Genecopoeia, along with appropriate empty vector controls.

Lentiviruses.

Lentiviral plasmids, packaging cells and reagents were from Genecopoeia. 48 hours after seeding, 293Ta packaging cells were transfected with lentiviral vectors encoding HMGCR or empty vector (EX-NEG-Lv105), using Lenti-Pac™ HIV Expression Packaging Kit according to the manufacturer's instructions. Two days post-transfection, lentivirus-containing culture medium was passed through a 0.45 µm filter and added to the target cells (MCF7 cells) in the presence of 5 µg/ml Polybrene. Infected cells were selected with a concentration of 1.5 µg/ml of puromycin.

Sulforhodamine B (SRB) assay.

SRB (S9012, Sigma) measures total biomass by staining cellular proteins. After 48 h treatment, cells were fixed in 10% trichloroacetic acid (T9159, Sigma) for 1h at 4°C, stained with SRB (S9012, Sigma) for 15 minutes, and washed 3 times with 1% acetic acid (27225, Sigma). The incorporated dye was solubilized with 10 mM Tris Base, pH 8.8 (T1503, Sigma). Absorbance was spectrophotometrically measured at 540 nm in a FluoStar Omega plate reader (BMG Labtech). Background measurements were subtracted from all values [20].

Label-free quantitative proteomics.

Chemicals and sample preparation. Formic acid, trifluoroacetic acid, ammonium formate (10 M), ammonium bicarbonate TCEP (Tris (2-carboxyethyl)phosphine hydrochloride), MMTS (Methyl methanethiosulfonate) and trypsin were all obtained from Sigma. HPLC gradient grade acetonitrile was obtained from Fisher Scientific. Briefly, 2×10^6 MCF-7 were seeded in 150 cm culture dishes coated with (2-hydroxyethylmethacrylate) (poly-HEMA, Sigma, #P3932) until cells were formed spheres (5days). As control, MCF-7 cells only attached, were processed in parallel. After 5 days, cells were lysed in RIPA buffer (R0278, Sigma) and kept at 4°C for 20 minutes with rotation. Lysates were cleared by centrifugation for 10 minutes at 10,000 x g and supernatants were collected and kept frozen at -80°C. *Protein digestion.* Lysate samples were thawed to room temperature and their concentrations equalised to 1 µg/µL

(50 μL volume) with RIPA buffer, and further processed for trypsin digestion by sequential reduction of disulphide bonds with TCEP and alkylation with MMTS. Briefly, 1 μL benzonase (Novagen) was added to the 50 μL aliquot and placed on ice for 15 minutes. The sample was then taken to dryness using a SpeedVac, and resuspended in 22.5 μL trypsin reaction buffer (40 mM ammonium bicarbonate and 9% acetonitrile). One μL of 50 mM TCEP solution was added to each sample, mixed briefly and placed on a heater block at 60°C for 60 minutes. After cooling to room temperature, 0.5 μL of 200 mM MMTS solution was added to each sample and allowed to react for 15 minutes. Trypsin was added in two waves to ensure efficient digestion of the sample. Firstly, 20 μg of sequencing grade trypsin was resuspended in 1800 μL of trypsin reaction buffer; 225 μL of this solution were added to each sample for digestion, and the reactions were left at 37°C overnight with shaking (600 rpm). The following morning, a further aliquot of trypsin was added. Two ml of trypsin reaction buffer was added to 20 μL of sequencing grade trypsin; 250 μL of this solution were added to each of the digest samples from overnight, and the reactions were left at 37°C for 4 hours with shaking (600 rpm). Thirty-five μL 10% formic acid were added to the 500 μL digest sample (0.7% final concentration of formic acid) to stop the digestion. The digested solution was diluted in 7.5 mL of acetonitrile containing 0.3% formic acid. *HILIC solid phase extraction (SPE) of peptides*. PolyhydroxyethylA SPE 12 μm , 300A, 300mg cartridges (obtained from PolyLC) were used for the HILIC procedure. Prior to use, cartridges required an overnight soak in 50 mM formic acid followed by rinsing with water the

following day. Cartridges were preconditioned with 2 mL of Buffer A (90% acetonitrile, 5 mM ammonium formate, pH 2.7) followed by 2 mL of Buffer B (5mM ammonium formate, pH 2.7) and finally re-equilibrated with 10 mL Buffer A. The diluted samples were loaded onto the cartridges and washed with a further 10 mL Buffer A. Finally, peptides were eluted in 1 mL Buffer C (9 parts Buffer B plus 1 part Buffer A) and the samples dried on a Speedvac to remove organic solvent prior to LC-MS/MS analysis.

LC-MS/MS analysis. Lyophilised digests were resuspended in 50 μ L of 0.1% TFA to give an approximate concentration of 1 μ g/ μ L. One μ L injection volumes were used throughout resulting in an on-column peptide loading of approximately 1 μ g per injection. Analysis was performed in quintuplicate for each sample. All LC-MS/MS analyses were performed on an LTQ Orbitrap XL mass spectrometer coupled to an Ultimate 3000 RSLCnano system (Thermo Scientific). One μ L injection volumes were used throughout and samples loaded directly onto the analytical column, PepMap RSLC C18, 2 μ m x 75 μ m id x 50 cm (Thermo Scientific). The composition (v/v) of LC buffers were as follows; Buffer A - 99.9% water plus 0.1% formic acid and Buffer B - 80% acetonitrile, 19.9% water and 0.1% formic acid. Peptides were loaded directly onto the column at a flow rate of 400 nl/min with an initial mobile phase composition of 1% B. The organic strength was increased linearly from 1% to 22.5% B over 22.5 minutes again at 400 nl/min, followed by an increase to 24.8% B over the next 2.6 minutes with a concomitant reduction in flow rate to 300 nl/min, and to 39% B over a further 14 minutes. A further increase to 60% B over the next 5 minutes was followed by a ramp to

95% B over 2.5 minutes where it was held for a further 2 minutes. The column was then allowed to re-equilibrate to 1% B for a total analysis time of 74 minutes. The mass spectrometer was instructed to perform data dependent acquisition on the top six precursor ions, which were measured in the Orbitrap FTMS detector over the mass range 370-1200 m/z, at a nominal resolution of 60,000. MS/MS spectra were acquired in the ion trap under CID conditions with normalized collision energy of 35, isolation width of 3 Th, Q value of 0.25 and 30 ms activation time. Gas-phase fractionation was performed on the five replicate injections such that MS/MS data was collected for precursor ion range 370-494 m/z Injection 1, 494-595 m/z Injection 2, 595-685 m/z Injection 3, 685-817 m/z Injection 4 and 817-1200 m/z Injection 5. *Statistical analysis.* Xcalibur raw data files acquired on the LTQ-Orbitrap XL were directly imported into Progenesis LCMS software (Waters Corp) for peak detection and alignment. Data were analysed using the Mascot search engine [21]. Three replicates were analysed for each sample type (N = 3). Statistical analyses were performed using ANOVA and only fold-changes in proteins with a p-value less than 0.05 were considered significant (Scheme 1).

Ingenuity pathway analyses.

Pathway and function analyses were generated using Ingenuity Pathway Analysis (IPA) (Ingenuity systems, <http://www.ingenuity.com>), which assists with proteomics data interpretation via grouping differentially expressed genes or proteins into known

functions and pathways. Pathways with a z score >1.9 were considered as significantly activated, and pathways with a z score <-1.9 were considered as significantly inhibited.

Cell Cycle.

Control and treated MCF7 cells were subjected to cell-cycle analysis by FACS. Briefly, 1×10^6 cells, per condition, were fixed with cold ethanol (80%) for 30 min on ice, centrifuged, and washed twice in cold PBS. The cells were incubated with 0.1% Triton X-100 and $1\mu\text{g/ml}$ DAPI (Invitrogen D1306). Following a 30-min incubation at room temperature, cells were analysed (50,000 events per condition) using FACS (BD Fortessa). Gated cells were manually categorised into cell-cycle stages .

Seahorse XFe-96 Metabolic Flux Analysis (OCR, ECAR and FAO).

Real-time oxygen consumption rates (OCR), extracellular acidification rates (ECAR) and fatty acid oxidation measurement (FAO) for MCF7 cells and fibroblasts (h-tert-BJ1 cells) treated with BMF, pravastatin and simvastatin were determined using the Seahorse Extracellular Flux (XFe-96) analyzer (Seahorse Bioscience, MA, USA) [22]. 1×10^4 cells per well were seeded into XFe-96 well cell culture plates, and incubated overnight to allow attachment. Then, cells were treated with BMF, pravastatin and simvastatin ($100\mu\text{M}$ and 1mM) for 72 hours. Vehicle alone (DMSO) control cells were processed in parallel. After 72 hours of incubation, cells were washed in pre-warmed

XF assay media (or for OCR measurement, XF assay media supplemented with 10mM glucose, 1mM Pyruvate, 2mM L-glutamine and adjusted at 7.4 pH). Cells were then maintained in 175 μ L/well of XF assay media at 37°C, in a non-CO₂ incubator for 1 hour. During the incubation time, we loaded 25 μ L of 80mM glucose, 9 μ M oligomycin, and 1M 2-deoxyglucose (for ECAR measurement) or 10 μ M oligomycin, 9 μ M FCCP, 10 μ M rotenone, 10 μ M antimycin A (for OCR measurement), in XF assay media into the injection ports in the XFe-96 sensor cartridge [22]. The fatty acid oxidation (FAO) was evaluated by XF assay for oxidation of exogenous and endogenous FAs. 1.5×10^3 cells were seeded in XF Cell Culture Microplates and allowed to grow overnight in typical growth medium. The growth medium was then replaced (after 24h) with substrate-limited medium contained BMF 1mM, glucose 0.5 mM, GlutaMAX 1 mM, carnitine 0.5 mM and 1% FBS to deplete endogenous substrates within the cell (glycogen, triglycerides, amino acids), thus priming the cells to oxidize exogenous FAs. Carnitine was added fresh the day of the media change. and serum to deplete endogenous substrates within the cell (glycogen, triglycerides, amino acids), thus priming the cells to oxidize exogenous FAs. Prior to the assay (45 minutes before) the cells were washed twice times with FAO Assay Medium contained NaCl 111mM, KCl 4.7mM, CaCl₂ 1.25mM, MgSO₄ 2mM, NaH₂PO₄ 1.2mM supplemented with 2.5mM glucose, 0.5mM carnitine, and 5mM HEPES on the day of the assay, adjusted to pH 7.4 at 37°C. The FAO assay medium was added to the plate (135 μ L/well) and incubated in a non-CO₂ incubator for 30 minutes at 37°C. The cartridge was loaded following OCR

protocol as described before. After 30 minutes 10mM stock solution of Etomoxir (Eto) was diluted to 400 μ M in FAO Assay Medium and was added 15 μ L to the appropriate wells. The final concentration of Eto in the wells was 40 μ M. The plate was incubated for 15 minutes at 37°C in a non-CO₂ incubator. Just prior to starting the assay 30 μ L of XF Palmitate-BSA FAO Substrate or BSA to the appropriate wells and immediately the XF Cell Culture Microplate was inserted into the XF96 Analyzer and was run the XF Cell Mito Stress Test with the command protocol. Measurements were normalized by protein content (SRB and Bradford assay). Data set was analyzed by XFe-96 software and GraphPad Prism software, using one-way ANOVA and Student's t-test calculations. All experiments were performed in quintuplicate, three times independently.

Evaluation of CSC signalling pathways.

The Signal Lenti reporter assay (luc) system (Qiagen) was chosen for monitoring the activity of several signal transduction pathways in MCF7 cells. The responsive luciferase constructs encode the firefly luciferase reporter gene under the control of a minimal (m)CMV promoter and tandem repeats of response elements for each pathway. The following constructs were used: TCF/LEF(luc) for Wnt signal transduction (CLS-018L); STAT3(luc) for transcriptional activity of STAT3 (CLS-6028L); RBP-Jk(luc) for Notch-induced signaling (CLS-014L); ARE(luc) for Nrf2- and Nrf1-mediated antioxidant response (CLS-2020L); GAS(luc) for Interferon gamma-induced Stat1-

signal transduction (CLS-009L); SMAD(luc) for TGF β -induced signal transduction (CLS-017L). Briefly, 1×10^5 MCF7 cells were seeded in 12-well plates. Once cells were attached, the viral particles were diluted 1:10 in complete culture media containing polybrene (sc-134220, Santa Cruz), and added to the cells. Puromycin treatment (P9620, Sigma) was started 48 hours later in order to select stably infected cells [9].

Luciferase assays.

The Luciferase Assay System (E1501, Promega Kit) was used on all luciferase reporter MCF7 cells treated with BMF [22]. Briefly, 6×10^3 MCF7 cells were seeded in black-walled 96-well plates and then were treated with BMF 1mM. As controls, vehicle-treated cells were run in parallel. Six replicates were used for each condition. After 72 hours of treatment, luciferase assays were performed according to the manufacturer's instructions. Light signal was acquired for 2 minutes in photons/second in the Xenogen VivoVision IVIS Lumina (Caliper Life Sciences), and the results were analysed using Living Image 3.2 software (Caliper Life Sciences). Luminescence was normalized using SRB (to determine total cellular protein), as a measure of MCF7 cell viability.

GM-CSF and IL-8 ELISA assays.

To evaluate the anti-inflammatory cancer progression related effects of BMF, we utilized the IL-8 Human SimpleStep (Ab 174442, Abcam) and GM-CSF Human SimpleStep (Ab 174448, Abcam) ELISA kits. The experiments were performed on pre-collect cellular media, after 72h of treatment with BMF and pravastatin, in MCF7 cells. The ELISA plate was pre-warmed a 25° for 30 minutes before to use. After 30 minutes, 50ul of media and 50ul of cocktail antibody were added in each well and leave in incubation at 25 °C for 1h mixing at 400 rpm. After 1h, each well was washed for three times 350ul of wash buffer and were added 100ul of TMB substrate in each well. The plate was incubated in a dark room for 10 minutes mixing at 400 rpm. After 10 minutes were added 100ul of stop solution and the plate was leaved to incubate for 1 minute. Lastly the plate was read at FLUOstar plate reader at 600nm.

Evaluation of HIF and NF- κ signaling pathways.

The Cignal Lenti reporter assay (Luc) system (Qiagen) was chosen for monitoring HIF- and NF B-Luc pathway activity in fibroblasts, as we previously described [9, 20]. Luciferase assay (E1501, Promega) was performed in luciferase reporter hTERT-BJ1 cells treated with atovaquone. Briefly, 1×10^4 hTERT-BJ1 reporter cells were seeded in black-walled 96-well plates and then were treated with BMF (100 μ M and 1mM) for 72 hours. Vehicle alone (DMSO) control cells were run in parallel. Six replicates were

used for each condition. After 72 hours, luciferase assay was performed according to the manufacturer's instructions. Light signal was acquired for 2 minutes in photons/second in the Xenogen VivoVision IVIS Lumina (Caliper Life Sciences), and the results were analyzed using the Living Image 3.2 software (Caliper Life Sciences). Luminescence was normalized using SRB (total proteins), as a measure of cell viability

MCF-7 spheres formation.

Culture. A single cell suspension was prepared using enzymatic (1x Trypsin-EDTA, Sigma Aldrich, #T3924), and manual disaggregation (25 gauge needle) to create a single cell suspension [23]. Cells were plated at a density of 500 cells/cm² in mammosphere medium (DMEM-F12/ B27/20ng/ml EGF/PenStrep) in non-adherent conditions, in culture dishes coated with (2-hydroxyethylmethacrylate) (poly-HEMA, Sigma, #P3932). Then, cells were treated with BMF (100µM and 1mM) and pravastatin (100µM and 1mM), in presence or absence of mevalonate 1mM and cholesterol 10µM. Vehicle alone (DMSO) control cells were processed in parallel. Cells were grown for 5 days and maintained in a humidified incubator at 37°C. After 5 days for culture, spheres >50 µm were counted using an eye piece graticule, and the percentage of cells plated which formed spheres was calculated and is referred to as percentage mammosphere formation, and was normalized to one (1 = 100% MSF).

ALDEFLUOR assay and separation of the ALDH-positive population by FACS.

ALDH activity was assessed in MCF-7 cells [24]. The ALDEFLUOR kit (StemCell technologies, Durham, NC, USA) was used to isolate the population with high ALDH enzymatic activity by FACS (Fortessa, BD Bioscience). Briefly, 1×10^5 were incubated in 1ml ALDEFLUOR assay buffer containing ALDH substrate (5 μ l/ml) for 40 minutes at 37°C. In each experiment a sample of cells was stained under identical conditions with 30mM of diethylaminobenzaldehyde (DEAB), a specific ALDH inhibitor, as negative control. The ALDH-positive population was established in according to the manufacturer's instructions and was evaluated in 20.000 cells. ALDEFLUOR-positive signal was detected in cell line treated with BMF (100 μ M and 1mM) and pravastatin (100 μ M and 1mM), compared with control. *Statistical Analysis.* Data is represented as the mean \pm standard error of the mean (SEM), taken over 3 independent experiments, with 3 technical replicates per experiment, unless otherwise stated. Statistical significance was measured using the analysis of variance (ANOVA) test or t-test. P 0.05 was considered significant and all statistical tests were two-sided.

RESULTS

BMF inhibits MCF7 and MCF7-HMGCR cell growth.

The effect of BMF on cell proliferation was examined in the mammalian cancer cell lines MCF7 and MCF7-HMGCR. The MCF7-HMGCR cell line was generated using Lenti-Pac™ HIV Expression Packaging Kit according to the manufacturer's instructions. As shown in Fig. 1A, the correct overexpression of the *hmgcr* protein in transfected cells was confirmed by western blotting analysis, compared with empty vector transfected cells (EV). The effect of BMF was compared with the effect of pravastatin and simvastatin, two different typologies of statins having different metabolism and half-life (Table 1) [25]. The cells were exposed to varying doses of BMF, pravastatin and simvastatin for 72h. As shown in Fig. 1B-1C, a significant decrease of growth was seen in the MCF7-HMGCR respect MCF7, co-incident with inhibition of proliferation. BMF effectively inhibited cell proliferation in a dose-dependent manner in both cancer cells, following the pravastatin trend. The mean IC_{50} value, for BMF and pravastatin of these cell lines was approximately between 100 μ M and 1mM respectively and 10 μ M for simvastatin. In order to ensure that BMF, pravastatin and simvastatin was not toxic was examined the effect on epithelial normal cell line h-tert-BJ1. As shown in Fig. 1D, after exposure to varying doses of BMF, pravastatin and simvastatin for 72 h, simvastatin resulted toxic for h-tert-BJ1 with a IC_{50} value between 10 μ M and 50 μ M. The results showed that the BMF followed the

pravastatin trend of inhibition on MCF7 and MCF7-HMGCR cell lines. Furthermore BMF and pravastatin showed a no toxic profile on h-tert-BJ1 after 72 h of treatment.

BMF reduce mitochondrial respiration in MCF7 cancer cell line increasing endogenous fatty acid oxidation.

The metabolic profile of MCF7 and MCF7-HMGCR cells was examined using the Seahorse XFe96 analyzer, by employing a mitochondrial stress test and a glycolytic stress test (Fig. 2A-2B). Notably, the oxygen consumption rate (OCR) was greatly increased in MCF7-HMGCR compared with MCF7-EV, while no differences was showed in extracellular acidification rate (ECAR). As shown in Fig. 2C, after treatment with BMF the OCR was decreased in MCF7-HMGCR cell line. Further quantification revealed significant reductions in basal and maximal respiration as well as ATP levels (Fig. 2C). The same experiment was repeated in MCF7 cell line upon BMF, pravastatin and simvastatin treatment, showing the same trend in OCR reduction (Fig. 2D-2E). Thus BMF significantly reduces the rates of oxidative mitochondrial metabolism. To further validate these results, a mitochondrial stress test was performed on h-tert-BJ1 treated with BMF, pravastatin and simvastatin. Notably, the OCR in h-tert-BJ1 was no affected by BMF 100 μ M and 1mM, contrary to simvastatin effects (Fig. 2E). The fatty acid oxidation (FAO) was evaluated after 72h of treatment with BMF and pravastatin (100 μ M and 1mM) compared with the control. As Fig. 2F shown, BMF and pravastatin reduced the FAO exogenous, suggested an increased FAO endogenous respectively to

control (vehicle alone: DMSO). These results confirmed that HMGCR is a gene involved in a cell survival and mitochondrial respiration. Furthermore BMF, pravastatin and simvastatin reduced the OCR and FAO exogenous in MCF7, while FAO endogenous was increasing compare to the control. The BMF showed no toxic effects on h-tert-BJ1 cell line.

BMF induced cell cycle arrest in G0/G1 phase.

To evaluate the underlying mechanism of growth inhibition by BMF, the cell cycle profile was analysed after treating MCF7 cells with 100 μ M and 1mM of BMF and pravastatin for 72h. BMF treatment resulted in G0/G1 cell cycle arrest and reduced S phase in a dose-dependent manner in the MCF7 cells (Fig. 3) following the same trend of pravastatin. Indeed, as shown in Fig. 3A, after treatment with pravastatin at the indicated concentrations for 72 h, the G0/G1 cell cycle phase was increased in MCF7 cells. Contrary reduced the G2/M and S phases were reduced (dose –dependent) in the MCF7 cells after treatment with BMF and pravastatin compared to control (vehicle alone: DMSO).

BMF modulates several signaling pathways involved in inflammation, proliferation and stemness.

To analyse in which metabolism-signaling pathway the BMF is involved, was analysed

the effects of BMF on a series of well-established signaling pathways, which have been shown to promote proliferation, inflammation and stemness [26-31]. For this purpose, was employed a panel of eight MCF7 cell lines (Table 2) carrying different luciferase reporters, to monitor the activation state of a variety of different signalling networks, including Sonic hedgehog, TGF β -SMAD, STAT3, Wnt, Interferon (IFN)- γ -STAT1/2, NRF2- dependent antioxidant responses, IFN- γ -STAT1 and Notch pathways. Notably, several pathways were significantly inhibited by BMF treatment, including stem cell signaling (Notch, STAT3, Wnt) and IFN- γ -STAT1/2 signaling (Fig. 4A). However, NRF2- dependent antioxidant responses and IFN- γ -STAT1 were significantly activated by BMF treatment. No effects were observed on Sonic hedgehog and TGF β -SMAD pathway. (Fig. 4B). Thus, BMF inhibits the activation of several signal transduction pathways related to cancer stem-like features and CSCs formation. The BMF activates antioxidant responses by Nrf2 and IFN- γ -STAT1/2 signaling triggering anti-proliferative and antiviral responses in target cells through signalling pathway modulation.

HMGCR inhibitors reduce the IL-8 and GM-CSF levels.

The secretion of IL-8/CXCL8 (pro-inflammatory cytokine) from cancer cells may have a profound effect on the tumor microenvironment (Diagram 1) [32]. Interestingly, granulocyte macrophage colony-stimulation factor (GM-CSF) signaling significantly is implicated in atherosclerosis and was identified as a factor responsible for expansion

and activation of granulocytes and macrophages, but has since been found to have many direct and indirect effects on multiple cell types, including cell proliferation, maturation, and survival in a cancer cells [33]. IL-8 and GM-CSF is known to stimulate malignant tumor cell growth and migration in vitro and to promote cancer progression in vivo (Diagram 2) [34-37]. IL-8 and GM-CSF releases in the cell culture media, after 72h of treatment with BMF and pravastatin, were detected by using IL-8 ELISA kit (sensitivity < 25 pg/ml) according to the manufacturer's instructions (IL-8 Abcam 174442) and GM-CSF ELISA kit (GM-CSF Abcam 174448). As Fig. 5A-5B shown, the GM-CSF and IL-8 levels were reduced by BMF and pravastatin treatment in MCF7 cancer cell line. This result confirm the ability of HMGCR inhibitors to decrease the pro-inflammatory cytokine and granulocyte macrophage activation reducing cancer progression and CSCs formation.

NF-k and HIF signalling pathways were inhibited by MVA pathway inhibitors.

The results of a recently published study have numerous implications for a number of pathologies where NF-k and HIF was deregulated, including cancer [38, 39]. Therefore, it is thought that understanding the cross-talk between these two key transcription factors, NF-k and HIF, will greatly enhance the process of drug development [40, 41]. HIF activity is involved in angiogenesis required for cancer tumor growth. The overexpression of HIF factor, modulated by NF-k, in stromal fibroblasts (h-tert-BJ1) around tumor bulk, help the tumor growth, cancer progression

and it is involved in CSCs formation. As shown in Fig. 6A-6B, BMF and pravastatin reduced the HIF and NF- κ B signalling pathway in h-tert-BJ1 after 72h of treatment, reducing two key factors involved in a cancer progression and stemness.

MCF7 and T47D tumorspheres shown an overexpression of enzymes involved in mevalonate metabolic pathways.

Proteomic analysis of MCF7 mammospheres monolayer and mammosphere cultures of MCF7 cells (an ER-positive luminal cell line), were subjected to quantitative label-free proteomics analysis. For simplicity, was focused on the proteins that were significantly upregulated in mammospheres, compared to monolayer cell cultures ($p < 0.05$) involved in MVA pathway and fatty acid synthase/oxidation. Immediately, was noticed that several metabolic enzyme involved in MVA pathway were highly upregulated in mammospheres. Table 2 showed a non-redundant list of 40 proteins that were selectively upregulated in MCF7 mammospheres respect monolayer adherent cells. A functional analysis of this list revealed that proteins were specifically related to beta-oxidation and MVA cascade. For comparison purposes, was performed unbiased label-free proteomic analysis on a second independent ER-positive breast cancer cell line, namely T47D cells [42]. The results are summarized in Table 2. Note that 30 proteins of the list were specifically over-expressed in T47D mammospheres, as compared with T47D monolayer cultures processed in parallel. Remarkably, 30 of these proteins overlapped with the proteins that were upregulated in MCF7 mammospheres (75%

overlap). Moreover, the 21 metabolic proteins involved in MVA pathway overlapped with the 24 proteins that were upregulated in MCF7 mammospheres (87,5% overlap). See the Venn diagram presented in Fig. 7A. Therefore, many of the same biological processes would be expected to be activated or enhanced. Thus, MVA cascade, beta-oxidation, mitochondrial biogenesis and fatty acid production are likely to be key biological features of both MCF7 and T47D mammospheres. Interestingly, MVA pathway was highly upregulated in both MCF7 and T47D data sets, representing a key role in tumorspheres growth and CSCs formation [16]. BMF and MVA metabolic pathways inhibitors could regulate the tumor growth rise CSCs mediated (Fig. 7B).

MVA Pathway inhibitors reduce Breast CSC Population in not mediated through cholesterol biosynthesis blockade.

To validate the role of MVA metabolism in the regulation of breast CSC biology, was performed a tumorspheres formation assay utilizing MCF7-HMGCR cell line [23]. As shown in Fig. 8A, the MCF7-HMGCR cell line was more able to form spheres compared with the control (MCF7-EV). To validate the role of HMGCR enzyme in the regulation of tumorspheres formation, the MCF7-HMGCR cells were treated with BMF and pravastatin, which blocks the biosynthesis of MVA. The tumorsphere (or mammosphere) formation efficiency (MFE) was highly reduced after BMF and pravastatin treatment (Fig. 8B) in MCF7-HMGCR cell line. The same experiment was performed in MCF7 cell line, where BMF and pravastatin showed a similar effect,

reducing MFE and CSC population (Fig. 8C). The effect of BMF and pravastatin treatment on the CSC population was measured by both the ALDEFLUOR assay and the tumorsphere formation assay[23]. In these cell lines, the ALDEFLUOR-positive population contains the CSC population [15]. BMF and pravastatin treatment reduced the CSC population, with 2.5 times less ALDEFLUOR-positive cells after 72 h of treatment (Fig. 8D). The addition of mevalonate, the product of HMGCR, to the culture medium, rescued the CSC population, with a complete restoration of both the ALDEFLUOR-positive population and the tumorsphere-initiating ability [16] (Fig. 8E-8F). Because MVA metabolism generates several endproducts [17] (cholesterol, isoprenoids), we examined the compensatory effect of exogenous cholesterol on BMF and pravastatin treatment. Addition of cholesterol did not prevent BMF and pravastatin effect on CSC population with a similar reduction in the ALDEFLUOR-positive population and MFE in MCF7 cell line (Fig. 8E-8F). These results confirm the essential role of MVA metabolism in the regulation of CSCs formation and CSC self-renewal.

FIGURE 1

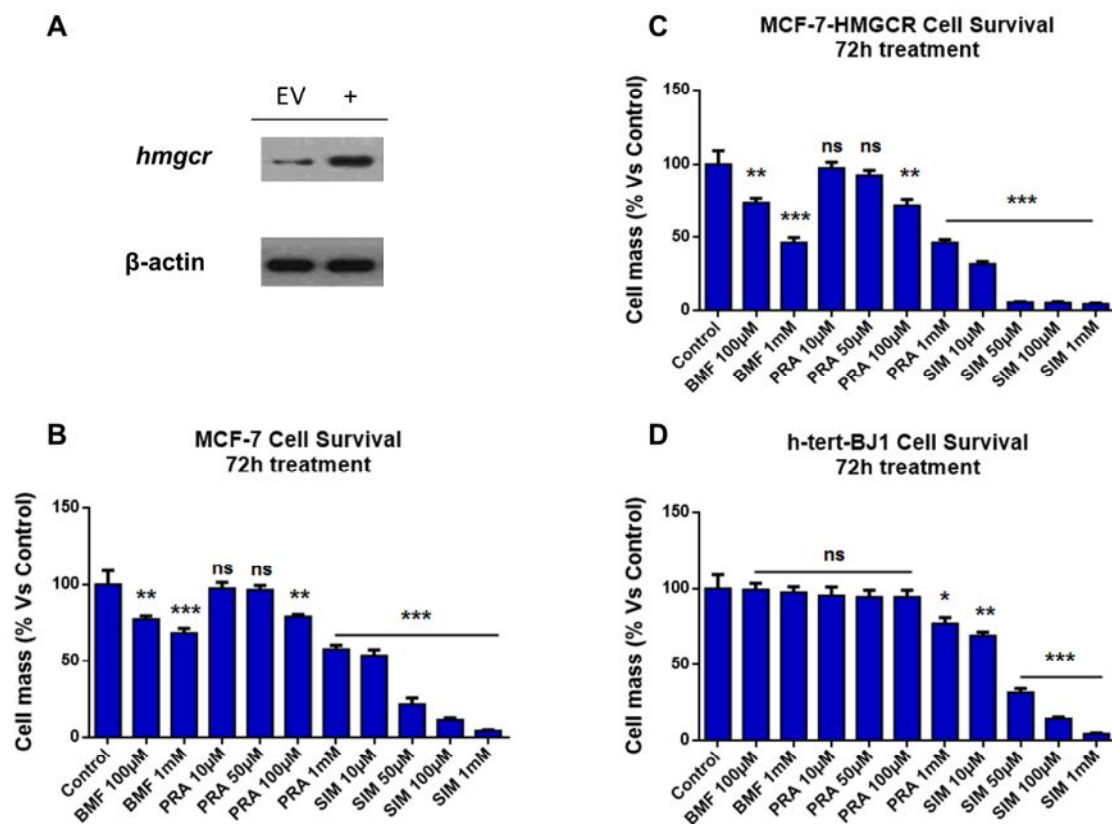
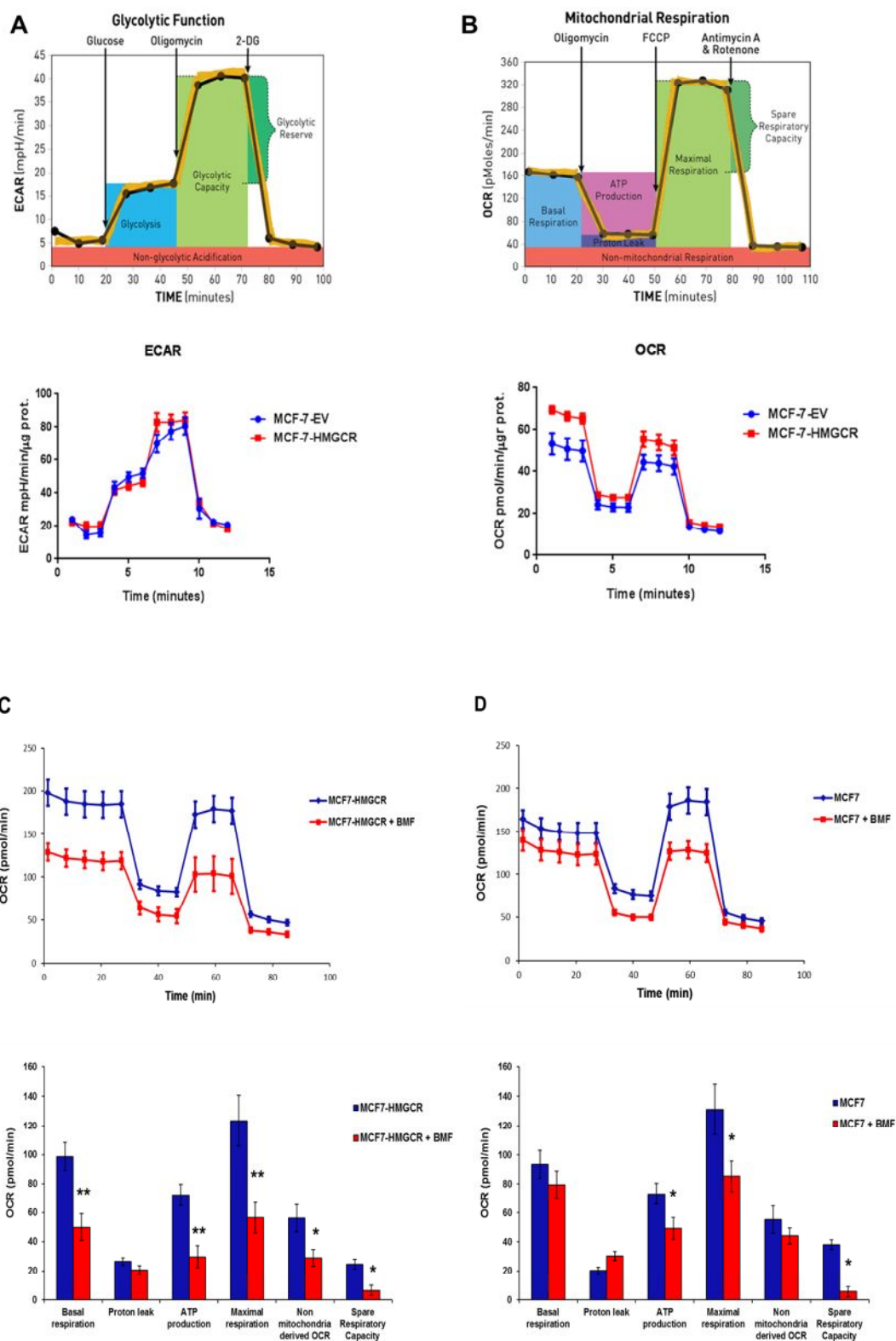


Fig. 1: BMF inhibited the growth of MCF7 and MCF7-HMGCR cell lines . To evaluate the anti-proliferative effect of BMF by HMGCR inhibition, MCF7 cells were transfected with HMGCR gene following the GENECOPOEIA manufacturer's instructions. **(A)** Western blotting analysis on 30 μ g of MCF7-EV (EV) and MCF7-HMGCR (+) cell lysates. The western blotting was performed utilizing HMGCR antibody (C-1 SantaCruz) diluted 1:500 in BSA 5% over night. The loading control was performed utilizing β -actin antibody (Ab8226 Abcam) diluted 1:5000 in BSA 5%. The result showed an overexpression of *hmgcr* protein in MCF7-HMGCR transfected cells. **(B-C)** The BMF, pravastatin and simvastatin significantly reduces cell survival in both MCF7 and MCF7-HMGCR cells. Note that after 72h of treatment, BMF

reduced cell viability, with an IC-50 of ~1mM in MCF7-HMGCR cells and > of 1mM in MCF7 cells, like pravastatin treatment. Simvastatin showed a strongly effect on both cell lines, with an IC-50 less of 10 μ M in MCF7-HMGCR cells and ~10 μ M in MCF7 cells. **(D)** BMF was not affect the cell viability normal fibroblasts (h-tert-BJ1) at 100 μ M and 1mM. Contrary simvastatin showed a strongly effect on normal fibroblasts cell viability, with a toxic effect already from 10 μ M. Pravastatin 1mM showed fewer toxic effects on normal fibroblast compare to simvastatin. Cell viability of MCF7, MCF-HMGCR and hTERT-BJ1 fibroblasts was assessed using an SRB assay. An ns indicates p = not significant, * indicates p < 0.05; ** indicates p < 0.005; *** indicates p < 0.0005 (One-way ANOVA t-test).

FIGURE 2



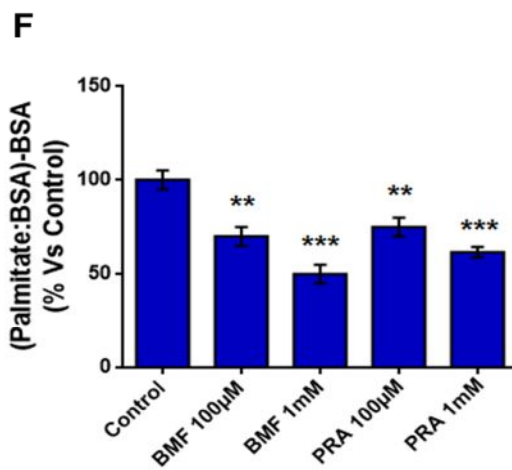
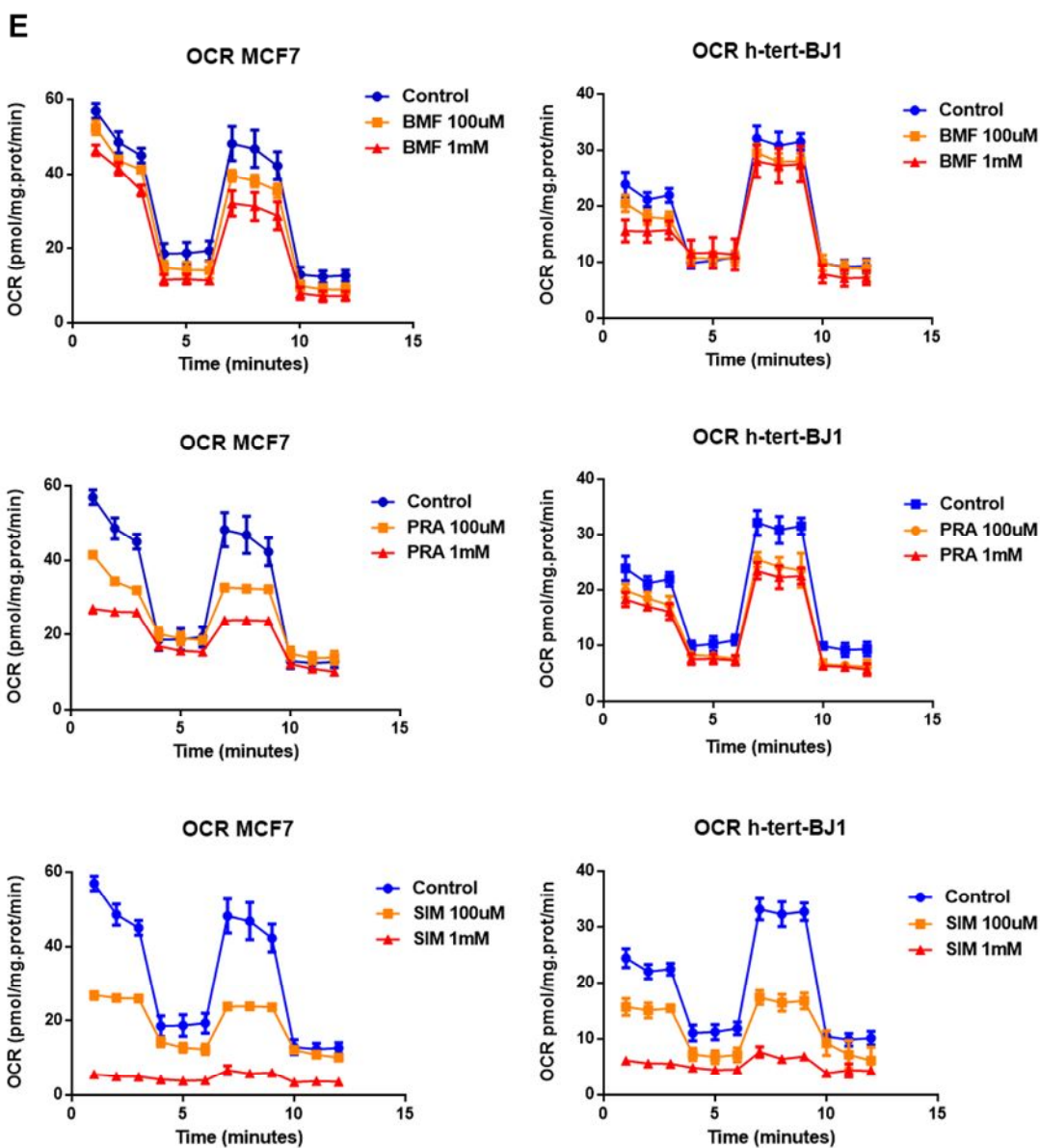


Fig. 2: Metabolic profiles of MCF7-HMGCR and MCF7 treated with BMF, pravastatin and simvastatin. (A-B) MCF7-HMGCR cells were examined using the Seahorse XFe96 analyzer, by employing a glycolytic function and a mitochondrial respiration. The extracellular acidification rate (ECAR mpH/min./ μ g prot.) and oxygen consumption rate (OCR pmol/min./ μ g prot.), were evaluated in 72h plated cells. (C-D) MCF7-HMGCR and MCF7 were treated for 72h with BMF 1mM and was examined the OCR and relative basal respiration, maximal respiration, ATP levels, proton leak, NON-mitochondrial derived OCR and spare respiratory capacity. After treatment with BMF 1mM the OCR and relative levels, were highly reduced in MCF7-HMGCR cells compare MCF7 cells. (E) The OCR was evaluated also in MCF7 and normal fibroblast (h-tert-BJ1) after treatment with BMF, pravastatin and simvastatin (100 μ M and 1mM each). The effects simvastatin 100 μ M and 1mM resulted toxic for normal fibroblast, strongly reducing the mitochondrial respiration. (F) The fatty acid oxidation was evaluated by Seahorse FAO assay kit. After 72h of treatment with BMF and pravastatin (100 μ M and 1mM) the exogenous consumption of palmitate level was lower compare to control (vehicle alone DMSO). The ratio Palmitate:BSA - BSA was calculate on mean values of FCCP injections in presence or absence of palmitate, in MCF7 cell line. The value obtained after treatment with BMF and pravastatin was compared to control (vehicle alone DMSO). This result suggested that BMF and pravastatin treatment increased the endogenous fatty acid oxidation compare to control. An * indicates $p < 0.05$; ** indicates $p < 0.005$; *** indicates $p < 0.0005$ (One-way ANOVA t-test).

FIGURE 3

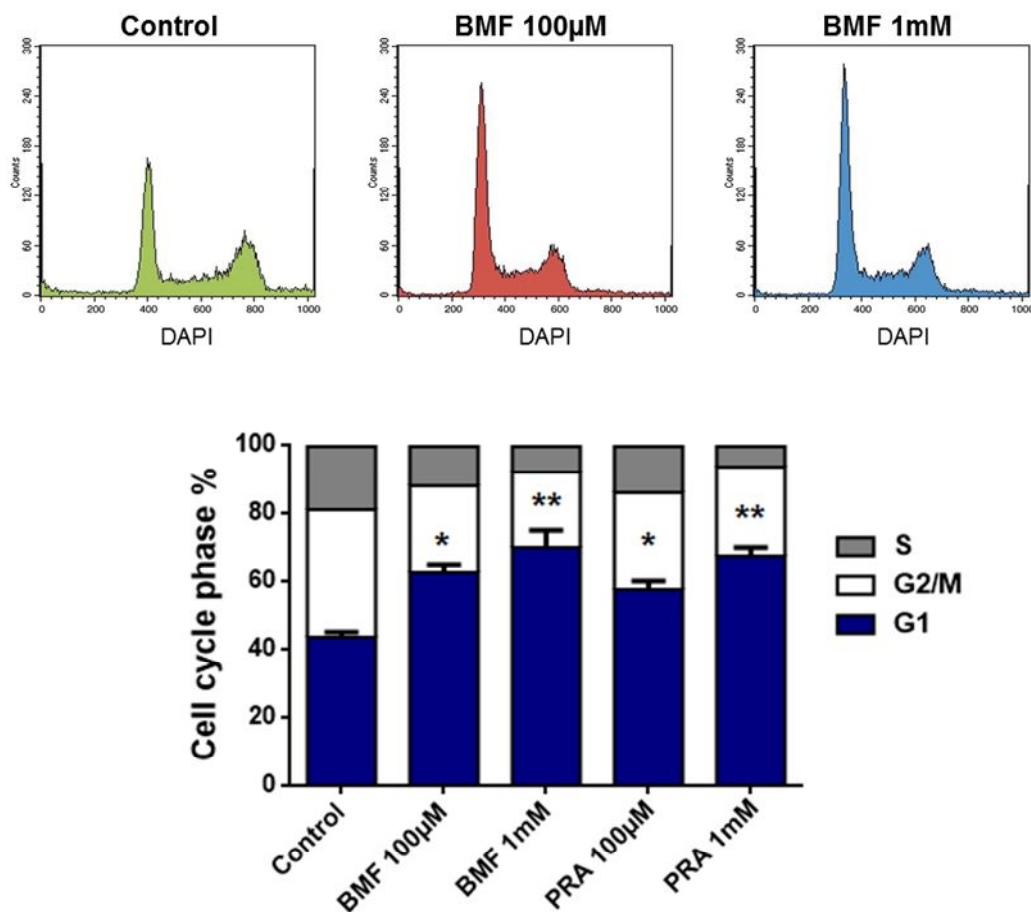


Fig. 3: BMF and pravastatin induced cell cycle G1 arrest in MCF7 cell line. MCF7 cell line was treated with the indicated doses of BMF and pravastatin (1 uM) for 72h. Cell cycle analysis was performed by FACS (BD Fortessa). BMF and pravastatin markedly induced cell cycle G1 arrest in both cell lines in a dose dependent manner, compare to control. Each experiment was performed three times. An * indicates $p < 0.05$; ** indicates $p < 0.005$ (One-way ANOVA t-test).

FIGURE 4

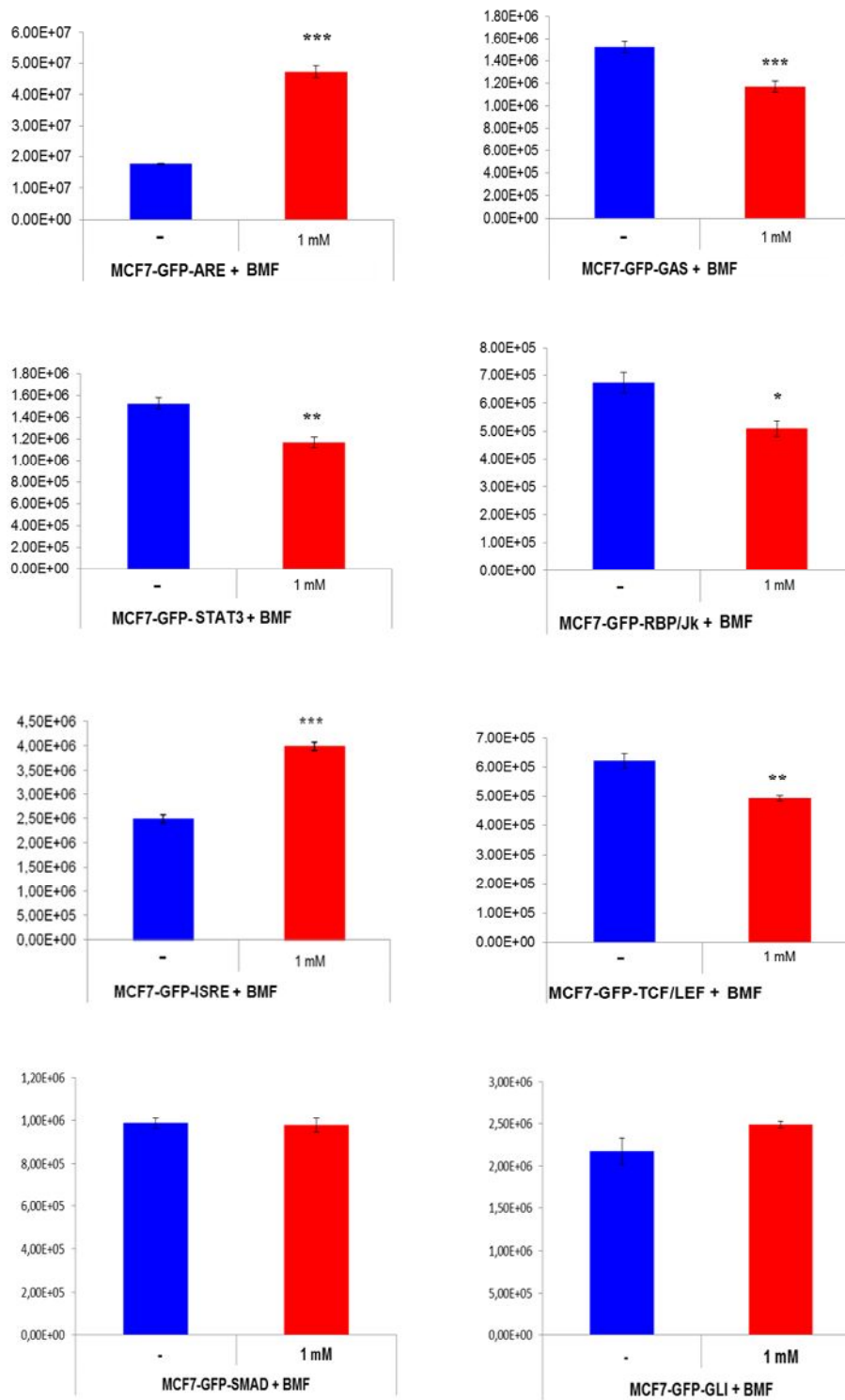


Fig. 4: BMF inhibited signaling pathways related to inflammation, proliferation and CSCs formation. MCF7 breast cancer cells carrying luciferase-reporters (Signal, QIAGEN) were generated to monitor the activation of a variety of signaling networks, including Wnt (TCF/LEF), STAT3, Notch (RBP/Jk), NRF2-dependent antioxidant responses, Hedgehog signalling pathway (GLI), Interferon γ -STAT1, Interferon 1 (ISRE) and SMAD-TGF β pathways. MCF7-Luc reporter cells were treated with BMF 1mM for 72 hours and luminescence was determined as a measure of pathway activation status. Note that BMF inhibited cancer stem cell signaling (WNT, STAT3 and Notch), as well as INF γ -STAT1 signaling and activated the NRF2-antioxidant responses and Interferon 1 signaling pathway. No effects were observed for the SMAD-TGF β -pathway and Hedgehog (GLI) pathway. Each experiment was performed three times. An * indicates $p < 0.05$; ** indicates $p < 0.005$; *** indicates $p < 0.0005$ (Student's t-test).

FIGURE 5

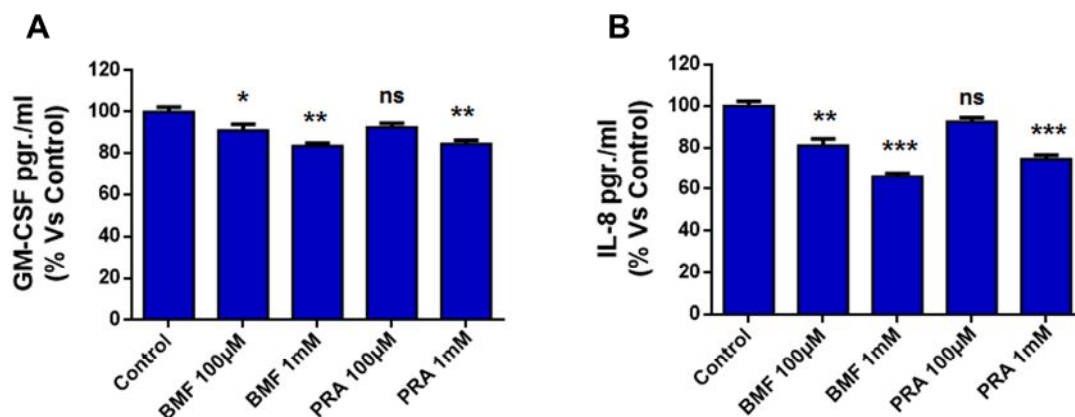


Fig. 5: BMF affected cancer pregression and CSCs formation by GM-CSF and IL-8 reduction. GM-CSF and IL-8 is known to stimulate malignant tumor cell growth and migration in vitro, to promote cancer progression in vivo an are involved in CSCs formation. To evaluate the effect of BMF on cancer pregression and CSCs formation, were seeded 1×10^5 MCF7 cells in 12 well plate and treated with BMF and pravastatin for 72h. After 72h the media was collected and analyzed follow the GM-CSF (Ab 174448) and IL-8 (Ab 174442) kit ELISA manufacturer's instructions. **(A)** The GM-CSF level was reduced after treatment with BMF in a dose dependent manner, compare to control (control $35,74 \pm 8,21$ pg/ml). The GM-CSF level was reduced also with pravastatin 1mM. **(B)** The IL-8 level was reduced after treatment with BMF in a dose dependent manner, compare to control (control $64,57 \pm 6,45$ pg/ml) . The IL-8 level was reduced also with pravastatin 1mM. An ns indicates $p =$ not significant; * indicates $p < 0.05$; ** indicates $p < 0.005$; *** indicates $p < 0.0005$ (One-way ANOVA t-test).

FIGURE 6

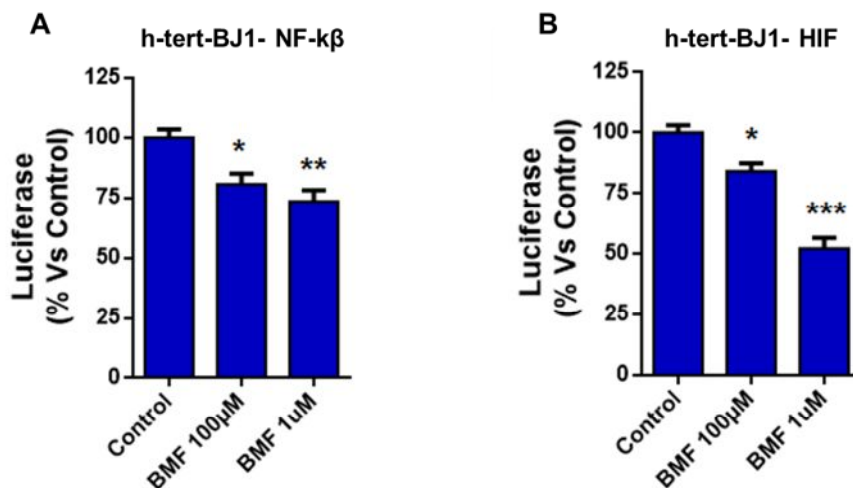


Fig. 6: BMF prevented cancer progression by HIF and NF-k modulation in stromal fibroblasts. The tumor growth and progression is helped by normal stromal cells around the tumor-bulk. The overexpression of HIF and NF-k factor in fibroblast is required by the tumor to growth. These two factor are also involved in cancer progression traffic signaling. h-tert-BJ1 cells carrying luciferase-reporters (Cignal, QIAGEN) were generated to monitor the activation of HIF and NF-k signaling networks. h-tert-BJ1-Luc reporter cells were treated with BMF and pravastatin (100µM and 1mM) for 72 hours and luminescence was determined as a measure of pathway activation status. **(A-B)** Note that BMF and pravastatin inhibited HIF and NF-k signalling pathways in a dose dependent manner, compare to control (vehicle alone DMSO). BMF and pravastatin reduced two key factors involved in cancer progression. An * indicates $p < 0.05$; ** indicates $p < 0.005$; *** indicates $p < 0.0005$ (Student's t-test).

FIGURE 7

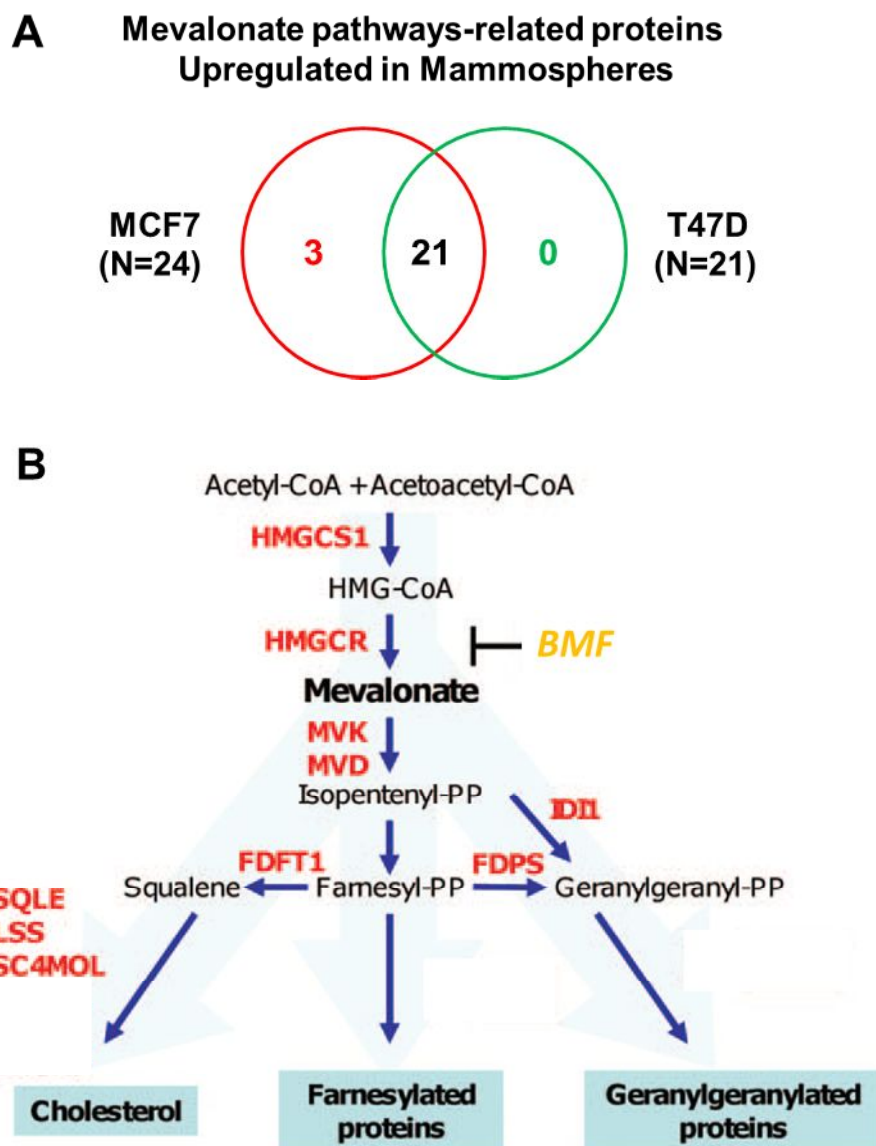


Fig. 7: Overview of proteins and pathways identified upregulated in the lysates of MCF7 and T47D mammospheres relative to monolayer cells by Ingenuity Pathway Analysis. (A) Venn diagram highlighting the conserved upregulation MVA pathways related proteins in both

MCF7 and T47D mammospheres. Overlap of differentially regulated proteins identified in MCF7 and T47D mammospheres compared to monolayer cells . Of all proteins identified by quantitative proteomics, 21 of 24 were proteins the expression of which was found upregulated in both mammosphere lines. **(B)** Schematic diagram of the MVA metabolism. Proteins significantly overexpressed in tumorspheres and involved in MVA metabolism were represented at their respective sites of action (in red). Similarly, the site of action of compounds BMF used to inhibit MVA metabolism by HMGCR blockade was represented.

FIGURE 8

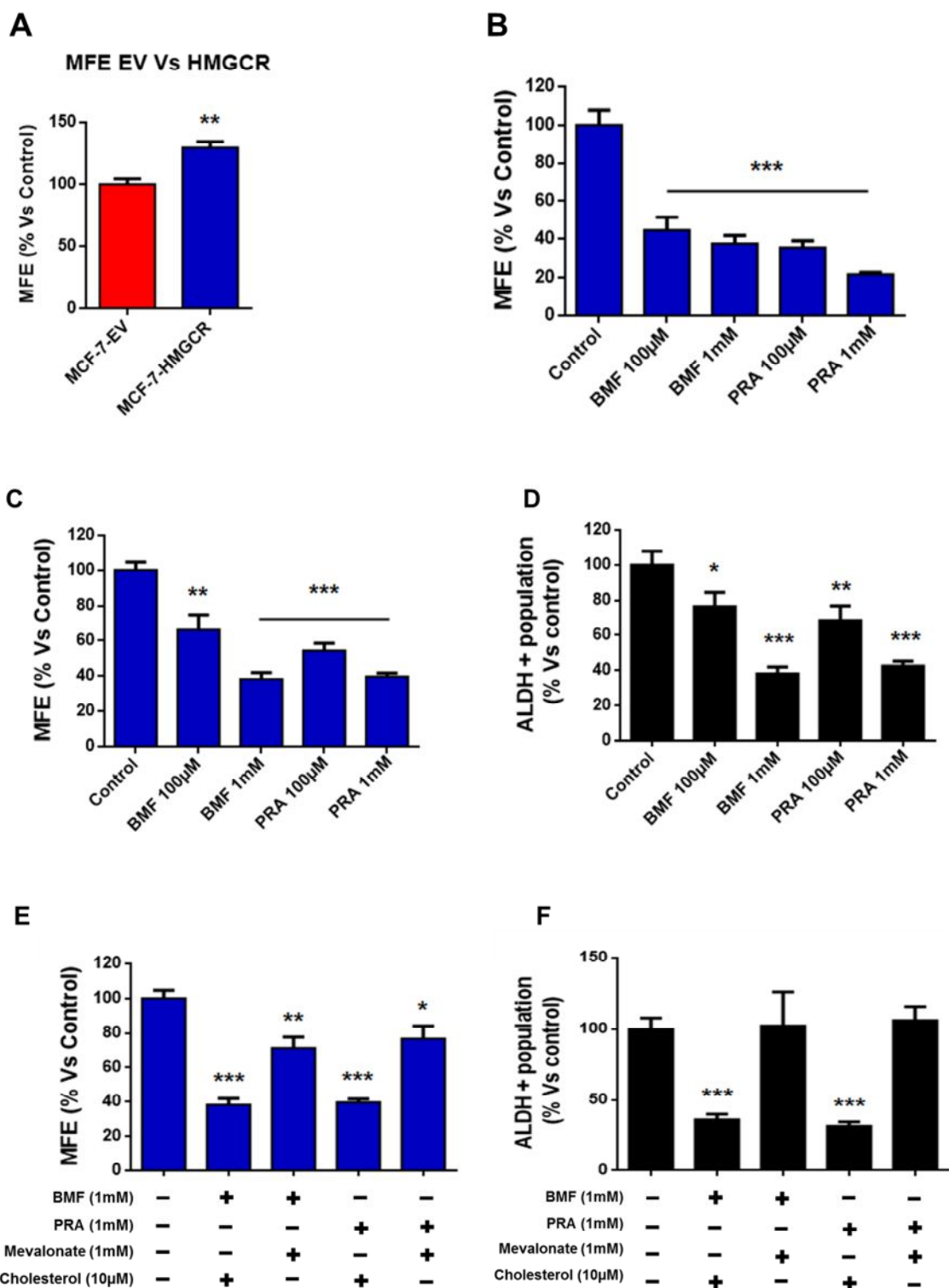
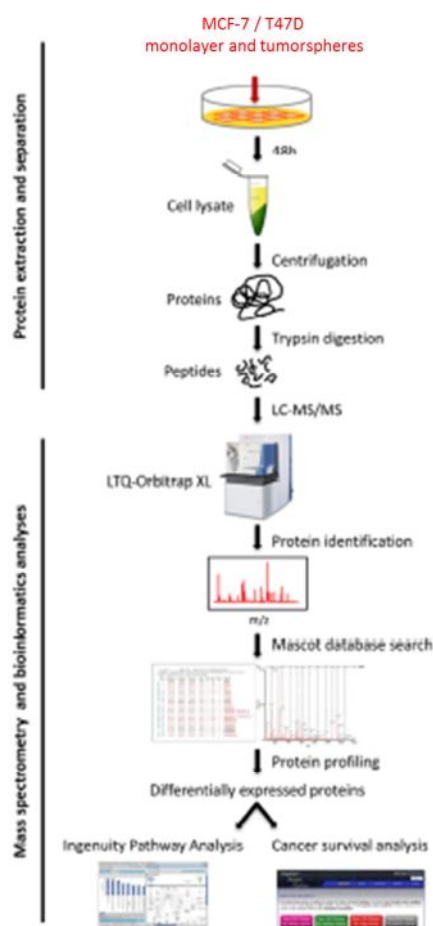


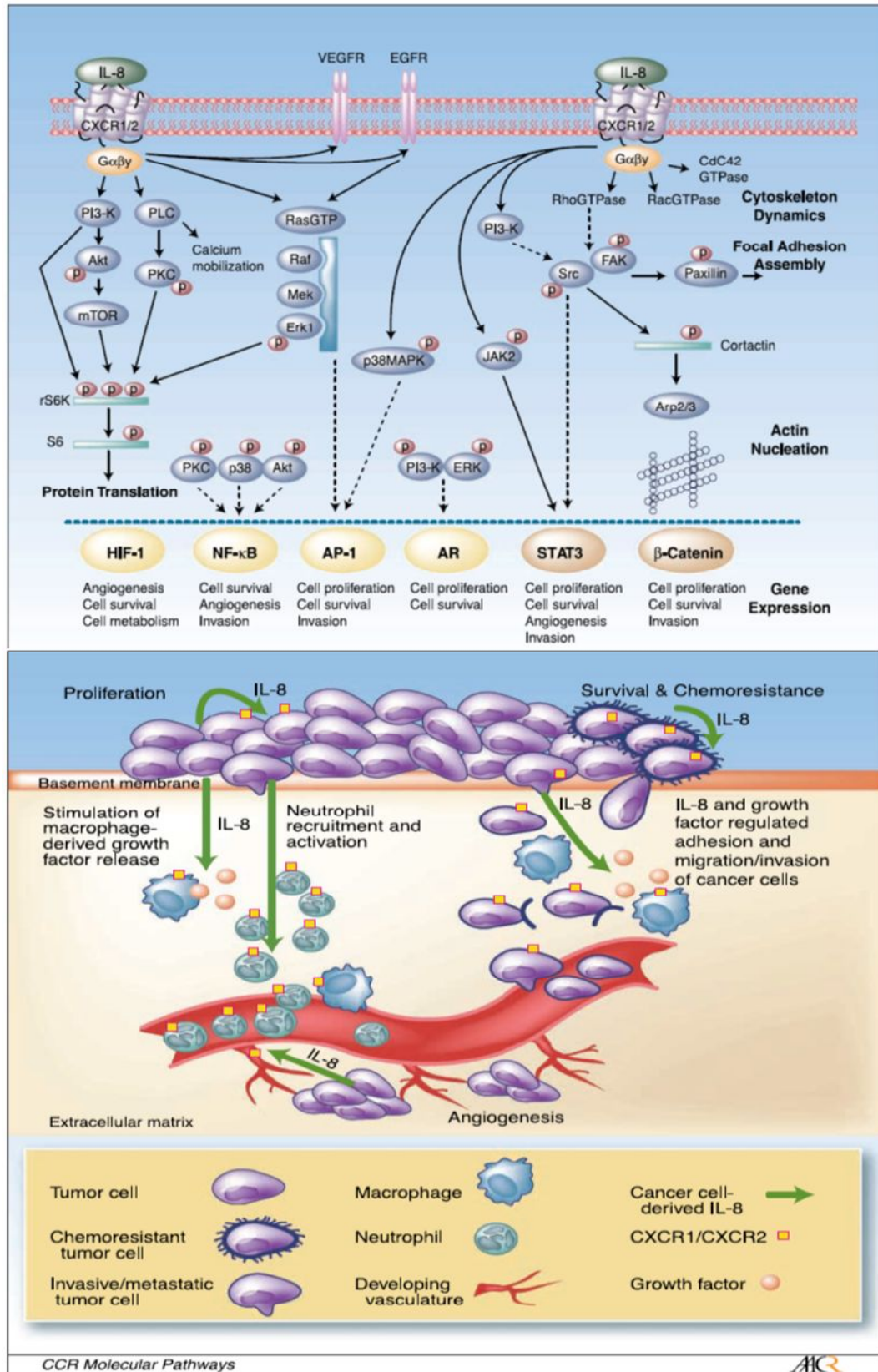
Fig. 8: Mevalonate (MVA) metabolism blockade reduces the breast cancer stem cell (CSC) populations independently of cholesterol biosynthesis. To evaluate the relevance of mevalonate in CSC formation, was performed a mammosphere assay using MCF7-HMGCR cells. **(A)** The mammosphere formation efficiency (MFE) was increased (35%) in MCF7-HMGCR compare to MCF7-EV. **(B)** The MVA pathways inhibitors significantly reduced mammosphere formation in MCF7-HMGCR cells. Note that BMF effectively reduced mammosphere formation, with an IC-50 of ~100 μ M in MCF7-HMGCR cells. The same experiment was repeated with MCF7 cells, treated with BMF and pravastatin. **(C)** The MFE was reduced after treatment with BMF and pravastatin also in MCF7 cells, with an $100 \mu\text{M} < \text{IC-50} < 1 \text{ mM}$ for both treatments. The effect BMF and pravastatin on the CSC population was assessed using ALDEFLUOR assay **(D)**. BMF and pravastatin treatment decreased significantly the ALDEFLUOR-positive population confirming the MFE reduce. **(E-F)** The addition of mevalonate (10 μ M), the product of HMGCR, to the culture medium, rescued the CSC population, with a complete restoration of both the ALDEFLUOR-positive population and the MFE in MCF7 cells. Addition of cholesterol (1mM) did not prevent BMF and pravastatin effect on CSC population with a similar reduction in the ALDEFLUOR-positive population and MFE in MCF7 cells. These results suggest that the BMF ability to affect the breast CSC population via MVA metabolism blockade is not related to cholesterol biosynthesis. Each experiments was repeated three times. An * indicates $p < 0.05$; ** indicates $p < 0.005$; *** indicates $p < 0.0005$ (Student's t-test).

SCHEME 1



Scheme 1: Workflow for the comparative proteome analysis of MCF7 and T47D monolayer cells and tumorspheres. Protein lysates were obtained from MCF7 and T47D after 5days for monolayer and tumorspheres plates .Peptides obtained after trypsin digestion were analysed via LC-MS/MS on an LTQ-Orbitrap XL mass spectrometer. Label-free quantitative proteomics was used to detect changes in protein abundances across monolayer and tumorspheres extracts. The proteomics data sets were further analysed using Ingenuity Pathway Analysis and a cancer survival analysis tool (kmplot.com).

DIAGRAM 1



Characterized IL-8 signaling pathways and the role of IL-8 and GM-CSF signaling in the tumor microenvironment. A schematic diagram illustrating the range of signaling pathways that are activated after stimulation of CXCR1 and/or CXCR2 receptors with IL-8. After activation of heterotrimeric small G proteins, IL-8 signaling promotes activation of the primary effectors phosphatidylinositol-3-kinase or phospholipase C, promoting the activation of Akt, PKC, calcium mobilization and/or MAPK signaling cascades. These signaling pathways have been shown to promote protein translation (left) and regulate the activity of a range of transcription factors (bottom). Solid gold lines, transcription factors whose activity has been shown to be positively regulated by IL-8 signaling using various reporter assays. In the case of signal transducers and activators of transcription 3 (STAT3) and h-catenin, IL-8 signaling has been shown to promote nuclear translocation of these factors; however, transcriptional activation of either factor remains to be shown. Dashed lines, the putative pathways through which IL-8 signaling regulates transcription factor activity. In addition, IL-8 signaling activates members of the RhoGTPase family and activates a number of nonreceptor tyrosine kinases (e.g., Src family kinases and FAK) that regulate the architecture of the cell cytoskeleton and its interaction with the surrounding extracellular environment (right). Tumor-derived IL-8 has the capacity to exert profound effects on the tumor microenvironment. For example, secretion of IL-8 from cancer cells can enhance the proliferation and survival of cancer cells through autocrine signalling pathways. In addition, tumor-derived IL-8 will activate endothelial cells in the tumor vasculature to promote angiogenesis and induce a chemotactic infiltration of neutrophils into the tumor site. Although IL-8 can promote cell invasion and migration, the

capacity of IL-8 to induce tumor-associated macrophages to secrete additional growth factors will further increase the rate of cell proliferation and cancer cell invasion at the tumor site. The multiple effects of IL-8 signaling upon different cell types present within the tumor microenvironment suggests that targeting of CXC-chemokine signaling (including but not limited to IL-8) may have important implications to halt disease progression and assist in sensitizing tumors to chemotherapeutic and biological agents [34]. Diagram and figure made and published by CCR molecular pathways in Waugh, D.J *et al.*, 2008 [32].

TABLE 1**Table 1** Clinical Pharmacokinetics of HMG-CoA Reductase Inhibitors

Parameter	Atorvastatin	Fluvastatin	Fluvastatin XL	Lovastatin	Pravastatin	Rosuvastatin	Simvastatin
T _{max} (h)	2–3	0.5–1	4	2–4	0.9–1.6	3	1.3–2.4
C _{max} (ng/mL)	27–66	448	55	10–20	45–55	37	10–34
Bioavailability (%)	12	19–29	6	5	18	20	5
Lipophilicity	Yes	Yes	Yes	Yes	No	No	Yes
Protein binding (%)	80–90	>99	>99	>95	43–55	88	94–98
Metabolism	CYP3A4	CYP2C9	CYP2C9	CYP3A4	Sulfation	CYP2C9, 2C19 (minor)	CYP3A4
Metabolites	Active	Inactive	Inactive	Active	Inactive	Active (minor)	Active
Transporter protein substrates	Yes	No	No	Yes	Yes/No	Yes	Yes
T _{1/2} (h)	15–30	0.5–2.3	4.7	2.9	1.3–2.8	20.8	2–3
Urinary excretion (%)	2	6	6	10	20	10	13
Fecal excretion (%)	70	90	90	83	71	90	58

Based on a 40-mg oral dose, with the exception of fluvastatin XL (80 mg).

Adapted from data in Corsini A, et al. *Pharmacol Ther.* 1999;84:413–428, and White CM. *J Clin Pharmacol.* 2002;42:963–970.

Table 1 : Clinical Pharmacokinetics of HMG-CoA Reductase Inhibitors [25]. In the table were indicated different HMG-CoA inhibitors. Pravastatin and simvastatin were chosen to performed the experiments like a control, compared with BMF. Pravastatin and simvastatin showed different pharmacokinetics properties from metabolism to lipophilicity, opportunely chosen to understand the behavior of BMF.

TABLE 2

Vector		Genecopoeia (ref.)	Cell line	Selection
GFP		EX-EGFP-Lv151	MCF7	G418 1mg/ml
Signal Lenti reporter assay (luc)	Qiagen (reference)	Pathway	Cell line	Selection
ARE(luc)	CLS-2020L	Nrf2- and Nrf1-mediated antioxidant response	MCF7-GFP	Puromycin 2 µg/ml
GAS(luc)	CLS-009L	Interferon gamma-induced signal transduction	MCF7-GFP	Puromycin 2 µg/ml
GLI(luc)	CLS-3030L	Hedgehog signaling pathway	MCF7-GFP	Puromycin 2 µg/ml
ISRE(luc)	CLS-008L	Type I interferon-induced signal transduction	MCF7-GFP	Puromycin 2 µg/ml
RBP-Jk(luc)	CLS-014L	Notch-induced signalling	MCF7-GFP	Puromycin 2 µg/ml
SMAD(luc)	CLS-017L	TGFβ-induced signal transduction	MCF7-GFP	Puromycin 2 µg/ml
STAT3(luc)	CLS-6028L	Transcriptional activity of STAT3	MCF7-GFP	Puromycin 2 µg/ml
TCF/LEF(luc)	CLS-018L	Wnt signal transduction	MCF7-GFP	Puromycin 2 µg/ml
HIF(luc)	CLS-007L	HIF-1 signal transduction	h-tert-BJ1	Puromycin 2 µg/ml
NFκβ(luc)	CLS-013L	Nf-Kβ-induced signal transduction	h-tert-BJ1	Puromycin 2 µg/ml

Tab. 2: Signal Lenti reporter assay and GFP vectors used in this study and cell line utilised for transduction for each of them.

TABLE 3

MCF7	Description	T47D
Infinity	Isopentenyl-diphosphate Delta-isomerase	Infinity
Infinity	Peroxisome proliferator activated receptor interacting complex protein	Infinity
Infinity	Ubiquitin carboxyl-terminal hydrolase	Infinity
Infinity	Adenylate kinase 2, mitochondrial	#N/D
Infinity	Glycerol-3-phosphate dehydrogenase, mitochondrial	#N/D
Infinity	Methylcrotonoyl-CoA carboxylase subunit alpha, mitochondrial	18,35
Infinity	ATP synthase subunit beta	#N/D
3642,09	Ubiquitin thioesterase	14,06
2592,84	D-beta-hydroxybutyrate dehydrogenase, mitochondrial	15,17
1124,93	Acetyl-CoA acetyltransferase, mitochondrial	49,45
975,80	NADH dehydrogenase [ubiquinone] 1 beta subcomplex subunit 10	2,97
522,86	Delta(24)-sterol reductase	30,01
355,26	2-oxoglutarate dehydrogenase E1 component DHKTD1, mitochondrial	17,54
292,09	6-phosphogluconate dehydrogenase, decarboxylating	23,93
224,71	Acetyl-Coenzyme A carboxylase alpha	34,85
158,10	Pyruvate carboxylase, mitochondrial	2,59
114,95	Delta(3,5)-Delta(2,4)-dienoyl-CoA isomerase, mitochondrial	10,49
114,95	Delta(3,5)-Delta(2,4)-dienoyl-CoA isomerase, mitochondrial	10,49
90,25	Pyruvate dehydrogenase (lipoamide) alpha 1	Infinity
38,50	Lanosterol synthase (2,3-oxidosqualene-lanosterol cyclase)	11,83
23,99	Dihydrolipoylysine-residue succinyltransferase, 2-oxoglutarate dehydrogenase complex	21,39
23,94	Dihydrolipoylysine-residue acetyltransferase, pyruvate dehydrogenase complex	4,31
20,60	Squalene synthase	7,00
17,47	NADH dehydrogenase [ubiquinone] 1 alpha subcomplex subunit 5	6,47
10,62	Succinate dehydrogenase (ubiquinone) flavoprotein subunit, mitochondrial	#N/D
8,32	Creatine kinase, ubiquitous mitochondrial (EC 2.7.3.2)	6,81
6,77	Fatty acid synthase (FASN)	8,53
6,37	3'-hydroxyisobutyrate dehydrogenase	#N/D
4,64	Pyruvate kinase	3,27
4,50	Enoyl-CoA hydratase, mitochondrial	2,95
3,57	Carnitine O-acetyltransferase	5,11
2,69	Ubiquinone biosynthesis protein COQ9, mitochondrial	#N/D
2,59	Isocitrate dehydrogenase	2,55
2,41	Malic enzyme	2,45
2,09	Glyoxylate reductase/hydroxypyruvate reductase	1,23
1,93	Mevalonate kinase	2,10
1,65	Acetoacetyl-CoA synthetase	#N/D
1,54	7-dehydrocholesterol reductase	#N/D
1,49	3-hydroxy-3-methylglutaryl-Coenzyme A synthase 1	6,28
1,43	Spermidine synthase	3,77
1,25	Diphosphomevalonate decarboxylase	2,34

Tab. 3: Fold-Upregulation of proteins involved in MVA cascade, -oxidation, fatty acid synthase/oxidation and mitochondrial biogenesis, in MCF7 and T47D mammospheres.

DISCUSSION

Targeting breast CSCs for cancer therapy is a promising and developing field [43]. Several studies have described an association between metabolism and CSC biology, but no therapy has ever been proposed so far. However, to develop an effective anticancer therapeutic strategy it will be necessary to take into account several parameters and differences [16, 44]. These differences may be, at least in part, due to different CSCs regulated by different signalling pathways. Statins are competitive inhibitors of HMGCR, which converts HMG-CoA to mevalonate. This is the rate-limiting step in cholesterol biosynthesis [17]. Cholesterol is an essential component of cell membrane; the rapidly growing cancer tumour cells require a high uptake of extracellular cholesterol, but many patients with cancer have reduced plasma levels of cholesterol [45, 46]. Therefore, statins can inhibit human cancer growth and thus reduce mortality by decreasing the locally synthesised or circulating cholesterol levels [18, 47]. In addition to cholesterol, HMGCR inhibition by statins also depletes several other important intermediates [48] may be involved in CSCs formation [16]. Here, was showed that treatment with BMF (100 μ M - 1mM) was efficient reduce tumorsphere formation in MCF7 cancer cell lines through HMGCR inhibition. The results showed that BMF efficacy reduced the tumor cell survival in MCF7 cells and MCF7-HMGCR transfected cells, targeting the HMGCR enzyme and arresting cell cycle in G0/G1 phase [19]. Moreover, using MCF7 cells expressing a panel of luciferase reporters, was observed that BMF treatment was indeed sufficient to inhibit a number of different

signal transduction pathways, including WNT, Notch, STAT1/3 and to activate the NRF2-antioxidant responses and Interferon 1 signaling pathway. No effects were observed for the SMAD-TGF β -pathway and Hedgehog pathway. Thus, BMF may reduce the number of CSCs that are capable of forming tumor-spheres, by inhibiting their proliferation. Importantly, results indicate that BMF treatment reduced the mitochondrial respiration in MCF7 cell line but not in normal fibroblast. Moreover, BMF increased the endogenous fatty acid oxidation in MCF7 cell line, suggesting the β -oxidation induction. The statins can inhibit “bulk” cancer cell migration or prevent tumor growth by reducing the network signaling pathway HIF and Nf- κ B related also, in normal cells surrounding the tumor [40, 49, 50]. Using h-tert-BJ1 cells expressing a luciferase reporters, was observed that BMF treatment was indeed sufficient to inhibit HIF and Nf- κ B, inhibiting the cancer progression. IL-8 and GM-CSF is known to stimulate malignant tumor cell growth and migration in vitro and to promote cancer progression in vivo [34-36]. Mostly, IL-8 is a tumor invasion key factor, covering a main role to active numerous cancer progression [34] and CSC formation pathways, including WNT, Notch, STAT1/3 pathway [51-53]. For these reasons, were evaluated the GM-CSF and IL-8 level in MCF7 culture media after 72h of treatment with BMF. The result showed that BMF inhibited the GM-CSF and IL-8 levels in a dose dependent manner. Further, proteomics analysis revealed significantly 41 overexpressed proteins associated with basal/mesenchymal tumorspheres (MCF7 and T47D), involved in MVA cascade, β -oxidation, fatty acid synthase/oxidation and mitochondrial biogenesis

compared to adherent cancer cells [42]. Both, MCF7 and T47D tumorsphere cell lines were highly enriched in enzymes involved in mevalonic acid (MVA) metabolism. This results confirm that this metabolic pathway, which starts by the conversion of 3-hydroxy-3-methylglutaryl CoA (HMGCoA) to mevalonate through HMG-CoA reductase (HMGCR) activity [19], has a key role in tumorsphere and CSC formation. Finally, using a specific breast CSC marker (ALDH) [24], was showed that BMF appears to reduce the number of CSCs, in MCF7 and MCF7-HMGCR cell lines. Indeed, the MCF7-HMGCR showed an increased ability to form CSCs, compare to MCF7-EV. Moreover, the addition of mevalonate, the product of HMGCR, to the culture medium, rescued the CSC population, with a complete restoration of both the ALDEFLUOR-positive population and the tumorsphere formation. These results confirm the essential role of MVA metabolism in the regulation of CSC self-renewal [16]. Contrary, the addition of cholesterol did not prevent BMF and pravastatin effect on CSC population with a similar reduction in the ALDEFLUOR-positive population and tumorsphere-initiating capacity in MCF7 cel line. These results suggest that the ability to affect the breast CSC population via MVA metabolism blockade is not related to cholesterol biosynthesis. These result candidates the BMF natural compound, to prevent the tumor proliferation, cancer progression and CSCs formation.

REFERENCES

1. Berry, D.A., et al., *Effect of screening and adjuvant therapy on mortality from breast cancer*. N Engl J Med, 2005. 353(17): p. 1784-92.
2. Liu, S. and M.S. Wicha, *Targeting breast cancer stem cells*. J Clin Oncol, 2010. 28(25): p. 4006-12.
3. Karsten, U. and S. Goletz, *What makes cancer stem cell markers different?* Springerplus, 2013. 2(1): p. 301.
4. Reya, T., et al., *Stem cells, cancer, and cancer stem cells*. Nature, 2001. 414(6859): p. 105-11.
5. Ginestier, C., E. Charafe-Jauffret, and D. Birnbaum, *Targeting breast cancer stem cells: fishing season open!* Breast Cancer Res, 2010. 12(5): p. 312.
6. Charafe-Jauffret, E., C. Ginestier, and D. Birnbaum, *Breast cancer stem cells: tools and models to rely on*. BMC Cancer, 2009. 9: p. 202.
7. Dontu, G., et al., *Stem cells in normal breast development and breast cancer*. Cell Prolif, 2003. 36 Suppl 1: p. 59-72.
8. Magee, J.A., E. Piskounova, and S.J. Morrison, *Cancer stem cells: impact, heterogeneity, and uncertainty*. Cancer Cell, 2012. 21(3): p. 283-96.
9. Fiorillo, M., et al., *Graphene oxide selectively targets cancer stem cells, across multiple tumor types: implications for non-toxic cancer treatment, via "differentiation-based nano-therapy"*. Oncotarget, 2015. 6(6): p. 3553-62.
10. Shaw, F.L., et al., *Treatment-related restoration of Langerhans cell migration in psoriasis*. J Invest Dermatol, 2014. 134(1): p. 268-71.
11. Fillmore, C.M. and C. Kuperwasser, *Human breast cancer cell lines contain stem-like cells that self-renew, give rise to phenotypically diverse progeny and survive chemotherapy*. Breast Cancer Res, 2008. 10(2): p. R25.
12. Cojoc, M., et al., *A role for cancer stem cells in therapy resistance: cellular and molecular mechanisms*. Semin Cancer Biol, 2015. 31: p. 16-27.

13. Skvortsov, S., et al., *Crosstalk between DNA repair and cancer stem cell (CSC) associated intracellular pathways*. *Semin Cancer Biol*, 2015. 31: p. 36-42.
14. Al-Hajj, M., et al., *Prospective identification of tumorigenic breast cancer cells*. *Proc Natl Acad Sci U S A*, 2003. 100(7): p. 3983-8.
15. Ginestier, C., et al., *ALDH1 is a marker of normal and malignant human mammary stem cells and a predictor of poor clinical outcome*. *Cell Stem Cell*, 2007. 1(5): p. 555-67.
16. Ginestier, C., et al., *Mevalonate metabolism regulates Basal breast cancer stem cells and is a potential therapeutic target*. *Stem Cells*, 2012. 30(7): p. 1327-37.
17. Thurnher, M., G. Gruenbacher, and O. Nussbaumer, *Regulation of mevalonate metabolism in cancer and immune cells*. *Biochim Biophys Acta*, 2013. 1831(6): p. 1009-15.
18. Pisanti, S., et al., *Novel prospects of statins as therapeutic agents in cancer*. *Pharmacol Res*, 2014. 88: p. 84-98.
19. Stine, J.E., et al., *The HMG-CoA reductase inhibitor, simvastatin, exhibits anti-metastatic and anti-tumorigenic effects in ovarian cancer*. *Oncotarget*, 2015.
20. Peiris-Pages, M., F. Sotgia, and M.P. Lisanti, *Chemotherapy induces the cancer-associated fibroblast phenotype, activating paracrine Hedgehog-GLI signalling in breast cancer cells*. *Oncotarget*, 2015. 6(13): p. 10728-45.
21. Peiris-Pages, M., et al., *Proteomic identification of prognostic tumour biomarkers, using chemotherapy-induced cancer-associated fibroblasts*. *Aging (Albany NY)*, 2015. 7(10): p. 816-38.
22. De Luca, A., et al., *Mitochondrial biogenesis is required for the anchorage-independent survival and propagation of stem-like cancer cells*. *Oncotarget*, 2015. 6(17): p. 14777-95.
23. Shaw, F.L., et al., *A detailed mammosphere assay protocol for the quantification of breast stem cell activity*. *J Mammary Gland Biol Neoplasia*, 2012. 17(2): p. 111-7.
24. Farnie, G., F. Sotgia, and M.P. Lisanti, *High mitochondrial mass identifies a sub-population of stem-like cancer cells that are chemo-resistant*. *Oncotarget*, 2015. 6(31): p. 30472-86.
25. Bellosta, S., R. Paoletti, and A. Corsini, *Safety of statins: focus on clinical pharmacokinetics and drug interactions*. *Circulation*, 2004. 109(23 Suppl 1): p. III50-7.

26. Soriano, J.V., et al., *Expression of an activated Notch4(int-3) oncoprotein disrupts morphogenesis and induces an invasive phenotype in mammary epithelial cells in vitro*. Int J Cancer, 2000. 86(5): p. 652-9.
27. Nefedova, Y., et al., *Hyperactivation of STAT3 is involved in abnormal differentiation of dendritic cells in cancer*. J Immunol, 2004. 172(1): p. 464-74.
28. Vorechovsky, I., K.P. Benediktsson, and R. Toftgard, *The patched/hedgehog/smoothened signalling pathway in human breast cancer: no evidence for H133Y SHH, PTCH and SMO mutations*. Eur J Cancer, 1999. 35(5): p. 711-3.
29. Kelly, O.G., K.I. Pinson, and W.C. Skarnes, *The Wnt co-receptors Lrp5 and Lrp6 are essential for gastrulation in mice*. Development, 2004. 131(12): p. 2803-15.
30. Huelsken, J., et al., *Requirement for beta-catenin in anterior-posterior axis formation in mice*. J Cell Biol, 2000. 148(3): p. 567-78.
31. Guo, S., et al., *Oncogenic role and therapeutic target of leptin signaling in breast cancer and cancer stem cells*. Biochim Biophys Acta, 2012. 1825(2): p. 207-22.
32. Waugh, D.J. and C. Wilson, *The interleukin-8 pathway in cancer*. Clin Cancer Res, 2008. 14(21): p. 6735-41.
33. Cimato, T.R. and B.A. Palka, *Fractalkine (CX3CL1), GM-CSF and VEGF-a levels are reduced by statins in adult patients*. Clin Transl Med, 2014. 3: p. 14.
34. Ginestier, C., et al., *CXCR1 blockade selectively targets human breast cancer stem cells in vitro and in xenografts*. J Clin Invest, 2010. 120(2): p. 485-97.
35. Kim, D.H., et al., *Comparative anticancer effects of flavonoids and diazepam in cultured cancer cells*. Biol Pharm Bull, 2008. 31(2): p. 255-9.
36. Lawicki, S., et al., *Hematopoietic cytokines as tumor markers in breast malignancies. A multivariate analysis with ROC curve in breast cancer patients*. Adv Med Sci, 2013. 58(2): p. 207-15.
37. Morales, J.K., et al., *GM-CSF is one of the main breast tumor-derived soluble factors involved in the differentiation of CD11b-Gr1- bone marrow progenitor cells into myeloid-derived suppressor cells*. Breast Cancer Res Treat, 2010. 123(1): p. 39-49.
38. Garcia, J.A., *HIFing the brakes: therapeutic opportunities for treatment of human malignancies*. Sci STKE, 2006. 2006(337): p. pe25.

39. Chung, S.S., C. Aroh, and J.V. Vadgama, *Constitutive activation of STAT3 signaling regulates hTERT and promotes stem cell-like traits in human breast cancer cells*. PLoS One, 2013. 8(12): p. e83971.
40. Guido, C., et al., *Mitochondrial fission induces glycolytic reprogramming in cancer-associated myofibroblasts, driving stromal lactate production, and early tumor growth*. Oncotarget, 2012. 3(8): p. 798-810.
41. Bardos, J.I. and M. Ashcroft, *Negative and positive regulation of HIF-1: a complex network*. Biochim Biophys Acta, 2005. 1755(2): p. 107-20.
42. Lamb, R., et al., *Mitochondria as new therapeutic targets for eradicating cancer stem cells: Quantitative proteomics and functional validation via MCT1/2 inhibition*. Oncotarget, 2014. 5(22): p. 11029-37.
43. McDermott, S.P. and M.S. Wicha, *Targeting breast cancer stem cells*. Mol Oncol, 2010. 4(5): p. 404-19.
44. Ginestier, C. and M.S. Wicha, *Mammary stem cell number as a determinate of breast cancer risk*. Breast Cancer Res, 2007. 9(4): p. 109.
45. Fiorenza, A.M., A. Branchi, and D. Sommariva, *Serum lipoprotein profile in patients with cancer. A comparison with non-cancer subjects*. Int J Clin Lab Res, 2000. 30(3): p. 141-5.
46. Benn, M., et al., *Low-density lipoprotein cholesterol and the risk of cancer: a mendelian randomization study*. J Natl Cancer Inst, 2011. 103(6): p. 508-19.
47. Yeganeh, B., et al., *Targeting the mevalonate cascade as a new therapeutic approach in heart disease, cancer and pulmonary disease*. Pharmacol Ther, 2014. 143(1): p. 87-110.
48. Kato, S., et al., *Lipophilic but not hydrophilic statins selectively induce cell death in gynaecological cancers expressing high levels of HMGCoA reductase*. J Cell Mol Med, 2010. 14(5): p. 1180-93.
49. Semenza, G.L., *Regulation of cancer cell metabolism by hypoxia-inducible factor 1*. Semin Cancer Biol, 2009. 19(1): p. 12-6.
50. Kim, Y., et al., *Statin pretreatment inhibits the LPS-induced EMT via the downregulation of TLR4 and NF-kappaB in human biliary epithelial cells*. J Gastroenterol Hepatol, 2015.

51. Kakarala, M., et al., *Targeting breast stem cells with the cancer preventive compounds curcumin and piperine*. Breast Cancer Res Treat, 2010. 122(3): p. 777-85.
52. Simoes, B.M., et al., *Anti-estrogen Resistance in Human Breast Tumors Is Driven by JAG1-NOTCH4-Dependent Cancer Stem Cell Activity*. Cell Rep, 2015. 12(12): p. 1968-77.
53. Chung, S.S. and J.V. Vadgama, *Curcumin and epigallocatechin gallate inhibit the cancer stem cell phenotype via down-regulation of STAT3-NFkappaB signaling*. Anticancer Res, 2015. 35(1): p. 39-46.

Mitochondrial mass, a new metabolic biomarker for stem-like cancer cells: Understanding WNT/FGF-driven anabolic signaling

Rebecca Lamb^{1,2,*}, Gloria Bonuccelli^{1,2,*}, Béla Ozsvári^{1,2}, Maria Peiris-Pagès^{1,2}, Marco Fiorillo^{1,2,3}, Duncan L. Smith⁴, Generoso Bevilacqua^{5,6}, Chiara Maria Mazzanti⁵, Liam A. McDonnell⁵, Antonio Giuseppe Naccarato⁶, Maybo Chiu^{1,2}, Luke Wynne^{1,2}, Ubaldo E. Martinez-Outschoorn⁷, Federica Sotgia^{1,2} and Michael P. Lisanti^{1,2}

¹ The Breast Cancer Now Research Unit, Institute of Cancer Sciences, University of Manchester, Manchester, UK

² The Manchester Centre for Cellular Metabolism (MCCM), Institute of Cancer Sciences, University of Manchester, Manchester, UK

³ The Department of Pharmacy, Health and Nutritional Sciences, The University of Calabria, Cosenza, Italy

⁴ The Cancer Research UK Manchester Institute, University of Manchester, Manchester, UK

⁵ FPS – The Pisa Science Foundation, Pisa, Italy

⁶ Department of Pathology, Pisa University Hospital, Pisa, Italy

⁷ The Sidney Kimmel Cancer Center, Philadelphia, PA, USA

* These authors should be considered as co-first authors

Correspondence to: Michael P. Lisanti, **email:** michaelp.lisanti@gmail.com

Federica Sotgia, **email:** fsotigia@gmail.com

Keywords: mitochondria, MitoTracker, MMTV, WNT, FGF

Received: July 21, 2015

Accepted: August 22, 2015

Published: September 28, 2015

This is an open-access article distributed under the terms of the Creative Commons Attribution License, which permits unrestricted use, distribution, and reproduction in any medium, provided the original author and source are credited.

ABSTRACT

Here, we developed an isogenic cell model of “stemness” to facilitate protein biomarker discovery in breast cancer. For this purpose, we used knowledge gained previously from the study of the mouse mammary tumor virus (MMTV). MMTV initiates mammary tumorigenesis in mice by promoter insertion adjacent to two main integration sites, namely Int-1 (Wnt1) and Int-2 (Fgf3), which ultimately activates Wnt/ β -catenin signaling, driving the propagation of mammary cancer stem cells (CSCs). Thus, to develop a humanized model of MMTV signaling, we over-expressed WNT1 and FGF3 in MCF7 cells, an ER(+) human breast cancer cell line. We then validated that MCF7 cells over-expressing both WNT1 and FGF3 show a 3.5-fold increase in mammosphere formation, and that conditioned media from these cells is also sufficient to promote stem cell activity in untransfected parental MCF7 and T47D cells, as WNT1 and FGF3 are secreted factors. Proteomic analysis of this model system revealed the induction of i) EMT markers, ii) mitochondrial proteins, iii) glycolytic enzymes and iv) protein synthesis machinery, consistent with an anabolic CSC phenotype. MitoTracker staining validated the expected WNT1/FGF3-induced increase in mitochondrial mass and activity, which presumably reflects increased mitochondrial biogenesis. Importantly, many of the proteins that were up-regulated by WNT/FGF-signaling in MCF7 cells, were also transcriptionally over-expressed in human breast cancer cells *in vivo*, based on the bioinformatic analysis of public gene expression datasets of laser-captured patient samples. As such, this isogenic cell model should accelerate the discovery of new biomarkers to predict clinical outcome in breast cancer, facilitating the development of personalized medicine.

Finally, we used mitochondrial mass as a surrogate marker for increased mitochondrial biogenesis in untransfected MCF7 cells. As predicted, metabolic

fractionation of parental MCF7 cells, via MitoTracker staining, indicated that high mitochondrial mass is a new metabolic biomarker for the enrichment of anabolic CSCs, as functionally assessed by mammosphere-forming activity. This observation has broad implications for understanding the role of mitochondrial biogenesis in the propagation of stem-like cancer cells. Technically, this general metabolic approach could be applied to any cancer type, to identify and target the mitochondrial-rich CSC population.

The implications of our work for understanding the role of mitochondrial metabolism in viral oncogenesis driven by random promoter insertions are also discussed, in the context of MMTV and ALV infections.

INTRODUCTION

The mouse mammary tumor virus (MMTV) is a saliva- and milk-transmitted retrovirus [1-5]; however, infected mice only develop mammary tumors in adulthood [4]. This long latency period makes MMTV an interesting virus for understanding the pathogenesis of human breast cancers [6]. The provirus inserts upstream of two key integration sites, named Int-1 and Int-2 [7-10]. This process of insertional mutagenesis is thought to be random, but involves the positive selection of genes that will ultimately provide an increase in “stemness”, a cellular growth-advantage, or perhaps both. MMTV tumors are oligo-clonal, suggesting that there is some synergy between these two different integration sites. These mammary proto-oncogenes Int-1 and Int-2 have been identified as WNT1 and FGF3 [11-13], two secreted growth factors normally involved in stem cell signaling pathways.

WNT1 is the first member of the WNT gene family, which is known to be involved in cell fate determination and patterning during embryogenesis [14, 15]. FGF3 is a member of the fibroblast growth factor family, which controls cell proliferation, morphogenesis and tissue repair [16]. Interestingly, WNT1 and FGF3 converge directly upon the WNT/ β -catenin signaling cascade [17, 18]. However, it remains largely unknown exactly how WNT1/FGF3 signaling induces mammary tumorigenesis.

Here, we have created a humanized model of MMTV signaling, by over-expressing WNT1 and FGF3 in human breast cancer cells, namely MCF7 cells, an ER(+) cell line. Unbiased label-free proteomic analysis of this model system reveals the induction of EMT markers, mitochondrial proteins, glycolytic enzymes and protein synthesis machinery, consistent with an anabolic CSC phenotype. The proteins that were up-regulated by WNT/FGF-signaling in MCF7 cells, were also transcriptionally over-expressed in human breast cancer cells *in vivo*. This isogenic cell model should accelerate the identification and development of new protein biomarkers to predict clinical outcomes in breast cancer patients.

Finally, we also show that mitochondrial mass is a new metabolic biomarker for anabolic CSCs, as assessed by MitoTracker vital-staining and metabolic cell

fractionation by flow-cytometry.

RESULTS

Generating a humanized model of MMTV signaling.

During MMTV infection of mammary epithelial cells, genomic viral integration occurs. This ultimately leads to mammary tumorigenesis in mice. Mechanistically,

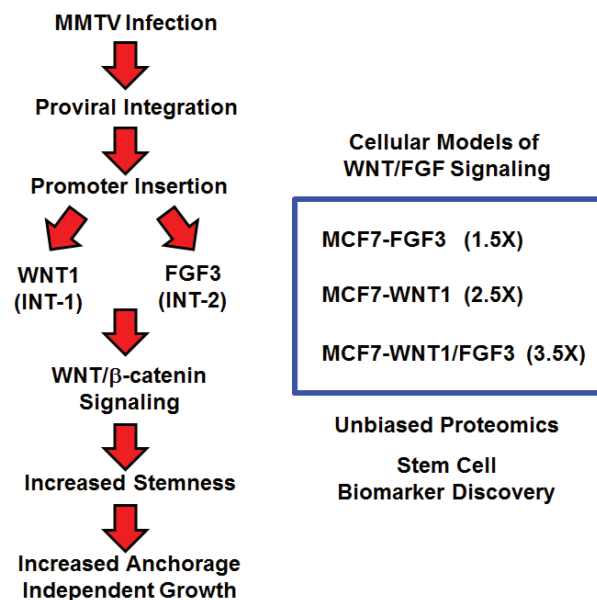


Figure 1: Creating a humanized experimental model for MMTV: Focus on WNT1 and FGF3 signaling.

To create a humanized model of MMTV signaling, we recombinantly over-expressed WNT1 and FGF3 in MCF7 cells, an ER(+) human breast cancer cell line. WNT1 and FGF3 were expressed either individually or in combination, using lenti-viral vectors carrying two different selection markers (puromycin or neomycin/G418). This isogenic cell model of “stemness” was generated to facilitate protein biomarker discovery in breast cancer, via unbiased label-free proteomics. Importantly, over-expression of FGF3, WNT1, or WNT1/FGF3 increases mammosphere formation by 1.5-, 2.5- and 3.5-fold, respectively (See Figure 2). Thus, we focused on MCF7-WNT1/FGF3 cells for further validation and proteomic analysis.

Table 1: MMTV common proviral integration sites and gene designations.

Integration site(s)	Gene Name
Int-1	Wnt-1
Int-2	Fgf-3
Int-3	Notch-4
Int-4	Wnt-3
Int-5	Aromatase; Cyp19a1
Int-6	Eukaryotic translation initiation factor 3; eIF3
Int-7	Rspo-2

Additional genes include Fgf-4, Wnt-3a and Wnt-10, among others.

the MMTV virus uses a promoter insertion mechanism of mutagenesis, to drive oncogenesis [19]. More specifically, the MMTV promoter inserts upstream of two main integration sites, namely Int-1 (Wnt1) or Int-2 (Fgf3), although a few other rare integration sites have been described [11-13, 20] (Table 1). As a consequence, the MMTV promoter drives the over-expression of these secreted stem cell associated growth factors, constitutively activating Wnt/ β -catenin signaling [11, 21, 22]. Thus, the MMTV model has been instrumental for understanding how “amplified” or “constitutive” stem cell signaling directly contributes to solid tumor formation (Figure 1). As such, it would be beneficial to create a humanized non-infectious model of MMTV signaling, to drive the discovery of new stem cell associated biomarkers, for predicting clinical outcome in human breast cancer

patients.

Thus, in order to create a humanized model of MMTV signaling, we recombinantly over-expressed WNT1 and FGF3 in MCF7 cells, an ER(+) human breast cancer cell line. WNT1 and FGF3 were expressed either individually or in combination, using lentiviral vectors carrying two different selection markers (puromycin or neomycin/G418). For comparison purposes, empty vector controls (EV) were generated in parallel (Figure 1).

Then, the various cell lines were screened for stem cell activity, using the mammosphere assay as a functional readout. Importantly, Figure 2A directly validates that over-expression of either WNT1 or FGF3 is sufficient to increase the clonal expansion of cancer stem cells. Interestingly, FGF3 and WNT1 significantly increased mammosphere formation by ~1.5-fold and ~2.5-fold,

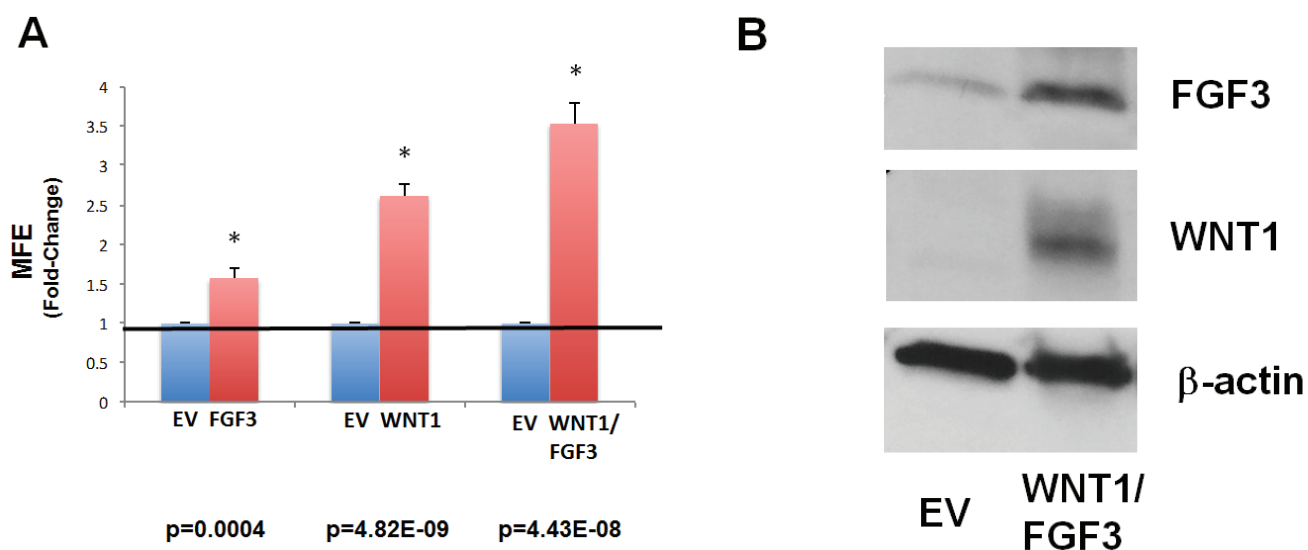


Figure 2: Recombinant over-expression of WNT1 and/or FGF3 in MCF7 cells significantly augments mammosphere formation. **A) Mammosphere formation.** The cell lines we generated were screened for stem cell activity, using the mammosphere assay as a functional readout. Note that over-expression of either WNT1 or FGF3 significantly increased mammosphere formation by ~1.5-fold and ~2.5-fold, respectively. However, MCF7 cells over-expressing both WNT1 and FGF3 showed the largest increase in mammosphere formation, by up to ~3.5-fold. Results were normalized to the three control cell lines harboring either i) EX-Neg-Lv105(puro), ii) EX-Neg-Lv151(neo) or iii) both control vectors. P-values are as indicated. Assays were performed in triplicate and repeated three times independently. MFE, mammosphere forming efficiency. **B) Immunoblot analysis.** Recombinant over-expression of WNT1 and FGF3 in these transfected cell models was validated by immunoblot analysis, with specific antibody probes. Beta-actin is shown as a control for equal loading.

respectively. However, MCF7 cells over-expressing both WNT1 and FGF3 showed the largest increase in mammosphere formation, by up to ~3.5-fold (Figure 2A).

We also validated the recombinant over-expression of WNT1 and FGF3 in these transfected cell models by immunoblot analysis, with specific antibody probes (Figure 2B).

Conditioned media from MCF7-WNT1/FGF3 cells is sufficient to increase mammosphere formation.

As WNT1 and FGF3 are secreted factors, it would be predicted that the increase in constitutive stem cell signaling could also act in a paracrine fashion on non-transfected cells. To test this hypothesis, we prepared conditioned media from MCF7-WNT1/FGF3 cells and the corresponding empty vector (MCF7-EV) control cells.

Then, we compared the ability of conditioned media to support mammosphere formation, in untransfected parental MCF7 cells. Figure 3 (Left) shows that conditioned media prepared from MCF7-WNT1/FGF3 cells significantly stimulated mammosphere formation by ~2-fold. Importantly, virtually identical results were obtained with untransfected parental T47D cells, a second independent ER(+) breast cancer cell line (Figure 3

(Right)).

Proteomics analysis of MCF7-WNT1/FGF3 cells reveals the upregulation of EMT markers, mitochondrial proteins, glycolytic enzymes, and the protein synthesis machinery.

To better understand how WNT and FGF signaling drive the expansion of CSCs, we used unbiased label-free proteomics analysis. The proteome of MCF7-WNT1/FGF3 cells was compared to MCF7-EV control cells. We restricted our analysis to protein products that were over-expressed by >1.5-fold. Overall, our results are detailed in Tables 2, 3 and 4.

Remarkably, >40 nuclear-encoded mitochondrial-related proteins were over-expressed in MCF7-WNT1/FGF3 cells (Table 2). Many of these proteins were related to the TCA cycle (ACO2), oxidative phosphorylation (MT-CO2), regenerating ATP (CKMT1/2) or mitochondrial biogenesis (TOMM34). In addition, MT-CO2 (a mitochondria-DNA encoded protein) was upregulated by >2.5-fold, indicative of the production of new mitochondria. In support of an anabolic phenotype, proteins related to glycolysis, the pentose phosphate pathway, glycogen metabolism and amino acid synthesis were upregulated (Table 2).

WNT1/FGF3 Conditioned Media Experiments

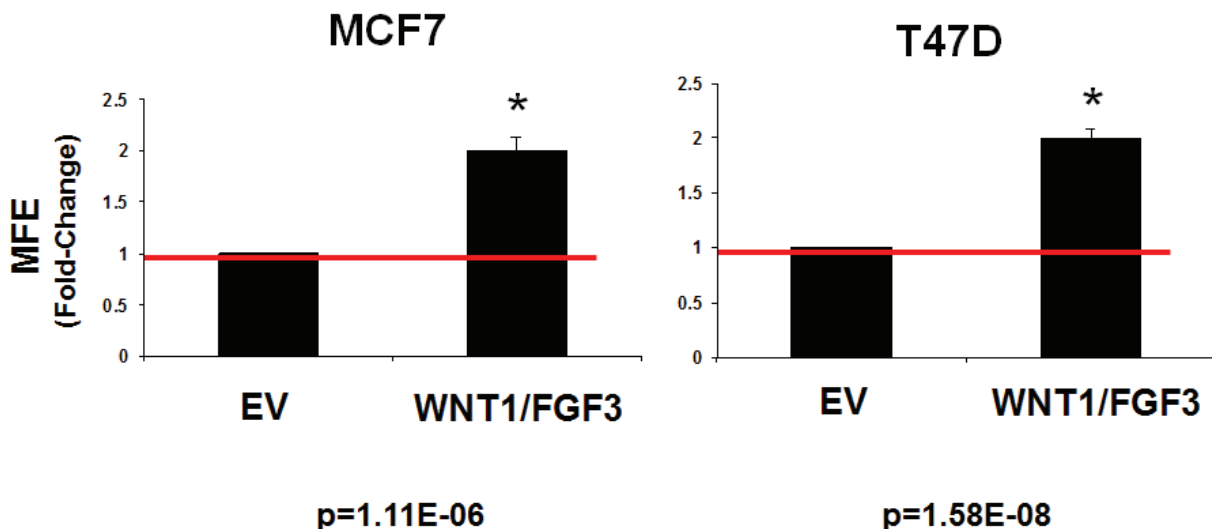


Figure 3: Conditioned media from WNT1/FGF3 expressing MCF7 cells increases mammosphere formation. Since WNT1 and FGF3 are secreted factors, they should act in a paracrine fashion on non-transfected cells. To test this hypothesis, we prepared conditioned media from MCF7-WNT1/FGF3 cells and the corresponding empty vector (MCF7-EV) control cells. Then, we compared the ability of this conditioned media to support mammosphere formation, in untransfected parental MCF7 cells (Left panel). Note that conditioned media prepared from MCF7-WNT1/FGF3 cells significantly stimulated mammosphere formation by ~2-fold. Nearly identical results were obtained with untransfected parental T47D cells, a second independent ER(+) breast cancer cell line (Right panel). Assays were performed in triplicate and repeated three times independently. MFE, mammosphere forming efficiency.

Table 2: Key Molecules Up-regulated by WNT1/FGF3 in MCF7 Cells: Mitochondria and Glycolysis.

Symbol	Description	Fold-Change	ANOVA
Mitochondrial-related Proteins/TCA Cycle (42)			
ACO2	Aconitase 2, mitochondrial	Infinity	1.61E-08
IDH1	Isocitrate dehydrogenase [NADP] 1	Infinity	0.004
MDH1	Malate dehydrogenase, cytoplasmic	28.32	2.11E-05
CKMT2	Creatine kinase S-type, mitochondrial	11.04	0.015
FASN	Fatty acid synthase	7.77	0.036
CKMT1	Creatine kinase U-type, mitochondrial	7.60	2.12E-05
CKMT1B	Creatine kinase U-type, mitochondrial	6.27	5.74E-05
CKMT1A	Creatine kinase U-type, mitochondrial	5.19	7.98E-05
OAT	Ornithine aminotransferase, mitochondrial	4.79	0.0003
PC	Pyruvate carboxylase, mitochondrial	4.63	0.0001
DUT	Deoxyuridine 5'-triphosphate nucleotidohydrolase, mitochondrial	3.85	0.0001
TOMM34	Translocase of outer mitochondrial membrane 34	2.89	0.0027
GLUD2	Glutamate dehydrogenase 2, mitochondrial	2.78	0.035
MT-CO2	Cytochrome c oxidase subunit 2 (COX2)	2.66	0.0017
NQO1	NAD(P)H dehydrogenase [quinone] 1	2.60	8.31E-05
ACADVL	Very long-chain-specific acyl-CoA dehydrogenase, mitochondrial	2.46	0.0007
C21orf33	ES1 protein homolog, mitochondrial	2.37	0.01
NDUFS1	Mitochondrial NADH-ubiquinone oxidoreductase 75 kDa subunit	2.27	0.0026
SCD	Acyl-CoA desaturase	2.25	3.93E-05
GPD2	Glycerol-3-phosphate dehydrogenase, mitochondrial	2.08	0.03
HSPA9	Stress-70 protein, mitochondrial	2.07	0.0498
IDH3A	Isocitrate dehydrogenase [NAD] subunit alpha, mitochondrial	1.96	0.001
HSPD1	60 kDa heat shock protein, mitochondrial	1.95	0.02
ETF A	Electron transfer flavoprotein subunit alpha, mitochondrial	1.91	0.03
ABAT	4-aminobutyrate aminotransferase, mitochondrial	1.85	0.03
PRDX5	Peroxioredoxin-5, mitochondrial	1.83	0.037
COX4I1	Cytochrome c oxidase subunit 4 isoform 1, mitochondrial	1.83	0.007
COX6A1	Cytochrome c oxidase subunit 6A, mitochondrial	1.81	0.002
TUFM	Elongation factor Tu, mitochondrial	1.78	0.02
ATP5O	ATP synthase subunit O, mitochondrial	1.77	0.004
CLPX	ATP-dependent Clp protease ATP-binding subunit clpX-like, mitochondrial	1.72	0.016
CS	Citrate synthase, mitochondrial	1.71	0.001
ECHS1	Enoyl-CoA hydratase, mitochondrial	1.70	0.004
ATP5B	ATP synthase subunit beta, mitochondrial	1.69	0.039
PCK2	Phosphoenolpyruvate carboxykinase [GTP], mitochondrial	1.66	0.001
AK2	Adenylate kinase 2, mitochondrial	1.65	0.004
ATP5A1	ATP synthase subunit alpha, mitochondrial	1.61	0.02
ETFB	Electron-transfer-flavoprotein, beta	1.60	0.02
PRKDC	DNA-dependent protein kinase catalytic subunit (maintains mt-DNA copy number)	1.58	0.03
CHCHD2P9	Coiled-coil-helix-coiled-coil-helix domain-protein CHCHD2P9, mitochondrial	1.57	0.02
AIFM1	Apoptosis-inducing factor 1, mitochondrial	1.53	0.006
UQCRCF1P1	Putative cytochrome b-c1 complex subunit Rieske-like protein 1	1.50	0.02
Enzymes Related to Glycolysis, the Pentose Phosphate Pathway, Glycogen, and Amino Acid Synthesis (Serine/Arginine) (14)			
PHGDH	D-3-phosphoglycerate dehydrogenase	Infinity	2.68E-13
ASS1	Argininosuccinate synthase	17.39	3.42E-09
HK2	Hexokinase-2	11.57	3.15E-08
PKM2	Pyruvate kinase	2.83	0.003
PYGB	Glycogen phosphorylase, brain form	2.23	0.01
PFKL	6-phosphofructokinase, liver type	2.17	0.004
CAD	Glutamine-dependent carbamoyl-phosphate synthase	2.08	0.0007
PKLR	Pyruvate kinase isozymes R/L	2.08	1.46E-05
PGAM4	Probable phosphoglycerate mutase 4	1.94	0.005
G6PD	Glucose-6-phosphate 1-dehydrogenase	1.89	0.005
TKT	Transketolase	1.64	0.003
PGK2	Phosphoglycerate kinase 2	1.57	0.006
ENO1	Enolase, alpha	1.51	0.007
PGK1	Phosphoglycerate kinase	1.50	0.04

Stem-like cancer cells also undergo an epithelial-mesenchymal transition (EMT), which promotes cell migration, invasion and distant metastasis [23]. Importantly, >45 proteins known to be associated with the EMT phenotype (cell migration or invasiveness) were upregulated in MCF7-WNT1/FGF3 cells (Table 3).

Examples include FRS2 (FGF receptor substrate-2; >10-fold) and β -catenin (>2-fold), which would be expected to further amplify WNT/FGF signaling, as these are downstream elements of these convergent signaling networks. Similarly, other signaling molecules that promote the EMT and cell migration were significantly upregulated, such as

Table 3: Key Molecules Up-regulated by WNT1/FGF3 in MCF7 Cells: The EMT and Cell Migration.

Symbol	Description	Fold-Change	ANOVA
EMT Markers, Extracellular Matrix, Cell Migration and Cytoskeletal proteins (47)			
MARCKS	Myristoylated alanine-rich C-kinase substrate	371.76	3.72E-05
S100A14	Protein S100-A14	96.23	0.0002
CDC42	Cell division control protein 42 homolog	68.67	5.27E-06
LGALS3BP	Galectin-3-binding protein	38.46	0.001
FRS2	Fibroblast growth factor receptor substrate 2	11.59	9.69E-05
MAST4	Microtubule-associated serine/threonine-protein kinase 4	10.81	2.62E-05
CALML5	Calmodulin-like protein 5	8.06	0.0007
CDV3	Carnitine deficiency-associated gene expressed in cardiac ventricle 3	7.67	7.58E-06
SCUBE1	Signal peptide, CUB domain, EGF-like 1	6.84	1.97E-05
S100A11	Protein S100-A11	6.66	0.026
S100A16	Protein S100-A16	6.41	0.0003
MERTK	Tyrosine-protein kinase MER	6.24	4.40E-05
NINJ1	Ninjurin-1	5.36	0.0001
TTBK2	Tau-tubulin kinase	5.31	4.15E-05
EMD	Emerin	4.38	0.0006
FLNB	Filamin-B	4.27	0.004
TTN	Titin	3.66	7.32E-05
CGNL1	Cingulin-like protein 1	3.62	0.005
TAGLN2	Transgelin-2	2.94	0.02
ACTA2	Actin, aortic smooth muscle	2.86	0.0002
TLN1	Talin-1	2.78	0.008
SEPT2	Septin-2	2.77	0.004
HMGB1	High mobility group protein B1	2.66	0.001
TPT1	Translationally-controlled tumor protein	2.54	0.028
AMOT	Angiomotin	2.40	0.008
CTNNB1	Catenin, beta-1	2.37	0.0003
TRIOBP	TRIO and F-actin-binding protein	2.35	0.003
ASAP2	Arf-GAP with SH3 domain, ANK repeat and PH domain-containing protein 2	2.23	0.01
MYH14	Myosin-14	2.20	0.02
S100A10	S100A10 protein	2.13	0.0002
TAX1BP3	Tax1-binding protein 3	2.13	0.0002
HMGB3	High mobility group protein B3	2.10	0.01
FLNA	Filamin-A	2.08	0.004
MYO18B	Myosin XVIIIIB	1.99	0.0005
IQGAP1	IQ motif containing GTPase activating protein 1 (scaffold protein for CDC42)	1.98	0.026
ACTN2	Alpha-actinin-2	1.96	1.64E-05
ANXA2	Annexin A2	1.90	0.01
TAGLN3	Transgelin-3	1.89	0.01
FAM129B	Niban-like protein 1 (associated with cell invasion)	1.88	0.0008
ACTN3	Alpha-actinin-3	1.81	0.025
FAM82B	Regulator of microtubule dynamics protein 1	1.80	0.02
MYH10	Myosin, heavy polypeptide 10, non-muscle	1.79	0.04
MYOF	Myoferlin	1.60	0.0026
CAPZB	F-actin-capping protein subunit beta	1.58	0.04
MTPN	Myotrophin	1.57	0.007
TUBB2A	Tubulin beta-2A chain	1.56	0.0045
EPPK1	Epiplakin	1.51	0.0485
Miscellaneous (17)			
CAST	Calpastatin A	21.60	0.005
SH3BGR1	SH3 domain-binding glutamic acid-rich-like protein	14.23	0.0003
SEC24A	Protein transport protein Sec24A	12.52	7.39E-05
PABPC4	Polyadenylate-binding protein 4	6.53	0.0006
C10orf12	Uncharacterized protein C10orf12	5.71	3.46E-05
TMED4	Transmembrane emp24 domain-containing protein 4	4.99	4.34E-05
PTMS	Parathyrosin	4.66	0.0001
HUWE1	E3 ubiquitin-protein ligase HUWE1	4.50	5.23E-05
PON2	Paraoxonase 2, isoform	4.28	0.003
AHNAK	Neuroblast differentiation-associated protein, AHNAK	3.68	0.0002
COMT	Soluble catechol-O-methyltransferase	3.66	0.002
STUB1	E3 ubiquitin-protein ligase CHIP	3.38	0.0001
TMEM205	Transmembrane protein 205 (chemo-resistance to cisplatin)	2.92	1.55E-05
TFF1	Trefoil factor 1	2.30	0.005
MATR3	Matrin-3	2.25	0.038
SRRM2	Serine/arginine repetitive matrix protein 2	2.19	0.03
ARF5	ADP-ribosylation factor 5	2.06	0.009

Genes encoding **FRS2** and **CTNNB1** are highlighted in **BOLD**, as they would be expected to amplify FGF and WNT signaling, respectively.

Table 4: Key Molecules Up-regulated by WNT1/FGF3 in MCF7 Cells: Ribosomes and Protein Synthesis.

Symbol	Description	Fold-Change	ANOVA
<u>Ribosome-related proteins (8)</u>			
RPL13	60S ribosomal protein L13	6.65	7.43E-07
NPM1	NPM1 protein	3.78	0.001
RPL14	60S ribosomal protein L14	3.41	0.001
SRPRB	Signal recognition particle receptor subunit beta	2.11	0.002
RPL4	60S ribosomal protein L4	2.04	0.01
RPS5	40S ribosomal protein S5	1.99	0.006
RPL15	60S ribosomal protein L15	1.99	0.004
RPL13	60S ribosomal protein L19	1.50	0.01
<u>Translation initiation factors (5)</u>			
EIF5A	Eukaryotic translation initiation factor 5A	7.22	0.03
EIF5B	Eukaryotic translation initiation factor 5B	2.25	3.38E-06
EIF6	Eukaryotic translation initiation factor 6	2.24	0.028
EIF2S1	Eukaryotic translation initiation factor 2, subunit 1 alpha, 35kDa	1.55	0.0035
EIF3D	Eukaryotic translation initiation factor 3 subunit D	1.51	0.03
<u>Elongation factors (4)</u>			
EEF1B2	Elongation factor 1-beta	1.95	0.0498
TUFM	Elongation factor Tu, mitochondrial	1.78	0.02
EEF1D	Elongation factor 1-delta	1.70	0.03
EEF1G	Elongation factor 1-gamma	1.52	0.001
<u>Enzymes for tRNA synthesis (6)</u>			
DARS	Aspartate--tRNA ligase, cytoplasmic	3.23	0.0001
WARS	Tryptophan--tRNA ligase, cytoplasmic	2.54	0.0016
LARS	Leucine--tRNA ligase, cytoplasmic	1.90	0.002
FARSB	Phenylalanine--tRNA ligase beta subunit	1.69	0.005
EPRS	Bifunctional aminoacyl-tRNA synthetase (Glutamyl-Prolyl-tRNA Synthetase)	1.65	0.006
C22orf28	tRNA-splicing ligase RtcB homolog	1.56	0.008
<u>Protein folding chaperones (heat shock proteins) (14)</u>			
PDIA3	Protein disulfide-isomerase A3	3.59	2.39E-05
PPIB	Peptidyl-prolyl cis-trans isomerase B	3.39	1.90E-06
CALU	Calumenin	2.93	0.0002
PDIA6	Protein disulfide-isomerase A6	2.82	0.001
PDIA4	Protein disulfide-isomerase A4	2.68	0.004
HSPA1B	Heat shock 70 kDa protein 1	2.43	0.0003
HSPD1	60 kDa heat shock protein, mitochondrial	1.95	0.02
HSP90AB3P	Putative heat shock protein HSP 90-beta-3	1.61	0.026
HSPA8	Heat shock cognate 71 kDa protein	1.60	0.02
HSP90B1	Endoplasmic	1.60	0.006
HSPH1	Heat shock protein 105 kDa	1.60	0.047
PPIA	Peptidyl-prolyl cis-trans isomerase A	1.60	0.02
HSP90AB1	Heat shock protein HSP 90-beta	1.57	0.049
CANX	Calnexin	1.54	0.01
<u>Amino acid transport (2)</u>			
SLC1A5	Neutral amino acid transporter B(0)	2.77	0.0004
SLC7A5	Solute carrier family 7 (Cationic amino acid transporter, y+ system), member 5	1.66	0.04

MARCKS (>370-fold) and CDC42 (>65-fold).

Finally, augmented protein synthesis is another characteristic of anabolic CSCs. Note that MCF7-WNT1/FGF3 cells show the upregulation of >35 proteins related to protein synthesis (Table 4). Examples include ribosome-related proteins (RPS and RPL), translation initiation factors (EIFs), peptide elongation factors (EEFs), enzymes for tRNA synthesis, as well as chaperones for protein folding (HSPs) and amino acid transporters (SLC).

Thus, MCF7-WNT1/FGF3 cells upregulate greater than 140 proteins that would be consistent with an overall anabolic phenotype (Figure 4).

Expression of WNT1/FGF3-related targets in patient-derived human breast cancer samples

To determine the possible translational significance of our results, we intersected our WNT-FGF proteomics data with human genome-wide transcriptional profiling data. These human clinical data were derived from publically available human breast cancer samples, in which breast cancer cells were separated by laser-capture microdissection from tumor stromal cells. Transcriptional profiles were analyzed from from N=28 human breast cancer patients (See the *Materials & Methods* section). In this data set, gene expression was previously determined

using Affymetrix U133A 2.0 GeneChips. A concise summary of these findings is presented in Tables 5, 6 and 7. Overall, greater than sixty WNT1/FGF3 targets (related to mitochondria, glycolysis, the EMT, and protein synthesis) that we identified in MCF7-WNT1/FGF3 cells were also transcriptionally elevated in human breast cancer cells *in vivo*. These new protein targets that we identified in MCF7-WNT1/FGF3 cells may be important for developing new strategies for the diagnosis and treatment of breast cancer.

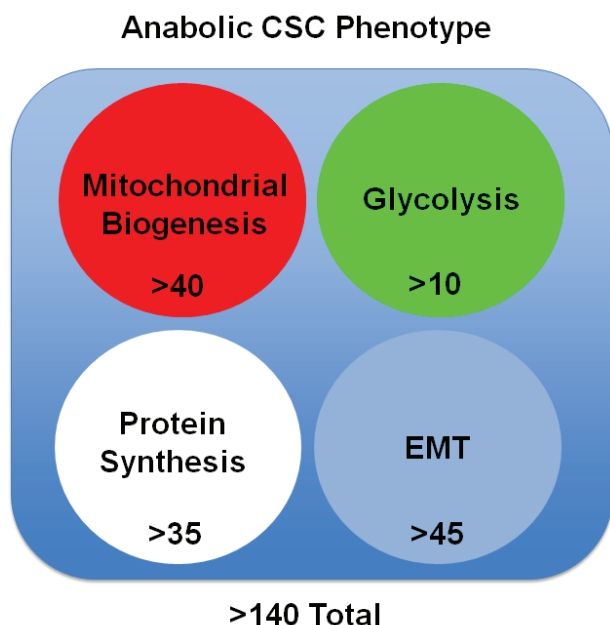


Figure 4: The anabolic CSC phenotype: Proteomics analysis. Unbiased label-free proteomics analysis of MCF7-WNT1/FGF3 cells revealed the induction of i) mitochondrial proteins, ii) glycolytic enzymes, iii) protein synthesis machinery and iv) EMT markers, consistent with an anabolic CSC phenotype. For specific details, see Tables 2, 3 and 4. *Mitochondrial proteins* – Greater than 40 nuclear-encoded mitochondrial-related proteins were over-expressed in MCF7-WNT1/FGF3 cells. Many of these proteins were related to the TCA cycle (ACO2), oxidative phosphorylation (MT-CO2), regenerating ATP (CKMT1/2) or mitochondrial biogenesis (TOMM34). In addition, MT-CO2 (a mitochondrial DNA encoded protein) was upregulated by >2.5-fold. *Glycolytic enzymes* – More than 10 enzymes related to glycolysis, the pentose phosphate pathway, glycogen metabolism and amino acid synthesis were all upregulated in MCF7-WNT1/FGF3 cells. *Protein synthesis machinery* – Over 35 proteins related to protein synthesis, including ribosome-related proteins, enzymes for tRNA synthesis, chaperones for protein folding and amino acid transporters, were all up upregulated in MCF7-WNT1/FGF3 cells. *EMT markers* – Greater than 45 proteins known to be associated with the EMT phenotype were upregulated in MCF7-WNT1/FGF3 cells. Examples include FRS2 (FGF receptor substrate-2; >10-fold) and β -catenin (>2-fold).

MCF7-WNT1/FGF3 cells show a functional increase in mitochondrial mass and mitochondrial membrane potential

To further validate the mitochondrial phenotype of MCF7-WNT1/FGF3 cells, we used fluorescent probes to quantitate mitochondrial mass and mitochondrial membrane potential by FACS analysis. For this purpose, we used MitoTracker Deep-Red (640-nm) to measure mitochondrial mass and MitoTracker Orange (561-nm), as a measure of mitochondrial membrane potential.

Figure 5 (Left panels) show that as compared to EV control MCF7 cells, MCF7 cells overexpressing WNT1/FGF3 show a clear shift to the right, for both mitochondrial mass and membrane potential. Furthermore, quantitation of fluorescence intensity (MFI) reveals that both of these mitochondrial parameters are significantly elevated in MCF7-WNT1/FGF3 cells (Figure 5 (Right panels)).

These results suggest that increased mitochondrial mass and function may be important features of the anabolic CSC phenotype.

High mitochondrial mass is a key determinant of mammosphere-forming activity in parental MCF7 cells

Based on our above observations with WNT1/FGF3 signaling, we would predict that mitochondrial biogenesis is critical for mammosphere forming activity. To test this hypothesis more directly, we metabolically fractionated untransfected parental MCF7 cells, using MitoTracker Deep-Red, as a measure of mitochondrial mass. In this context, we chose to analyze three distinct metabolic phenotypic sub-groups: i) negative cells (little or no positive staining; mito-negative group); ii) bottom 5% (mito-low group); and top 5% (mito-high group). Only live cells in each group were selected for this analysis.

Five thousand live cells from each group were then seeded per well, in 6-well low attachment plates, to measure mammosphere-forming efficiency. Remarkably, Figures 6 and 7 directly show that increasing mitochondrial mass results in a 3.0 to 5.5-fold increase in mammosphere-forming activity, depending on which gating parameters are used (singlet-gating vs. all live cells). A comparison with all live cells is also shown because mammary stem cells tend to be larger than non-stem cells (See Ref # 37 for a discussion of this point).

As such, the mito-negative group showed the least 3-D sphere-forming activity, while the mito-high group showed the highest 3-D sphere-forming efficiency. Thus, we conclude that mitochondrial mass can be used to enrich for stem-like cancer cells that are able to undergo anchorage-independent propagation, under low-attachment conditions.

DISCUSSION

The mouse mammary tumor virus (MMTV) initiates mammary tumorigenesis in mice by promoter insertion adjacent to two main integration sites, namely Int-1 (Wnt1) and Int-2 (Fgf3), driving the propagation of mammary cancer stem cells [11-13, 20]. Here, we developed an isogenic cell model of MMTV signaling to facilitate protein biomarker discovery in breast cancer (Figure 8). More specifically, we over-expressed WNT1 and FGF3 in MCF7 cells, an ER(+) human breast cancer cell line. Importantly, MCF7 cells over-expressing both WNT1 and FGF3 showed a 3.5-fold increase in mammosphere formation. Proteomic analysis of this model system revealed the induction of EMT markers, mitochondrial proteins, glycolytic enzymes and protein synthesis machinery, consistent with an anabolic phenotype. The WNT1/FGF3-induced increases in

mitochondrial function were validated by MitoTracker staining. Proteins up-regulated by WNT/FGF-signaling in MCF7 cells, were also transcriptionally over-expressed in breast cancer cells *in vivo*, based on the bioinformatic analysis of public datasets of laser-captured epithelial tumor cells from breast cancer patients. We believe that this isogenic cell model will accelerate the identification of new protein biomarkers to predict clinical outcomes in breast cancer patients. Remarkably, metabolic fractionation of parental MCF7 cells, via MitoTracker staining, indicated that mitochondrial mass is a key determinant of mammosphere-forming activity. The mito-negative group showed the least sphere-forming activity, while the mito-high group showed the highest sphere-forming efficiency. Thus, new mitochondrial biogenesis is critical for the successful propagation of stem-like cancer cells.

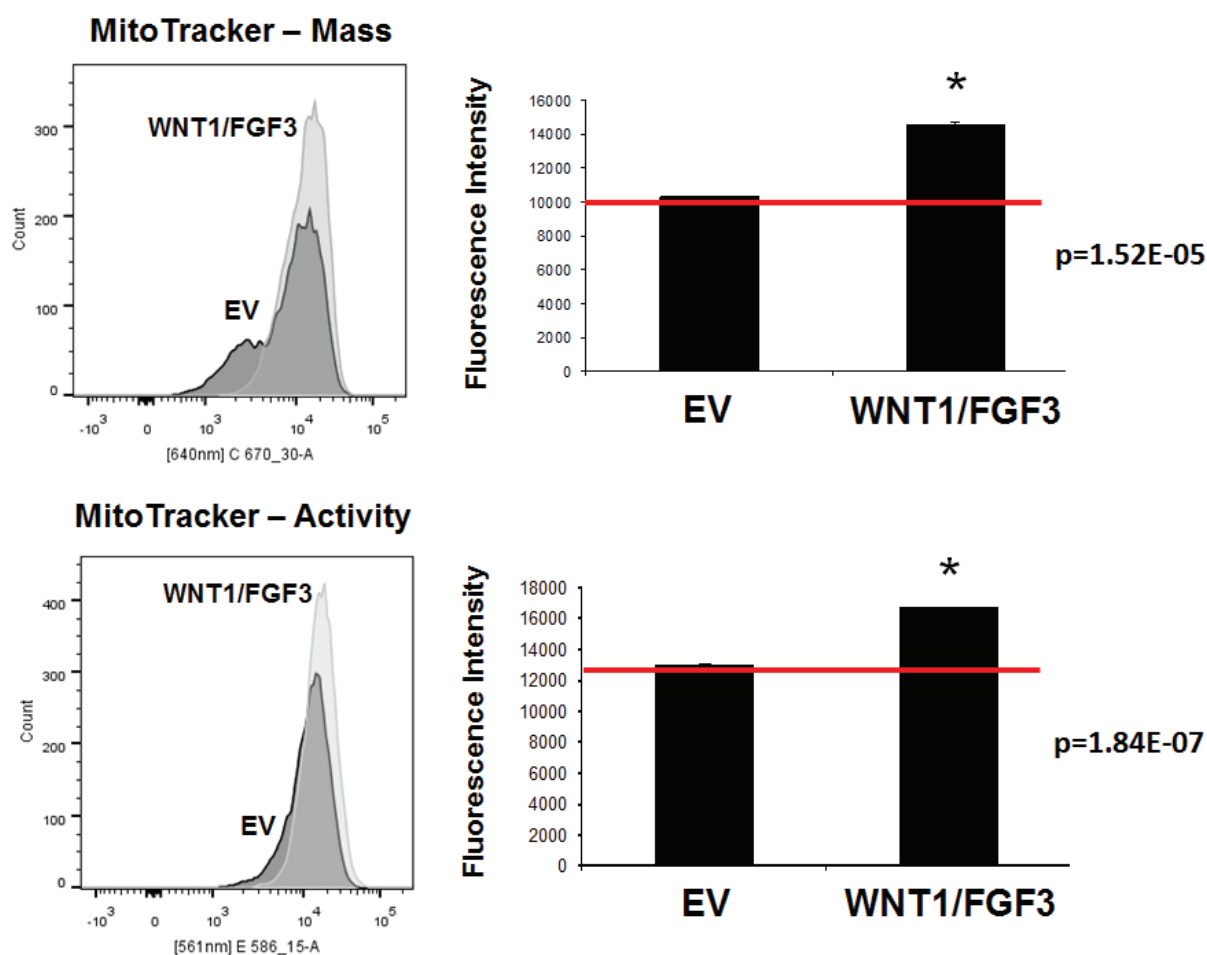


Figure 5: WNT1/FGF3 over-expressing MCF7 cells have increased mitochondrial mass and activity. We used two different fluorescent probes to quantitate mitochondrial mass and mitochondrial membrane potential by FACS analysis. Briefly, we employed MitoTracker Deep-Red (640-nm) to measure mitochondrial mass and MitoTracker Orange (561-nm), as a measure of mitochondrial membrane potential. Note that as compared to EV control MCF7 cells, MCF7 cells overexpressing WNT1/FGF3 show a clear shift to the right, for both mitochondrial mass (Lower panels) and membrane potential (Upper panels). Quantitation of fluorescence intensity (MFI) reveals that both of these mitochondrial parameters are significantly elevated in MCF7-WNT1/FGF3 cells. P-values are as shown. These results suggest that both mitochondrial mass and function may be critical features of the CSC phenotype.

Table 5: WNT1/FGF3 Targets Increased in Human Breast Cancer Cells in Vivo: Mitochondria and Glycolysis.

Symbol	Description	Fold-Change	P-value
Mitochondrial-related Proteins/TCA Cycle (26)			
ATP5O	ATP synthase subunit O, mitochondrial	5.12	2.13E-06
ATP5B	ATP synthase subunit beta, mitochondrial	5.04	2.75E-06
ATP5A1	ATP synthase subunit alpha, mitochondrial	5.01	3.09E-06
COX6A1	Cytochrome c oxidase subunit 6A, mitochondrial	4.46	2.07E-05
ECHS1	Enoyl-CoA hydratase, mitochondrial	4.05	8.22E-05
MDH1	Malate dehydrogenase, cytoplasmic	3.99	9.88E-05
PCK2	Phosphoenolpyruvate carboxykinase [GTP], mitochondrial	3.88	1.43E-04
SCD	Acyl-CoA desaturase	3.70	2.55E-04
HSPA9	Stress-70 protein, mitochondrial	3.69	2.64E-04
NQO1	NAD(P)H dehydrogenase [quinone] 1	3.49	4.81E-04
HSPD1	60 kDa heat shock protein, mitochondrial	3.42	5.93E-04
COX4I1	Cytochrome c oxidase subunit 4 isoform 1, mitochondrial	3.39	6.61E-04
TUFM	Elongation factor Tu, mitochondrial	3.38	6.74E-04
C21orf33	ES1 protein homolog, mitochondrial	3.31	8.40E-04
NDUFS1	Mitochondrial NADH-ubiquinone oxidoreductase 75 kDa subunit	3.20	1.15E-03
IDH1	Isocitrate dehydrogenase [NADP] 1	3.18	1.22E-03
OAT	Ornithine aminotransferase, mitochondrial	3.17	1.25E-03
CS	Citrate synthase, mitochondrial	2.66	5.13E-03
AK2	Adenylate kinase 2, mitochondrial	2.20	1.59E-02
IDH3A	Isocitrate dehydrogenase [NAD] subunit alpha, mitochondrial	2.16	1.78E-02
PRKDC	DNA-dependent protein kinase catalytic subunit (maintains mt-DNA copy number)	2.14	1.85E-02
CLPX	ATP-dependent Clp protease ATP-binding subunit clpX-like, mitochondrial	2.11	1.96E-02
ABAT	4-aminobutyrate aminotransferase, mitochondrial	2.08	2.14E-02
ACO2	Aconitase 2, mitochondrial	1.83	3.64E-02
DUT	Deoxyuridine 5'-triphosphate nucleotidohydrolase, mitochondrial	1.87	3.37E-02
ETFA	Electron transfer flavoprotein subunit alpha, mitochondrial	1.76	4.25E-02
Enzymes Related to Glycolysis, the Pentose Phosphate Pathway, Glycogen, and Amino Acid Synthesis (Serine/Arginine) (4)			
PKM2	Pyruvate kinase	3.26	9.79E-04
PGK1	Phosphoglycerate kinase	2.46	8.66E-03
TKT	Transketolase	2.20	1.60E-02
ENO1	Enolase, alpha	1.96	2.75E-02

-Transcriptional profiling data derived from the analysis of N=28 breast cancer patients are shown, high-lighting the levels of fold-upregulation observed in the epithelial cancer cell compartment (relative to the tumor stroma), and corresponding p-values derived from the analysis of these clinical samples.

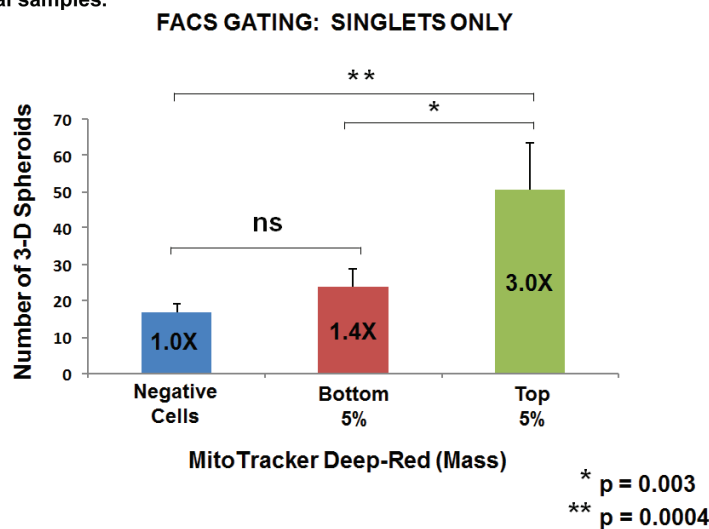


Figure 6: Metabolic fractionation of parental MCF7 cells directly correlates with mammosphere-forming activity: Gating for singlet cells. We metabolically fractionated parental MCF7 cells, using MitoTracker Deep-Red, as a measure of mitochondrial mass. In this context, we chose to analyze three distinct metabolic phenotypic groups: i) negative cells (little or no positive staining; mito-negative group); ii) bottom 5% (mito-low group); and top 5% (mito-high group). Only live cells in each group were selected for this analysis. Five thousand live cells from each group were then seeded per well, in 6-well low attachment plates, to measure mammosphere-forming efficiency. Note that increasing mitochondrial mass results in a 3.0-fold increase in mammosphere-forming activity. Thus, the mito-deficient group showed the least sphere-forming activity, while the mito-high group showed the highest sphere-forming efficiency. Assays were performed in triplicate and repeated three times independently. The mean number of mammospheres (3-D spheroids) formed is shown.

Table 6: WNT1/FGF3 Targets Increased in Human Breast Cancer Cells in Vivo: The EMT and Cell Migration.

Symbol	Description	Fold-Change	P-value
EMT Markers, Extracellular Matrix, Cell Migration and Cytoskeletal proteins (15)			
FLNB	Filamin-B	4.81	6.21E-06
TPT1	Translationally-controlled tumor protein	3.43	5.81E-04
CDC42	Cell division control protein 42 homolog	3.11	1.48E-03
S100A11	Protein S100-A11	2.88	2.81E-03
ANXA2	Annexin A2	2.83	3.28E-03
MYOF	Myoferlin	2.67	5.00E-03
TUBB2A	Tubulin beta-2A chain	2.63	5.56E-03
SEPT2	Septin-2	2.56	6.60E-03
TAGLN2	Transgelin-2	2.42	9.47E-03
IQGAP1	IQ motif containing GTPase activating protein 1 (scaffold protein for CDC42)	2.32	1.19E-02
HMGB1	High mobility group protein B1	2.21	1.57E-02
CAPZB	F-actin-capping protein subunit beta	2.19	1.66E-02
CDV3	Carnitine deficiency-associated gene expressed in cardiac ventricle 3	2.04	2.30E-02
FAM82B	Regulator of microtubule dynamics protein 1	1.97	2.72E-02
MYH10	Myosin, heavy polypeptide 10, non-muscle	1.82	3.69E-02
Miscellaneous (11)			
PON2	Paraoxonase 2, isoform	4.02	9.25E-05
MATR3	Matrin-3	3.45	5.56E-04
SH3BGR1	SH3 domain-binding glutamic acid-rich-like protein	3.12	1.43E-03
AHNAK	Neuroblast differentiation-associated protein, AHNAK	2.57	6.41E-03
CAST	Calpastatin A	2.54	7.08E-03
SEC24A	Protein transport protein Sec24A	2.19	1.65E-02
PABPC4	Polyadenylate-binding protein 4	2.15	1.78E-02
COMT	Soluble catechol-O-methyltransferase	2.10	2.04E-02
STUB1	E3 ubiquitin-protein ligase CHIP	1.95	2.79E-02
TFF1	Trefoil factor 1	1.76	4.17E-02
HUWE1	E3 ubiquitin-protein ligase HUWE1	1.75	4.33E-02

-Transcriptional profiling data derived from the analysis of N=28 breast cancer patients are shown, high-lighting the levels of fold-upregulation observed in the epithelial cancer cell compartment (relative to the tumor stroma), and corresponding p-values derived from the analysis of these clinical samples.

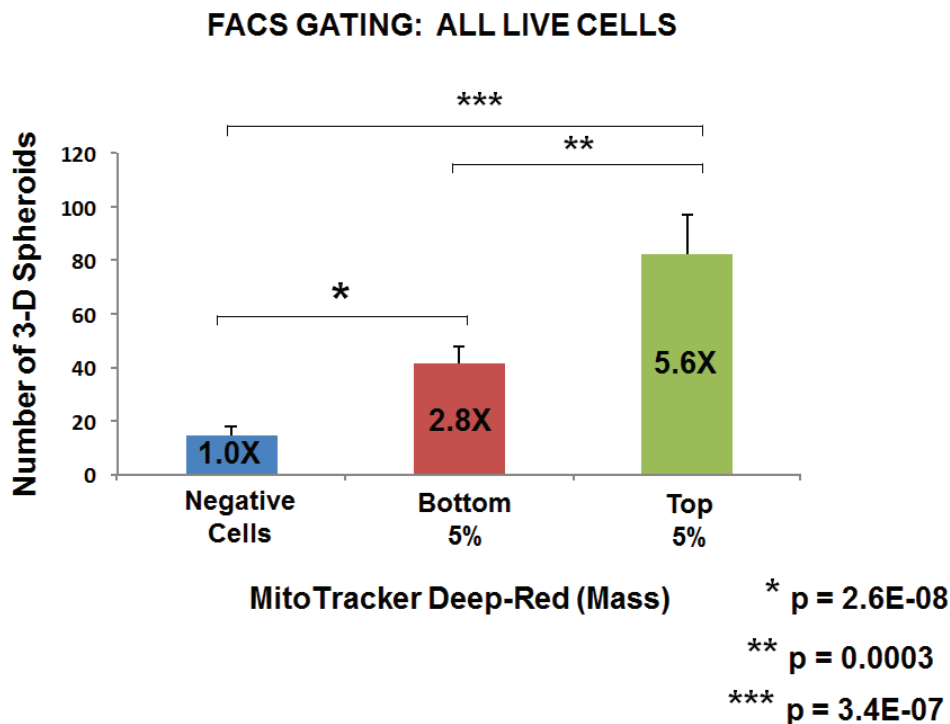


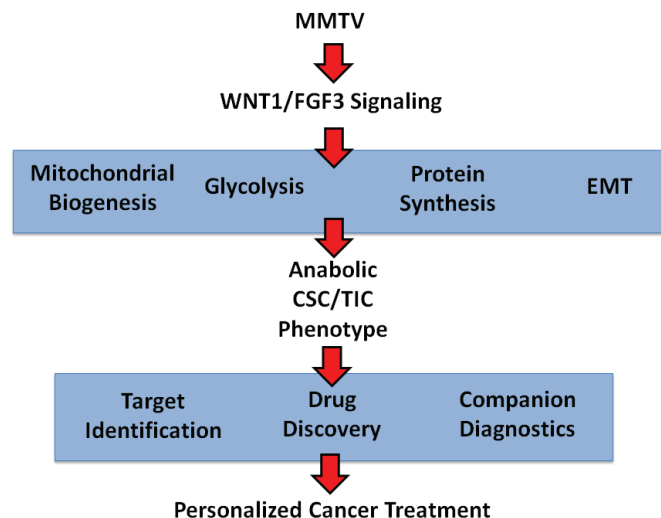
Figure 7: Metabolic fractionation of parental MCF7 cells directly correlates with mammosphere-forming activity: Gating for all live cells. As in Figure 6, except that FACS gating included all live cells, not only live singlets. Under these conditions, note that increasing mitochondrial mass results in a >5.5-fold increase in mammosphere-forming activity. Assays were performed in triplicate and repeated three times independently. The mean number of mammospheres (3-D spheroids) formed is shown.

Table 7: WNT1/FGF3 Targets Increased in Human Breast Cancer Cells in Vivo: Ribosomes and Protein Synthesis.

Symbol	Description	Fold-Change	P-value
Ribosome-related proteins (8)			
SRPRB	Signal recognition particle receptor subunit beta	4.68	9.97E-06
RPL15	60S ribosomal protein L15	4.60	1.28E-05
RPL13	60S ribosomal protein L19	4.48	1.98E-05
RPL13	60S ribosomal protein L13	4.48	1.98E-05
RPL14	60S ribosomal protein L14	4.45	2.15E-05
RPS5	40S ribosomal protein S5	4.41	2.45E-05
RPL4	60S ribosomal protein L4	3.05	1.79E-03
NPM1	NPM1 protein	2.42	9.50E-03
Translation initiation factors (3)			
EIF2S1	Eukaryotic translation initiation factor 2, subunit 1 alpha, 35kDa	3.98	1.04E-04
EIF3D	Eukaryotic translation initiation factor 3 subunit D	2.85	3.13E-03
EIF5B	Eukaryotic translation initiation factor 5B	2.58	6.29E-03
Elongation factors (4)			
EEF1B2	Elongation factor 1-beta	4.08	7.56E-05
EEF1G	Elongation factor 1-gamma	3.71	2.44E-04
TUFM	Elongation factor Tu, mitochondrial	3.38	6.74E-04
EEF1D	Elongation factor 1-delta	2.50	7.67E-03
Enzymes for tRNA synthesis (4)			
C22orf28	tRNA-splicing ligase RtcB homolog	4.59	1.37E-05
EPRS	Bifunctional aminoacyl-tRNA synthetase (Glutamyl-Prolyl-tRNA Synthetase)	4.06	8.10E-05
DARS	Aspartate--tRNA ligase, cytoplasmic	3.43	5.87E-04
WARS	Tryptophan--tRNA ligase, cytoplasmic	2.48	8.17E-03
Protein folding chaperones (heat shock proteins) (11)			
HSP90AB1	Heat shock protein HSP 90-beta	4.94	4.03E-06
PPIA	Peptidyl-prolyl cis-trans isomerase A	4.29	3.74E-05
CANX	Calnexin	3.99	9.88E-05
PDIA6	Protein disulfide-isomerase A6	3.62	3.22E-04
HSPD1	60 kDa heat shock protein, mitochondrial	3.42	5.93E-04
PPIB	Peptidyl-prolyl cis-trans isomerase B	3.28	9.25E-04
HSPH1	Heat shock protein 105 kDa	3.18	1.22E-03
HSPA8	Heat shock cognate 71 kDa protein	3.11	1.49E-03
PDIA3	Protein disulfide-isomerase A3	2.53	7.22E-03
HSP90B1	Endoplasmin	2.43	9.33E-03
PDIA4	Protein disulfide-isomerase A4	2.13	1.89E-02

-Transcriptional profiling data derived from the analysis of N=28 breast cancer patients are shown, high-lighting the levels of fold-upregulation observed in the epithelial cancer cell compartment (relative to the tumor stroma), and corresponding p-values derived from the analysis of these clinical samples.

Figure 8: Anabolic CSC signaling: Exploiting a humanized model of MMTV signaling to identify the characteristics of anabolic CSCs and achieve the goals of personalized medicine. A humanized isogenic model of MMTV-signaling was generated by co-expressing WNT1 and FGF3 in MCF7 cells, an ER(+) human breast cancer cell line. This model was first validated using the mammosphere assay to measure stem cell activity and then subjected to unbiased label-free proteomics analysis. WNT1/FGF3 protein targets identified in this manner were found to be transcriptionally over-expressed in human breast cancer cells *in vivo*, providing clinical validation of the success of our approach. Thus, we established that the anabolic CSC phenotype is characterized by the induction of EMT markers, mitochondrial proteins, glycolytic enzymes and protein synthesis machinery. These represent new classes of identified protein targets for drug discovery and the identification of companion diagnostics, to eradicate anabolic CSCs.



Role of new mitochondrial biogenesis in WNT-signaling and asymmetric cell division in stem cells

Interestingly, two previous studies have also linked WNT signaling to new mitochondrial biogenesis, in the context of skeletal muscle function and osteoblastic differentiation [24, 25]. For example, Yoon et al performed an si-RNA screen to identify novel protein targets that are critical for driving mitochondrial biogenesis in skeletal muscle cells [24]. For this purpose, they screened the effects of si-RNAs on C2C12 cells, representing >6,300 genes, using a high-throughput FACS-based assay to measure mitochondrial function. Overall, they identified >150 proteins not previously recognized to be involved in the regulation of mitochondrial biogenesis. Bioinformatics analysis of this data set identified WNT/ β -catenin signaling as a key regulator of mitochondrial biogenesis. This was functionally validated by using si-RNAs targeting β -catenin and Axin2. Moreover, treatment of C2C12 cells with Wnt3a increased mitochondrial biogenesis by nearly 2-fold, which also directly correlated with a functional increase in oxygen consumption. Expression of a dominant-negative form of TCF4 blocked the effects of Wnt3a on mitochondrial biogenesis, indicating that the canonical Wnt-pathway was responsible for the metabolic effects of Wnt3a. Interestingly, Wnt3a mediated mitochondrial biogenesis also appeared to be dependent

Viral Promoter Insertion and Energy Metabolism

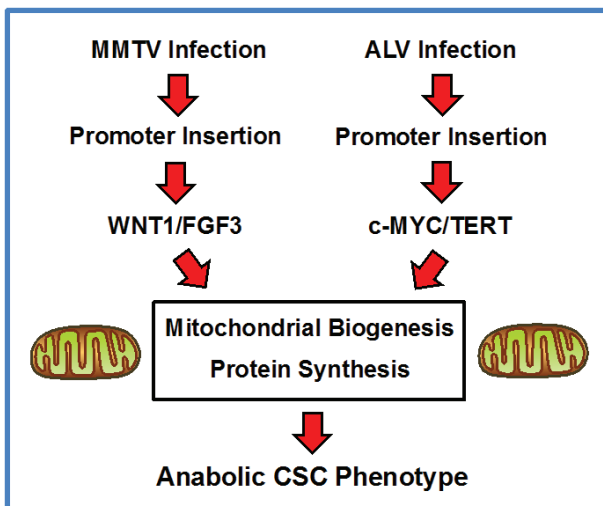


Figure 9: Convergent role of energy metabolism in the pathogenesis of viral oncogenesis, driven by promoter insertion: A new metabolic hypothesis. We propose that MMTV and ALV may induce oncogenesis by a convergent metabolic mechanism, which relies on an anabolic CSC phenotype, characterized by increased mitochondrial biogenesis and augmented protein synthesis. See the Discussion section for further details. ALV, avian leukosis virus; MMTV, mouse mammary tumor virus.

on down-stream effectors, such as IRS-1 and c-MYC [24]. Therefore, the effects of WNT/ β -catenin signaling on mitochondrial biogenesis, may ultimately be mediated by the c-MYC proto-oncogene.

Asymmetric cell division is required for the maintenance of the stem cell phenotype and also occurs in stem-like cancer cells. Recently, Weinberg and Sabatini assessed how mitochondria are apportioned during asymmetric cell division, using an immortalized model of mammary epithelial stem cells [26]. Interestingly, they observed that “newly-synthesized” mitochondria were concentrated in stem cells during asymmetric cell division, while “old” mitochondria were segregated into daughter cells. As such, asymmetric cell division requires new mitochondrial biogenesis, for the propagation the stem cell phenotype. These findings could mechanistically explain our current results, that high-mitochondrial mass (Figures 6 and 7) directly correlates with “stemness” and mammosphere-forming efficiency.

Role of mitochondrial biogenesis in anchorage-independent growth, in transformed fibroblasts and CSCs

In 1984, Klebe and Harriss described the use of a colorimetric tetrazolium dye, namely MTT, to distinguish between normal and transformed fibroblasts, when the two different immortal isogenic cell lines were co-cultured [27]. More specifically, they showed that SV40-transformed BALB/3T3 fibroblasts, which were undergoing anchorage-independent growth (foci-formation), were highly MTT-positive [27]. In contrast, non-transformed quiescent BALB/3T3 cells were MTT-negative, showing little or no staining [27]. As MTT-staining has largely been attributed to mitochondrial oxidative function and redox activity, these results may be the first description of an association between anchorage-independent growth and mitochondrial function.

In accordance with these findings, Fisher et al., 2011 [28] demonstrated that PGC1- α mediated activation of mitochondrial biogenesis is indeed required for the anchorage-independent growth of RAS-transformed fibroblasts. Moreover, recent studies with XCT790, a chemical inhibitor of the ERR- α /PGC1- α signaling network, directly showed that blocking mitochondrial biogenesis is sufficient to effectively prevent the anchorage-independent survival and propagation of epithelial CSCs [29]. Quantitatively similar results were also obtained with azithromycin and doxycycline [29, 31], two well-established antibiotic inhibitors of mitochondrial biogenesis, which target mitochondrial protein translation.

Thus, our current results are also consistent with the idea that mitochondrial power somehow helps to energize anchorage-independent growth, which is a key characteristic of CSCs.

Viral oncogenesis, promoter insertion and energy metabolism

MMTV is known to cause the development of mammary tumors by promoter insertion proximal to cellular proto-oncogenes, that when over-expressed, confer an oncogenic phenotype. This appears to be largely through the constitutive activation of WNT/ β -catenin signaling. Here, we show that this signal transduction process also leads to the activation of mitochondrial biogenesis and an increase in the machinery necessary for protein synthesis, which is characteristic of an anabolic CSC phenotype. Previous studies have also shown that the ability of WNT/ β -catenin signaling to increase mitochondrial biogenesis is dependent on c-MYC activation, but in the context of skeletal muscle cells [24]. In further support of these ideas, MMTV Int-6 is eukaryotic translation initiation factor 3 (eIF3), which serves as a scaffolding protein to increase protein synthesis (Table 1).

Avian leukosis virus (ALV) is another pathogen that induces cancer, via a promoter insertion-based mechanism [32, 33]. More specifically, ALV infection leads to proviral integration and promoter insertion, driving the development of myeloid leukemia and, ultimately, frank leukemia in chickens. Interestingly, the most common ALV integration sites include c-MYC and hTERT, as well as other gene products related to mitochondrial biogenesis and function (NDUFS6 and PARK2) [34].

Taken together, these data imply that MMTV and ALV may induce oncogenesis by a convergent metabolic mechanism, which relies on the down-stream activation of c-MYC, driving increased mitochondrial biogenesis. Interestingly, c-MYC is also known to increase protein synthesis, by targeting translation initiation, as well as by directly increasing ribosomal biogenesis [35, 36]. As such, MMTV and ALV may both ultimately induce the anabolic CSC phenotype, via increased mitochondrial biogenesis and increased protein synthesis (Figure 9). In further support of this idea, hTERT over-expression also appears to be directly associated with an anabolic CSC phenotype, driving increased mitochondrial biogenesis and augmented protein synthesis [37]. Thus, this intriguing hypothesis, regarding the existence of a convergent metabolic mechanism, underlying MMTV and ALV oncogenesis, undoubtedly deserves further study.

Mitochondrial DNA content and mitochondrial mass both increase during the transition from normal tissue to hyperplasia and malignancy

Interestingly, previous studies in human endometrial cancer have monitored i) mt-DNA content (by RT-PCR) and ii) mitochondrial mass (using the enzyme activity of citrate synthase), during the transition to malignancy. More

specifically, they observed that both of these parameters increased by up to 2 to 3 fold, when normal endometrial tissue was directly compared to endometrial cancer [38]. Similarly, they also observed that the protein expression levels of three mitochondrial-related transcription factors (TFAM, NRF1 and PGC1-alpha) were all significantly increased by nearly 2-fold [39]. Taken together, these results are all consistent with an increase in mitochondrial biogenesis, during the pathogenesis of tumor initiation.

Similarly, we have previously shown that markers of mitochondrial mass and mitochondrial activity are specifically localized to the basal stem cell layer in normal human mucosa, which co-localizes with Ki67, an established marker of cell proliferation [40]. In addition, this mitochondria-rich population of cells is dramatically expanded in head and neck cancers [40] and breast cancers [41-43]. Moreover, recombinant over-expression of mitochondrial-related proteins, such as PGC1-alpha/beta, POLRMT, MitoNEET or GOLPH3, is sufficient to promote tumor growth, by up to 3-fold, in xenografted pre-clinical models of human breast cancers [44, 45]. Finally, mitochondrial biogenesis and mass are also significantly increased in hematological malignancies, such as in chronic lymphocytic leukemia (CLL) and acute myeloid leukemia (AML) [46-49].

This increase in mitochondrial mass also appears to be part of a normal developmental process, as mitochondrial biogenesis increases between 25 to 50 fold, during mammalian embryogenesis, especially from the two-cell stage to the early blastocyst [50]. This early stage of embryogenesis reflects the proliferative expansion normal progenitor cells. Interestingly, pluripotent ES cell lines are derived from the inner cell mass of the blastocyst.

CONCLUSIONS

In summary, the use of mitochondrial mass as a surrogate metabolic biomarker of mitochondrial biogenesis allows for the identification of stem-like cancer cells, facilitating CSC enrichment for future biomarker studies and aiding in the design of novel therapeutic interventions. In this context, MCF7 cells over-expressing WNT1/FGF3 will provide a novel model system for these ongoing investigations.

MATERIALS AND METHODS

Materials

Breast cancer cell lines (MCF7 and T47D) were originally purchased from the ATCC. Gibco-brand cell culture media (DMEM and DMEM/F12) was purchased from Life Technologies. Lentiviral vectors encoding WNT1 [EX-B0110-Lv105(puro)] and FGF3 [EX-

A0154-Lv151(neo)] were obtained commercially from Genecopoeia (USA), along with appropriate empty vector controls [EX-Neg-Lv105(puro) and EX-Neg-Lv151(neo)]. Antibodies directed against FGF3 (# HPA012692, Sigma) and WNT1 (# ab15251, Abcam) were also obtained commercially. MitoTracker probes (Deep-Red and Orange) were purchased from Molecular Probes, via Life Technologies.

MCF7 cell viral transduction and antibiotic selection

Lentiviral particles harboring human WNT1 [EX-B0110-Lv105(puro)] or human FGF3 [EX-A0154-Lv151(neo)] were prepared and used to stably transduce MCF7 cells, according to the manufacturer's protocol. After 24 hours, media containing the virus was removed and replaced with standard media. Cells were then selected with puromycin (2 µg/ml) or G418 (2 mg/ml), for up to 10 days. MCF7 cells harboring the empty vector alone controls were generated at the same time in parallel. MCF7-WNT1/FGF3 cells were generated by serial transduction with both WNT1 and FGF3 lentiviral vectors.

WNT1 and FGF3 immunoblotting

Transduced MCF7 cells were seeded in 10 cm dishes for 72 hrs. Then, cells were lysed in RIPA buffer (Sigma), containing proteinase inhibitors (Roche) and kept at 4°C for 30 minutes. Lysates were collected by centrifugation for 10 minutes at 10,000 x g, and protein concentration were determined using the BCA protein assay kit (Pierce). Samples were diluted into SDS-PAGE sample buffer and were boiled for 5 minutes before being separated by SDS-PAGE, using a 4-15% gradient Mini-PROTEAN TGX Gel (Biorad). Samples were then transferred onto a nitrocellulose membrane (Biorad), blocked in 5% milk in TBS-Tween 20 (Sigma) and probed with antibodies directed against WNT1 or FGF3 and β-actin (Santa Cruz Biotechnology, #sc-1616), using a secondary antibody at a dilution of 1 to 5000. Bound antibodies were detected using the Supersignal West Pico Chemiluminiscent substrate (ThermoScientific). Alternatively, in the laboratory, blots were also routinely processed with a blocking solution containing BSA, as a blocking agent. Similarly, other comparable antibodies directed against β-actin were used, but were obtained from different commercial sources, such as Sigma.

Assessment of mammosphere forming activity

Mammosphere formation was carried out, essentially as described previously by Clarke and colleagues, without any significant modifications [51]. MCF7 cells were plated

at a density of 500 cells/cm² in mammosphere medium in culture dishes coated with poly-HEMA (Sigma, #P3932). After 5 days, 3D spheroids with a diameter greater than 50 µm were counted using a microscope, fitted with a graticule eye-piece, and the percentage of cells which formed spheroids was calculated and normalized to one (1 = 100 % MSE; mammosphere forming efficiency). Mammosphere assays were performed in triplicate and repeated three times independently.

Conditioned media experiments

One million MCF7 cells transfected with WNT1/FGF3 or empty vector alone controls were plated for 24 hours in DMEM (10% FCS). Cells were then washed in PBS, the subsequently cultured for 72 hours in 10 ml of DMEM/F12 phenol-red free media (mammosphere media). Media was then collected and cells were removed by centrifugation at 1800 rpm for 10 minutes. Conditioned media was then added directly to mammosphere assays of parental untransfected breast cancer cell lines (MCF7 and T47D) in a ratio of 1:1 with fresh mammosphere formation media.

Unbiased label-free proteomics analysis

Proteomics analysis was carried out essentially as we previously described, with minor modifications [52, 53]. Statistical analyses were performed using ANOVA and only fold-changes in proteins with a p-value less than 0.05 were considered significant. Unbiased proteomics and the statistical analysis of the results were performed by the Biological Mass Spectrometry Core Facility, at the Cancer Research UK Manchester Institute, under the supervision of Dr. Duncan L. Smith.

Bioinformatics analysis with publically available human breast cancer clinical data

To determine the possible translational significance of our proteomics analysis, we intersected our MCF7-based WNT/FGF proteomics data with human genome-wide transcriptional profiling data. These human clinical data were derived from publically available human breast cancer samples, in which breast cancer cells were separated by laser-capture microdissection from tumor stromal cells. Transcriptional profiles were analyzed from N=28 human breast cancer patients [54].

Analysis of mitochondrial mass and membrane potential

To measure mitochondrial activity, cells were stained with MitoTracker Orange (#M7510, Invitrogen),

whose accumulation in mitochondria is dependent upon membrane potential. To measure mitochondrial mass, cells were stained with MitoTracker Deep Red (#M22426, Invitrogen), localizing to mitochondria regardless of mitochondrial membrane potential. Cells were incubated with pre-warmed MitoTracker staining solution (diluted in PBS/CM to a final concentration of 10 nM) for 30-60 min at 37 °C. All subsequent steps were performed in the dark. Cells were washed in PBS, harvested, and re-suspended in 300 µL of PBS. Cells were then analyzed by flow cytometry. Data analysis was performed using FlowJo software.

Metabolic fractionation of parental MCF7 cells using MitoTracker

Using MitoTracker Deep-Red staining as a marker of mitochondrial mass, we metabolically fractionated parental MCF7 cells, using FACS analysis and cell collection. In these experiments, we analyzed three different metabolic sub-groups: i) negative cells (little or no positive staining; mito-negative group); ii) bottom 5% (mito-low group); and top 5% (mito-high group). Only live cells in each group were selected for this analysis. Five thousand live cells from each group (performed in triplicate) were then seeded per well, in 6-well low attachment plates, to measure mammosphere-forming efficiency. Gating for cell size was varied to take into account the observation that stem-like mammary cells may be physically larger than “bulk” cancer cells, as was previously suggested.

This method is a further refinement of a protocol used by Farnie, Sotgia and Lisanti, in a companion study published in parallel [55]. Importantly, very similar results were obtained here, indicating that the method is operator independent. For example, see Figure 4 (Panel A) in Farnie et al., 2015, for comparison purposes [55]; however, in this companion paper, the mito-negative group was not analyzed.

Statistical analyses

Statistical significance was determined using the Student's t-test or ANOVA, where appropriate. Values of less than 0.05 were considered significant. Data in figures are shown as the mean ± SEM, unless stated otherwise.

ACKNOWLEDGEMENTS

We thank the University of Manchester for providing start-up funds that contributed to the success of this study. The Sotgia and Lisanti Laboratories were supported, in part, by funding from the European Union (ERC Advanced Grant), Breast Cancer Now, and the Manchester Cancer Research Centre (MCRC). DLS

was core-funded by CRUK. Dr. Ubaldo E. Martinez-Outschoorn was supported by the National Cancer Institute (NCI) of the National Institutes of Health (NIH), under Award Number K08-CA175193-01A1. Drs. Bevilacqua, Mazzanti and McDonnell were supported by the Pisa Science Foundation.

CONFLICTS OF INTEREST

There is no conflict of interest.

Author Contributions

MPL initiated and coordinated this internationally collaborative project (UK, US and Italy). RL, MC, LW, DLS and GB performed all the experiments, analyzed the data and generated the figures with experimental data. MPL and FS wrote the first draft of the manuscript, which was extensively edited by the other authors, who also contributed ideas and suggestions for the discussion topics. RL also contributed heavily to the writing of the Material and Methods section and the figure legends. MPL generated the schematic summary diagrams. Unbiased proteomics and the statistical analysis of the proteomic results were performed by the Biological Mass Spectrometry Core Facility, at the Cancer Research UK Manchester Institute, under the supervision of DLS.

Abbreviations

CSCs, cancer stem-like cells; MMTV, mouse mammary tumor virus; TICs, tumor-initiating cells; EMT, epithelial-mesenchymal transition; ALV, avian leukosis virus; MTT, 3-(4,5-dimethylthiazol-2-yl)-2,5-diphenyltetrazolium bromide

REFERENCES

1. Kilham L. Isolation in suckling mice of a virus from C3H mice harboring Bittner milk agent. *Science*. 1952; 116:391-392.
2. Moore R, Dixon M, Smith R, Peters G and Dickson C. Complete nucleotide sequence of a milk-transmitted mouse mammary tumor virus: two frameshift suppression events are required for translation of gag and pol. *Journal of virology*. 1987; 61:480-490.
3. Cohen JC. Methylation of milk-borne and genetically transmitted mouse mammary tumor proviral DNA. *Cell*. 1980; 19:653-662.
4. Cohen JC and Varmus HE. Proviruses of mouse mammary tumor virus in normal and neoplastic tissues from GR and C3Hf mouse strains. *Journal of virology*. 1980; 35:298-305.
5. Mazzanti CM, Lessi F, Armogida I, Zavaglia K, Franceschi S, Hamad MA, Roncella M, Ghilli M, Boldrini A,

- Aretini P, Fanelli G, Marchetti I, Scatena C, Hochman J, Naccarato AG and Bevilacqua G. Human saliva as route of inter-human infection for mouse mammary tumor virus. *Oncotarget*. 2015; 6: 18355-18363.
6. Mazzanti CM, Al Hamad M, Fanelli G, Scatena C, Zammarchi F, Zavaglia K, Lessi F, Pistello M, Naccarato AG and Bevilacqua G. A mouse mammary tumor virus env-like exogenous sequence is strictly related to progression of human sporadic breast carcinoma. *The American journal of pathology*. 2011; 179:2083-2090.
 7. Nusse R, Theunissen H, Wagenaar E, Rijsewijk F, Gennissen A, Otte A, Schuurin E and van Ooyen A. The Wnt-1 (int-1) oncogene promoter and its mechanism of activation by insertion of proviral DNA of the mouse mammary tumor virus. *Molecular and cellular biology*. 1990; 10:4170-4179.
 8. Nusse R, van Ooyen A, Cox D, Fung YK and Varmus H. Mode of proviral activation of a putative mammary oncogene (int-1) on mouse chromosome 15. *Nature*. 1984; 307:131-136.
 9. van Ooyen A and Nusse R. Structure and nucleotide sequence of the putative mammary oncogene int-1; proviral insertions leave the protein-encoding domain intact. *Cell*. 1984; 39:233-240.
 10. Dickson C, Smith R, Brookes S and Peters G. Tumorigenesis by mouse mammary tumor virus: proviral activation of a cellular gene in the common integration region int-2. *Cell*. 1984; 37:529-536.
 11. Li Y, Hively WP and Varmus HE. Use of MMTV-Wnt-1 transgenic mice for studying the genetic basis of breast cancer. *Oncogene*. 2000; 19:1002-1009.
 12. Peters G, Brookes S, Smith R, Placzek M and Dickson C. The mouse homolog of the hst/k-FGF gene is adjacent to int-2 and is activated by proviral insertion in some virally induced mammary tumors. *Proceedings of the National Academy of Sciences of the United States of America*. 1989; 86:5678-5682.
 13. Kwan H, Pecanka V, Tsukamoto A, Parslow TG, Guzman R, Lin TP, Muller WJ, Lee FS, Leder P and Varmus HE. Transgenes expressing the Wnt-1 and int-2 proto-oncogenes cooperate during mammary carcinogenesis in doubly transgenic mice. *Molecular and cellular biology*. 1992; 12:147-154.
 14. Klaus A and Birchmeier W. Wnt signalling and its impact on development and cancer. *Nature reviews Cancer*. 2008; 8:387-398.
 15. Cadigan KM and Nusse R. Wnt signaling: a common theme in animal development. *Genes & development*. 1997; 11:3286-3305.
 16. Hatch EP, Noyes CA, Wang X, Wright TJ and Mansour SL. Fgf3 is required for dorsal patterning and morphogenesis of the inner ear epithelium. *Development*. 2007; 134:3615-3625.
 17. Katoh M and Katoh M. Cross-talk of WNT and FGF signaling pathways at GSK3beta to regulate beta-catenin and SNAIL signaling cascades. *Cancer biology & therapy*. 2006; 5:1059-1064.
 18. Katoh Y and Katoh M. FGF signaling inhibitor, SPRY4, is evolutionarily conserved target of WNT signaling pathway in progenitor cells. *International journal of molecular medicine*. 2006; 17:529-532.
 19. Ross SR. Mouse mammary tumor virus molecular biology and oncogenesis. *Viruses*. 2010; 2:2000-2012.
 20. Callahan R and Smith GH. Common integration sites for MMTV in viral induced mouse mammary tumors. *Journal of mammary gland biology and neoplasia*. 2008; 13:309-321.
 21. Callahan R and Smith GH. MMTV-induced mammary tumorigenesis: gene discovery, progression to malignancy and cellular pathways. *Oncogene*. 2000; 19:992-1001.
 22. Cho RW, Wang X, Diehn M, Shedden K, Chen GY, Sherlock G, Gurney A, Lewicki J and Clarke MF. Isolation and molecular characterization of cancer stem cells in MMTV-Wnt-1 murine breast tumors. *Stem cells*. 2008; 26:364-371.
 23. Mani SA, Guo W, Liao MJ, Eaton EN, Ayyanan A, Zhou AY, Brooks M, Reinhard F, Zhang CC, Shipitsin M, Campbell LL, Polyak K, Brisken C, Yang J and Weinberg RA. The epithelial-mesenchymal transition generates cells with properties of stem cells. *Cell*. 2008; 133:704-715.
 24. Yoon JC, Ng A, Kim BH, Bianco A, Xavier RJ and Elledge SJ. Wnt signaling regulates mitochondrial physiology and insulin sensitivity. *Genes & development*. 2010; 24:1507-1518.
 25. An JH, Yang JY, Ahn BY, Cho SW, Jung JY, Cho HY, Cho YM, Kim SW, Park KS, Kim SY, Lee HK and Shin CS. Enhanced mitochondrial biogenesis contributes to Wnt induced osteoblastic differentiation of C3H10T1/2 cells. *Bone*. 2010; 47:140-150.
 26. Katajisto P, Dohla J, Chaffer CL, Pentimikko N, Marjanovic N, Iqbal S, Zoncu R, Chen W, Weinberg RA and Sabatini DM. Stem cells. Asymmetric apportioning of aged mitochondria between daughter cells is required for stemness. *Science*. 2015; 348:340-343.
 27. Klebe RJ and Harriss JV. A technically simple "non-lethal" vital staining procedure for viral plaque and cell transformation assays. *Arch Virol*. 1984; 81:359-62.
 28. Fisher KW, Das B, Kortum RL, Chaika OV and Lewis RE. Kinase suppressor of ras 1 (KSR1) regulates PGC1 α and estrogen-related receptor α to promote oncogenic Ras-dependent anchorage-independent growth. *Mol Cell Biol*. 2011; 31:2453-61.
 29. De Luca A, Fiorillo M, Peiris-Pagès M, Ozsvári B, Smith DL, Sanchez-Alvarez R, Martínez-Outschoorn UE, Cappello AR, Pezzi V, Lisanti MP and Sotgia F. Mitochondrial biogenesis is required for the anchorage-independent survival and propagation of stem-like cancer cells. *Oncotarget*. 2015; 6:14777-95.

30. Lamb R, Fiorillo M, Chadwick A, Ozsvári B, Reeves KJ, Smith DL, Clarke RB, Howell SJ, Cappello AR, Martínez-Outschoorn UE, Peiris-Pagès M, Sotgia F and Lisanti MP. Doxycycline down-regulates DNA-PK and radiosensitizes tumor initiating cells: Implications for more effective radiation therapy. *Oncotarget*. 2015; 6:14005-25.
31. Lamb R, Ozsvári B, Lisanti CL, Tanowitz HB, Howell A, Martínez-Outschoorn UE, Sotgia F and Lisanti MP. Antibiotics that target mitochondria effectively eradicate cancer stem cells, across multiple tumor types: treating cancer like an infectious disease. *Oncotarget*. 2015; 6:4569-84.
32. Neel BG, Hayward WS, Robinson HL, Fang J and Astrin SM. Avian leukosis virus-induced tumors have common proviral integration sites and synthesize discrete new RNAs: oncogenesis by promoter insertion. *Cell*. 1981; 23:323-34.
33. Hayward WS, Neel BG and Astrin SM. Activation of a cellular onc gene by promoter insertion in ALV-induced lymphoid leukosis. *Nature*. 1981; 290: 475-80.
34. Li Y1, Liu X, Yang Z, Xu C, Liu D, Qin J, Dai M, Hao J, Feng M, Huang X, Tan L, Cao W and Liao M. The MYC, TERT, and ZIC1 genes are common targets of viral integration and transcriptional deregulation in avian leukosis virus subgroup J-induced myeloid leukosis. *J Virol*. 2014; 88:3182-91.
35. Meyer N and Penn LZ. Reflecting on 25 years with MYC. *Nat Rev Cancer*. 2008; 8: 976-90.
36. Schmidt EV. The role of c-myc in regulation of translation initiation. *Oncogene*. 2004; 23:3217-21.
37. Lamb R, Ozsvári B, Bonuccelli G, Smith DL, Pestell RG, Martínez-Outschoorn UE, Clarke RB, Sotgia F, and Lisanti MP. Dissecting tumor metabolic heterogeneity: Telomerase and large cell size metabolically define a sub-population of stem-like, mitochondrial-rich, cancer cells. *Oncotarget*, 2015; 6:21892-905. doi: 10.18632/oncotarget.5260.
38. Cormio A, Guerra F, Cormio G, Pesce V, Fracasso F, Loizzi V, Resta L, Putignano G, Cantatore P, Selvaggi LE, Gadaleta MN. Mitochondrial DNA content and mass increase in progression from normal to hyperplastic to cancer endometrium. *BMC Res Notes*. 2012; 5:279.
39. Cormio A, Guerra F, Cormio G, Pesce V, Fracasso F, Loizzi V, Cantatore P, Selvaggi L, Gadaleta MN. The PGC-1alpha-dependent pathway of mitochondrial biogenesis is upregulated in type I endometrial cancer. *Biochem Biophys Res Commun*. 2009; 390:1182-5.
40. Curry JM, Tuluc M, Whitaker-Menezes D, Ames JA, Anantharaman A, Butera A, Leiby B, Cognetti DM, Sotgia F, Lisanti MP and Martínez-Outschoorn UE. Cancer metabolism, stemness and tumor recurrence: MCT1 and MCT4 are functional biomarkers of metabolic symbiosis in head and neck cancer. *Cell Cycle*; 12: 1371-84.
41. Whitaker-Menezes D1, Martínez-Outschoorn UE, Flomenberg N, Birbe RC, Witkiewicz AK, Howell A, Pavlides S, Tsirigos A, Ertel A, Pestell RG, Broda P, Minetti C, Lisanti MP and Sotgia F. Hyperactivation of oxidative mitochondrial metabolism in epithelial cancer cells in situ: Visualizing the therapeutic effects of metformin in tumor tissue. *Cell Cycle*. 2011; 10: 4047-64.
42. Sotgia F, Whitaker-Menezes D, Martínez-Outschoorn UE, Flomenberg N, Birbe RC, Witkiewicz AK, Howell A, Philp NJ, Pestell RG and Lisanti MP. Mitochondrial metabolism in cancer metastasis: Visualizing tumor cell mitochondria and the “reverse Warburg effect” in positive lymph node tissue. *Cell Cycle*. 2012; 11:1445-54.
43. Ertel A, Tsirigos A, Whitaker-Menezes D, Birbe RC, Pavlides S, Martínez-Outschoorn UE, Pestell RG, Howell A, Sotgia F and Lisanti MP. Is cancer a metabolic rebellion against host aging? In the quest for immortality, tumor cells try to save themselves by boosting mitochondrial metabolism. *Cell Cycle*. 2012; 11:253-63.
44. Salem AF, Whitaker-Menezes D, Howell A, Sotgia F and Lisanti MP. Mitochondrial biogenesis in epithelial cancer cells promotes breast cancer tumor growth and confers autophagy resistance. *Cell Cycle*. 2012; 11:4174-80.
45. Salem AF, Whitaker-Menezes D, Lin Z, Martínez-Outschoorn UE, Tanowitz HB, Al-Zoubi MS, Howell A, Pestell RG, Sotgia F and Lisanti MP. Two-compartment tumor metabolism: autophagy in the tumor microenvironment and oxidative mitochondrial metabolism (OXPHOS) in cancer cells. *Cell Cycle*. 2012;11:2545-56.
46. Jitschin R, Hofmann AD, Bruns H, Giessl A, Bricks J, Berger J, Saul D, Eckart MJ, Mackensen A, Mougiakakos D. Mitochondrial metabolism contributes to oxidative stress and reveals therapeutic targets in chronic lymphocytic leukemia. *Blood*. 2014; 123: 2663-72.
47. Jia L, Gribben JG. Dangerous power: mitochondria in CLL cells. *Blood*. 2014 ;123:2596-7.
48. Carew JS, Nawrocki ST, Xu RH, Dunner K, McConkey DJ, Wierda WG, Keating MJ, Huang P. Increased mitochondrial biogenesis in primary leukemia cells: the role of endogenous nitric oxide and impact on sensitivity to fludarabine. *Leukemia*. 2004; 18:1934-40.
49. Schimmer AD, Skrtić M. Therapeutic potential of mitochondrial translation inhibition for treatment of acute myeloid leukemia. *Expert Rev Hematol*. 2012; 5: 117-9.
50. Pikó L and Taylor KD. Amounts of mitochondrial DNA and abundance of some mitochondrial gene transcripts in early mouse embryos. *Dev Biol*. 1987;123:364-74.
51. Shaw FL, Harrison H, Spence K, Ablett MP, Simoes BM, Farnie G and Clarke RB. A detailed mammosphere assay protocol for the quantification of breast stem cell activity. *Journal of mammary gland biology and neoplasia*. 2012; 17:111-117.
52. Holland M, Castro FV, Alexander S, Smith D, Liu J, Walker M, Bitton D, Mulryan K, Ashton G, Blaylock M, Bagley S, Connolly Y, Bridgeman J, Miller C, Krishnan S, Dempsey C, et al. RAC2, AEP, and ICAM1 expression are associated with CNS disease in a mouse model of pre-B childhood

acute lymphoblastic leukemia. *Blood*. 2011; 118:638-649.

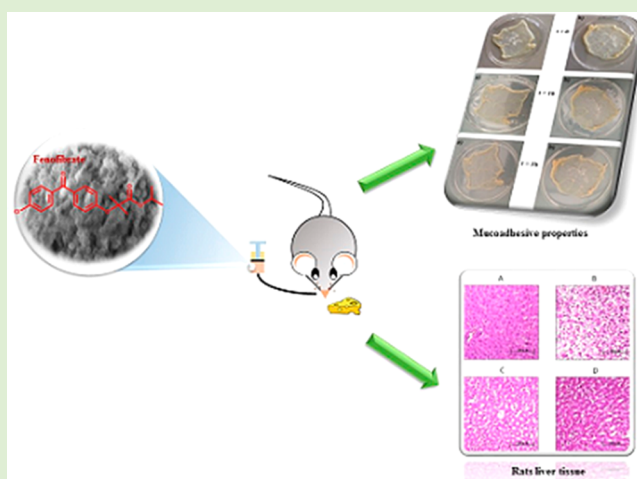
53. Lamb R, Harrison H, Hulit J, Smith DL, Lisanti MP, Sotgia F. Mitochondria as new therapeutic targets for eradicating cancer stem cells: Quantitative proteomics and functional validation via MCT1/2 inhibition. *Oncotarget*. 2014; 5:11029-37.
54. Casey T, Bond J, Tighe S, Hunter T, Lintault L, Patel O, Eneman J, Crocker A, White J, Tessitore J, Stanley M, Harlow S, Weaver D, Muss H and Plaut K. Molecular signatures suggest a major role for stromal cells in development of invasive breast cancer. *Breast cancer research and treatment*. 2009; 114:47-62.
55. Farnie G, Sotgia F and Lisanti MP. High mitochondrial mass identifies a sub-population of stem-like cancer cells that are chemo-resistant. *Oncotarget* 2015 Sep 30. doi: 10.18632/oncotarget.5401.

Sericin/Poly(ethylcyanoacrylate) Nanospheres by Interfacial Polymerization for Enhanced Bioefficacy of Fenofibrate: In Vitro and In Vivo Studies

Ortensia I. Parisi,^{†,‡,§} Marco Fiorillo,^{†,‡} Luca Scrivano,[‡] Maria S. Sinicropi,[‡] Vincenza Dolce,[‡] Domenico Iacopetta,[‡] Francesco Puoci,^{*,‡,||} and Anna R. Cappello^{*,‡,||}

[†]Department of Pharmacy, Health and Nutritional Sciences, and [§]Department of Informatics, Modeling, Electronics and Systems Engineering, University of Calabria, 87036 Rende (CS), Italy

ABSTRACT: Fenofibrate is a lipophilic drug used in hypercholesterolemia and hypertriglyceridemia as a lipid-regulating agent; however, it is characterized by poor water solubility and low dissolution rate, which result in a low oral bioavailability. In the present study, sericin/poly(ethylcyanoacrylate) nanospheres are synthesized by interfacial polymerization in aqueous media and investigated as a novel sericin-based delivery system for improved and enhanced oral bioefficacy of fenofibrate. The incorporation of sericin into the prepared cyanoacrylate nanoparticles and their spherical shape are confirmed by Lowry assay and scanning electron microscopy, respectively. Hydrophilic and mucoadhesive properties of the synthesized nanospheres are also evaluated. Finally, both in vitro release and in vivo studies are performed and the oral absorbable amount of fenofibrate is calculated to be higher than 70% when incorporated into the polymeric material, reducing the levels of total cholesterol (TC), triacylglycerols (TG), very low-density lipoproteins (VLDL), and low-density lipoproteins (LDL) compared to fenofibrate alone.



INTRODUCTION

Oral administration, which allows the release therapeutic agents into the gastrointestinal tract, represents the most common and convenient route for drugs administration due to its ease, safety, and cheapness. This way, by which most drugs are given, results in enhanced patient compliance; however, a large number of therapeutics are poorly soluble in water leading to a limited oral bioavailability because of their low dissolution rate and low absorption.¹

Researchers have explored different strategies in the aim to develop novel delivery systems able to improve oral bioavailability by enhancing drug solubility or increasing the surface area available for dissolution and,² among polymeric materials, the use of poly(alkylcyanoacrylate) nanoparticles as carriers for drug controlled release is attracting significant interest. This kind of material, indeed, is able to modify the body distribution of incorporated therapeutic agents,³ protect them against enzymatic degradation,⁴ and reduce the toxic effects.⁵ The coupling of poly(alkylcyanoacrylates) with mucoadhesive proteins, such as sericin, could be a promising approach to obtain an innovative drug device able to overcome the drawbacks associated with the low water solubility.

Sericin (SER) is a component of silk protein and contains 18 amino acids, including mainly glycine, serine, and aspartic acid. Among them, most are characterized by the presence of strong

polar side groups, such as hydroxyl, carboxyl, amine,⁶ and serine, having an aliphatic alcohol moiety, occupied 33 mol % of the protein structure.⁷ This natural polymer presents several interesting properties, including aqueous-based purification, water solubility, antibacterial activity, UV and oxidation resistance,⁸ mucoadhesion, biocompatibility, and biodegradability.⁹ All these features contribute to make sericin a very attractive biomaterial in drug delivery formulation. SER, indeed, could impart mucoadhesive properties to poly(alkylcyanoacrylate) nanospheres reaching a suitable balance between the lipophilicity of cyanoacrylate nanoparticles, obtaining a stable drug/carrier association, and mucoadhesion capacity, which allows the particles to be retained for a longer period of time in the gastrointestinal tract, resulting in an improved drug adsorption.

In the present study, sericin/poly(ethylcyanoacrylate) nanospheres were prepared by interfacial polymerization in aqueous media in order to improve the gastrointestinal absorbable amount of the poorly water-soluble fenofibrate and enhance its bioefficacy.

Received: June 3, 2015

Revised: September 2, 2015

Published: September 8, 2015

Fenofibrate (FF) is a lipophilic drug used in hypercholesterolemia and hypertriglyceridemia as a lipid-regulating agent. This compound is able to decrease low-density lipoprotein (LDL) and very-low-density lipoprotein (VLDL) levels and increase high-density lipoprotein (HDL) level. In addition, it increases the LDL clearance and reduces small and dense LDL through the modulation of the synthesis and catabolism of VLDL fractions in patients at risk for coronary heart disease.^{10,11} However, fenofibrate is characterized by poor water solubility and low dissolution rate, which result in a low oral bioavailability.¹² Therefore, the synthesized sericin/poly(ethylcyanoacrylate) nanospheres were employed as delivery system in the aim to improve the amount of the considered therapeutic agent reaching the gastrointestinal mucosa, leading to an enhanced bioefficacy.

■ EXPERIMENTAL SECTION

Materials. Ethyl 2-cyanoacrylate (ECA), sericin *Bombyx mori* (SER, silkworm), hydrochloric acid (HCl), sodium hydroxide (NaOH), disodium hydrogen phosphate (Na_2HPO_4), sodium dihydrogen phosphate (NaH_2PO_4), phosphoric acid (H_3PO_4), pepsin from porcine gastric mucosa, sodium cholate, α -amylase from porcine pancreas type VI-B, esterase from porcine liver, sodium bicarbonate (NaHCO_3), pancreatin from porcine pancreas, hydrogen peroxide (H_2O_2), sodium potassium tartrate ($\text{KNaC}_4\text{H}_4\text{O}_6 \cdot 4\text{H}_2\text{O}$), copper sulfate (CuSO_4), sodium carbonate (Na_2CO_3), Folin and Ciocalteu's phenol reagent, and fenofibrate (FF) were purchased from Sigma-Aldrich (Sigma Chemical Co., St Louis, MO, U.S.A.).

All solvents were reagent grade or HPLC-grade and provided by Carlo Erba reagents (Milan, Italy).

Pig intestinal membrane from freshly slaughtered animal was purchased from the local slaughterhouse.

Animals and Diet. Male Wistar strain rats, weighing about 100 g each, were purchased from Charles River (Lecco, Italy). All of the animal experiment protocols followed the institutional guidelines of the Italian Ministry of Health for Animal Care (D.M. 116/1992). The animals were housed in rooms maintained at $23 \pm 1^\circ\text{C}$ and $55 \pm 5\%$ relative humidity and were allowed free access to water, a standard rodent chow diet during acclimatization. They were then randomly divided into five groups of nine animals each: Group I (controls, N) received the regular diet for 6 weeks; Group II (hypercholesterolemic, H) received the hypercholesterolemic diet (regular diet + 2% cholesterol + 0.2% cholic acid) for 6 weeks; Group III (H + FF) received the hypercholesterolemic diet (regular diet + 2% cholesterol + 0.2% cholic acid) for 6 weeks (fenofibrate was not used as such, but formulated before administration to animals); from the second to the sixth week, each rat was administered by gavage with fenofibrate (5 mg/kg bw/day); Group IV (H + FFV) received the hypercholesterolemic diet (regular diet + 2% cholesterol + 0.2% cholic acid) for 6 weeks; from the second to the sixth week each rat was administered by gavage with the fenofibrate (5 mg/kg bw/day) plus delivery system (PolyECA-SER nanospheres); Group V (H + V) received the hypercholesterolemic diet (regular diet + 2% cholesterol + 0.2% cholic acid) for 6 weeks; from the second to the sixth week each rat was administered by gavage with delivery system alone, at the same amount employed with fenofibrate. Regular and hypercholesterolemic diets were supplied by Charles River (Lecco, Italy). During the experiment, rats were weighed daily and the 24 h food consumption was recorded, then fasted for 24 h before experiments. At the end of the treatment, blood samples were collected, respectively, in EDTA-treated tubes and silica-treated tubes for plasma and serum detentation, and centrifuged at 2500g for 15 min; the serum was separated and stored at -20°C until analyzed. The animals were anesthetized with chloral hydrate (400 mg/kg, i.p.) and killed by perfusion through the left ventricle of the heart with 100 mL of heparinized saline (pH 7.4). The liver was excised and immediately frozen in liquid nitrogen, then stored at -80°C until required.

Instrumentation. The scanning electron microscopy (SEM) photographs were obtained with a Jeol JSMT 300 A; the surface of the samples was made conductive by the deposition of a gold layer on the samples in a vacuum chamber. Approximate range in particle size was determined, employing an image processing and analysis system, a Leica DMRB equipped with a LEICA Wild 3D stereomicroscope.

The liquid chromatography consisted of a Jasco BIP-I pump and a Jasco UVDEC-100-V detector set at 286 nm. A 250 mm \times 4 mm C-18 Hibar column, particle size 5 μm (Merck, Darmstadt, Germany), was employed. As reported in literature,¹³ the adopted mobile phase was acetonitrile and 0.1% (v/v) H_3PO_4 (75:25, v/v) and run isocratically at a flow rate of 2.0 mL min^{-1} . The sample injection volume was 20 μL for fenofibrate concentration measurement.

The zeta potential of the synthesized nanospheres was measured with the laser Doppler electrophoretic mobility measurements using the Zetasizer 2000 (Malvern Instruments Ltd., Malvern, U.K.), at 25°C . Analyses were done in triplicate and zeta potential values and standard deviations ($\pm\text{SD}$) were elaborated directly from the instrument.

UV-vis absorption spectra were obtained with a Jasco V-530 UV-vis spectrometer.

Synthesis of PolyECA-SER Nanospheres by Interfacial Polymerization. In the aim to synthesize PolyECA-SER nanospheres, 400 mg of sericin were dissolved in 50 mL of an HCl solution (pH 4.0) at 50°C under magnetic stirring and, then, ethyl 2-cyanoacrylate (5 g) was added dropwise to the aqueous polymerization medium. After monomer addition, the polymerization reaction was left to proceed at 50°C with continuous stirring (~ 600 rpm) for 2.5 h. Then, the nanoparticles suspension was neutralized with 0.1 M NaOH until it reached pH 6.0. The resulting nanospheres were collected from the suspension by centrifugation at 7000 rpm for 10 min, washed with distilled water, and finally, dried overnight at 40°C under vacuum.

For a comparison, PolyECA nanoparticles were also prepared, to act as a control, in the absence of sericin during the polymerization process and treated in the same conditions.

Protein Assay According to the Lowry Method. The incorporation of sericin into the synthesized nanospheres was evaluated by protein assay according to the Lowry method and using SER as a standard.¹⁴ The test was performed using previously oxidized nanoparticles in order to avoid the interference on the protein assay due to the presence of cyano groups.

Oxidation. A total of 50 mg of nanospheres were added to 10 mL of H_2O_2 (5% w/w) and allowed to react at room temperature under stirring. After 1 h, the sample was purified by successive washing steps with distilled water and ethanol, recovered by filtration, and finally, dried overnight in a vacuum oven set at 40°C .

Lowry Assay. A total of 10 mg of the obtained oxidized nanospheres were added to 4 mL of freshly prepared Lowry reagent (made by adding 1 mL of 1% sodium potassium tartrate and 1 mL of 0.5% copper sulfate to 50 mL of 2% sodium carbonate in 0.1 M NaOH) and 0.5 mL of water. After mixing, the sample was allowed to stand for 10 min before the addition of 0.4 mL of Folin and Ciocalteu's phenol reagent solution. The sample was mixed and placed at room temperature for 30 min, and then, absorbance was determined spectrophotometrically at 600 nm.

The same reaction conditions were applied on the control polymer in the aim to evaluate the interference of the polymeric material on the protein assay.

Swelling Behavior. Aliquots (50 mg) of nanospheres dried to constant weight were placed in a tared 5 mL sintered glass filter ($\text{O}10$ mm; porosity, G3), weighed, and left to swell by immersing the filter plus support in a beaker containing 0.1 N HCl (pH 1.0, simulated gastric fluid) as the swelling media for the first 2 h and phosphate buffer (pH 6.8, simulated intestinal fluid) as the swelling media for the next 4 h. At predetermined times (2 and 6 h, respectively), the excess water was removed by percolation at atmospheric pressure. Then, the filter was placed in a properly sized centrifuge test tube by fixing it with the help of a bored silicone stopper, centrifuged at 2000 rpm for 5 min,

and weighed. The filter tare was determined after centrifugation with only water.

The weight recorded was used to give the water content percentage (WR%) by the following eq 1:

$$WR\% = \frac{W_s - W_d}{W_d} \times 100 \quad (1)$$

where W_s and W_d are weights of swollen and dried spherical nanoparticles, respectively.

Each experiment was carried out in triplicate.

Drug Loading by the Soaking Procedure. A total of 1.5 g of nanoparticles were immersed in an isopropyl alcohol solution containing 455 mg of fenofibrate and soaked for 3 days at room temperature. During this time, the mixture was continuously stirred, and then, the solvent was removed under reduced pressure.

Evaluation of the Mucoadhesive Properties: In Vitro Wash-Off Test. The mucoadhesive properties and the mucoadhesive strength of the synthesized polymeric nanomaterials were evaluated by performing a modified version of the in vitro wash-off adhesion test.¹⁵ The mucoadhesion of the PolyECA-SER nanoparticles was compared with that of a nonmucoadhesive material, such as PolyECA nanoparticles prepared following the same reaction conditions but in the absence of sericin.

Freshly excised pieces of pig intestinal mucosa (2 × 2 cm) were tightened onto glass slides (3 × 1 in.) with thread. An amount of 50 mg of nanoparticles loaded with the drug was spread onto each wet-rinsed tissue specimen and immediately incubated at 37 °C. The tissue specimens were taken out at 1 and 3 h. The samples were washed with 10 mL of PBS (pH 7.4) at each time interval. The results were evaluated based on the comparison between PolyECA-SER and PolyECA samples.

Determination of the Mucoadhesive Strength. In order to evaluate the mucoadhesive strength, the concentration of the nonadhered fenofibrate eluted in the buffer (PBS pH 7.4) was measured by HPLC analysis. The remaining drug was assumed to be present in PolyECA-SER nanoparticles adhered to the intestinal mucosa.

The mucoadhesive strength was expressed as percentage and was calculated by the following eq 2:

$$\text{mucoadhesion}(\%) = \left[\frac{\text{amt of drug adhering to the mucosa}}{\text{amt of drug used in the test}} \right] \times 100 \quad (2)$$

In Vitro Drug Release Studies. In vitro drug release studies in simulated gastric and intestinal fluids were carried out by performing a slight modified version of the dialysis tubing procedure.¹⁶ The dialysis tubing method is characterized by two consecutive enzymatic digestions, such as pepsin and pancreatin digestion, respectively, and these two steps are described as follows.

Pepsin Digestion. A total of 100 mg of PolyECA-SER nanoparticles loaded with fenofibrate were mixed with 1.0 mL of a 0.85 N HCl solution containing 24000 U of porcine pepsin per mL and 3 mL of a sodium cholate solution (2% w/v in distilled water). The obtained mixture was introduced into a dialysis bag (Spectrum Laboratories Inc., MWCO: 12–14000 Da, U.S.A.), which was then carefully closed and immersed inside a flask containing 10 mL of a 0.85 N HCl solution (pH 1.0). The flask was then incubated into a shaking water bath at 37 °C to simulate the human body conditions of temperature for 2 h.

Pancreatin Digestion. At the end of the 2 h pepsin digestion, the dialysis bag was opened and 11 mg of amylase, 11 mg of esterase, and 1.3 mL of a 0.8 M NaHCO₃ solution containing 22.60 mg porcine pancreatin/mL were added to the peptic digesta. After the digesta and enzyme solution were well-mixed, the dialysis bag was sealed on each end with clamps and placed into a flask with 10 mL of buffer solution at pH 7.0. The flask was incubated into the shaking water bath at 37 °C for an additional 4 h.

In the aim to evaluate the amount of free undigested drug released from the system, 2 mL of the medium were withdrawn from the flask for sample analysis at the time points of 2 and 6 h, after pepsin and pancreatin digestions, respectively, and the concentration of the samples was determined by HPLC analysis.

The amount of unmodified drug obtained after the two digestion phases is thought to be the available amount of FF that can potentially reach the bloodstream after absorption.

The in vitro digestion of fenofibrate from the synthesized nanoparticles was compared to that of free drug by performing the same experimental procedure. For this purpose, an amount of FF, which was equal to that loaded onto 100 mg of PolyECA-SER, was treated under the same conditions.

Each experiment was performed in triplicate.

Animal Studies. Biochemical Value. The livers were cut into small pieces, washed several times in a cold buffer (0.25 M sucrose, 3 mM EDTA, 20 mMTris-HCl, pH 7.0), homogenized in the same buffer, and treated as described in Muciet al.¹⁷ for TC extraction. Briefly, an aliquot of 10 mg protein sample was saponified with alcoholic KOH for 90 min at 85–90 °C. Nonsaponifiable constituents were extracted three times (5 mL each) with light petroleum (bp 40–60 °C). The pooled extracts were then evaporated to dryness under N₂, and the residue was dissolved in 2-propanol. Total lipids were extracted from liver homogenate (10 mg protein) with chloroform/methanol (1:1 v/v) according to Di Donna et al.¹⁸ The levels of hepatic TG and TC were measured, respectively, by Triglyceride Quantification Kit ab65336 (Abcam, Toronto Canada), Total Cholesterol Assay Kits (Cell Biolabs, Inc. San Diego, USA), and HPLC analysis, as described in Di Donna et al.¹⁸ The TG, TC, HDL, LDL, and VLDL levels were evaluated by direct enzymatic assays using Total Cholesterol Assay Kits Cell Biolabs, Inc., San Diego, U.S.A.), Triglyceride Quantification Kit ab65336 (Abcam, Toronto Canada), HDL, and LDL/VLDL Cholesterol Assay Kit ab65390 (Abcam, Toronto Canada), respectively, according to the manufacturer's instruction. Alanine transaminase (ALT), aspartate transaminase (AST), bilirubin, and creatinine were measured using reagent kits from Alanine Transaminase Colorimetric Assay kit (CaymanChem, Michigan, U.S.A.), Aspartate Aminotransferase Activity Assay kit (CaymanChem, Michigan, U.S.A.), Bilirubin Assay kit (Abnova, Taiwan), and Creatinine Colorimetric Assay kit (CaymanChem, Michigan, U.S.A.).

Morphological Analysis. After treatment, rats were anesthetized with chloral hydrate (400 mg/kg, i.p.) and perfused through the left ventricle of the heart with 100 mL of heparinized saline (pH 7.4), followed by 200 mL of 4% paraformaldehyde (PFA). Livers were explanted, fixed for 2 h in 4% PFA at 4 °C, and cryopreserved in 30% sucrose overnight. Specimens were frozen in Optimal Cutting Temperature compound (Tissue-Tek, Sakura Finetek Europe, Alphen aan den Rijn, The Netherlands), and 20 μm cryostat sections were cut, mounted onto Superfrost ultra plus glass slide (Menzel-Gläser, Braunschweig, Germany), and stored at –80 °C until required.¹⁹ Liver sections were stained with hematoxylin and eosin (H&E),²⁰ then the morphological characteristics of the tissue sections were assessed using light microscopy (40× magnification).

Statistical Analysis. All data are presented as means ± SD for the number of experiments indicated in each case. Data were analyzed by Student's *t* test using the GraphPAD Prism5 software (GraphPad Software, U.S.A.). Differences were considered statistically significant at *P* < 0.05.

RESULTS AND DISCUSSION

Synthesis and Characterization of PolyECA-SER Nanospheres. In the present study, PolyECA-SER nanoparticles were synthesized by interfacial polymerization technique involving the dropwise addition of ECA monomer into an acidic aqueous solution.

It has been reported that polymerization of alkylcyanoacrylates might occur through an anionic mechanism, a zwitterionic mechanism, or both of them.²¹ In the first case, hydroxyl anions

from water are the initiating species and lead to chain elongation followed by aggregation of the oligomers to form the polymeric nanoparticles; in the second case, molecules, characterized by the presence of nucleophilic groups, could act as initiators leading to the covalent insertion of the respective compound into the polymer backbone.²² This mechanism involves initiator addition across the alkyl cyanoacrylate double bond, according to a Michael-type addition, to produce a zwitterion that reacts with additional monomer.²³ It can be reasonably hypothesized that the insertion of sericin into the growing polymer backbone occurs according to the above-mentioned zwitterionic mechanism involving the nucleophilic moieties (pendant amino and hydroxyl groups) present in the protein structure.

The incorporation of SER into the synthesized cyanoacrylate nanospheres was confirmed by protein assay according to the Lowry method, which allows to obtain a crude estimate of the amount of incorporated protein. This value was equal to 5.64 ± 0.6 mg of sericin per gram of nanospheres. The adopted conditions of pH and temperature represent the most appropriate ones in the aim to obtain poly(ethylcyanoacrylate) nanospheres incorporating SER and characterized by nanometer size and an unimodal size distribution. Spherical geometry and the practical monodispersity of the prepared nanospheres were, indeed, confirmed by scanning electron micrographs (Figure 1). The mean diameter of the nanospheres

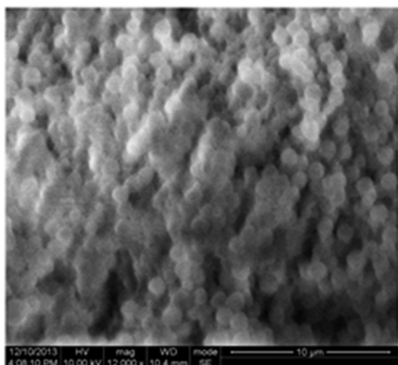


Figure 1. Scanning electron micrographs of PolyECA-SER nanospheres.

was obtained following the instructions given in the [Experimental Section](#). It was found to be 175 ± 12 nm with polydispersity index (PDI) equals to 0.201 (PDI value lower than 0.300 indicates the presence of a homogeneous population of particles).

Zeta potential represents a measure of the electrical charge close to the surface of the nanospheres and, therefore, allows to characterize the electrostatic properties of the synthesized polymeric particles. From zeta potential analysis, pure sericin, PolyECA and PolyECA-SER are characterized by a negative charge on their surfaces of -22.4 ± 0.7 , -31.0 ± 0.6 and -32.8 ± 1.0 mV, respectively. According to literature, SER surface is negatively charged above pH 3.5 due to deprotonated amino and carboxyl groups,²⁴ while PolyECA does not contain ionic functional groups; however, some of the ester bonds of the polymer may be hydrolyzed to acrylic carboxyl groups.²² Nanoparticles characterized by high absolute values of zeta potential (>30 mV) have high degrees of stability in aqueous media; on the other hand, low zeta potential value (<5 mV) can lead to agglomeration.

Swelling Behavior. The swelling properties in water media of the synthesized PolyECA-SER nanospheres and, thus, their hydrophilic properties play a key role in affecting the biocompatibility of the prepared polymeric carrier.

In the aim to evaluate the swelling behavior of PolyECA-SER, aliquots of nanospheres were immersed in 0.1 N HCl for the first 2 h and, then, in a phosphate buffer solution at pH 6.8 for the next 4 h, simulating gastric and intestinal fluids, respectively. The same water uptake experiments were performed using PolyECA as control material and the obtained results were expressed as water content percentage and reported in [Table 1](#).

Table 1. Hydrophilic Properties of PolyECA and PolyECA-SER Nanospheres: Water Content (%)

sample	water content (%)	
	pH 1.0	pH 6.8
PolyECA	32 ± 0.2	58 ± 0.5
PolyECA-SER	225 ± 0.5	250 ± 0.3

In both gastric and intestinal simulating fluids, PolyECA-SER showed good hydrophilic properties ascribable to the presence of sericin; contrariwise, PolyECA exhibited low water content percentages in both the tested media confirming its hydrophobic nature.

In Vitro Mucoadhesive Properties of PolyECA-SER Nanospheres. The in vitro assay for the evaluation of the mucoadhesive properties and mucoadhesive strength was carried out by performing a modified version of the wash-off method on pork intestine. For this purpose, the mucoadhesion of PolyECA-SER nanospheres was compared with that of a nonmucoadhesive material, such as PolyECA nanoparticles prepared following the same reaction conditions but in the absence of sericin.

The tissue specimens were washed with a buffer solution at pH 7.4 after 1 and 3 h of incubation at 37 °C, and particles adhesion was evaluated macroscopically. As it is possible to note in [Figure 2](#), PolyECA-SER nanospheres remained adherent to the intestinal mucosa also after 3 h; on the other hand, the control material did not adhere to the tissue already in the first hour.

The percentage of PolyECA-SER mucoadhesive strength was calculated by [eq 2](#) and, after 3 h of incubation, about 61% of the originally loaded fenofibrate was retained on the intestinal mucosa.

The obtained results can be explained due to the presence of sericin, which confers mucoadhesive properties to the synthesized cyanoacrylate nanospheres. Mucins are glycoproteins that represent the main components of the mucus that covers the mucosal surfaces of human body and have lubricating and cell-protective functions.²⁵ The presence of SER allows the formation of electrostatic interactions with mucin, which are responsible for mucoadhesive features.

In Vitro Drug Release Studies. Dialysis tubing procedure represents a fast and low cost method to evaluate the amount of drug released, undigested and free to be absorbed by gastrointestinal mucosa. Different kinds of molecules can be tested and, in the present study, it was employed in order to evaluate the in vitro release of fenofibrate from the synthesized PolyECA-SER nanospheres compared to that of free drug.

The amount of drug free to be absorbed has been defined as the percentage of the tested therapeutic agent recovered in the

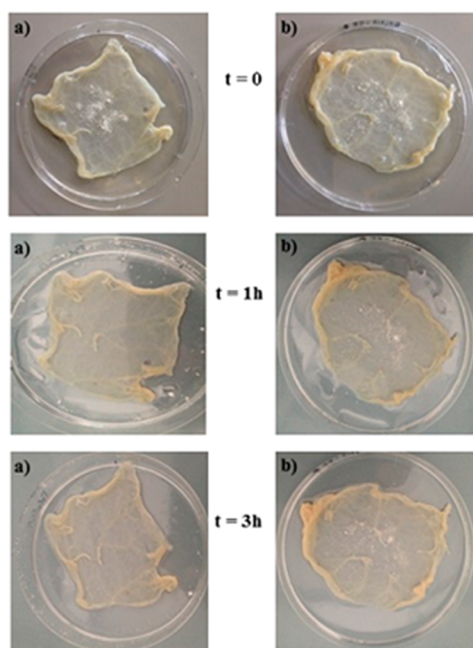


Figure 2. (a) PolyECA nanospheres as control nonmucoadhesive material; (b) PolyECA-SER nanospheres.

bioaccessible fraction, after in vitro digestion, in relation to the original nondigested sample, and it can be calculated by the following eq 3:

$$\text{absorbable drug}(\%) = \frac{\text{bioaccessible content}}{\text{total content}} \times 100 \quad (3)$$

Fenofibrate is characterized by a low bioavailability after oral administration due to its poor aqueous solubility ($3 \mu\text{g/L}$)²⁶ and low dissolution rate.²⁷

The obtained results (Table 2) showed that the amount of FF within the bioaccessible medium has been increased when PolyECA-SER nanospheres were employed as delivery system.

Table 2. Absorbable Drug (%) of Free Fenofibrate and Fenofibrate from PolyECA-SER after Pepsin (2 h) and Pancreatin (4 h) Digestions

sample	absorbable drug (%)		
	pepsin digestion (2 h)	pancreatin digestion (4 h)	total absorbable drug (6 h)
free FF	12 ± 0.4	26 ± 0.7	38 ± 0.8
PolyECA-SER	24 ± 0.8	48 ± 0.5	72 ± 0.9

Animal Studies. Food Intake and Body Weight Gain. The data on food intake and body weight are shown in Figure 3. Figure 3A summarizes the daily food intake that took place during the entire period of treatment, for each group of rats. No significant alteration in food intake was observed for each group (i.e., fenofibrate alone, H + FF, or delivery system alone, H + V, or fenofibrate plus delivery system, H + FFV, treated rats vs control). There were no differences in body weight gain between groups, during the experimental phase (Figure 3B). These observations indicate that the diet and treatments used in these studies were well tolerated in rats, given that no physical alteration, body weight loss, or food intake reduction occurred over the period of study. Two groups of rats were fed a regular and hypercholesterolemic diet, respectively. These

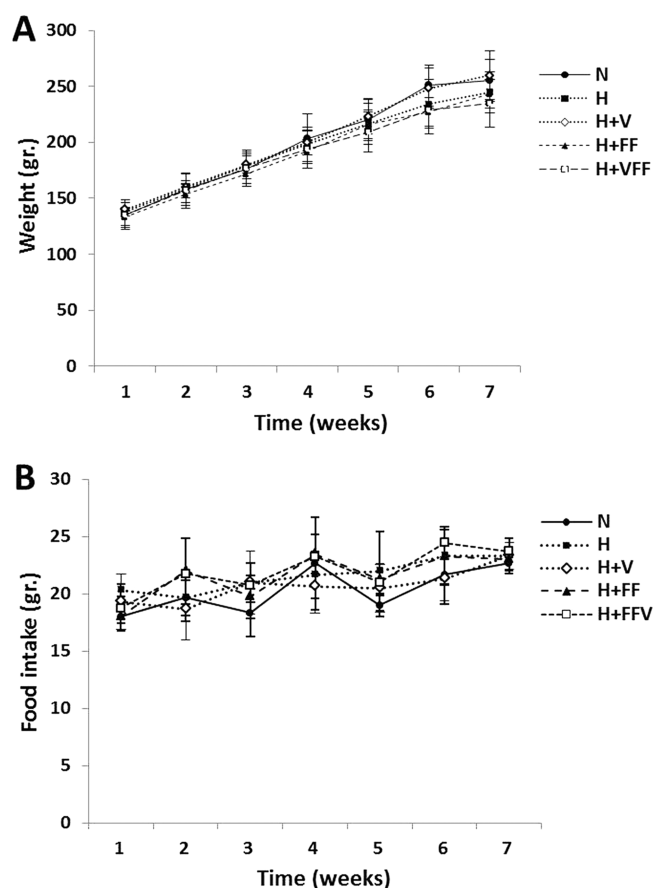


Figure 3. Summary of daily food intake and body weight changes over the study period for each group. Hypercholesterolemic group (filled squares, H) was fed and treated with (H + V), fenofibrate treated (triangles, H + FF), and fenofibrate treated with delivery system (blank squares) described in Food Intake and Body Weight Gain. Regular diet fed rats group is indicated as N (dots). Values represent the mean ± SD of the daily chow intake (A) and of the daily weight (B) for each rat respect to the group.

two groups were used as control; in particular, the first group was used to verify the induced hypercholesterolemia, while the second group was used to test the hypothetical activity of the delivery system.

Effect of Fenofibrate and Fenofibrate Plus Vehicle on Serum and Hepatic Lipid Content. First, in order to establish whether the hypercholesterolemic rat model has been achieved, we compared the serum and hepatic lipid profile of the regular diet fed rats (group N) and the hypercholesterolemic ones (group H). The TC, TG, VLDL, LDL, and HDL levels, in rat serum (Figure 4A), showed a significant increase (100, 32, 53, and 82%, respectively) with respect to the group N, whose values were $105.85 \pm 5.6 \text{ mg/dl}$ for TC, $204.7 \pm 12.3 \text{ mg/dl}$ for TG, $39.02 \pm 1.5 \text{ mg/dl}$ for VLDL, and $49.03 \pm 3.1 \text{ mg/dl}$ for LDL, whereas no significant variation has been found for HDL levels (in group N, the HDL value was $45.52 \pm 3.3 \text{ mg/dl}$). Furthermore, a strong increase of the hepatic TC and TG levels (Figure 4B) has been observed in group H (150 and 300%, respectively) compared to group N, whose values were $1.98 \pm 0.9 \text{ mg/g}$ liver for TC and $4.87 \pm 0.39 \text{ mg/g}$ liver for TG. These results confirmed that the H group can be used as a hypercholesterolemic and hyperlipidemic model in the following experiments.

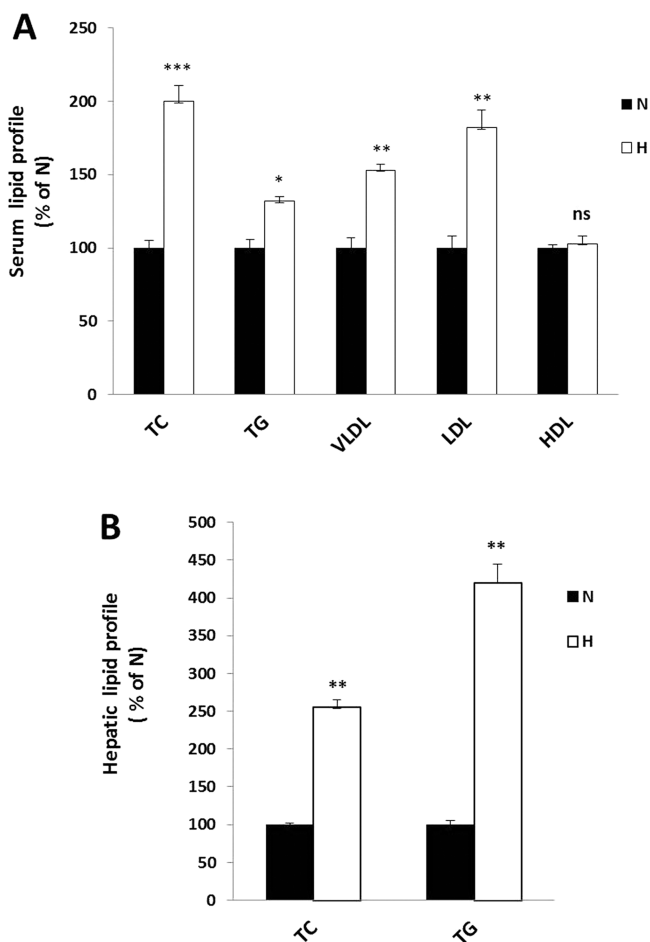


Figure 4. Serum and hepatic lipid profile variations between normal and hypercholesterolemic rats: normal (black bars, N); hypercholesterolemic (white bars, H). The groups were fed as described in [Food Intake and Body Weight Gain](#). The total cholesterol (TC), triglycerides (TG), very low density lipoproteins (VLDL), low density lipoproteins (LDL), and high density lipoproteins (HDL) levels were measured in N and H serum (A). TC and TG were also measured in N and H liver (B). The obtained results were plotted as percentage and columns are mean \pm SD of three independent experiments performed in duplicate. * $P = 0.01$ vs control; ** $P < 0.05$ vs control; *** $P < 0.005$ vs control; ns, no significant.

Then, we investigated the effects triggered by fenofibrate (FF) and fenofibrate plus delivery system (FF + V) treatments on serum and hepatic TC of hypercholesterolemic rats, compared to group H. We observed a significant decrease of the serum TC that was more evident after FF + V treatments (of about 25 and 45%, respectively). No change was detected in rats treated with the delivery system alone, compared to the hypercholesterolemic ones ([Figure 5A](#)). Moreover, the liver TC content showed an even more pronounced reduction in H + FF and H + FFV groups, of 30 and 50%, respectively ([Figure 5B](#)). The direct correlation between an increase in the concentration of LDL in serum and the risk that the incidence of atherosclerosis and cardiovascular disease/cerebrovascular becomes higher is well-known.²⁸ Besides, the HDL concentration has been correlated inversely with the onset of atherosclerosis associated diseases,²⁹ whereas the data concerning the VLDL role in atherosclerotic plaque formation are still controversial.³⁰ For the above reason, we evaluated serum levels of LDL, HDL, and VLDL. A significant reduction of VLDL and

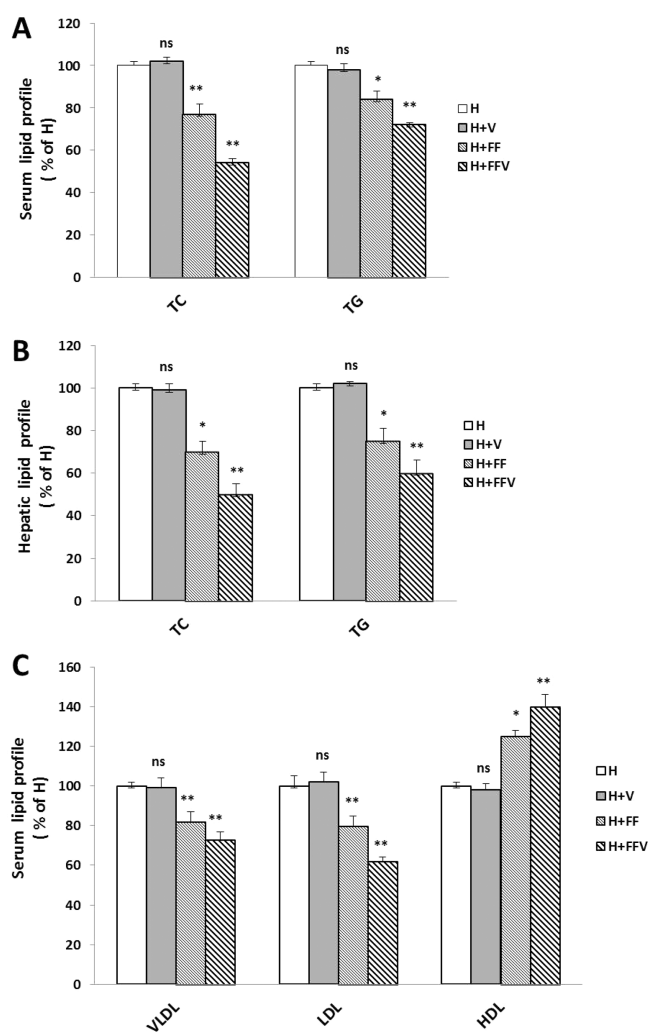


Figure 5. Serum and hepatic lipid profile variations between hypercholesterolemic and treated rats: hypercholesterolemic (white bars, H), delivery system treated (gray bars, H + V), fenofibrate treated (striped bars, H + FF), and fenofibrate with delivery system (big striped bars, H + FFV). The groups were fed as described in [Food Intake and Body Weight Gain](#). The total cholesterol (TC) and triglycerides (TG) were measured in serum (A). Very low density lipoproteins (VLDL), low density lipoproteins (LDL), and high density lipoproteins (HDL) levels were measured in serum (C; H as control). TC and TG were also measured in liver (C; H as control). The obtained results were plotted as percentage and columns are mean \pm SD of three independent experiments performed in duplicate. * $P = 0.01$ vs control; ** $P < 0.05$ vs control; *** $P < 0.005$ vs control; ns, nonsignificant.

LDL was measured in H + FF (20 and 24% lower, respectively) and H + FFV groups (28 and 40% lower, respectively; [Figure 5C](#)). Conversely, an increase of 23% was found in the levels of HDL of rats belonging to group H + FF with respect to those of rats of group H ([Figure 5C](#)). The increase exceeded 38% in rats of group H + FFV. Since fibrates and their derivatives have been shown to be particularly effective at reducing serum triacylglycerols, in experimental animals,³¹ we measured serum and hepatic TG content, in our model. The obtained results showed that relative to H, groups H + FF and H + FFV have their TG levels reduced by 18 and 28%, respectively, for serum TG ([Figure 5A](#)) and of about 30 and 40%, respectively, for hepatic TG ([Figure 5B](#)).

Liver Microscopic Examination. As shown in Figure 6, in the hepatocytes of group H (Figure 6B) there is a lipid

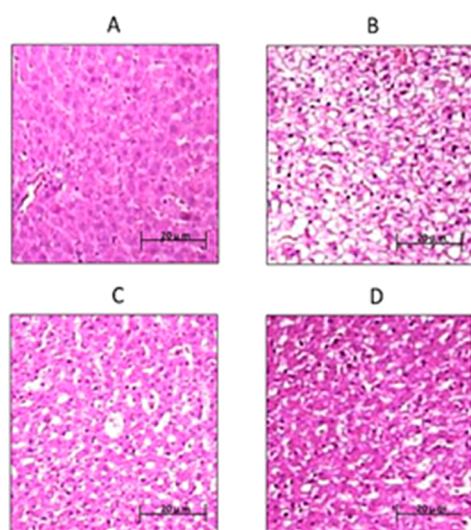


Figure 6. Image showing liver tissue of rats: normal liver (A), hypercholesterolemic liver (B), hypercholesterolemic liver after treatment with fenofibrate (C), and hypercholesterolemic liver after treatment with fenofibrate plus delivery system (D).

accumulation that is absent in hepatocytes of group N (Figure 6A). This accumulation is less noticeable after the fenofibrate treatment, as demonstrated in the hepatocytes of H + FF group (Figure 6C), the disappearance was more relevant in group H + FFV (Figure 6D).

Influence of Fenofibrate and Fenofibrate Plus Vehicle on Rat ALT, AST, Bilirubin, and Creatinine Levels. At last, we investigated, in rat, the effects caused by fenofibrate and fenofibrate plus delivery system on hepatic and renal functional parameters, (e.g., ALT, AST, bilirubin and creatinine). The creatinine levels decreased in FF treated rats by 14% compared to those of hypercholesterolemic rats. This reduction is even more pronounced, reaching 29%, in FFV treated rats; this latter treatment brings the creatinine level to normal values (group N values). Conversely, no significant difference was found for serum total bilirubin in FF and FFV treated rats, with respect to the rats of groups N and H (Table 3).

Compared with the N group, the serum ALT and AST levels of the H group rats have had a greater increase, of 83% and 51% respectively. Serum ALT and AST levels were lowered significantly in rats treated with fenofibrate (28 and 21%, respectively) when comparing them to the hypercholesterolemic rats. This reduction was greater, by 40 and 30%, respectively, in rats belonging to H + FFV group (Table 3). No significant difference was found for serum total bilirubin, creatinin, ALT, and AST levels in rats belonging to group H + V compared to those of the H group.

Table 3. Bilirubin, Creatinine, ALT, and AST Serum Levels in Rats^a

group	total bilirubin (mg/dl)	creatinin (mg/dl)	ALT (U/L)	AST (U/L)
N	0.29 ± 0.05	0.5 ± 0.06	41.391 ± 2.730	103.696 ± 5.018
H	0.31 ± 0.04	0.7 ± 0.03	75.832 ± 3.654	156.929 ± 4.673
H + FF	0.30 ± 0.06	0.6 ± 0.04	54.269 ± 4.002	124.125 ± 5.329
H + FFV	0.29 ± 0.05	0.5 ± 0.02	45.678 ± 3.423	109.375 ± 4.997

^aALT: alanine transferase; AST: aspartate transferase; Values are means ± SD.

CONCLUSIONS

In the present research study, a novel sericin-based delivery system for improved and enhanced oral bioefficacy of fenofibrate was synthesized by interfacial polymerization in aqueous media.

The prepared sericin/poly(ethylcyanoacrylate) nanospheres showed good hydrophilic and mucoadhesive properties, and the in vitro studies highlighted an improved percentage of absorbable therapeutic agent in the gastrointestinal tract (higher than 70%) when incorporated into the synthesized nanoparticles. All these parameters lead to an enhanced bioefficacy of fenofibrate, which was confirmed by the performed in vivo studies. Indeed, in rats, the daily supplement of fenofibrate incorporated in the new synthesized nanoparticles in their diet was able to significantly reduce the levels of TC, TG, VLDL, and LDL. More importantly, the microscopic examination of liver showed that the lipid accumulation present in hepatocytes of group H is strikingly reduced in the hepatocytes of group H + FFV. Therefore, the obtained results clearly indicate the efficiency of the adopted synthetic strategy and the potential application of the synthesized sericin/poly(ethylcyanoacrylate) nanospheres as delivery system for poorly water-soluble drugs.

Furthermore, the results presented here establish in a model that is highly related to humans that the synthesized delivery system employed in this study is a promising strategy to improve the effectiveness of fenofibrate in the therapy of hyperlipidemia.

AUTHOR INFORMATION

Corresponding Authors

*Tel.: +39 0984 493151. Fax: +39 0984 493298. E-mail: francesco.puoci@unical.it.

*E-mail: annarita.cappello@unical.it.

Author Contributions

†These authors contributed equally to the manuscript (O.I.P. and M.F.).

Notes

The authors declare no competing financial interest.

‡These authors are joint senior authors (F.P. and A.R.C.).

ACKNOWLEDGMENTS

The financial support of the Italian Minister of University and Research and University of Calabria is most gratefully acknowledged. The authors thank Dr. F. Cavaliere and Dr. M. Certo for technical assistance in morphological analysis and Dr. G. Fico for animal care assistance.

REFERENCES

- (1) Leuner, C.; Dressman, J. B. *Eur. J. Pharm. Biopharm.* **2000**, *50*, 47–60.
- (2) Cho, Y.-D.; Park, Y.-J. *Arch. Pharmacol. Res.* **2014**, *37*, 193–203.

- (3) Grislain, L.; Couvreur, P.; Lenaerts, V.; Roland, M.; Deprez-Decampeneere, D.; Speiser, P. *Int. J. Pharm.* **1983**, *15*, 335–345.
- (4) Lowe, P. J.; Temple, C. S. *J. Pharm. Pharmacol.* **1994**, *46*, 547–552.
- (5) Harivardhan Reddy, L.; Murthy, R. S. R. *Biomed. Pap.* **2004**, *148*, 161–166.
- (6) Zhang, Y.-Q. *Biotechnol. Adv.* **2002**, *20*, 91–100.
- (7) Shen, Y.; Johnson, M. A.; Martin, D. *Macromolecules* **1998**, *31*, 8857–8864.
- (8) Doakhan, S.; Montazer, M.; Rashidi, A.; Moniri, R.; Moghadam, M. B. *Carbohydr. Polym.* **2013**, *94*, 737–748.
- (9) Yucel, T.; Lovett, M. L.; Kaplana, D. L. *J. Controlled Release* **2014**, *190*, 381–397.
- (10) Staels, B.; Dallongeville, J.; Auwerx, J.; Schoonjans, K.; Leitersdorf, E.; Fruchart, J. C. *Circulation* **1998**, *98* (19), 2088–2093.
- (11) McKeage, K.; Keating, G. M.; Bhatnagar, D.; Elam, M. B.; Farnier, M.; Mohiuddin, S. M. *Drugs* **2011**, *71* (14), 1917–1946.
- (12) Ige, P. P.; Baria, R. K.; Gattani, S. G. *Colloids Surf., B* **2013**, *108*, 366–373.
- (13) Yousaf, A.; Kim, D.; Choi, H.-G.; Oh, E. *Curr. Pharm. Anal.* **2014**, *10*, 97–104.
- (14) Sepehrimanesh, M.; Aminlari, M. *Comp. Clin. Pathol.* **2014**, *23*, 353–356.
- (15) Karn, P. R.; Vanic, Z.; Pepic, I.; Škalko-Basnet, N. *Drug Dev. Ind. Pharm.* **2011**, *37*, 482–488.
- (16) Chimento, A.; Sala, M.; Gomez-Monterrey, I. M.; Musella, S.; Bertamino, A.; Caruso, A.; Sinicropi, M. S.; Sirianni, R.; Puoci, F.; Parisi, O. I.; Campana, C.; Martire, E.; Novellino, E.; Saturnino, C.; Campiglia, P.; Pezzi, V. *Bioorg. Med. Chem. Lett.* **2013**, *23*, 6401–6405.
- (17) Muci, M. R.; Cappello, A. R.; Vonghia, G.; Bellitti, E.; Zezza, L.; Gnoni, G. V. *Int. J. Vitam. Nutr. Res.* **1992**, *62*, 330–333.
- (18) Di Donna, L.; Iacopetta, D.; Cappello, A. R.; Gallucci, G.; Martello, E.; Fiorillo, M. *J. Funct. Foods* **2014**, *7*, 558–568.
- (19) Viscomi, M. T.; Florenzano, F.; Latini, L.; Amantea, D.; Bernardi, G.; Molinari, M. *Neuroscience* **2008**, *154*, 1267–1282.
- (20) Nucci, C.; Tartaglione, R.; Cerulli, A.; Mancino, R.; Spanò, A.; Cavaliere, F.; Rombolà, L.; Bagetta, G.; Corasaniti, M. T.; Morrone, L. A. *Int. Rev. Neurobiol.* **2007**, *82*, 397–406.
- (21) Graf, A.; McDowell, A.; Rades, T. *Expert Opin. Drug Delivery* **2009**, *6*, 371–387.
- (22) Yordanov, G.; Bedzhova, Z. *Cent. Eur. J. Chem.* **2011**, *9*, 1062–1070.
- (23) Klemarczyk, P. *Polymer* **2001**, *42*, 2837–2848.
- (24) Chen, X.; Lam, K. F.; Mak, S. F.; Ching, W. K.; Ng, T. N.; Yeung, K. L. *Chin. J. Chem. Eng.* **2012**, *20*, 426–432.
- (25) Bäckström, M.; Ambort, D.; Thomsson, E.; Johansson, M. E.; Hansson, G. C. *Mol. Biotechnol.* **2013**, *54*, 250–256.
- (26) Mohsin, K. *AAPS PharmSciTech* **2012**, *13*, 637–646.
- (27) Kasim, N. A.; Whitehouse, M.; Ramachandran, C.; Bermejo, M.; Lennernäs, H.; Hussain, A. S.; Junginger, H. E.; Stavchansky, S. A.; Midha, K. K.; Shah, V. P.; Amidon, G. L. *Mol. Pharmaceutics* **2004**, *1*, 85–96.
- (28) Steinberg, D. *Circulation* **1987**, *76*, 508–514.
- (29) Arsenaault, B. J.; Rana, J. S.; Stroes, E. S.; Després, J. P.; Shah, P. K.; Kastelein, J. J.; Wareham, N. J.; Boekholdt, S. M.; Khaw, K. T. *J. Am. Coll. Cardiol.* **2009**, *55*, 35–41.
- (30) Stancu, C. S.; Toma, L.; Sima, A. V. *Cell Tissue Res.* **2012**, *349*, 433–446.
- (31) Ferreira, E. S.; Silva, M. A.; Demonte, A.; Neves, V. A. *Lipids Health Dis.* **2012**, *11*, 11.

Estrogen related receptor α (ERR α) a promising target for the therapy of adrenocortical carcinoma (ACC)

Ivan Casaburi^{1,*}, Paola Avena^{1,*}, Arianna De Luca^{1,*}, Adele Chimento¹, Rosa Sirianni¹, Rocco Malivindi¹, Vittoria Rago¹, Marco Fiorillo¹, Francesco Domanico¹, Carmela Campana¹, Anna Rita Cappello¹, Federica Sotgia², Michael P. Lisanti², Vincenzo Pezzi¹

¹Department of Pharmacy, Health and Nutritional Sciences, University of Calabria, Italy

²The Breakthrough Breast Cancer Research Unit and the Manchester Centre for Cellular Metabolism, Institute of Cancer Sciences, University of Manchester, UK

*These authors have contributed equally to this work

Correspondence to:

Vincenzo Pezzi, e-mail: v.pezzi@unical.it

Keywords: ERR α , adrenocortical cancer, mitochondria, ATP depletion

Received: May 21, 2015

Accepted: July 17, 2015

Published: July 29, 2015

ABSTRACT

The pathogenesis of the adrenocortical cancer (ACC) involves integration of molecular signals and the interplay of different downstream pathways (i.e. IGFII/IGF1R, β -catenin, Wnt, ESR1). This tumor is characterized by limited therapeutic options and unsuccessful treatments. A useful strategy to develop an effective therapy for ACC is to identify a common downstream target of these multiple pathways. A good candidate could be the transcription factor estrogen-related receptor alpha (ERR α) because of its ability to regulate energy metabolism, mitochondrial biogenesis and signalings related to cancer progression.

In this study we tested the effect of ERR α inverse agonist, XCT790, on the proliferation of H295R adrenocortical cancer cell line. Results from *in vitro* and *in vivo* experiments showed that XCT790 reduced H295R cell growth. The inhibitory effect was associated with impaired cell cycle progression which was not followed by any apoptotic event. Instead, incomplete autophagy and cell death by a necrotic processes, as a consequence of the cell energy failure, induced by pharmacological reduction of ERR α was evidenced.

Our results indicate that therapeutic strategies targeting key factors such as ERR α that control the activity and signaling of bioenergetics processes in high-energy demanding tumors could represent an innovative/alternative therapy for the treatment of ACC.

INTRODUCTION

Adrenocortical carcinoma (ACC) is a very rare and aggressive disease with a high risk of relapse after radical surgery. Treatment options in advanced, metastatic stages are limited, since cytotoxic chemotherapy options are poor and radiotherapy is mostly ineffective [1]. The drug mitotane (o, p'-dichlorodiphenyldichloroethane (o, p'-DDD)) with its adrenolytic activity is the only adrenal specific drug that is currently used for ACC treatment. However, toxicity, narrow therapeutic window and side effects are the major limitation to its use as well as therapeutic success [2].

Given the high mortality and aggressiveness of ACC, more effective and specific treatment options are needed. Recently, monoclonal antibodies targeting insulin-like growth factor II (IGFII) receptor (IGF1R) have been tested in clinical trials, however they provided a limited effectiveness in refractory patients [3]. Rationale for targeting IGF1R comes from the observation that IGFII gene is overexpressed in ACC [4]. We have recently demonstrated that IGFII/IGF1R pathway can be activated by the estrogen receptor alpha (ESR1), a gene overexpressed in ACC that mediates estrogen-dependent proliferative effects [5, 6]. ESR1 knock down was more effective than an IGF1R antibody in reducing H295R cell

proliferation *in vitro* [5] and the selective estrogen receptor modulator (SERM) tamoxifen prevented the growth of H295R both *in vitro* [7] and as xenografts *in vivo* [5]. Thus, ESR1 could be a promising target to reduce ACC growth.

Indeed, a recent study [8], investigating a large cohort of advanced ACC, confirmed the presence of a large number of potentially targetable molecules involved in ACC progression. These observations confirm that ACC is an extremely heterogeneous disease and that its pathogenesis involves integration of signals and the interplay of downstream pathways. It is currently accepted that these changes are also associated with a profound reprogramming of cellular metabolism [9]. Consequently, one potential strategy to develop an effective therapy for ACC could be the identification of a common downstream target of multiple pathways capable of controlling expression and activity of various bioenergetic factors.

Estrogen Related Receptor α (ERR α) is an orphan member of the nuclear hormone receptor superfamily of transcription factors that has been identified on the basis of its high level of sequence identity to ER α and for which an endogenous ligand has yet to be defined [10]. ERR α functions downstream of the peroxisome proliferator-activated receptor gamma coactivator-1 alpha and beta (PGC-1 α and PGC-1 β) and regulates the expression of genes involved in energy metabolism and mitochondrial biogenesis such as genes encoding enzymes and proteins of the tricarboxylic acid cycle, pyruvate metabolism, oxidative phosphorylation, and electron transport [11]. Research to understand how changes in cell metabolism promote tumor growth has accelerated in recent years [12]. As a consequence, research has focused on targeting metabolic dependencies of cancer cells, an approach with the potential to have a major impact on patient care. Notably, ERR α has recently been associated with dysregulated cell metabolism and cancer progression. Accordingly, increased expression of ERR α has been shown in several cancerous tissues including breast [13], ovary [14] prostate [15] and colon [16]. Several signaling pathways, also relevant to ACC development have been shown to converge upon and regulate the expression and activity of ERR α together with its coactivators such as PGC-1 α and β in others tumor types [17]. Several studies have reported that ERR α inverse agonist XCT-790 [18] can induce cell growth arrest in different tumor cell lines [19, 20]. To date, few studies have investigated the role of ERR α in adrenal gland and ACC. ERR α is expressed in normal adult adrenal and regulates the expression of enzymes involved in steroidogenesis [21]. Moreover, ERR α seems to be more expressed in ACC compared to normal adrenal and adenoma [22].

The aim of this study was to establish if ERR α depletion using XCT790 can induce growth arrest in ACC cells. The data obtained support the hypothesis that ERR α could be a promising target for the treatment of adrenocortical cancer.

RESULTS

ERR α inverse agonist XCT790 decreases ERR α protein content and inhibits ACC cells proliferation *in vitro*

First, we verified that ERR α is expressed in H295R adrenocortical cancer cells. MCF-7 breast cancer cells were used as positive control [23] (Figure 1A). Moreover, we also demonstrated that in both H295R and MCF-7 cells, XCT790 treatment decreased ERR α protein levels in a dose-dependent manner (Figure 1B). The latter results confirmed the ability of XCT790 to reduce the expression of ERR α most probably by proteasome degradation [23]. Next, we evaluated the effects of different concentrations of ERR α inverse agonist XCT790 on ACC cell growth. Results from MTT assay revealed that XCT790 treatment exerted a dose- and time-dependent inhibition on H295R cell proliferation compared to vehicle-treated cells (Figure 1C). The maximum inhibitory effect on ACC cell proliferation was seen at 10 μ M XCT790 that was then used for all the following experiments.

ERR α inverse agonist XCT790 inhibits ACC cells proliferation *in vivo*

We next established H295R cell xenograft tumors in immunocompromised mice to investigate the ability of XCT790 to reduce tumor growth *in vivo*. To this aim, H295R cells were injected into the intrascapular region of mice. When tumors reached an average volume of 200 mm³, animals were randomized into two groups to be treated with either vehicle or XCT790 (2,5 mg/Kg). As shown in Figure 2A, mice treated with XCT790 displayed a significant tumor growth reduction compared to the vehicle treated control group. Accordingly, tumor reduction upon XCT790 treatment is evidenced both in terms of tumor mass (Figure 2B) and proliferation as seen in Figure 2C, showing a strong decrease in Ki67staining (value score control: $7.2 \pm 0,46$ (SD); value score XCT790 treated cells: $4.7 \pm 0.53^*$ (SD), $*p < 0.05$).

ERR α inverse agonist XCT790 blocks G1/S transition of ACC cells without inducing apoptosis

The observed effects of XCT790 on ACC cells proliferation led us to evaluate XCT790 action on H295R cell cycle progression.

First, by analyzing PI staining with FACSJazz flow cytometer, we investigated whether XCT790 treatment could affect the distribution of cells within the three major phases of the cycle. To this aim, H295R cells were grown for 24 h in 5% CS-FBS and then treated with either vehicle (DMSO) or 10 μ M XCT790. 48 hours later, FACS analysis revealed that XCT790 treated cells accumulated

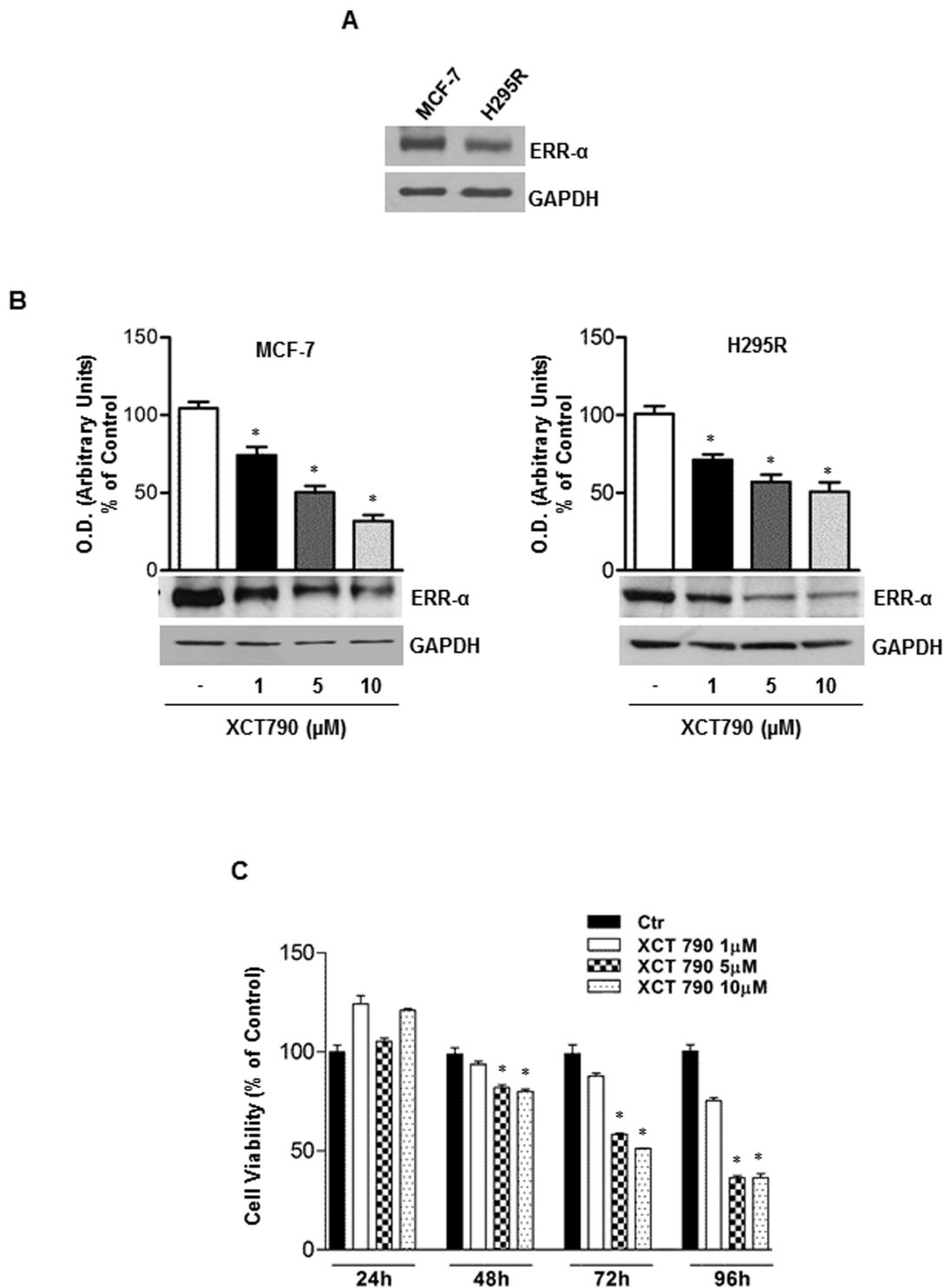


Figure 1: ERR α inverse agonist XCT790 decreases ERR α protein content and H295R cells growth *in vitro*. A. Western blot analysis of ERR α was performed on 50 μ g of total proteins extracted from H295R and MCF-7 cells. Blots are representative of three independent experiments with similar results. (B. lower left and right panel), protein extracts from MCF-7 and H295R cells left untreated (-) or treated for 48 h with different doses of XCT790 were resolved by SDS-PAGE and subjected to immunoblot against ERR α . GAPDH served as loading control. (b, upper left and right panel), graphs represent means of ERR α optical density (O.D.) from three independent experiments with similar results normalized to GAPDH content (* p < 0.001 compared to untreated control sample assumed as 100). C. Cell viability after XCT790 treatment was measured using MTT assay. Cells were plated in triplicate in 24-well plates and were untreated (Ctr) or treated with increasing concentrations of XCT790 for the indicate times in DMEM supplemented with 2,5% Charcoal-Stripped FBS. Absorbance at 570 nm was measured on a multiwell-plate reader. Cell viability was expressed as a percentage of control, (* p < 0.001).

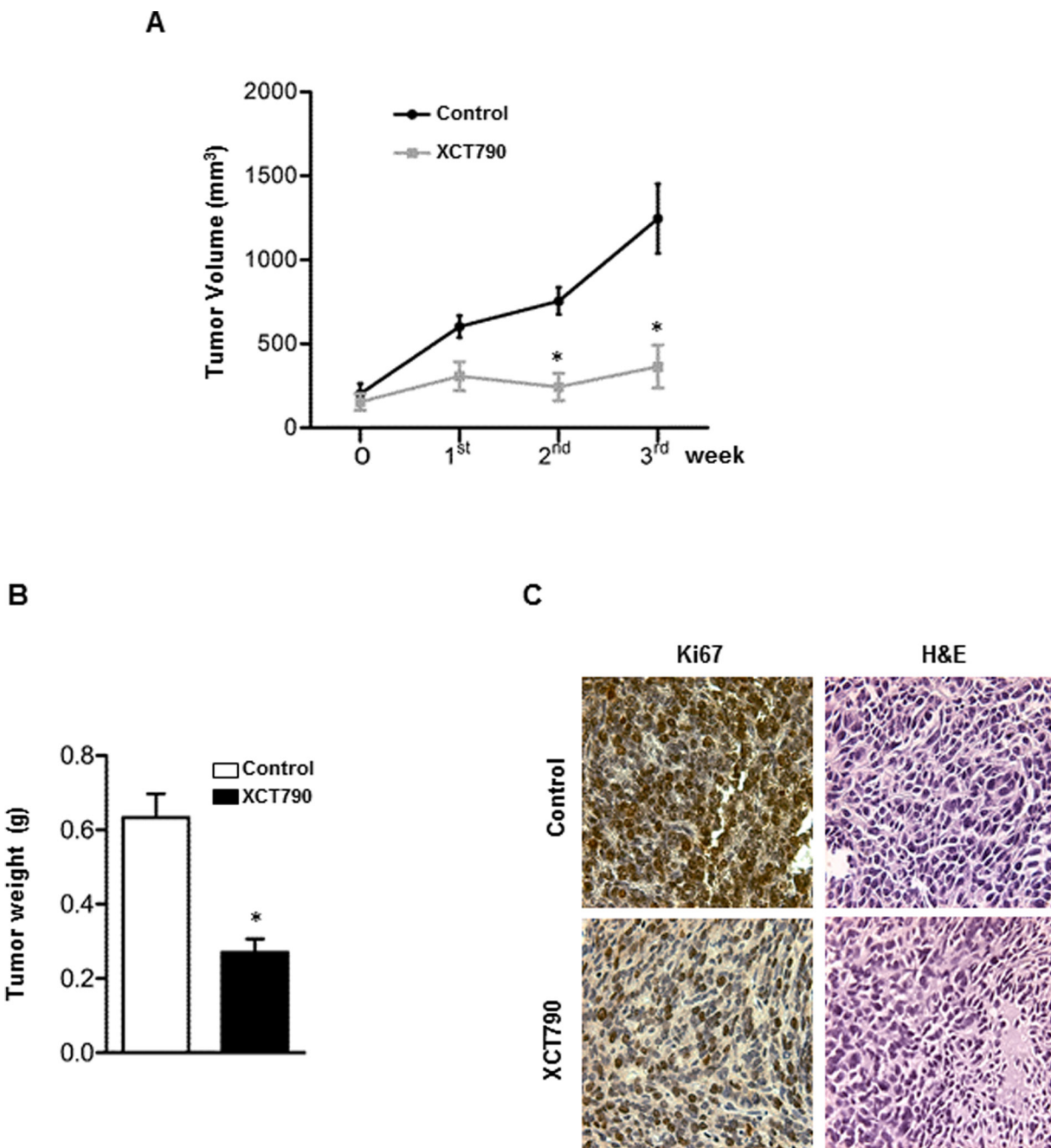


Figure 2: ERRA inverse agonist XCT790 decreases H295R cells proliferation *in vivo*. **A.** 6×10^6 H295R cells were injected subcutaneously onto the intrascapular region of immunocompromised mice and the resulting tumors were grown to an average of 200 mm^3 . The animals were randomized to vehicle controls or XCT790 treatment for twenty one days. Tumor volumes were calculated, as indicated in Materials and Methods. Values represent the mean \pm SE of measured tumor volume over time in the control group (filled circles, $n = 10$) and in the XCT790-treated group (filled squares, $n = 10$). **B.** After 21 days (3 weeks) tumors were harvested and weighed. Values represent the mean \pm SE of measured tumour weight ($n = 10$) * $P < 0.05$ versus control at the same day of treatment. **C.** Ki67 immunohistochemical and H & E staining: histologic images of H295R explanted from xenograft tumors (magnification X 400).

in the G0/G1-phase of the cell cycle while the fraction of cells in S phase decreased compared with vehicle treated cells (Figure 3A).

In order to define the molecular mechanisms involved in XCT790-dependent cell cycle arrest, changes in levels of protein involved in cell cycle regulation were investigated by Western blotting analysis. After

48 h treatment, XCT790 reduced Cyclin D1 and Cyclin E protein content while expression levels of CDK2 and CDK4 proteins were unaffected. Consistently with the observed G1/S transition arrest of the cell cycle, Rb protein showed a hypophosphorylated status (Figure 3B–3C). As the analysis of the cell cycle revealed a minimal increase of the sub-G1 fraction (Figure 3A), a known

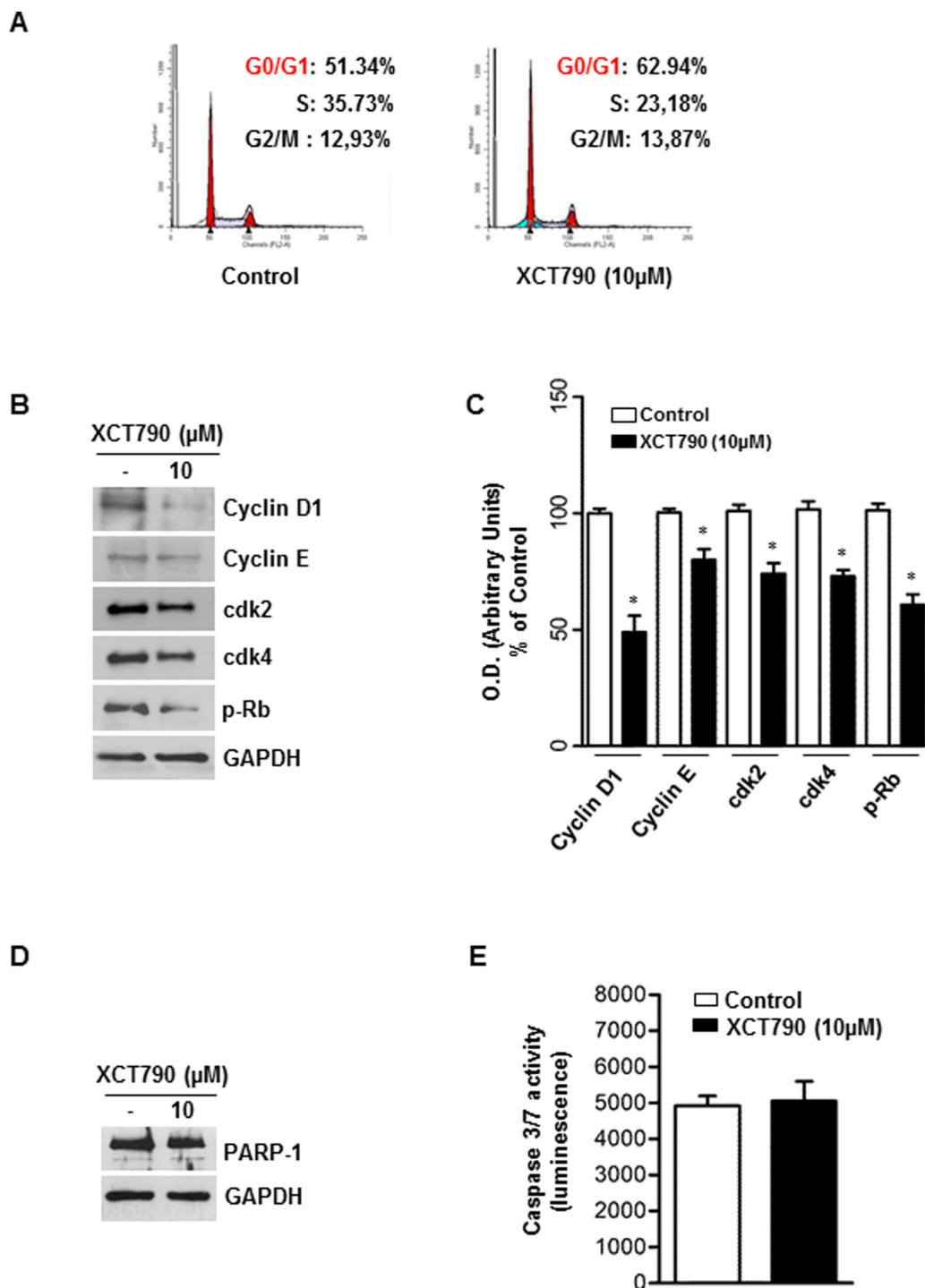


Figure 3: ERR α inverse agonist XCT790 impairs G1/S transition of ACC cells without inducing apoptosis. **A.** The distribution of H295R cells in the cycle was determined by Flow Cytometry using Propidium-iodide (PI) stained nuclei. The graph shows the distribution of H295R cell population (%) in the various phases of cell cycle. **B.** Total proteins from H295R cells left untreated (–) or treated with XCT790 for 48 h were resolved by SDS-PAGE and subjected to immunoblot analysis using specific antibodies against human Cyclin D1, Cyclin E, cdk2, cdk4, p-Rb. **C.** Graphs represent means of Cyclin D1, Cyclin E, cdk2, cdk4, p-Rb optical densities (O.D.) from three independent experiments with similar results normalized to GAPDH content, (* $p < 0.001$ compared to each untreated control assumed as 100); **D.** Total proteins were analyzed by Western blot for PARP-1. Blots are representative of three independent experiments with similar results. GAPDH served as loading control. **E.** Cellular caspase 3/7 activity was determined by Caspase-Glo assay system using the substrate Ac-DEVD-pNA and expressed as relative luminescence units (RLU) of treated cell to untreated control cell. Each column represents the mean \pm SD of three independent experiments (* $p < 0.001$ compared to untreated control sample).

marker of apoptotic events, we next attempted to verify the presence of apoptotic features such as PARP-1 cleavage and caspase 3/7 activation, all well-known biochemical markers of programmed cell death. Surprisingly, results from Western blotting analysis for PARP-1 (Figure 3D) and caspase 3/7 activity assay (Figure 3E) clearly showed that XCT790 did not activate an apoptotic pathway.

XCT-790 decreased mitochondrial mass and function in ACC cells

The activity of $ERR\alpha$ is highly dependent on the presence of coactivator proteins, most notably PGC-1 α and PGC-1 β [24], both known for their crucial role in regulating energy metabolism and mitochondrial biogenesis [24]. Moreover, it has been observed that XCT790 treatment, causing $ERR\alpha$ proteasome degradation, also down-regulates PGC-1 α [24]. Based on these observations, we first checked if XCT790 treatment regulates PGC-1 α expression in H295R cells. To this aim, ACC cells were left untreated or treated with 10 μ M XCT790 for 48 h. Results from Western blotting showed (Figure 4A–4B) that XCT790 treated cells display a reduced expression of PGC-1 α , with no effect on PGC-1 β levels. We then asked whether reduced levels of PGC-1 α would lead to reduction of mitochondrial mass. To this purpose we treated cells with MitoTracker deep red FM that stains specifically mitochondria independently of their membrane potential. Using flow cytometric analysis (Figure 4C), fluorescent imaging (Figure 4D) and fluorescent plate reader (Figure 4E), we found that XCT790 significantly decreased mitochondrial mass.

The mitochondrial citrate carrier CIC is a protein that belongs to a family of metabolites transporters embedded in the inner mitochondrial membrane [25, 26] and has been recently highlighted as important component in maintaining mitochondrial integrity and bioenergetics in normal and particularly in tumor cells [27]. We used CIC protein expression as a marker of both mitochondrial mass and function and found that XCT790 decreased mitochondrial CIC expression (Figure 4F–4G) as well as its transport activity (Figure 4H) in H295R-treated cells compared to vehicle-treated control cells.

To extend these findings, we used immunoblotting to monitor the abundance of a known reliable marker of mitochondrial mass, TOM20, in response to 10 μ M XCT790 treatment. We found that XCT790 treated-H295R cells displayed a reduced expression of $ERR\alpha$, as expected, concomitantly with a drastic decline of TOM20 protein expression (Figure 5A–5B). Similarly, the analysis of the expression of the mitochondrial oxidative pathway (OXPHOS) enzymes showed a substantial reduction of all the complexes (Figure 5C). In agreement with these findings, the reduction in the ATP content reveals a bioenergetics failure induced by XCT790 in treated cells (Figure 5D).

XCT790 induce cell death by necrosis in ACC cells

Very recent data revealed that low levels of CIC or its impaired expression induce mitochondrial dysfunction followed by enhanced mitochondrial turnover via autophagy/mitophagy mechanism [27]. Based on this observation and accordingly to our above reported results showing the ability of XCT790 to down-regulate CIC expression in H295R cells, we wanted to verify if autophagic features were detected in our experimental conditions. Autophagy is characterized by acidic vacuoles (AVO) formation, which can be measured by acridine orange (AO) vital staining. AO moves freely to cross biological membranes and accumulates in acidic compartment, where it is seen as bright red fluorescence [28]. As shown in Figure 6A (upper panel), AO vital staining of 48 h XCT790-treated H295R cells showed the accumulation of AVO in the cytoplasm. To quantify the accumulation of the acidic component, we performed FACS analysis of acridine orange-stained cells using FL3 mode (> 650 nm) to quantify the bright red fluorescence and FL1 mode (500–550 nm) for the green fluorescence. As shown in Figure 6A (lower panel), XCT790 treatment raised the strength of red fluorescence from 7,5% to 51%. These results corroborate the observation that XCT790, increases the formation of AVOs which suggests autophagy/mitophagy as possible mechanisms to explain the reduced mitochondrial mass. This latter event could be responsible for the inhibitory effects on cell growth elicited by XCT790 on adrenocortical cancer cells. A careful evaluation of the autophagic/mitophagic process by investigating changes in autophagic markers such as Beclin 1, LC3B, BNIP3 and Cathepsin B (Figure 6B), suggested that XCT790 treatment promotes the initial stages of the autophagic process. This is supported by the evidence of increased Beclin 1 expression and the presence of the cleaved LC3B form [29]. However, autophagy fails to terminate as indicated by decreased BNIP3, Cathepsin B and Lamp1 proteins expression [29]. Therefore, we evaluated XCT790 ability to induce H295R cells death by necrosis. To this aim, Trypan blue exclusion test was performed after 48 h of XCT790 treatment. As shown in Figure 6C, H295R displayed a significant increase in the number of positive stained cells compared to control cells indicating that membrane integrity and permeability were lost accounting for a necrotic event following a bioenergetic failure triggered by $ERR\alpha$ depletion.

DISCUSSION

The molecular heterogeneity and complexity that characterize adrenocortical cancer biology combined with lack of an effective treatment, drive towards the discovery of new therapeutic targets. Advances in the understanding of the molecular pathogenesis of ACC have

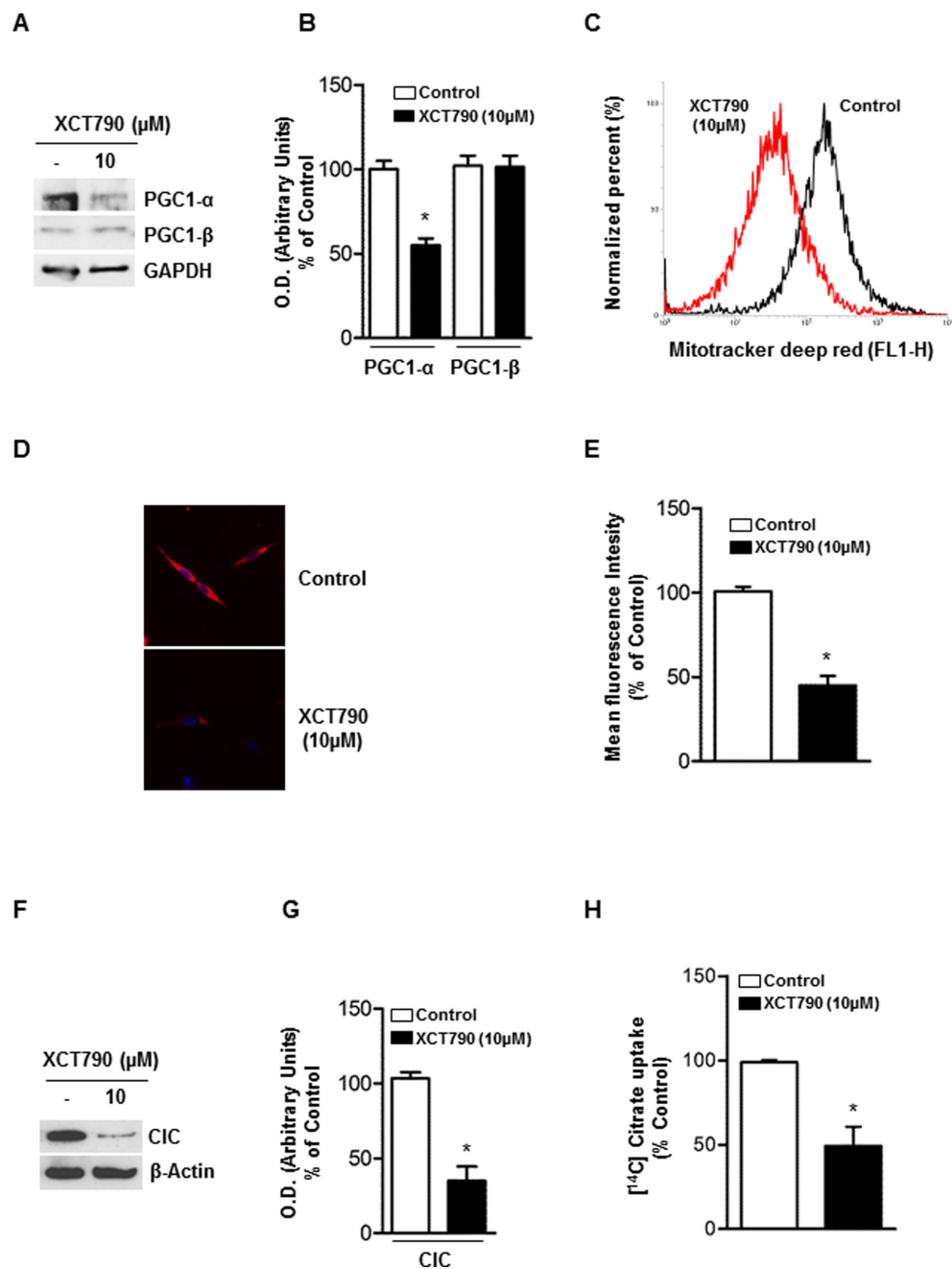


Figure 4: XCT-790 decreases mitochondrial mass and function in H295R cells. **A.** Total protein extracts from H295R cells, left untreated (-) or XCT790 treated in 2.5% DCC-FBS medium for 48 h were analyzed by Western blot with antibodies against PGC-1 α and PGC-1 β . GAPDH was used as loading control. **B.** Graphs represent means of PGC-1 α and β optical densities (O.D.) from three independent experiments with similar results normalized to GAPDH content ($*p < 0.001$ compared to each untreated control sample assumed as 100). **C.** H295R cells were right untreated (control) or treated with XCT790. 48 h later, absorption of MitoTracker deep red FM was determined by FACS analysis. The uptake of MitoTracker was used as an indicator for the mitochondrial mass. **D.** Reduction in mitochondrial mass was further evaluated by fluorescence microscopy of MitoTracker-stained cells. **E.** Quantification of Mito-Tracker fluorescent signal intensity in untreated (control) or XCT790-treated H295R cells was evaluated measuring red fluorescent signal by a fluorescent plate reader (ex. 644; em. 665) $*p < 0.001$ compared to untreated control sample. **F.** Immunoblots for CIC expression from mitochondrial extracts in untreated (-) or XCT-790 treated H295R cells for 48 h. β -Actin served as loading control. Blots are representative of three independent experiments with similar results. **G.** Graph represent means of CIC density (O.D.) from three independent experiments with similar results normalized to β -Actin content ($*p < 0.001$ compared to untreated control sample assumed as 100). **H.** CIC activity was measured at 20 min as steady-state levels of citrate/citrate exchange. Transport was started by adding 0.5 mM [¹⁴C]Citrate to proteoliposomes preloaded internally with 10 mM citrate and reconstituted with mitochondria isolated from untreated H295R cells (Control; white column) and H295R-treated cells (black column). The transport reaction was stopped at 20 minutes. Results are expressed as percentage of the control. The data represent means \pm SD of at least three independent experiments.

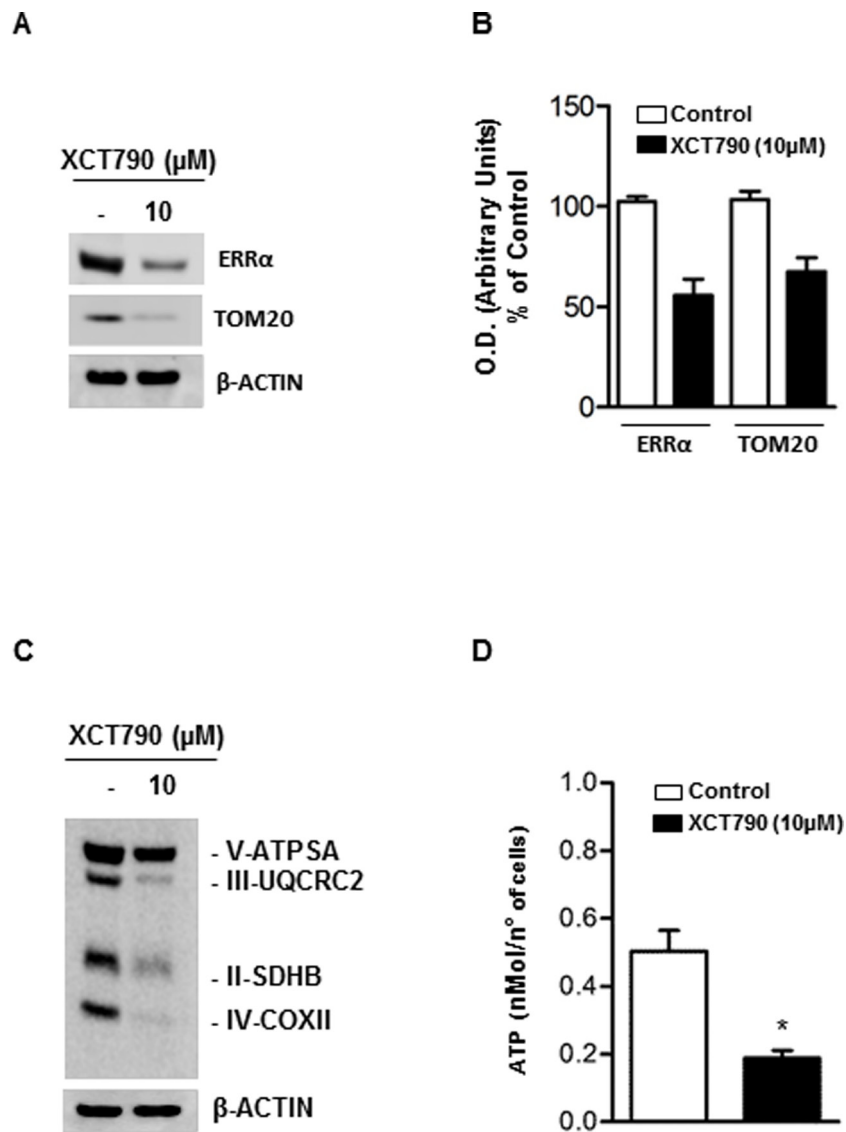


Figure 5: XCT790 decreased OXPHOS protein content and ATP concentration in H295R cells. **A.** Total protein extracts from H295R cells, left untreated (-) or treated for 48 h in 2.5% DCC-FBS medium with 10 μM XCT790, were analyzed by Western blot using antibodies against ERRα and TOM20. β-actin was used as loading control. **B.** Graphs represent means of ERRα and TOM20 optical densities (O.D.) from three independent experiments with similar results normalized to β-Actin content (**p* < 0.001 compared to each untreated control sample assumed as 100). **C.** Total protein extracts from H295R cells left untreated (-) or treated for 48 h in 2.5% DCC-FBS medium with 10 μM XCT790, were analyzed by Western blot experiments using antibodies against OXPHOS subunits. β-Actin was used as loading control. Blots are representative of three independent experiments with similar results. **D.** ATP concentrations in H295R cells untreated (-) or treated with XCT790 were determined as described in Material and Methods and expressed as nmol/number of cells. Each column represents the mean ± SD of three independent experiments (**p* < 0, 001).

been made based on studies of gene expression profiling and genetic syndromes associated with the development of ACC [30]. Results from these studies have highlighted the presence of different and important modifications such as somatic TP53 mutations, alterations at 11p15, a chromosomal locus of IGFII, H19 and cyclin-dependent kinase inhibitor 1C, β-catenin accumulation and activation of the Wnt signaling pathway and overexpression of SF-1 protein [30]. Moreover we have recently demonstrated the involvement of ESR1 in ACC cell growth regulation [5]. Genetic modifications and molecular pathways alterations

have as a common purpose the survival and proliferation of the transformed phenotype. It is currently accepted that these changes are associated with a concurrent adaptation and reprogramming of cellular metabolism [31]. In this scenario adrenocortical tumors are not an exception and the metabolic receptor ERRα represents a good therapeutic target. In fact, ERRα is a common downstream target of multiple pathways and a key factor in controlling the expression and activity of various bioenergetics processes. Indeed, it has already been observed that high ERRα gene expression correlates with unfavorable clinical outcomes

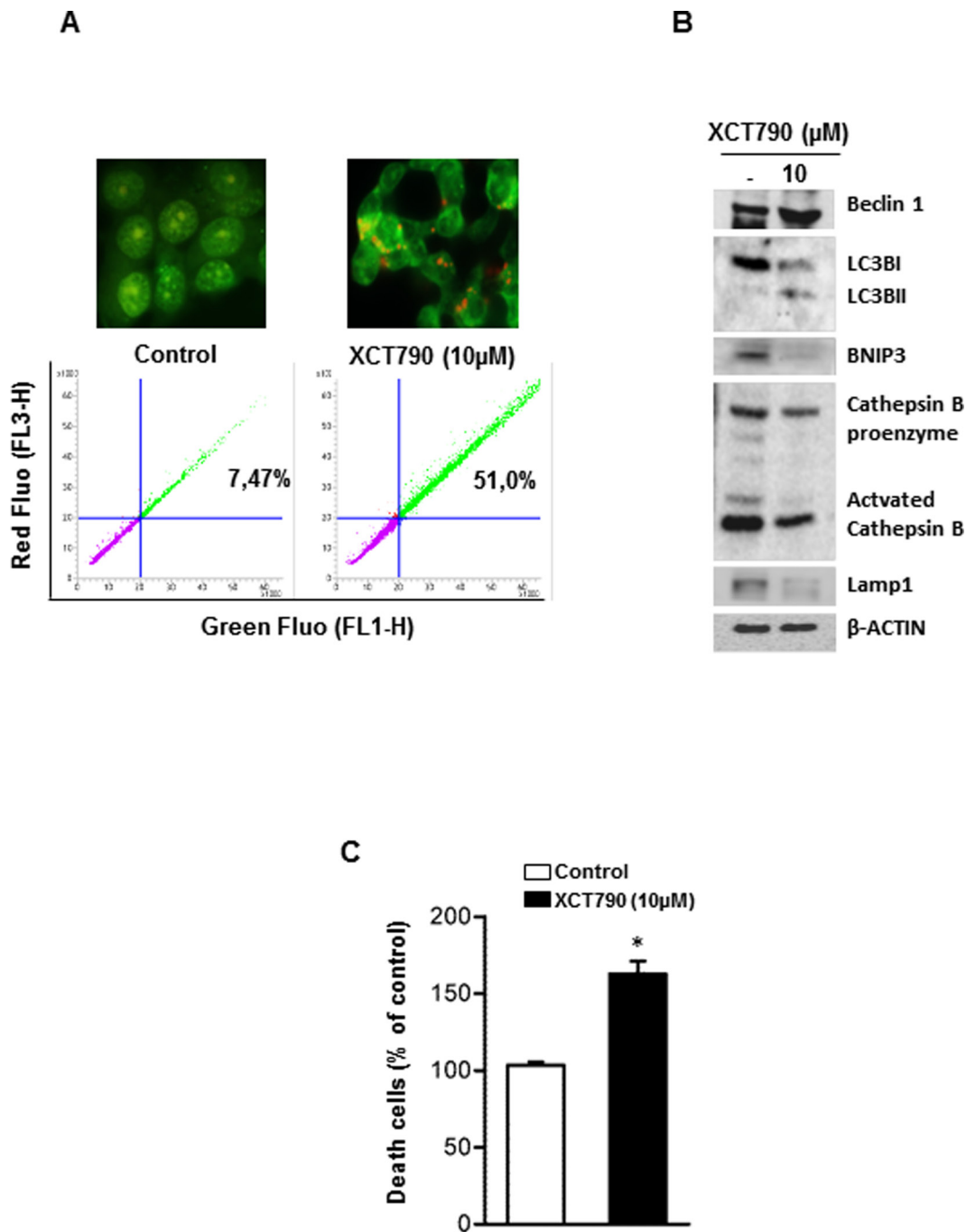


Figure 6: XCT790 induces necrosis in H295R cells. A. H295R cells were left untreated (control) or treated with XCT790 10 μ M. After 48 h, cells were incubated with (1 μ g/mL) acridine orange (AO) solution for 30 min at 37°C. Absorption of AO was determined by FACS analysis (lower panel). In the same experimental conditions, treated or untreated H295R cells were stained with acridine orange, mounted and immediately analyzed by fluorescent microscope (upper panel). B. Total protein extracts from H295R cells left untreated (-) or treated in 2.5% DCC-FBS medium with XCT790, as indicated, for 48 h were analyzed by Western blot experiments using antibodies against Beclin 1, LC3B, BNIP3, Cathepsin B, Lamp1. β -Actin was used as loading control. Blots are representative of three independent experiments with similar results. C. Cell death by necrosis was assessed by Trypan blue-exclusion assay in H295R cells untreated (-) or treated with XCT790. The mean \pm SD of three replicates are shown. Cell death was expressed as a percentage of control, (* $p < 0.001$).

in breast [32] and ovarian cancer [14, 33] and that breast cancer cells exhibiting high $ERR\alpha$ activity are more sensitive to growth inhibition by an $ERR\alpha$ inverse agonist such as XCT790 [34]. Consistent with this findings and

with very recent data reporting high $ERR\alpha$ expression in adrenal tumors compared to benign and normal adrenal gland [22], here we report that $ERR\alpha$ is expressed in H295R cells, the most valid cell model to study ACC

biology. Moreover, our data show that pharmacological down-regulation of $ERR\alpha$ expression impaired H295R cell proliferation *in vitro* in a dose-dependent fashion. Most importantly, the same inhibitory effect was obtained also in *in vivo* experiments using H295R cells as xenograft model. At the molecular level, the growth inhibition is associated with a G0/G1 cell cycle arrest and by the decreased levels of G1-phase markers such as Cyclin D1 and pRb while CDKs protein levels were unaffected. Noteworthy, cell cycle arrest was not followed by any apoptotic event since we were unable to detect any morphological data (data not shown) or biochemical events such as caspase activation and PARP-1 cleavage.

Accumulating data provide evidence that a caspase-independent form of programmed cell death such as autophagy can be at play under certain conditions [35]. Therefore we investigated whether the inhibitory effects induced by XCT790 treatment could be linked to autophagy. Our results indicated that XCT790 caused a significant increase in autophagic vesicles. Concomitantly, we observed a drastic reduction in the expression of PGC1- α protein, which plays a key role in mitochondrial biogenesis, and of mitochondrial carrier CIC. The reduction of mitochondrial mass, also confirmed by the reduction of TOM20 protein expression, is followed by a considerable and significant decrease in the ATP concentration. Despite the presence of some autophagic markers such as the up-regulation of Beclin 1 and the cleaved form of LC3 protein, the formation of autophagolysosomes seems to be incomplete as evidenced by the reduction in LAMP1 protein, known to play an important role during the final steps of autophagy process [36]. A possible explanation could be a considerable reduction in the availability of intracellular ATP, required to drive forward the active cell death mechanism including autophagy. On the other hand, we cannot exclude that the observed initial steps of autophagy are a defense cell response to keep cells alive during energy failure to counteract the reduced expression and activity of the master bioenergetic executor $ERR\alpha$. Moreover, the bioenergetics crisis following treatment with $ERR\alpha$ inverse agonist might be responsible for the loss of plasma membrane integrity, a key signature for a necrotic cell death, allowing the significant increase in the number of Trypan blue stained cells.

However, our most significant finding is that in ACC cells $ERR\alpha$ depletion after XCT790 treatment clearly caused a reduction of mitochondrial function and mass leading to the activation of a number of cellular mechanisms that result in tumor cell death.

It's now well known that mitochondria with its direct involvement in bioenergetics, biosynthesis and cell signaling are mandatory for tumorigenesis. Thus, it's not surprising that many studies have begun to demonstrate that mitochondrial metabolism and signaling is potentially a successful avenue for cancer therapy. Moreover, ACC

is (in most cases) characterized by steroids producing/secreting cancer cells highly dependent on functioning mitochondria to ensure steroidogenic processes. For these reasons, strategies using mitochondrial metabolism and signaling as targets should be particularly effective for ACC treatment. Moreover, our current data obtained performing *in vivo* experiments by using H295R cells as xenograft model and according to previous *in vivo* studies performed in breast [37] and leukemia [38] tumor cells also suggest that chemical depletion of $ERR\alpha$ may be specific for high energy demanding cells such as tumor cells without exerting any toxic effect on other tissues.

In conclusion, our study supports the hypothesis that $ERR\alpha$ represents a valid innovative/alternative target for the treatment of adrenocortical cancer.

MATERIALS AND METHODS

Cell culture

H295R adrenocortical cancer cells were obtained from Dr. Antonio Stigliano (University of Rome, Italy) and cultured in DMEM/F12 supplemented with 1% ITS Liquid Media Supplement, 10% fetal bovine serum (FBS), 1% glutamine, 2% penicillin/streptomycin (complete medium) MCF7 breast cancer cells were maintained in monolayer cultures DMEM/F12, supplemented with 10% FBS, 1% glutamine, 2% penicillin/streptomycin. Both cell lines were cultured at 37°C in 5% CO₂ in a humidified atmosphere. All media and supplements were from Sigma-Aldrich, Milano, Italy.

Western blot analysis

Whole cell lysate were prepared in RIPA buffer (50 mM Tris-HCl, 150 mM NaCl, 1% NP-40, 0.5% sodium deoxycholate, 2 mM sodium fluoride, 2 mM EDTA, 0.1% SDS and a mixture of protease inhibitors) or in ice-cold lysis buffer (10 mM Tris-HCl pH 8, 150 mM NaCl, 1% Triton X-100, 60 mM octylglucoside). Samples were analyzed by 11% SDS-PAGE and blotted onto a nitrocellulose membrane. Blots were incubated overnight at 4°C with anti- $ERR\alpha$ polyclonal antibody, anti-cyclin D1, anti-cyclin E, anti-cdk2, anti-cdk4, anti-p-Rb, anti-PARP, anti-cathepsin B, anti-LAMP1, anti-Tom20 (all from Santa Cruz Biotechnology), anti-Beclin 1 (Novus Biological), anti-LC3B antibody, anti-BNIP3 antibody, Mitoprofile Total OXPHOS Human WB Antibody Cocktail (Abcam) and then incubated with appropriate horseradish peroxidase conjugated secondary antibodies for 1 h at room temperature. The immunoreactive products were detected by the ECL Western blotting detection system (Amersham Pharmacia Biotech, Piscataway, NJ). GAPDH antibody (Santa Cruz Biotechnology) or anti- β -Actin antibody (Sigma-Aldrich) were used as internal control.

Cell viability assay

H295R cells were seeded in 12-well plates at a density of 1×10^5 cells per well and cultured in complete medium overnight. Before treatment culture medium was switched into in DMEM F-12 supplemented with 2.5% charcoal stripped (CS) FBS and cells were untreated or treated with different concentration of XCT790 (Tocris Bioscience, Bristol, UK) for the indicated time. DMSO (Sigma-Aldrich) was used as vehicle control. Cell viability was measured using MTT assay (Sigma-Aldrich). Each experiment was performed in triplicate and the optical density was measured at 570 nm in a spectrophotometer. Experiments were repeated three times.

Trypan blue assay

Trypan blue stain was prepared freshly as a 0.4% solution in 0.9% sodium chloride before each experiment. After trypsinization, 20 μ l cell suspension was added to 20 μ l of Trypan blue solution and mixed thoroughly. Triplicate wells of dye positive cells from untreated or XCT790 treated were counted using a hemocytometer and the experiment was repeated three times.

Xenograft model

Athymic Nude- Foxn1^{nu} mouse 4–6 weeks old from Charles River Laboratories [Calco (LC), Italy] were maintained in groups of five or less and quarantined for one week. Mice were kept on a 12 h light/dark cycle with ad libitum access to food and water.

6×10^6 H295R cells suspended in 100 μ l of sterile PBS (*Dulbecco's* Phosphate Buffered Saline) and mixed with 100 μ l of matrigel, were injected subcutaneously into the intrascapular region of each animal. When tumor size reached a volume of about 200 mm³ mice were randomly divided in 2 groups. Animals were injected every other day with vehicle (soy oil) or XCT790 (2,5 mg/Kg) over a 21 day period. Tumors were measured with a caliper every two days, volumes were calculated using the formula $V = a b^2/2$ (V :volume; a is the length of the long axis, and b is the length of the short axis). At the end of the treatment period tumors were harvested and tumor weight and volumes were evaluated. All animal procedures were approved by the local Ethics Committee for Animal Research.

Immunohistochemical analysis

5 μ m thick paraffin-embedded sections were mounted on slides precoated with poly-lysine, and then they were deparaffinized and dehydrated (seven to eight serial sections). Immuno-histochemical experiments were performed using rabbit polyclonal Ki67 primary antibody (Dako, Denmark) at 4°C over-night. Then, a biotinylated goat-anti-rabbit IgG was applied for

1 h at room temperature, followed by avidin biotin-horseradish peroxidase reaction (Vector Laboratories, CA). Immunoreactivity was visualized by using the diaminobenzidine chromogen (Sigma-Aldrich). Counterstaining was carried out with methylene-blue (Sigma-Aldrich). Hematoxylin and eosin Y staining was performed as suggested by the manufacturer (Bio-Optica, Milan, Italy).

Scoring system

The immunostained slides of tumor samples were evaluated by light microscopy using the Allred Score [39] which combines a proportion score and an intensity score. A proportion score was assigned representing the estimated proportion of positively stained tumor cells (0 = none; 1 = 1/100; 2 = 1/100 to <1/10; 3 = 1/10 to <1/3; 4 = 1/3 to 2/3; 5 = >2/3). An intensity score was assigned by the average estimated intensity of staining in positive cells (0 = none; 1 = weak; 2 = moderate; 3 = strong). Proportion score and intensity score were added to obtain a total score that ranged from 0 to 8. A minimum of 100 cells were evaluated in each slide. Six to seven serial sections were scored in a blinded manner for each sample.

Cell cycle analysis

H295R cells treated with different doses of XCT790 were fixed, treated with RNase A (20 μ g/ml), stained with Propidium iodide (100 μ g/ml) (Sigma-Aldrich) and analyzed by Flow Cytometry using BD FACSJazz™ Cell Sorter (Becton, Dickinson and Co) for DNA content and cell cycle status.

Caspases 3/7 activity assay

Caspases activity was measured with Caspase-Glo Assay Kit (Promega Italia SRL, Milano, Italy) following the manufacturer instruction. The luminescence of each sample was measured in a plate-reading luminometer (Gen5 2.01) with Synergy H1 Hybrid Reader. Each experiment was performed on triplicate wells per condition.

Mitochondrial mass determination

XCT790 treated or untreated H295R cells were incubated in serum free medium with 200 nM Mitotracker deep red (Invitrogen, USA) for 30 min at 37°C in the dark. After staining, cells were washed twice with cold PBS, trypsinized, centrifuged at 1200 rpm for 5 min and then resuspended in PBS. Absorption of MitoTracker deep red FM was determined by FACS analysis and by fluorescence microscopy. In the same experimental conditions, fluorescent signal intensity was also assessed using a fluorescent plate reader (ex. 644 nm; em. 665 nm).

Detection of acidic vesicular organelles (AVOs) with acridine orange

H295R cells were cultured on 6 well plates and treated in 2.5% CS-FBS with or without 10 μ M XCT790. After 48 h, cells were washed with PBS and stained for 30 min at 37°C with 1 μ g/mL acridine orange solution (Sigma-Aldrich). Cells were then washed three times with cold PBS and one drop of mounting solution was added. Cell were observed and imaged by an inverted fluorescence microscope (100X magnification). Accumulation of the acidic vacuoles was also determined by FACS analysis.

ATP Determination

1×10^5 cells were seeded in 96 white clear bottom multi-well plates in complete medium. Two days later, cells were treated in DMEM F-12 supplemented with 2.5% CS FBS containing 10 μ M XCT790. After 48 h, ATP concentrations were determined using the CellTiter-Glo luminescent cell viability assay (Promega) following the manufacturer instruction. Results were normalized to the cell number evaluated by HOECHST staining (Sigma-Aldrich) and expressed as nMol/number of cells.

Mitochondria reconstitution and transport measurements

The transport activity was carried out as described previously [40]. Briefly, isolated mitochondria from untreated (control) or XCT790 treated H295R cells were solubilized in a buffer containing 3% Triton X, 114, 4 mg/ml cardiolipin, 10 mM Na₂SO₄, 0.5 mM EDTA, 5 mM PIPES pH 7. The mixture was incubated for 20 min and centrifuged at 138,000 \times g for 10 min. The supernatant was incorporated into phospholipid vesicles by cyclic removal of the detergent [41]. The reconstitution mixture consisted of 0.04 mg protein solution, 10% Triton X-114, 10% phospholipids (egg lecithin from Fluka, Milan, Italy) as sonicated liposomes, 10 mM citrate, 0.85 mg/ml cardiolipin (Sigma) and 20 mM PIPES, pH 7.0. The citrate transport was measured after external substrate removal from proteoliposomes on Sephadex G-75 columns, pre-equilibrated with buffer A (50 mM NaCl and 10 mM PIPES, pH 7.0). Transport at 25°C was started by the addition of 0.5 mM [¹⁴C] citrate (Amersham) to the eluted proteoliposomes and terminated by the addition of 20 mM 1,2,3-benzene-tricarboxylate. Finally, the external radioactivity was removed from the Sephadex G-75 columns, liposomes radioactivity was measured and transport activity was calculated [41].

Statistics

All experiments were performed at least three times. Data were expressed as mean values \pm standard deviation (SD), statistical significance between control and treated samples was analyzed using GraphPad Prism 5.0

(GraphPad Software, Inc.; La Jolla, CA) software. Control and treated groups were compared using the analysis of variance (ANOVA). A comparison of individual treatments was also performed, using Student's t test. Significance was defined as $p < 0.05$.

ACKNOWLEDGMENTS

We are grateful to Prof. F. Palmieri for the kind gift of antibody against CIC and Prof. A. Stigliano for H295R cells.

FUNDING

This work was supported by Associazione Italiana per la Ricerca sul Cancro (AIRC) projects n. IG14433 to Vincenzo Pezzi. This work was also supported by Fondo Investimenti Ricerca di Base (FIRB) Accordi di Programma 2011, RBAP1153LS-02 from the Ministry of Education, University and Research, Rome, Italy. The funders had no role in study design, data collection and analysis, decision to publish, or preparation of the manuscript.

CONFLICTS OF INTEREST

The authors declare no conflicts of interest.

REFERENCES

1. Glover AR, Ip JC, Zhao JT, Soon PS, Robinson BG, Sidhu SB. Current management options for recurrent adrenocortical carcinoma. *OncoTargets and therapy*. 2013; 6:635–643.
2. Ronchi CL, Kroiss M, Sbiera S, Deutschbein T, Fassnacht M. EJE prize 2014: current and evolving treatment options in adrenocortical carcinoma: where do we stand and where do we want to go? *European journal of endocrinology / European Federation of Endocrine Societies*. 2014; 171:R1–R11.
3. Naing A, Lorusso P, Fu S, Hong D, Chen HX, Doyle LA, Phan AT, Habra MA, Kurzrock R. Insulin growth factor receptor (IGF-1R) antibody cixutumumab combined with the mTOR inhibitor temsirolimus in patients with metastatic adrenocortical carcinoma. *British journal of cancer*. 2013; 108:826–830.
4. Gicquel C, Bertagna X, Schneid H, Francillard-Leblond M, Luton JP, Girard F, Le Bouc Y. Rearrangements at the 11p15 locus and overexpression of insulin-like growth factor-II gene in sporadic adrenocortical tumors. *The Journal of clinical endocrinology and metabolism*. 1994; 78:1444–1453.
5. Sirianni R, Zolea F, Chimento A, Ruggiero C, Cerquetti L, Fallo F, Pilon C, Arnaldi G, Carpinelli G, Stigliano A, Pezzi V. Targeting estrogen receptor-alpha reduces adrenocortical cancer (ACC) cell growth *in vitro* and *in vivo*: potential therapeutic role of selective estrogen receptor modulators (SERMs) for ACC treatment. *The Journal of clinical endocrinology and metabolism*. 2012; 97:E2238–2250.

6. Barzon L, Masi G, Pacenti M, Trevisan M, Fallo F, Remo A, Martignoni G, Montanaro D, Pezzi V, Palu G. Expression of aromatase and estrogen receptors in human adrenocortical tumors. *Virchows Archiv : an international journal of pathology*. 2008; 452:181–191.
7. Montanaro D, Maggiolini M, Recchia AG, Sirianni R, Aquila S, Barzon L, Fallo F, Ando S, Pezzi V. Antiestrogens upregulate estrogen receptor {beta} expression and inhibit adrenocortical H295R cell proliferation. *Journal of molecular endocrinology*. 2005; 35:245–256.
8. De Martino MC, Al Ghuzlan A, Aubert S, Assie G, Scoazec JY, Leboulleux S, Do Cao C, Libe R, Nozieres C, Lombes M, Pattou F, Borson-Chazot F, Hescot S, Mazoyer C, Young J, Borget I, et al. Molecular screening for a personalized treatment approach in advanced adrenocortical cancer. *The Journal of clinical endocrinology and metabolism*. 2013; 98:4080–4088.
9. Cairns RA, Harris IS, Mak TW. Regulation of cancer cell metabolism. *Nature reviews Cancer*. 2011; 11:85–95.
10. Giguere V, Yang N, Segui P, Evans RM. Identification of a new class of steroid hormone receptors. *Nature*. 1988; 331:91–94.
11. Deblois G, Giguere V. Functional and physiological genomics of estrogen-related receptors (ERRs) in health and disease. *Biochimica et biophysica acta*. 2011; 1812:1032–1040.
12. Galluzzi L, Kepp O, Vander Heiden MG, Kroemer G. Metabolic targets for cancer therapy. *Nature reviews Drug discovery*. 2013; 12:829–846.
13. Ariazi EA, Jordan VC. Estrogen-related receptors as emerging targets in cancer and metabolic disorders. *Current topics in medicinal chemistry*. 2006; 6:203–215.
14. Fujimoto J, Alam SM, Jahan I, Sato E, Sakaguchi H, Tamaya T. Clinical implication of estrogen-related receptor (ERR) expression in ovarian cancers. *J Steroid Biochem Mol Biol*. 2007; 104:301–304.
15. Fujimura T, Takahashi S, Urano T, Kumagai J, Ogushi T, Horie-Inoue K, Ouchi Y, Kitamura T, Muramatsu M, Inoue S. Increased expression of estrogen-related receptor alpha (ERRalpha) is a negative prognostic predictor in human prostate cancer. *International journal of cancer Journal international du cancer*. 2007; 120:2325–2330.
16. Bernatchez G, Giroux V, Lassalle T, Carpentier AC, Rivard N, Carrier JC. ERRalpha metabolic nuclear receptor controls growth of colon cancer cells. *Carcinogenesis*. 2013; 34:2253–2261.
17. Deblois G, St-Pierre J, Giguere V. The PGC-1/ERR signaling axis in cancer. *Oncogene*. 2013; 32:3483–3490.
18. Busch BB, Stevens WC Jr, Martin R, Ordentlich P, Zhou S, Sapp DW, Horlick RA, Mohan R. Identification of a selective inverse agonist for the orphan nuclear receptor estrogen-related receptor alpha. *Journal of medicinal chemistry*. 2004; 47:5593–5596.
19. Wang J, Wang Y, Wong C. Oestrogen-related receptor alpha inverse agonist XCT-790 arrests A549 lung cancer cell population growth by inducing mitochondrial reactive oxygen species production. *Cell proliferation*. 2010; 43:103–113.
20. May FE. Novel drugs that target the estrogen-related receptor alpha: their therapeutic potential in breast cancer. *Cancer management and research*. 2014; 6:225–252.
21. Seely J, Amigh KS, Suzuki T, Mayhew B, Sasano H, Giguere V, Laganier J, Carr BR, Rainey WE. Transcriptional regulation of dehydroepiandrosterone sulfotransferase (SULT2A1) by estrogen-related receptor alpha. *Endocrinology*. 2005; 146:3605–3613.
22. Felizola SJ, Nakamura Y, Hui XG, Satoh F, Morimoto R, K MM, Midorikawa S, Suzuki S, Rainey WE, Sasano H. Estrogen-related receptor alpha in normal adrenal cortex and adrenocortical tumors: involvement in development and oncogenesis. *Molecular and cellular endocrinology*. 2013; 365:207–211.
23. Lanvin O, Bianco S, Kersual N, Chalbos D, Vanacker JM. Potentiation of ICI182,780 (Fulvestrant)-induced estrogen receptor-alpha degradation by the estrogen receptor-related receptor-alpha inverse agonist XCT790. *The Journal of biological chemistry*. 2007; 282:28328–28334.
24. Chang CY, McDonnell DP. Molecular pathways: the metabolic regulator estrogen-related receptor alpha as a therapeutic target in cancer. *Clinical cancer research : an official journal of the American Association for Cancer Research*. 2012; 18:6089–6095.
25. Palmieri F. The mitochondrial transporter family SLC25: identification, properties and physiopathology. *Molecular aspects of medicine*. 2013; 34:465–484.
26. Dolce V, Rita Cappello A, Capobianco L. Mitochondrial tri-carboxylate and dicarboxylate-tricarboxylate carriers: from animals to plants. *IUBMB life*. 2014; 66:462–471.
27. Catalina-Rodriguez O, Kolukula VK, Tomita Y, Preet A, Palmieri F, Wellstein A, Byers S, Giaccia AJ, Glasgow E, Albanese C, Avantiaggiati ML. The mitochondrial citrate transporter, CIC, is essential for mitochondrial homeostasis. *Oncotarget*. 2012; 3:1220–1235.
28. Paglin S, Hollister T, Delohery T, Hackett N, McMhill M, Sphicas E, Domingo D, Yahalom J. A Novel Response of Cancer Cells to Radiation Involves Autophagy and Formation of Acidic Vesicles. *Cancer research*. 2001; 61:439–444.
29. Capparelli C, Whitaker-Menezes D, Guido C, Balliet R, Pestell TG, Howell A, Sneddon S, Pestell RG, Martinez-Outschoorn U, Lisanti MP, Sotgia F. CTGF drives autophagy, glycolysis and senescence in cancer-associated fibroblasts via HIF1 activation, metabolically promoting tumor growth. *Cell Cycle*. 2012; 11:2272–2284.
30. Xu Y, Qi Y, Zhu Y, Ning G, Huang Y. Molecular markers and targeted therapies for adrenocortical carcinoma. *Clinical endocrinology*. 2014; 80:159–168.

31. Cantor JR, Sabatini DM. Cancer cell metabolism: one hallmark, many faces. *Cancer discovery*. 2012; 2:881–898.
32. Deblois G, Giguere V. Oestrogen-related receptors in breast cancer: control of cellular metabolism and beyond. *Nature reviews Cancer*. 2013; 13:27–36.
33. Lam SS, Mak AS, Yam JW, Cheung AN, Ngan HY, Wong AS. Targeting estrogen-related receptor alpha inhibits epithelial-to-mesenchymal transition and stem cell properties of ovarian cancer cells. *Molecular therapy : the journal of the American Society of Gene Therapy*. 2014; 22:743–751.
34. Chang CY, Kazmin D, Jasper JS, Kunder R, Zuercher WJ, McDonnell DP. The metabolic regulator ERRalpha, a downstream target of HER2/IGF-1R, as a therapeutic target in breast cancer. *Cancer cell*. 2011; 20:500–510.
35. Parzych KR, Klionsky DJ. An overview of autophagy: morphology, mechanism, and regulation. *Antioxidants & redox signaling*. 2014; 20:460–473.
36. Eskelinen EL. Roles of LAMP-1 and LAMP-2 in lysosome biogenesis and autophagy. *Molecular aspects of medicine*. 2006; 27:495–502.
37. Chisamore MJ, Wilkinson HA, Flores O, Chen JD. Estrogen-related receptor-alpha antagonist inhibits both estrogen receptor-positive and estrogen receptor-negative breast tumor growth in mouse xenografts. *Molecular cancer therapeutics*. 2009; 8:672–681.
38. Michalek RD, Gerriets VA, Nichols AG, Inoue M, Kazmin D, Chang CY, Dwyer MA, Nelson ER, Pollizzi KN, Ilkayeva O, Giguere V, Zuercher WJ, Powell JD, Shinohara ML, McDonnell DP, Rathmell JC. Estrogen-related receptor-alpha is a metabolic regulator of effector T-cell activation and differentiation. *Proceedings of the National Academy of Sciences of the United States of America*. 2011; 108:18348–18353.
39. Allred DC, Harvey JM, Berardo M, Clark GM. Prognostic and predictive factors in breast cancer by immunohistochemical analysis. *Modern pathology : an official journal of the United States and Canadian Academy of Pathology, Inc.* 1998; 11:155–168.
40. Bonofiglio D, Santoro A, Martello E, Vizza D, Rovito D, Cappello AR, Barone I, Giordano C, Panza S, Catalano S, Iacobazzi V, Dolce V, Ando S. Mechanisms of divergent effects of activated peroxisome proliferator-activated receptor-gamma on mitochondrial citrate carrier expression in 3T3-L1 fibroblasts and mature adipocytes. *Biochimica et biophysica acta*. 2013; 1831:1027–1036.
41. Palmieri F, Indiveri C, Bisaccia F, Iacobazzi V. Mitochondrial metabolite carrier proteins: purification, reconstitution, and transport studies. *Methods in enzymology*. 1995; 260:349–369.

Bergamot (*Citrus bergamia* Risso) Flavonoids and Their Potential Benefits in Human Hyperlipidemia and Atherosclerosis: an Overview

A.R. Cappello^{*,#}, V. Dolce^{*,#}, D. Iacopetta, M. Martello, M. Fiorillo, R. Curcio, L. Muto and D. Dhanyalayam



A.R. Cappello

Department of Pharmacy, Health and Nutritional Sciences, University of Calabria, 87036 Arcavacata di Rende (Cosenza) Italy

Abstract: Elevated serum cholesterol, triglycerides and LDL levels are often associated with an increased incidence of atherosclerosis and coronary artery disease. The most effective therapeutic strategy against these diseases is based on statins administration, nevertheless some patients, especially those with metabolic syndrome fail to achieve their recommended LDL targets with statin therapy, moreover, it may induce many serious side effects. Several scientific studies have highlighted a strong correlation between diets rich in flavonoids and cardiovascular risk reduction. In

particular, *Citrus bergamia* Risso, also known as bergamot, has shown a significant degree of hypocholesterolemic and antioxidant/radical scavenging activities. In addition, this fruit has attracted considerable attention due to its peculiar flavonoid composition, since it contains some flavanones that can act as natural statins. Hence, the study of bergamot flavonoids as metabolic regulators offers a great opportunity for screening and discovery of new therapeutic agents. Cholesterol metabolism, flavonoid composition and potential therapeutic use of *C. bergamia* Risso will be discussed in the following review.



D. Dhanyalayam

Keywords: Bergamot fruit, flavonoids, hyperlipidemia, atherosclerosis, 3-hydroxy-3-methylglutaryl-CoA reductase enzyme.

INTRODUCTION

The risk for atherosclerosis and coronary heart disease is increased in patients with elevated serum concentrations of low-density lipoproteins cholesterol (LDL), total cholesterol (TC) and triglycerides (TG) [1-5]. Several meta-analysis studies showed that statin therapy can reduce the 5-year incidence of cardiovascular diseases, by about one fifth per mmol/L reduction in LDL cholesterol [6-8].

It is well-known that statins are able to inhibit 3-hydroxy-3-methylglutaryl-CoA reductase (HMGR) activity, the rate-limiting enzyme of cholesterol biosynthesis [9]. Statin administration is one of the most widely used approaches to lower serum LDL level and to reduce cardiovascular event rates [10-12]. However, many patients, especially those with the dyslipidemia associated with metabolic syndrome, are unable to reach their lipid treatment goals on statins alone [2]. Furthermore, patients might be statin-intolerant and experience significant side-effects [3], hence the importance of finding new drugs acting as statins.

Some foods were shown to possess these therapeutic properties; in particular, daily consumption of *Citrus* fruit

juice was shown to positively influence serum lipid levels and to decrease coronary heart disease risk [13]. Their hypolipidemic effects can be due to the presence of flavonoids, pectins and ascorbic acid, which have a high antioxidant potential and may interfere with cholesterol metabolism [14-19].

Flavonoids are aromatic secondary plant metabolites, having strong antioxidant and radical scavenging activities [15, 20]. Their intake was associated with a reduced risk for certain chronic diseases such as cardiovascular disorders and cancerous processes [21-23]. Flavonoids exhibited antiviral, antimicrobial and anti-inflammatory activities [23-25], moreover, they were able to inhibit human platelet aggregation [26] and to support a correct immune response [27].

Bergamot, the common name of *Citrus bergamia* Risso, belongs to the family Rutaceae, subfamily Esperidea and it has been widespread in the Mediterranean area for centuries. Over the past few years, thanks to the growing interest in bioactive compounds, bergamot fruit has attracted attention for its remarkable flavonoid composition. The first part of this review will report an overview on cholesterol metabolism, in the second part, literature data regarding flavonoid composition and distribution in bergamot fruit will be analysed. The last part will focus on the scientific evidence concerning the bioactivities of bergamot flavonoids and their potential utility for human health as well as their uses in atherosclerosis and coronary heart disease treatments.

*Address correspondence to these authors at the Department of Pharmacy, Health and Nutritional Sciences, University of Calabria 87036 Arcavacata di Rende (Cosenza) Italy; Tel: +39 0 984493177; Fax: +39 0 984493107; E-mail: annarita.cappello@unical.it; and Tel: +39 0 984493119; Fax: +39 0 984493107; E-mail: vincenza.dolce@unical.it;

[#]These authors contributed equally to this work.

1. CHOLESTEROL HOMEOSTASIS AND REGULATION

Cholesterol body homeostasis is mainly due to the regulation of its endogenous synthesis, intestinal absorption, excretion and hepatic conversion (Fig. 1).

Cholesterol *de novo* synthesis occurs mainly in the liver and, in human, it accounts for more than 70% of body cholesterol. Cholesterol intestinal absorption depends on diet composition. Excess liver cholesterol can be directly excreted as biliary sterols or converted into bile acids, both are eliminated via feces.

Cholesterol absorption is controlled by at least two types of transporters, Niemann-Pick C1-Like 1 (NPC1L1) as influx transporter and ATP-Binding Cassette (ABC) proteins as efflux transporters [28]. NPC1L1 transports cholesterol from intestinal lumen into enterocytes and it reabsorbs free

cholesterol back into hepatocyte from bile [29]. ABCG5 and ABCG8 reduce cholesterol absorption in the intestinal lumen and exclude cholesterol from liver to the bile duct (Fig. 1). ABCG1 and ABCA1 are involved in reverse cholesterol transport, the pathway by which peripheral cell cholesterol can be returned to the liver for excretion [30].

Regulation of cholesterol homeostasis is achieved by proteins such as sterol regulatory element-binding proteins (SREBPs) and AMP-Activated Protein Kinase (AMPK); by nuclear receptors such as peroxisome proliferator activated receptors (PPARs) and liver X receptors (LXRs); by microRNAs (miRNAs).

SREBPs are key transcription regulators encoded by two genes, SREBP-1 and SREBP-2. SREBP-1 upregulates the transcription of some hepatic lipogenic genes [31-35]. SREBP-2 modulates the transcription of some sterol

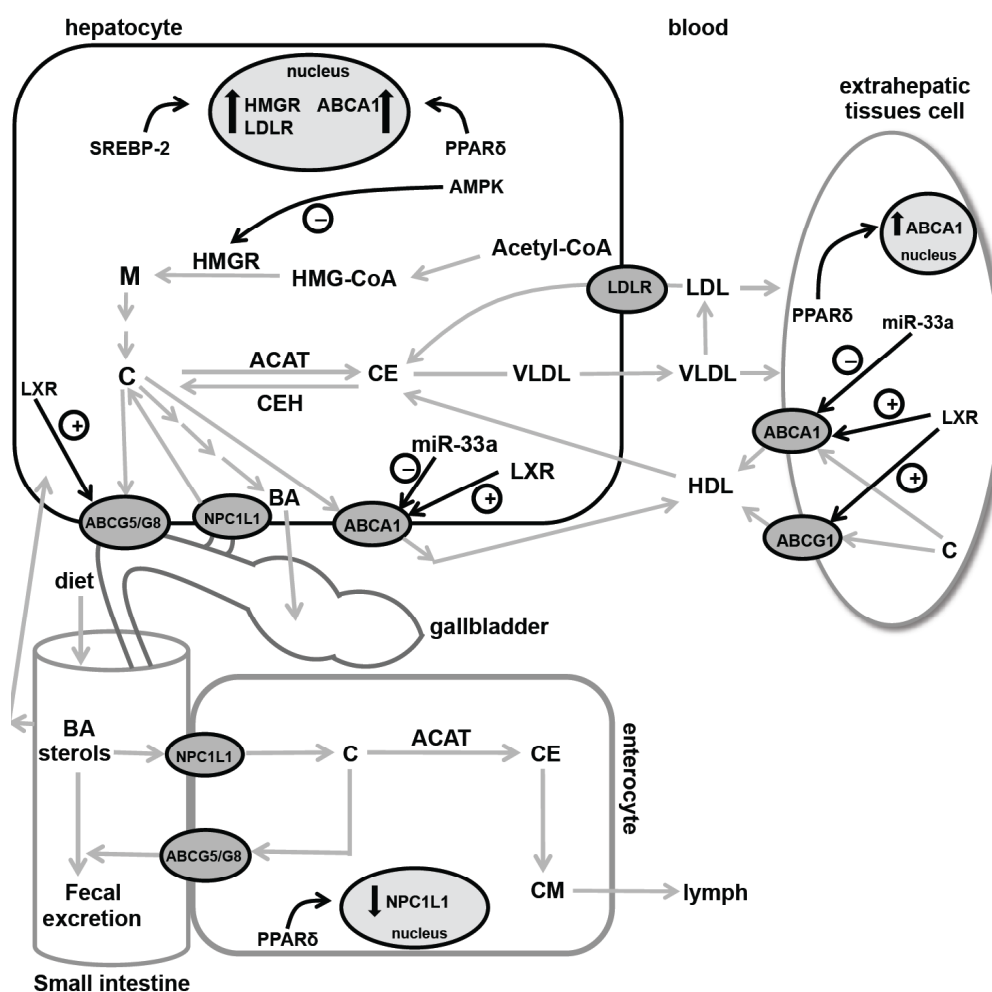


Fig. (1). Overview of cholesterol homeostasis and regulation in liver, small intestine, extrahepatic tissues, and plasma. The regulation is indicated with black arrows. \oplus indicates activation while \ominus indicates inhibition. ABCA1, ABCG1, and ABCG5/G8: ATP-binding cassette transporters; ACAT: acyl CoA:cholesterol acyltransferase; AMPK: AMP-activated protein kinase; BA: bile acid; C: cholesterol; CE: cholesteryl ester; CEH: cholesteryl ester hydrolase; CM: chylomicrons; HDL: high-density lipoprotein; HMGR: 3-hydroxy-3-methylglutaryl-CoA reductase; LDL: low-density lipoprotein; LDLR: low-density lipoprotein receptor; LXR: liver X receptor; M: mevalonate; miR-33a: microRNA-33a; MTP: microsomal triglyceride transfer protein; NPC1L1: Niemann-Pick C1-Like 1; PPAR δ : peroxisome proliferator activated receptor delta; SREBP2: sterol regulatory element binding protein-2; VLDL: very low density lipoprotein.

biosynthetic genes [36], for instance, when hepatocyte cholesterol content is low, expressions of HMGCR and LDLR are upregulated [36] (Fig. 1).

AMPK is a critical player in energy homeostasis at both cellular and whole body levels. An increased AMP to ATP ratio leads to AMPK activation through phosphorylation by at least three different upstream kinases [37]; in particular, when cellular cholesterol content is high, AMPK inactivates HMGCR by phosphorylation (Fig. 1) [38].

PPARs are members of nuclear hormone receptors superfamily that act as ligand-dependent transcription factors [39, 40]. PPAR α directly upregulates the transcription of genes involved in cholesterol catabolism [41]. PPAR γ integrates the control of energy, lipid and glucose homeostasis [42-44] and its activation also redirects effluxed cholesterol from liver toward adipose tissue uptake via scavenger receptor type-BI [45]. PPAR δ activation elevates serum HDL levels by increasing the expression of ABCA1 [30], it can reduce cholesterol absorption by decreasing NPC1L1 intestinal expression [29] and it also potentiates fecal neutral sterol secretion by increasing transintestinal cholesterol efflux [46].

LXRs play a primary role in reverse cholesterol transport, modulating the expression of several target genes as ABCA1, ABCG1, ABCG4 ABCG5, ABCG8 and apoE [47-50]. In the liver, when cellular cholesterol content is high, LXRs activation induces cholesterol excretion and/or efflux [50, 51].

MicroRNAs promote the down-regulation of their target genes by binding to specific regions located in the 3' UTR of their target mRNA [52]. MIR-33a is believed to minimize cholesterol export by the post-transcriptional repression of ABCA1 transporter (Fig. 1) [53, 54].

2. FLAVONOIDS IN BERGAMOT TISSUES

Plant flavonoids are a large group of very different compounds sharing the common feature of phenolic moieties [55]. The presence of a relatively large number of flavonoids is the result of many different possible combinations among polyhydroxylated aglycones and a limited number of mono- and disaccharides. The most commonly found sugars are hexoses, such as glucose, galactose and rhamnose or pentoses such as arabinose and xylose. They are, with a few notable exceptions, plant metabolites deriving from the shikimate pathway and the phenylpropanoid metabolism [56]. In recent years, flavonoids have attracted tremendous attention due to the protection that they provide against some types of cardiovascular diseases [57]. As a consequence, many studies have been directed to the characterization of the flavonoid fractions and to the isolation of the most representative flavonoids present in the most common *Citrus* species, as well as of flavonoids present in many local species such as *C. bergamia* Risso [58, 59]. Bergamot fruit presents an external part, epicarp or flavedo yellow coloured; a middle part, mesocarp or albedo, that is a spongy white inner layer and an inner part, endocarp or pulp. Albedo and flavedo peeled off together are called peel. Bergamot

essential oil is obtained from this fraction by cold press; it is composed of a volatile (93–96%) and a non-volatile fraction (4–7%).

The classes of flavonoids present in *C. bergamia* Risso fractions are flavanones and flavones. Flavanones are present as flavanone-O-glycosides, recently, flavanones diglycosides carrying the 3-hydroxy-3-methylglutaric acid (HMG) moiety have also been detected [60-62]. Flavones are present as flavone-O-glycosides, flavone-C-glycosides or polymethoxy-flavones (Table 1).

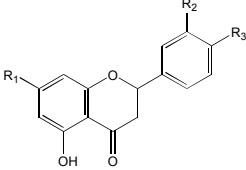
A comparative study on flavonoid composition in fruit tissues of different *Citrus* species has been reported by Nogata *et al.* [59], showing that bergamot fruit has a peculiar flavonoid composition. In particular, it contains neoerioditrin in exceptionally large amount (288 mg/100 g fresh weight) and it is relatively rich in neohesperidin, naringin, poncirin, rhoifolin, and neodiosmin (590, 438, 1240, 43 and 33 mg/100 g fresh weight, respectively) with respect to the other *Citrus* fruits analyzed. Furthermore, it contains very little amount of hesperidin (2 mg/100 g fresh weight).

Table 1 lists structure and tissue distribution of flavonoids, in *C. bergamia* Risso as described in literature.

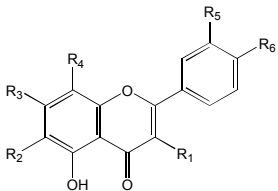
Flavanone-O-glycosides are present in all the analysed parts, in particular the most abundant are naringin, neoerioditrin, neohesperidin and poncirin, whereas hesperidin and neoponcirin have been detected in a very low amount [59]. They are also present in the peel, but it could be noted that when it is splitted into albedo and flavedo, these compounds are mainly present in albedo [59]. Moreover, poncirin, which is present in huge amount in hand-squeezed juice, is absent in industrial juice, this may be due to the pressing process used to extract industrial juices [58]. In addition, three acylated flavanones, which seem to correspond to di-oxalate derivatives of neoerioditrin, naringin and neohesperidin, have been identified in bergamot juice [63]. The HMG-conjugated flavanones, brutieridin, melitidin and HMG-neoerioditrin have also been detected at different concentrations depending on the ripening stage; they may be found in bergamot fruit either in juice or in albedo and flavedo [60-62].

Flavone-O-glycosides present a different tissue distribution. All these compounds are present in the peel, with the exception of chrysoeriol 7-O-neohesperidoside, chrysoeriol 7-O-neohesperidoside-4'-glucoside and rhoifolin 4'-glucoside [59, 64]. Diosmetin mono-glucoside, diosmetin mono-rhamnoside and apigenin mono-glucoside/mono-rhamnoside has been detected in bergamot peel [64] but not in albedo and flavedo. It could be explained because, according to this author, bergamot peel is a mix of seeds, pulp and deoiled flavedo after essential oil and juice extraction. Furthermore, rutin, that is absent in albedo, has been found in large amount in flavedo [64]. All these compounds have been revealed in the juice [58, 59, 63, 65-67], with the exception of diosmetin mono-rhamnoside and diosmetin mono-glucoside; this latter has been detected in industrial juice, probably because fruit industrial processing leads to juices contaminated with peel constituents [58].

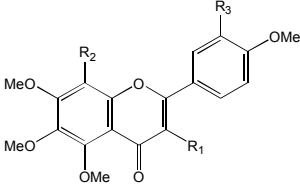
Table 1. Flavonoids identified in bergamot fruit.

Flavanone-O-glycosides	Peel	Albedo	Flavedo	Juice	Industrial juice
	[59, 84, 92]	[59, 60, 79]	[59, 60, 79]	[58-60, 64-67, 79]	[58]
Eriocitrin (eriodictyol 7-O-rutinoside) R ₁ =O-rutinoside, R ₂ =OH, R ₃ =OH	X	X	X	X	X
Eriodictyol mono-rhamnoside Most likely 7-O-substituted	X				
Hesperidin (hesperetin 7-O-rutinoside) R ₁ =O-rutinoside, R ₂ =OH, R ₃ =OCH ₃	X	X		X	
Hesperetin mono-rhamnoside Most likely 7-O-substituted	X				
Naringin (naringenin 7-O-neohesperidoside) R ₁ =O-neohesperidose, R ₂ =H, R ₃ =OH	X	X	X	X	X
Naringenin mono-rhamnoside Most likely 7-O-substituted	X	X	X	X	X
Narirutin (naringenin 7-O-rutinoside) R ₁ =O-rutinoside, R ₂ =H, R ₃ =OH	X	X	X	X	
Neoeriocitrin (eriodictyol 7-O-neohesperidoside) R ₁ =O-neohesperidose, R ₂ =OH, R ₃ =OH	X	X	X	X	X
Neohesperidin (hesperetin 7-O-neohesperidoside) R ₁ =O-neohesperidose, R ₂ =OH, R ₃ =OCH ₃	X	X	X	X	X
Neoponcirin (isosakuranetin 7-O-rutinoside) R ₁ =O-rutinoside, R ₂ =H, R ₃ =OCH ₃	X	X	X	X	
Poncirin (isosakuranetin 7-O-neohesperidoside) R ₁ =O-neohesperidose, R ₂ =H, R ₃ =OCH ₃	X	X	X	X	
Neoeriocitrin di-oxalate R ₁ =O-neohesperidose -di-oxalate, R ₂ =OH, R ₃ =OH				X	
Naringin di-oxalate R ₁ =O-neohesperidose-di-oxalate R ₂ =OH, R ₃ =OH				X	
Neohesperidin di-oxalate R ₁ =O-neohesperidose -di-oxalate R ₂ =OCH ₃ , R ₃ =OH				X	
Brutieridin (hesperetin 7-2''-α-rhamnosyl-6''-3'''-hydroxy-3'''-methylglutaryl)-β-glucoside) R ₁ =O-rhamnosyl-HMG, R ₂ =OH, R ₃ =OCH ₃		X	X	X	
Melitidin (naringenin 7-2''-α-rhamnosyl-6''-3'''-hydroxy-3'''-methylglutaryl)-β-glucoside) R ₁ =O-rhamnosyl-HMG, R ₂ =H, R ₃ =OH		X	X	X	
Neoeriocitrin HMG conjugated		X	X	X	

(Table 1) Contd....

Flavone O-glycosides and C-glycosides	Peel	Albedo	Flavedo	Juice	Industrial juice
	[59, 84, 92]	[59, 60, 79]	[59, 60, 79]	[58-60, 64-67, 79]	[58]
Apigenin	X				
Mono-glucoside/mono-rhamnoside					
Chrysoeriol 7-O-neohesperidoside R ₁ =H, R ₂ =H, R ₃ =O-neohesperidose, R ₄ =H, R ₅ =OCH ₃ , R ₆ =OH				X	X
Chrysoeriol 7-O-neohesperidoside-4'-glucoside R ₁ =H, R ₂ =H, R ₃ =O-neohesperidose, R ₄ =H, R ₅ =OCH ₃ , R ₆ =O-glucoside				X	X
Diosmetin mono glucoside	X				X
Diosmetin mono rhamnoside	X				
Diosmin (diosmetin 7-O-rutinoside) R ₁ =H, R ₂ =H, R ₃ =O-rutinoside, R ₄ =H, R ₅ =OH, R ₆ =OCH ₃	X	X	X	X	
Neodiosmin (diosmetin 7-O-neohesperidoside) R ₁ =H, R ₂ =H, R ₃ =O-neohesperidose, R ₄ =H, R ₅ =OH, R ₆ =OCH ₃	X	X	X	X	X
Rhoifolin (apigenin 7-O-neohesperidoside) R ₁ =H, R ₂ =H, R ₃ =O-neohesperidose, R ₄ =H, R ₅ =OH, R ₆ =OH	X	X	X	X	X
Rhoifolin 4'-glucoside (apigenin 7-O-neohesperidoside 4'-glucoside) R ₁ =H, R ₂ =H, R ₃ =O-neohesperidose, R ₄ =H, R ₅ =OH, R ₆ =O-glucoside				X	X
Rutin (quercetin 3-O-rutinoside) R ₁ =O-rutinoside, R ₂ =H, R ₃ =OH, R ₄ =H, R ₅ =OH, R ₆ =OH	X		X	X	
Isovitexin (apigenin 6-C-glucoside) R ₁ =H, R ₂ =glucoside, R ₃ =OH, R ₄ =H, R ₅ =H, R ₆ =OH				X	X
Luteolin	X				
Mono-glucoside/mono-rhamnoside					
Lucenin-2 (luteolin 6,8-di-C-glucoside) R ₁ =H, R ₂ =glucoside, R ₃ =OH, R ₄ =glucoside, R ₅ =OH, R ₆ =OH				X	X
Lucenin-2 4'-methyl ether (diosmetin 6,8-di-C-glucoside) R ₁ =H, R ₂ =glucoside, R ₃ =OH, R ₄ =glucoside, R ₅ =OH, R ₆ =OCH ₃	X			X	X
Stellarin-2 (chrysoeriol 6,8-di-C-glucoside) R ₁ =H, R ₂ =glucoside, R ₃ =OH, R ₄ =glucoside, R ₅ =OCH ₃ , R ₆ =OH				X	X
Scoparin (chrysoeriol 8-C-glucoside) R ₁ =H, R ₂ =H, R ₃ =OH, R ₄ =glucoside, R ₅ =OCH ₃ , R ₆ =OH				X	X
Orientin 4'-methyl ether (diosmetin 8-C-glucoside) R ₁ =H, R ₂ =H, R ₃ =OH, R ₄ =glucoside, R ₅ =OH, R ₆ =OCH ₃				X	
Vicenin-2 (apigenin 6,8-di-C-glucoside) R ₁ =H, R ₂ =glucoside, R ₃ =OH, R ₄ =glucoside, R ₅ =H, R ₆ =OH	X			X	

(Table 1) Contd....

Polymethoxy flavones	Peel	Albedo	Flavedo	Juice	Industrial juice
	[59, 84, 92]	[59, 60, 79]	[59, 60, 79]	[58-60, 64-67, 79]	[58]
Sinensetin (3',4',5,6,7-pentamethoxyflavone) R ₁ =H, R ₂ =H, R ₃ =OCH ₃	X		X		
Nobiletin (3',4',5,6,7,8,-esamethoxyflavone) R ₁ =H, R ₂ =OCH ₃ , R ₃ =OCH ₃	X	X	X		
Tangeretin (4',5,6,7,8-pentamethoxyflavone) R ₁ =H, R ₂ =OCH ₃ , R ₃ =H	X		X		

Flavone-C-glycosides are mainly present in the juice, similarly to flavanone-O-glycosides some of these compounds lack in industrial juice [58, 63, 65-68]. In bergamot essential oil (data not showed) only two flavonoids have been detected: sinensetin and tetra-O-methylscutellarein. This latter has been detected in essential oil [69].

3. HYPOLIPIDEMIC AND ANTIATHEROSCLEROTIC PROPERTIES OF BERGAMOT DERIVATIVES

Hypolipidemic effects of *Citrus* species are due to several components, such as flavonoids, pectins and ascorbic acid. Flavonoids are believed to inhibit LDL oxidation and to increase LDL reuptake, furthermore, they can interfere with fecal excretion of bile acids and with HMGR, LDLR and FASN functions [14, 70-72]. In particular, naringin seems to be active on atherosclerosis, as demonstrated by animal studies [73], neoeriocitrin is believed to strongly inhibit LDL oxidation [74] whereas, HMG-flavonoids could be able to inhibit HMGR [60]. These observations have provided the rationale to investigate the protective hypolipidemic effect of bergamot extracts in animal models and in human patients.

Miceli *et al.* [75] demonstrated that daily administration of bergamot juice to hypercholesterolemic rats caused a significant reduction in TC, TG and LDL levels, an increase in serum HDL levels and a protective effect on hepatic parenchyma. In addition, fecal output of total bile acids and neutral sterols was enhanced in the bergamot juice treated group in comparison with the hyperlipidemic group. These results are in agree with previous studies, which hypothesized that pectins and flavonoids were able to lower serum cholesterol levels by modulating hepatic HMG-CoA concentration. It could be noted that in this study, the potential side-effect due to bergamottin presence in bergamot juice was not investigated. Bergamot juice is rich in bergamottin (ranging from 18 to 61 mg/L) [63, 66], a furanocoumarin compound that inhibits cytochrome P450 3A4 enzyme activity, significantly increasing the oral bioavailability of several drugs metabolized primarily by this cytochrome [74, 76].

This problem was overcome by Mollace *et al.* [77], that analyzed the hypolipidemic effect of a defurocoumarinized bergamot-derived polyphenolic fraction supplemented with ascorbic acid on animal models of diet-induced hyperlipidemia and in patients suffering from metabolic syndrome [77]. They found that oral administration of this fraction both in animal and in patients, caused a significant reduction of TC, TG and glycemia with a concomitant increase of HDL levels. In particular, in 59 patients with metabolic syndrome a 30-days treatment period with bergamot-derived polyphenolic fraction, administered at the dose of 1 g/die, reduced the serum levels of TC, LDL and TG by 30%, 33% and 41%, respectively [26]. This effect was associated with a significant improvement in vascular reactivity in patients with both hyperlipidemia and hyperglycemia, suggesting a potential protective role for the use of bergamot-derived polyphenolic fraction in these patients.

Recent prospective studies, led on patients with hyperlipidemia demonstrated that administration of a defurocoumarinized bergamot-derived polyphenolic fraction was able to reduce TC level by 31%. In the same conditions, rosuvastatin administration (10 mg/die) caused a similar reduction of TC content (30%). Their association produced a considerable enhancement of rosuvastatin hypolipidemic effect, causing a reduction of TC level by 38%, normalizing the serum lipid profile [78].

The authors suggested that the observed hypolipidemic effect could be mainly due to the presence in bergamot-derived polyphenolic fraction of melitidin, brutieridin and HMG-neoeriocitrin. This hypothesis was investigated by Di Donna *et al.* [79] in a hypercholesterolemic rat model, by measuring the effects on lipid profile of administration of HMG-flavanones enriched fraction (62% of brutieridin, 14% of melitidin and 15% of HMG-neoeriocitrin), extracted from bergamot fruit, in comparison with simvastatin. HMGR, LDLR and FASN transcription levels and their correlated protein amounts were evaluated.

In this study, simvastatin and HMG-flavanones enriched fraction singularly administrated reduced levels of TC (30%, 20% respectively), TG (32%, 20% respectively), VLDL (33%, 28% respectively) and LDL (24%, 40% respectively), whereas an increase of 20% in HDL content was observed exclusively in rats treated by HMG-flavanones enriched fraction [61]. Furthermore, according to the previously published data, HMGR, LDLR and FAS transcription levels were found up-regulated. An increased amount of their corresponding proteins was detected [80]. Genotoxicity and toxicity were not observed by testing HMG-flavanones enriched fraction *in vitro*. The authors hypothesized that HMGR inhibition leads to a reduction of endogenous cholesterol level which, in turn, is responsible of HMGR and LDLR transcriptional up-regulation, as well of the higher LDLR exposure within the hepatocytes membrane, through a compensatory mechanism based on SREBPs pathway. Furthermore, it was highlighted that cholesterol depletion below a certain threshold is known to be responsible for FASN genic transcription increase, via SREBPs activation, which is one of the observed effects. It was suggested that transcriptional up-regulation of these genes and the corresponding increased protein amounts could be occurred via SREBPs pathway (Fig. 2).

Beside the already described hypolipidemic effect, flavonoids, in particular naringin, have received considerable attention because of their antioxidant/radical scavenging properties [15, 20]. Increasing clinical evidences support the hypothesis that phospholipid oxidation products may play a role in atherosclerosis. This was firstly suggested by demonstrating that mildly oxidized LDL proatherogenic activities were present in the fraction containing oxidized phospholipids. Subsequently, phospholipid oxidation products

were reported to accumulate in hyperlipidemic plasma, atherosclerotic lesions and in several diseases that predispose to stroke [81-83].

Trombetta *et al.* [84] reported that two flavonoid-rich extracts from bergamot peel, endowed with radical-scavenging properties and lacking genotoxic activity, were able to prevent alterations induced by the pleiotropic inflammatory cytokine tumor necrosis factor- α (TNF- α) on human umbilical vein endothelial cells (HUVECs). This study was led by monitoring intracellular levels of malondialdehyde, reduced and oxidized glutathione levels, superoxide dismutase activity and the activation status of nuclear factor- κ B. To clarify the mechanisms involved in flavonoid protective activity, flavonoid-rich extracts were tested *in vitro* for their ability to inhibit cyclooxygenase-1 (COX-1) and cyclooxygenase-2 (COX-2) activity, in a human whole blood model. Conversely to literature data [85], authors excluded that the protective effect of bergamot peel extracts against TNF- α -induced changes in HUVECs might be due to their capability to inhibit COX-1 or COX-2 pathways, because these phytocomplexes were unable to modify prostaglandin E2 and tromboxan B2 release when they were tested on human whole blood.

Several investigations suggested that phospholipid oxidation products may play a pathogenic role in progressive renal damage [86, 87]. A prominent mechanism probably involved in the deleterious effects of hypercholesterolemia on the kidney was an increased formation of reactive oxygen species. In addition, oxidized LDL particles were injurious to renal tubular epithelial cells and they might contribute to tubulointerstitial damage and glomerulosclerosis [88]. In an experimental model of short-term diet-induced

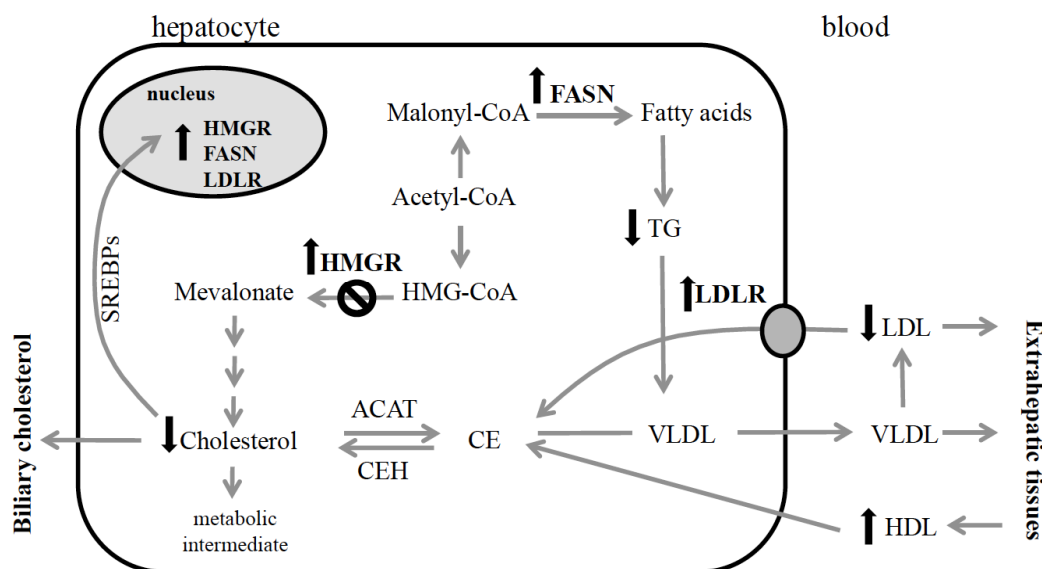


Fig. (2). Model depicting HMG flavanones enriched fraction effects on lipids metabolism elicited in rat hepatocytes (from Di Donna *et al* 2014 [61]). Black arrows indicate HMG flavanones enriched fraction effects on genes, enzymes and metabolites levels. ⊙ indicates enzymatic inhibition. ACAT: Acyl-CoA:cholesterol acyltransferase; CE: cholesteryl ester; CEH: cholesteryl ester hydrolase; FASN: fatty acid synthase; HDL: high-density lipoprotein; HMG-CoA: 3-hydroxy-3-methylglutaryl-CoA; HMGR: 3-hydroxy-3-methylglutaryl-CoA reductase; LDL: low density lipoprotein; LDLR: low density lipoprotein receptor; SREBPs: sterol response element binding proteins; TG: triglycerides; VLDL: very low density lipoprotein.

hypercholesterolemia [89], a significant decrease in renal lipid peroxidation was observed after bergamot juice administration, as shown by the low malondialdehyde levels found. Furthermore, analysis of kidney histopathological sections supported the biochemical data, indicating a protective effect of bergamot juice on the development of kidney injury induced by the hypercholesterolemic diet. The authors hypothesized that the beneficial effect on renal parenchyma was due to the great abundance of flavonoids in bergamot juice, believed to reduce oxidative damage *in vivo*.

CONCLUSION

HMGR inhibitors (statins) are the most effective, practical and largely prescribed class of drugs for reducing LDL concentrations [10, 11]. Nevertheless some patients, especially those with metabolic syndrome do not achieve their recommended LDL targets with statin therapy [77, 90]. Moreover, statins may induce many side effects, including myalgia, myopathy, liver diseases and rhabdomyolysis [91]. Many studies demonstrated a relationship between the intake of flavonoid-rich foods and a reduced risk for cardiovascular disease [13]. Bergamot fruit is very rich in many peculiar bioactive flavonoids compared to other *Citrus* fruits [15-18], hence their evaluation as metabolic regulators might represent an attractive strategy in drug discovery. The aim of this review is to provide an overview on all flavonoids detected in *C. bergamia* Risso and on the current knowledge of their hypolipidemic effects [58-69], summarizing the results obtained from different *in vivo* studies [61, 75, 77, 89].

All data reported suggest that *C. bergamia* Risso flavonoids might be used in nutraceutical products or in functional foods, even if additional studies are needed to fully reveal their interaction with upstream mediators of lipid metabolism pathways. Furthermore, since only few studies on flavonoids administration in humans are available, further clinical studies are required to focus on dose, bioavailability, efficacy and safety of this class of flavonoids in humans.

LIST OF ABBREVIATIONS

ABC	=	ATP-Binding Cassette
AMPK	=	AMP- activated protein kinase
COX-1	=	cyclooxygenase-1
COX-2	=	cyclooxygenase-2
FASN	=	fatty acid synthase
HDL	=	high-density lipoprotein
HMG-CoA	=	3-hydroxy-3-methylglutaryl-CoA
HMGR	=	3-hydroxy-3-methylglutaryl-CoA reductase
HUVECs	=	human umbilical vein endothelial cells
LDL	=	low-density lipoprotein
LDLR	=	low-density lipoprotein receptor
LXRs	=	liver X receptors
microRNAs	=	miRNAs

NPC1L1	=	Niemann-Pick C1-Like 1
PPARs	=	peroxisome proliferator activated receptors
SREBPs	=	sterol regulatory element-binding proteins
TC	=	total cholesterol
TG	=	triglycerides
TNF- α	=	tumor necrosis factor- α
VLDL	=	very low-density lipoprotein

CONFLICT OF INTEREST

The author(s) confirm that this article content has no conflict of interest.

ACKNOWLEDGEMENTS

We thank Dr. Bela Oszvari for critical reading of the manuscript.

SUPPLEMENTARY MATERIALS

Supplementary material is available on the publisher's web site along with the published article.

REFERENCES

- Balbisi, E.A. Management of hyperlipidemia: new LDL-C targets for persons at high-risk for cardiovascular events. *Med. Sci. Monit.*, **2006**, 12(2), RA34-39.
- Maxfield, F.R. Tabas, I. Role of cholesterol and lipid organization in disease. *Nature*, **2005**, 438(7068), 612-621.
- Gielen, S.; Sandri, M.; Schuler, G. Teupser, D. Risk factor management: antiatherogenic therapies. *Eur. J. Cardiovasc. Prev. Rehabil.*, **2009**, 16 Suppl 2(S29-36).
- Stamler, J.; Neaton, J.D.; Cohen, J.D.; Cutler, J.; Eberly, L.; Grandits, G.; Kuller, L.H.; Ockene, J.; Prineas, R. Group, M.R. Multiple risk factor intervention trial revisited: a new perspective based on nonfatal and fatal composite endpoints, coronary and cardiovascular, during the trial. *J. Am. Heart Assoc.*, **2012**, 1(5), e003640.
- Stamler, J. Neaton, J.D. The Multiple Risk Factor Intervention Trial (MRFIT)--importance then and now. *JAMA*, **2008**, 300(11), 1343-1345.
- Baigent, C.; Keech, A.; Kearney, P.M.; Blackwell, L.; Buck, G.; Pollicino, C.; Kirby, A.; Sourjina, T.; Peto, R.; Collins, R.; Simes, R. Cholesterol Treatment Trialists, C. Efficacy and safety of cholesterol-lowering treatment: prospective meta-analysis of data from 90,056 participants in 14 randomised trials of statins. *Lancet*, **2005**, 366(9493), 1267-1278.
- Boekholdt, S.M.; Hovingh, G.K.; Mora, S.; Arsenault, B.J.; Amarenco, P.; Pedersen, T.R.; LaRosa, J.C.; Waters, D.D.; DeMicco, D.A.; Simes, R.J.; Keech, A.C.; Colquhoun, D.; Hitman, G.A.; Betteridge, D.J.; Clearfield, M.B.; Downs, J.R.; Colhoun, H.M.; Gotto, A.M., Jr.; Ridker, P.M.; Grundy, S.M. Kastelein, J.J. Very low levels of atherogenic lipoproteins and the risk for cardiovascular events: a meta-analysis of statin trials. *J. Am. Coll. Cardiol.*, **2014**, 64(5), 485-494.
- Boekholdt, S.M.; Arsenault, B.J.; Mora, S.; Pedersen, T.R.; LaRosa, J.C.; Nestel, P.J.; Simes, R.J.; Durrington, P.; Hitman, G.A.; Welch, K.M.; DeMicco, D.A.; Zwiderman, A.H.; Clearfield, M.B.; Downs, J.R.; Tonkin, A.M.; Colhoun, H.M.; Gotto, A.M., Jr.; Ridker, P.M. Kastelein, J.J. Association of LDL cholesterol, non-HDL cholesterol, and apolipoprotein B levels with risk of cardiovascular events among patients treated with statins: a meta-analysis. *JAMA*, **2012**, 307(12), 1302-1309.
- Goldstein, J.L. Brown, M.S. Regulation of the mevalonate pathway. *Nature*, **1990**, 343(6257), 425-430.

- [10] Ross, S.D.; Allen, I.E.; Connelly, J.E.; Korenblat, B.M.; Smith, M.E.; Bishop, D. Luo, D. Clinical outcomes in statin treatment trials: a meta-analysis. *Arch. Intern. Med.*, **1999**, 159(15), 1793-1802.
- [11] Scharnagl, H.; Schinker, R.; Gierens, H.; Nauck, M.; Wieland, H. Marz, W. Effect of atorvastatin, simvastatin, and lovastatin on the metabolism of cholesterol and triacylglycerides in HepG2 cells. *Biochem. Pharmacol.*, **2001**, 62(11), 1545-1555.
- [12] Stone, N.J.; Robinson, J.G.; Lichtenstein, A.H.; Bairey Merz, C.N.; Blum, C.B.; Eckel, R.H.; Goldberg, A.C.; Gordon, D.; Levy, D.; Lloyd-Jones, D.M.; McBride, P.; Schwartz, J.S.; Shero, S.T.; Smith, S.C., Jr.; Watson, K.; Wilson, P.W.; Eddleman, K.M.; Jarrett, N.M.; LaBresh, K.; Nevo, L.; Wnek, J.; Anderson, J.L.; Halperin, J.L.; Albert, N.M.; Bozkurt, B.; Brindis, R.G.; Curtis, L.H.; DeMets, D.; Hochman, J.S.; Kovacs, R.J.; Ohman, E.M.; Pressler, S.J.; Sellke, F.W.; Shen, W.K.; Smith, S.C., Jr.; Tomaselli, G.F. American College of Cardiology/American Heart Association Task Force on Practice, G. 2013 ACC/AHA guideline on the treatment of blood cholesterol to reduce atherosclerotic cardiovascular risk in adults: a report of the American College of Cardiology/American Heart Association Task Force on Practice Guidelines. *Circulation*, **2014**, 129(25 Suppl 2), S1-45.
- [13] Assini, J.M.; Mulvihill, E.E. Huff, M.W. Citrus flavonoids and lipid metabolism. *Curr. Opin. Lipidol.*, **2013**, 24(1), 34-40.
- [14] Gorinstein, S.; Leontowicz, H.; Leontowicz, M.; Krzeminski, R.; Gralak, M.; Martin-Belloso, O.; Delgado-Licon, E.; Haruenkit, R.; Katrich, E.; Park, Y.S.; Jung, S.T. Trakhtenberg, S. Fresh Israeli Jaffa blond (Shamouti) orange and Israeli Jaffa red Star Ruby (Sunrise) grapefruit juices affect plasma lipid metabolism and antioxidant capacity in rats fed added cholesterol. *J. Agric. Food Chem.*, **2004**, 52(15), 4853-4859.
- [15] Gorinstein, S.; Leontowicz, H.; Leontowicz, M.; Krzeminski, R.; Gralak, M.; Delgado-Licon, E.; Martinez Ayala, A.L.; Katrich, E. Trakhtenberg, S. Changes in plasma lipid and antioxidant activity in rats as a result of naringin and red grapefruit supplementation. *J. Agric. Food Chem.*, **2005**, 53(8), 3223-3228.
- [16] Monforte, M.T.; Trovato, A.; Kirjavainen, S.; Forestieri, A.M.; Galati, E.M. Lo Curto, R.B. Biological effects of hesperidin, a Citrus flavonoid. (note II): hypolipidemic activity on experimental hypercholesterolemia in rat. *Farmaco*, **1995**, 50(9), 595-599.
- [17] Srinivasan, S. Pani, L. Antihyperlipidemic effect of diosmin: A citrus flavonoid on lipid metabolism in experimental diabetic rats. *Journal of Functional Foods*, **2013**, 5(1), 484-492.
- [18] Marounek, M.; Volek, Z.; Synytsya, A. Copikova, J. Effect of pectin and amidated pectin on cholesterol homeostasis and cecal metabolism in rats fed a high-cholesterol diet. *Physiol. Res.*, **2007**, 56(4), 433-442.
- [19] Lappano, R.; Rosano, C.; Madeo, A.; Albanito, L.; Plastina, P.; Gabriele, B.; Forti, L.; Stivala, L.A.; Iacopetta, D.; Dolce, V.; Ando, S.; Pezzi, V. Maggiolini, M. Structure-activity relationships of resveratrol and derivatives in breast cancer cells. *Mol. Nutr. Food Res.*, **2009**, 53(7), 845-858.
- [20] Burda, S. Oleszek, W. Antioxidant and antiradical activities of flavonoids. *J. Agric. Food Chem.*, **2001**, 49(6), 2774-2779.
- [21] Peterson, J.J.; Dwyer, J.T.; Jacques, P.F. McCullough, M.L. Associations between flavonoids and cardiovascular disease incidence or mortality in European and US populations. *Nutr. Rev.*, **2012**, 70(9), 491-508.
- [22] Garcia-Lafuente, A.; Guillamon, E.; Villares, A.; Rostagno, M.A. Martinez, J.A. Flavonoids as anti-inflammatory agents: implications in cancer and cardiovascular disease. *Inflamm. Res.*, **2009**, 58(9), 537-552.
- [23] Kim, H.P.; Son, K.H.; Chang, H.W. Kang, S.S. Anti-inflammatory plant flavonoids and cellular action mechanisms. *J. Pharmacol. Sci.*, **2004**, 96(3), 229-245.
- [24] Yin, D.; Li, J.; Lei, X.; Liu, Y.; Yang, Z. Chen, K. Antiviral Activity of Total Flavonoid Extracts from *Selaginella moellendorffii* Hieron against Coxsackie Virus B3 In Vitro and In Vivo. *Evid. Based Complement Alternat. Med.*, **2014**, 2014(950817).
- [25] Mandalari, G.; Bennett, R.N.; Bisignano, G.; Trombetta, D.; Saija, A.; Faulds, C.B.; Gasson, M.J. Narbad, A. Antimicrobial activity of flavonoids extracted from bergamot (*Citrus bergamia* Risso) peel, a byproduct of the essential oil industry. *J. Appl. Microbiol.*, **2007**, 103(6), 2056-2064.
- [26] Tijburg, L.B.; Mattern, T.; Folts, J.D.; Weisgerber, U.M. Katan, M.B. Tea flavonoids and cardiovascular disease: a review. *Crit. Rev. Food Sci. Nutr.*, **1997**, 37(8), 771-785.
- [27] Peluso, I.; Miglio, C.; Morabito, G.; Ioannone, F. Serafini, M. Flavonoids and immune function in human: a systematic review. *Crit. Rev. Food Sci. Nutr.*, **2015**, 55(3), 383-395.
- [28] Matsuo, M. ATP-binding cassette proteins involved in glucose and lipid homeostasis. *Biosci. Biotechnol. Biochem.*, **2010**, 74(5), 899-907.
- [29] Jia, L.; Betters, J.L. Yu, L. Niemann-pick C1-like 1 (NPC1L1) protein in intestinal and hepatic cholesterol transport. *Annu. Rev. Physiol.*, **2011**, 73(239-259).
- [30] Attie, A.D. ABCA1: at the nexus of cholesterol, HDL and atherosclerosis. *Trends Biochem. Sci.*, **2007**, 32(4), 172-179.
- [31] Sampath, H. Ntambi, J.M. Polyunsaturated fatty acid regulation of genes of lipid metabolism. *Annu. Rev. Nutr.*, **2005**, 25(317-340).
- [32] Santolla, M.F.; Lappano, R.; De Marco, P.; Pupo, M.; Vivacqua, A.; Sisci, D.; Abonante, S.; Iacopetta, D.; Cappello, A.R.; Dolce, V. Maggiolini, M. G protein-coupled estrogen receptor mediates the up-regulation of fatty acid synthase induced by 17beta-estradiol in cancer cells and cancer-associated fibroblasts. *J. Biol. Chem.*, **2012**, 287(52), 43234-43245.
- [33] Dolce, V.; Capobianco, L. Cappello, A.R. Mitochondrial tricarboxylate and dicarboxylate-tricarboxylate carriers: from animals to plants. *IUBMB Life*, **2014**, 66(7), 462-671.
- [34] Dolce, V.; Cappello, A.R.; Lappano, R. Maggiolini, M. Glycerophospholipid synthesis as a novel drug target against cancer. *Curr. Mol. Pharmacol.*, **2011**, 4(3), 167-175.
- [35] Cappello, A.R.; Guido, C.; Santoro, A.; Santoro, M.; Capobianco, L.; Montanaro, D.; Madeo, M.; Ando, S.; Dolce, V. Aquila, S. The mitochondrial citrate carrier (CIC) is present and regulates insulin secretion by human male gamete. *Endocrinology*, **2012**, 153(4), 1743-1754.
- [36] Goldstein, J.L. Brown, M.S. The LDL receptor. *Arterioscler. Thromb. Vasc. Biol.*, **2009**, 29(4), 431-438.
- [37] Steinberg, G.R. Kemp, B.E. AMPK in Health and Disease. *Physiol. Rev.*, **2009**, 89(3), 1025-1078.
- [38] Steck, T.L. Lange, Y. Cell cholesterol homeostasis: mediation by active cholesterol. *Trends Cell Bio.l.*, **2010**, 20(11), 680-687.
- [39] Desvergne, B. Wahli, W. Peroxisome proliferator-activated receptors: nuclear control of metabolism. *Endocr. Rev.*, **1999**, 20(5), 649-688.
- [40] Braissant, O.; Fougelle, F.; Scotto, C.; Dauca, M. Wahli, W. Differential expression of peroxisome proliferator-activated receptors (PPARs): tissue distribution of PPAR-alpha, -beta, and -gamma in the adult rat. *Endocrinology*, **1996**, 137(1), 354-366.
- [41] Bensinger, S.J. Tontonoz, P. Integration of metabolism and inflammation by lipid-activated nuclear receptors. *Nature*, **2008**, 454(7203), 470-477.
- [42] Chawla, A.; Repa, J.J.; Evans, R.M. Mangelsdorf, D.J. Nuclear receptors and lipid physiology: opening the X-files. *Science*, **2001**, 294(5548), 1866-1870.
- [43] Bonfiglio, D.; Santoro, A.; Martello, E.; Vizza, D.; Rovito, D.; Cappello, A.R.; Barone, I.; Giordano, C.; Panza, S.; Catalano, S.; Iacobazzi, V.; Dolce, V. Ando, S. Mechanisms of divergent effects of activated peroxisome proliferator-activated receptor-gamma on mitochondrial citrate carrier expression in 3T3-L1 fibroblasts and mature adipocytes. *Biochim. Biophys. Acta*, **2013**, 1831(6), 1027-1036.
- [44] Francis, G.A.; Fayard, E.; Picard, F. Auwerx, J. Nuclear receptors and the control of metabolism. *Annu. Rev. Physiol.*, **2003**, 65(261-311).
- [45] Toh, S.A.; Millar, J.S.; Billheimer, J.; Fuki, I.; Naik, S.U.; Macphee, C.; Walker, M. Rader, D.J. PPARgamma activation redirects macrophage cholesterol from fecal excretion to adipose tissue uptake in mice via SR-BI. *Biochem. Pharmacol.*, **2011**, 81(7), 934-941.
- [46] Vrins, C.L.; van der Velde, A.E.; van den Oever, K.; Levels, J.H.; Huet, S.; Oude Elferink, R.P.; Kuipers, F. Groen, A.K. Peroxisome proliferator-activated receptor delta activation leads to increased transintestinal cholesterol efflux. *J. Lipid Res.*, **2009**, 50(10), 2046-2054.
- [47] Kennedy, M.A.; Venkateswaran, A.; Tarr, P.T.; Xenarios, I.; Kudoh, J.; Shimizu, N. Edwards, P.A. Characterization of the human ABCG1 gene: liver X receptor activates an internal

- promoter that produces a novel transcript encoding an alternative form of the protein. *J. Biol. Chem.*, **2001**, 276(42), 39438-39447.
- [48] Wagner, B.L.; Valledor, A.F.; Shao, G.; Daige, C.L.; Bischoff, E.D.; Petrowski, M.; Jepsen, K.; Baek, S.H.; Heyman, R.A.; Rosenfeld, M.G.; Schulman, I.G. Glass, C.K. Promoter-specific roles for liver X receptor/corepressor complexes in the regulation of ABCA1 and SREBP1 gene expression. *Mol. Cell Biol.*, **2003**, 23(16), 5780-5789.
- [49] Laffitte, B.A.; Repa, J.J.; Joseph, S.B.; Wilpitz, D.C.; Kast, H.R.; Mangelsdorf, D.J. Tontonoz, P. LXRs control lipid-inducible expression of the apolipoprotein E gene in macrophages and adipocytes. *Proc. Natl. Acad. Sci. U S A*, **2001**, 98(2), 507-512.
- [50] Repa, J.J.; Berge, K.E.; Pomajzl, C.; Richardson, J.A.; Hobbs, H. Mangelsdorf, D.J. Regulation of ATP-binding cassette sterol transporters ABCG5 and ABCG8 by the liver X receptors alpha and beta. *J. Biol. Chem.*, **2002**, 277(21), 18793-18800.
- [51] Peet, D.J.; Turley, S.D.; Ma, W.; Janowski, B.A.; Lobaccaro, J.M.; Hammer, R.E. Mangelsdorf, D.J. Cholesterol and bile acid metabolism are impaired in mice lacking the nuclear oxysterol receptor LXR alpha. *Cell*, **1998**, 93(5), 693-704.
- [52] Shukla, G.C.; Singh, J. Barik, S. MicroRNAs: Processing, Maturation, Target Recognition and Regulatory Functions. *Mol. Cell Pharmacol.*, **2011**, 3(3), 83-92.
- [53] Najafi-Shoushtari, S.H.; Kristo, F.; Li, Y.; Shioda, T.; Cohen, D.E.; Gerszten, R.E. Naar, A.M. MicroRNA-33 and the SREBP host genes cooperate to control cholesterol homeostasis. *Science*, **2010**, 328(5985), 1566-1569.
- [54] Rayner, K.J.; Suarez, Y.; Davalos, A.; Parathath, S.; Fitzgerald, M.L.; Tamehiro, N.; Fisher, E.A.; Moore, K.J. Fernandez-Hernando, C. MiR-33 contributes to the regulation of cholesterol homeostasis. *Science*, **2010**, 328(5985), 1570-1573.
- [55] Harborne, J.B. Williams, C.A. Advances in flavonoid research since 1992. *Phytochemistry*, **2000**, 55(6), 481-504.
- [56] Vogt, T. Phenylpropanoid biosynthesis. *Mol. Plant*, **2010**, 3(1), 2-20.
- [57] Benavente-Garcia, O. Castillo, J. Update on uses and properties of citrus flavonoids: new findings in anticancer, cardiovascular, and anti-inflammatory activity. *J. Agric. Food Chem.*, **2008**, 56(15), 6185-6205.
- [58] Gattuso, G.; Barreca, D.; Gargiulli, C.; Leuzzi, U. Caristi, C. Flavonoid composition of Citrus juices. *Molecules*, **2007**, 12(8), 1641-1673.
- [59] Nogata, Y.; Sakamoto, K.; Shiratsuchi, H.; Ishii, T.; Yano, M. Ohta, H. Flavonoid composition of fruit tissues of citrus species. *Biosci. Biotechnol. Biochem.*, **2006**, 70(1), 178-192.
- [60] Di Donna, L.; De Luca, G.; Mazzotti, F.; Napoli, A.; Salerno, R.; Taverna, D. Sindona, G. Statin-like principles of bergamot fruit (Citrus bergamia): isolation of 3-hydroxymethylglutaryl flavonoid glycosides. *J. Nat. Prod.*, **2009**, 72(7), 1352-1354.
- [61] Di Donna, L.; Iacopetta, D.; Cappello, A.R.; Gallucci, G.; Martello, E.; Fiorillo, M.; Dolce, V. Sindona, G. Hypocholesterolaemic activity of 3-hydroxy-3-methyl-glutaryl flavanones enriched fraction from bergamot fruit (Citrus bergamia): "In vivo" studies. *J. Funct. Foods*, **2014**, 7(558-568).
- [62] Sindona, G.; Di Donna, L. Dolce, V. Natural molecules extracted from bergamot tissues, extraction process and pharmaceutical use., **April 15, 2010**, WO/2010/041290 A1(WO/2010/041290 A1).
- [63] Gardana, C.; Nalin, F. Simonetti, P. Evaluation of flavonoids and furanocoumarins from Citrus bergamia (Bergamot) juice and identification of new compounds. *Molecules*, **2008**, 13(9), 2220-2228.
- [64] Mandalari, G.; Bennett, R.N.; Bisignano, G.; Saija, A.; Dugo, G.; Lo Curto, R.B.; Faulds, C.B. Waldron, K.W. Characterization of flavonoids and pectins from bergamot (Citrus bergamia Risso) peel, a major byproduct of essential oil extraction. *J. Agric. Food Chem.*, **2006**, 54(1), 197-203.
- [65] Dugo, P.; Presti, M.L.; Ohman, M.; Fazio, A.; Dugo, G. Mondello, L. Determination of flavonoids in citrus juices by micro-HPLC-ESI/MS. *J. Sep. Sci.*, **2005**, 28(11), 1149-1156.
- [66] Gattuso, G.; Barreca, D.; Caristi, C.; Gargiulli, C. Leuzzi, U. Distribution of flavonoids and furocoumarins in juices from cultivars of Citrus bergamia Risso. *J. Agric. Food Chem.*, **2007**, 55(24), 9921-9927.
- [67] Gattuso, G.; Caristi, C.; Gargiulli, C.; Bellocco, E.; Toscano, G. Leuzzi, U. Flavonoid glycosides in bergamot juice (Citrus bergamia Risso). *J. Agric. Food Chem.*, **2006**, 54(11), 3929-3935.
- [68] Caristi, C.; Bellocco, E.; Gargiulli, C.; Toscano, G. Leuzzi, U. Flavone-di-C-glycosides in citrus juices from Southern Italy. *Food Chem.*, **2006**, 95(3), 431-437.
- [69] Dugo, P.; Mondello, L.; Dugo, L.; Stancanelli, R. Dugo, G. LC-MS for the identification of oxygen heterocyclic compounds in citrus essential oils. *J. Pharm. Biomed. Anal.*, **2000**, 24(1), 147-154.
- [70] Barreca, D.; Bellocco, E.; Caristi, C.; Leuzzi, U. Gattuso, G. Flavonoid composition and antioxidant activity of juices from Chinotto (Citrus x myrtifolia Raf.) fruits at different ripening stages. *J. Agric. Food Chem.*, **2010**, 58(5), 3031-3036.
- [71] Morin, B.; Nichols, L.A.; Zalasky, K.M.; Davis, J.W.; Manthey, J.A. Holland, L.J. The citrus flavonoids hesperetin and nobiletin differentially regulate low density lipoprotein receptor gene transcription in HepG2 liver cells. *J. Nutr.*, **2008**, 138(7), 1274-1281.
- [72] Kou, M.C.; Fu, S.H.; Yen, J.H.; Weng, C.Y.; Li, S.; Ho, C.T. Wu, M.J. Effects of citrus flavonoids, 5-hydroxy-3,6,7,8,3',4'-hexamethoxyflavone and 3,5,6,7,8,3',4'-heptamethoxyflavone, on the activities of macrophage scavenger receptors and the hepatic LDL receptor. *Food Funct.*, **2013**, 4(4), 602-609.
- [73] Choe, S.C.; Kim, H.S.; Jeong, T.S.; Bok, S.H. Park, Y.B. Naringin has an antiatherogenic effect with the inhibition of intercellular adhesion molecule-1 in hypercholesterolemic rabbits. *J. Cardiovasc. Pharmacol.*, **2001**, 38(6), 947-955.
- [74] Yu, J.; Wang, L.; Walzem, R.L.; Miller, E.G.; Pike, L.M. Patil, B.S. Antioxidant activity of citrus limonoids, flavonoids, and coumarins. *J. Agric. Food Chem.*, **2005**, 53(6), 2009-2014.
- [75] Miceli, N.; Mondello, M.R.; Monforte, M.T.; Sdrafkakis, V.; Dugo, P.; Crupi, M.L.; Taviano, M.F.; De Pasquale, R. Trovato, A. Hypolipidemic effects of Citrus bergamia Risso et Poiteau juice in rats fed a hypercholesterolemic diet. *J. Agric. Food Chem.*, **2007**, 55(26), 10671-10677.
- [76] Paine, M.F.; Criss, A.B. Watkins, P.B. Two major grapefruit juice components differ in time to onset of intestinal CYP3A4 inhibition. *J. Pharmacol. Exp. Ther.*, **2005**, 312(3), 1151-1160.
- [77] Mollace, V.; Sacco, I.; Janda, E.; Malara, C.; Ventrice, D.; Colica, C.; Visalli, V.; Muscoli, S.; Ragusa, S.; Muscoli, C.; Rotiroli, D. Romeo, F. Hypolipemic and hypoglycaemic activity of bergamot polyphenols: from animal models to human studies. *Fitoterapia*, **2011**, 82(3), 309-316.
- [78] Gliozzi, M.; Walker, R.; Muscoli, S.; Vitale, C.; Gratteri, S.; Carresi, C.; Musolino, V.; Russo, V.; Janda, E.; Ragusa, S.; Aloe, A.; Palma, E.; Muscoli, C.; Romeo, F. Mollace, V. Bergamot polyphenolic fraction enhances rosuvastatin-induced effect on LDL-cholesterol, LOX-1 expression and protein kinase B phosphorylation in patients with hyperlipidemia. *Int. J. Cardiol.*, **2013**, 170(2), 140-145.
- [79] Di Donna, L.; Iacopetta, D.; Cappello, A.R.; Gallucci, G.; Martello, E.; Fiorillo, M.; Dolce, V. Sindona, G. Hypocholesterolaemic activity of 3-hydroxy-3-methyl-glutaryl flavanones enriched fraction from bergamot fruit (Citrus bergamia): "In vivo" studies. *J. Funct. Foods*, **2014**, 7(558-568).
- [80] Kong, W.J.; Wei, J.; Zuo, Z.Y.; Wang, Y.M.; Song, D.Q.; You, X.F.; Zhao, L.X.; Pan, H.N. Jiang, J.D. Combination of simvastatin with berberine improves the lipid-lowering efficacy. *Metabolism*, **2008**, 57(8), 1029-1037.
- [81] Lee, S.; Birukov, K.G.; Romanoski, C.E.; Springstead, J.R.; Lusic, A.J. Berliner, J.A. Role of phospholipid oxidation products in atherosclerosis. *Circ. Res.*, **2012**, 111(6), 778-799.
- [82] Bochkov, V.N.; Oskolkova, O.V.; Birukov, K.G.; Levonen, A.L.; Binder, C.J. Stockl, J. Generation and biological activities of oxidized phospholipids. *Antioxid. Redox Signal*, **2010**, 12(8), 1009-1059.
- [83] Berliner, J.A.; Leitinger, N. Tsimikas, S. The role of oxidized phospholipids in atherosclerosis. *J. Lipid Res.*, **2009**, 50 Suppl(S207-212).
- [84] Trombetta, D.; Cimino, F.; Cristani, M.; Mandalari, G.; Saija, A.; Ginestra, G.; Speciale, A.; Chirafisi, J.; Bisignano, G.; Waldron, K.; Nardad, A. Faulds, C.B. In vitro protective effects of two extracts from bergamot peels on human endothelial cells exposed to tumor necrosis factor-alpha (TNF-alpha). *J. Agric. Food Chem.*, **2010**, 58(14), 8430-8436.
- [85] Kim, Y.S.; Ahn, Y.; Hong, M.H.; Joo, S.Y.; Kim, K.H.; Sohn, I.S.; Park, H.W.; Hong, Y.J.; Kim, J.H.; Kim, W.; Jeong, M.H.; Cho, J.G.; Park, J.C. Kang, J.C. Curcumin attenuates inflammatory

- responses of TNF-alpha-stimulated human endothelial cells. *J. Cardiovasc. Pharmacol.*, **2007**, 50(1), 41-49.
- [86] Scheuer, H.; Gwinner, W.; Hohbach, J.; Grone, E.F.; Brandes, R.P.; Malle, E.; Olbricht, C.J.; Walli, A.K. Grone, H.J. Oxidant stress in hyperlipidemia-induced renal damage. *Am. J. Physiol. Renal Physiol.*, **2000**, 278(1), F63-74.
- [87] Chade, A.R.; Rodriguez-Porcel, M.; Grande, J.P.; Krier, J.D.; Lerman, A.; Romero, J.C.; Napoli, C. Lerman, L.O. Distinct renal injury in early atherosclerosis and renovascular disease. *Circulation*, **2002**, 106(9), 1165-1171.
- [88] Stulak, J.M.; Lerman, A.; Porcel, M.R.; Caccitolo, J.A.; Romero, J.C.; Schaff, H.V.; Napoli, C. Lerman, L.O. Renal vascular function in hypercholesterolemia is preserved by chronic antioxidant supplementation. *J. Am. Soc. Nephrol.*, **2001**, 12(9), 1882-1891.
- [89] Trovato, A.; Taviano, M.F.; Pergolizzi, S.; Campolo, L.; De Pasquale, R. Miceli, N. Citrus bergamia Risso & Poiteau juice protects against renal injury of diet-induced hypercholesterolemia in rats. *Phytother. Res.*, **2010**, 24(4), 514-519.
- [90] Jones, P.H. Expert perspective: reducing cardiovascular risk in metabolic syndrome and type 2 diabetes mellitus beyond low-density lipoprotein cholesterol lowering. *Am. J. Cardiol.*, **2008**, 102(12A), 41L-47L.
- [91] Joy, T.R. Hegele, R.A. Narrative review: statin-related myopathy. *Ann. Intern. Med.*, **2009**, 150(12), 858-868.

Mitochondrial biogenesis is required for the anchorage-independent survival and propagation of stem-like cancer cells

Arianna De Luca^{1,2,3,*}, Marco Fiorillo^{1,2,3,*}, Maria Peiris-Pagès^{1,2}, Bela Ozsvari^{1,2}, Duncan L. Smith⁴, Rosa Sanchez-Alvarez^{1,2}, Ubaldo E. Martinez-Outschoorn⁵, Anna Rita Cappello³, Vincenzo Pezzi³, Michael P. Lisanti^{1,2} and Federica Sotgia^{1,2}

¹ The Breakthrough Breast Cancer Research Unit, Institute of Cancer Sciences, University of Manchester, UK

² The Manchester Centre for Cellular Metabolism (MCCM), Institute of Cancer Sciences, University of Manchester, UK

³ Department of Pharmacy, Health and Nutritional Sciences, University of Calabria, Arcavacata di Rende (CS), Italy

⁴ The Cancer Research UK Manchester Institute, University of Manchester, UK

⁵ The Sidney Kimmel Cancer Center, Philadelphia, PA, USA

* These authors contributed equally and should be considered co-first authors

Correspondence to: Michael P. Lisanti, **email:** michaelp.lisanti@gmail.com

Federica Sotgia, **email:** fsotigia@gmail.com

Keywords: XCT790, doxycycline, drug repurposing, ERR-α, PGC1-α/β

Abbreviations: CSCs, cancer stem-like cells; TICs, tumor-initiating stem-like cells.

Received: February 05, 2015

Accepted: May 30, 2015

Published: June 09, 2015

This is an open-access article distributed under the terms of the Creative Commons Attribution License, which permits unrestricted use, distribution, and reproduction in any medium, provided the original author and source are credited.

ABSTRACT

Here, we show that new mitochondrial biogenesis is required for the anchorage independent survival and propagation of cancer stem-like cells (CSCs). More specifically, we used the drug XCT790 as an investigational tool, as it functions as a specific inhibitor of the ERRα-PGC1 signaling pathway, which governs mitochondrial biogenesis. Interestingly, our results directly demonstrate that XCT790 efficiently blocks both the survival and propagation of tumor initiating stem-like cells (TICs), using the MCF7 cell line as a model system. Mechanistically, we show that XCT790 suppresses the activity of several independent signaling pathways that are normally required for the survival of CSCs, such as Sonic hedgehog, TGFβ-SMAD, STAT3, and Wnt signaling. We also show that XCT790 markedly reduces oxidative mitochondrial metabolism (OXPHOS) and that XCT790-mediated inhibition of CSC propagation can be prevented or reversed by Acetyl-L-Carnitine (ALCAR), a mitochondrial fuel. Consistent with our findings, over-expression of ERRα significantly enhances the efficiency of mammosphere formation, which can be blocked by treatment with mitochondrial inhibitors. Similarly, mammosphere formation augmented by FOXM1, a downstream target of Wnt/β-catenin signaling, can also be blocked by treatment with three different classes of mitochondrial inhibitors (XCT790, oligomycin A, or doxycycline). In this context, our unbiased proteomics analysis reveals that FOXM1 drives the expression of >90 protein targets associated with mitochondrial biogenesis, glycolysis, the EMT and protein synthesis in MCF7 cells, processes which are characteristic of an anabolic CSC phenotype. Finally, doxycycline is an FDA-approved antibiotic, which is very well-tolerated in patients. As such, doxycycline could be re-purposed clinically as a 'safe' mitochondrial inhibitor, to target FOXM1 and mitochondrial biogenesis in CSCs, to prevent tumor recurrence and distant metastasis, thereby avoiding patient relapse.

INTRODUCTION

Tumor-initiating stem-like cells (TICs) are a small sub-population of tumor cells that are resistant to most anti-cancer therapies, including radio- and chemotherapy, and are able to expand and regenerate tumors, after conventional therapy is completed [1-4]. As such, TICs are responsible for tumor recurrence, metastatic dissemination, and, ultimately, patient death. As a consequence, TICs have become very attractive targets for novel cancer therapies. TICs share some features with stem cells, and many studies have investigated the signaling pathways regulating their proliferation, asymmetric cell division and migrating properties, as well as their ability to undergo proliferation under anchorage-independent conditions [5-7]. In fact, this latter property is being widely exploited to isolate TICs, which are able to survive and clonally expand as tumor-spheres, when placed in non-adherent settings [8]. Tumor-spheres generated from breast cancer cells are known as mammospheres.

The metabolic requirements of TICs remain a fairly unexplored area of investigation. We and others have recently shown that TICs rely mainly on mitochondrial metabolism, as compared to the more differentiated tumor cell population [9-12]. Also, it was previously shown that the radio-resistance of TICs from gliomas [13] and breast cancers [14] correlates with higher mitochondrial respiration.

We have demonstrated that >60 mitochondrial proteins are up-regulated in mammospheres derived from breast cancer cell lines (MCF7 and T47D), relative to cells grown in monolayers. Furthermore, pharmacological inhibition with oligomycin A, an inhibitor of the ATP synthase, greatly reduced mammosphere formation [11]. More importantly, treatment with doxycycline, an FDA-approved antibiotic targeting mitochondrial ribosomes as a known 'side effect', inhibited the formation of tumor-spheres generated from cell lines across several different tumor types, as well as from primary tumor samples [12].

These studies indicate that mitochondria in TICs are potentially druggable targets for the prevention of tumor recurrence and metastasis. The aim of our current study was to further validate mitochondrial function as a critical target for the development of new anti-cancer therapies. Here, we employed XCT790 as an investigational compound to inhibit mitochondrial oxidative phosphorylation [15]. XCT790 is a well-established inverse agonist of Estrogen-Related Receptor α (ERR α), which functions as an essential cofactor of PGC1 α . Importantly, PGC1 α is required for the transcription of nuclear-encoded mitochondrial genes and drives mitochondrial biogenesis [16, 17]. XCT790 has been shown to inhibit colony formation in soft agar induced by PGC1 α [18], and to induce cell death in chemo-resistant cancer cells [19]. However, to our knowledge, no studies have previously investigated the effects of XCT790 on the

propagation and survival of TICs.

Here, our results show that XCT790 inhibits the proliferation of TICs from MCF7 breast cancer cells, as assessed using i) mammosphere formation and by ii) CD44/CD24 immuno-staining, coupled with FACS analysis. We also demonstrate that XCT790 suppresses the activation of well-established pathways governing TIC proliferation and survival, including Sonic hedgehog, TGF β -SMAD, STAT3, and Wnt signaling. As expected, XCT790 profoundly reduced mitochondrial respiration. Importantly, XCT790-induced TIC inhibition could be rescued by treatment with Acetyl-L-Carnitine (ALCAR), a mitochondrial fuel and cofactor, which enhances mitochondrial oxidative metabolism and biogenesis [20]. We also show that overexpression of ERR α is sufficient to augment MCF7 cell mammosphere formation, which can be blocked by treatment with mitochondrial inhibitors, such as XCT790 and oligomycin A, an inhibitor of ATP synthase. Finally, we show that mammosphere formation driven by FOXM1, a transcription factor downstream of Wnt/ β -catenin signaling that governs stemness [21-24], can also be blocked by treatment with three different classes of mitochondrial inhibitors (XCT790, oligomycin A, or doxycycline).

Thus, our results firmly establish that mitochondrial biogenesis and metabolism are required for the survival of TICs, indicating that mitochondrial-targeted therapies are a promising novel strategy for targeting TICs for the treatment of relapsed and resistant cancers. Mitochondrial-targeted therapies should also be considered for cancer prevention.

RESULTS

Mammosphere formation in MCF7 cells depends on mitochondrial function

We have previously shown that mitochondrial proteins are up-regulated in mammospheres derived from breast cancer cell lines (MCF7 and T47D), relative to cells grown in monolayers [11]. Furthermore, pharmacological inhibition with oligomycin A, an inhibitor of ATP synthase, greatly reduced mammosphere formation [11]. More importantly, treatment with doxycycline, an FDA-approved antibiotic that targets mitochondrial ribosomes as a known 'side effect', inhibited the formation of tumor-spheres derived from 12 cell lines across eight different tumor types, as well as from primary tumor samples [12].

To further investigate the role of mitochondria in TICs, here we employed a well-established inverse agonist of ERR α , namely XCT790. ERR α is a cofactor of PGC1 α/β , which is required for the transcription of nuclear mitochondrial genes and mitochondrial biogenesis [16, 17]. As such, XCT790 is believed to

suppress mitochondrial function. Notably, treatment with XCT790 dose-dependently inhibits MCF7 mammosphere formation, with an IC-50 of 10 μM (Figure 1A). We also validated that XCT790 dose-dependently reduces the protein expression of PGC1 α in MCF7 cell monolayers by immuno-blot analysis (data not shown), by up to 70-80%, over this concentration range.

These results were independently confirmed by evaluating the expression of *bona-fide* TIC markers CD44/CD24 by FACS. Under these conditions, CD44(+)/high/CD24(-)/low cells are considered to represent the TIC sub-population. XCT790 treatment significantly reduced

the number of CD44(+)/high/CD24(-)/low cells in a dose-dependent fashion, relative to vehicle alone controls (Figure 1B).

We next set out to investigate if XCT790 can target TICs in the presence of the total cancer cell population. To this end, MCF7 cells were treated with XCT790 (at 5 or 10 μM) as monolayers for 2 days and then re-plated on low-attachment plates in the absence of XCT790, to generate mammospheres for 5 days. Under these conditions, XCT790 pre-treatment dose-dependently reduced MCF7 cell mammosphere formation, by up to ~70% (Figure 1C), indicating that XCT790 can target the TIC population also

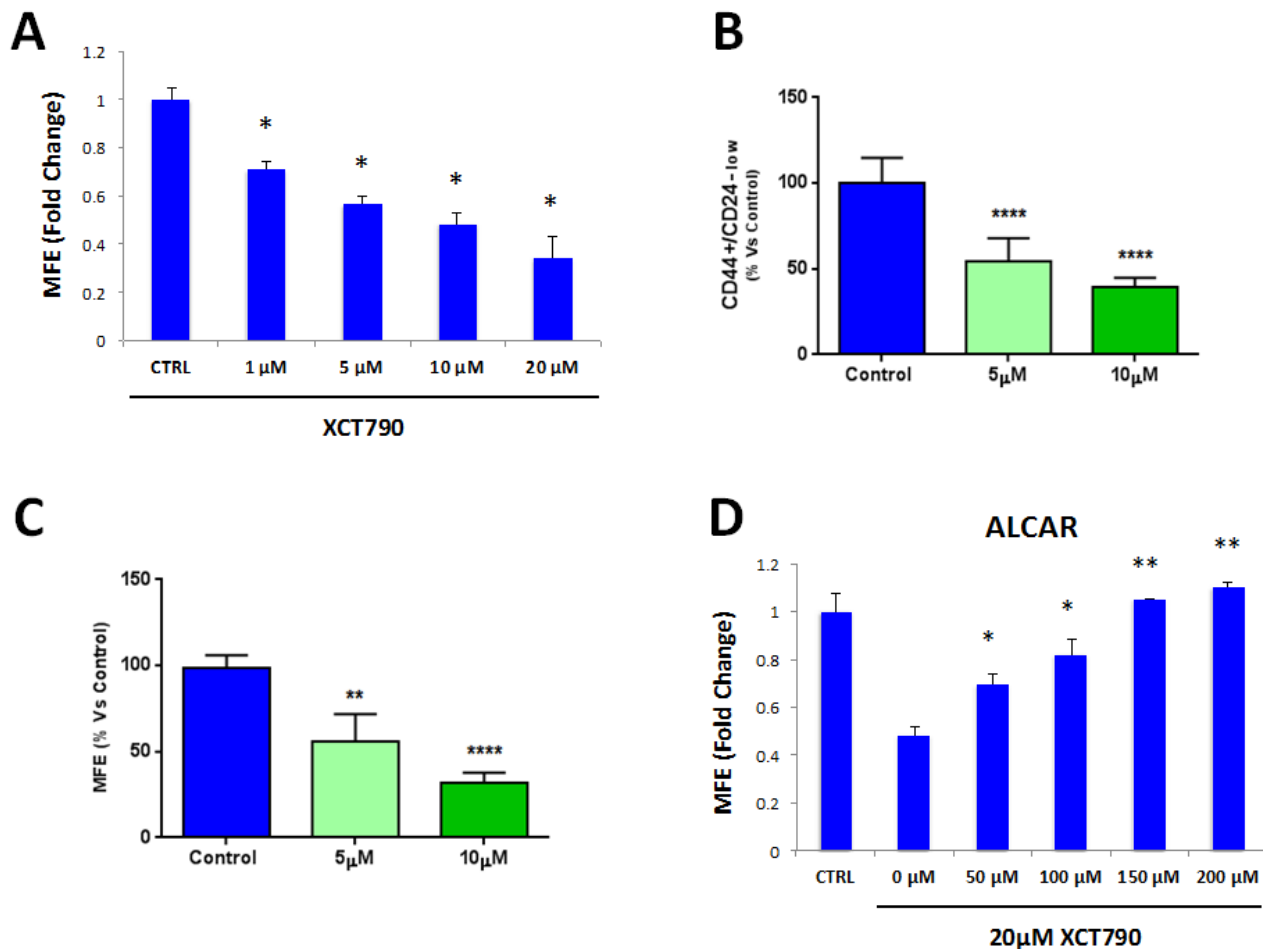


Figure 1: MCF7 cell 3D-spheroid formation depends on mitochondrial function. **A.** The well-established ERR α inverse agonist, namely XCT790, dose-dependently inhibits MCF7 mammosphere formation, with an IC-50 of 10 μM . ERR α is a cofactor of PGC1 α , which is required for the transcription of mitochondrial genes and mitochondrial biogenesis. * p < 0.01 evaluated by Student's t test. **B.** MCF7 cells were pre-treated with XCT790 (at 5 or 10 μM) as monolayers for 2 days and then re-plated on low-attachment plates in the absence of XCT790, for anoikis assay for 10 hours. Expression of TIC markers CD24 and CD44 was analyzed by FACS. Note that XCT790 pre-treatment dose-dependently reduced the number of CD44(+)/high/CD24(-)/low cells, which are considered the TICs population. **** p < 0.00001 evaluated with one-way ANOVA. **C.** MCF7 cells were pre-treated with XCT790 (at 5 or 10 μM) as monolayers for 2 days and then re-plated on low-attachment plates in the absence of XCT790, for mammosphere assay for 5 days. Under these conditions, XCT790 pre-treatment dose-dependently reduced MCF7 cell mammosphere formation, by up to ~70%. ** p < 0.001 and **** p < 0.00001 evaluated with one-way ANOVA. **D.** Treatment with the mitochondrial cofactor Acetyl L-Carnitine (ALCAR) rescues the decreased mammosphere formation induced by XCT790. Mammosphere formation was assessed upon treatment with 20 μM XCT790 and increasing concentration of ALCAR. Thus, mitochondrial function is required for the efficient clonal expansion and anchorage-independent growth of TICs. * p < 0.05; ** p < 0.001, relative to XCT790 only treated cells (0 μM ALCAR) evaluated by Student's t test. MFE: mammosphere forming efficiency.

when present in a heterogeneous cell population.

Also, we asked if decreased mammosphere formation induced by XCT790 could be rescued by treatment with the mitochondrial cofactor Acetyl-L-Carnitine (ALCAR). ALCAR plays a key role in mitochondrial oxidative metabolism, by enhancing fatty acid β -oxidation [20]. ALCAR stimulates mitochondrial biogenesis and is also directly converted to acetyl-CoA, a mitochondrial fuel [20]. To this end, mammosphere formation was assessed after treatment with XCT790 (at 20 μ M) and increasing concentrations of ALCAR. Figure 1D shows that ALCAR rescues the decrease in mammosphere formation induced by XCT790, in a dose-dependent manner. Thus, mitochondrial function is required for the efficient clonal expansion and anchorage-independent growth of TICs.

We then examined if XCT790 affects the viability of the total cancer cell population, or if it specifically inhibits the viability of MCF7 cells in mammospheres. To this end, MCF7 cells were treated with increasing concentrations of XCT790 as monolayers for 3 days (Figure 2A) or 5 days (Figure 2B). Cell viability was then assessed using the SRB assay. Note that 5-day treatment did not affect the viability of the MCF7 cell monolayers, as profoundly as MCF7 cell mammospheres (Figure 2B). For example, treatment with 10 μ M XCT790 reduces mammosphere formation by 50% (Figure 1A), whereas the viability of monolayer cells is reduced by only 20%. Thus, XCT790 preferentially reduces the viability of MCF7 cell mammospheres, relative to bulk cancer cells.

XCT790 inhibits the activation of several stem cell related signaling pathways

To further corroborate the idea that XCT790 inhibits cancer stem cell-like features, we next analyzed the effects of XCT790 on a series of well-established signaling pathways, which have been shown to promote stemness. For this purpose, we employed a panel of eight MCF7 cell lines carrying different luciferase reporters [25], to monitor the activation state of a variety of different signaling networks, including Sonic hedgehog, TGF β -SMAD, STAT3, Wnt, Interferon (IFN)- α/β -STAT1/2, NRF2-dependent antioxidant responses, IFN- γ -STAT1 and Notch pathways. Notably, several pathways were significantly inhibited by XCT790 treatment, including stem cell signaling (Sonic hedgehog, TGF β -SMAD, STAT3, Wnt) and IFN- α/β -STAT1/2 signaling (Figure 3A). However, no effects were observed on the NRF2-antioxidant response, IFN- γ -STAT1 and the Notch pathways (Figure 3B). Thus, XCT790 inhibits the activation of several signal transduction pathways related to cancer stem-like features.

XCT790 inhibits mitochondrial respiration

Next, we set out to investigate the mechanism(s) by which XCT790 inhibits mammosphere formation and CSC features. XCT790 is an inverse agonist of ERR α , which is a cofactor of PGC1 α required for the transcription of mitochondrial genes and mitochondrial biogenesis. Thus, the metabolic profile of MCF7 cells treated with XCT790 was analyzed. To this end, MCF7 cells were treated with XCT790 for 48 hours, stained with various MitoTracker

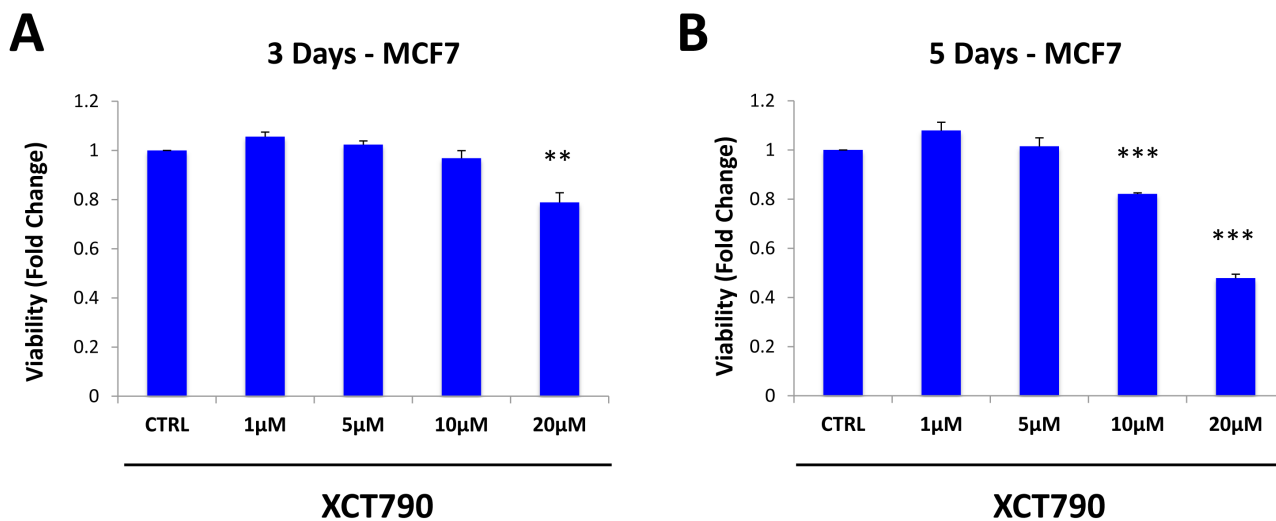


Figure 2: XCT790 preferentially reduces the viability of MCF7 cells in mammospheres, relative to bulk cancer cells. MCF7 cells were treated with XCT790 (1, 5, 10, 20 μ M) as monolayers for 3 days **A.** or 5 days **B.** Cell viability was assessed by SRB assay. Note that 5-day treatment did not affect the viability of the MCF7 cell monolayers as profoundly as MCF7 cell mammospheres. For example, treatment with 10 μ M XCT790 reduces mammosphere formation by 50% (Figure 1A), whereas viability of monolayer cells is reduced by 20%. ** $p < 0.01$; *** $p < 0.001$ evaluated by Student's t test.

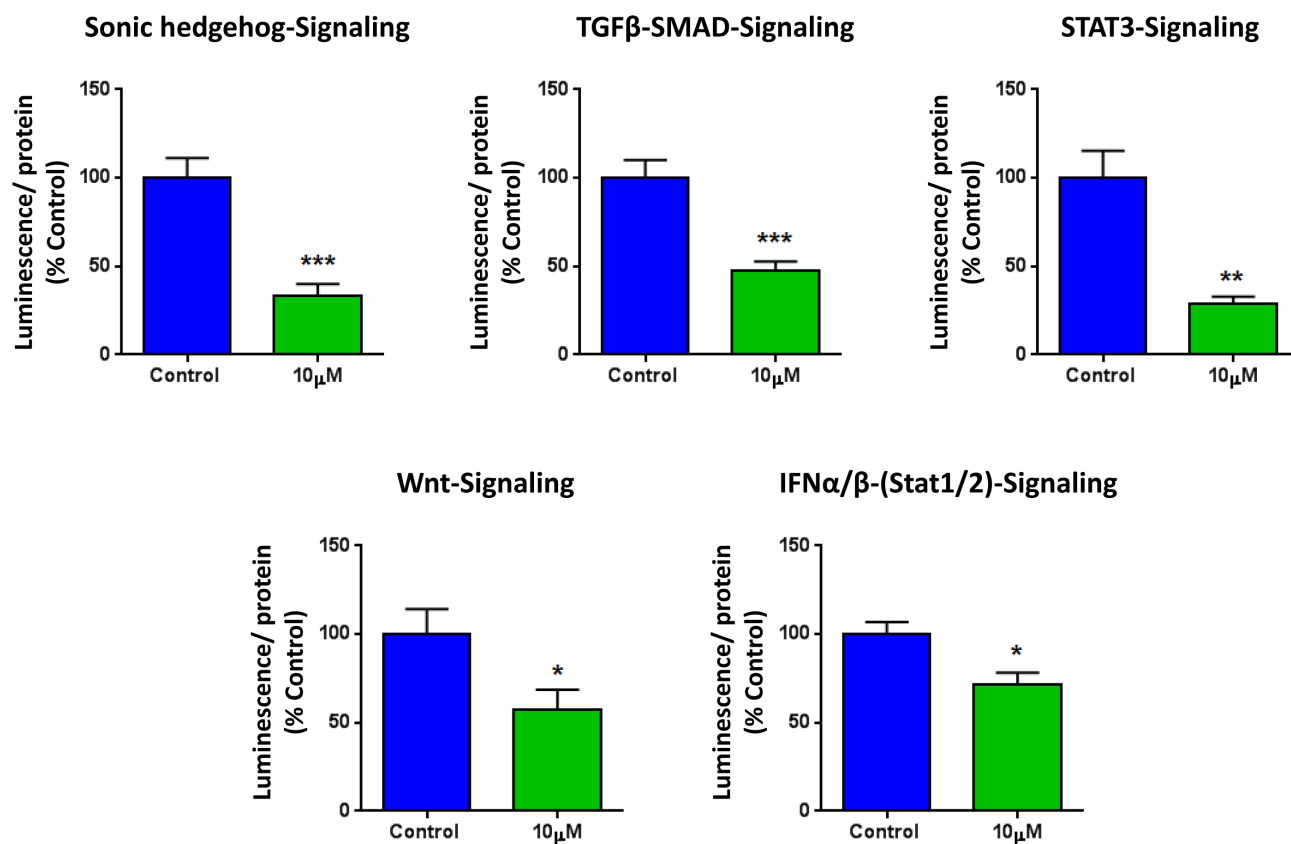
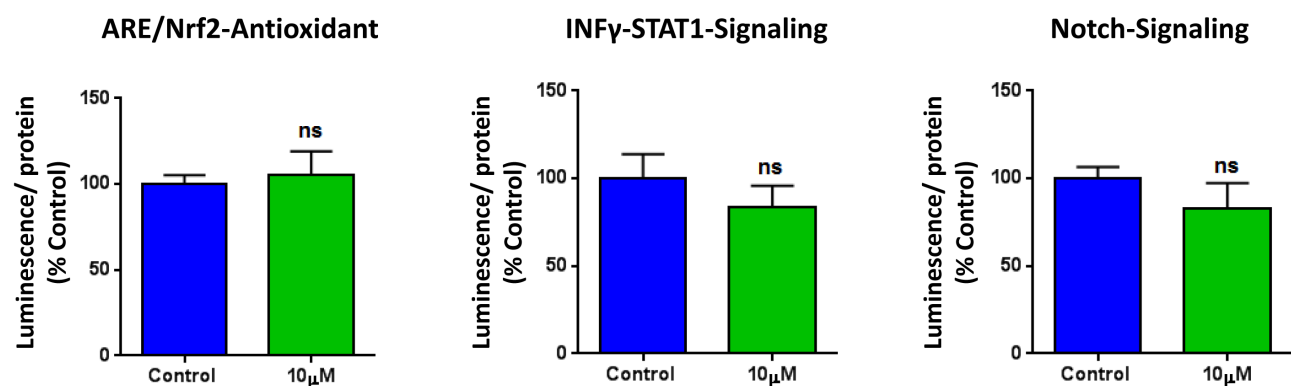
A**B**

Figure 3: XCT790 inhibits signaling pathways related to cancer stem cells, and interferon. MCF7 breast cancer cells carrying luciferase-reporters (Cignal, QIAGEN) were generated to monitor the activation of a variety of signaling networks, including Sonic hedgehog TGFβ-SMAD, STAT3, Wnt, Interferon (IFN)-α/β-STAT1/2, NRF2-dependent antioxidant responses, IFN-γ-STAT1 and Notch pathways. MCF7-Luc reporter cells were treated with XCT790 for 48 hours and luminescence was determined as a measure of pathway activation status. Luminescence was normalized by protein content. **A.** Note that XCT790 inhibits cancer stem cell signaling (Sonic hedgehog TGFβ-SMAD, STAT3, Wnt), as well as IFN-α/β-STAT1/2 signaling. **B.** No effects were observed for the NRF2-antioxidant responses, IFN-γ-STAT1 and Notch pathways. * $p < 0.01$; ** $p < 0.001$; *** $p < 0.0001$, using Student's t test.

probes and analyzed by FACS. Figure 4A shows that XCT790 induces a decrease in mitochondrial membrane potential, as assessed with MitoTracker Orange, which accumulates in mitochondria with an active mitochondrial potential. Surprisingly, XCT790 induces also an increase in mitochondrial mass, as assessed with MitoTracker Green (Figure 4B), localizing to mitochondria regardless of mitochondrial membrane potential. Similar results were obtained with MitoTracker Deep Red, which also measures mitochondria mass (data not shown). Analysis of the ratio of mitochondrial membrane potential versus mitochondrial mass indicates that XCT790 induces a profound decrease in mitochondrial membrane potential per mitochondria (Figure 4C).

Also, the metabolic profile of MCF7 cells treated with XCT790 was examined using the Seahorse XFe96 analyzer, by employing a mitochondrial stress test. Notably, the oxygen consumption rate (OCR) was greatly reduced by treatment with XCT790 (Figure 5A). Further quantification revealed significant reductions in basal and maximal respiration (Figure 5B-5C), as well as ATP levels (Figure 5D), upon XCT790 treatment. Thus, XCT790 significantly reduces the rates of oxidative mitochondrial metabolism. To further validate these results, a glycolytic stress test was performed using the Seahorse XFe96 analyzer, by measuring the extracellular acidification rate (ECAR) of MCF7 cells treated with XCT790. Notably, XCT790 also significantly reduces ECAR, a marker of glycolysis (Figure 6A). Finally, plotting the ratio of OCR to ECAR demonstrates that XCT790 shifts MCF7 cells from a highly energetic to a metabolically quiescent state (Figure 6B).

ERR α expression is both necessary and sufficient to increase mammosphere formation in MCF7 cells

XCT790 is an inverse agonist of ERR α . As XCT790 inhibits mammosphere formation, we then asked if ERR α expression is sufficient to promote 3D-spheroid formation in MCF7 cells. To this end, ERR α was over-expressed in MCF7 cells using a lentiviral approach. Empty Vector (EV) cells were generated in parallel. Figure 7A shows that MCF7 cells over-expressing ERR α show a 50% increase in mammosphere forming capacity. Notably, MCF7 cells over-expressing ERR α show increased mitochondrial membrane potential, as assessed by MitoTracker Orange, as well as increased mitochondrial mass, as assessed by MitoTracker Green and MitoTracker Deep Red, as expected (Figure 7B).

We then used a pharmacological approach to inhibit ERR α -driven mammosphere formation, using oligomycin A, a mitochondrial inhibitor, as well as XCT790, a specific ERR α inverse agonist. Importantly, mammosphere formation induced by ERR α expression was inhibited by either treatment with oligomycin A (Figure 7C), or XCT790 (Figure 7D). These results indicate that ERR α activity and mitochondrial function are normally required for the clonal expansion of TICs.

Mammosphere formation driven by FOXM1 requires mitochondrial function

To examine if mitochondrial function is essential for TIC expansion driven by well-established stem-like signaling, we decided to overexpress FOXM1 in

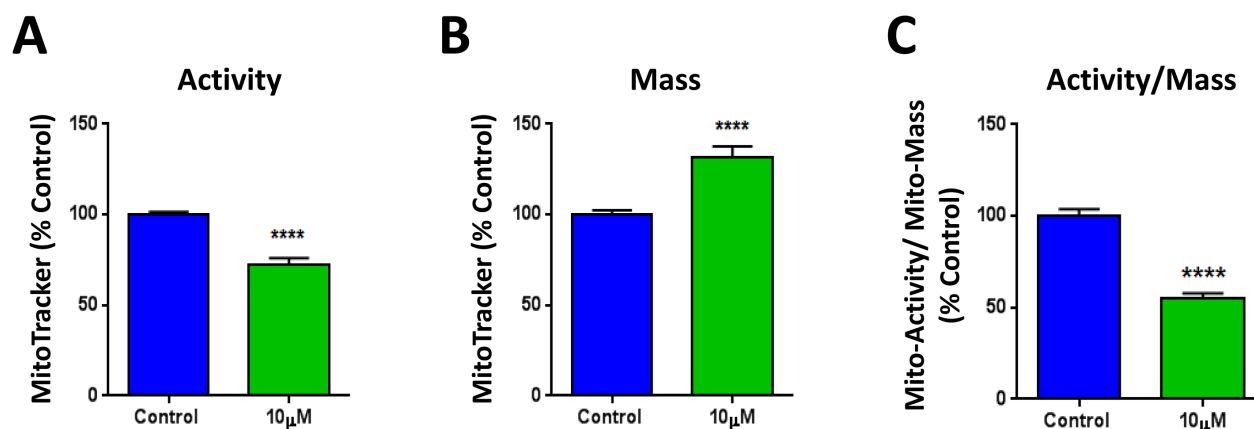


Figure 4: XCT790 induces a decrease in mitochondrial membrane potential, with an unexpected increase in mitochondrial mass. MCF7 cells were treated with XCT790 (10 μ M) as monolayers for 48 hours, stained with various MitoTracker probes and analyzed by FACS. **A.** XCT790 induces a decrease in mitochondrial membrane potential, as assessed with MitoTracker Orange, which accumulates in mitochondria with an active mitochondrial potential. **B.** XCT790 induces an unexpected increase in mitochondrial mass, as assessed with MitoTracker Green, which localizes to mitochondria regardless of mitochondrial membrane potential. **C.** Ratio of mitochondrial membrane potential (MitoTracker Orange), versus mitochondrial mass (MitoTracker Green) demonstrates that XCT790 induces a large decrease in mitochondrial membrane potential per mitochondria. **** $p < 0.00001$ evaluated with Student's *t* test.

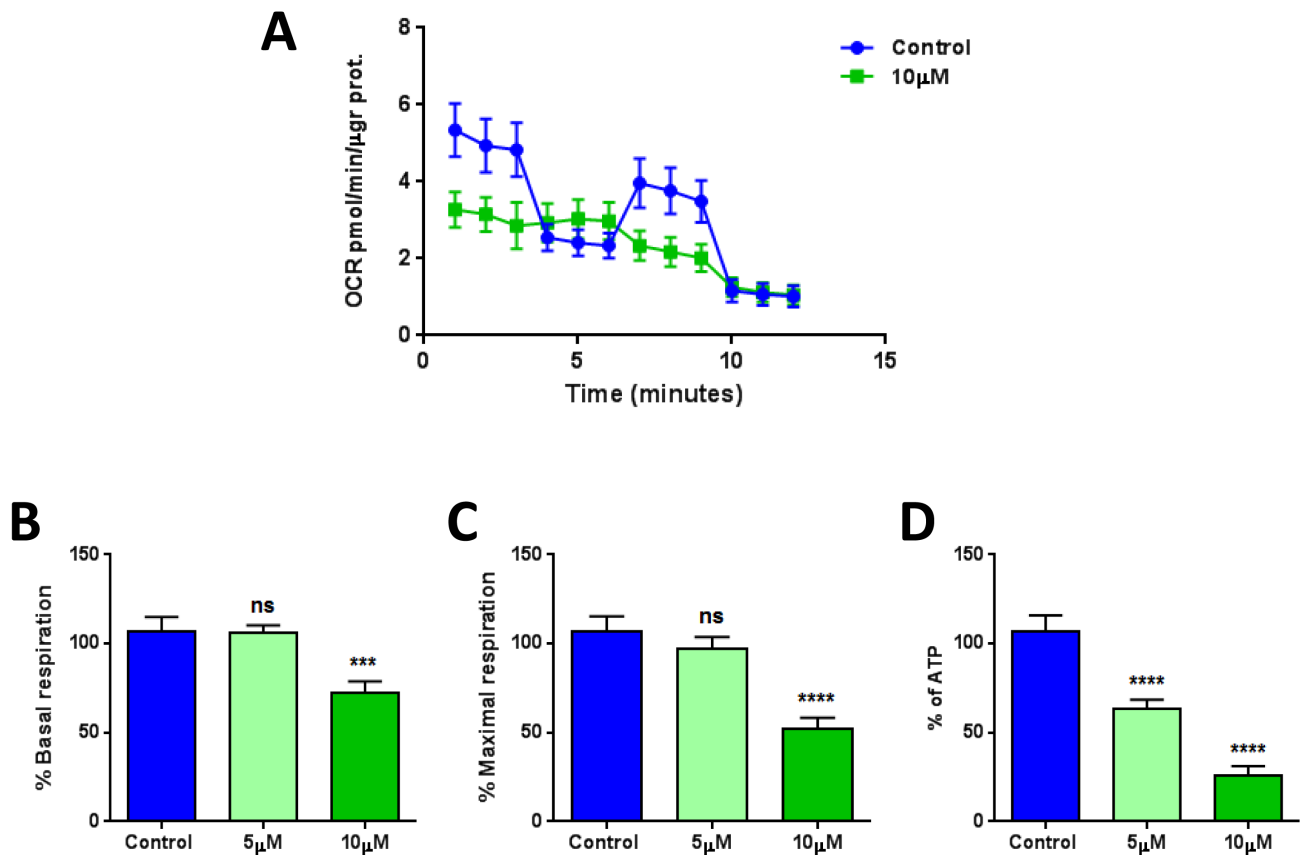


Figure 5: XCT790 quantitatively reduces mitochondrial respiration. The metabolic profile of MCF7 cell monolayers treated with XCT790 (5 or 10 μM) for 2-days was examined using the Seahorse XFe96 analyzer. **A.** Oxygen consumption rate (OCR) is significantly reduced by treatment with 10 μM XCT790. **B., C., D.** Significant reductions in respiration (basal and maximal) and in ATP levels were observed upon XCT790 treatment. Thus, the rates of oxidative mitochondrial metabolism were significantly reduced by XCT790 treatment. *** $p < 0.0001$, **** $p < 0.00001$ evaluated with one-way ANOVA.

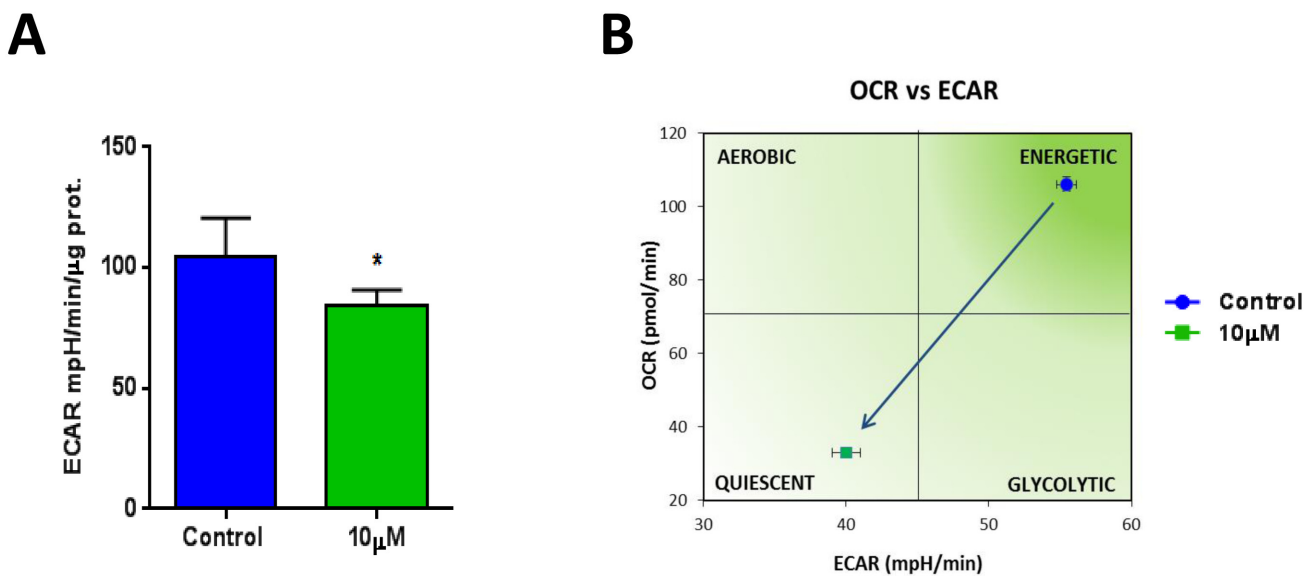


Figure 6: XCT790 shifts MCF7 cells from a highly energetic to a metabolically quiescent state. **A.** Extracellular acidification rate (ECAR) of MCF7 cell monolayers treated with XCT790 (10 μM) for 2-days was assessed using the Seahorse XFe96 analyzer. Note that XCT790 significantly reduces ECAR, a marker of glycolysis. * $p < 0.01$ evaluated with Student's t test. **B.** OCR plotted against ECAR. Note that MCF7 cells treated with XCT790 were shifted towards a more metabolically quiescent state.

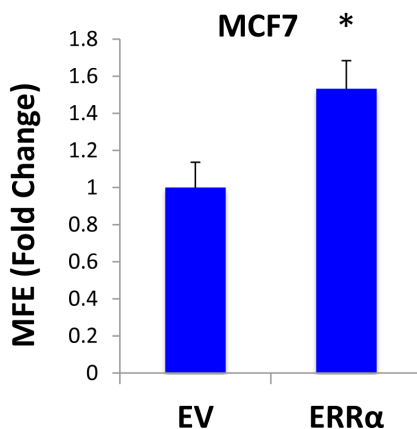
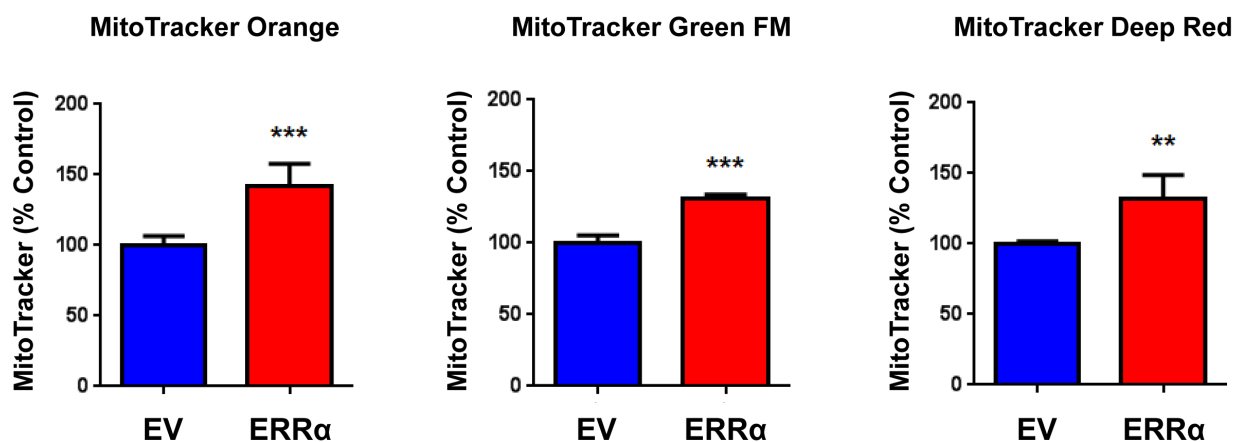
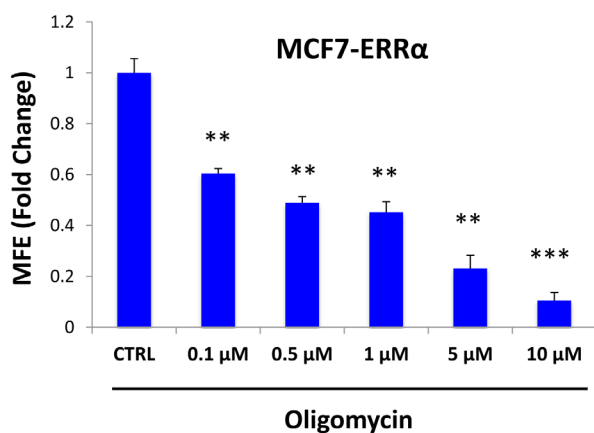
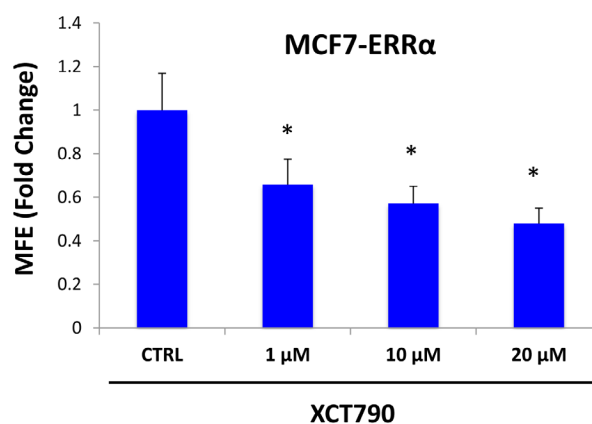
A**B****C****D**

Figure 7: ERRα expression is required for 3D-spheroid formation in MCF7 cells. ERRα was over-expressed in MCF7 cells using a lentiviral approach. Empty Vector (EV) cells were generated in parallel. **A.** MCF7 cells overexpressing ERRα show a 50% increase in mammosphere forming capacity, relative to EV controls. **B.** MCF7 cells over-expressing ERRα show an increase of mitochondrial membrane potential, as assessed by MitoTracker Orange staining, as well as an increase in mitochondrial mass, as assessed by MitoTracker Green and MitoTracker Deep Red staining, as expected. **C.** Oligomycin A, an inhibitor of mitochondrial ATP synthase, inhibits mammosphere formation in MCF7 cells overexpressing ERRα, indicating that mitochondrial function is required for ERRα-driven mammosphere formation. **D.** XCT790, an ERRα inverse agonist, inhibits mammosphere formation in MCF7 cells over-expressing ERRα. Thus, ERRα activity is required for the efficient clonal expansion of TICs. EV: Empty Vector. * $p < 0.05$, ** $p < 0.01$, *** $p < 0.001$ evaluated by Student's t test.

Table 1: MCF7-FOXM1 Cells Over-express Key Protein Molecules Functionally Related to Mitochondria, Glycolysis and the EMT.

Symbol	Description	Fold-Upregulation	ANOVA
Mitochondrial-related proteins (27)			
HSPD1	HSP60, 60 kDa heat shock protein, mitochondrial	12.35	0.02
ACADVL	Acyl-Coenzyme A dehydrogenase, very long chain, mitochondrial	12.14	0.001
ATP5B	ATP synthase subunit beta, mitochondrial	10.74	0.0006
COX4I1	Cytochrome c oxidase subunit 4 isoform 1, mitochondrial	9.44	0.002
SLC25A4	Solute carrier family 25 (ADP/ATP translocase), member 4, mitochondrial	5.97	0.003
PRKDC	DNA-dependent protein kinase, catalytic (maintains mt-DNA copy number)	2.43	0.0005
ABAT	4-aminobutyrate aminotransferase, mitochondrial	2.28	0.0002
PMPCA	Mitochondrial-processing peptidase alpha subunit	2.21	0.03
CHCHD3	MICOS complex subunit MIC19, mitochondrial	2.04	0.03
NDUFS1	Mitochondrial NADH-ubiquinone oxidoreductase 75 kDa subunit	1.99	7.61E-05
HSPA9	Heat shock 70kDa protein 9 (Mortalin), mitochondrial	1.90	0.049
SUCLG2	Succinate-CoA ligase, GDP-forming, beta subunit	1.88	0.01
SLC25A3	Solute carrier family 25 (mitochondrial phosphate carrier), member 3	1.84	0.037
MTHFD2	methylene tetrahydrofolate dehydrogenase (NAD+dependent), mitochondrial	1.83	0.046
MDH2	Malate dehydrogenase 2, NAD (mitochondrial)	1.79	0.03
COX5A	Cytochrome c oxidase subunit 5A, mitochondrial	1.78	0.0045
TIMM9	Translocase of inner mitochondrial membrane 9	1.78	0.04
IDH2	Isocitrate dehydrogenase [NADP], mitochondrial	1.70	0.01
PDHA1	Pyruvate dehydrogenase E1 component subunit alpha, mitochondrial	1.67	0.037
MRPL49	39S ribosomal protein L49, mitochondrial	1.63	0.04
ATP5A1	ATP synthase subunit alpha, mitochondrial	1.60	0.03
HADH2	Hydroxyacyl-Coenzyme A dehydrogenase, type II, mitochondrial (HSD17B10)	1.55	0.04
HADHB	Trifunctional enzyme subunit beta, mitochondrial	1.55	0.049
ALDH18A1	Delta-1-pyrroline-5-carboxylate synthase, mitochondrial	1.55	0.02
GLRX5	Glutaredoxin-related protein 5, mitochondrial	1.97	0.03
PMPCB	Mitochondrial-processing peptidase subunit beta	1.69	0.03
MRPS22	28S ribosomal protein S22, mitochondrial	1.51	0.049
Glycolysis and PPP (10)			
G6PD	Glucose-6-phosphate 1-dehydrogenase	10.02	0.0003
GAPDH	Glyceraldehyde-3-phosphate dehydrogenase	8.35	0.003
ENO2	Gamma-enolase	7.72	6.65E-05
PKM1/2	Pyruvate kinase, muscle	5.49	0.0002
ALDOA	Fructose-bisphosphate aldolase	5.44	6.37E-05
ENO1	Alpha-enolase	2.81	0.02
PGD	6-phosphogluconate dehydrogenase, decarboxylating	1.86	0.005
TKT	Transketolase	1.81	0.004
TPI1	Triosephosphate isomerase 1	1.74	0.04
PGAM1	Phosphoglycerate mutase 1 (Brain)	1.62	0.0001
EMT markers and Cytoskeletal proteins (31)			
KRT19	Keratin, type I cytoskeletal 19	23.94	7.17E-06
PFN1	Profilin 1	10.85	0.046
ACTB	Actin, cytoplasmic 1	8.11	0.0002
ACTC1	Actin, alpha cardiac muscle 1	6.37	9.67E-05
ESPNL	Espin-like protein	5.74	2.35E-05
ACTBL2	Beta-actin-like protein 2	4.87	4.54E-06
TUBB2A	Tubulin beta-2A chain	4.70	0.0005
MYL6	Myosin light polypeptide 6	4.70	0.006
TUBB7	Tubulin beta-7 chain	4.40	0.003
EPPK1	Epiplakin	4.32	0.05
AGR2	Anterior gradient protein 2	3.84	0.0007
PAK2	Serine/threonine-protein kinase PAK 2	3.47	4.69E-05
PLEC	Plectin	3.12	0.001
CROCC	Rootletin	2.44	0.007
SPTBN1	Spectrin beta chain, non-erythrocytic 1	2.38	0.01
TPM2	Tropomyosin beta	2.35	0.002
TLN2	Talin-2	2.29	0.02
FLNB	Filamin-B	2.11	0.03
TUBB4	Tubulin beta-4 chain	2.05	0.03
DYNC1I2	Cytoplasmic dynein 1 intermediate chain 2	2.04	0.03
TMOD3	Tropomodulin-3	2.01	2.01E-05
FLNC	Filamin-C	1.93	0.008
ARPC2	Actin related protein 2/3 complex, subunit 2, 34kDa, isoform	1.84	0.047
APC	Adenomatosis polyposis coli	1.82	0.05
DSP	Desmoplakin	1.81	0.009
MYH14	Myosin-14	1.80	0.0006
TLN1	Talin-1	1.68	0.04
MYO1B	Myosin 1B	1.65	0.04
MSN	Moesin	1.59	0.02
TUBA1C	Tubulin alpha-1C	1.54	0.04
DYNLL2	Dynein light chain 2, cytoplasmic	1.52	0.048

Table 2: MCF7-FOXM1 Cells Over-express Key Protein Molecules Functionally Related to Ribosomes and Protein Synthesis.

Symbol	Description	Fold-Upregulation	ANOVA
Ribosome-related proteins (9)			
RPL15	60S ribosomal protein L15	5.49	0.003
RPL8	60S ribosomal protein L8	4.41	0.01
RPS3A	40S ribosomal protein S3A	1.78	0.046
RPL7	60S ribosomal protein L7	1.71	0.02
RPL10A	60S ribosomal protein L10A	1.69	0.006
RPL7A	60S ribosomal protein L7A	1.68	0.02
RRP1B	Ribosomal RNA processing protein 1 homolog B	1.66	0.05
MRPL49	39S ribosomal protein L49, mitochondrial	1.63	0.04
MRPS22	28S ribosomal protein S22, mitochondrial	1.51	0.049
Translation initiation factors (4)			
EIF4G3	Eukaryotic translation initiation factor 4 gamma 3	5.72	3.19E-06
EIF3C	Eukaryotic translation initiation factor 3 subunit C	2.44	0.001
EIF4B	Eukaryotic translation initiation factor 4B	1.83	0.04
EIF3S4	Eukaryotic translation initiation factor 3 subunit G	1.55	0.04
Elongation factors (5)			
EEF1A1	Elongation factor 1-alpha 1	5.63	0.0004
EEF1A2	Elongation factor 1-alpha 2	4.36	0.05
EEF1G	Elongation factor 1-gamma	3.03	0.003
EFTUD2	Elongation factor Tu GTP binding domain containing 2	2.84	4.94E-05
EEF1D	Elongation factor 1-delta	2.16	0.003
Enzymes for tRNA synthesis (6)			
GARS	Glycine--tRNA ligase	4.50	0.0006
DARS	Aspartate--tRNA ligase, cytoplasmic	2.28	0.01
TARS	Threonyl-tRNA synthetase, cytoplasmic	1.82	0.01
HARS	Histidine--tRNA ligase, cytoplasmic	1.82	0.03
RARS	Arginine--tRNA ligase, cytoplasmic	1.70	0.01
AARS	Alanine--tRNA ligase, cytoplasmic	1.56	0.03
Protein folding chaperones (heat shock proteins) (8)			
HSPD1	Heat shock 60kDa protein 1 (Chaperonin), mitochondrial	12.35	0.02
HSPB1	Heat shock protein beta-1	3.00	0.009
HSPA8	Heat shock cognate 71 kDa protein	2.20	0.002
HSP90AB1	Heat shock protein HSP 90-beta	1.97	9.13E-07
CLGN	Calmegin (ER chaperone)	1.59	0.026
HSPA1A	Heat shock 70 kDa protein 1	1.57	0.002
HSPH1	Heat shock 105kDa/110kDa protein 1	1.55	0.02
HSPA6	Heat shock 70 kDa protein 6	1.55	0.006

MCF7 cells. Empty Vector (EV) control cells were generated in parallel. The transcription factor FOXM1 was recently shown to induce the expansion of human normal stem cells, as well as of cancer stem-like cells [21-24]. Mechanistically, it is believed that FOXM1 acts downstream of key signaling pathways essential for stem cell regulation and tumorigenesis, such as Wnt/ β -catenin and 14-3-3 ζ signaling cells [22, 26].

MCF7 cells over-expressing FOXM1 show a 3.3-fold increase in mammosphere formation, relative to empty-vector controls, as expected (Figure 8A). In order to better dissect the molecular changes driven by FOXM1, MCF7 cell monolayers over-expressing FOXM1 and EV control cells were subjected to proteomics analysis. Proteomic datasets of up-regulated proteins in the MCF7-FOXM1 cells were then analyzed with respect to their metabolic protein profiles.

Table 1 shows that several key molecules related to mitochondria, glycolysis and the EMT are up-regulated in FOXM1-over-expressing MCF7 cells, indicating that FOXM1-induced stemness is associated with increased

metabolic flexibility. Notably, keratin-19 (KRT19), a well-established marker of circulating tumor cells and CSCs, is increased by >20-fold in MCF7-FOXM1 cells. Also, four key mitochondrial proteins (HSPD1, ACADVL, ATP5B, COX4I1) are increased by >10-fold each in MCF7-FOXM1 cells; SLC25A4 (the mitochondrial ATP/ADP exchanger) is increased by nearly 6-fold. Similarly, twenty-two other mitochondrial proteins are increased by >1.5 fold.

Moreover, Table 2 shows that several key molecules related to protein synthesis are also up-regulated in FOXM1-overexpressing MCF7 cells. We have previously shown that protein synthesis is a mechanism for enhancing the proliferation of TICs, and that known inhibitors of protein synthesis, such as puromycin and rapamycin, are very effective at reducing mammosphere formation [27]. Similarly, the EMT is also regarded as a key feature of TICs [28, 29]. Consistent with the notion that FOXM1 drives stemness, ribosome-related proteins and EMT markers are increased by FOXM1 expression (Tables 1 and 2).

Table 3. FOXM1 Targets are Transcriptionally Up-regulated in Human Breast Cancer: Mitochondria, Glycolysis and the EMT.

Symbol	Gene Description	Up-regulation (fold-change)	P-value
Mitochondrial-related proteins (23)			
ATP5B	ATP synthase subunit beta, mitochondrial	5.04	2.75E-06
ATP5A1	ATP synthase subunit alpha, mitochondrial	5.01	3.09E-06
MRPL49	39S ribosomal protein L49, mitochondrial	4.94	3.93E-06
MDH2	Malate dehydrogenase 2, NAD (mitochondrial)	4.18	5.32E-05
GLRX5	Glutaredoxin-related protein 5, mitochondrial	4.07	7.83E-05
PMPCB	Mitochondrial-processing peptidase subunit beta	3.81	1.77E-04
SLC25A3	Solute carrier family 25 (mitochondrial phosphate carrier), member 3	3.76	2.09E-04
HSPA9	Heat shock 70kDa protein 9 (Mortalin), mitochondrial	3.69	2.64E-04
COX5A	Cytochrome c oxidase subunit 5A, mitochondrial	3.62	3.22E-04
TIMM9	Translocase of inner mitochondrial membrane 9	3.58	3.69E-04
HSPD1	HSP60, 60 kDa heat shock protein, mitochondrial	3.42	5.93E-04
COX4I1	Cytochrome c oxidase subunit 4 isoform 1, mitochondrial	3.39	6.61E-04
MRPS22	28S ribosomal protein S22, mitochondrial	3.27	9.31E-04
NDUFS1	Mitochondrial NADH-ubiquinone oxidoreductase 75 kDa subunit	3.20	1.15E-03
HADHB	Trifunctional enzyme subunit beta, mitochondrial	3.06	1.73E-03
SUCLG2	Succinate-CoA ligase, GDP-forming, beta subunit	3.03	1.89E-03
CHCHD3	MICOS complex subunit MIC19, mitochondrial	2.74	4.14E-03
MTHFD2	methylene tetrahydrofolate dehydrogenase (NAD ⁺ dependent), mitochondrial	2.67	4.98E-03
IDH2	Isocitrate dehydrogenase [NADP], mitochondrial	2.46	8.55E-03
PRKDC	DNA-dependent protein kinase, catalytic (maintains mt-DNA copy number)	2.14	1.85E-02
ABAT	4-aminobutyrate aminotransferase, mitochondrial	2.08	2.14E-02
PDHA1	Pyruvate dehydrogenase E1 component subunit alpha, mitochondrial	1.89	3.21E-02
Glycolysis and PPP (7)			
TPI1	Triosephosphate isomerase 1	4.21	4.88E-05
ALDOA	Fructose-bisphosphate aldolase	3.60	3.45E-04
PKM1/2	Pyruvate kinase, muscle	3.26	9.79E-04
GAPDH	Glyceraldehyde-3-phosphate dehydrogenase	2.97	2.22E-03
PGAM1	Phosphoglycerate mutase 1 (Brain)	2.55	6.87E-03
TKT	Transketolase	2.20	1.60E-02
ENO1	Alpha-enolase	1.96	2.75E-02
EMT markers and Cytoskeletal proteins (11)			
DSP	Desmoplakin	5.27	1.24E-06
FLNB	Filamin-B	4.81	6.21E-06
KRT19	Keratin, type I cytoskeletal 19	4.39	2.66E-05
DYNC1I2	Cytoplasmic dynein 1 intermediate chain 2	3.90	1.33E-04
MYL6	Myosin light polypeptide 6	3.74	2.22E-04
TUBA1C	Tubulin alpha-1C	3.30	8.64E-04
AGR2	Anterior gradient protein 2	2.94	2.44E-03
PAK2	Serine/threonine-protein kinase PAK 2	2.88	2.86E-03
TUBB2A	Tubulin beta-2A chain	2.63	5.56E-03
PFN1	Profilin 1	2.27	1.36E-02
ARPC2	Actin related protein 2/3 complex, subunit 2, 34kDa, isoform	2.04	2.33E-02

-Transcriptional profiling data derived from the analysis of N=28 breast cancer patients are shown, high-lighting the levels of fold-upregulation observed in the epithelial cancer cell compartment (relative to the tumor stroma), and corresponding p-values derived from the analysis of these clinical samples.

To test if mitochondrial inhibitors could block FOXM1-driven mammosphere formation, we then used several independent pharmacological approaches. Interestingly, formation of FOXM1-driven mammospheres was inhibited by treatment with oligomycin A (Figure 8B), XCT790 (Figure 8C), and doxycycline (Figure 8D). Doxycycline is an FDA-approved antibiotic that we have recently shown to inhibit proliferation of TICs, by targeting their mitochondrial ribosomes [12]. Thus, mitochondrial protein translation and function are required for FOXM1-driven mammosphere formation.

Mitochondrial function is required for 3D-spheroid formation using H295R cells

Finally, we asked if mitochondrial function is required for 3D-spheroid formation of other cell lines, such as H295R adrenocortical carcinoma cells. Figure 9 shows that XCT790 dose-dependently inhibits 3D-spheroid formation of the H295R adrenocortical carcinoma cell line, with an IC₅₀ of 10 μ M. These results indicate that mitochondrial function is required for the 3D-spheroid formation of cell lines other than MCF7 breast cancer cells.

Quantitatively similar results were obtained when XCT790 was tested on several other epithelial cancer

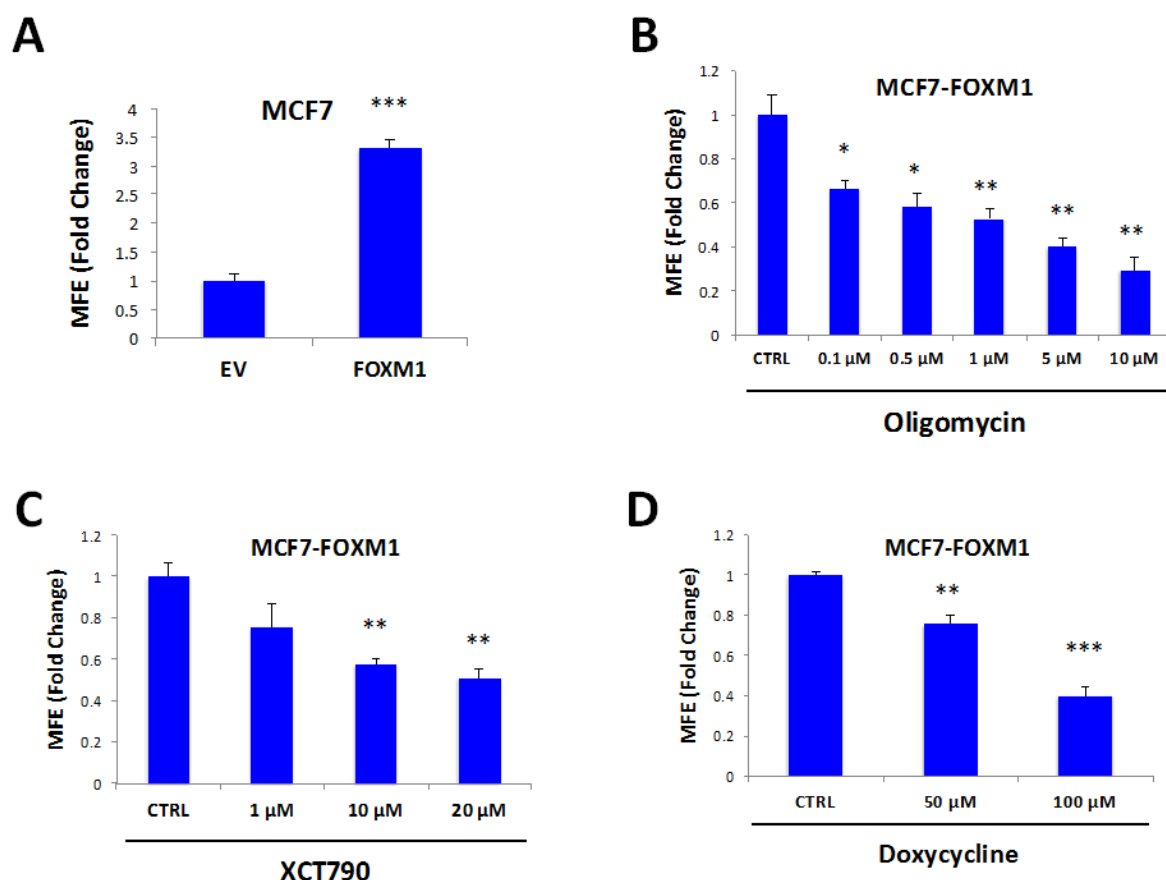


Figure 8: Mammosphere formation driven by FOXM1 requires mitochondrial function. FOXM1 was over-expressed in MCF7 cells using a lentiviral approach. Empty Vector (EV) cells were generated in parallel. **A.** MCF7 cells over-expressing FOXM1 show a >3.3-fold increase in mammosphere formation. **B.** Treatment with oligomycin A, an inhibitor of the mitochondrial ATP synthase, inhibits mammosphere formation in MCF7 cells over-expressing FOXM1. **C.** Treatment with XCT790 inhibits mammosphere formation in MCF7 cells over-expressing FOXM1. **D.** Treatment with doxycycline, an FDA-approved antibiotic that we have recently shown to inhibit proliferation of TICs by targeting TIC mitochondria, inhibits mammosphere formation in MCF7 cells over-expressing FOXM1. Thus, mitochondrial function is required for FOXM1-driven mammosphere formation. EV: Empty Vector. * $p < 0.05$, ** $p < 0.01$, *** $p < 0.001$ evaluated by Student's t test.

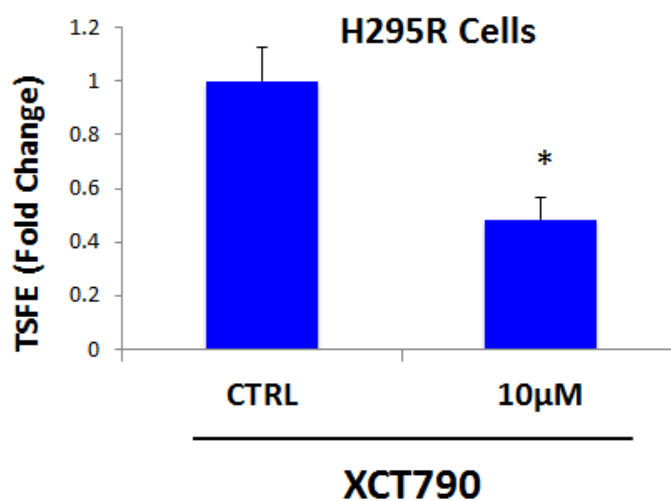


Figure 9: 3D-spheroid formation in H295R cells is dependent upon mitochondrial function. XCT790 dose-dependently inhibits 3D-spheroid formation in H295R cells, an adrenocortical carcinoma cell line, with an IC-50 of 10 μ M. These results indicate that mitochondrial function is required for the 3D-spheroid formation in cell lines other than MCF7 breast cancer cells. TSFE, tumor-sphere forming efficiency; * $p < 0.05$ evaluated by Student's t test.

Table 4: FOXM1 Targets are Transcriptionally Up-regulated in Human Breast Cancer: Ribosomes and Protein Synthesis.

Symbol	Gene Description	Up-regulation (fold-change)	P-value
Ribosome-related proteins (9)			
RPL7A	60S ribosomal protein L7A	5.23	1.41E-06
RPL7	60S ribosomal protein L7	5.21	1.53E-06
RPL10A	60S ribosomal protein L10A	5.09	2.35E-06
MRPL49	39S ribosomal protein L49, mitochondrial	4.94	3.93E-06
RPL15	60S ribosomal protein L15	4.60	1.28E-05
RPS3A	40S ribosomal protein S3A	4.59	1.35E-05
RPL8	60S ribosomal protein L8	3.86	1.51E-04
MRPS22	28S ribosomal protein S22, mitochondrial	3.27	9.31E-04
RRP1B	Ribosomal RNA processing protein 1 homolog B	2.21	1.58E-02
Translation initiation factors (2)			
EIF3C	Eukaryotic translation initiation factor 3 subunit C	4.48	1.94E-05
EIF4B	Eukaryotic translation initiation factor 4B	3.17	1.27E-03
Elongation factors (3)			
EEF1G	Elongation factor 1-gamma	3.71	2.44E-04
EEF1A1	Elongation factor 1-alpha 1	3.16	1.30E-03
EEF1D	Elongation factor 1-delta	2.50	7.67E-03
Enzymes for tRNA synthesis (2)			
DARS	Aspartate--tRNA ligase, cytoplasmic	3.43	5.87E-04
HARS	Histidine--tRNA ligase, cytoplasmic	2.42	9.55E-03
Protein folding chaperones (heat shock proteins) (5)			
HSP90AB1	Heat shock protein HSP 90-beta	4.93	5.93E-06
HSPD1	Heat shock 60kDa protein 1 (Chaperonin), mitochondrial	3.42	5.93E-04
HSPB1	Heat shock protein beta-1	3.27	9.51E-04
HSPH1	Heat shock 105kDa/110kDa protein 1	3.18	1.22E-03
HSPA8	Heat shock cognate 71 kDa protein	2.54	7.06E-03

-Transcriptional profiling data derived from the analysis of N=28 breast cancer patients are shown, high-lighting the levels of fold-upregulation observed in the epithelial cancer cell compartment (relative to the tumor stroma), and corresponding p-values derived from the analysis of these clinical samples.

cell lines, indicating that the ability of XCT790 to inhibit 3D-spheroid formation reflects a general property of CSCs (data not shown).

Relevance of FOXM1-related targets in human breast cancers

To assess the possible clinical relevance of our results, we also determined whether the proteomic targets that we identified in MCF7-FOXM1 cells were transcriptionally over-expressed in human breast cancer cells *in vivo*. Towards this end, we exploited a clinical data set of tumor samples from 28 breast cancer patients. These tumor samples were subjected to laser-capture micro-dissection, to separate epithelial cancer cells from adjacent tumor stroma [30].

Tables 3 and 4 present a summary of these findings. Overall, greater than fifty FOXM1 targets (related to mitochondria, glycolysis, the EMT, and protein synthesis) that we identified in MCF7-FOXM1 cells were also transcriptionally elevated in human breast cancer cells *in vivo*. As such, the new FOXM1 protein targets that we identified in MCF7-FOXM1 cells may be especially relevant for improving human breast cancer diagnosis and therapy.

DISCUSSION

Here, we specifically tested the hypothesis that new mitochondrial biogenesis is required for the survival and propagation of stem-like cancer cells. For this purpose, we used an investigational inhibitor of the $ERR\alpha$ -PGC1 α / β signaling pathway, namely XCT790, to interrogate the role of mitochondrial biogenesis and function in the anchorage-independent growth of CSCs. Importantly, treatment with XCT790 blocked mammosphere formation and prevented anoikis-resistance in CD44(+)/high/CD24(-)/low MCF7 cells. Mechanistically, XCT790 inhibited mitochondrial function (OCR) and effectively reduced signaling along a number of classical stem cell transduction pathways, such as the Hedgehog/GLI, TGF β /SMAD, and Wnt/ β -catenin signaling. Overexpression of either $ERR\alpha$ or FOXM1 (a down-stream target of Wnt-signaling [22]) in MCF7 cells significantly augmented mammosphere formation, which could be prevented by a number of mitochondrial inhibitors. In this regard, doxycycline treatment was sufficient to overcome the effects of FOXM1 on mammosphere formation. Interestingly, doxycycline is an FDA-approved antibiotic that has been used for nearly 50 years to treat a wide variety of bacterial and parasitic infections, without significant side effects. Finally, unbiased proteomics analysis of

MCF7-FOXM1 cells revealed the up-regulation of specific mitochondrial proteins, glycolytic enzymes, EMT markers and components of the protein synthesis machinery. Importantly, these FOXM1 target proteins were also transcriptionally up-regulated in patient samples *in vivo*, in human breast cancer epithelial cells isolated by laser-capture micro-dissection, highlighting their clinical relevance.

Many other recent studies have also directly implicated augmented mitochondrial function in resistance to chemotherapy and radiation [31-36], in the survival of treatment-resistant cancer stem-like cells [37], in the propagation and motility of circulating tumor cells [38], as well as in tumor growth and cancer cell metastasis in pre-clinical animal models *in vivo* [39-44].

Consistent with our current findings, we have previously shown that a PGC1/NRF1 gene signature predicts tumor recurrence, metastasis and poor overall survival in ER(+)/Luminal-A breast cancer patients [45]. This PGC1/NRF1 gene signature was also elevated in >2,000 human tumors excised from breast cancer patients, including both ER(+) and ER(-) cases [45]. Moreover,

recombinant over-expression of PGC1 α/β , or other genes that promote mitochondrial biogenesis (MitoNEET/POLRMT), in MDA-MB-231 cells, was indeed sufficient to functionally increase tumor growth by up to ~3-fold [43].

Asymmetric cell division is an essential characteristic of stem cells. Interestingly, Sabatini, Weinberg and colleagues examined the segregation of “newly-synthesized” and “older” mitochondria in immortalized mammary epithelial cells, during asymmetric cell division, a property that is also a characteristic of CSCs [46]. They observed that “newly-synthesized” mitochondria were preferentially enriched in stem cells during asymmetric cell division, while “old” mitochondria were segregated into the daughter cells [46]. These results imply that asymmetric cell division in stem cells somehow requires new mitochondrial biogenesis, for the propagation and maintenance of the stem cell phenotype.

As such, these findings may help to mechanistically explain our current results that new mitochondrial biogenesis is required for the efficient propagation of and

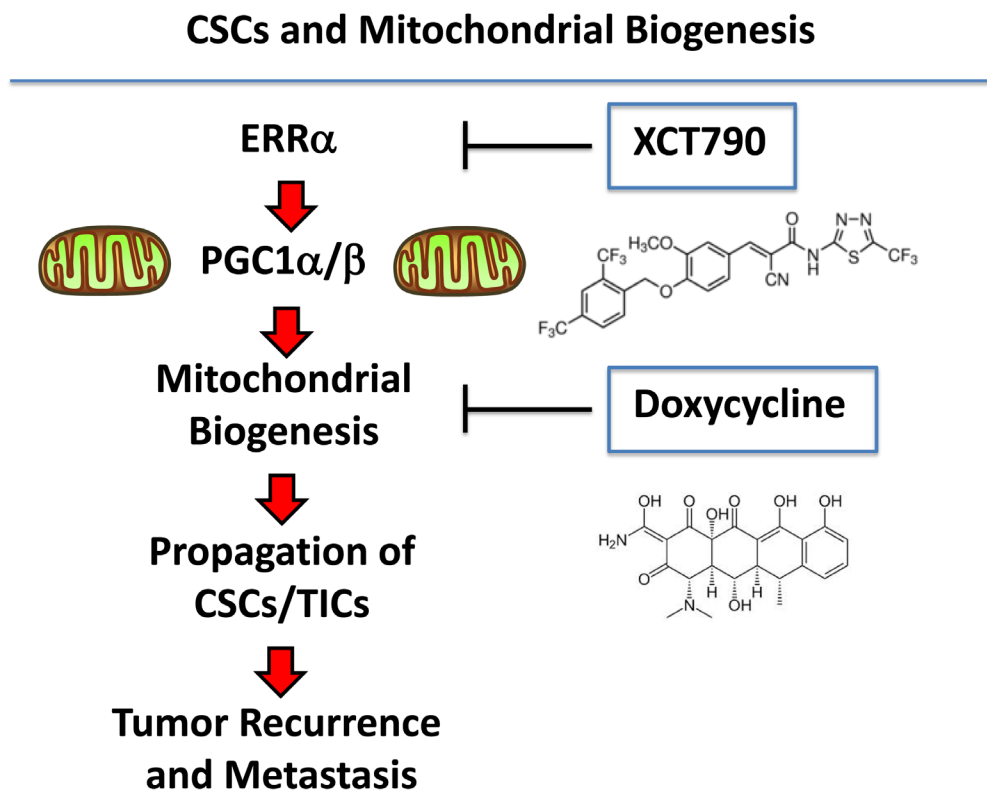


Figure 10: Understanding the role of mitochondrial biogenesis and function in the propagation of CSCs/TICs. ERR α is a co-factor for PGC1 α/β , which is a well-established transcription factor that is critical for driving new mitochondrial biogenesis. Here, we show that three different classes of mitochondrial inhibitors (XCT790, oligomycin A and doxycycline) all prevent the propagation of CSCs/TICs. XCT790 is an inverse agonist of ERR α . Oligomycin A is an inhibitor of the mitochondrial ATP-synthase (complex V) (not shown). Finally, doxycycline is an inhibitor of mitochondrial protein synthesis, as it binds directly to the small subunit of the mitochondrial ribosome. This reflects the fact that mitochondria were originally derived from aerobic bacteria that evolved over millions of years, to establish a symbiotic relationship with the host cell. The chemical structures of XCT790 and doxycycline are also shown.

survival of CSCs (Figure 10), as we have seen using the mammosphere and anoikis-resistance assays, to measure stem cell activity. Taken together, these data implicate mitochondrial biogenesis and mitochondrial function as critical targets for new drug discovery, to overcome tumor recurrence, distant metastasis and drug-resistance, especially in cancer patients with clinically advanced disease.

MATERIALS AND METHODS

Materials

MCF7 breast cancer cells were purchased from the ATCC. H295R adrenocortical carcinoma cells were a generous gift of Dr. Antonio Stigliano (University of Rome). Gibco-brand cell culture media (DMEM/F12) was purchased from Life Technologies. XCT790 was purchased from Tocris, oligomycin A and doxycycline were purchased from Sigma-Aldrich. Lentiviral vectors for the expression of ERR α (#Z1441) and FOXM1 (#U1376) were obtained commercially from Genecopoeia, along with the appropriate empty vector controls, in the Lv-105 (Puro^R) vector system.

Mammosphere culture

A single cell suspension was prepared using enzymatic (1x Trypsin-EDTA, Sigma Aldrich, #T3924), and manual disaggregation (25 gauge needle) to create a single cell suspension [8]. Cells were plated at a density of 500 cells/cm² in mammosphere medium (DMEM-F12/ B27/ EGF(20ng/ml)/ Pen-Strep) in non-adherent conditions, in culture dishes coated with (2-hydroxyethylmethacrylate) (poly-HEMA, Sigma, #P3932). Cells were grown for 5 days and maintained in a humidified incubator at 37°C at an atmospheric pressure in 5% (v/v) carbon dioxide/air. After 5 days for culture, spheres >50 μ m were counted using an eye piece graticule, and the percentage of cells plated which formed spheres was calculated and is referred to as percentage mammosphere formation, and was normalized to one (1 = 100 %MSE, mammosphere forming efficiency). For pharmacological inhibition of mammosphere formation, cells were directly seeded on low-attachment plates in the presence of XCT790 or oligomycin or doxycycline at the indicated concentrations.

Pre-treatment of monolayers with XCT790

After incubation with XCT790 (5 or 10 μ M for 48 hours), MCF7 cell monolayers were trypsinized and seeded for mammosphere cultures for 5 days, without

XCT790.

Lentiviruses

Lentiviral plasmids, packaging cells and reagents were from Genecopoeia. 48 hours after seeding, 293Ta packaging cells were transfected with lentiviral vectors encoding ERR α , FOXM1 or empty vector (EX-NEG-Lv105), using Lenti-PacTM HIV Expression Packaging Kit according to the manufacturer's instructions. Two days post-transfection, lentivirus-containing culture medium was passed through a 0.45 μ m filter and added to the target cells (MCF7 cells) in the presence of 5 μ g/ml Polybrene. Infected cells were selected with a concentration of 1.5 μ g/ml of puromycin.

CD44/CD24 analysis

Following XCT790 treatment for 48 hours, the TIC population was enriched by seeding on low-attachment plates. Under these conditions, the non-TIC population undergoes anoikis (a form of apoptosis induced by a lack of cell-substrate attachment) and TICs are believed to survive. The surviving TIC fraction was analyzed by FACS analysis. Briefly, 1 x 10⁴ MCF7 monolayer cells were treated with XCT790 (5 μ M and 10 μ M) for 48h in 6-well plates. Then, cells were trypsinized and seeded in low-attachment plates in mammosphere media. After 10h, MCF7 cells were spun down and incubated with CD24 (IOtest CD24-PE, Beckman Coulter) and CD44 (APC mouse Anti-Human CD44, BD Pharmingen cat.559942) antibodies for 15 minutes on ice. Cells were rinsed twice and incubated with LIVE/DEAD dye (Fixable Dead Violet reactive dye; Invitrogen) for 10 minutes. Samples were then analyzed by FACS (Fortessa, BD Bioscience). Only the live population, as identified by the LIVE/DEAD dye staining, was analyzed for CD24/CD44 expression. Data were analyzed using FlowJo software.

Viability assay

Cell viability was assessed by sulphorhodamine (SRB) assay, based on the measurement of cellular protein content. After treatment with XCT790 for 3 or 5 days in 96 well plates, cells were fixed with 10% trichloroacetic acid (TCA) for 1h in cold room, and dried overnight at room temperature. Then, cells were incubated with SRB for 15 min, washed twice with 1% acetic acid, and air dried for at least 1h. Finally, the protein-bound dye was dissolved in 10 mM Tris pH 8.8 solution and read using the plate reader at 540 nm.

Evaluation of CSC signalling pathways

The Cignal Lenti reporter assay (luc) system (Qiagen) was chosen for monitoring the activity of several signaling pathways in MCF7 cells [25]. The responsive luciferase constructs encode the firefly luciferase reporter gene under the control of a minimal (m)CMV promoter and tandem repeats of response elements for each pathway. The following constructs were used: TCF/LEF(luc) for Wnt signaling (CLS-018L); STAT3(luc) for transcriptional activity of STAT3 (CLS-6028L); RBP-Jk(luc) for Notch-induced signaling (CLS-014L); ARE(luc) for Nrf2- and Nrf1-mediated antioxidant response (CLS-2020L); GAS(luc) for IFN γ -induced Stat1-signaling (CLS-009L); ISRE(luc) for (IFN)- α/β -STAT1/2 signaling (CLS-008L); SMAD(luc) for TGF β -induced signaling (CLS-017L); GLI(luc) for Sonic hedgehog signaling (CLS-6030L). Briefly, 1×10^5 MCF7 cells were seeded in 12-well plates. Once cells were attached, the viral particles were diluted 1:10 in complete culture media containing polybrene (sc-134220, Santa Cruz), and added to the cells. Puromycin treatment (#P9620, Sigma) was started 48 hours later in order to select stably infected cells.

Luciferase assay

Luciferase Assay System (E1501, Promega) was performed in all luciferase reporter MCF7 cells treated with XCT790. Briefly, 6×10^3 MCF7 cells were seeded in black-walled 96-well plates and then were treated with XCT790 (10 μ g/ml). As control, vehicle-treated cells were run in parallel. Four replicates were used for each condition. After 48 hours of treatment, luciferase assay was performed according to the manufacturer's instructions. Light signal was acquired for 2 minutes in photons/second in the Xenogen VivoVision IVIS Lumina (Caliper Life Sciences), and the results were analysed using the Living Image 3.2 software (Caliper Life Sciences). Luminescence was normalized using total proteins, as assessed with the Bradford protein assay.

Mitochondrial staining

To measure mitochondrial activity, cells were stained with MitoTracker Orange (#M7510, Invitrogen), whose accumulation in mitochondria is dependent upon membrane potential. To measure mitochondrial mass, cells were stained with MitoTracker Green (#M7514 Invitrogen), or MitoTracker Deep Red (#M22426, Invitrogen), both localizing to mitochondria regardless of mitochondrial membrane potential. Briefly, MCF7 cells were treated with XCT790 for 48 hours. Cells were then incubated with pre-warmed MitoTracker staining solution (diluted in PBS/CM to a final concentration of 10 nM) for

30-60 min at 37 °C. All subsequent steps were performed in the dark. Cells were washed in PBS, harvested, and resuspended in 300 μ L of PBS. Cells were then analyzed by flow cytometry. Data analysis was performed using FlowJo software.

Seahorse XFe96 metabolic flux analysis

Extracellular acidification rates (ECAR) and real-time oxygen consumption rates (OCR) for MCF7 cells treated with XCT790 or vehicle alone control were determined using the Seahorse Extracellular Flux (XF96) analyzer (Seahorse Bioscience, MA, USA). MCF7 cells were maintained in DMEM supplemented with 10% FBS (fetal bovine serum), 2 mM GlutaMAX, and 1% Pen-Strep. 7,000 cells were seeded per well into XF96-well cell culture plates, and incubated overnight at 37°C in a 5% CO $_2$ humidified atmosphere. After 24h, cells were treated with XCT790 (5 μ M or 10 μ M) for 48h. After 48h of treatment, cells were washed in pre-warmed XF assay media (for OCR measurement, XF assay media was supplemented with 10mM glucose, 1mM Pyruvate, 2mM L-glutamine and adjusted at pH 7.4). Cells were then maintained in 175 μ L/well of XF assay media at 37°C, in a non-CO $_2$ incubator for 1h. During the cell incubation time, we loaded 25 μ L each of 80mM glucose, 9 μ M oligomycin, 1M 2-deoxyglucose (for ECAR measurement) and 25 μ L each of 10 μ M oligomycin, 9 μ M FCCP, 10 μ M rotenone, 10 μ M antimycin A (for OCR measurement), in XF assay media into the injection ports in the XFe-96 sensor cartridge. ECAR and OCR measurements were normalized by protein content. Data set was analyzed by XFe-96 software and GraphPad Prism software, using one-way ANOVA and Student's t-test calculations. All experiments were performed in quintuplicate, three times independently, such that each data point represents the average of 15 replicates.

Label-free quantitative proteomics analysis

Cell lysates were prepared for trypsin digestion by sequential reduction of disulphide bonds with TCEP and alkylation with MMTS [47]. Then, the peptides were extracted and prepared for LC-MS/MS. All LC-MS/MS analyses were performed on an LTQ Orbitrap XL mass spectrometer (Thermo Scientific, San Jose, CA) coupled to an Ultimate 3000 RSLCnano system (Thermo Scientific, formerly Dionex, The Netherlands). Xcalibur raw data files acquired on the LTQ-Orbitrap XL were directly imported into Progenesis LCMS software (Waters Corp., Milford, MA, formerly Non-linear dynamics, Newcastle upon Tyne, UK) for peak detection and alignment. Data were analyzed using the Mascot search engine. Five replicates were analyzed for each sample type ($N = 5$). Statistical analyses were performed using ANOVA and

only fold-changes in proteins with a p-value less than 0.05 were considered significant.

Data mining

To firmly establish the clinical relevance of our results from the quantitative proteomics analysis of mammospheres, we re-analyzed the transcriptional profiles of epithelial breast cancer cells and adjacent tumor stromal cells that were physically separated by laser-capture microdissection (from $N = 28$ human breast cancer patients) [30].

ACKNOWLEDGMENTS

We thank the University of Manchester for providing start-up funds that contributed to the success of this study. FS and MPL were supported, in part, by funding from the European Union (ERC Advanced Grant), Breakthrough Breast Cancer, and the Manchester Cancer Research Centre (MCRC). DLS was core-funded by CRUK. ADL was supported by an E.U. grant for post-doctoral associates: Unical (POR Calabria FSE 2007-2013). VP was funded by a grant from the Associazione Italiana per la Ricerca sul Cancro (AIRC), project n. IG14433.

CONFLICTS OF INTEREST

There is no conflict of interest.

REFERENCES

1. Sinha N, Mukhopadhyay S, Das DN, Panda PK and Bhutia SK. Relevance of cancer initiating/stem cells in carcinogenesis and therapy resistance in oral cancer. *Oral oncology*. 2013; 49:854-862.
2. Scopelliti A, Cammareri P, Catalano V, Saladino V, Todaro M and Stassi G. Therapeutic implications of Cancer Initiating Cells. *Expert opinion on biological therapy*. 2009; 9:1005-1016.
3. Xin H, Kong Y, Jiang X, Wang K, Qin X, Miao ZH, Zhu Y and Tan W. Multi-drug-resistant cells enriched from chronic myeloid leukemia cells by Doxorubicin possess tumor-initiating-cell properties. *Journal of pharmacological sciences*. 2013; 122:299-304.
4. Easwaran H, Tsai HC and Baylin SB. Cancer epigenetics: tumor heterogeneity, plasticity of stem-like states, and drug resistance. *Molecular cell*. 2014; 54:716-727.
5. Takebe N, Miele L, Harris PJ, Jeong W, Bando H, Kahn M, Yang SX and Ivy SP. Targeting Notch, Hedgehog, and Wnt pathways in cancer stem cells: clinical update. *Nature reviews Clinical oncology*. 2015.
6. Angeloni V, Tiberio P, Appierto V and Daidone MG. Implications of stemness-related signaling pathways in breast cancer response to therapy. *Seminars in cancer biology*. 2015; 31:43-51.
7. Maccalli C and De Maria R. Cancer stem cells: perspectives for therapeutic targeting. *Cancer immunology, immunotherapy* : CII. 2015; 64:91-97.
8. Shaw FL, Harrison H, Spence K, Ablett MP, Simoes BM, Farnie G and Clarke RB. A detailed mammosphere assay protocol for the quantification of breast stem cell activity. *Journal of mammary gland biology and neoplasia*. 2012; 17:111-117.
9. Alvero AB, Montagna MK, Holmberg JC, Craveiro V, Brown D and Mor G. Targeting the mitochondria activates two independent cell death pathways in ovarian cancer stem cells. *Molecular cancer therapeutics*. 2011; 10:1385-1393.
10. Pasto A, Bellio C, Pilotto G, Ciminale V, Silic-Benussi M, Guzzo G, Rasola A, Frasson C, Nardo G, Zulato E, Nicoletto MO, Manicone M, Indraccolo S and Amadori A. Cancer stem cells from epithelial ovarian cancer patients privilege oxidative phosphorylation, and resist glucose deprivation. *Oncotarget*. 2014; 5:4305-4319.
11. Lamb R, Harrison H, Hulit J, Smith DL, Lisanti MP and Sotgia F. Mitochondria as new therapeutic targets for eradicating cancer stem cells: Quantitative proteomics and functional validation via MCT1/2 inhibition. *Oncotarget*. 2014; 5:11029-11037.
12. Lamb R, Ozsvari B, Lisanti CL, Tanowitz HB, Howell A, Martinez-Outschoorn UE, Sotgia F and Lisanti MP. Antibiotics that target mitochondria effectively eradicate cancer stem cells, across multiple tumor types: Treating cancer like an infectious disease. *Oncotarget*. 6:4569-4584.
13. Vlashi E, Lagadec C, Vergnes L, Matsutani T, Masui K, Poulou M, Popescu R, Della Donna L, Evers P, Dekmezian C, Reue K, Christofk H, Mischel PS and Pajonk F. Metabolic state of glioma stem cells and nontumorigenic cells. *Proceedings of the National Academy of Sciences of the United States of America*. 2011; 108:16062-16067.
14. Vlashi E, Lagadec C, Vergnes L, Reue K, Frohnen P, Chan M, Alhiyari Y, Dratver MB and Pajonk F. Metabolic differences in breast cancer stem cells and differentiated progeny. *Breast cancer research and treatment*. 2014; 146:525-534.
15. Busch BB, Stevens WC, Jr., Martin R, Ordentlich P, Zhou S, Sapp DW, Horlick RA and Mohan R. Identification of a selective inverse agonist for the orphan nuclear receptor estrogen-related receptor alpha. *Journal of medicinal chemistry*. 2004; 47:5593-5596.
16. Deblois G and Giguere V. Functional and physiological genomics of estrogen-related receptors (ERRs) in health and disease. *Biochimica et biophysica acta*. 2011; 1812:1032-1040.
17. Deblois G, St-Pierre J and Giguere V. The PGC-1/ERR signaling axis in cancer. *Oncogene*. 2013; 32:3483-3490.
18. Fisher KW, Das B, Kortum RL, Chaika OV and Lewis RE. Kinase suppressor of ras 1 (KSR1) regulates PGC1alpha

- and estrogen-related receptor alpha to promote oncogenic Ras-dependent anchorage-independent growth. *Molecular and cellular biology*. 2011; 31:2453-2461.
19. Wu F, Wang J, Wang Y, Kwok TT, Kong SK and Wong C. Estrogen-related receptor alpha (ERRalpha) inverse agonist XCT-790 induces cell death in chemotherapeutic resistant cancer cells. *Chemico-biological interactions*. 2009; 181:236-242.
 20. Cassano P, Sciancalepore AG, Pesce V, Fluck M, Hoppeler H, Calvani M, Mosconi L, Cantatore P and Gadaleta MN. Acetyl-L-carnitine feeding to unloaded rats triggers in soleus muscle the coordinated expression of genes involved in mitochondrial biogenesis. *Biochimica et biophysica acta*. 2006; 1757:1421-1428.
 21. Gemenetzidis E, Elena-Costea D, Parkinson EK, Waseem A, Wan H and Teh MT. Induction of human epithelial stem/progenitor expansion by FOXM1. *Cancer research*. 2010; 70:9515-9526.
 22. Zhang N, Wei P, Gong A, Chiu WT, Lee HT, Colman H, Huang H, Xue J, Liu M, Wang Y, Sawaya R, Xie K, Yung WK, Medema RH, He X and Huang S. FoxM1 promotes beta-catenin nuclear localization and controls Wnt target-gene expression and glioma tumorigenesis. *Cancer cell*. 2011; 20:427-442.
 23. Bao B, Wang Z, Ali S, Kong D, Banerjee S, Ahmad A, Li Y, Azmi AS, Miele L and Sarkar FH. Over-expression of FoxM1 leads to epithelial-mesenchymal transition and cancer stem cell phenotype in pancreatic cancer cells. *Journal of cellular biochemistry*. 2011; 112:2296-2306.
 24. Chiu WT, Huang YF, Tsai HY, Chen CC, Chang CH, Huang SC, Hsu KF and Chou CY. FOXM1 confers to epithelial-mesenchymal transition, stemness and chemoresistance in epithelial ovarian carcinoma cells. *Oncotarget*. 2015; 6:2349-2365.
 25. Peiris-Pages M, Sotgia F and Lisanti MP. Chemotherapy induces the cancer-associated fibroblast phenotype, activating paracrine hedgehog-GLI signaling in breast cancer cells. *Oncotarget*. 6:10728-10745.
 26. Bergamaschi A, Christensen BL and Katzenellenbogen BS. Reversal of endocrine resistance in breast cancer: interrelationships among 14-3-3zeta, FOXM1, and a gene signature associated with mitosis. *Breast cancer research : BCR*. 2011; 13:R70.
 27. Lamb R, Harrison H, Smith DL, Townsend PA, Jackson T, Ozsvari B, Martinez-Outschoorn UE, Pestell RG, Howell A, Lisanti MP and Sotgia F. Targeting tumor-initiating cells: eliminating anabolic cancer stem cells with inhibitors of protein synthesis or by mimicking caloric restriction. *Oncotarget*. 2015; 6:4585-4601.
 28. Scheel C, Eaton EN, Li SH, Chaffer CL, Reinhardt F, Kah KJ, Bell G, Guo W, Rubin J, Richardson AL and Weinberg RA. Paracrine and autocrine signals induce and maintain mesenchymal and stem cell states in the breast. *Cell*. 2011; 145:926-940.
 29. Mani SA, Guo W, Liao MJ, Eaton EN, Ayyanan A, Zhou AY, Brooks M, Reinhard F, Zhang CC, Shipitsin M, Campbell LL, Polyak K, Brisken C, Yang J and Weinberg RA. The epithelial-mesenchymal transition generates cells with properties of stem cells. *Cell*. 2008; 133:704-715.
 30. Casey T, Bond J, Tighe S, Hunter T, Lintault L, Patel O, Eneman J, Crocker A, White J, Tessitore J, Stanley M, Harlow S, Weaver D, Muss H and Plaut K. Molecular signatures suggest a major role for stromal cells in development of invasive breast cancer. *Breast cancer research and treatment*. 2009; 114:47-62.
 31. Bowling BD, Doudican N, Manga P and Orlow SJ. Inhibition of mitochondrial protein translation sensitizes melanoma cells to arsenic trioxide cytotoxicity via a reactive oxygen species dependent mechanism. *Cancer chemotherapy and pharmacology*. 2008; 63:37-43.
 32. Martinez-Outschoorn UE, Goldberg A, Lin Z, Ko YH, Flomenberg N, Wang C, Pavlides S, Pestell RG, Howell A, Sotgia F and Lisanti MP. Anti-estrogen resistance in breast cancer is induced by the tumor microenvironment and can be overcome by inhibiting mitochondrial function in epithelial cancer cells. *Cancer biology & therapy*. 2011; 12:924-938.
 33. Martinez-Outschoorn UE, Prisco M, Ertel A, Tsirigos A, Lin Z, Pavlides S, Wang C, Flomenberg N, Knudsen ES, Howell A, Pestell RG, Sotgia F and Lisanti MP. Ketones and lactate increase cancer cell "stemness," driving recurrence, metastasis and poor clinical outcome in breast cancer: achieving personalized medicine via Metabolo-Genomics. *Cell cycle*. 2011; 10:1271-1286.
 34. Lu CL, Qin L, Liu HC, Candas D, Fan M and Li JJ. Tumor cells switch to mitochondrial oxidative phosphorylation under radiation via mTOR-mediated hexokinase II inhibition--a Warburg-reversing effect. *PloS one*. 2015; 10:e0121046.
 35. Whitaker-Menezes D, Martinez-Outschoorn UE, Flomenberg N, Birbe RC, Witkiewicz AK, Howell A, Pavlides S, Tsirigos A, Ertel A, Pestell RG, Broda P, Minetti C, Lisanti MP and Sotgia F. Hyperactivation of oxidative mitochondrial metabolism in epithelial cancer cells in situ: visualizing the therapeutic effects of metformin in tumor tissue. *Cell cycle*. 2011; 10:4047-4064.
 36. Ko YH, Lin Z, Flomenberg N, Pestell RG, Howell A, Sotgia F, Lisanti MP and Martinez-Outschoorn UE. Glutamine fuels a vicious cycle of autophagy in the tumor stroma and oxidative mitochondrial metabolism in epithelial cancer cells: implications for preventing chemotherapy resistance. *Cancer biology & therapy*. 2011; 12:1085-1097.
 37. Viale A, Pettazoni P, Lyssiotis CA, Ying H, Sanchez N, Marchesini M, Carugo A, Green T, Seth S, Giuliani V, Kost-Alimova M, Muller F, Colla S, Nezi L, Genovese G, Deem AK, et al. Oncogene ablation-resistant pancreatic cancer cells depend on mitochondrial function. *Nature*. 2014; 514:628-632.
 38. LeBleu VS, O'Connell JT, Gonzalez Herrera KN, Wikman

- H, Pantel K, Haigis MC, de Carvalho FM, Damascena A, Domingos Chinen LT, Rocha RM, Asara JM and Kalluri R. PGC-1 α mediates mitochondrial biogenesis and oxidative phosphorylation in cancer cells to promote metastasis. *Nature cell biology*. 2014; 16:992-1003, 1001-1015.
39. Bonucci G, Tsirogos A, Whitaker-Menezes D, Pavlides S, Pestell RG, Chiavarina B, Frank PG, Flomenberg N, Howell A, Martinez-Outschoorn UE, Sotgia F and Lisanti MP. Ketones and lactate “fuel” tumor growth and metastasis: Evidence that epithelial cancer cells use oxidative mitochondrial metabolism. *Cell cycle*. 2010; 9:3506-3514.
 40. Martinez-Outschoorn UE, Sotgia F and Lisanti MP. Power surge: supporting cells “fuel” cancer cell mitochondria. *Cell metabolism*. 2012; 15:4-5.
 41. Son J, Lyssiotis CA, Ying H, Wang X, Hua S, Ligorio M, Perera RM, Ferrone CR, Mullarky E, Shyh-Chang N, Kang Y, Fleming JB, Bardeesy N, Asara JM, Haigis MC, DePinho RA, et al. Glutamine supports pancreatic cancer growth through a KRAS-regulated metabolic pathway. *Nature*. 2013; 496:101-105.
 42. Tan AS, Baty JW, Dong LF, Bezawork-Geleta A, Endaya B, Goodwin J, Bajzikova M, Kovarova J, Peterka M, Yan B, Pesdar EA, Sobol M, Filimonenko A, Stuart S, Vondrusova M, Kluckova K, et al. Mitochondrial genome acquisition restores respiratory function and tumorigenic potential of cancer cells without mitochondrial DNA. *Cell metabolism*. 2015; 21:81-94.
 43. Salem AF, Whitaker-Menezes D, Howell A, Sotgia F and Lisanti MP. Mitochondrial biogenesis in epithelial cancer cells promotes breast cancer tumor growth and confers autophagy resistance. *Cell cycle*. 2012; 11:4174-4180.
 44. Martinez-Outschoorn UE, Sotgia F and Lisanti MP. Caveolae and signalling in cancer. *Nature reviews Cancer*. 2015; 15:225-237.
 45. Ertel A, Tsirogos A, Whitaker-Menezes D, Birbe RC, Pavlides S, Martinez-Outschoorn UE, Pestell RG, Howell A, Sotgia F and Lisanti MP. Is cancer a metabolic rebellion against host aging? In the quest for immortality, tumor cells try to save themselves by boosting mitochondrial metabolism. *Cell Cycle*. 2012; 11:253-63.
 46. Katajisto P, Dohla J, Chaffer CL, Pentimikko N, Marjanovic N, Iqbal S, Zoncu R, Chen W, Weinberg RA and Sabatini DM. Stem cells. Asymmetric apportioning of aged mitochondria between daughter cells is required for stemness. *Science*. 2015; 348:340-343.
 47. Holland M, Castro FV, Alexander S, Smith D, Liu J, Walker M, Bitton D, Mulryan K, Ashton G, Blaylock M, Bagley S, Connolly Y, Bridgeman J, Miller C, Krishnan S, Dempsey C, et al. RAC2, AEP, and ICAM1 expression are associated with CNS disease in a mouse model of pre-B childhood acute lymphoblastic leukemia. *Blood*. 2011; 118:638-649.

Doxycycline down-regulates DNA-PK and radiosensitizes tumor initiating cells: Implications for more effective radiation therapy

Rebecca Lamb^{1,2}, Marco Fiorillo^{1,2,3}, Amy Chadwick^{1,2}, Bela Ozsvari^{1,2}, Kimberly J. Reeves^{1,2}, Duncan L. Smith⁴, Robert B. Clarke¹, Sacha J. Howell¹, Anna Rita Cappello³, Ubaldo E. Martinez-Outschoorn⁵, Maria Peiris-Pagès^{1,2}, Federica Sotgia^{1,2}, Michael P. Lisanti^{1,2}

¹The Breakthrough Breast Cancer Research Unit, Institute of Cancer Sciences, University of Manchester, UK

²The Manchester Centre for Cellular Metabolism (MCCM), Institute of Cancer Sciences, University of Manchester, UK

³The Department of Pharmacy, Health and Nutritional Sciences, The University of Calabria, Italy

⁴The Cancer Research UK Manchester Institute, University of Manchester, UK

⁵The Sidney Kimmel Cancer Center, Philadelphia, PA, USA

Correspondence to:

Michael P. Lisanti, **e-mail:** michaelp.lisanti@gmail.com

Federica Sotgia, **e-mail:** fsotgia@gmail.com

Keywords: doxycycline, mitochondrial biogenesis, radiation resistance, proteomic analysis, DNA-PK

Abbreviations: CSCs, cancer stem-like cells; TICs, tumor-initiating cells

Received: February 21, 2015

Accepted: June 01, 2015

Published: June 13, 2015

ABSTRACT

DNA-PK is an enzyme that is required for proper DNA-repair and is thought to confer radio-resistance in cancer cells. As a consequence, it is a high-profile validated target for new pharmaceutical development. However, no FDA-approved DNA-PK inhibitors have emerged, despite many years of drug discovery and lead optimization. This is largely because existing DNA-PK inhibitors suffer from poor pharmacokinetics. They are not well absorbed and/or are unstable, with a short plasma half-life. Here, we identified the first FDA-approved DNA-PK inhibitor by "chemical proteomics". In an effort to understand how doxycycline targets cancer stem-like cells (CSCs), we serendipitously discovered that doxycycline reduces DNA-PK protein expression by nearly 15-fold (> 90%). In accordance with these observations, we show that doxycycline functionally radiosensitizes breast CSCs, by up to 4.5-fold. Moreover, we demonstrate that DNA-PK is highly over-expressed in both MCF7- and T47D-derived mammospheres. Interestingly, genetic or pharmacological inhibition of DNA-PK in MCF7 cells is sufficient to functionally block mammosphere formation. Thus, it appears that active DNA-repair is required for the clonal expansion of CSCs. Mechanistically, doxycycline treatment dramatically reduced the oxidative mitochondrial capacity and the glycolytic activity of cancer cells, consistent with previous studies linking DNA-PK expression to the proper maintenance of mitochondrial DNA integrity and copy number. Using a luciferase-based assay, we observed that doxycycline treatment quantitatively reduces the anti-oxidant response (NRF1/2) and effectively blocks signaling along multiple independent pathways normally associated with stem cells, including STAT1/3, Sonic Hedgehog (Shh), Notch, WNT and TGF-beta signaling. In conclusion, we propose that the efficacy of doxycycline as a DNA-PK inhibitor should be tested in Phase-II clinical trials, in combination with radio-therapy. Doxycycline has excellent pharmacokinetics, with nearly 100% oral absorption and a long serum half-life (18–22 hours), at a standard dose of 200-mg per day. In further support of this idea, we show that doxycycline effectively inhibits the mammosphere-forming activity of primary breast cancer samples, derived from metastatic disease sites (pleural effusions or ascites fluid). Our results also have

possible implications for the radio-therapy of brain tumors and/or brain metastases, as doxycycline is known to effectively cross the blood-brain barrier. Further studies will be needed to determine if other tetracycline family members also confer radio-sensitivity.

INTRODUCTION

Recently, we employed a label-free quantitative proteomics approach to discover new therapeutic targets in tumor-initiating cells (TICs) and/or cancer stem-like cells (CSCs) [1]. Briefly, ER-positive breast cancer lines were cultured under suspension conditions, allowing for the formation of mammospheres (a.k.a., tumor-spheres). Then, we compared the proteome of these tumor-spheres directly to attached monolayer cells grown in parallel. Using this approach, we identified several functional groups of proteins that were specifically up-regulated in tumor-spheres, relative to epithelial monolayers. More specifically, mitochondrial proteins were dramatically over-expressed, including key enzymes related to beta-oxidation and ketone metabolism, as well as proteins involved in mitochondrial biogenesis, and specific protein inhibitors of mitophagy [1]. Interestingly, our approach revealed > 60 mitochondrial-related target proteins that were significantly over-expressed in tumor-spheres. These mitochondrial proteins were also transcriptionally over-expressed in human breast cancer samples, highlighting their potential clinical importance. As such, we believe that increased mitochondrial biogenesis could provide a new mechanism for the accumulation of mitochondrial mass in CSCs.

We also utilized a pharmacological approach to functionally validate the importance of mitochondrial fuels, by employing a specific MCT1/2 inhibitor, which prevents the uptake of two mitochondrial fuels, ketone bodies and L-lactate. Notably, inhibition of MCT function significantly inhibited tumor-sphere formation in both ER-positive and ER-negative breast cancer cell lines, with an IC-50 of ~1–2 μ M [1]. Oligomycin A, an inhibitor of Complex V, the mitochondrial ATP-synthase, showed very similar inhibitory activity. Taken together, these results provide suggestive evidence that the proliferative expansion of CSCs strictly depends upon oxidative mitochondrial metabolism [1]. These findings could have future clinical implications for eradicating CSCs, to minimize or prevent tumor recurrence, metastasis and drug resistance. Of course, this would depend on the clinical development of new non-toxic mitochondrial inhibitors that are safe for the treatment of breast cancer patients, which could require 10–15 years of intensive pharmaceutical development and investment.

In summary, using this unbiased proteomic approach, we identified a conserved dependence on mitochondrial biogenesis for the clonal expansion and survival of CSCs. Interestingly, it is well-known that certain FDA-approved antibiotics inhibit mitochondrial biogenesis as a mild, clinically manageable, side-effect [2–6]. Thus, we recently proposed that these antibiotics could be re-purposed as a relatively non-toxic approach to target CSCs. This approach

would dramatically accelerate the potential use of mitochondrial inhibitors in cancer patients [7].

Using this strategy, we experimentally identified 5 different classes of mitochondrially-targeted antibiotics that successfully targeted CSCs [7]. Importantly, these FDA-approved drugs inhibited the growth of CSCs in 12 different cancer cell lines, across 8 different tumor types (breast, DCIS, ovarian, prostate, lung, pancreatic, melanoma, and glioblastoma (brain)). The use of generic antibiotics for cancer therapy could significantly reduce the costs of patient care, making treatment more accessible.

Doxycycline is one of the most promising drugs that emerged from these studies [7]. Since its FDA-approval in 1967, it has been successfully used as a broad-spectrum antibiotic for nearly 50 years, without any major side-effects. Currently, acne patients use doxycycline safely for chronic therapy, for up to 6 months at a time, at a standard dose of 200-mg per day [8, 9].

Mechanistically, in mammalian cells, doxycycline functions as an inhibitor of mitochondrial biogenesis, by binding to the small subunit of the mitochondrial ribosome [2–4, 10, 11]. Doxycycline targets the mitochondrial ribosome, as mitochondria evolved from bacteria over millions of years of evolution [12, 13]. Therefore, bacterial ribosomes and mitochondrial ribosomes show many conserved properties and protein homologies. Recent clinical trials with doxycycline (intended to target cancer-associated infections, but not cancer cells) have already shown positive therapeutic effects in lymphoma patients, although their ability to eradicate CSCs was not yet appreciated [14–15].

Here, to better understand the mechanism(s) of action of doxycycline on cancer cell metabolism, we used an unbiased proteomics approach to identify which proteins are effectively down-regulated by doxycycline. This led to identification of doxycycline as the first FDA-approved inhibitor of DNA-PK, which has broad clinical implications for the use of doxycycline as a radio-sensitizer, to overcome radio-resistance in CSCs.

Throughout this paper, we have used the term cancer stem-like cells (CSCs) or tumor-initiating cells (TICs). For a very insightful discussion of the emerging terminology surrounding the definition of CSCs or TICs, please see the following review (16).

RESULTS

Doxycycline inhibits mammosphere formation, as assessed using primary breast cancer samples derived from metastatic disease sites

Previously, we established that the antibiotic doxycycline effectively inhibits tumor-sphere formation

in 12 different cell lines, across eight different cancer types, including breast cancer. More specifically, both ER-positive (MCF7/T47D) and ER-negative (MDA-MB-231) cell lines were all sensitive to doxycycline treatment [7]. Interestingly, all three of these cell lines were originally derived from the pleural effusions of breast cancer patients, with metastatic disease. Thus, we next tested if primary breast cancer samples derived from metastatic disease sites were also sensitive to doxycycline.

Importantly, Figure 1 shows that doxycycline dose-dependently inhibits mammosphere formation in primary patient samples derived from metastatic disease sites (either pleural effusions or ascites fluid). Moreover, doxycycline appeared to work equally well in samples derived from either ER-positive or ER-negative patients ($N = 4$ patients in total) (See also Supplemental Figure 1). As such, we obtained quantitatively similar results with both well-established cell lines and primary breast cancer samples.

Primary Cancer Samples from Metastatic Disease Sites

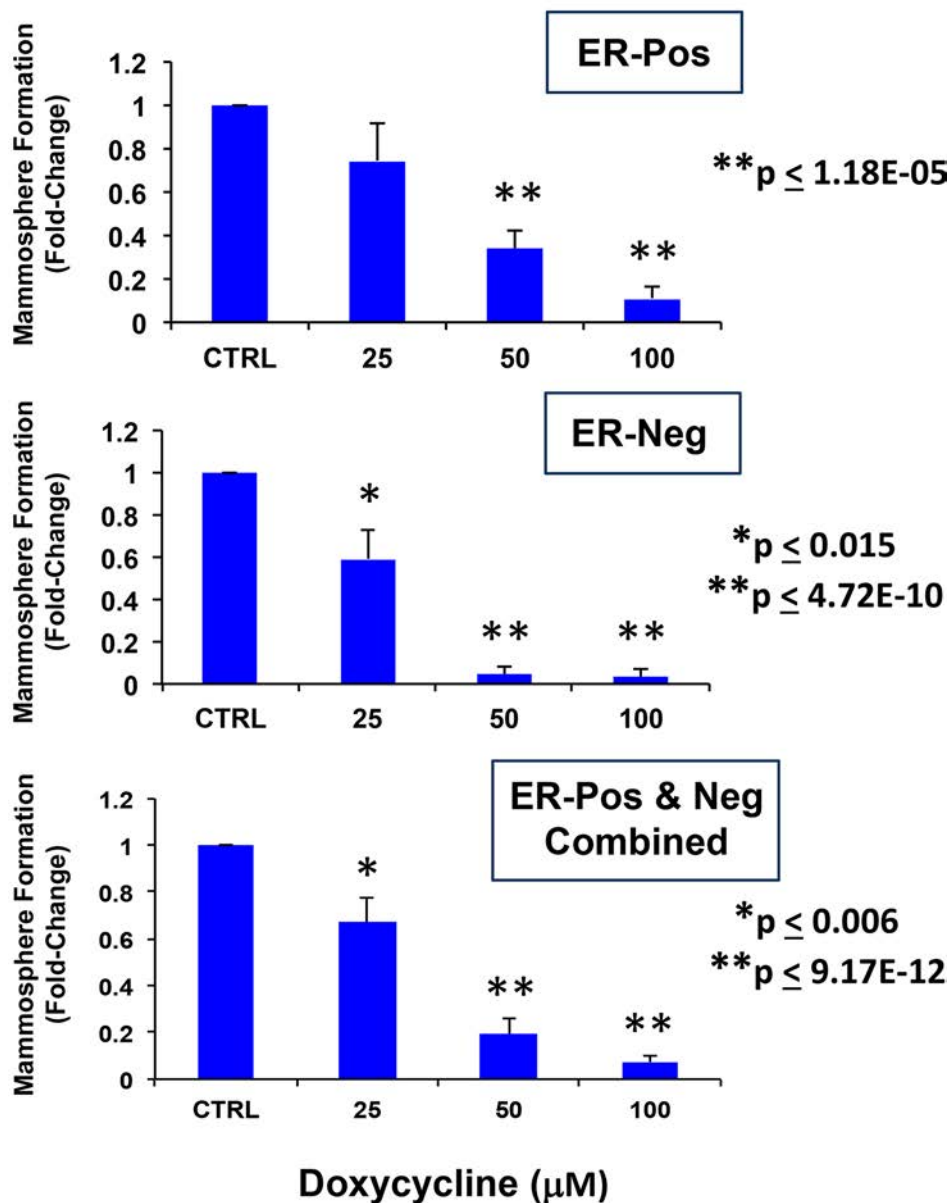


Figure 1: Doxycycline inhibits mammosphere formation, as assessed using primary breast cancer samples derived from metastatic disease sites. Upper panel: ER-positive ($N = 2$ patients); Middle panel: ER-negative ($N = 2$ patients); Lower panel: ER-positive and negative samples combined ($N = 4$ patients). Note that doxycycline dose-dependently inhibits mammosphere formation in primary patient's samples derived from metastatic disease sites (either pleural effusions or ascites). Doxycycline appears to work equally well in samples derived from either ER-positive or ER-negative patients. All experiments were performed in triplicate.

These results are consistent with previous studies showing that doxycycline dramatically inhibits the *in vivo* growth of metastatic lesions (bone and soft tissue) in a mouse model of breast cancer, by up to 60-to-80% [17].

Doxycycline pre-treatment reduces the mammosphere forming capacity of MCF7 monolayer cells

To better understand how doxycycline inhibits the growth of CSCs, we used an unbiased proteomic approach to identify its potential molecular targets. For this purpose, we established conditions under which doxycycline selectively inhibits the proliferation of CSCs, but not “bulk” cancer cells.

First, MCF7 cells were pre-treated with doxycycline (50 μ M) as monolayers for 7- days and then re-plated for the mammosphere assay, in the absence of doxycycline. Figure 2 shows that pre-treatment with doxycycline, under these conditions, is sufficient to significantly reduce mammosphere forming capacity. However, this 7-day treatment also significantly reduced proliferation in MCF7 cell monolayers to a similar extent, but did not affect the viability of the remaining cells.

Therefore, we next shortened the pre-treatment period to 3-days. Importantly, under these new conditions, doxycycline (50 μ M) reduced the mammosphere forming capacity of MCF7 cells by \sim 50%, without affecting the proliferation of the bulk monolayer cells (Figure 3). Thus, doxycycline can be used to selectively reduce “stemness” in MCF7 monolayers.

Identification of the molecular targets of doxycycline, using unbiased label-free proteomics analysis: DNA-PK emerges as a new target

Next, to begin to understand the molecular basis of this selectively, we used these culture conditions to perform unbiased proteomics analysis on MCF7 monolayers (treated with doxycycline for 3-days). The results of this analysis are summarized in Table 1. Only proteins reduced by \geq 1.5-fold ($p < 0.05$) were considered in the analysis. Importantly, Table 1 clearly highlights that doxycycline pre-treatment of MCF7 cell monolayers significantly reduced the expression of many key protein targets functionally associated with mitochondrial metabolism, glycolysis, the EMT, protein synthesis and the DNA damage response, as well as inflammation and protein degradation, in human breast cancer cells.

Interestingly, using this approach, we identified DNA-PK as the protein target that was most dramatically down-regulated by doxycycline, by nearly 15-fold ($> 90\%$ reduction) (Table 1). DNA-PK (also known as PRKDC) is the catalytic subunit of the DNA-dependent protein kinase involved in DNA-repair. DNA-PK is

required for DNA-repair using the mechanism of NHEJ (non-homologous end joining) [18] [19]. DNA-PK also functions to maintain the integrity and copy number of mt-DNA, so there is a clear link with mitochondrial metabolic function, as well [20].

Consistent with our current findings, we also observed that DNA-PK is significantly over-expressed in both MCF7 and T47D mammospheres (Table 2). Remarkably, DNA-PK is infinitely upregulated in MCF7 mammospheres and nearly 15-fold increased in T47D mammospheres, relative to monolayer cultures.

Clinical relevance of “doxycycline reduced targets” in human breast cancers

To determine the potential clinical relevance of our proteomic findings, we next assessed whether the protein targets reduced by doxycycline were transcriptionally upregulated in human breast cancer cells *in vivo*.

For this purpose, we employed a published clinical data set of $N = 28$ breast cancer patients in which their tumor samples were subjected to laser-capture microdissection, to physically separate epithelial cancer cells from their adjacent tumor stroma [21]. Table 3 presents a summary of these findings. Importantly, most of the protein targets reduced by doxycycline were transcriptionally upregulated in human breast cancer cells in tumors excised from patients.

In light of these findings, the new “doxycycline reduced targets” that we identified may be particularly relevant, for improving both the diagnosis and treatment of human breast cancers.

Validation of DNA-PK as a therapeutic target in CSCs

To validate the potential relevance of DNA-PK for maintaining the growth of CSCs, we next used an sh-RNA-approach. Briefly, MCF7 cells were transduced with lentiviral vectors harboring either control sh-RNA or sh-RNA species targeting the expression of DNA-PK. Figure 4A illustrates that MCF7 cells harboring the DNA-PK sh-RNA show a 50% reduction in mammosphere forming capacity, as predicted. Loss of DNA-PK expression was indeed confirmed by immunoblot analysis, using specific antibody probes (Figure 4A).

Validation was also performed using a well-established DNA-PK inhibitor, namely KU-57788 [NU-7441] [22, 23]. Figure 4B directly shows that KU-57788 [NU-7441] dose-dependently inhibits MCF7 mammosphere formations, with an IC-50 between 100 nM and 1 μ M.

Thus, DNA-PK activity appears to be required for the efficient clonal expansion and anchorage-independent growth of CSCs, as observed using the mammosphere assay.

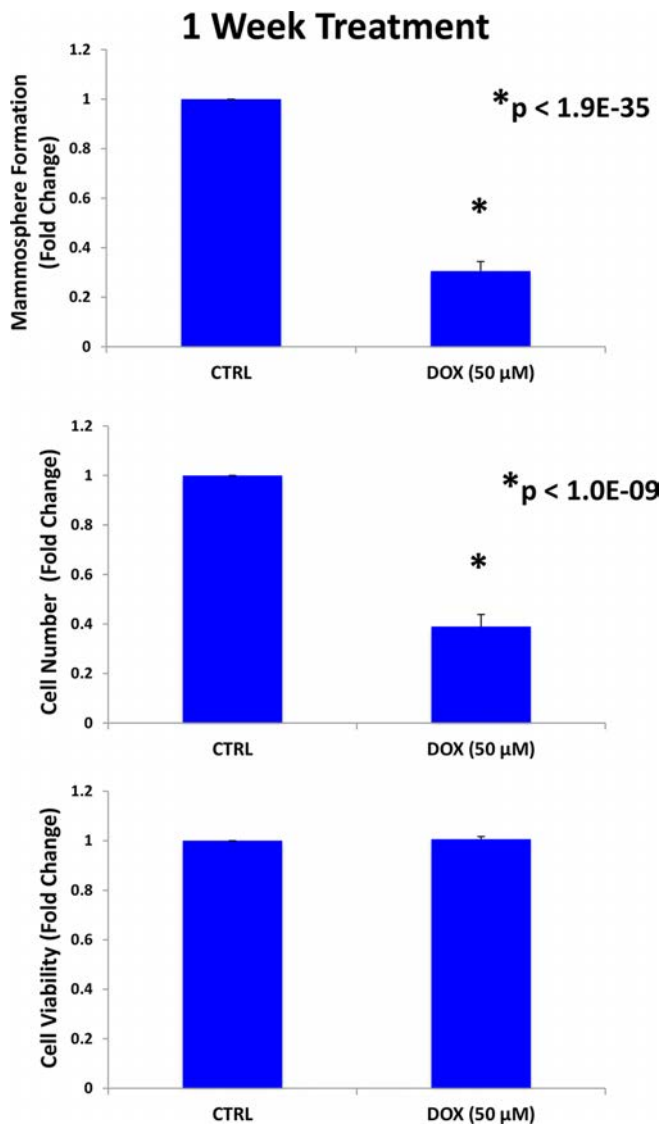


Figure 2: Doxycycline pre-treatment of MCF7 monolayers inhibits mammosphere formation: Effects at 7-days. MCF7 cells were pre-treated with doxycycline (50 μM) as monolayers for 7-days and then re-plated for the mammsphere assay, in the absence of doxycycline. Note that pre-treatment with doxycycline, under these conditions, is sufficient to significantly reduce mammosphere forming capacity. However, this 7-day treatment also reduced proliferation in MCF7 cell monolayers to a similar extent, but did not affect the viability of the remaining cells. Each data point in this figure is the average of 9 replicates.

Doxycycline pre-treatment sensitizes CSCs to radiation treatment

Since DNA-PK has been previously implicated in the radio-resistance of cancer cells [24, 25] and we show here that doxycycline functionally reduces the expression of DNA-PK, we would predict that doxycycline treatment should radio-sensitize CSCs.

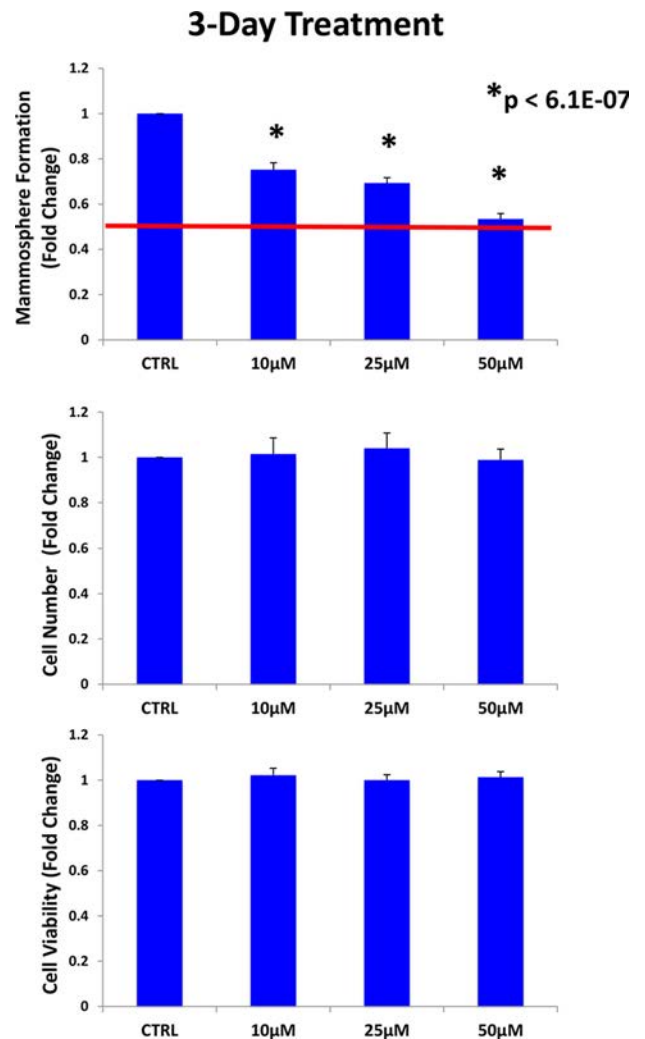


Figure 3: Doxycycline pre-treatment of MCF7 monolayers inhibits mammosphere formation: Effects at 3-days. MCF7 cells were pre-treated with doxycycline (50 μM) as monolayers for 3-days and then re-plated for the mammosphere assay, in the absence of doxycycline. Under these conditions, doxycycline (50 μM) reduced the mammosphere forming capacity of MCF7 cells by ~ 50%, without affecting the proliferation of the bulk monolayer cells. As such, doxycycline can be used to selectively reduce “stemness” in MCF7 monolayers. Each data point in this figure is the average of 9 replicates.

To test this hypothesis directly, MCF7 cell monolayers were pre-treated with doxycycline (50 μM) for 3-days and then irradiated. After radiation treatment, monolayers were trypsinized and re-plated to evaluate mammosphere growth over a 5-day period. Figure 5 shows that radiation treatment significantly increases the growth of CSCs by up to 1.45-fold, as expected. In contrast, doxycycline pre-treatment increased the sensitivity of CSCs to radiation by up to 4.5-fold. However, under these conditions, doxycycline pre-treatment (with or without radiation) had little or no effect on the proliferation or viability of the “bulk” cancer cells (Figure 6A, 6B).

Thus, doxycycline pre-treatment functionally sensitizes CSCs to radiation, as predicted based on its ability to reduce DNA-PK expression.

Validation of the metabolic phenotype induced by doxycycline pre-treatment

Based on our proteomics analysis presented in Table 1, both the levels of key mitochondrial proteins and glycolytic enzymes were significantly reduced by doxycycline pre-treatment. Thus, these results suggest that doxycycline should reduce overall metabolic activity in cancer cells.

To test this hypothesis further, we next examined the metabolic profile of MCF7 cell monolayers pre-treated with doxycycline (50 μ M) for 2-days. Interestingly, Figure 7 shows that the rates of both oxidative mitochondrial metabolism and glycolysis were dramatically reduced by doxycycline pre-treatment, as measured using the Seahorse XFe96 analyzer to measure metabolic flux. This resulted in significant reductions in respiration (basal and maximal), as well as reduced ATP levels (Figure 8). Finally, as seen in Figure 9, MCF7 cancer cells were shifted from a highly energetic to a metabolically quiescent state.

Doxycycline reduces the anoikis-resistance of MCF7 cells, prior to mammosphere formation

Anoikis is a specific type of programmed cell death (apoptosis) that is induced in certain cell types, under anchorage-independent growth conditions [26, 27]. Interestingly, epithelial CSCs show anoikis-resistance, and are able to undergo mammosphere formation under these anchorage-independent conditions [28].

Next, to determine the possible effects on anoikis-resistance, MCF7 cells were pre-treated with doxycycline (at 25 or 50 μ M) as monolayers for 2-days and then replated on low-attachment plates, for either the anoikis assay or the mammosphere assay, in the absence of doxycycline.

Importantly, Figure 10 shows that doxycycline pre-treatment dose-dependently reduced the number of live cells remaining after 10 hours of seeding on low-attachment plates. Under these conditions, doxycycline pre-treatment also dose-dependently reduced the mammosphere forming capacity of MCF7 cells, by up to ~50%. Thus, doxycycline may exert its inhibitory effects on mammosphere formation, in part, by effectively reducing anoikis-resistance, during the initial time spent under low-attachment conditions.

Doxycycline simultaneously inhibits the functional activity of multiple stem-cell associated signal transduction pathways

To better understand which signaling pathways are affected by doxycycline treatment, we used a panel of eight MCF7-GFP cell lines engineered to express different luciferase-based transcriptional reporters. The functional activation state of these reporters was then normalized by GFP expression, to account for cell number.

Interestingly, Figure 11 directly shows that doxycycline treatment of MCF7 monolayer cultures inhibits both the anti-oxidant response (NRF1/2) and STAT1/3 signaling, especially at 72 and 96 hours. Similarly, Figure 12 illustrates that doxycycline also dampens signaling along four other stem-cell associated pathways, including Sonic Hedgehog, Notch, WNT and TGF-beta signaling, again most prominently at 72 and 96 hours. Interestingly, in several cases, a bi-phasic response was noted, with activation of signaling at 24 hours, and progressive inhibition from 48-to-96 hours.

These results directly support our observation that doxycycline potently inhibits mammosphere formation, by blocking the clonal expansion of CSCs and reduces anoikis-resistance. Indeed, it has been reported that most of these signaling pathways such as Notch, Hedgehog, WNT, TGF β , STAT3 or NRF1/2 are able to confer anoikis-resistance, and inhibition of these pathways sensitizes CSCs to anoikis.

Table 1: MCF7 cell proteins down-regulated in response to doxycycline treatment of monolayer cultures (3-days at 50 μ M)

Symbol	Gene Description	Down-regulation (fold-change)	ANOVA
Mitochondrial-related Proteins			
PRKDC	DNA-dependent protein kinase catalytic subunit (maintains mt-DNA integrity & copy number)	14.71	0.02
GPD2	Glycerol-3-phosphate dehydrogenase, mitochondrial	5.29	1.55E-06

(Continued)

Symbol	Gene Description	Down-regulation (fold-change)	ANOVA
MDH2	Malate dehydrogenase 2, mitochondrial	3.08	4.01E-06
EC1I	Enoyl-CoA delta isomerase 1, mitochondrial	2.95	0.018
VDAC1	Voltage-dependent anion-selective channel protein 1	2.71	9.65E-05
HSPD1	60 kDa heat shock protein, mitochondrial	2.24	0.004
DECR1	2,4-dienoyl CoA reductase 1, mitochondrial	1.94	0.02
UQCRC2	Cytochrome b-c1 complex subunit 2, mitochondrial	1.91	0.002
SDHA	Succinate dehydrogenase complex subunit A	1.88	0.0001
ALDH18A1	Delta-1-pyrroline-5-carboxylate synthase, mitochondrial	1.88	0.006
COX6A	Cytochrome c oxidase subunit 6A, mitochondrial	1.84	0.008
FASN	Fatty acid synthase	1.83	0.02
LRPPRC	Leucine-rich PPR-motif containing (inhibitor of mitophagy)	1.72	0.002
ORP150	150 kDa oxygen-regulated protein	1.70	0.02
NDUFA4	NADH dehydrogenase (Ubiquinone) 1 alpha-subcomplex, 4	1.68	0.0007
COX5B	Cytochrome c oxidase subunit 5B, mitochondrial	1.66	0.0008
ATP5F1	ATP synthase, H ⁺ transporting, mitochondrial F0 complex, subunit b	1.57	0.02
Glycolytic Enzymes			
GPI	Glucose-6-phosphate isomerase	3.82	8.06E-05
LDHA	L-lactate dehydrogenase A	2.26	0.02
TPI1	Triosephosphate isomerase 1	2.25	0.004
ENO1	Enolase 1	1.71	0.005
ALDOA	Fructose-bisphosphate aldolase A	1.57	0.007
PGK1	Phosphoglycerate kinase 1	1.57	0.037
LDHB	L-lactate dehydrogenase B	1.53	0.03
PKM1/2	Pyruvate kinase	1.45	0.03
EMT-markers/Muscle-related proteins (cytoskeletal)/Extracellular Matrix/Angiogenesis			
SMOC2	SPARC-related modular calcium-binding protein 2	7.01	5.17E-06
MYO18B	Unconventional myosin-XVIIIb	6.48	0.0002
TUBB1	Tubulin beta-1 chain	3.72	3.09E-05
ADAM22	A disintegrin and metalloproteinase domain 22	3.49	8.96E-05
PLEC1	Plectin 1, intermediate filament binding protein 500kDa	2.86	0.0001
ATP2A2	Sarcoplasmic/endoplasmic reticulum calcium ATPase 2	2.37	0.035
ACTBL2	Beta-actin-like protein 2	2.28	0.008
CTNNA1	Catenin (Cadherin-associated protein), beta 1, 88kDa	2.07	0.02
CFL2	Cofilin-2	2.11	0.0004
CFL1	Cofilin-1 (Non-muscle), isoform	2.01	0.04

(Continued)

Symbol	Gene Description	Down-regulation (fold-change)	ANOVA
DYNC1H1	Cytoplasmic dynein 1 heavy chain 1	1.91	0.04
SRRM2	Serine/arginine repetitive matrix protein 2	1.85	0.006
AMOT	Angiomotin	1.79	0.0005
MYH15	Myosin-15	1.76	0.0003
MYH10	Myosin-10	1.73	0.02
TUBA4B	Putative tubulin-like protein alpha-4B	1.67	0.003
USMG5	Up-regulated during skeletal muscle growth protein 5	1.58	0.02
KIF5C	Kinesin heavy chain isoform 5C	1.58	0.009
TUBA1A	Tubulin alpha-1A chain	1.50	0.01
Protein Synthesis and Transport, Glycosylation and Glycosaminoglycan Synthesis (GAGs)			
EIF3C	Eukaryotic translation initiation factor 3 subunit C	7.24	0.0002
VCP	Valosin-containing protein	4.95	7.38E-06
RPL9	60S ribosomal protein L9	4.94	6.46E-05
SARS	Seryl (serine)-tRNA synthetase	4.85	0.0002
PMM2	Phosphomannomutase 2	4.45	1.43E-05
SURF4	Surfeit locus protein 4	3.53	5.63E-05
EEF1G	Elongation factor 1-gamma	3.18	7.42E-05
EIF3A	Eukaryotic translation initiation factor 3 subunit A	3.04	0.0007
RPB4	60S ribosomal protein L4	2.81	0.02
EIF3G	Eukaryotic translation initiation factor 3 subunit G	2.77	7.33E-06
RAB2	RAB2, member RAS oncogene family	2.59	0.03
COPG1	Coatomer subunit gamma-1	2.34	0.003
HSP90AB1	Heat shock protein 90kDa alpha (Cytosolic), class B member 1	2.29	0.02
UGDH	UDP-glucose 6-dehydrogenase	2.28	0.03
EEF1A1	Eukaryotic translation elongation factor 1 alpha 1	2.21	0.004
RRBP1	p180/ribosome receptor	2.19	0.04
AP1G1	AP-1 complex subunit gamma-1	1.98	0.002
RPS18	40S ribosomal protein S18	1.97	0.007
RAB21	RAB21, member RAS oncogene family	1.88	0.02
RPL15	60S ribosomal protein L15	1.82	0.026
RPL7	60S ribosomal protein L7	1.75	0.03
STIP1	Stress-induced-phosphoprotein 1 (Hsp70/Hsp90-organizing protein)	1.72	0.003
P4HB	Protein disulfide-isomerase	1.69	0.02
RPS16	40S ribosomal protein S16	1.59	0.015
RPS2	40S ribosomal protein S2	1.57	0.008

(Continued)

Symbol	Gene Description	Down-regulation (fold-change)	ANOVA
RPL35	60S ribosomal protein L35	1.55	0.02
SEC22B	Vesicle-trafficking protein SEC22b	1.50	0.037
DNA-binding, Nuclear-related, and Cell Cycle Control			
PRKDC	DNA-dependent protein kinase catalytic subunit (non-homologous end joining (NHEJ))	14.71	0.02
XRN2	5'-3' exoribonuclease 2	5.53	0.0006
NAP1L4	Nucleosome assembly protein 1-like 4	4.46	0.002
ESF1	Nucleolar Pre-RRNA Processing Protein, Homolog	4.30	2.00E-08
NASP	Nuclear autoantigenic sperm protein	4.12	0.009
HNRNPA1	Heterogeneous nuclear ribonucleoprotein A1	3.85	9.30E-05
FUBP1	Far upstream element-binding protein 1	3.21	1.44E-05
POLD3	DNA polymerase delta subunit 3	3.09	0.0007
RPA1	Replication protein A 70 kDa DNA-binding subunit	2.80	0.02
CHD4	Chromodomain-helicase-DNA-binding protein 4	2.62	5.68E-05
CTPS1	CTP synthase	2.37	0.0003
LMNA	Prelamin-A/C	2.22	0.01
CEP110	Centrosomal protein 110kDa	2.02	0.03
MCM7	MCM7 minichromosome maintenance deficient 7	1.96	0.03
NAP1L1	Nucleosome assembly protein 1-like 1	1.86	0.015
HDAC1	Histone deacetylase 1	1.71	0.045
SP100	Nuclear autoantigen Sp-100	1.64	0.03
DHX9	ATP-dependent RNA helicase A	1.47	0.02
Inflammation/Immune Function			
LTA4H	Leukotriene A(4) hydrolase	3.52	1.16E-06
CCT4	T-complex protein 1 subunit delta	2.13	0.0003
CCT2	T-complex protein 1 subunit beta	1.53	0.04
Protein Degradation			
UBR4	E3 ubiquitin-protein ligase UBR4	3.47	0.002
STUB1	E3 ubiquitin-protein ligase CHIP	2.55	0.01
PSMC3	Proteasome (prosome, macropain) 26S subunit, ATPase 3	1.79	0.04
PSMB4	Proteasome subunit beta type-4	1.72	0.003
PSMD2	Proteasome 26S non-ATPase subunit 2	1.58	0.04
UBE1	Ubiquitin-activating enzyme E1 (A1S9T and BN75 temperature sensitivity complementing)	1.55	0.003
UBE2V1	Ubiquitin-conjugating enzyme E2 variant 1	1.47	0.03
USP14	Ubiquitin carboxyl-terminal hydrolase 14	1.47	0.007

Note that doxycycline targets mitochondrial metabolism, glycolysis, the EMT, protein synthesis and the DNA damage response, as well as inflammation and protein degradation, in human breast cancer cells.

Table 2: DNA-PK is highly up-regulated in both MCF7 and T47D mammospheres, as compared with monolayer cultures

Cell Line	Symbol	Gene Description	Up-regulation (fold-change)	ANOVA
MCF7	PRKDC	DNA-dependent protein kinase, catalytic subunit	Infinity	1.13E-10
T47D	PRKDC	DNA-dependent protein kinase, catalytic subunit	14.85	2.60E-05

Table 3: Doxycycline-targets normally up-regulated in human breast cancer cells *in vivo*

Symbol	Gene Description	Up-regulation (fold-change)	P-value
Mitochondrial-related Proteins			
ATP5F1	ATP synthase, H ⁺ transporting, mitochondrial F0 complex, subunit b	5.39	7.83E-07
COX5B	Cytochrome c oxidase subunit 5B, mitochondrial	5.03	2.86E-06
UQCRC2	Cytochrome b-c1 complex subunit 2, mitochondrial	4.84	5.73E-06
COX6A	Cytochrome c oxidase subunit 6A, mitochondrial	4.46	2.07E-05
LRPPRC	Leucine-rich PPR-motif containing (inhibitor of mitophagy)	4.34	3.15E-05
NDUFA4	NADH dehydrogenase (Ubiquinone) 1 alpha-subcomplex, 4	4.25	4.29E-05
MDH2	Malate dehydrogenase 2, mitochondrial	4.18	5.32E-05
HSPD1	60 kDa heat shock protein, mitochondrial	3.42	5.93E-04
DECR1	2,4-dienoyl CoA reductase 1, mitochondrial	3.38	6.86E-04
VDAC1	Voltage-dependent anion-selective channel protein 1	2.64	5.35E-03
PRKDC	DNA-dependent protein kinase catalytic subunit (maintains mt-DNA integrity & copy number)	2.14	0.02
Glycolytic Enzymes			
TPI1	Triosephosphate isomerase 1	4.21	4.88E-05
ALDOA	Fructose-bisphosphate aldolase A	3.60	3.45E-04
GPI	Glucose-6-phosphate isomerase	3.36	7.28E-04
PKM2	Pyruvate kinase	3.26	9.79E-04
PGK1	Phosphoglycerate kinase 1	2.46	8.66E-03
LDHA	L-lactate dehydrogenase A	2.42	9.42E-03
ENO1	Enolase 1	1.96	0.03
EMT-markers/Muscle-related proteins (cytoskeletal)			
CFL1	Cofilin-1 (Non-muscle), isoform	2.39	0.01
TUBB1	Tubulin beta-1 chain	2.32	0.01
TUBA1A	Tubulin alpha-1A chain	2.17	0.02
ATP2A2	Sarcoplasmic/endoplasmic reticulum calcium ATPase 2	2.07	0.02
CTNNB1	Catenin (Cadherin-associated protein), beta 1, 88kDa	2.05	0.02
MYH10	Myosin-10	1.82	0.037
KIF5C	Kinesin heavy chain isoform 5C	1.82	0.037
Protein Synthesis and Transport			
RPL7	60S ribosomal protein L7	5.21	1.53E-06

(Continued)

Symbol	Gene Description	Up-regulation (fold-change)	P-value
RPS18	40S ribosomal protein S18	4.96	3.71E-06
HSP90AB1	Heat shock protein 90kDa alpha (Cytosolic), class B member 1	4.94	4.03E-06
RPS2	40S ribosomal protein S2	4.77	7.21E-06
RPL15	60S ribosomal protein L15	4.60	1.28E-05
EIF3C	Eukaryotic translation initiation factor 3 subunit C	4.48	1.94E-05
RPL35	60S ribosomal protein L35	4.10	7.05E-05
RAB2	RAB2, member RAS oncogene family	3.73	2.29E-04
RPL9	60S ribosomal protein L9	3.71	2.49E-04
EEF1G	Elongation factor 1-gamma	3.71	2.44E-04
EEF1A1	Eukaryotic translation elongation factor 1 alpha 1	3.16	1.30E-03
RPS16	40S ribosomal protein S16	3.05	1.77E-03
RPL4	60S ribosomal protein L4	3.05	1.79E-03
SEC22B	Vesicle-trafficking protein SEC22b	3.04	1.81E-03
EIF3A	Eukaryotic translation initiation factor 3 subunit A	2.51	7.57E-03
SARS	Seryl (serine)-tRNA synthetase	2.15	0.02
P4HB	Protein disulfide-isomerase	2.15	0.02
EIF3G	Eukaryotic translation initiation factor 3 subunit G	1.92	0.03
DNA-binding, Nuclear-related, and Cell cycle control			
HDAC1	Histone deacetylase 1	4.15	6.02E-05
NAP1L4	Nucleosome assembly protein 1-like 4	4.07	7.61E-05
HNRNPA1	Heterogeneous nuclear ribonucleoprotein A1	4.03	8.90E-05
RPA1	Replication protein A 70 kDa DNA-binding subunit	2.52	7.30E-03
MCM7	MCM7 minichromosome maintenance deficient 7	2.23	0.015
NAP1L1	Nucleosome assembly protein 1-like 1	2.19	0.017
PRKDC	DNA-dependent protein kinase catalytic subunit (non-homologous end joining (NHEJ))	2.14	0.02
CTPS1	CTP synthase	2.09	0.02
CHD4	Chromodomain-helicase-DNA-binding protein 4	1.87	0.034
Inflammation/Immune Function			
CCT4	T-complex protein 1 subunit delta	3.25	1.00E-03
LTA4H	Leukotriene A(4) hydrolase	2.94	2.40E-03
CCT2	T-complex protein 1 subunit beta	2.85	3.06E-03
Protein Degradation			
PSMB4	Proteasome subunit beta type-4	4.16	5.70E-05
PSMD2	Proteasome 26S non-ATPase subunit 2	3.31	8.29E-04
USP14	Ubiquitin carboxyl-terminal hydrolase 14	3.23	1.05E-03
STUB1	E3 ubiquitin-protein ligase CHIP	1.95	0.03
UBR4	E3 ubiquitin-protein ligase UBR4	1.77	0.04

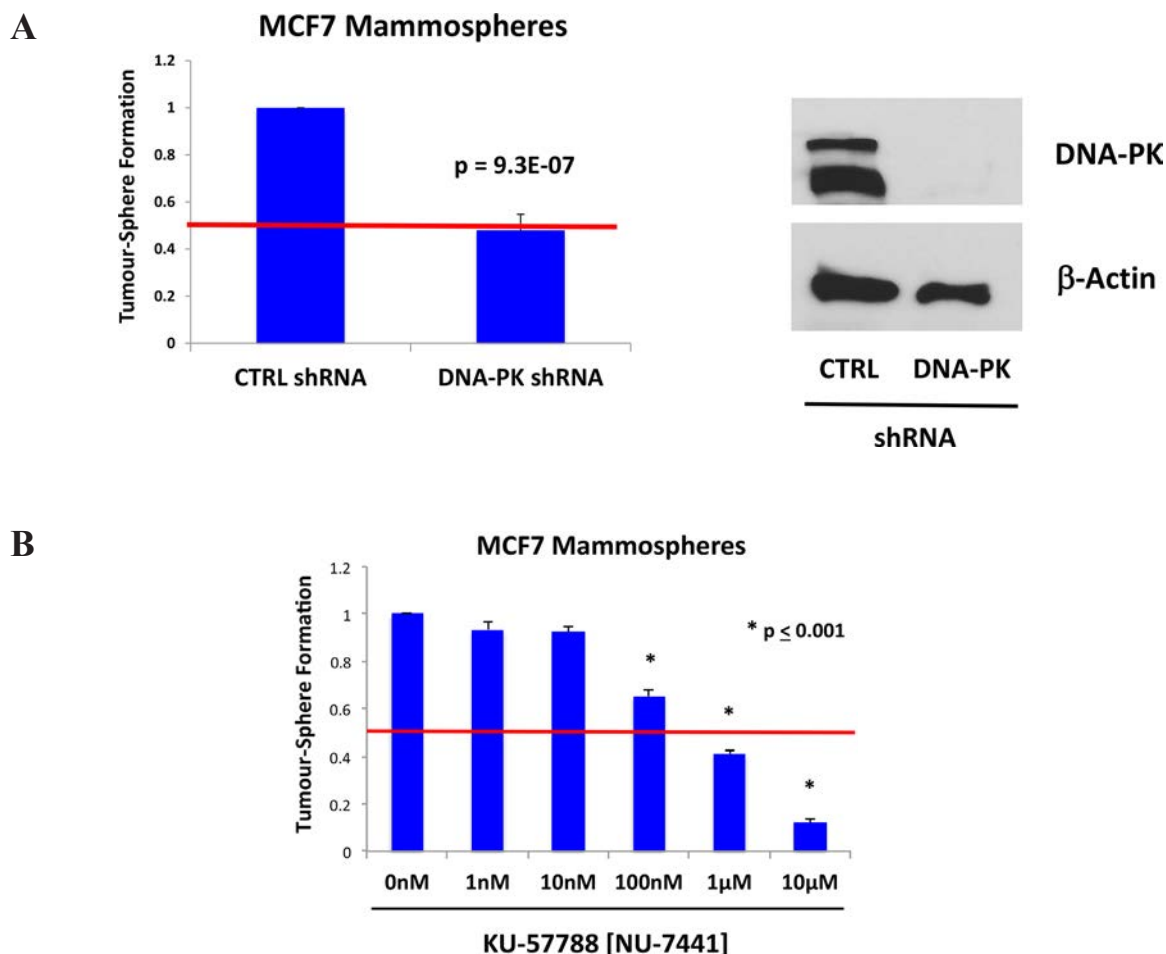


Figure 4: DNA-PK is required for mammosphere formation in MCF7 cells. **A.** Genetic approach. MCF7 cells were transduced with lentiviral vectors harboring either control sh-RNA or sh-RNA species targeting the expression of DNA-PK. Note that MCF7 cells harboring the DNA-PK sh-RNA show a 50% reduction in mammosphere forming capacity, as predicted. **B.** Pharmacological approach. Note that the well-established DNA-PK inhibitor, namely KU-57788 [NU-7441], dose-dependently inhibits MCF7 mammosphere formations, with an IC₅₀ between 100 nM and 1 µM. As such, DNA-PK activity is required for the efficient clonal expansion and anchorage-independent growth of CSCs, as observed using the mammosphere assay. Each data point in this figure is the average of 9 replicates.

DISCUSSION

Recently, we proposed that FDA-approved antibiotics that adversely effect mitochondria could be used to effectively target the cancer stem cell population, by inhibiting mitochondrial biogenesis in tumor-initiating cells (TICs) [7]. One of these promising antibiotics is doxycycline, a member of the tetracycline class, with excellent pharmacokinetics.

To better understand how doxycycline exerts its therapeutic effects, here we used a chemical proteomics approach [29, 30] to more effectively interrogate the target-phenotype relationship. Our results directly show that doxycycline treatment significantly reduced the expression of many key protein targets

functionally associated with mitochondrial metabolism, glycolysis, the EMT, protein synthesis and the DNA damage response, as well as inflammation and protein degradation, in human breast cancer cells. We further validated that doxycycline suppresses both oxidative mitochondrial metabolism and glycolysis, using metabolic flux analysis. Doxycycline also inhibited signal transduction along multiple stem-cell associated communication pathways, namely Sonic Hedgehog, Notch, WNT and TGF-beta signaling.

Interestingly, using this approach, we also identified DNA-PK as the protein target that was most dramatically down-regulated by doxycycline, by nearly 15-fold (> 90% reduction) (Figure 13). DNA-PK is required for effective cellular DNA-repair and also maintains the integrity and

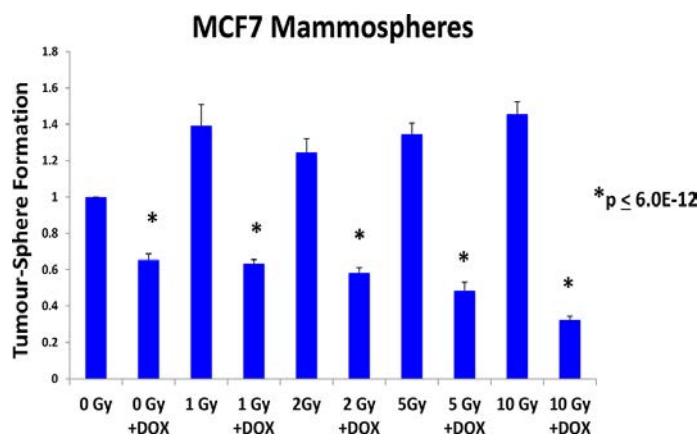
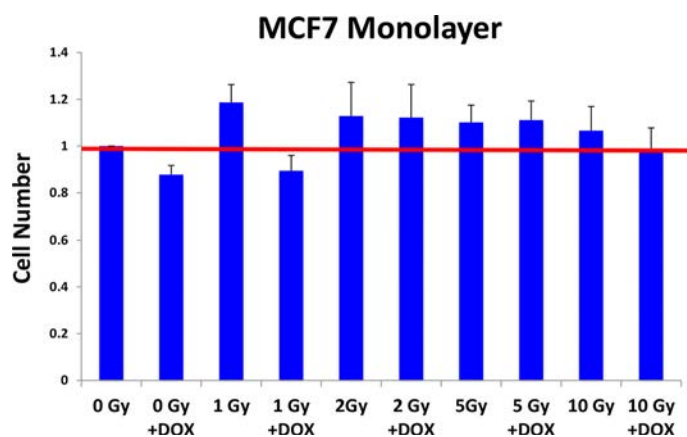


Figure 5: Doxycycline pre-treatment sensitizes cancer stem cells to radiation treatment. MCF7 cell monolayers were pre-treated with doxycycline (50 μ M) for 3-days and then irradiated. After radiation treatment, monolayers were trypsinized and re-plated to evaluate mammosphere growth over a 5-day period. Note that radiation treatment significantly increases the growth of CSCs by up to 1.45-fold, as expected. In contrast, doxycycline pre-treatment increased the sensitivity of CSCs to radiation by up to 4.5-fold. In conclusion, doxycycline pre-treatment functionally sensitizes CSCs to radiation, as predicted based on its ability to reduce DNA-PK expression. Each data point in this experiment is the average of 18 replicates.

A



B

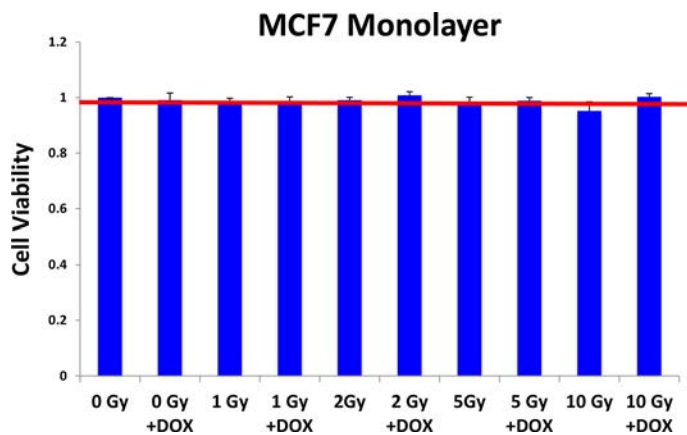


Figure 6: Doxycycline pre-treatment does not inhibit the growth and viability of MCF7 cell monolayers. As in Figure 4, MCF7 cell monolayers were pre-treated with doxycycline (50 μ M) for 3-days and then irradiated. However, note that under these conditions doxycycline pre-treatment (with or without radiation), had little or no effect on the proliferation or viability of the “bulk” cancer cells. Each data point in this experiment is the average of 18 replicates.

DOX Pre-treatment (48-hours)

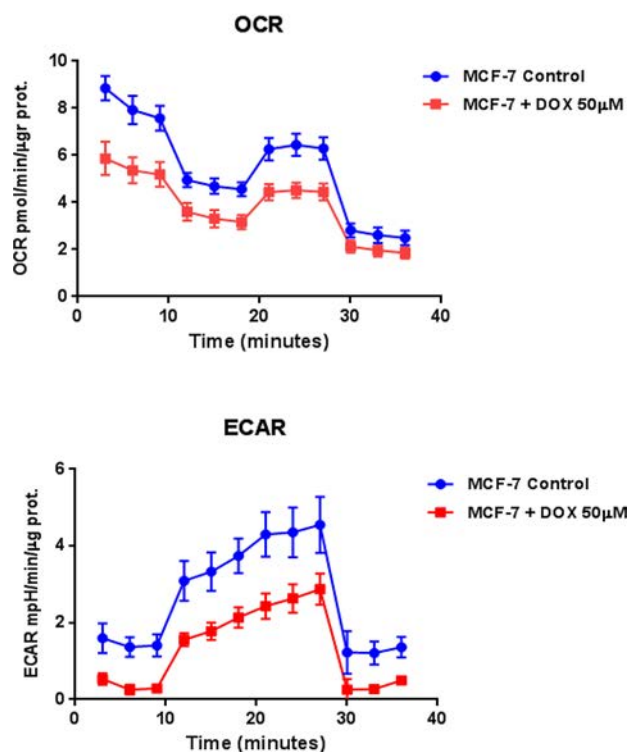


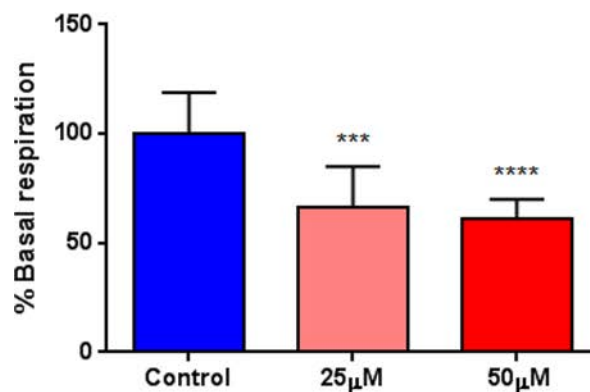
Figure 7: Doxycycline treatment reduces the rates of both oxidative mitochondrial metabolism and glycolysis. We examined the metabolic profile of MCF7 cell monolayers pre-treated with doxycycline (50 µM) for 2-days. Note that the rates of both oxidative mitochondrial metabolism and glycolysis were significantly reduced by doxycycline pre-treatment, as measured using the Seahorse XFe96 analyzer to measure metabolic flux.

copy number of mitochondrial DNA [20, 31, 32]. DNA-PK is thought to confer radiation resistance in cancer cells [33–35], but has never been previously implicated in the growth of CSCs.

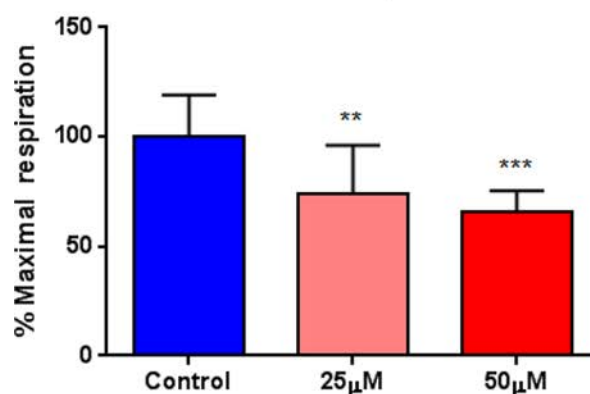
Additional validation experiments, using both genetic (DNA-PK sh-RNA) and pharmacological (DNA-PK inhibitor: NU-7441) approaches directly showed that DNA-PK expression or activity is required for MCF7 cells to efficiently form mammospheres. This is the first demonstration that DNA-PK is required for the clonal expansion and survival of CSCs. Most importantly, however, pre-treatment of MCF7 cell monolayers with doxycycline was sufficient to increase the sensitivity of CSCs to radiation treatment, by up to 4.5-fold.

Unfortunately, no FDA-approved DNA-PK inhibitors have emerged, despite many years of drug discovery and lead optimization. This is largely because existing DNA-PK inhibitors suffer from poor pharmacokinetics. They are not well absorbed and/or are unstable, with a short plasma half-life [36–38]. In contrast, doxycycline

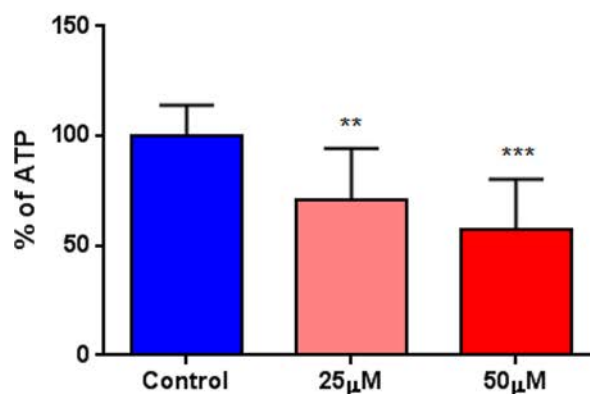
Basal respiration



Maximal respiration



ATP



** p<0.005; *** p<0.0005; **** p<0.00005

Figure 8: Doxycycline quantitatively reduces respiration (basal and maximal) and ATP levels. We examined the metabolic profile of MCF7 cell monolayers pre-treated with doxycycline (50 µM) for 2-days, using the Seahorse XFe96 analyzer to measure metabolic flux. Note that significant reductions in respiration (basal and maximal), as well as reduced ATP levels, were observed experimentally. Each data point in this figure is the average of 9 replicates.

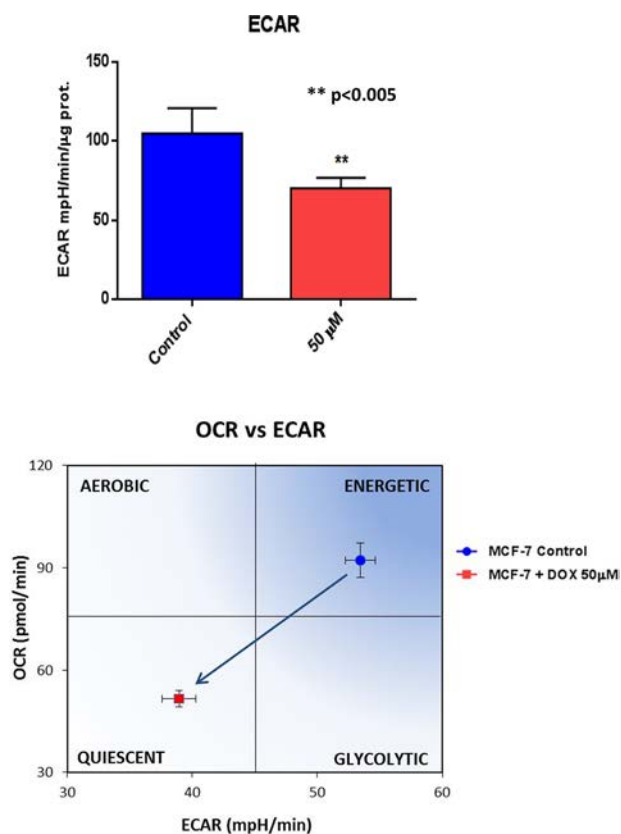


Figure 9: Doxycycline shifts MCF7 cancer cells from a highly energetic to a metabolically quiescent state. We examined the metabolic profile of MCF7 cell monolayers pre-treated with doxycycline (50 μ M) for 2-days, using the Seahorse XFe96 analyzer to measure metabolic flux. Note that MCF7 cancer cells were shifted towards a metabolically quiescent state. Each data point in this figure is the average of 9 replicates.

has excellent pharmacokinetics, with nearly 100% oral absorption and a long serum half-life (18–22 hours), at a standard dose of 200-mg per day [39, 40].

Thus, we propose that the efficacy of doxycycline as a DNA-PK inhibitor should be tested in Phase-II clinical trials, in combination with radio-therapy. In further support of this idea, we show that doxycycline effectively inhibits the mammosphere-forming activity of primary breast cancer samples, derived from metastatic disease sites (pleural effusions or ascites fluid).

MATERIALS AND METHODS

Materials

Breast cancer cell lines (MCF7 and T47D) were purchased from the ATCC. Gibco-brand cell culture media (DMEM and DMEM/F12) was purchased from Life Technologies. Doxycycline was purchased from Sigma-Aldrich. Sh-RNA lentiviral particles targeting DNA-PK (sc-35200-V) were obtained commercially from Santa

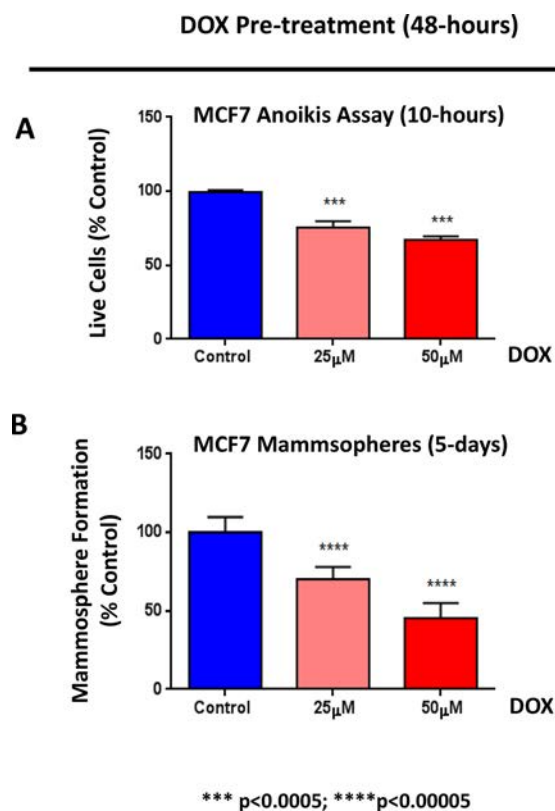


Figure 10: Doxycycline reduces the anoikis-resistance of MCF7 cells, prior to mammosphere formation. MCF7 cells were pre-treated with doxycycline (at 25 or 50 μ M) as monolayers for 2-days and then re-plated on low-attachment plates, for the anoikis assay or the mammosphere assay, in the absence of doxycycline. **A. Anoikis Assay.** Note that doxycycline pre-treatment dose-dependently reduced the number of live cells remaining after 10 hours of seeding on low-attachment plates. **B. Mammosphere formation.** Note that, under these conditions, doxycycline pre-treatment dose-dependently reduced the mammosphere forming capacity of MCF7 cells, by up to ~ 50%. Each data point in this figure is the average of 9 replicates.

Cruz Biotech (USA), along with appropriate sh-RNA control particles (sc-108080). Antibodies directed against DNA-PK (MS-423-P0) for immunoblot analysis were obtained from Thermo Scientific. KU-57788 [NU-7441] was obtained from Selleckchem.

Description of primary tumor samples from metastatic disease sites

Ethical approval was granted by the Central Office for Research Ethics Committee (study numbers: 05/Q1402/25 and 05/Q1403/159) and patients gave written informed consent. Metastatic fluid samples were obtained from 4 patients undergoing palliative drainage of symptomatic ascites or pleural effusions at The Christie Hospital, Manchester, UK. Estrogen, progesterone, and HER2 receptor status of the primary

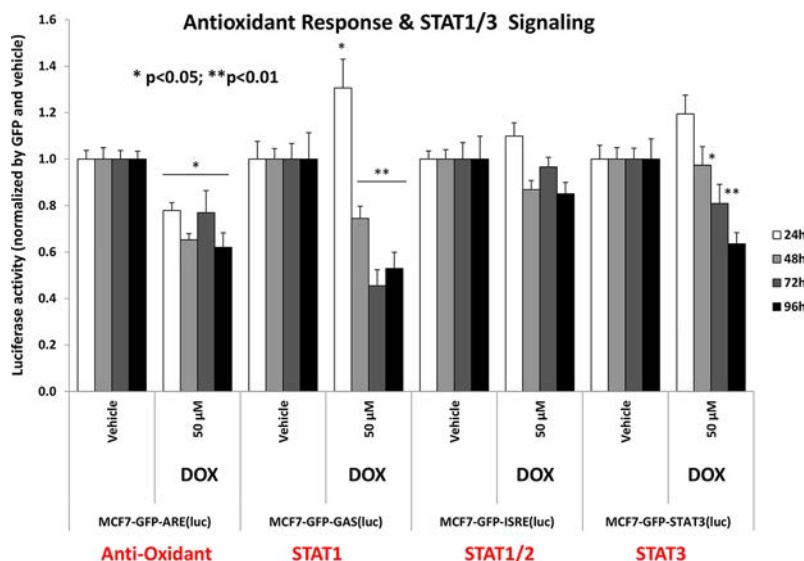


Figure 11: Doxycycline treatment of MCF7 monolayers inhibits the anti-oxidant response (NRF1/2) and STAT1/3 signaling. Note that doxycycline is especially effective at 72 and 96 hours. Each data point in this figure is the average of at least 8 replicates.

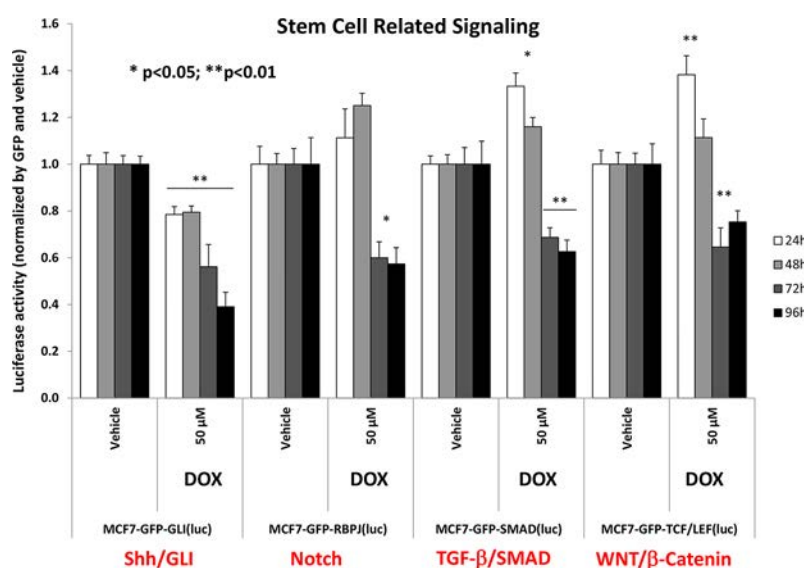


Figure 12: Doxycycline dampens signaling along four major stem-cell associated pathways in MCF7 cells, namely Sonic Hedgehog, Notch, WNT and TGF-beta signaling. Note that the functional effects of doxycycline were most prominent at 72 and 96 hours. In several cases, a bi-phasic response was noted, with activation of signaling at 24 hours, and progressive inhibition from 48-to-96 hours. Each data point in this figure is the average of at least 8 replicates.

tumors were reported by the Department of Pathology at The Christie, according to established criteria [41].

Isolation of breast cancer epithelial cells

Metastatic breast cancer cells were harvested as previously described, with minor modifications [42]. Invasive breast cancer tissue (1–2 cm³) was collected, dissected into 1–2 mm³ cubes, and digested in media

comprised of Dulbecco's Modified Eagle's Media (DMEM), 15 mM HEPES, and 10% collagenase/hyaluronidase (Stem Cell Technologies) (supplemented with Pen-Strep) at 37°C for 16 hours. Digested tissue was filtered sequentially through 100, 70, and 40 µm sieves. Red blood cells were removed using Lymphoprep (Axis-Shield), and leukocytes were removed with CD45-negative magnetic sorting according to the manufacturer's instructions (Miltenyi Biotec).

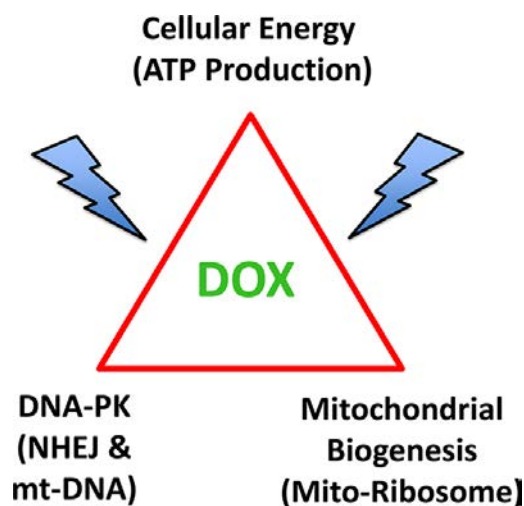


Figure 13: Doxycycline targets mitochondrial biogenesis and DNA-repair, ultimately converging on ATP production and energy metabolism in cancer cells. DNA-PK activity is normally required for repairing mt-DNA and maintaining mt-DNA copy number. Mitochondrial biogenesis is dependent on mitochondrial protein synthesis, which is carried out, in part, by mitochondrial ribosomes, which share significant homology with bacterial ribosomes. Doxycycline targets both mitochondrial ribosomes and DNA-PK, thereby reducing ATP levels, as observed experimentally.

Pre-treatment of monolayers with doxycycline, with and without radiation treatment

MCF7 cells were plated in normal medium (DMEM, 10% FCS, L-glutamine, supplemented with Pen-Strep) for 24-hr. Cells were then treated, initially for 7 days with doxycycline, with media changed every 3 days. For subsequent experiments, cells were treated for 72-hr. For radiation experiments, monolayer cells pre-treated with doxycycline, were exposed to increasing levels of radiation, and the cells collected by trypsinization and centrifugation. To quantitatively determine cell growth, the number of cells remaining after treatment was counted using an automatic cell counter (Biorad), compared to untreated cells and expressed as fold-change. To assess cell viability, cells were incubated for 1 minute with Trypan Blue (Sigma, #T8145) using a 1:1 ratio. The number of Trypan Blue positive cells (non-viable) was measured using an automatic cell counter (Biorad) and compared to untreated controls. Cells were also plated into mammosphere cultures to assess stem cell-like activity with no further drug treatment. All experiments were performed in triplicate and repeated at least three times independently.

Irradiation of MCF7 monolayers using a cell x-ray unit

MCF7 cells were pre-treated at a monolayer for 3 days, with either doxycycline (50 μ M) or with

vehicle-alone, and then were irradiated with 0–10 Gy at room temperature, using an X-ray unit, at a dose-rate of 1.37 Gy/min. More specifically, irradiation was performed using a free-standing 320 kV x-ray system (Gulmay Medical Ltd, now Xstrahl Ltd, Camberley, UK). The machine was operated at 300 kV, 10 mA with the addition of a 0.75 mm Cu filter to give a beam quality with half-value layer (HVL) of 2.3 mm Cu. Samples were positioned at a distance of 500 mm from the x-ray focus and a backscatter block was utilised to ensure good dose uniformity. The dose rate to samples was determined to be 1.37 Gy/min [43]. This dose rate was checked regularly using the IPEM 2005 protocol and equipment whose calibration was traceable to UK national standards.

Lentiviral transduction

Lentiviral particles harboring human DNA-PK sh-RNA (#sc-35200-V, Santa Cruz) or control shRNA lentiviral Particles (#sc-108080, Santa Cruz), were used to stably transduce MCF7 cells, according to the manufacturer's protocol (in the presence of 5 μ g/ml polybrene). Twenty-four hours post-infection, media containing the virus was removed and replaced with standard media. Cells were then selected with 2 μ g/ml puromycin, for up to 10 days.

Immunoblot analysis

MCF7 cells were seeded in 10 cm dishes for 72 hrs. Then, cells were lysed in RIPA buffer (Sigma), containing proteinase inhibitors (Roche) and kept at 4°C for 30 minutes. Lysates were collected by centrifugation for 10 minutes at 10,000 \times g, and protein concentration were determined using the BCA protein assay kit (Pierce). Samples were diluted into SDS-PAGE sample buffer and were boiled for 5 minutes before being separated by SDS-PAGE, using a 4–15% gradient Mini-PROTEAN TGX Gel (Biorad). Samples were then transferred onto a nitrocellulose membrane (Biorad), blocked in 5% milk in TBS-Tween 20 (Sigma) and probed with antibodies directed against DNA-PK (ThermoScientific, #MS-423-P0) and β -actin (Santa Cruz Biotechnology, #sc-1616), using a secondary antibody at a dilution of 1 to 5000. Bound antibodies were detected using the Supersignal West Pico Chemiluminescent substrate (ThermoScientific).

Mammosphere culture

A single cell suspension was prepared using enzymatic (1x Trypsin-EDTA, Sigma Aldrich, #T3924), and manual disaggregation (25 gauge needle) to create a single cell suspension [44]. Cells were plated at a density of 500 cells/cm² in mammosphere medium (DMEM-F12/B27/20 ng/ml EGF/PenStrep) in non-adherent conditions, in culture dishes coated with (2-hydroxyethylmethacrylate)

(poly-HEMA, Sigma, #P3932). Cells were grown for 5 days and maintained in a humidified incubator at 37°C at an atmospheric pressure in 5% (v/v) carbon dioxide/air. After 5 days for culture, spheres > 50 µm were counted using an eye piece graticule, and the percentage of cells plated which formed spheres was calculated and is referred to as percentage mammosphere formation, and was normalized to one (1 = 100% MSF). For proteomic analysis, mammospheres were collected by centrifugation at 800 rpm for 10 minutes and compared to monolayer cells grown for 5 days.

Label-free quantitative proteomics analysis

Cell lysates were prepared for trypsin digestion by sequential reduction of disulphide bonds with TCEP and alkylation with MMTS [45]. Then, the peptides were extracted and prepared for LC-MS/MS. All LC-MS/MS analyses were performed on an LTQ Orbitrap XL mass spectrometer (Thermo Scientific, San Jose, CA) coupled to an Ultimate 3000 RSLCnano system (Thermo Scientific, formerly Dionex, The Netherlands). Xcalibur raw data files acquired on the LTQ-Orbitrap XL were directly imported into Progenesis LCMS software (Waters Corp., Milford, MA, formerly Non-linear dynamics, Newcastle upon Tyne, UK) for peak detection and alignment. Data were analyzed using the Mascot search engine. Five replicates were analyzed for each sample type ($N = 5$). Statistical analyses were performed using ANOVA and only fold-changes in proteins with a p -value less than 0.05 were considered significant.

Data mining

To firmly establish the clinical relevance of our results from the quantitative proteomics analysis of mammospheres, we re-analyzed the transcriptional profiles of epithelial breast cancer cells and adjacent tumor stromal cells that were physically separated by laser-capture microdissection (from $N = 28$ human breast cancer patients) [21].

Seahorse XFe96 metabolic flux analysis

Extracellular acidification rates (ECAR) and real-time oxygen consumption rates (OCR) for MCF7 and MCF7 treated with doxycycline were determined using the Seahorse Extracellular Flux (XFe96) analyzer (Seahorse Bioscience, MA, USA). MCF7 cells were maintained in DMEM supplemented with 10% FBS (fetal bovine serum), 2 mM GlutaMAX, and 1% Pen-Strep. We seeded 7,000 cells per well into XFe96 well cell culture plates and they were incubated overnight at 37°C in a 5% CO₂ humidified atmosphere. After 24 h, the cells were treated with DOX

(25 µM and 50 µM) for 48 h in XFe96 cell culture plates. After 48 h of incubation in DMEM media, MCF-7 cells were washed in XF assay media (or for OCR measurement, XF assay media supplemented with 10 mM glucose, 1 mM Pyruvate, 2 mM L-glutamine and adjusted at 7.4 pH), which were pre-warmed to 37°C. MCF7 cells were then maintained in 175 µL/well of XF assay media at 37°C, in a non-CO₂ incubator for 1 h. During the cell incubation time, we loaded 25 µL of 80 mM glucose, 9 µM oligomycin, 1M 2-deoxyglucose (for ECAR measurement) and 10 µM oligomycin, 9 µM FCCP, 10 µM rotenone, 10 µM antimycin A (for OCR measurement), in XF assay media into the injection ports in the XFe96 sensor cartridge. Measurements were normalized by protein content. Data set was analyzed by XFe96 software and GraphPad Prism software, using one-way ANOVA and Student's t -test calculations. All experiments were performed in quintuplicate, three times independently, such that each data point represents the average of 15 replicates.

Anoikis assay

Following doxycycline treatment, the CSC population was enriched by seeding on low-attachment plates. Under these conditions, the non-CSCs undergo anoikis (a form of apoptosis induced by a lack of cell-substrate attachment) and CSCs are believed to survive. The surviving "CSC fraction" was analyzed by FACS analysis. Briefly, 1×10^4 MCF7 cells were treated with doxycycline (25 µM and 50 µM) for 48 h in 6-well plates, grown as a monolayer. Then, the monolayer cells were trypsinized and seeded in low-attachment plates in mammosphere media. After 10 h under low-attachment conditions, MCF7 cells were spun down and incubated with LIVE/DEAD dye (Fixable Dead Violet reactive dye; Invitrogen) for 20 minutes to distinguish between the live and dead populations of cells (cell viability), during anoikis. Samples were then analyzed by FACS (Fortessa, BD Bioscience) and the data were analysed using FlowJo software.

Monitoring cell signal transduction pathways

The Signal Lenti luciferase reporter assay was used to monitor the activity of several signaling pathways in MCF7-GFP cells, essentially as previously described [46, 47]. Briefly, viral particles diluted 1:10 in complete media containing polybrene (sc-134220, Santa Cruz) were added to the cells. Puromycin treatment (P9620, Sigma) was added 48 h later in order to stably select infected cells. Luciferase assays (E1501, Promega) were performed according to manufacturer's instructions. Approximately 6×10^3 MCF7 cells were seeded in black-walled 96 well plates. When cells were attached, drug treatments were added for 24, 48, 72 and 96 h. Four replicates were used for each condition. After

treatment, the luciferase assay was performed according to manufacturer's instructions and light signal was acquired in the Xenogen VivoVision IVIS Lumina. Results were normalized by GFP fluorescence.

ACKNOWLEDGMENTS

We thank the University of Manchester for providing start-up funds that contributed to the success of this study. The Sotgia and Lisanti Laboratories were supported, in part, by funding from the European Union (ERC Advanced Grant), Breakthrough Breast Cancer, and the Manchester Cancer Research Centre (MCRC). DLS was core-funded by CRUK.

REFERENCES

1. Lamb R, Harrison H, Hulit J, Smith DL, Lisanti MP, Sotgia F. Mitochondria as new therapeutic targets for eradicating cancer stem cells: Quantitative proteomics and functional validation via MCT1/2 inhibition. *Oncotarget*. 2014; 5:11029–11037.
2. McKee EE, Ferguson M, Bentley AT, Marks TA. Inhibition of mammalian mitochondrial protein synthesis by oxazolidinones. *Antimicrobial agents and chemotherapy*. 2006; 50:2042–2049.
3. Moullan N, Mouchiroud L, Wang X, Ryu D, Williams EG, Mottis A, Jovaisaite V, Frochoux MV, Quiros PM, Deplancke B, Houtkooper RH, Auwerx J. Tetracyclines Disturb Mitochondrial Function across Eukaryotic Models: A Call for Caution in Biomedical Research. *Cell reports*. 2015; 10:1681–1691.
4. Riesbeck K, Bredberg A, Forsgren A. Ciprofloxacin does not inhibit mitochondrial functions but other antibiotics do. *Antimicrobial agents and chemotherapy*. 1990; 34:167–169.
5. Bottger EC, Springer B, Prammananan T, Kidan Y, Sander P. Structural basis for selectivity and toxicity of ribosomal antibiotics. *EMBO reports*. 2001; 2:318–323.
6. Leach KL, Swaney SM, Colca JR, McDonald WG, Blinn JR, Thomasco LM, Gadwood RC, Shinabarger D, Xiong L, Mankin AS. The site of action of oxazolidinone antibiotics in living bacteria and in human mitochondria. *Molecular cell*. 2007; 26:393–402.
7. Lamb R, Ozsvari B, Lisanti CL, Tanowitz HB, Howell A, Martinez-Outschoorn UE, Sotgia F, Lisanti MP. Antibiotics that target mitochondria effectively eradicate cancer stem cells, across multiple tumor types: Treating cancer like an infectious disease. *Oncotarget*. 2015.
8. Kircik LH. Doxycycline and minocycline for the management of acne: a review of efficacy and safety with emphasis on clinical implications. *Journal of drugs in dermatology: JDD*. 2010; 6:4569–4584.
9. Maibach H. Second-generation tetracyclines, a dermatologic overview: clinical uses and pharmacology. *Cutis*. 1991; 48:411–417.
10. Ahler E, Sullivan WJ, Cass A, Braas D, York AG, Bensinger SJ, Graeber TG, Christofk HR. Doxycycline alters metabolism and proliferation of human cell lines. *PloS one*. 2013; 8:e64561.
11. Zhang L, Ging NC, Komoda T, Hanada T, Suzuki T, Watanabe K. Antibiotic susceptibility of mammalian mitochondrial translation. *FEBS letters*. 2005; 579:6423–6427.
12. Zimorski V, Ku C, Martin WF, Gould SB. Endosymbiotic theory for organelle origins. *Current opinion in microbiology*. 2014; 22:38–48.
13. Degli Esposti M, Chouaia B, Comandatore F, Crotti E, Sasser D, Lievens PM, Daffonchio D, Bandi C. Evolution of mitochondria reconstructed from the energy metabolism of living bacteria. *PloS one*. 2014; 9:e96566.
14. Ferreri AJ, Dolcetti R, Magnino S, Doglioni C, Cangini MG, Pecciarini L, Ghia P, Dagklis A, Pasini E, Vicari N, Dognini GP, Resti AG, Ponzoni M. A woman and her canary: a tale of chlamydiae and lymphomas. *Journal of the National Cancer Institute*. 2007; 99:1418–1419.
15. Ferreri AJ, Ponzoni M, Guidoboni M, Resti AG, Politi LS, Cortelazzo S, Demeter J, Zallio F, Palmas A, Muti G, Dognini GP, Pasini E, Lettini AA, Sacchetti F, De Conciliis C, Doglioni C, et al. Bacteria-eradicating therapy with doxycycline in ocular adnexal MALT lymphoma: a multicenter prospective trial. *Journal of the National Cancer Institute*. 2006; 98:1375–1382.
16. Blagosklonny MV. Cancer stem cell and cancer stem-loids: from biology to therapy. *Cancer Biol Ther*. 2007; 6:1684–90.
17. Duivenvoorden WC, Popovic SV, Lhotak S, Seidlitz E, Hirte HW, Tozer RG, Singh G. Doxycycline decreases tumor burden in a bone metastasis model of human breast cancer. *Cancer research*. 2002; 62:1588–1591.
18. Davis AJ, Lee KJ, Chen DJ. The N-terminal region of the DNA-dependent protein kinase catalytic subunit is required for its DNA double-stranded break-mediated activation. *The Journal of biological chemistry*. 2013; 288:7037–7046.
19. Davis AJ, Chen BP, Chen DJ. DNA-PK: a dynamic enzyme in a versatile DSB repair pathway. *DNA repair*. 2014; 17:21–29.
20. Papeta N, Zheng Z, Schon EA, Brosel S, Altintas MM, Nasr SH, Reiser J, D'Agati VD, Gharavi AG. Prkdc participates in mitochondrial genome maintenance and prevents Adriamycin-induced nephropathy in mice. *The Journal of clinical investigation*. 2010; 120:4055–4064.
21. Casey T, Bond J, Tighe S, Hunter T, Lintault L, Patel O, Eneman J, Crocker A, White J, Tessitore J, Stanley M, Harlow S, Weaver D, Muss H, Plaut K. Molecular signatures suggest a major role for stromal cells in development

- of invasive breast cancer. *Breast cancer research and treatment*. 2009; 114:47–62.
22. Hardcastle IR, Cockcroft X, Curtin NJ, El-Murr MD, Leahy JJ, Stockley M, Golding BT, Rigoreau L, Richardson C, Smith GC, Griffin RJ. Discovery of potent chromen-4-one inhibitors of the DNA-dependent protein kinase (DNA-PK) using a small-molecule library approach. *Journal of medicinal chemistry*. 2005; 48:7829–7846.
 23. Zhao Y, Thomas HD, Batey MA, Cowell IG, Richardson CJ, Griffin RJ, Calvert AH, Newell DR, Smith GC, Curtin NJ. Preclinical evaluation of a potent novel DNA-dependent protein kinase inhibitor NU7441. *Cancer research*. 2006; 66:5354–5362.
 24. Ciszewski WM, Tavecchio M, Dastyk J, Curtin NJ. DNA-PK inhibition by NU7441 sensitizes breast cancer cells to ionizing radiation and doxorubicin. *Breast cancer research and treatment*. 2014; 143:47–55.
 25. Hsu FM, Zhang S, Chen BP. Role of DNA-dependent protein kinase catalytic subunit in cancer development and treatment. *Translational cancer research*. 2012; 1:22–34.
 26. Chiarugi P, Giannoni E. Anoikis: a necessary death program for anchorage-dependent cells. *Biochemical pharmacology*. 2008; 76:1352–1364.
 27. Taddei ML, Giannoni E, Fiaschi T, Chiarugi P. Anoikis: an emerging hallmark in health and diseases. *The Journal of pathology*. 2012; 226:380–393.
 28. Kwon OJ, Valdez JM, Zhang L, Zhang B, Wei X, Su Q, Ittmann MM, Creighton CJ, Xin L. Increased Notch signaling inhibits anoikis and stimulates proliferation of prostate luminal epithelial cells. *Nature communications*. 2014; 5:4416.
 29. Rix U and Superti-furga, G. Target profiling of small molecules by chemical proteomics. *Nature chemical biology*. 2009; 5:616–624.
 30. Jeffery DA, Bogoy M. Chemical proteomics and its application to drug discovery. *Current opinion in biotechnology*. 2003; 14:87–95.
 31. O'Connor MJ, Martin NM, Smith GC. Targeted cancer therapies based on the inhibition of DNA strand break repair. *Oncogene*. 2007; 26:7816–7824.
 32. Kashishian A, Douangpanya H, Clark D, Schlachter ST, Eary CT, Schiro JG, Huang H, Burgess LE, Kesicki EA, Halbrook J. DNA-dependent protein kinase inhibitors as drug candidates for the treatment of cancer. *Molecular cancer therapeutics*. 2003; 2:1257–1264.
 33. An J, Xu QZ, Sui JL, Bai B, Zhou PK. Downregulation of c-myc protein by siRNA-mediated silencing of DNA-PKcs in HeLa cells. *International journal of cancer*. 2005; 117:531–537.
 34. Peng Y, Zhang Q, Nagasawa H, Okayasu R, Liber HL, Bedford JS. Silencing expression of the catalytic subunit of DNA-dependent protein kinase by small interfering RNA sensitizes human cells for radiation-induced chromosome damage, cell killing, and mutation. *Cancer research*. 2002; 62:6400–6404.
 35. Novotna E, Tichy A, Pejchal J, Lukasova E, Salovska B, Vavrova J. DNA-dependent protein kinase and its inhibition in support of radiotherapy. *International journal of radiation biology*. 2013; 89:416–423.
 36. Nutley BP, Smith NF, Hayes A, Kelland LR, Brunton L, Golding BT, Smith GC, Martin NM, Workman P, Raynaud FI. Preclinical pharmacokinetics and metabolism of a novel prototype DNA-PK inhibitor NU7026. *British journal of cancer*. 2005; 93:1011–1018.
 37. Davidson D, Amrein L, Panasci L, Aloyz R. Small Molecules, Inhibitors of DNA-PK, Targeting DNA Repair, and Beyond. *Frontiers in pharmacology*. 2013; 4:5.
 38. Goodwin JF, Knudsen KE. Beyond DNA repair: DNA-PK function in cancer. *Cancer discovery*. 2014; 4:1126–1139.
 39. Bahrami F, Morris DL, Pourgholami MH. Tetracyclines: drugs with huge therapeutic potential. *Mini reviews in medicinal chemistry*. 2012; 12:44–52.
 40. Welling PG, Koch PA, Lau CC, Craig WA. Bioavailability of tetracycline and doxycycline in fasted and nonfasted subjects. *Antimicrobial agents and chemotherapy*. 1977; 11:462–469.
 41. Singh JK, Farnie G, Bundred NJ, Simoes BM, Shergill A, Landberg G, Howell SJ, Clarke RB. Targeting CXCR1/2 significantly reduces breast cancer stem cell activity and increases the efficacy of inhibiting HER2 via HER2-dependent and -independent mechanisms. *Clinical cancer research: an official journal of the American Association for Cancer Research*. 2013; 19:643–656.
 42. Harrison H, Farnie G, Howell SJ, Rock RE, Stylianou S, Brennan KR, Bundred NJ, Clarke RB. Regulation of breast cancer stem cell activity by signaling through the Notch4 receptor. *Cancer research*. 2010; 70:709–718.
 43. Aukett RJ, Burns JE, Greener AG, Harrison RM, Moretti C, Nahum AE, Rosser KE, Party IW. Addendum to the IPEMB code of practice for the determination of absorbed dose for x-rays below 300 kV generating potential. 0.035 mm Al-4 mm Cu HVL. *Physics in medicine and biology*. 2005; 50:2739–2748.
 44. Shaw FL, Harrison H, Spence K, Ablett MP, Simoes BM, Farnie G, Clarke RB. A detailed mammosphere assay protocol for the quantification of breast stem cell activity. *Journal of mammary gland biology and neoplasia*. 2012; 17:111–117.
 45. Holland M, Castro FV, Alexander S, Smith D, Liu J, Walker M, Bitton D, Mulryan K, Ashton G, Blaylock M, Bagley S, Connolly Y, Bridgeman J, Miller C, Krishnan S, Dempsey C, et al. RAC2, AEP, and ICAM1 expression are

- associated with CNS disease in a mouse model of pre-B childhood acute lymphoblastic leukemia. *Blood*. 2011; 118:638–649.
46. Peiris-Pagès M, Sotgia F, Lisanti MP. Chemotherapy induces the cancer-associated fibroblast phenotype, activating paracrine Hedgehog-GLI signaling in breast cancer cells. *Oncotarget*. 2015; 6:10728–107245.
47. Fiorillo M, Verre AF, Iliut M, Peiris-Pagès M, Ozsvári B, Gandara R, Cappello AR, Sotgia F, Vijayaraghavan A, Lisanti MP. Graphene oxide selectively targets cancer stem cells, across multiple tumor types: Implications for non-toxic cancer treatment, via “differentiation-based nanotherapy”. *Oncotarget*. 2015; 6:3553–62.

Graphene oxide selectively targets cancer stem cells, across multiple tumor types: Implications for non-toxic cancer treatment, via “differentiation-based nano-therapy”

Marco Fiorillo^{1,2,3}, Andrea F. Verre⁴, Maria Iliut⁴, Maria Peiris-Pagés^{1,2}, Bela Ozsvári^{1,2}, Ricardo Gandara^{1,2}, Anna Rita Cappello³, Federica Sotgia^{1,2}, Aravind Vijayaraghavan⁴ and Michael P. Lisanti^{1,2}

¹ The Manchester Centre for Cellular Metabolism (MCCM), Institute of Cancer Sciences, University of Manchester, UK

² The Breakthrough Breast Cancer Research Unit, Institute of Cancer Sciences, University of Manchester, UK

³ The Department of Pharmacy, Health and Nutritional Sciences, The University of Calabria, Italy

⁴ School of Materials and National Graphene Institute, University of Manchester, UK

Correspondence to: Michael P. Lisanti, **email:** michael.lisanti@manchester.ac.uk

Aravind Vijayaraghavan, **email:** aravind@manchester.ac.uk

Keywords: nanomaterials, graphene oxide, cancer stem cells, multiple cancer types: breast, ovarian

Received: January 01, 2015

Accepted: February 12, 2015

Published: February 24, 2015

This is an open-access article distributed under the terms of the Creative Commons Attribution License, which permits unrestricted use, distribution, and reproduction in any medium, provided the original author and source are credited.

ABSTRACT

Tumor-initiating cells (TICs), a.k.a. cancer stem cells (CSCs), are difficult to eradicate with conventional approaches to cancer treatment, such as chemo-therapy and radiation. As a consequence, the survival of residual CSCs is thought to drive the onset of tumor recurrence, distant metastasis, and drug-resistance, which is a significant clinical problem for the effective treatment of cancer. Thus, novel approaches to cancer therapy are needed urgently, to address this clinical need. Towards this end, here we have investigated the therapeutic potential of graphene oxide to target cancer stem cells. Graphene and its derivatives are well-known, relatively inert and potentially non-toxic nano-materials that form stable dispersions in a variety of solvents. Here, we show that graphene oxide (of both big and small flake sizes) can be used to selectively inhibit the proliferative expansion of cancer stem cells, across multiple tumor types. For this purpose, we employed the tumor-sphere assay, which functionally measures the clonal expansion of single cancer stem cells under anchorage-independent conditions. More specifically, we show that graphene oxide effectively inhibits tumor-sphere formation in multiple cell lines, across 6 different cancer types, including breast, ovarian, prostate, lung and pancreatic cancers, as well as glioblastoma (brain). In striking contrast, graphene oxide is non-toxic for “bulk” cancer cells (non-stem) and normal fibroblasts. Mechanistically, we present evidence that GO exerts its striking effects on CSCs by inhibiting several key signal transduction pathways (WNT, Notch and STAT-signaling) and thereby inducing CSC differentiation. Thus, graphene oxide may be an effective non-toxic therapeutic strategy for the eradication of cancer stem cells, via differentiation-based nano-therapy.

INTRODUCTION

Cancer stem cells (CSCs) are resistant to conventional therapeutic approaches [1-3]. As a

consequence, they have been directly implicated in the disease pathogenesis of tumor recurrence and distant metastasis [4, 5]. In addition, drug-resistant CSCs have been linked to unfavorable clinical outcomes,

across different tumor types [6-8]. As only a very small percentage of cancer cells have “stem-like” and “tumor-initiating” properties, they are difficult to study and their key distinguishing features remain relatively uncharacterized, although they appears to resist both chemo-therapy and radiation.

Interestingly, CSCs share many properties with normal stem cells, including immortality and resistance to stress, as well as asymmetric cell division [9, 10]. A particular distinguishing characteristic of CSCs is their ability to initiate tumors and to undergo anchorage-independent growth, when cultured in suspension [11]. Under these particular cell culture conditions, CSCs proliferate and form 3D-spheroid-like structures, containing CSCs and progenitor cells, which are known as “tumor-spheres” or “onco-spheres” [12, 13]. In striking contrast, the vast majority of non-CSCs undergo a specialized form of apoptosis in suspension cultures, called anoikis. Importantly, each 3D-spheroid originates from the clonal proliferation of a single CSC, is not due to the self-aggregation of cancer cells. Thus, tumor-sphere formation is an efficient means to selectively enrich for CSCs. The CSC population is resistant to DNA-damage, and shows lower levels of ROS production, as well [14, 15]. 3D-tumor-spheres derived from breast cancer cells are also known as mammo-spheres [12, 13].

Clinically, there is an urgent need to identify new therapeutic strategies for selectively targeting CSCs. Here, we show that graphene oxide (GO) demonstrates this selectivity. As such, our current study provides a new rationale for exploiting graphene oxide itself as an anti-cancer therapeutic, rather than simply as a drug-delivery agent [16].

RESULTS

GO flakes target breast cancer stem cells

Here, we tested the efficacy of graphene oxide as a potential new anti-cancer agent, for the selective targeting of CSCs. Graphene, described as two-dimensional sheets of carbon atoms without any additional functional groups, does not form stable dispersions in water or other biologically relevant solvents [17]. On the other hand, graphene oxide [18] is the water-soluble derivative of graphene which can be produced with various sizes and bearing varied functional groups and which can be more easily manipulated experimentally, especially in biological systems. Sterile GO dispersions were prepared in a 5% mixture of DMSO in double-distilled water for these studies.

Initially, we tested the ability of GO to affect CSC proliferation, using MCF7 cells, a well-established ER(+) breast cancer cell line. Two grades of GO were used, small GO (s-GO) with flake sizes of 0.2–2 μm and big GO (b-GO) with flake sizes of 5–20 μm , to represent two size classes, where the flakes are either smaller or larger than the target cells (Figure 1). For this purpose, we assessed the effects of graphene oxide on the anchorage-independent clonal expansion of MCF7 CSCs, using the tumor-sphere assay. This functional assay directly measures CSCs proliferative expansion [12]. Figure 2 shows the results of this analysis. Using s-GO flakes, we observed a dose-dependent inhibition of tumor-sphere formation, in the range of 1.25 to 25 $\mu\text{g/ml}$, with an IC-

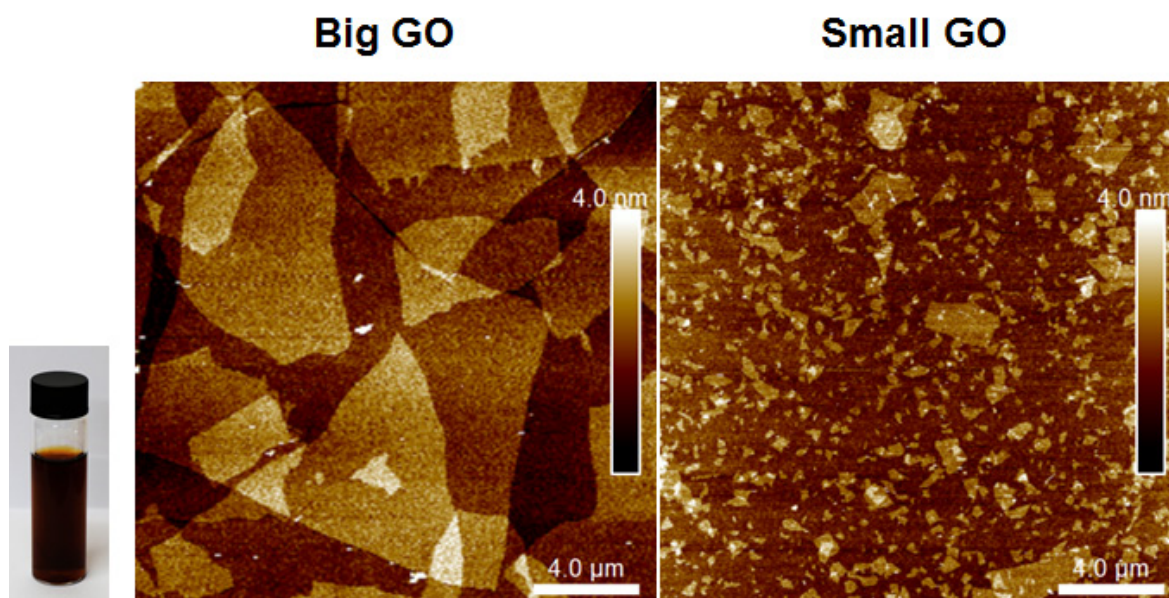


Figure 1: Graphene oxide (GO) grades. Left and Right panels show atomic force microscopy images of graphene oxide on a silicon dioxide substrate indicating the flake size distribution and monolayer thickness of the flakes. Inset shows a vial of b-GO stock dispersion in DMSO and water, at concentration of 2.3 mg/ml.

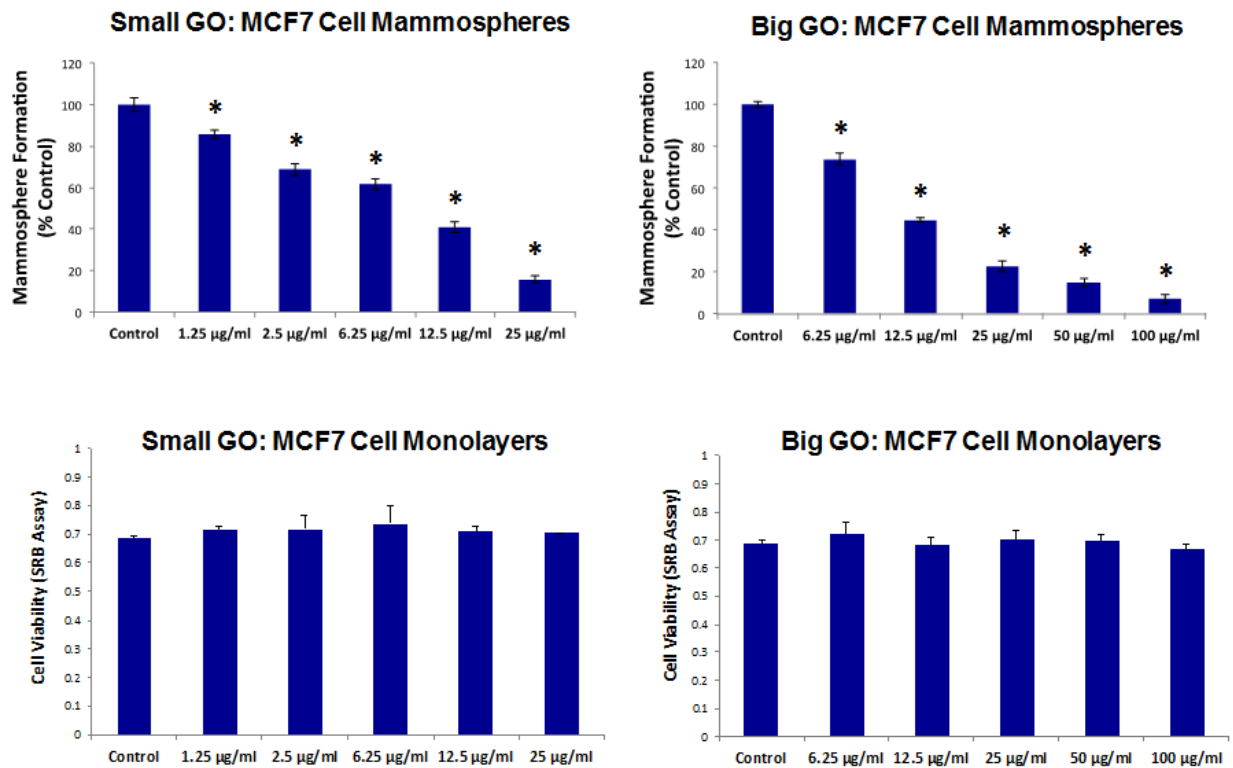


Figure 2: Graphene oxide (GO) selectively targets cancer stem cells (CSCs) in breast cancer cells. Upper Panels. Note that GO (big and small flakes) inhibits the anchorage-independent proliferation of MCF7 CSCs, as evidenced by inhibition of mammosphere formation. Lower Panels. In contrast, GO (big and small flakes) does not affect cell viability of the total MCF7 cell population. An * indicates $p < 0.05$ (Student's t-test).

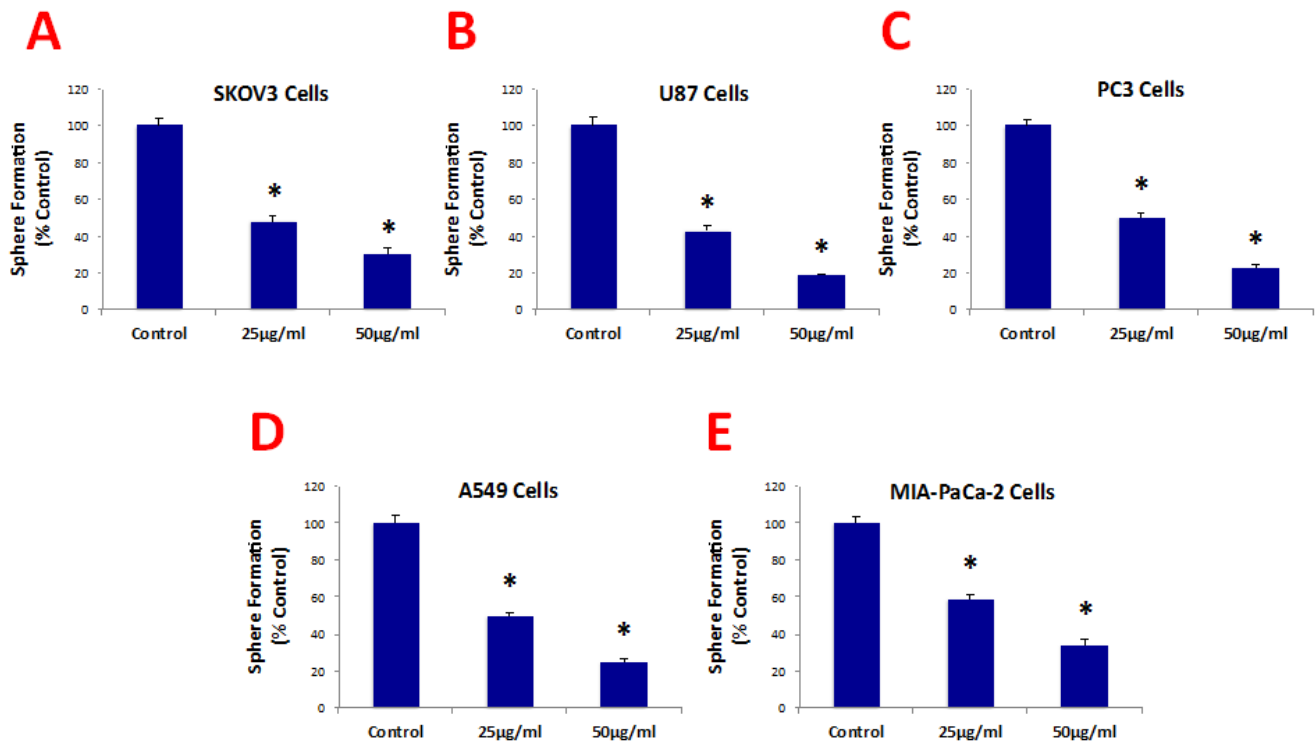


Figure 3: Graphene oxide (GO) selectively targets cancer stem cells (CSCs) of multiple cancer cell types. GO (big flakes) inhibits the anchorage-independent proliferation of SKOV3 ovarian cancer cells (A), U87 glioblastoma cells (B), PC3 prostate cancer cells (C), A549 lung cancer cells (D), as well as pancreatic cancer cells (E), in a concentration-independent manner. These results indicate that GO inhibits sphere formations of multiple cancer types. An * indicates $p < 0.05$ (Student's t-test).

Table 1: Six Cancer Cell Models with Broad Applicability.

Cancer Types	Cell Lines
Breast(ER+)	MCF7
Ovarian	SKOV3
Prostate	PC3
Pancreatic	MIA-PaCa-2
Lung	A549
Glioblastoma	U87 MG

50 of ~12.5 µg/ml. Similarly, using b-GO flakes, we also observed a dose-dependent inhibition of tumor-sphere formation, in the range of 6.25 to 100 µg/ml, again with an IC-50 of ~12.5 µg/ml. Importantly, both small and big GO flakes did not affect the viability of the bulk non-CSC population of MCF7 cells, indicating selectivity towards CSCs (Figure 2).

GO flakes target CSCs, across multiple cancer types

Since both the small and big GO flakes showed similar potency, we focused more on evaluating the efficacy of b-GO flakes. We next evaluated whether GO also showed efficacy against CSCs from multiple cancer types, such as ovarian, prostate, pancreatic and lung cancers, as well as glioblastoma (brain) (the six cell lines tested are summarized in Table 1). For simplicity, we tested b-GO flakes at two doses, namely 25 and 50 µg/ml.

Figure 3 shows that b-GO flakes also effectively inhibited tumor-sphere formation in these 5 other cell lines. Thus, our results indicate that GO must be targeting a relatively specific and highly-conserved phenotypic property of CSCs, across multiple cancer types. Representative images of tumor-sphere inhibition by GO treatment are shown in Figure 4. Interestingly, the viability of bulk non-CSCs from these five cancer cell lines (SKOV3, PC3, A549, Mia PaCa2, and U-87) was not affected by GO (Figure 5), further highlighting its specificity and selectivity for CSCs.

Importantly, b-GO flakes also did not affect the viability of a normal skin fibroblast cell line (hTERT-BJ1), indicating that GO is relatively non-toxic for normal body cells (Figure 6). This is consistent with the findings of many other laboratories, i.e., that GO is non-toxic for multiple normal cell types [19, 20].

GO-based mechanistic studies: Effects on well-established CSC signaling pathways

To gain mechanistic insights into how GO flakes target cancer stem cells, we next analyzed their effects on a series of well-established signal transduction pathways, which have been shown to contribute towards “stemness” [21-23].

For this purpose, we used a panel of MCF7 cell lines that were stably-transfected with different luciferase reporters, that allows one to quantitatively measure the activation-state of a given signal transduction pathway. Interestingly, Figure 7 shows that a number of signaling pathways were significantly inhibited by GO treatment. More specifically, GO treatment inhibited WNT- and Notch-driven signaling, as well as STAT1/3 signaling and the NRF2-dependent anti-oxidant response. However, little or no effect was observed on TGF-beta/SMAD-

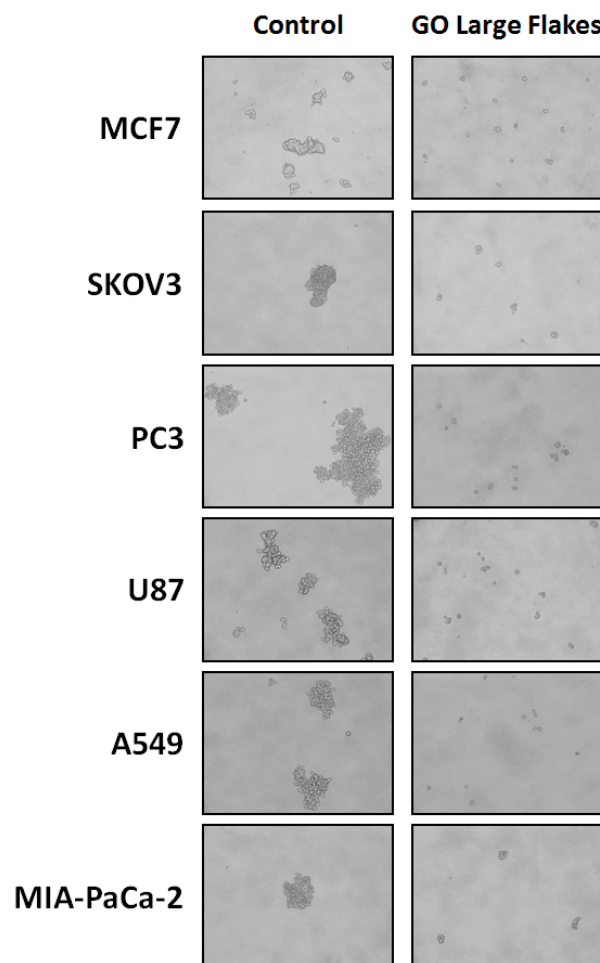


Figure 4: Graphene oxide (GO) selectively targets cancer stem cells (CSCs) of multiple cancer cell types. Representative images showing that GO (big flakes, 25µg/ml) inhibits the anchorage-independent proliferation of MCF7 breast cancer cells, SKOV3 ovarian cancer cells, PC3 prostate cancer cells, U87 glioblastoma cells, A549 lung cancer cells as well as MIA-PaCa-2 pancreatic cancer cells.

signaling (Figure 7).

Thus, it appears that GO treatment somehow targets several different signal transduction pathways in cancer cells, to reduce overall “stemness”.

GO promotes the differentiation of breast cancer stem cells

To further validate the idea GO was reducing stemness in MCF7-derived CSCs, we used a series of well-established breast cancer stem cell markers (CD44

and CD24), and quantitatively analyzed their expression by FACS analysis. The results of these studies are presented in Figure 8.

Briefly, MCF7 cells were treated as monolayer cultures with GO (50µg/ml) for 48 hours or left untreated (vehicle alone control). Then, cells were trypsinized and plated on low-attachment plates for 10 hours to induce anoikis and enrich for CSCs. Single cells were then analysed by FACS to quantitate the CD44(+)/CD24-/low population, which represents the breast CSCs. As predicted, the CD44(+)/CD24-/low population is greatly enriched after 10 hours in low-attachment conditions

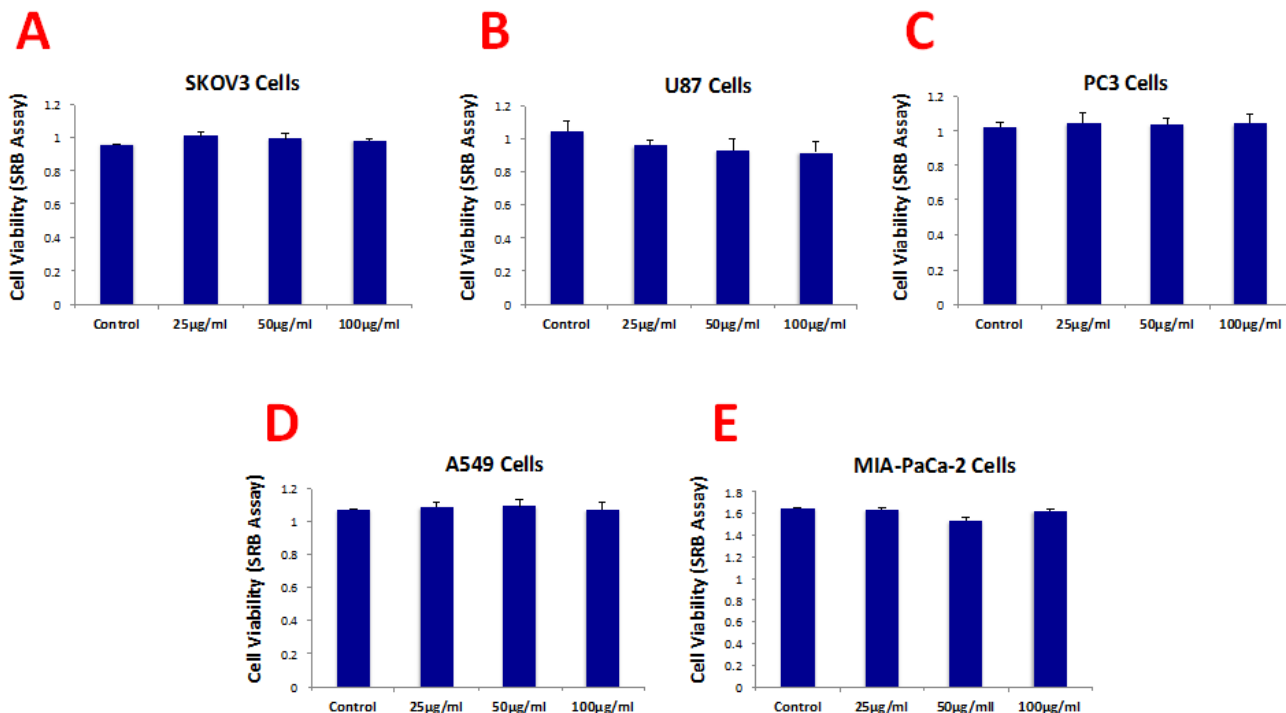


Figure 5: Graphene oxide (GO) does not affect cell viability of the total population of cancer cells. Cell viability was assessed using an SRB assay. Note that GO (big flakes) does not affect cell viability of the total cell population of SKOV3 ovarian cancer cells (A), U87 glioblastoma cells (B), PC3 prostate cancer cells (C), A540 lung cancer cells (D) as well as MIA-PaCa-2 pancreatic cancer cells.

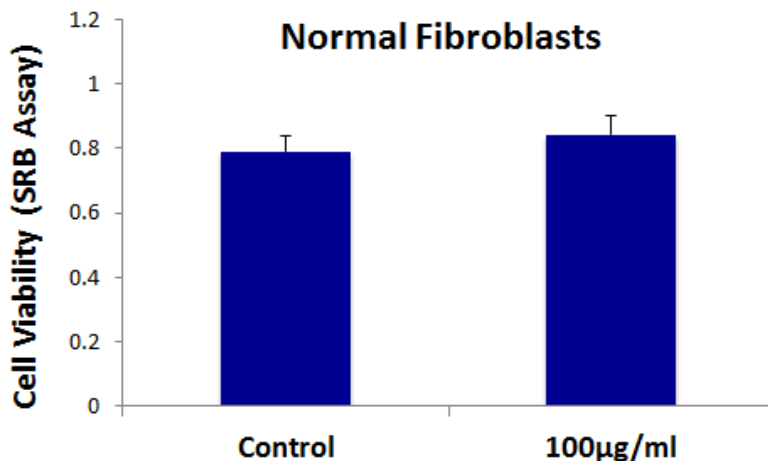


Figure 6: Graphene oxide (GO) does not affect the cell viability normal fibroblasts. Cell viability of hTERT-BJ1 fibroblasts was assessed using an SRB assay. Note that GO (big flakes) does not affect cell viability of the total cell population of normal fibroblasts.

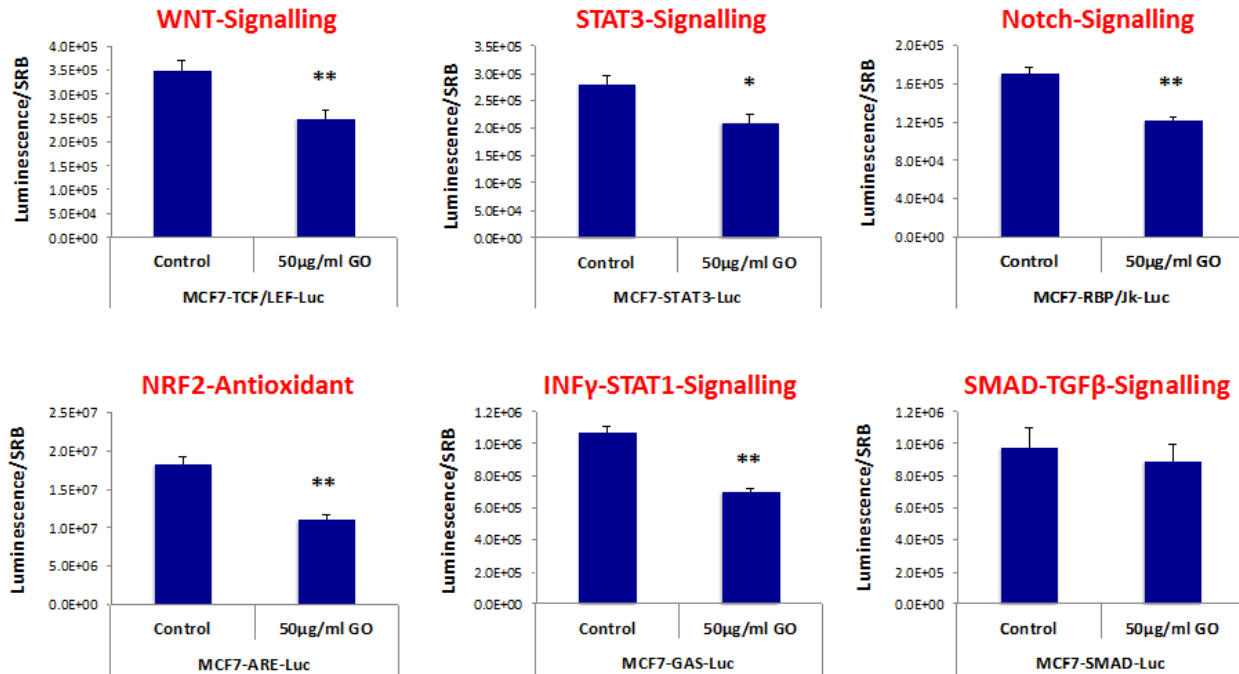


Figure 7: Graphene oxide (GO) inhibits signaling pathways related to cancer stem cells, antioxidant responses and interferon. MCF7 breast cancer cells carrying luciferase-reporters (Signal, QIAGEN) were generated to monitor the activation of a variety of signaling networks, including Wnt, STAT3, Notch, NRF2-dependent antioxidant responses, Interferon-STAT1 and SMAD-TGFβ pathways. MCF7-Luc reporter cells were treated with GO (big flakes) for 48 hours and luminescence was determined as a measure of pathway activation status. Note that GO inhibits cancer stem cell signaling (WNT, STAT3 and Notch), NRF2-antioxidant responses, as well as INFY-STAT1 signaling. No effects were observed for the SMAD-TGFβ-pathway. An * indicates $p < 0.05$; ** indicates $p < 0.01$ (Student's t-test).

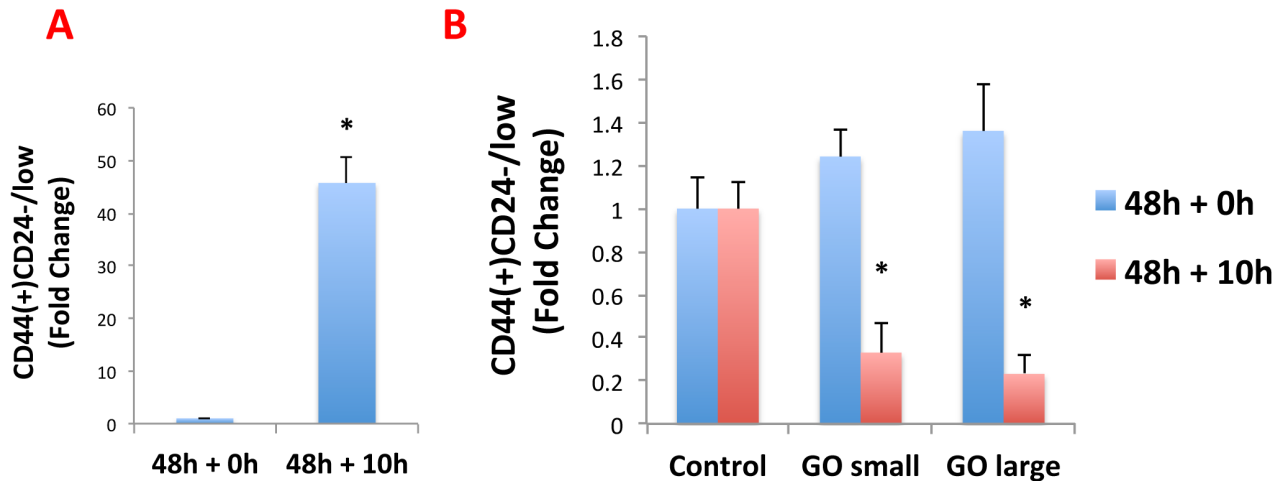


Figure 8: Graphene oxide (GO) promotes the differentiation of breast cancer stem cells. MCF7 cells were treated as monolayer cultures with small or big GO (50µg/ml) for 48 hours or left untreated (vehicle alone control). Then, cells were trypsinized and plated on low-attachment plates for 10 hours to induce anoikis and enrich for cancer stem cells. Single cells were then analyzed by FACS to quantitate the CD44(+)CD24-/low population, which represents the cancer stem cells. A. Note that, as expected, the CD44(+)CD24-/low population is greatly enriched after 10 hours in low-attachment conditions (vehicle alone control). B. Interestingly, GO does not reduce the total number of anoikis-resistant cells (data not shown), but rather induces the expression of CD24, thereby significantly reducing the CD44(+)CD24-/low population. This suggests that GO inhibits mammosphere formation by promoting the differentiation of breast cancer stem cells. An * indicates $p < 0.05$ (Student's t-test).

(vehicle alone control) (Figure 8A).

Interestingly, GO does not reduce the total number of anoikis-resistant cells (data not shown), but rather induces the expression of CD24, thereby significantly reducing the CD44(+)CD24-/low population (Figure 8B). This suggests that GO inhibits mammosphere formation by promoting the differentiation of breast cancer stem cells, supporting our results from the analysis of multiple signal transduction pathways

DISCUSSION

Here, we show that treatment with GO is sufficient to inhibit tumor-sphere formation in six independent cancer cell lines, across multiple tumor types (breast, ovarian, prostate, lung, and pancreatic cancer, as well glioblastoma (brain cancer)). These results suggest that GO specifically targets a global phenotypic property of CSCs that is highly conserved in multiple tumor types. Moreover, using MCF7 cells expressing a panel of luciferase reporters, we observed that GO treatment was indeed sufficient to inhibit a number of different signal transduction pathways, including WNT, Notch, STAT1/3 and NRF-2, but did not effect TGB-beta/SMAD signaling. Finally, using a panel of specific well-established breast CSC markers (namely CD44 and CD24), we show that GO appears to reduce the number of CSCs by inducing their differentiation, as they now begin to express CD24.

Thus, GO may reduce the number of bonafide CSCs that are capable of forming tumor-spheres, by inducing their differentiation and inhibiting their proliferation. However, additional mechanistic studies are clearly warranted.

Importantly, our preliminary results indicate that GO treatment does not significantly affect oxidative mitochondrial metabolism (OXPHOS) in this context (data not shown), suggesting that GO does not target mitochondria. This is in contrast to our previous studies where a number of mitochondrially-targeted FDA-approved antibiotics effectively eradicated CSCs [24]. Thus, GO and mitochondrially-targeted antibiotics appear to work differently, via separate and distinct molecular mechanism(s).

Also, since b-GO flakes are 5-to-20 μ m in size, they must be exerting their effects at the cell surface, as they are too large to be internalized within cells and are actually larger than a single cell. This is consistent with our findings that GO-treatment dampens the activation of several stem cell associated signal transduction pathways, which are initiated at the cell surface. This could then mechanistically induce CSC differentiation, which we observed experimentally (summarized in Figure 9).

Previous studies have shown that GO (or its related derivatives) can inhibit “bulk” cancer cell migration or prevent tumor growth in xenograft models [25-28]. However, none of these studies connected GO treatment to the CSC phenotype or indicated that it could be used for “differentiation” therapy.

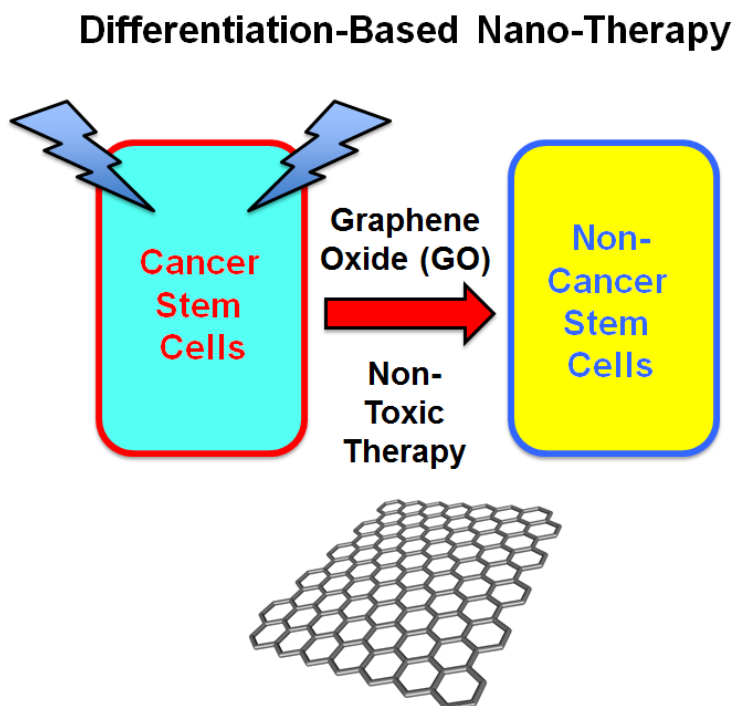


Figure 9: Graphene oxide (GO): Targeting cancer stem cells with differentiation-based nano-therapy. Our current mechanistic studies suggest that GO could directly be used as a therapeutic for targeting CSCs, because of its ability to induce differentiation. In this context, we might envision that GO could be used to clear residual CSCs, with the aim of preventing tumor recurrence and distant metastasis, thereby providing a practical means for achieving “differentiation-based nano-therapy”.

Interestingly, several studies have shown that GO is non-toxic for normal stem cells, and indeed GO promotes their differentiation. More specifically, it was demonstrated that culturing normal pluripotent stem cells on GO as a substrate induces their terminal differentiation towards multiple cell lineages, including neurons, chondrocytes and adipocytes [29-33]. These properties are currently being actively exploited for tissue engineering and regenerative medicine, by using GO as a scaffold for bone reconstruction and neural regeneration.

Our new mechanistic studies suggest that GO could directly be used as a therapeutic for targeting CSCs, possibly as a differentiation agent. In this context, we envision that GO could be delivered i.v. or p.o., as a new anti-cancer therapeutic, depending on the location of the tumor. Alternatively, GO flakes could also be used as a lavage solution during surgery, to clear the tumor excision site or the peritoneal cavity (as in ovarian or other peritoneal cancers) of residual CSCs, with the aim of preventing tumor recurrence and distant metastasis, via differentiation-based nano-therapy (Figure 9).

MATERIALS & METHODS

Materials

Cancer cell lines were purchased from the ATCC or other commercially available sources. Gibco-brand cell culture media (DMEM/F12) was purchased from Life Technologies.

Graphene oxide

Graphene oxide was prepared by using the Hummers method with modifications [34, 35]. The individual graphite oxide flakes contain carboxyl groups mainly at the edges, and epoxide, hydroxide and ketone groups mainly on the basal plane. The C to O ratio is usually slightly lower or slightly higher than 1 as determined by X-ray photoemission spectroscopy. The graphene oxide flakes of different sizes were separated by centrifuging graphene oxide suspensions at various rpm and collecting different phases of the suspension. The AFM characterization of graphene oxide flakes was performed on a Bruker Dimension FastScan AFM system by using tapping mode. The substrates were prepared by spin-casting the suspension on a Si/SiO₂ substrate to yield monolayer film, followed by AFM imaging. Concentrations were obtained from UV-Vis spectra, which were recorded in 10 mm path length quartz cells using a PerkinElmer Lambda – 1050 UV-Vis-NIR spectrometer. The dispersions were diluted to give the absorption intensity lower than 1.

Tumor-sphere culture

A single cell suspension was prepared using enzymatic (1x Trypsin-EDTA, Sigma Aldrich, #T3924), and manual disaggregation (25 gauge needle) to create a single cell suspension. Cells were plated at a density of 500 cells/cm² in mammosphere medium (DMEM-F12/B27/20ng/ml EGF/PenStrep) in non-adherent conditions, in culture dishes coated with (2-hydroxyethylmethacrylate) (poly-HEMA, Sigma, #P3932) [12]. Cells were grown for 5 days and maintained in a humidified incubator at 37°C at an atmospheric pressure in 5% (v/v) carbon dioxide/air. After 5 days for culture, spheres >50 μm were counted using an eye graticule, and the percentage of tumor-sphere formation was normalized to 100% for vehicle alone control (1 = 100 % TSF) [12]. All experiments were performed in triplicate, three times independently, such that each data point represents the average of 9 replicates.

Evaluation of CSC signalling pathways

The Cignal Lenti reporter assay (luc) system (Qiagen) was chosen for monitoring the activity of several signal transduction pathways in MCF7 cells. The responsive luciferase constructs encode the firefly luciferase reporter gene under the control of a minimal (m) CMV promoter and tandem repeats of response elements for each pathway. The following constructs were used: TCF/LEF(luc) for Wnt signal transduction (CLS-018L); STAT3(luc) for transcriptional activity of STAT3 (CLS-6028L); RBP-Jk(luc) for Notch-induced signaling (CLS-014L); ARE(luc) for Nrf2- and Nrf1-mediated antioxidant response (CLS-2020L); GAS(luc) for Interferon gamma-induced Stat1-signal transduction (CLS-009L); SMAD(luc) for TGFβ-induced signal transduction (CLS-017L). Briefly, 1 x 10⁵ MCF7-GFP cells were seeded in 12-well plates. Once cells were attached, the viral particles were diluted 1:10 in complete culture media containing polybrene (sc-134220, Santa Cruz), and added to the cells. Puromycin treatment (P9620, Sigma) was started 48 hours later in order to select stably infected cells.

Luciferase assays

The Luciferase Assay System (E1501, Promega Kit) was used on all luciferase reporter MCF7 cells treated with GO. Briefly, 6 × 10³ MCF7-GFP cells were seeded in black-walled 96-well plates and then were treated with GO (50 μg/ml). As controls, vehicle-treated cells were run in parallel. Four replicates were used for each condition. After 48 hours of treatment, luciferase assays were performed according to the manufacturer's instructions. Light signal was acquired for 2 minutes in photons/second in the Xenogen VivoVision IVIS Lumina (Caliper Life

Sciences), and the results were analysed using Living Image 3.2 software (Caliper Life Sciences). Luminescence was normalized using SRB (to determine total cellular protein), as a measure of MCF7 cell viability.

Anoikis and CSC differentiation analysis

Following GO treatment, the CSC population was enriched by seeding on low-attachment plates. Under these conditions, the non-CSCs undergo anoikis (a form of apoptosis induced by lack of proper attachment) and CSCs are believed to survive. The expression of differentiation markers by the surviving “CSC fraction” was analyzed by FACS analysis. Briefly, 1×10^4 MCF7 cells were treated with GO (50 μ g/ml) for 48h in 6-well plates, grown as a monolayer. Then, the monolayer cells were trypsinized and seeded in low-attachment plates in mammosphere media. After 10h under low-attachment conditions, MCF7 cells were spun down and incubated with CD24 (IOtest CD24-PE, Beckman Coulter) and CD44 (APC mouse Anti-Human CD44, BD Pharmingen cat.559942) antibodies for 15 minutes on ice. Cells were rinsed twice and incubated with LIVE/DEAD dye (Fixable Dead Violet reactive dye; Invitrogen) for 10 minutes. Samples were then analyzed by FACS (Fortessa, BD Bioscience). Only the live population, as identified by the LIVE/DEAD dye staining, was analyzed for CD24/CD44 expression. Data were analysed using FlowJo software. Virtually identical results were also obtained using 7-AAD (7-Aminoactinomycin D; Life Technologies) to distinguish between the live and dead populations of cells (cell viability), during anoikis.

ACKNOWLEDGEMENTS

We thank the University of Manchester for providing start-up funds that contributed to the success of this study (to Federica Sotgia and Michael P. Lisanti). Aravind Vijayaraghavan, Maria Iliut and Andrea F. Verre were supported by Engineering and Physical Sciences Research Council (EPSRC) grants EP/G03737X/1 and EP/G035954/1.

REFERENCES

1. Sinha N, Mukhopadhyay S, Das DN, Panda PK and Bhutia SK. Relevance of cancer initiating/stem cells in carcinogenesis and therapy resistance in oral cancer. *Oral oncology*. 2013; 49(9):854-862.
2. Xin H, Kong Y, Jiang X, Wang K, Qin X, Miao ZH, Zhu Y and Tan W. Multi-drug-resistant cells enriched from chronic myeloid leukemia cells by Doxorubicin possess tumor-initiating-cell properties. *Journal of pharmacological sciences*. 2013; 122(4):299-304.
3. Easwaran H, Tsai HC and Baylin SB. Cancer epigenetics: tumor heterogeneity, plasticity of stem-like states, and drug

- resistance. *Molecular cell*. 2014; 54(5):716-727.
4. Dawood S, Austin L and Cristofanilli M. Cancer Stem Cells: Implications for Cancer Therapy. *Oncology*. 2014; 28(12).
5. Colak S and Medema JP. Cancer stem cells--important players in tumor therapy resistance. *The FEBS journal*. 2014; 281(21):4779-4791.
6. Filipova A, Seifrtova M, Mokry J, Dvorak J, Rezacova M, Filip S and Diaz-Garcia D. Breast cancer and cancer stem cells: a mini-review. *Tumori*. 2014; 100(4):363-369.
7. Scopelliti A, Cammareri P, Catalano V, Saladino V, Todaro M and Stassi G. Therapeutic implications of Cancer Initiating Cells. *Expert opinion on biological therapy*. 2009; 9(8):1005-1016.
8. Dean M. ABC transporters, drug resistance, and cancer stem cells. *Journal of mammary gland biology and neoplasia*. 2009; 14(1):3-9.
9. Reya T, Morrison SJ, Clarke MF and Weissman IL. Stem cells, cancer, and cancer stem cells. *Nature*. 2001; 414(6859):105-111.
10. Karsten U and Goletz S. What makes cancer stem cell markers different? *SpringerPlus*. 2013; 2(1):301.
11. Magee JA, Piskounova E and Morrison SJ. Cancer stem cells: impact, heterogeneity, and uncertainty. *Cancer cell*. 2012; 21(3):283-296.
12. Shaw FL, Harrison H, Spence K, Ablett MP, Simoes BM, Farnie G and Clarke RB. A detailed mammosphere assay protocol for the quantification of breast stem cell activity. *Journal of mammary gland biology and neoplasia*. 2012; 17(2):111-117.
13. Fillmore CM and Kuperwasser C. Human breast cancer cell lines contain stem-like cells that self-renew, give rise to phenotypically diverse progeny and survive chemotherapy. *Breast cancer research : BCR*. 2008; 10(2):R25.
14. Cojoc M, Mabert K, Muders MH and Dubrovska A. A role for cancer stem cells in therapy resistance: Cellular and molecular mechanisms. *Seminars in cancer biology*. 2014.
15. Skvortsov S, Debbage P, Lukas P and Skvortsova I. Crosstalk between DNA repair and cancer stem cell (CSC) associated intracellular pathways. *Seminars in cancer biology*. 2014.
16. Liu Z, Robinson JT, Sun X and Dai H. PEGylated nanographene oxide for delivery of water-insoluble cancer drugs. *Journal of the American Chemical Society*. 2008; 130(33):10876-10877.
17. Hernandez Y, Lotya M, Rickard D, Bergin SD and Coleman JN. Measurement of Multicomponent Solubility Parameters for Graphene Facilitates Solvent Discovery. *Langmuir*. 2010; 26(5):3208-3213.
18. Dreyer DR, Park S, Bielawski CW and Ruoff RS. The chemistry of graphene oxide. *Chem Soc Rev*. 2010; 39(1):228-240.
19. Liao KH, Lin YS, Macosko CW and Haynes CL. Cytotoxicity of graphene oxide and graphene in human

- erythrocytes and skin fibroblasts. *ACS applied materials & interfaces*. 2011; 3(7):2607-2615.
20. Ruiz ON, Fernando KA, Wang B, Brown NA, Luo PG, McNamara ND, Vangsness M, Sun YP and Bunker CE. Graphene oxide: a nonspecific enhancer of cellular growth. *ACS nano*. 2011; 5(10):8100-8107.
 21. Angeloni V, Tiberio P, Appierto V and Daidone MG. Implications of stemness-related signaling pathways in breast cancer response to therapy. *Seminars in cancer biology*. 2014.
 22. Li D, Masiero M, Banham AH and Harris AL. The notch ligand JAGGED1 as a target for anti-tumor therapy. *Frontiers in oncology*. 2014; 4:254.
 23. Yu H, Lee H, Herrmann A, Buettner R and Jove R. Revisiting STAT3 signalling in cancer: new and unexpected biological functions. *Nature reviews Cancer*. 2014; 14(11):736-746.
 24. Lamb R, Ozsvari B, Lisanti CL, Tanowitz HB, Howell A, Martinez-Outschoorn UE, Sotgia F and Lisanti MP. Antibiotics that target mitochondria effectively eradicate cancer stem cells, across multiple tumor types: Treating cancer like an infectious disease. *Oncotarget*. 2015.
 25. Zhou T, Zhang B, Wei P, Du Y, Zhou H, Yu M, Yan L, Zhang W, Nie G, Chen C, Tu Y and Wei T. Energy metabolism analysis reveals the mechanism of inhibition of breast cancer cell metastasis by PEG-modified graphene oxide nanosheets. *Biomaterials*. 2014; 35(37):9833-9843.
 26. Chen GY, Chen CL, Tuan HY, Yuan PX, Li KC, Yang HJ and Hu YC. Graphene oxide triggers toll-like receptors/autophagy responses *in vitro* and inhibits tumor growth *in vivo*. *Advanced healthcare materials*. 2014; 3(9):1486-1495.
 27. Zhou H, Zhang B, Zheng J, Yu M, Zhou T, Zhao K, Jia Y, Gao X, Chen C and Wei T. The inhibition of migration and invasion of cancer cells by graphene via the impairment of mitochondrial respiration. *Biomaterials*. 2014; 35(5):1597-1607.
 28. Chen GY, Meng CL, Lin KC, Tuan HY, Yang HJ, Chen CL, Li KC, Chiang CS and Hu YC. Graphene oxide as a chemosensitizer: diverted autophagic flux, enhanced nuclear import, elevated necrosis and improved antitumor effects. *Biomaterials*. 2015; 40:12-22.
 29. Bressan E, Ferroni L, Gardin C, Sbricoli L, Gobbato L, Ludovichetti F, Tocco I, Carraro A, Piattelli A and Zavan B. Graphene based scaffolds effects on stem cells commitment. *Journal of translational medicine*. 2014; 12(1):296.
 30. Ku SH and Park CB. Myoblast differentiation on graphene oxide. *Biomaterials*. 2013; 34(8):2017-2023.
 31. Lee WC, Lim CH, Shi H, Tang LA, Wang Y, Lim CT and Loh KP. Origin of enhanced stem cell growth and differentiation on graphene and graphene oxide. *ACS nano*. 2011; 5(9):7334-7341.
 32. Yang D, Li T, Xu M, Gao F, Yang J, Yang Z and Le W. Graphene oxide promotes the differentiation of mouse embryonic stem cells to dopamine neurons. *Nanomedicine*. 2014; 9(16):2445-2455.
 33. Yoon HH, Bhang SH, Kim T, Yu T, Hyeon T and Kim BS. Dual Roles of Graphene Oxide in Chondrogenic Differentiation of Adult Stem Cells: Cell-Adhesion Substrate and Growth Factor-Delivery Carrier. *Adv Funct Mater*. 2014; 24(41):6455-6464.
 34. Hummers WS and Offeman RE. Preparation of Graphitic Oxide. *Journal of the American Chemical Society*. 1958; 80(6):1339-1339.
 35. Marcano DC, Kosynkin DV, Berlin JM, Sinitskii A, Sun ZZ, Slesarev A, Alemany LB, Lu W and Tour JM. Improved Synthesis of Graphene Oxide. *ACS nano*. 2010; 4(8):4806-4814.



Enhanced cellular uptake by “pharmaceutically oriented devices” of new simplified analogs of Linezolid with antimicrobial activity



Ortensia Ilaria Parisi^{a,d,1}, Marco Fiorillo^{a,1}, Anna Caruso^{a,d,1}, Anna Rita Cappello^a, Carmela Saturnino^b, Francesco Puoci^{a,*}, Antonella Panno^a, Vincenza Dolce^a, Hussein El-Kashef^c, Maria Stefania Sinicropi^a

^a Department of Pharmacy, Health and Nutritional Sciences, University of Calabria, 87036 Rende (CS), Italy

^b Department of Pharmaceutical and Biomedical Sciences, University of Salerno, 84084 Fisciano (SA), Italy

^c Department of Chemistry, Faculty of Science, Assiut University, 71516, Assiut, Egypt

^d Department of Computer Engineering, Modeling, Electronics and Systems, University of Calabria, 87036 Rende (CS), Italy

ARTICLE INFO

Article history:

Received 4 October 2013

Received in revised form

19 November 2013

Accepted 23 November 2013

Available online 1 December 2013

Keywords:

Drug carriers

Enhanced cellular uptake

Oxazolidinones

Antimicrobial activity

Simplified analogs of Linezolid

ABSTRACT

The aim of the present study was to enhance cellular uptake of simplified analogs of Linezolid by their incorporation into suitable delivery devices in order to improve the antimicrobial activity of these novel synthesized oxazolidin-2-one derivatives.

The oxazolidin-2-one derivatives were synthesized by developing a rather simple one-pot reaction starting from oxiranylmethanol and several primary amines. Three delivery devices were prepared by following different synthetic approaches, such as single-step free radical grafting, precipitation polymerization and nano-emulsion. Finally, the antimicrobial activity of the novel synthesized compounds, without any vehicle and after their incorporation into the delivery devices, was evaluated against *Escherichia coli* and *Saccharomyces cerevisiae* by performing time-kill analyses.

The synthesized oxazolidinones exhibited modest antimicrobial activity against *E. coli* and *S. cerevisiae* (MIC 16 µg/mL). A good activity was, instead, highlighted after their incorporation into the prepared delivery devices (lecithin-based nano-emulsion, poly(N-vinyl-pyrrolidone)-methacrylic acid grafted copolymer and spherical polymeric nanoparticles) (MIC ≤ 4 µg/mL). The incorporation into suitable vehicles, indeed, reduced by 4 times the normal MICs of the newly synthesized oxazolidin-2-ones and represents an effective strategy to overcome cellular penetration constraints.

© 2013 Elsevier B.V. All rights reserved.

1. Introduction

The oxazolidinones, a new class of synthetic clinically important antimicrobial agents, are active against the sensitive and resistant Gram +ve organisms.

Initial studies designed to elucidate the oxazolidinones mechanism of action evidenced that these drugs inhibit the formation of the initiation complex in bacterial translation systems by preventing the formation of the N-formylmethionyl-tRNA ribosome-mRNA ternary complex (Swaney et al., 1998). The identification of the drug-binding site at the ribosome, as well as the mechanism of action of these antimicrobial agents, is not fully understood. However, recent works have highlighted the interaction of

oxazolidinones (e.g. Linezolid, Fig. 1.) with the 50S A-site pocket at the peptidyltransferase center (PTC) of the ribosome, which overlaps the aminoacyl moiety of an A-site bound tRNA, inhibiting the protein synthesis process in whole cells of Gram +ve bacteria (Wilson et al., 2008). On the other hand, the inhibition of protein synthesis of Gram –ve bacteria, such as *Escherichia coli* (*E. coli*), has been observed only at higher doses (Muller and Schimz, 1999).

Keeping in mind the aforementioned interesting antimicrobial activities of oxazolidinones and that the infections caused by Gram –ve bacteria are emerging nowadays (Michalska et al., 2013), the preparation of some new oxazolidin-2-ones potentially active against this kind of microorganisms and investigate their formulation and cellular uptake could be of relevant interest.

Since the main target sites for antibacterial agents are located within the cell, at the cytoplasmic membrane level or within the cytoplasm, the wall structure of Gram –ve bacteria offers a complex barrier system to these compounds (Denyer and Maillard, 2002). The phenomenon of cellular impermeability, indeed, is due to the presence of an outer envelope represented by a bilayer structure

* Corresponding author. Tel.: +39 0984 493151; fax: +39 0984 493298.

E-mail addresses: francescopuoci@gmail.com, francesco.puoci@unical.it (F. Puoci).

¹ These authors equally contributed to the manuscript.

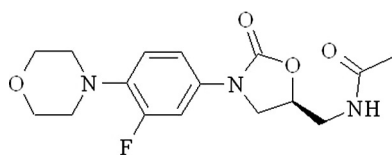


Fig. 1. Chemical structure of Linezolid.

consisting of lipopolysaccharides and phospholipids. Thus, antimicrobial agents have to cross this outer membrane in order to get their principal target site.

Limited cellular penetration could reduce the effectiveness of many antimicrobial treatments and, in view of this fact, the present study was focused on the exploration of antimicrobial activity of the synthesized therapeutic agents alone and after their incorporation into “pharmaceutically oriented devices”.

In order to modulate the cellular uptake of these compounds, three different strategies were adopted. The novel synthesized oxazolidin-2-ones were, indeed, incorporated into drug delivery carriers of different nature and structure, such as lecithin-based nano-emulsion, poly(*N*-vinyl-pyrrolidone)-methacrylic acid grafted copolymer (PVP-MAA) and spherical nanoparticles (SNs).

The antimicrobial activity of the compounds, without any vehicle and after their incorporation into the delivery devices, was evaluated against *E. coli* and *Saccharomyces cerevisiae* (*S. cerevisiae*) by performing time-kill analyses according to the method of the Clinical and Laboratory Standards Institute (Clinical and Laboratory Standards Institute, 1999).

The choice of these kinds of vectors, characterized by such a different construction, allows to hypothesize several possible mechanisms involved in the enhancement of cellular uptake and, consequently, in the improvement of the antimicrobial activity.

2. Materials and methods

2.1. Materials and instrumentation

Commercial reagents were purchased from Aldrich, Acros Organics and Alfa Aesar and were used without additional purification.

Melting points were determined on a Gallenkamp melting point apparatus.

The IR spectra were recorded on a Fourier Transform Infrared Spectrometer FT/IR-4200 for KBr pellets.

GC/MS analyses were performed using a 17AA-V3 230 VLV spectrometer or a 6890N Network GC System (Agilent Technologies Inc., Palo Alto, CA, USA) equipped with an HP-5MS (30 m × 0.25 mm, PhMesiloxane 5%) capillary column. The mass detector was operated in the ionization chemical mode (CI-CH₄).

ESI-MS was performed using a spectrometer LC-MS Waters alliance 2695 (ESI+).

¹H NMR (300 MHz) and ¹³C NMR (100 MHz) spectra were recorded on a Bruker 300 spectrometer. Chemical shifts are expressed in parts per million downfield from tetramethylsilane as an internal standard.

Thin layer chromatography (TLC) was performed on silica gel 60F-264 (Merck).

The scanning electron microscopy (SEM) photographs were obtained with a Jeol JSMT 300 A; the surface of the samples was made conductive by the deposition of a gold layer on the samples in a vacuum chamber. Approximate range in particle size was determined employing an image processing and analysis system, a Leica DMRB equipped with a LEICA Wild 3D stereomicroscope.

Dynamic light scattering (DLS) analysis was performed using a 90 Plus Particle Size Analyzer (Brookhaven Instruments

Corporation, New York USA) at 25.0 ± 0.1 °C by measuring the auto-correlation function at 90°. The laser was operating at 658 nm.

2.2. Synthesis of simplified analogs of Linezolid

2.2.1. Preparation of (*RS*)-3-alkyl (or aryl)-5-hydroxymethyloxazolidin-2-ones (**5a,b**) (general method)

To a stirred solution of the appropriate primary amines **3a,b** (8.62 mmol) in MeOH (3 mL), (*RS*)-oxiranylmethanol **2** (7.84 mmol) was slowly added. The reaction mixture was stirred further at room temperature for 12 h to give intermediates **4a,b**. Diethylcarbonate (9.09 mmol) and anhydrous MeONa (0.74 mmol) were then added and the resulting mixture was heated under reflux for 12 h. After cooling to room temperature, the reaction mixture was evaporated under reduced pressure to afford an oil residue. This oil was taken up with EtOAc and the organic layer washed with water. Then it was separated, dried (Na₂SO₄) and concentrated under reduced pressure to give a solid or oil product, which was purified using silica gel column chromatography.

2.2.2. (*RS*)-3-Allyl-5-hydroxymethyl-oxazolidin-2-one (**5a**)

White solid, using CHCl₃:MeOH (9:1) as eluent, yield 45%; mp 82 °C. IR spectrum, ν , cm⁻¹: 3413, 2924, 1733, 1645, 1263, 765. ¹H NMR spectrum (CDCl₃), δ , ppm: 3.18 (1H, br.s, OH); 3.33–3.61 (4H, m, CH₂NCH₂); 3.77–3.86 (2H, m, CH₂OH); 4.51–4.59 (1H, m, CHCH₂OH); 5.14–5.26 (2H, m, CH₂CH=CH₂); 5.63–5.78 (1H, m, CH₂CH=CH₂). ¹³C NMR spectrum (CDCl₃), δ , ppm: 154.69; 133.85; 119.54; 76.03; 67.38; 59.61; 42.60. Mass spectrum (EI, 70 eV), m/z (*I*_{rel}, %): 157 [M]⁺ (100), 126 (74), 98 (89), 82 (98), 68 (88), 56 (44). Found, %: C 53.46; H 7.01; N 8.88. C₇H₁₁NO₃. Calculated, %: C 53.49; H 7.05; N 8.91.

2.2.3. (*RS*)-5-Hydroxymethyl-3-phenethyl-oxazolidin-2-one (**5b**)

White solid, using EtOAc:hexane (4:1) as eluent, yield 50%; mp 93 °C. IR spectrum, ν , cm⁻¹: 3444, 2927, 1735, 1603, 752. ¹H NMR spectrum (CDCl₃), δ , ppm (*J*, Hz): 2.78–2.86 (2H, t, CH₂Ph); 3.22–3.53 (6H, m, CH₂NCH₂, CHOH, OH); 3.69–3.77 (1H, dd, *J* = 3.30; *J* = 12.60, CHOH); 4.41–4.50 (1H, m, CHCH₂OH); 7.11–7.26 (5H, m, Ar). ¹³C NMR spectrum (CDCl₃), δ , ppm: 158.16, 138.25, 128.66, 128.59, 126.58, 73.72, 62.64, 46.09, 45.35, 33.72. Mass spectrum (EI, 70 eV), m/z (*I*_{rel}, %): 221 [M]⁺ (36), 130 (100), 104 (55), 77 (19), 56 (18). Found, %: C 65.18; H 6.79; N 6.29. C₁₂H₁₅NO₃. Calculated, %: C 65.14; H 6.83; N 6.33.

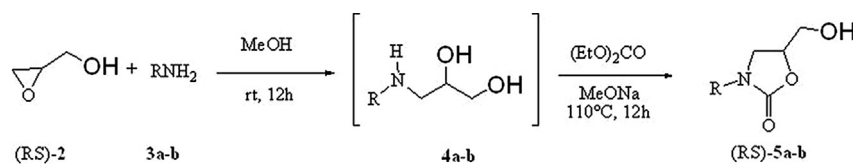
2.3. Synthesis of “pharmaceutically oriented delivery devices”

2.3.1. Poly(*N*-vinyl-pyrrolidone)-methacrylic acid (PVP-MAA) grafted copolymer

Single-step grafting of methacrylic acid (MAA) onto poly(*N*-vinyl-pyrrolidone) (PVP, average M.W. 360,000, Sigma-Aldrich) was carried out by employing hydrogen peroxide/ascorbic acid as biocompatible and water soluble redox pair (Parisi et al., 2013).

In a 25 mL glass tube, 4.0 g of PVP were dissolved in 15 mL of distilled water, then 1 mL of distilled MAA and 0.5 mL of H₂O₂ 1.0 M containing 0.025 g of ascorbic acid were added. The mixture was maintained under stirring at 25 °C for 3 h under atmospheric air. The resulting PVP-MAA grafted copolymer was purified by successive washing steps with distilled water, recovered by filtration and, finally, dried overnight in a vacuum oven set at 40 °C.

An amount of the synthesized PVP-MAA copolymer (128 mg) was immersed in 7.7 mL of a phosphate buffer solution (pH 7.4). Then, 0.3 mL of a solution in DMSO containing 32 mg of the antimicrobial agent were added and the obtained mixture was sonicated for 30 min.



Scheme 1. Synthesis of oxazolidinones **5a** and **5b**.

2.3.2. Spherical nanoparticles (SNs)

Spherical polymeric nanoparticles were prepared by precipitation polymerization employing methacrylic acid and ethylene glycol dimethacrylate (EGDMA) as functional monomer and cross-linking agent, respectively (Puoci et al., 2004).

In a 100 mL round bottom flask, distilled MAA (8 mmol) were dissolved in a mixture of acetonitrile (20 mL) and methanol (20 mL), then EGDMA (10 mmol) and 2,2-azoisobutyronitrile (AIBN, 50 mg) were added. The polymerization mixture was degassed in a sonicating water bath, purged with nitrogen for 10 min cooling with an ice bath. The flask was then gently agitated (40 rpm) in an oil bath. The temperature was increased from room temperature to 60 °C within 2 h, and then kept at 60 °C for 24 h. At the end of the reaction, the resulting nanoparticles were filtered, washed with 100 mL of ethanol, 100 mL of acetone and 100 mL of diethyl ether and, successively, dried overnight under vacuum at 40 °C.

An amount of the resulting SNs (128 mg) was immersed in 3 mL of a solution in ethanol containing 32 mg of the antimicrobial agent and soaked for 3 days at room temperature. Then the solvent was removed under reduced pressure.

2.3.3. Nano-emulsion based on soybean lecithin

Nano-emulsion containing the antimicrobial agent was prepared by the following procedure.

The emulsifier and the emulsifier adjuvant, such as soybean lecithin (1.2%, w/w) and tween 80 (1.2%, w/w) respectively, were added to soybean oil as the oil phase (10%, w/w). Lecithin was stirred with heating to 80 °C until it was completely dissolved in the oil phase and the obtained mixture was cooled to room temperature. Then, 0.3 mL of a solution in DMSO containing the antimicrobial agent (0.24%, w/w) was added and mixed homogeneously. The mixture was added dropwise into a 2.25% glycerol solution preheated at 40 °C, and then homogenized for 10 min at 24,000 rpm using a homogenizer. After the completion of the emulsification, the pH was adjusted to neutrality with NaOH (Kim and Lee, 1999).

2.4. Biological analyses

2.4.1. Yeast and bacterial strains

Yeast strains Y10000, wild-type, was provided by the EUROFAN resource center EUROSCARF (Frankfurt, Germany). The cells were grown in rich medium containing 2% Bactopeptone and 1% yeast extract (YP), supplemented with fermentable 2% glucose carbon sources (Iacopetta et al., 2010). The final pH was adjusted to 4.8.

The *E. coli* strains ATCC 8739 was provided by REMEL. The cells were grown in LB medium containing 10 g/L Tryptone, 5 g/L yeast extract and 0.5 g/L NaCl (Iacopetta et al., 2010; Santoro et al., 2011). The final pH was adjusted to 7.4.

Minimum inhibitory concentrations (MICs) were determined by the agar dilution method as described by the Clinical and Laboratory Standards Institute (CLSI) (Clinical and Laboratory Standards Institute, 2012).

2.4.2. Time-kill studies

Time-kill analyses were performed according to the method of the CLSI (Clinical and Laboratory Standards Institute, 1999).

Test organisms incubated in appropriate medium over night at 30 °C (yeast) or 35 °C (bacteria) were diluted with fresh medium to ca. 10⁴ CFU/mL and the diluted cultures were pre-incubated for 2 h. Each drug, solubilized in dimethyl sulfoxide (DMSO) was added to the cultures at concentrations of 1 × MIC. Samples (0.1 mL) of the cultures were removed at 0, 2, 4, 6 and 24 h of incubation and serial 10-fold dilutions were prepared in saline. The number of viable cells was determined as described in the literature (Jung et al., 2012).

3. Results and discussion

3.1. Chemistry

Different methods for the synthesis of oxazolidin-2-one compounds were reported in the literature (Lamanna et al., 2004; Osa et al., 2005; Robles-Machín et al., 2006; Ella-Menyea and Wang, 2007; Adibpour et al., 2010; Lancelot et al., 1993, 1996; Saturnino et al., 2000, 2004).

In the present study, we report a rather simple one-pot synthesis of two compounds (**5a,b**) starting from racemic (RS)-oxiranylmethanol (**2**) and different primary amines (**3a,b**) (Scheme 1). Thus, compound **2** was allowed to react with different primary amines (**3a,b**) in methanol, to give the corresponding 3-substituted-amino-1,2-propanediols intermediates (**4a,b**). The latter were then treated with equimolar amounts of diethylcarbonate in the presence of catalytic amounts of sodium methoxide to give N-substituted-5-hydroxymethyl-oxazolidin-2-ones (**5a,b**) in 45–87% yield (Table 1).

3.2. Synthesis of “pharmaceutically oriented delivery devices”

3.2.1. PVP-MAA grafted copolymer

Methacrylic acid was grafted onto a preformed polymeric backbone, such as poly(N-vinyl-pyrrolidone), by a free radical procedure involving a one-pot reaction at room temperature. Hydrogen peroxide/ascorbic acid redox pair was employed as water-soluble and biocompatible initiator system allowing to perform the grafting process in aqueous media. In view of this fact, the use of organic solvents and the generation of any kind of toxic reaction byproducts are avoided.

The mechanism of redox pair reaction (Fig. 2.) consists of the oxidation of ascorbic acid (AA) by hydrogen peroxide with the formation of hydroxyl and ascorbate radicals (Curcio et al., 2009). Hydroxyl radical represents the most reactive radical among the reactive oxygen species and its reaction with PVP chain generates macroradicals centered in three possible positions according to the lability of the hydrogen atoms present in the polymeric

Table 1
Synthesized oxazolidinones.

Cpd	RNH ₂	Rdt %
5a	3a	45
5b	3b	50

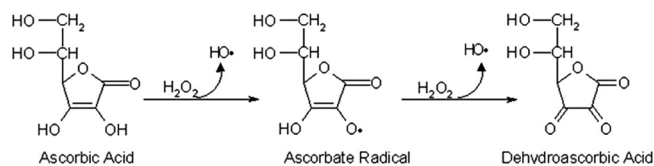


Fig. 2. Mechanism of AA/H₂O₂ redox pair reaction.

structure. Literature (Barros et al., 2006), indeed, reported that C–H bonds of PVP α -positioned to a heteroatom or a carbonyl are lower in energy, mainly due to the stabilization of the radical product. Generated macroradicals react with MAA monomer which is graft-copolymerized onto the PVP preformed polymeric chain.

Poly(*N*-vinyl-pyrrolidone) is a polymeric material characterized by chemical stability, low toxicity, biocompatibility with living tissues, general bioinertness and water solubility due to the presence of the polar lactam group which increases its hydrophilicity (Liu et al., 2013). On the other hand, the non-polar methylene groups make this material lipophilic. All these features make PVP widely employed as biomaterial and excipient in various fields, such as pharmaceutical, cosmetic, biomedical and food.

The grafting of hydrophilic molecules onto the surface of a material could improve its biocompatibility regulating protein adsorption and cell adhesion. In this study, the conjugation of PVP with methacrylic acid aimed to increase the hydrophilicity of the copolymer, providing pH-sensitivity to the system, and the choice of MAA was dictated to the broad applications of methacrylate polymers in biotechnology and biomedicine (Pérez et al., 2006).

PVP-MAA and the respective control polymer (PVP) were characterized by Fourier Transform IR spectrophotometry. By comparing the two IR spectra (Fig. 3), the PVP-MAA spectrum (trace B) showed the appearance of a new signal at 1717 cm⁻¹ ascribable to the C=O stretching vibration of the carboxylic groups of methacrylic acid.

3.2.2. Spherical nanoparticles (SNs)

In the last years, polymeric nanoparticles have received considerable attention due to their potential applications as drug delivery systems.

Precipitation polymerization represents a simple and efficient method to obtain uniform polymeric particles in the absence of any stabilizer. The size and size distribution of particles are involved in size-dependent cellular uptake (Zhang et al., 2009) and this polymerization technique allows to have a better control on size and shape.

The polymerization system consists of only monomer, cross-linker, initiator and solvent as components (Li and Stover, 1993) and, in the first stage of the process, monomers form oligomer radicals. Then, the formed oligomers crosslink and the obtained crosslinked nuclei aggregate into larger particles leading to the formation of the final polymer beads.

In a precipitation polymerization process, the adopted concentrations of monomer, cross-linking agent and initiator affect the size of synthesized particles. The diameter of polymeric spheres, indeed, increases with increasing monomer or initiator concentration (Puoci et al., 2004); on the other hand, the particles size decreases as the cross-linker percentage increases (Shim et al., 2004).

In the present study, spherical nanoparticles (SNs) were prepared by precipitation polymerization employing MAA, EGDMA and AIBN as functional monomer, cross-linking agent and initiator, respectively. For this purpose, in the prepolymerization feed the employed MAA/EGDMA molar ratio was equal to 8:10 (Cirillo et al., 2009). This ratio represents, indeed, the optimal value to obtain nanospheres with the desired characteristics such as spherical shape and nanometer size.

Spherical geometry and the practical monodispersity of the prepared nanospheres were confirmed by scanning electron micrographs (Fig. 4).

3.2.3. Nano-emulsion based on soybean lecithin

An emulsion is a mixture of two immiscible liquids, such as water and oil, with one dispersed in the other (Leal-Calderon et al., 2007). The preparation of emulsions requires the use of surfactants in the aim to decrease the interfacial tension and maintain the stability of the formulation.

Nano-emulsions represent promising drug delivery vehicles due to their small size, biocompatibility, relative stability and ability to protect drugs from hydrolysis and enzymatic degradation under physiological conditions (Jafari et al., 2007).

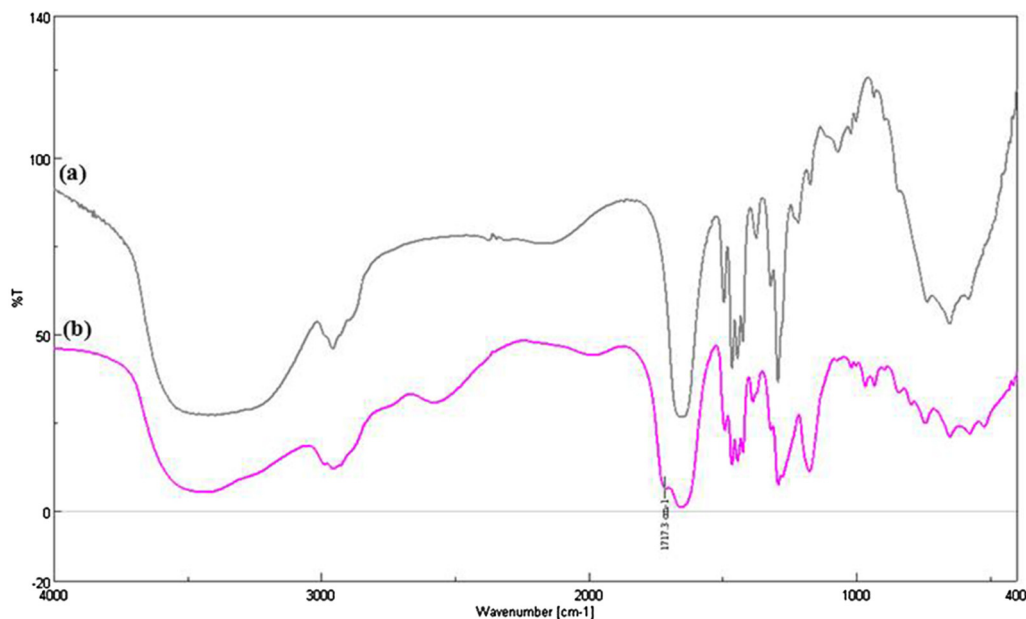


Fig. 3. FT-IR spectra of PVP (a) and PVP-MAA (b).

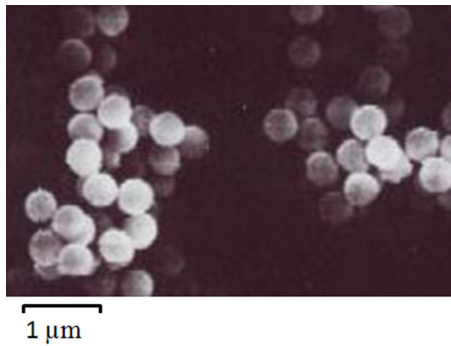


Fig. 4. Scanning electron micrograph of SNs.

In this report, nano-emulsions containing the antimicrobial agents were prepared using soybean lecithin and tween 80 as emulsifier and emulsifier adjuvant, respectively. The droplet size distribution was measured by dynamic light scattering (DLS) and it was found to be 259.6 nm (effective diameter) with a PDI of 0.268 (Fig. 5).

3.3. Time-kill curves

The oxazolidinones represent a novel chemical class of synthetic antimicrobial agents active against a large spectrum of sensitive and resistant Gram +ve organisms due to a unique mechanism of protein synthesis inhibition involving the binding at the P site of the ribosomal 50S subunit (Bozdogan and Appelbaum, 2004). However, protein synthesis of Gram –ve bacteria was affected only at higher doses by these molecules.

In this study, new oxazolidin-2-ones potentially active against Gram –ve bacteria were synthesized by following a simple one-step reaction and their formulation and cellular uptake were investigated.

Two different kinds of microorganisms, such as *E. coli* and *S. cerevisiae*, were chosen to evaluate the antimicrobial activity by performing time-kill analyses. The first one was chosen because it is a common type of bacteria and represents one of the most

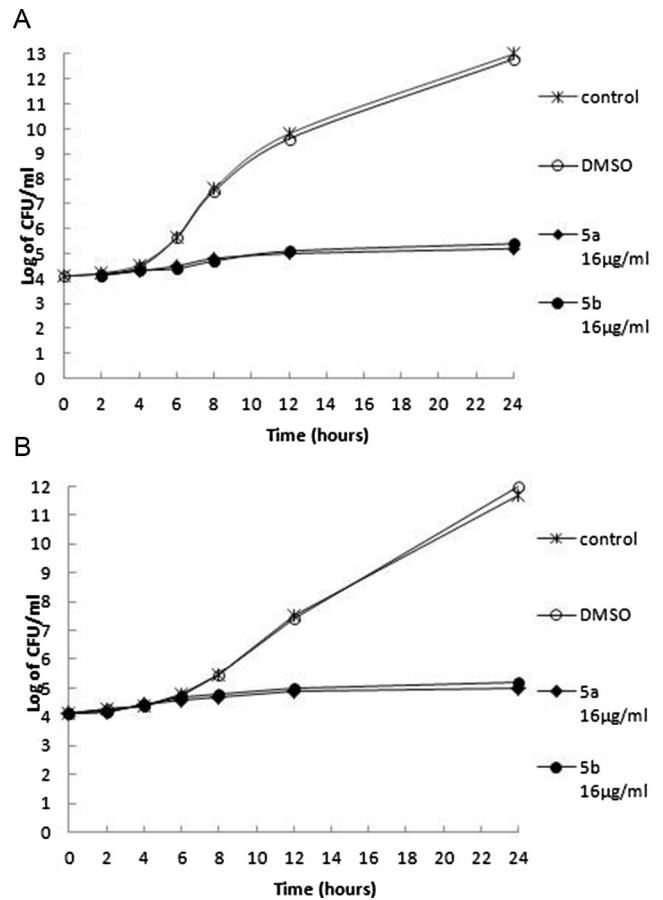


Fig. 6. Time-kill curve profiles of 5a and 5b against *E. coli* (panel A) and *S. cerevisiae* (panel B).

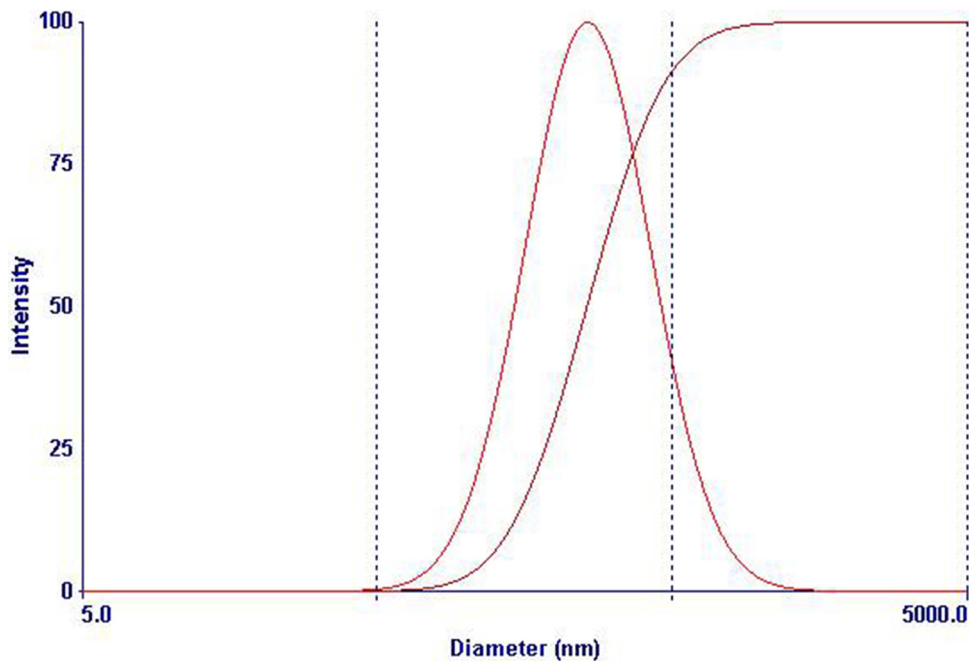


Fig. 5. Droplet size distributions of lecithin-based nano-emulsion determined by dynamic light scattering.

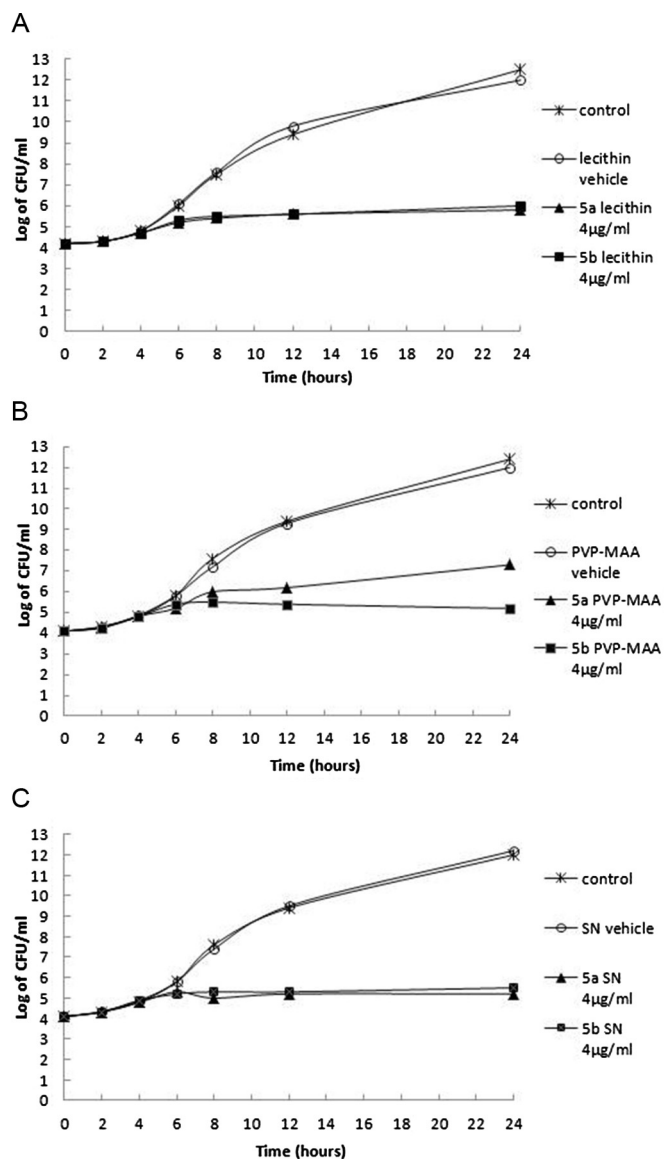


Fig. 7. Time-kill curve profiles of **5a** and **5b** against *E. coli*, after incorporation into lecithin-based nano-emulsion (panel A), PVP-MAA (panel B) and SNs (panel C).

frequent causes of many widespread bacterial infections; *S. cerevisiae* was selected due to the construction of its cell wall which is typical of other relevant and dangerous Saccharomycetes such as *Saccharomyces albicans*.

The synthesized oxazolidin-2-ones (**5a** and **5b**), without any vehicle, showed modest antimicrobial activity against *E. coli* (Fig. 6, panel A) and *S. cerevisiae* (Fig. 6, panel B) (MIC 16 µg/mL) in comparison with the results obtained using the microorganisms alone.

The problem could be probably due to the cellular impermeability of these microorganisms to the antimicrobial agents. Poor cellular uptake, indeed, could be responsible for the disappointing activity against bacteria that the synthesized compounds exhibited.

In order to overcome this drawback, **5a** and **5b** molecules were incorporated into three different carriers prepared according to reported literature: nano-emulsion based on soybean lecithin (Kim and Lee, 1999), PVP-MAA grafted copolymer (Parisi et al., 2013) and spherical polymeric nanoparticles (Puoci et al., 2004).

We supposed that the chosen vehicles have the ability to improve the cellular uptake of the synthesized oxazolidin-2-ones derivatives by several possible mechanisms.

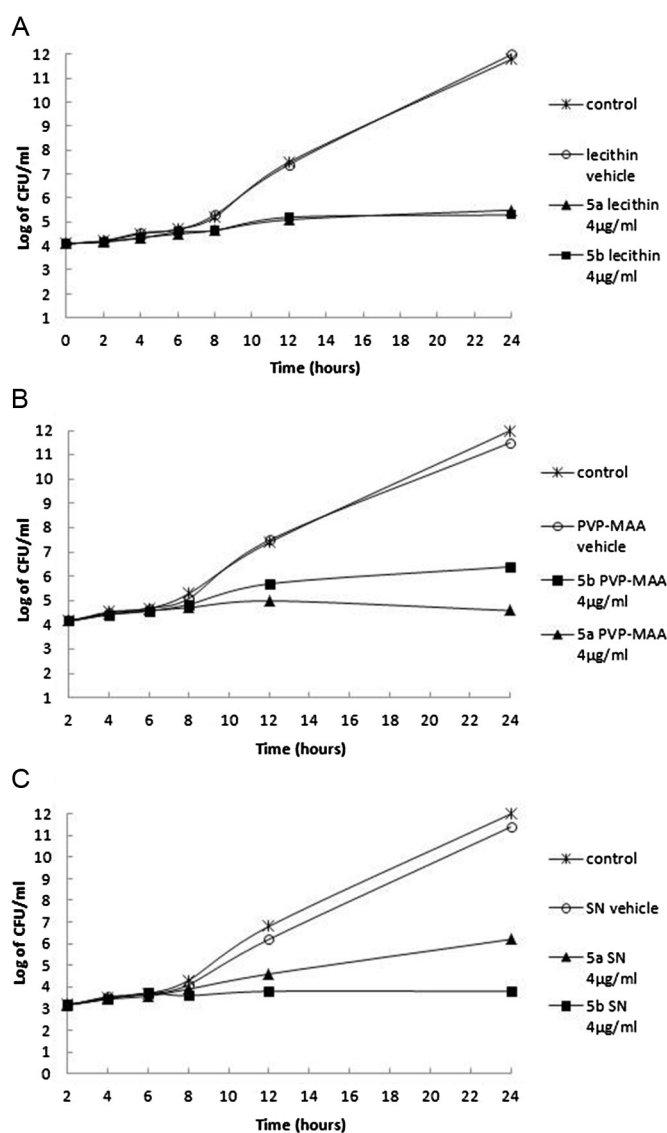


Fig. 8. Time-kill curve profiles of **5a** and **5b** against *S. cerevisiae*, after incorporation into lecithin-based nano-emulsion (panel A), PVP-MAA (panel B) and SNs (panel C).

PVP-MAA copolymer is characterized by a poly(N-vinylpyrrolidone) backbone with polymethacrylic acid grafted side chains attached to it. PVP is an interesting material from a biological point of view due to the presence of the lactam group in the pyrrolidone moiety which makes its structural feature similar to those of proteins (Liu et al., 2013). The performance of the prepared grafted copolymer as drug device depends on its lipophilicity/hydrophilicity ratio. Since membrane proteins also have hydrophilic and hydrophobic domains, these structural features may influence protein interactions with the copolymer.

Nano-emulsions containing the antimicrobial agents were, instead, prepared using soybean lecithin and tween 80 as emulsifier and emulsifier adjuvant, respectively. The results obtained employing this formulation could be attributed to its cellular permeability due to the presence of lecithin which is a complex mixture containing phospholipids, the main components of the biological membranes. Furthermore, the use of delivery systems at the nanoscale may potentially increase the passive cellular absorption mechanisms allowing the antimicrobial agent to act from the inner side on the cytoplasmic membrane.

Finally, spherical nanoparticles (SNs) were prepared by precipitation polymerization employing MAA and EGDMA as

functional monomer and cross-linking agent, respectively. Polymeric nanoparticles, indeed, are attracting significant research interest due to their unique properties and potential applications in different fields such as drug delivery and therapy. Their application in biomedical field involves the interaction with cells, which is influenced by the small size and the possibility to overcome cellular barriers by different endocytic pathways including phagocytosis (the uptake of large particles) (Sahay et al., 2010). Based on these considerations, the enhanced antimicrobial effect of novel synthesized Linezolid analogs observed employing SNs as carrier could be ascribable to the endocytic uptake of particulate systems which provides improved access for drugs.

The time-kill curve profiles of compounds **5a** and **5b**, after their incorporation into the carriers, confirmed our supposition showing significant activity against *E. coli* and *S. cerevisiae* (Fig. 7 and Fig. 8, respectively).

The obtained results, indeed, evidenced the efficiency of all the tested carriers in improving the antimicrobial activity and could be attributed to the different nature of the prepared delivery devices.

Significant differences were observed, between the log₁₀ CFU per milliliter counts at 24 h for all killing curves versus those for the growth controls and to those of vehicle alone (Fig. 7), with nanoemulsion (Fig. 7, panel A) and SNs formulations (Fig. 7, panel C). Although PVP-MAA vehicle, **5b** loaded, showed a similar behavior compared to other formulations, it proved to be less efficient for **5a** (Fig. 7, panel B). Therefore, the results of time-kill analyses showed that **5b** (with every vehicle) and **5a** (only with lecithin or SNs vehicles) has antibacterial activity against *E. coli* that begins to be evident after six hours from the addition of formulations and it remains for 24 h.

The time-kill effect of **5a** and **5b** against *S. cerevisiae* was similar to that against *E. coli*, only when lecithin was used as vehicle (Fig. 8, panel A). Conversely, PVP-MAA and SNs vehicles have been found to be less efficient for **5b** and **5a**, respectively (Fig. 8, panel B and C).

4. Conclusion

In the present study, we reported the synthesis of new oxazolidin-2-ones (**5a** and **5b**), as simplified analogs of Linezolid, and their incorporation into suitable “pharmaceutically oriented devices” in the aim to enhance their cellular uptake and improve the antimicrobial activity.

The synthesized derivatives showed modest antimicrobial activity against *E. coli* and *S. cerevisiae* (MIC 16 µg/mL). As hypothesized, a good activity was instead highlighted after their incorporation into the prepared delivery devices such as lecithin-based nano-emulsion, PVP-MAA grafted copolymer and SNs (MIC ≤ 4 µg/mL).

The obtained results clearly indicated that the incorporation into suitable drug carriers could be an effective and very promising strategy to enhance the cellular uptake of the synthesized therapeutic agents and, consequently, improve their antimicrobial effect. The presence of vehicles, indeed, reduced by 4 times the normal MIC values of the newly synthesized compounds improving their antimicrobial activity against two different kinds of microorganisms, Gram –ve bacteria and yeasts, at the same time.

Conflict of interest

The authors report no declarations of interest.

Acknowledgments

We wish to thank Italian Minister of University and Research for financial support of this work.

References

- Adibpour, N., Khalaj, A., Rajabalian, S., 2010. Synthesis and antibacterial activity of isothiazolyl oxazolidinones and analogous 3(2H)-isothiazolones. *Eur. J. Med. Chem.* 45, 19–24.
- Barros, J.A.G., Fechine, G.J.M., Alcantara, M.R., Catalani, L.H., 2006. Poly(N-vinyl-2-pyrrolidone) hydrogels produced by Fenton reaction. *Polymer* 47, 8414–8419.
- Bozdogan, B., Appelbaum, P.C., 2004. Oxazolidinones: activity, mode of action, and mechanism of resistance. *Int. J. Antimicrob. Agents* 23, 113–119.
- Cirillo, G., Iemma, F., Puoci, F., Parisi, O.I., Curcio, M., Spizzirri, U.G., Picci, N., 2009. Imprinted hydrophilic nanospheres as drug delivery systems for 5-fluorouracil sustained release. *J. Drug Target.* 17, 72–77.
- Clinical and Laboratory Standards Institute, 1999. Methods for determining bactericidal activity of antimicrobial agents: approved guideline. Document M26-A. CLSI, Wayne, PA.
- Clinical and Laboratory Standards Institute, 2012. Methods for dilution antimicrobial susceptibility test for bacteria that grow aerobically; approved standards. 9th ed. Document M07-A9. CLSI, Wayne, PA.
- Curcio, M., Puoci, F., Iemma, F., Parisi, O.I., Cirillo, G., Spizzirri, U.G., Picci, N., 2009. Covalent insertion of antioxidant molecules on chitosan by a free radical grafting procedure. *J. Agric. Food. Chem.* 57, 5933–5938.
- Denyer, S.P., Maillard, J.Y., 2002. Cellular impermeability and uptake of biocides and antibiotics in Gram –ve bacteria. *J. Appl. Microbiol.* 92, 355–455.
- Ella-Menyea, J.R., Wang, G., 2007. Synthesis of chiral 2-oxazolidinones, 2-oxazolines, and their analogs. *Tetrahedron* 63, 10034–10041.
- Iacopetta, D., Carrisi, C., De Filippis, G., Calcagnile, V.M., Cappello, A.R., Chimento, A., Curcio, R., Santoro, A., Vozza, A., Dolce, V., Palmieri, F., Capobianco, L., 2010. The biochemical properties of the mitochondrial thiamine pyrophosphate carrier from *Drosophila melanogaster*. *FEBS J.* 277, 1172–1181.
- Jafari, S.M., He, Y., Bhandari, B., 2007. Effectiveness of encapsulating biopolymers to produce sub-micron emulsions by high energy emulsification techniques. *Food Res. Int.* 40, 862–873.
- Jung, S.J., Yun, I.N., Park, H.S., Lee, H.H., Jeong, J.W., Kim, Y.Z., Cho, Y.L., Kwak, J.H., 2012. Antibacterial activity of LCB01-0062, a novel oxazolidinone. *Int J Antimicrob Agents* 40, 539–543.
- Kim, S.Y., Lee, Y.M.J., 1999. Lipid nanospheres containing vitamin A or vitamin E: evaluation of their stabilities and in vitro skin permeability. *Ind. Eng. Chem.* 5, 306–313.
- Lamanna, C., Sinicropi, M.S., Pietrangeli, P., Corbo, F., Franchini, Mondovi, C.B., Perrone, M.G., Scilimati, A., 2004. Synthesis and biological evaluation of 3-alkyloxazolidin-2-ones as reversible MAO inhibitors. *ARKIVOC* 5, 118–130.
- Lancelot, J.C., Letois, B., Saturnino, C., Perrine, D., Robba, M., 1993. Efficient synthesis of new β-lactams. *Synth. Commun.* 23, 1535–1542.
- Lancelot, J.C., Saturnino, C., El-Kashef, H., Perrine, D., Mahatsekake, M., Prunier, H., Robba, M., 1996. A facile synthesis of new β-lactams. *J. Heterocycl. Chem.* 33, 427–430.
- Leal-Calderon, F., Thivilliers, F., Schmitt, V., 2007. Structured emulsions. *Curr. Opin. Colloid Interface Sci.* 12, 206–212.
- Li, K., Stover, H.D.H.J., 1993. Synthesis of monodisperse poly(divinylbenzene) microspheres. *Polym. Sci., Polym. Chem. Ed.* 31, 3257–3263.
- Liu, X., Xu, Y., Wu, Z., Chen, H., 2013. Poly(N-vinylpyrrolidone)-modified surfaces for biomedical applications. *Macromol. Biosci.* 13, 147–154.
- Michalska, K., Karpiuk, I., Król, M., Tyski, S., 2013. Recent development of potent analogues of oxazolidinone antibacterial agents. *Bioorgan. Med. Chem.* 21, 577–591.
- Muller, M., Schimz, K.L., 1999. Oxazolidinones: a novel class of antibiotics. *Cell. Mol. Life Sci.* 56, 280–285.
- Osa, Y., Hikima, Y., Sato, Y., Takino, K., Ida, Y., Hirono, S., Nagase, H., 2005. Convenient synthesis of oxazolinones by the use of halomethylloxirane, primary amines and carbonate salt. *J. Org. Chem.* 70, 5737–5740.
- Parisi, O.I., Puoci, F., Iemma, F., Curcio, M., Cirillo, G., Spizzirri, U.G., Picci, N., 2013. Flavonoids preservation and release by methacrylic acid-grafted (N-vinylpyrrolidone). *Pharm. Dev. Technol.* 18, 1058–1065.
- Pérez, J.P., López-Cabarcos, E., López-Ruiz, B., 2006. The application of methacrylate-based polymers to enzyme biosensors. *Biomol. Eng.* 23, 233–245.
- Puoci, F., Iemma, F., Muzzalupo, R., Spizzirri, U.G., Trombone, S., Cassano, R., Picci, N., 2004. Spherical molecularly imprinted polymers (SMIPs) via a novel precipitation polymerization in the controlled delivery of sulfasalazine. *Macromol. Biosci.* 4, 22–26.
- Robles-Machín, R., Adrio, J., Carretero, J.C., 2006. Gold-catalyzed synthesis of alkyldiene 2-oxazolidinones and 1,3-oxazin-2-ones. *J. Org. Chem.* 71, 5023–5026.
- Sahay, G., Alakhova, D.Y., Kabanov, A.V., 2010. Endocytosis of nanomedicines. *J. Control. Release* 145, 182–195.
- Santoro, A., Cappello, A.R., Madeo, M., Martello, E., Iacopetta, D., Dolce, V., 2011. Interaction of fosfomicin with the glycerol 3-phosphate transporter of *Escherichia coli*. *Biochim. Biophys. Acta* 1810, 1323–1329.
- Saturnino, C., Buonerba, M., Capasso, A., Lancelot, J.C., De Martino, G., 2004. Evaluation of analgesic and anti-inflammatory profile of beta-lactam monocyclic compounds. *Biomed. Res.* 15, 26–30.
- Saturnino, C., Saturnino, P., Fusco, B.M., De Martino, G., Rocco, F., Lancelot, J.C., 2000. Evaluation of analgesic and anti-inflammatory activity of novel beta-lactam monocyclic compounds. *Biol. Pharm. Bull.* 23, 654–656.

- Shim, S.E., Yang, S.H., Choi, H.H., Choe, S.J., 2004. Fully crosslinked poly(styrene-co-divinylbenzene) microspheres by precipitation polymerization and their superior thermal properties. *Polym. Sci., Polym. Chem. Ed.* 42, 835–845.
- Swaney, S.M., Aoki, H., Ganoza, M.C., Shinabarger, D.L., 1998. The oxazolidinone linezolid inhibits initiation of protein synthesis in bacteria. *Antimicrob. Agents Chemother.* 42, 3251–3255.
- Wilson, D.N., Schluenzen, F., Harms, J.M., Starosta, A.L., Connell, S.R., Fucini, P., 2008. The oxazolidinone antibiotics perturb the ribosomal peptidyl-transferase center and effect tRNA positioning. *Proc. Natl. Acad. Sci. U.S.A.* 105, 13339–13344.
- Zhang, S.L., Li, J., Lykotrafitis, G., Bao, G., Suresh, S., 2009. Size-dependent endocytosis of nanoparticles. *Adv. Mater.* 21, 419–424.

Mass Spectrometry-Based Proteomic Approach in *Oenococcus oeni* Enological Starter

Anna Napoli,^{*,†} Donatella Aiello,[†] Gilda Aiello,[†] Maria Stella Cappello,[‡] Leonardo Di Donna,[‡] Fabio Mazzotti,[†] Stefano Materazzi,[§] Marco Fiorillo,[†] and Giovanni Sindona[†]

[†]Department of Chemistry and Chemical Technologies, University of Calabria, Via P. Bucci, Cubo 12/D, 87036 Arcavacata di Rende (CS), Italy

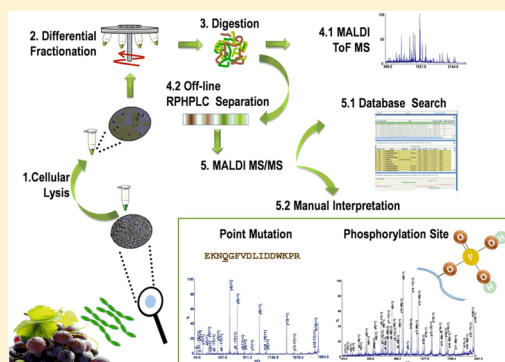
[‡]CNR, Institute of Science of Food Production (ISPA), Lecce, Italy

[§]Department of Chemistry, "Sapienza" University of Rome, Rome, Italy

Supporting Information

ABSTRACT: A simple procedure is proposed for selective protein solubilization and trypsin digestion, followed by off-line liquid chromatography–matrix assisted laser desorption ionization mass spectrometry (LC–MALDI MS) analysis of *Oenococcus oeni* (*O. oeni*) bacterium. Peptides were identified from tryptic digests using sequencing by tandem mass spectrometry and database searches. Cytoplasmic and membrane related proteins (MRP) were identified in the *O. oeni* bacterium. MS/MS data analysis points out 13 peptides having one point mutation from 9 proteins. The major microheterogeneity was found for Zn-dependent alcohol dehydrogenase (Zn-ADH, Q04GE6) and 60 kDa chaperonin (GroEL, Q04E64) that are involved in methionine catabolism and post-translational protein folding, respectively. MS/MS data processing also leads to the identification of 34 unique phosphorylation sites from 19 phosphoproteins.

KEYWORDS: *Oenococcus oeni*, MALDI, mass spectrometry, enzymes, phosphorylation, point mutation, shotgun approach, bacteria



INTRODUCTION

Oenococcus oeni (*O. oeni*) is an autochthonous alcohol-tolerant, acidophilic lactic bacterium species (LAB) naturally present in grapes.¹ The *O. oeni* population is characterized by genetic and biochemical variability, and it is deeply studied in order to confirm the genetic diversity and enological potential. It is also characterized by high population complexity. The strain discrimination is carried out by genotyping and by evaluating enzymatic activities, related to esterase, glucosidase, and protease as well as catabolic performances (degradation of L-malic acid, citric acid, acetaldehyde, and arginine).^{2,3} *O. oeni* owns peculiar physiological and biochemical properties, such as the production of volatile compounds, growth rate, interaction with yeasts, that are responsible for alcoholic fermentation and cold/ethanol shock resistance.⁴ Thus, it plays an important role in the improvement of the organoleptic quality and sensorial properties of wines.⁵ It is more used in winemaking as a starter culture to improve the spontaneous course of malolactic fermentation (MLF) and also to minimize the risk of wine to spoilage.^{6,7} The commercial availability of several starter cultures allowed the widespread of this practice among wineries.⁸ This bacterium survives on direct inoculation in wine and modulates the synthesis of proteins involved in amino acid metabolism, in sugar transport and catabolism, and in flavor metabolism.⁹ It is well-known that *O. oeni* is able to maintain the efficiency of cytoplasmic membrane during

ethanol and acid challenge by adjusting the membrane fluidity¹⁰ and protein composition.^{11,12} The development of new malolactic starters is a multiphase approach, because the resistance to wine conditions is strictly strain dependent. The use of selected strains allows control over the sensory impact of the wine, because significant hydrolysis of aroma precursors may occur during MLF as a result of metabolic activity.

In bacteria, protein phosphorylation is a reversible covalent post-translational modification that is utilized in the regulation of various cellular activities, e.g., metabolism, biosynthesis, stress, transport, and adaptation to diverse environmental conditions. In *Escherichia coli*, *Bacillus subtilis*, and *Lactococcus lactis*, many enzymes implicated in carbon metabolism and in the glycolytic pathway were found to be phosphorylated on S/T/Y residues.¹³ For example, the transcriptional regulation in *L. lactis* determines metabolic flux activities to some extent considering that the cellular regulation takes place after gene transcription. Thus, a MS-based proteomics study of the naturally occurring *O. oeni* strain which has gone spontaneous MLF in wine could constitute a significant contribute.

The conventional method for proteome analysis involves two-dimensional gel (2D) as the final purification step followed by in-gel digestion and mass spectrometric analysis.¹⁴ The

Received: December 26, 2013

Published: April 28, 2014

limitations in resolving certain classes of protein by 2D gels has been well-documented, and this drawback becomes increasingly apparent in microorganism proteome isoelectrofocusing (IEF), since the formation of cell wall polysaccharide/nucleic acid complexes results in streaks and smears.^{9,15,16} Mass spectrometric methodologies provide a rapid and sensitive tool for the identification¹⁷ and quantitation of metabolites,^{18–20} amino acids,^{21,22} and proteins²³ and their post-translational modification.^{24,25} Recent trends in proteomics suggest direct analysis of protein mixtures, with less emphasis on preliminary protein purification steps.²⁶ A rapid and highly reliable characterization of bacteria involving a brief *in situ* proteolytic digestion of small acid soluble proteins²⁷ (SASPs), matrix-assisted laser desorption ionization (MALDI) desorption of the resulting peptides, and subsequent analysis by tandem mass spectrometry was proposed earlier.^{28–30} The reliable detection of species-specific proteins and peptides, which are unique in mass and amino acid sequence, relies on proper protein solubilization, digestion, and sensitive MS analysis.

In this study, a simple procedure for selective protein solubilization and trypsin digestion, liquid chromatography (LC)–MALDI time of flight (TOF)/TOF mass spectrometry is applied to *O. oeni* strain. We applied this procedure to analyze a well identified, and isolated *O. oeni* strain (ITEM 8261) naturally occurring in “Primitivo”, an economically important red wine of the Salento Region.⁷

■ EXPERIMENTAL SECTION

Chemicals

Trifluoroacetic acid (TFA), methanol (MeOH), acetonitrile (ACN), H₂O, ammonium bicarbonate (NH₄HCO₃, 99.5%), trypsin, α -cyano-4-hydroxy-trans-cinnamic acid (α -CHCA, 99.0%), and glass beads (150–212 μ m) were purchased from Sigma-Aldrich Fluka (Milano, Italy).

Bacteria strain and growth conditions

The *O. oeni* strain used in this study is named ITEM 8261 and is from the culture collection form (ITEM) of Agri-Food Important Toxicogenic fungi, yeast, and bacteria, deposited at the Institute of Sciences of Food Production (ISPA), Bari, Italy (<http://server.ispa.cnr.it/ITEM/Collection/>). ITEM 8261 was isolated from “Primitivo” wine (Salento Region, Apulia, Italy). The strain was produced during natural must fermentation in an experimental cellar in the 2005 vintage; the genotypic characterization was carried out by Amplified Fragment Length Polymorphism (AFLP) analysis. In the present work, the bacterial strain was grown anaerobically (in a 5% CO₂ atmosphere conditions, using the Anaerogen 2.5 L System, Oxoid, U.K.) at 28 °C for 7–10 days in MRS broth (Oxoid), supplemented with 2% tomato juice (MRS-tj). pH was adjusted to 4.8 with 1 M KOH. The bacterial strain was isolated, dried, and stored at –80 °C until further processing.

Protein Extraction

The dehydrated cell culture *O. oeni* strain (7 mg) was suspended in 1 mL of NH₄HCO₃ (50 mM, pH 8.0) solution and incubated on an overhead stirrer for 30 min at room temperature. The cellular lysis was performed through the use of pressure waves and the frictional action of glass beads. A small amount of glass beads (order of 3–5 mg) was added to the cell solution, and the sample was shaken for 3 min on the vortex. The cell suspension was then sonicated by a probe at 4 °C for 10 min. The resulting sample was centrifuged for 5 min

at 250g, and then the pellet (P1) containing the cell debris was discarded. The supernatant (S1) was incubated for 10 min by continuously rocking and centrifuged for 10 min at 3000g. Then, the pellet (P2) containing the membrane related proteins was recovered. The suspension was centrifuged for 10 min at 26 000g. The cytosolic fraction (S2) was recovered, while the respective pellet was discarded. Centrifugation and incubation were carried out at 4 °C. All fractions obtained were stored at –20 °C until further use. The cellular lysis was monitored by using an optical microscope at a resolution of 100 \times by acquiring optical images before and after cellular lysis.

Protein Digestion

The microwaves assisted digestion on samples S2 and P2 was performed by trypsin. The completely digested samples were obtained after three simultaneous treatments in the microwave (MWD 246 SL, Whirlpool Europe, Italy) at 250 W irradiation power each lasting for 3 min. An aliquot (600 μ L) of S2 was digested with 5 μ L of trypsin (8 pmol/ μ L) solution. The complete solubilization of the P2 was obtained by adding 600 μ L of 0.5% SDS in NH₄HCO₃ (50 mM). The resulting solution (600 μ L) was digested with 5 μ L of trypsin (8 pmol/ μ L) solution.

HPLC Separation

Separation of the peptides derived from the S2 and P2 digests were carried out using HPLC (Agilent 1100 Germania) equipped with a C18 column (Hypersyl Gold 100 mm \times 4.6 mm i.d., Thermo, Bellefonte, PA). Dried peptides were dissolved in 50 μ L of TFA 0.1% and injected. The flow rate was set at 1 mL/min by using the following gradients: solvent A (H₂O, 0.1% TFA), solvent B (CH₃CN); from 10% B to 100% B in 35 min, 2 min at 100% B isocratic.³¹ The column effluent was collected at 0.5 min intervals resulting in 80 fractions.

Protein Identification by MALDI MS and MS/MS Analysis

Each of the RP-LC fractions were completely dried by Speed vac (Eppendorf, Hamburg, German) and resuspended in 10 μ L of α -CHCA. A 1 μ L portion of sample–matrix solution was spotted on a MALDI matrix target, dried at room temperature, and directly analyzed by MALDI mass spectrometry. Mass spectrometry analyses were performed using a 5800 MALDI-TOF/TOF analyzer (AB SCIEX, Darmstadt, Germany) equipped with a neodymium: yttrium-aluminum-garnet laser (349 nm), in reflectron positive mode with a mass accuracy of 5 ppm. At least 4000 laser shots were typically accumulated with a laser pulse rate of 400 Hz in the MS mode, whereas in the MS/MS mode spectra up to 5000 laser shots were acquired and averaged with a pulse rate of 1000 Hz. MS/MS experiments were performed at a collision energy of 1 kV, and ambient air was used as the collision gas with a medium pressure of 10^{–6} Torr.

Protein identification was performed with the ProteinPilot 4.0 software program (AB Sciex) using the Paragon (AB Sciex) protein database search algorithm.³² The data analysis parameters were as follows: **Sample type:** Identification; **Cys Alkylation:** None; **Digestion:** Trypsin; **Instrument:** 5800; **Special factors:** Phosphorylation emphasis; **Species:** None; **ID Focus:** Biological modifications –Amino acid substitution; **Database:** Uniprot_Oenococcus oeni_181.fasta; **Search Effort:** Thorough ID; **FDR analysis:** Yes; **Detected Protein Threshold [Unused ProtScore (Conf)]:** 1.5 (95.0%).

After acquisition, spectra were handled using Data Explorer version 4.11 (AB Sciex). The MS/MS data were also processed

Table 1. Proteins Identified of *O. oeni* by MS/MS Data Processing^a

accession no. ^a	metabolic classes ^b	short name ^b	MW ^b	pI ^c	biological function ^b	location ^b
Amino Acid Metabolism/Catabolism						
Q04D18	pyruvate oxidase	POX	63.614	6.08	oxidoreductase	unknown
Q04DB8	2-keto-4-methylthiobutyrate/aminotransferase/fructokinase	2k4MeAF	32.106	6.00	amminotransferasi	unknown
Q04GE6	Zn-dependent alcohol dehydrogenase	Zn-ADH	40.921	5.17	nucleotide binding	unknown
Q04EB7	1,3-propanediol dehydrogenase		42.239	5.23	oxidoreductase	unknown
Q04GX2	lactaldehyde dehydrogenase		52.531	5.03	oxidoreductase	unknown
Q04GQ8	glyceraldehyde-3-phosphate dehydrogenase	GapA	37.120	5.53	oxidoreductase	unknown
Q04EF1	NAD-dependent aldehyde dehydrogenase	GabD	51.533	5.02	oxidoreductase	unknown
Q04EJ8	acetaldehyde dehydrogenase/alcoholdehydrogenase		99.100	6.04	oxidoreductase	unknown
Q04D72	cystein synthase	CysK	32.758	6.98	lyase/transferase	unknown
Q04DQ5	S-ribosylhomocysteine lyase	LuxS	17.665	5.35	lyase	unknown
Q04D47	CTP synthase	pyrG	60.106	5.52	glutamine metabolic process	unknown
Q04FD8	phenylalanine-tRNA ligase alpha subunit	PheRS	39.705	5.53	protein biosynthesis	cytoplasm
Glycolysis, Pyruvate, and Carbohydrate Metabolism						
Q04FG3	6-phosphogluconate dehydrogenase decarboxylating	Gld	53.024	5.43	D-gluconate metabolic process in pentose-phosphate shunt	unknown
Q04G42	phosphoglycerate kinase	PGK	43.019	5.49	glycolysis	cytoplasm
Q04DH2	enolase	NNE	48.449	4.72	glycolysis	cytoplasm
Q04F61	pyruvate kinase	Pyk	52.239	5.96	glycolysis	unknown
Q04G44	glucosio-6-phosphato isomerase	GPI	48.668	4.99	glycolysis	cytoplasm
Q04D23	phosphoketolase	Xfp	92.306	5.08	aldehyde-lyase activity	unknown
Q04H39	mannose-6-phosphate isomerase, type 1	Man6P	36.619	6.90	carbohydrate metabolic process	unknown
Q04HE3	glucose 6-phosphate-1-dehydrogenase	G6PD	55.667	6.44	NADP Binding in pentose phosphate pathway	unknown
Q04HF5	2,3-bisphosphoglycerate-dependent phosphoglycerate mutase	GpmA	27.127	5.50	glycolysis	unknown
Q04G34	phosphoenolpyruvate-protein phosphotransferase	PtsI	63.219	5.11	sugar transport, kinase activity	cytoplasm
Q04GQ0	phosphoglycerate dehydrogenase-like dehydrogenase	GAPDH	36.556	5.59	oxidoreductase	unknown
Q04HJ9	aldo/ketoreductase related enzyme	DkgA	31.677	5.59	oxidoreductase	unknown
Other						
Q04FQ4	elongation factor Tu	EF-T	43.625	5.01	GTP binding	cytoplasm
Q04ED6	elongation Factor G	EF-G	77.965	4.82	GTP binding	cytoplasm
Q04G77	50S ribosomal protein L29	rpmC	7.844	9.40	translation	ribosome
P94898	heat shock protein Hsp18	Hsp18	16.938	5.10	stress response	unknown
Q04E64	60 kDa chaperonin	GroEL	57.288	4.85	prevents misfolding and promotes the refolding	cytoplasm
Q04EE1	chaperone protein DnaK	DnaK	66.200	4.86		
Q04GA6	ATP-binding subunit of Clp protease and DnaK/DnaJ chaperones	ClpP	79.031	5.74	hydrolase/Protease	unknown
Q04G86	30S ribosomal protein S10	rpsJ	11.690	10.05	RNA binding	ribosome
Q04G81	30S ribosomal protein S19	rpsS	10.504	10.3	RNA binding	ribosome
Q04G51	30S ribosomal protein S9	rpsI	14.028	11.46	translation	ribosome
Q04EQ1	cyclopropane-fatty-acyl-phospholipid synthase	CFA	45.436	6.21	lipid biosynthesis	unknown
Q04G20	ATP synthase subunit beta	atpD	50.704	4.69	ATP synthesis	membrane
Q04G23	ATP synthase subunit delta	atpH	20.146	6.92	ATP synthesis	membrane
Q04EY2	putative uncharacterized protein		19.425	9.78	FMN binding	membrane
Q04H48	putative uncharacterized protein		10.841	4.93		unknown
Q04HJ7	putative uncharacterized protein		4.639	9.30		unknown
Q04HG0	predicted GTPase, probable translation factor	predicted GTPases				
Q04GT1	Uvr ABC system protein A	UvrA	104.721	8.3	excision nuclease	cytoplasm
Q04H97	transcription-repair coupling factor	TRCF	134.984	6.0	ATP-binding	unknown
Q04F00	exonuclease RecJ	RecJ	69.964	8.45	hydrolase/exonuclease	unknown
DNA Binding						
Q04HR5	DNA polymerase III subunit beta	rpoB	40.742	4.98	DNA replication	cytoplasm
Q04F53	Bacterial nucleoid protein Hbs	Hbs	9.733	9.74	DNA condensation	unknown
Q04GT5	NAD/NADP transhydrogenase alpha subunit		41.049	8.67	nucleotide binding	unknown
Q04GM3	serine-tRNA ligase	SerRS	49.861	5.68	protein biosynthesis	cytoplasm
Q04HR4	S4-like RNA binding protein		8.237	8.01	RNA binding	ribosome

Table 1. continued

^aThe identification of protein parent was performed using the Protein Pilot Paragon Method. The MS/MS data were processed using a mass tolerance of 10 ppm and 0.2 Da for the precursor and fragment ions, respectively. ^bAccording to “UniProtKB” (<http://www.uniprot.org/>). ^cAccording to “Compute pI/MW” (http://web.expasy.org/compute_pi/).

Table 2. Identified Peptides from *O. oeni* Containing a Point Mutation^a

	protein ^b	accession no. ^b	start–end	peptide sequence ^c	<i>m/z</i> ^d	PM
1	Zn-ADH	Q04GE6	36–51	EKNQGFVDLIDDWKPR	1960.00	D → Q(39)
2			315–323	TVNDGIEVR	1002.53	L → N(317)
3			335–344	EAFQFGAEGK	1083.52	D → E(335)
			352–372	DDLNDINDVIEEMKEGTpITGR	2457.09	V → D(352)
4	GapA	Q04GQ8	221–239	AIGLVCPPEVDGKLNHQAQR	1977.05	V → C(226)
5	NNE	Q04DH2	17–34	GNtTVEAEVYSEDGFFGR	1977.89	P → T(19)
6	Xfp	Q04D23	301–319	GWGGVYKFDEEDGNPIENSFR	2123.02	P → V(305)
7	G6PD	Q04HE3	266–281	AAKNTVFSpKLLQYDER	1977.99	M → Q(277)
8	GroEL	Q04E64	452–467	LIVENAGLEGSVIAQR	1668.93	Q → L(452)
9			285–308	AQLMDIAILTGATVVTEDLGLQLK	2513.40	Q → M(288)
10	rpsJ	Q04G86	73–88	LIDMVNPTDKTpVDSpLR	1976.89	LM(76)
11	CFA	Q04EQ1	84–92	SAGSFLTDK	925.47	N → S(84)
12	atpD	Q04G20	252–265	FTQPGSEVSpALLGR	1541.74	A → P(255)
13	atpH	Q04G23	142–159	NVVDPNVIFGVILTAGSpK	1923.00	A → F(150)

^aFor detailed MS/MS data, see the Supporting Information. ^bAccording to “UniProtKB” (<http://www.uniprot.org/>). ^cTp, phosphothreonine; Sp, phosphoserine. ^dThe charge state of all peptides was 1+.

to assign candidate peptides in the NCBI, SwissProt database using the MASCOT search program (<http://www.matrixscience.com>). The mass tolerance of the parent and fragments for MS/MS data search was set at 10 ppm and 0.20 Da, respectively. The query was made for “Other Firmicutes” taxonomy allowing 2 missed cleavage. A Peaklist of 50 ions of intensity higher 10% above the noise level were generically used for the database search. The phosphorylation of serine and threonine were included in the variable modifications. Most of the MS/MS spectra showed intense and well resolved ion signals. However, all spectra were manually checked to verify the validity of the MASCOT results. The MASCOT results of MS/MS fragmentation are provided as Supporting Information (Supporting Information Figures 1–5).

RESULTS AND DISCUSSION

A simple and rapid protocol has been developed for selective protein solubilization from *O. oeni* cell lysates, followed by HPLC fractionation and MALDI MS/MS analysis. In silico proteome of LAB has displayed a biphasic pattern, since most proteins are in the pH range of 4–6 or 9–11.³³ We hypothesized that a simple acid or basic treatment followed by enzyme digestion and MALDI MS, MS/MS is not sufficient to detect the number of individual proteins either attached to and/or protected by the cell wall. Therefore, we decided to perform cell wall disruption by ammonium bicarbonate (50 mM, pH 8) coupled with glass beads. The choice of ammonium bicarbonate is favored by its ability to promote the formation of carboxylate/ammonium ion pairs and the solubility of the proteins.³⁴ Furthermore, the use of a saline solution (NH₄HCO₃, 50 mM, pH 8) would allow the extraction of a subproteome denoted by chemically homogeneous protein families.^{35,36} In order to carry out a more detailed analysis, we decided to fractionate the crude extract. This process prevents the linkage of proteins to the compartment in which they exert their activity. The fractionation of the sample prior to analysis enhances the proteome coverage and reproducibility.³⁷ The

adopted method relies on cell lysis through sequential addition of buffer to the cell pellet, followed by incubation and centrifugation at different speeds. Cytosol (S2) and membrane related (P2) fractions were only used. The hydrophilic S2 and lipophilic P2 fractions contain base-soluble proteins and hydrophobic proteins, respectively. Membrane related protein (MRP) enriched fraction (P2) is generally solubilized using a strong surfactant like SDS, which ensures proteins are highly charged and they will not be lost during the sample processing. Therefore, P2 fraction was solubilized in 0.5% SDS. An aliquot of the SDS-solubilized protein mixture P2 and hydrophilic S2 fractions were used for a solution-based shotgun proteomics approach. Trypsin was then added and digested under microwave irradiation conditions. Trypsin-digested P2 sample was analyzed by MALDI MS using a two-layer sample/matrix preparation method, which allows the analysis of protein and peptide samples containing up to 2% SDS. Peptides generated by trypsin-digested fractions were loaded on to the C18 column and a linear gradient elution was performed. All the collected fractions were lyophilized and resuspended in 20 μL of CH₃CN/H₂O, 40:60 (v:v). A volume of 1 μL of the resulting solution was loaded onto the MALDI plate.

Protonated tryptic peptides from each LC fraction were used to identify bacterial proteins after MS/MS fragmentation. The identification of the protein parent was performed using the Protein Pilot Paragon Method, and the results of the database search are summarized in Table 1. The MS/MS data were processed using a mass tolerance of 10 ppm and 0.2 Da for the precursor and fragment ions, respectively. The phosphorylation of serine and threonine were included in the variable modifications, and all spectra were manually evaluated. For this experiment, the database search resulted in 222 peptide and 48 protein (Supporting Information Table 1). Supporting Information Table 1 shows peptides that are originated from deamidation of the native peptides during sample preparation and peptide pairs [³⁴⁵VTPIVEKVDLNDINDVIEEMKEGT-ITGR]³⁷², *m/z* 3128.68 and [³⁴⁵VTPIVEKVDLNDINDV-

Table 3. Identified Phosphopeptides from *O. oeni* Proteins

	protein ^a	accession no. ^a	start–end	phosphopeptide sequence ^b	<i>m/z</i> ^c	phosphosite
1	2k4MeAF	Q04DB8	230–246	IVFGGGVVS _p EEFLKKVR	1944.07	S(238)
2	Zn-ADH	Q04GE6	352–372	DDLNDINDVIEEMKEGT _p ITGR	2457.09	T(368)
3	GapA	Q04GQ8	240–250	VAVVDGSpVTEL	1168.57	S(46)
4	GabD	Q04EF1	28–37	ALSpQGHT _p LYKK	1405.64	S(30), T(34)
			39–56	WRNGPLDKRVAT _p LHTIAK	2157.15	T(50)
5	ALDH	Q04EJ8	250–258	AAEDLLS _p KR	1195.61	S(257)
			311–323	HAVNGPVAGM _s SpGR	1332.60	S(321)
6	pyrG	Q04D47	32–44	LLK _s SpRGLAVTVQK	1492.87	S(35)
7	PheRS	Q04FD8	14–31	VSVEIDK _s SpSVDLIENIR	2163.00	S(21), S(22)
8	Gld	Q04FG3	193–206	GDEELIDET _p YNIMR	1777.74	T(201)
	NNE	Q04DH2	1–16	MSLIASIVAREVLDS _p R	1885.94	S(15) Dehyd S(2)
			17–34	GNPTVEAEVY _s SpEDGFFGR	2053.87	S(27)
			83–106	FDVADQRGIDLAMIALDGT _p PNKGGK	2625.31	T(101)
9	Xfp	Q04D23	579–596	PADGNELLAVAS _p RALVDR	1946.98	S(590)
10	Man6P	Q04H39	151–175	LLRKVPVKAGDFVYV _s SpGTIHALNK	2802.55	T(167)
			212–222	EpyroSpIDVTT _p VPPFR	1405.58	S(213), T(18)
11	G6PD	Q04HE3	266–281	AAKNTVFS _p KLKQYDER	1977.99	S(273)
			323–338	LQFENDRW _T pGVPFYIR	2121.00	T(331)
12	GroEL	Q04E64	7–14	FSpEDARTR	1061.45	S(8)
			267–282	GT _p FNVAAVKAPGFGDR	1686.81	T(268)
			309–320	DVT _p IDQLGQANR	1409.65	T(311)
			427–451	VADSLQGDVAT _p GARIVLRALEEPLR	2729.46	T(437)
13	rpsI	Q04G51	21–33	LTPGSpGKITINNR	1451.74	S(25)
14	rpsJ	Q04G86	73–88	LIDM _v VNPTDKT _p VDS _p LR	1976.89	T(83), S(86)
15	rpsS	Q04G81	28–37	KPVIRTWS _p RR	1378.75	S(35)
16	CFA	Q04EQ1	5–13	TIYRRLS _p R	1257.69	S(12)
17	atpD	Q04G20	71–89	VLDTGAPIEVPVGEAT _p LGR	1974.00	T(86)
			252–265	FTQPGEV _s SpALLGR	1541.74	S(560)
18	atpH	Q04G23	142–159	NVVDPNVIFGVILTAGS _p K	1923.00	S(158)
19	S4RNA	Q04HR4	35–52	ENANSFFVNGES _p ENRRGR	2162.95	S(46)

^aAccording to “UniProtKB” (<http://www.uniprot.org/>). ^bT_p, phosphothreonine, Sp phosphoserine. ^cThe charge state of all peptides were 1+.

IEEMKEGTITGR³⁷², *m/z* 3127.68, N(355)] that overlap significant mass spectrometric domains. The mass difference between these two peptides is only 1 Da showing a more complex isotopic pattern of peaks, and this suggests the possibility of originating from deamidation of the native peptide during sample preparation. The theoretically calculated isotopic distribution and the sum of the isotopic distributions of both peptides were evaluated before sequence validation. The protein identified by MS/MS analysis are the ones that are involved in amino acid metabolism/catabolism, glycolysis, pyruvate and carbohydrate metabolism, and stress response (Table 1). Table 1 lists the *pI*, the biological function, and location for every possible match in the database. It can be seen that most of the proteins are acidic (*pI* 4–6) and the subcellular location for about a half of the proteins matched is unknown. Most the protein reported in Table 1 are cytoplasmic and MRP; hence, the conditions chosen for cell disruption and the successive fractionation of the sample were well adopted.

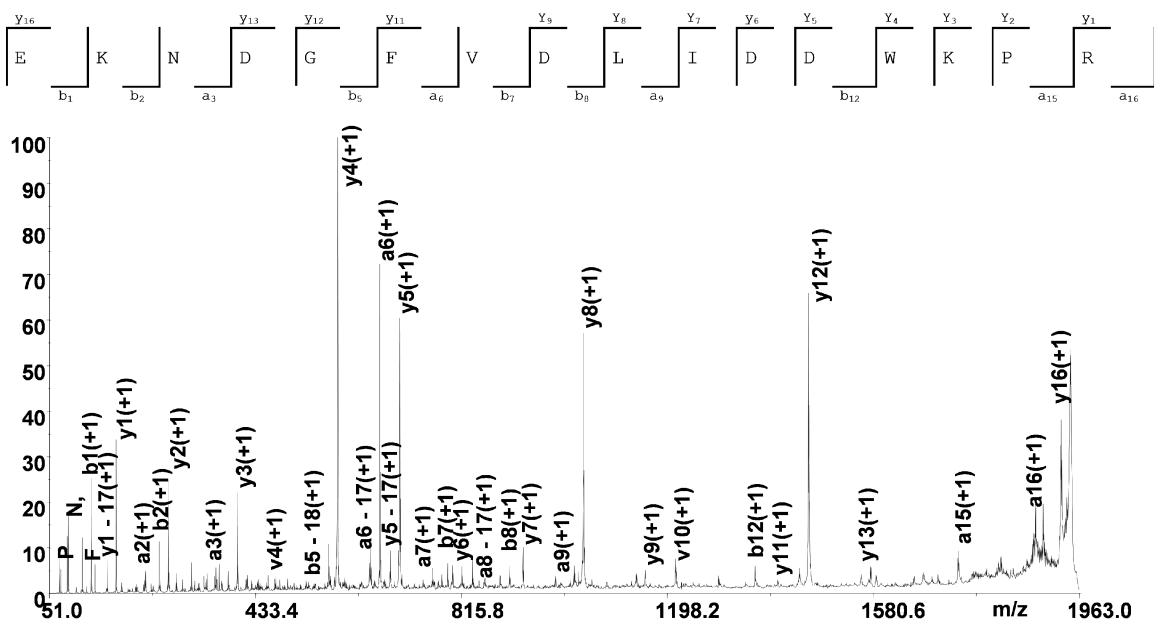
Tables 2 and 3 list the identified peptides highlighting the supposed point mutations and the post-translational modifications for each protein, respectively. In total, 13 peptides containing point mutation were identified from 9 proteins indicating a major microheterogeneity for Zn-dependent alcohol dehydrogenase (Zn-ADH) and 60 kDa chaperonin (GroEL). The adopted criteria to discriminate the protein variants are represented by the number of peptides matching the conservative domain. Zn-dependent alcohol dehydrogenase (Supporting Information Table 1) was in fact identified by

matching 19 peptides with 99% confidence (37% of sequence coverage, Supporting Information Figure 6). A difference of 13 mass units between the peaks *m/z* 1946.99 and 1960.00 suggests that the sample contains a mixture of at least two variants of Zn-ADH (Figure 1A,B and Table 2).

The exchange of an amino acid at the position 39 (D → Q) leads to a mass difference of 13 Da. The MS/MS experiments of the peaks *m/z* 1946.99 and 1960.00 validated the sequences ³⁶EKNDGFVDLIDDWKPR⁵¹ (Peptide A) and ³⁶EKNQG-FVDLIDDWKPR⁵¹ (Peptide B) that belong to Zn-ADH (Q04GE6) and the variant Zn-ADH_1, respectively (Figure 1A,B). The CID spectrum of peptide A (*m/z* 1946.99) is shown in Figure 1A. For this peptide, the MS/MS spectrum showed y and b ion series, allowing complete sequence coverage. It should be noted that the y13 (*m/z* 1575.8) ion is found 13 Da lower than the equivalent ion in peptide B (*m/z* 1588.8), indicating the change at the fourth residue from the N-terminus. In addition, the exchange of D → Q is also reliable with a mass difference of 128.1 Da between y13 (*m/z* 1588.8) and y12 (*m/z* 1460.7) ions. A similar manual interpretation process was carried out to sequence all peptides obtained by tryptic digestion (Table 2). Methionine residues were found to be oxidized, and their position was also confirmed by identifying the corresponding mass increase (16 Da).

Zn-dependent alcohol dehydrogenase was found phosphorylated at T368 (Table 3). The CID spectrum of segment ³⁵²DDLNDINDVIEEMKEGT_pITGR³⁷² (*m/z* 2457.13) from Zn-ADH is given in Figure 2A. For this segment, the MS/MS

A



B

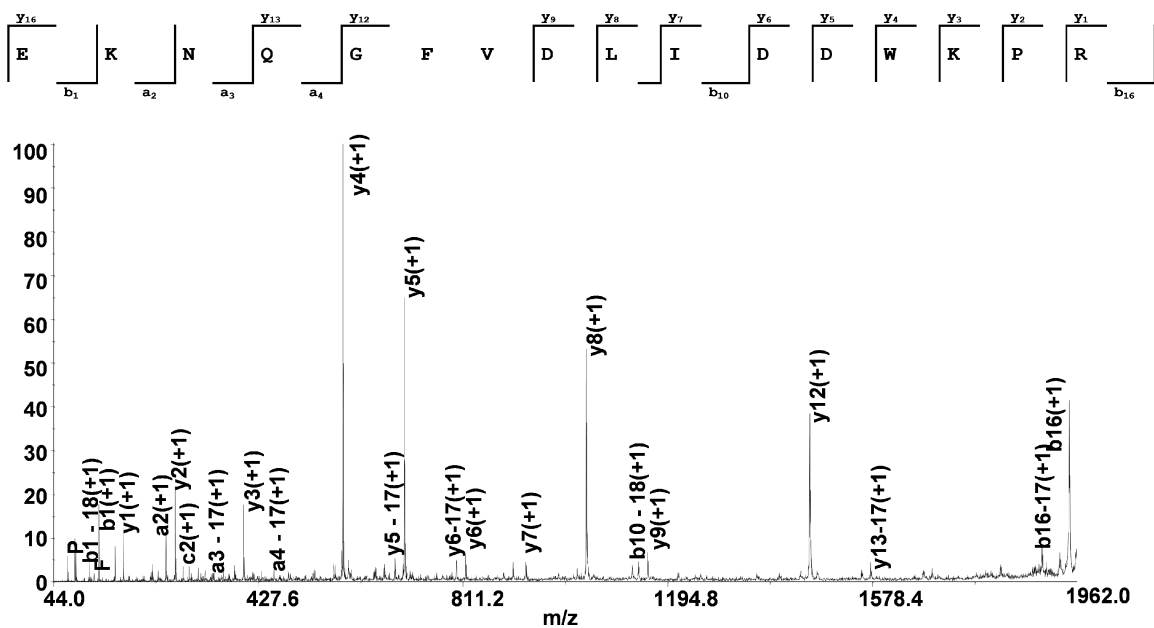
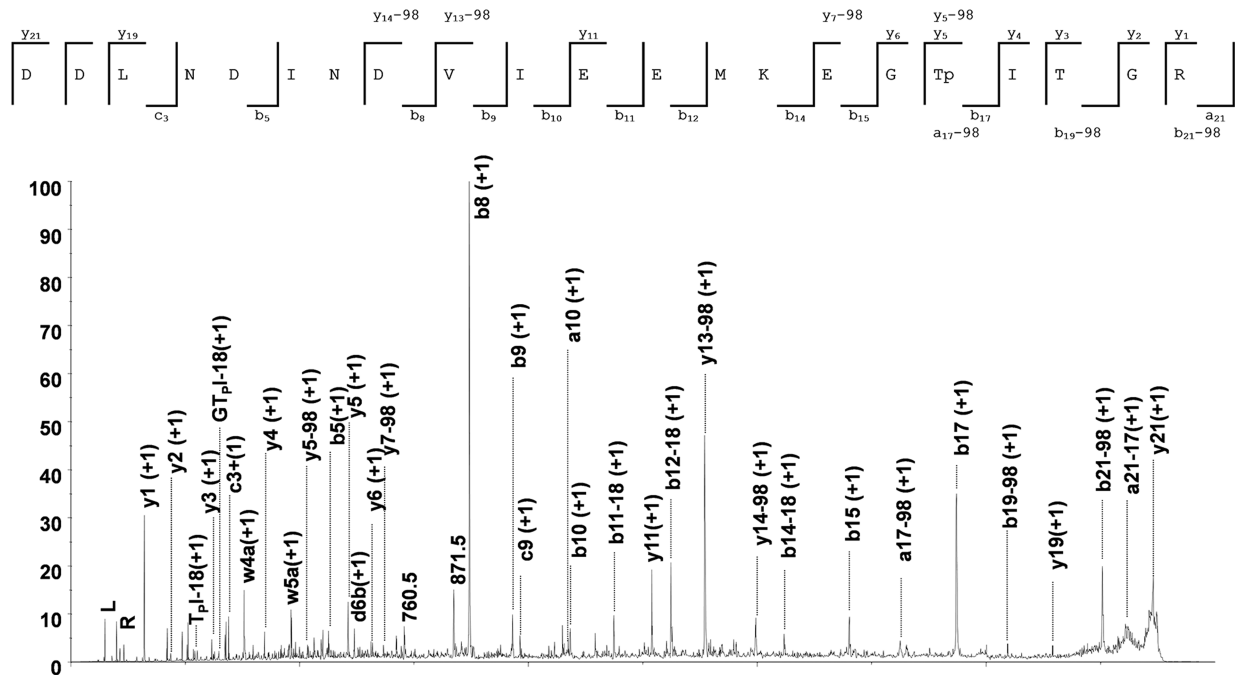


Figure 1. CID (1KeV) spectra of the sequences (A) $^{36}\text{EKNDGFVDLIDDWKPR}^{51}$ (m/z 1946.99) (B) $^{36}\text{EKNQGFVDLIDDWKPR}^{51}$ (m/z 1960.00) belonging to Zn-dependent alcohol dehydrogenase (Q04GE6) and variant 1 (Zn-dependent alcohol dehydrogenase_1), respectively.

spectrum showed N- (a, a-H₃PO₄, b and b-H₃PO₄) and carboxy-terminal (y and y-H₃PO₄) ion series, allowing the complete sequence coverage with the phosphorylation site at the T368 residue. The y-series ions down to y₅ (m/z 626.4) showed the ability to lose H₃PO₄ (98 Da), whereas, the b₁₅ (m/z 1774.7) and b₁₇ (m/z 2012.0) ions are present only in a nonphosphorylated state indicating that the 16th or 17th residue from the N-terminus is phosphorylated. Apart from that, the mass difference between the y₅ (m/z 626.4) and y₄ (m/z 446.5) ions is consistent with a phosphorylated T368 residue.

Only mannose-6-phosphate isomerase, type 1 (Man6P), 30S ribosomal protein S10 (rpsJ), and phenylalanine-tRNA ligase alpha subunit (PheRS) were found with a doubly phosphorylated peptides (Supporting Information Table 1). In particular, the segment $^{14}\text{VSVEIDKSpSpSVDLIENIR}^{31}$ of PheRS was found phosphorylated at S21 and S22. The CID spectrum of segment 14–31 (m/z 2163.00) is shown in Figure 2B. For this segment, the MS/MS spectrum showed b (b-H₃PO₄) and y ion series, allowing the sequence coverage with phosphorylation sites at the S21 and S22 residues. All b-series ions down to b₈ (m/z 938.9) showed the ability to lose H₃PO₄ (98 Da),

A



B

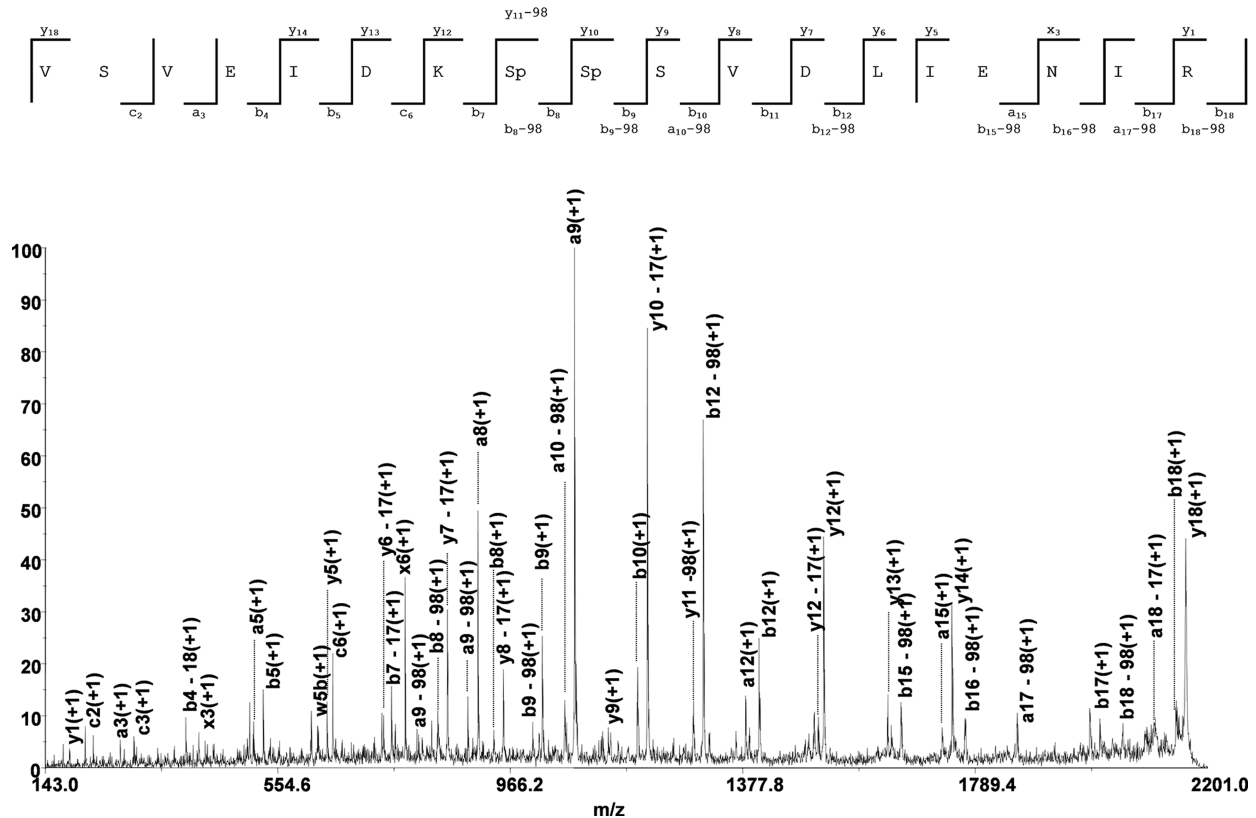


Figure 2. CID (1 keV) spectra of monophosphorylated peptide (A) 352 DDLNDINDVIEEMKEGTpITGR 372 (m/z 2457.13) belonging to Zn-dependent alcohol dehydrogenase (Q04GE6) and doubly phosphorylated peptide (B) 14 VSVEIDKSpSpSVDLIENIR 31 (m/z 2163.00) belonging to phenylalanine-tRNA ligase alpha subunit (Q04FD8).

whereas the b7 (m/z 771.8) ion is present only in the nonphosphorylated state indicating that the eighth residue from

the N-terminus (S21) is phosphorylated. In addition, the mass difference between the b7 (m/z 771.7) and b8 (m/z 938.9)

ions as well as the b8 (m/z 938.9) and b9 (m/z 1105.9) ions is consistent with the mass of a phosphoserine residue (167 Da). Furthermore, the presence of the ion peaks b9 (m/z 1105.9), b9–98 (m/z 1007.9), and the unmodified counterpart γ 8 (m/z 972.0) are consistent with a phosphorylated S22 residue. The presence of S21 phosphorylation is also reliable with the mass difference between the γ 11–98 (m/z 1294.9) and the unmodified counterpart b7 (m/z 771.7) ions. A similar set of b ($\text{b-H}_3\text{PO}_4$) and γ ($\gamma\text{-H}_3\text{PO}_4$) ions was observed for the mono-peptides and doubly-phosphorylated peptides allowing the assignment of serine and/or threonine phosphorylations (Table 3). Interestingly, the results indicate that 34 unique phosphorylation sites were identified from 19 phosphoproteins: 12 on threonine and 22 on serine (Table 3). The identified phosphorylated proteins take part in various cellular mechanisms, such as amino acid metabolism/catabolism, glycolysis, pyruvate and carbohydrate metabolism, and stress response.

Free amino acids produced by proteolysis are converted to various flavor compounds through amino acid catabolism. The branched-chain, the aromatic, and the sulfur-containing amino acids are known to be precursors of many flavor compounds.^{38,39} The conversion of these amino acids into flavors proceeds via two distinct routes: transamination and elimination. This approach leads to the identification of several enzymes involved in the amino acids catabolism. The aminotransferases (phenylalanine–tRNA ligase alpha subunit-POX, 2-keto-4-methyl-thiobutyrate-aminotransferase/fructokinase, Table 1) are involved in the conversion of amino acids into flavors via transamination route. They catalyze the transamination of branched-chain amino acids and methionine, converting them into corresponding α -keto acids. These species are further converted to aldehydes, alcohols, and esters, which are the important aroma compounds. Alcohol dehydrogenase (ADH) and aldehyde dehydrogenase (ALDH) families catalyze the conversion of aldehydes to alcohols and carboxylic acids, respectively. Zn-dependent alcohol dehydrogenase (Zn-ADH, Table 1) is involved in the formation of volatile sulfur compounds from methionine. The last enzymatic step of the methionine catabolism is the reduction of methional in methionol, which is catalyzed by Zn-ADH. Biochemical investigations have revealed that the Zn-ADH enzyme carries out the reduction of acetaldehyde and methional, showing high affinity for aldehydes containing one sulfur atom such as 3-(methylthio)butanal and methional.^{40,41} Lactaldehyde dehydrogenase and 1,3-propanediol dehydrogenase belong to NAD(P)-dependent group III aldehyde dehydrogenase (ALDH3).⁴² ALDH3 members are capable of processing a wide variety of substrates including linear, branched, primary, secondary alcohols in addition to their corresponding aldehydes and ketones. Some components of the ALDH family, like lactaldehyde dehydrogenase, are mainly involved in aldehyde reduction in bacterial species rather than alcohol turnover. 1,3-Propanediol dehydrogenases from *O. oeni* catalyzes the oxidation of several alcohols and the reduction of aldehydes in a broad pH range.⁴³ Cystein synthase (CysK) and S-ribosylhomocysteine lyase (LuxS) (Table 1) are involved in the conversion of amino acids into flavors via elimination route. They belong to the so-called pyridoxal phosphate-dependent β -family and convert methionine to cysteine showing an O-acetylserine-thiol-lyase (cysteine synthase) activity.

Many wine volatile compounds can be released from their flavorless glycoconjugate precursors by enzyme hydrolysis. The breakdown of β -glucosides can occur in bacteria through two

systems: extracellular or cell wall associated β -glucosidases and intracellular phospho- β -glucosidases/phosphoenolpyruvate dependent phospho transferase system (PEP–PTS). Phosphoenolpyruvate dependent phospho transferase (PtsI) is “non sugar specific” component of PTS system. This enzyme was identified using 6 peptides (Supporting Information Table 1), while for the glycosyl hydrolase family (GHF) and phospho- β -glucosidases no were found, as they are soluble in a hydrophobic environment and localized on the cell membrane.⁴⁴ The utilization of sugars as carbon and energy sources by wine LAB during MLF has been demonstrated in a number of studies. However, there are some differences in sugar utilization between species and strain.⁴⁵ Enzymes such as 6-phosphogluconate dehydrogenase decarboxylating (Gld), glyceraldehyde-3-phosphate dehydrogenase (GapA), phosphoglycerate kinase (PGK), enolase (NNE), pyruvate kinase (Pyk), acetaldehyde dehydrogenase/alcoholdehydrogenase, glucose-6-phosphate isomerase (GPI), lactaldehyde dehydrogenase, and phosphoketolase (Xfp) are detected; and these are engaged in glycolysis and pyruvate metabolism, while mannose-6-phosphate isomerase type1 (Man6P), glucose 6-phosphate-1-dehydrogenase (G6PD), and 2,3-bisphosphoglycerate-dependent phosphoglycerate mutase (GpmA) are involved in carbohydrate metabolism. Glucose 6-phosphate isomerase is the key enzyme in the formation of the erythritol pathway from glucose that leads to the isomerization of glucose 6-phosphate to fructose 6-phosphate.

A relationship between stress related gene, MLF performance, and growth in wine-like conditions has been reported.⁴⁶ Bacteria can adapt themselves to adverse conditions by modifying the fatty acid composition of their cell membrane. The ethanol-adapted *O. oeni* cells are characterized by an increased biosynthesis of cyclopropane fatty acids (CFAs). The presence of CFAs in the membrane could reduce proton permeability⁴⁷ and increase membrane rigidity.⁴⁸ CFAs are synthesized *in situ* by the transfer of methylene group from S-adenosyl- L-methionine to a double bond of unsaturated fatty acid chains of membrane phospholipids by CFA synthase (Table 2). The key enzyme of this process was detected and identified phosphorylated at S12 (Table 3). The heat shock protein Hsp18 (Hsp18, Table 1) has been defined as one of the stress proteins of *O. oeni*, playing an important role in the response to different environmental conditions.^{49,50} Furthermore, the evaluation of the abundance of Hsp18 and its gene expression has been successfully used as a parameter for assessing the state of adaptation of different strains.^{51,52} Stress responsive protease ATP-binding subunit of Clp protease and DnaK/DnaJ chaperones (ClpP, Table 1) can act independently or in association with ClpX ATPase to degrade larger specific substrates.⁵³ GroEL contributes to the initial folding of a significant portion of cellular proteins (20–30% of all proteins in the prokaryotic cytoplasm) and to the post-translational protein folding. In spite of their basic nature (pI value 11), some ribosomal proteins (30S ribosomal protein S9, 30S ribosomal protein S10, 30S ribosomal protein S19 and 50S ribosomal protein L29) are also detected (Table 1). These species represent a very high abundant family since almost half of the mass of growing cells corresponds to ribosomes. Furthermore, the related peptides have been detected with a very good intensity because of their propensity to become charged by proton transfer during the ionization process.⁵⁴

Several glycolytic enzymes (Gld, NNE, Xfp, Man6-P, G6PD, Table 3) were found to be phosphorylated on S/T residues. In

E. coli, *B. subtilis*, and *L. lactis*, many enzymes implicated in carbon metabolism including those involved in the glycolytic pathway were found to be phosphorylated.¹³ In *L. rhamnosus* GG, a growth pH-dependent protein phosphorylation was observed and the phosphorylation of glycolytic enzymes was found to be especially extensive. Our data set represents the in vivo phosphoproteome, since bacterial cells were grown in normal laboratory conditions and were not treated prior to harvesting. The phosphorylation processes could occur as an intermediate step in catalysis and thereby regulate the activity of the these proteins.⁵⁵ Therefore, the phosphorylated proteins should get different functions in their different phosphorylation states and at their different subcellular localizations.⁵⁶ These results are in agreement with findings already reported on *L. lactis*^{57,58} for which extensive phosphorylation on glycolytic enzymes, aminoacyl-tRNA synthetases, and ribosomal proteins was found.⁵⁹ This is a remarkable result, even though there it is lack of information on how phosphorylation affect the function of glycolytic enzymes in bacteria.

CONCLUSIONS

A shotgun solution based strategy have successfully used for the identification of proteins from *O. oeni*. Our data set represents the in vivo proteome, since bacterial cells were grown in normal laboratory conditions. The experimental approach exploited provides a tool to achieve deeper insight into the protein composition, opening up interesting possibilities for further research of *O. oeni* proteins involved in metabolic networks under specific stress conditions. The attractive feature of the proposed approach is its potential capabilities to obtain a specific subproteome containing several enzymes involved in different metabolic pathways. The next step should be the determination of the Ser/Thr/Tyr phosphoproteome of *O. oeni* in specific context, where protein phosphorylation has barely been studied before. Furthermore, the particular choice of sample preparation is not restrictive for the specific micro-organism, which also has a potential to be used for characterization of other bacteria proteome.

ASSOCIATED CONTENT

Supporting Information

Supporting Information Figure 1, (a) MS/MS spectrum of the ion species of m/z 2121.83 and (b) sequence identification by database search; Supporting Information Figure 2, (a) MS/MS spectrum of the ion species of m/z 1946.97 and (b) sequence identification by database search; Supporting Information Figure 3, (a) MS/MS spectrum of the ion species of m/z 1973.90 and (b) sequence identification by database search; Supporting Information Figure 4, (a) MS/MS spectrum of the ion species of m/z 1396.66 and (b) sequence identification by database search; Supporting Information Figure 5, (a) MS/MS spectrum of the ion species of m/z 1904.90 and (b) sequence identification by database search; Supporting Information Figure 6, Protein sequence coverage of Zn-dependent alcohol dehydrogenase [*Oenococcus oeni* PSU-1]; Supporting Information Table 1, Peptides identified of *O. oeni* by MS/MS data processing. The identification was performed using Protein Pilot Paragon Method. The MS/MS data were processed using a mass tolerance of 10 ppm and 0.2 Da for the precursor and fragment ions, respectively. This material is available free of charge via the Internet at <http://pubs.acs.org>.

AUTHOR INFORMATION

Corresponding Author

*E-mail: amc.napoli@unical.it. Fax: +39 0984 493307.

Notes

The authors declare no competing financial interest.

ACKNOWLEDGMENTS

This paper was supported by Grant PRIN 2009 KW27KE_005 and the QUASIORA project of the Calabria APQ-RAC network.

REFERENCES

- (1) Barata, A.; Malfeito-Ferreira, M.; Loureiro, V. The microbial ecology of wine grape berries. *Int. J. Food Microbiol.* **2012**, *153*, 243–259.
- (2) Cappello, M. S.; Stefani, D.; Grieco, F.; Logrieco, A.; Zapparoli, G. Genotyping by Amplified Fragment Length Polymorphism and malate metabolism performances of indigenous *Oenococcus oeni* strains isolated from Primitivo wine. *Int. J. Food Microbiol.* **2008**, *127*, 241–245.
- (3) Van Hoorde, K.; Vandamme, P.; Huys, G. Molecular identification and typing of lactic acid bacteria associated with the production of two artisanal raw milk cheeses. *Dairy Sci. Technol.* **2008**, *88*, 445–455.
- (4) Chu-Ky, S.; Tourdot-Maréchal, R.; Marechal, P. A.; Guzzo, J. Combined cold, acid, ethanol shocks in *Oenococcus oeni*: Effects on membrane fluidity and cell viability. *Biochim. Biophys. Acta* **2005**, *1717*, 118–124.
- (5) Bartowsky, E. J. *Oenococcus oeni* and malolactic fermentation – moving into the molecular arena. *Aust. J. Grape Wine Res.* **2005**, *11*, 174–187.
- (6) Mills, D. A.; Rawsthorne, H.; Parker, C.; Tamir, D.; Makarova, K. Genomic analysis of *Oenococcus oeni* PSU-1 and its relevance to winemaking. *FEMS Microbiol. Rev.* **2005**, *29*, 465–475.
- (7) Cappello, M. S.; Zapparoli, G.; Stefani, D.; Logrieco, A. Molecular and biochemical diversity of *Oenococcus oeni* strains isolated during spontaneous malolactic fermentation of Malvasia Nera wine. *Syst. Appl. Microbiol.* **2010**, *33*, 461–467.
- (8) Capozzi, V.; Russo, P.; Beneduce, L.; Weidmann, S.; Grieco, F.; Guzzo, J.; Spano, G. Technological properties of *Oenococcus oeni* strains isolated from typical southern Italian wines. *Let. Appl. Microbiol.* **2010**, *50*, 327–334.
- (9) Cecconi, D.; Milli, A.; Rinalducci, S.; Zolla, L.; Zapparoli, G. Proteomic analysis of *Oenococcus oeni* freeze-dried culture to assess the importance of cell acclimation to conduct malolactic fermentation in wine. *Electrophoresis* **2009**, *30*, 2988–2995.
- (10) Tourdot-Maréchal, R.; Gaboriau, D.; Beney, L.; Diviès, C. Membrane fluidity of stressed cells of *Oenococcus oeni*. *Int. J. Food Microbiol.* **2000**, *55*, 269–273.
- (11) Silveira, M. G.; Baumgärtner, M.; Rombouts, F. M.; Abee, T. Effect of Adaptation to Ethanol on Cytoplasmic and Membrane Protein Profiles of *Oenococcus oeni*. *Appl. Environ. Microbiol.* **2004**, *70*, 2748–2755.
- (12) Grandvalet, C.; Assad-García, J. S.; Chu-Ky, S.; Tollot, M.; Guzzo, J.; Gresti, J.; Tourdot-Maréchal, R. Changes in membrane lipid composition in ethanol- and acid-adapted *Oenococcus oeni* cells: characterization of the *cfa* gene by heterologous complementation. *Microbiology* **2008**, *154*, 2611–2619.
- (13) Koponen, J.; Laakso, K.; Koskenniemi, K.; Kankainen, M.; Savijoki, K.; Nyman, T. A.; de Vosc, W. M.; Tynkkynen, S.; Kalkkinen, N.; Varmanen, P. Effect of acid stress on protein expression and phosphorylation in *Lactobacillus rhamnosus* GG. *J. Proteomics* **2012**, *75*, 1357–1374.
- (14) Polati, R.; Zapparoli, G.; Giudici, P.; Bossi, A. A CTAB based method for the preparation of total protein extract of wine spoilage microorganisms for proteomic analysis. *J. Chromatogr., B: Anal. Technol. Biomed. Life Sci.* **2009**, *877*, 887–891.

- (15) Fountoulakis, M.; Langen, H.; Evers, S.; Gray, C. P.; Takács, B. Two-dimensional map of Haemophilus influenzae following protein enrichment by heparin chromatography. *Electrophoresis* **1997**, *18*, 1193–1202.
- (16) Tonella, L.; Hoogland, C.; Binz, P. A.; Appel, R. D.; Hochstrasser, D. F.; Sanchez, J. C. New perspectives in the Escherichia coli proteome investigation. *Proteomics* **2001**, *1*, 409–423.
- (17) Mazzotti, F.; Di Donna, L.; Taverna, D.; Nardi, M.; Aiello, D.; Napoli, A.; Sindona, G. Evaluation of dialdehydic anti-inflammatory active principles in extra-virgin olive oil by reactive paper spray mass spectrometry. *Int. J. Mass Spectrom.* **2013**, *352*, 87–91.
- (18) Di Donna, L.; Benabdelkamel, H.; Mazzotti, F.; Napoli, A.; Nardi, M.; Sindona, G. High-Throughput Assay of Oleopentanedialdehydes in Extra Virgin Olive Oil by the UHPLC-ESI-MS/MS and Isotope Dilution Methods. *Anal. Chem.* **2011**, *83* (6), 1990–1995.
- (19) Di Donna, L.; Mazzotti, F.; Napoli, A.; Salerno, R.; Sajjad, A.; Sindona, G. Secondary metabolism of olive secoiridoids. New microcomponents detected in drupes by electrospray ionization and high-resolution tandem mass spectrometry. *Rapid Mass Commun. Mass Spectrom.* **2007**, *21* (3), 273–278.
- (20) Mazzotti, F.; Benabdelkamel, H.; Di Donna, L.; Maiuolo, L.; Napoli, A.; Sindona, G. Assay of tyrosol and hydroxytyrosol in olive oil by tandem mass spectrometry and isotope dilution method. *Food Chem.* **2012**, *135* (3), 1006–1010.
- (21) Mazzotti, F.; Benabdelkamel, H.; Di Donna, L.; Athanassopoulos, C. M.; Napoli, A.; Sindona, G. Light and heavy dansyl reporter groups in food chemistry: amino acid assay in beverages. *J. Mass Spectrom.* **2012**, *47* (7), 932–939.
- (22) Cardiano, P.; Falcone, G.; Foti, C.; Giuffrè, O.; Napoli, A. Binding ability of glutathione towards alkyltin(IV) compounds in aqueous solution. *J. Inorg. Biochem.* **2013**, *129*, 84–93.
- (23) Napoli, A.; Athanassopoulos, C. M.; Moschidis, P.; Aiello, D.; Di Donna, L.; Mazzotti, F.; Sindona, G. Solid Phase Isobaric Mass Tag Reagent for Simultaneous Protein Identification and Assay. *Anal. Chem.* **2010**, *82* (13), 5552–5560.
- (24) Reddy, C. E.; Albanito, L.; De Marco, P.; Aiello, D.; Napoli, A.; Musti, A. M. Multisite phosphorylation of c-Jun at threonine 91/93/95 triggers the onset of c-Jun pro-apoptotic activity in cerebellar granule neurons. *Cell. Death Dis.* **2013**, *4*, e852.
- (25) Napoli, A.; Aiello, D.; Di Donna, L.; Moschidis, P.; Sindona, G. Vegetable proteomics: the detection of Ole e 1 isoallergens by peptide matching of MALDI MS/MS spectra of underivatized and dansylated glycopeptides. *J. Proteome Res.* **2008**, *7*, 2723–2732.
- (26) Aiello, D.; De Luca, D.; Gionfriddo, E.; Naccarato, A.; Napoli, A.; Romano, E.; Russo, A.; Tagarelli, A.; Sindona, G. Multistage mass spectrometry in quality, safety and origin of foods. *Eur. J. Mass Spectrom.* **2011**, *17* (1), 1–31.
- (27) Pribil, P.; Fenselau, C. Characterization of enterobacteria using MALDI-TOF mass spectrometry. *Anal. Chem.* **2005**, *77* (18), 6092–6095.
- (28) Warscheid, B.; Fenselau, C. Characterization of Bacillus spore species and their mixtures using post-source decay with a curved-field reflectron. *Anal. Chem.* **2003**, *75*, 5618–5627.
- (29) Warscheid, B.; Jackson, K.; Sutton, C.; Fenselau, C. MALDI analysis of Bacilli in spore mixtures by applying a quadrupole ion trap time-of-flight tandem mass spectrometer. *Anal. Chem.* **2003**, *75*, 5608–5617.
- (30) Pribil, P. A.; Patton, E.; Black, G.; Doroshenko, V.; Fenselau, C. Rapid characterization of Bacillus spores targeting species-unique peptides produced with an atmospheric pressure matrix-assisted laser desorption/ionization source. *J. Mass Spectrom.* **2005**, *40*, 464–474.
- (31) Di Donna, L.; Mazzotti, F.; Taverna, D.; Napoli, A.; Sindona, G. Structural Characterisation of Malonyl Flavonols in Leek (Allium porrum L.) Using High-performance Liquid Chromatography and Mass Spectrometry. *Phytochem. Anal.* **2014**, *25* (3), 207–212.
- (32) Shilov, I. V.; Seymour, S. L.; Patel, A. A.; Loboda, A.; Tang, W. H.; Keating, S. P.; Hunter, C. L.; Nuwaysir, L. M.; Schaeffer, D. A. The Paragon Algorithm, a Next Generation Search Engine That Uses Sequence Temperature Values and Feature Probabilities to Identify Peptides from Tandem Mass Spectra. *Mol. Cell. Proteomics* **2007**, *6* (9), 1638–1655.
- (33) Drews, O.; Reil, G.; Parlar, H.; Gorg, A. Setting up standards and a reference map for the alkaline proteome of the Gram-positive bacterium Lactococcus lactis. *Proteomics* **2004**, *4*, 1293–1304.
- (34) Rajnarayanan, R. V.; Wang, K. Ion-pair assisted recovery of matrix-assisted laser desorption/ionization mass spectral signals from SDS-containing peptide-protein mixtures. *J. Mass Spectrom.* **2004**, *39*, 79–85.
- (35) Napoli, A.; Aiello, D.; Di Donna, L.; Sajjad, A.; Perri, E.; Sindona, G. Profiling of Hydrophilic Proteins from Olea europaea Olive Pollen by MALDI TOF Mass Spectrometry. *Anal. Chem.* **2006**, *78* (10), 3434–3443.
- (36) Napoli, A.; Aiello, D.; Di Donna, L.; Prendushi, H.; Sindona, G. Exploitation of Endogenous Protease Activity in Raw Mastitic Milk by MALDI TOF/TOF. *Anal. Chem.* **2007**, *79* (15), 5941–5948.
- (37) Rockstroh, M.; Müller, S. A.; Jende, C.; Kerzhner, A.; Von Bergen, M.; Tomm, J. M. Cell fraction – an important tool for compartment proteomics. *J. Integr. Omics* **2011**, *1* (1), 135–143.
- (38) D’Incecco, N.; Bartowsky, E.; Kassara, S.; Lante, A.; Spettoli, P.; Henschke, P. Release of glycosidically bound flavour compounds of Chardonnay by Oenococcus oeni during malolactic fermentation. *Food Microbiol.* **2004**, *21*, 257–265.
- (39) Liu, M.; Nauta, A.; Francke, C.; Siezen, R. J. Comparative Genomics of Enzymes in Flavor-Forming Pathways from Amino Acids in Lactic Acid Bacteria. *Appl. Environ. Microbiol.* **2008**, *74* (15), 4590–4600.
- (40) Elleuche, S.; Fodor, K.; Klippel, B.; von der Heyde, A.; Wilmanns, M.; Antranikian, G. Structural and biochemical characterization of a NAD(+)-dependent alcohol dehydrogenase from Oenococcus oeni as a new model molecule for industrial biotechnology applications. *Appl. Microbiol. Biotechnol.* **2013**, *97* (20), 8963–8975.
- (41) Vallet, A.; Santarelli, X.; Lonvaud-Funel, A.; de Revel, G.; Cabanne, C. Purification of an alcohol dehydrogenase involved in the conversion of methional to methionol in Oenococcus oeni IOEB 8406. *Appl. Microbiol. Biotechnol.* **2009**, *82*, 87–94.
- (42) Elleuche, S.; Antranikian, G. Bacterial group III alcohol dehydrogenases - function, evolution and biotechnological applications. *OA Alcohol* **2013**, *1* (1), 2–6.
- (43) Marçal, D.; Toste Rêgo, A.; Carrondo, M. A.; Enguita, F. J. 1,3-Propanediol Dehydrogenase from Klebsiella pneumoniae: Decameric Quaternary Structure and Possible Subunit Cooperativity. *J. Bacteriol.* **2009**, *191* (4), 1143–1151.
- (44) Capaldo, A.; Walker, M. E.; Ford, C. M.; Jiranek, V. β -Glucosidase metabolism in Oenococcus oeni: Cloning and characterisation of the phospho- β -glucosidase bglD. *Food Chem.* **2011**, *125*, 476–482.
- (45) Salou, P.; Loubiere, P.; Pareilleux, A. Growth and energetics of Leuconostoc oenos during cometabolism of glucose with citrate or fructose. *Appl. Environ. Microbiol.* **1994**, *60*, 1459–1466.
- (46) Olguín, N.; Bordons, A.; Reguant, C. Multigenic expression analysis as an approach to understanding the behaviour of Oenococcus oeni in wine-like conditions. *Int. J. Food Microbiol.* **2010**, *144*, 88–95.
- (47) Da Silveira, M. G.; San Romão, M. V.; Loureiro-Dias, M. C.; Rombouts, F. M.; Abee, T. Flow Cytometric Assessment of Membrane Integrity of Ethanol-Stressed Oenococcus oeni Cells. *Appl. Environ. Microbiol.* **2002**, *68*, 6087–6093.
- (48) Da Silveira, M. G.; Golovina, E. A.; Hoekstra, F. A.; Rombouts, F. M.; Abee, T. Membrane Fluidity Adjustments in Ethanol-Stressed Oenococcus oeni Cells. *Appl. Environ. Microbiol.* **2003**, *69*, 5826–5832.
- (49) Guzzo, J.; Delmas, J. F.; Pierre, F.; Jobin, M. P.; Samyn, B.; Van Beeumen, J.; Cavin, J. F.; Diviès, C. A small heat shock protein from Leuconostoc oenos induced by multiple stresses and during stationary growth phase. *Let. Appl. Microbiol.* **1997**, *24*, 393–396.
- (50) Guzzo, J.; Jobin, M. P.; Diviès, C. Increase of sulfite tolerance in Oenococcus oeni by means of acidic adaptation. *FEMS Microbiol. Lett.* **1998**, *160*, 43–47.

(51) Coucheney, F.; Desroche, N.; Bou, M.; Tourdot-Maréchal, R.; Dulau, L.; Guzzo, J. A new approach for selection of *Oenococcus oeni* strains in order to produce malolactic starters. *Int. J. Food Microbiol.* **2005**, *105* (3), 463–470.

(52) Grandvalet, C.; Coucheney, F.; Beltramo, C.; Guzzo, J. CtsR Is the Master Regulator of Stress Response Gene Expression in *Oenococcus oeni*. *J. Bacteriol.* **2005**, *187* (16), 5614–5623.

(53) Makovets, S.; Titheradge, A. J. B.; Murray, N. E. ClpX and ClpP are essential for the efficient acquisition of genes specifying type IA and IB restriction systems. *Mol. Microbiol.* **1998**, *28*¹ (1), 25–35.

(54) Cohen, S. L.; Chait, B. T. Influence of Matrix Solution Conditions on the MALDI-MS Analysis of Peptides and Proteins. *Anal. Chem.* **1996**, *68*, 31–37.

(55) Macek, B.; Mijakovic, I.; Olsen, J. V.; Gnad, F.; Kumar, C.; Jensen, P. R.; Mann, M. The Serine/Threonine/Tyrosine Phosphoproteome of the Model Bacterium *Bacillus subtilis*. *Mol. Cell. Proteomics* **2007**, *6*, 697–707.

(56) Huberts, D. H.; van der Klei, I. J. Moonlighting proteins: an intriguing mode of multitasking. *Biochim. Biophys. Acta* **2010**, *1803* (4), 520–525.

(57) Guillot, A.; Gitton, C.; Anglade, P.; Mistou, M. Y. Proteomic analysis of *Lactococcus lactis*, a lactic acid bacterium. *Proteomics* **2003**, *3*, 337–354.

(58) Jers, C.; Soufi, B.; Grangeasse, C.; Deutscher, J.; Mijakovic, I. Phosphoproteomics in bacteria: towards a systemic understanding of bacterial phosphorylation networks. *Expert Rev. Proteomics* **2008**, *5*, 619–627.

(59) Soufi, B.; Gnad, F.; Jensen, P. R.; Petranovic, D.; Mann, M.; Mijakovic, I.; Macek, B. The Ser/Thr/Tyr phosphoproteome of *Lactococcus lactis* IL1403 reveals multiply phosphorylated proteins. *Proteomics* **2008**, *8*, 3486–3493.

Available at www.sciencedirect.com

ScienceDirect

journal homepage: www.elsevier.com/locate/jff

Hypocholesterolaemic activity of 3-hydroxy-3-methyl-glutaryl flavanones enriched fraction from bergamot fruit (*Citrus bergamia*): “In vivo” studies

Leonardo Di Donna^{a,1}, Domenico Iacopetta^{b,1}, Anna R. Cappello^b, Giselda Gallucci^a, Emanuela Martello^b, Marco Fiorillo^b, Vincenza Dolce^{b,*,2}, Giovanni Sindona^{a,*,2}

^aDept. of Chemistry, University of Calabria, 87036 Arcavacata di Rende, (CS), Italy

^bDept. of Pharmacy, Health and Nutritional Sciences, University of Calabria, 87036 Arcavacata di Rende, (CS), Italy

ARTICLE INFO

Article history:

Received 30 July 2013

Received in revised form

20 December 2013

Accepted 23 December 2013

Available online 1 February 2014

Keywords:

Bergamot fruit

Brutieridin

High-density lipoprotein

Low-density lipoprotein

Melitidin

Statin like compounds

ABSTRACT

Statins are the pharmacological inhibitors of cholesterol biosynthesis, acting on key enzyme 3-hydroxy-3-methylglutaryl-CoA reductase (HMGR). They are the most effective class of drugs used to treat cardiovascular disease, the main cause of mortality in westernized countries. Our major goal was to investigate the hypocholesterolaemic effects of the 3-hydroxy-3-methyl-glutaryl flavanones enriched fraction (HMGF), extracted from bergamot fruit, in comparison with one of the most used statins, i.e. simvastatin, in a rat model. HMGF and simvastatin reduced the total cholesterol (TC), triacylglycerols (TG), very low-density lipoproteins (VLDL) and low-density lipoproteins (LDL) levels, whereas an increase of the high-density lipoproteins (HDL) content was observed exclusively in the HMGF treated rats. Additionally, an appreciable increase of HMGR, LDL receptor (LDLR) and fatty acid synthase (FASN) was evidenced, at mRNA and protein levels. HMGF did not exhibit genotoxic effects and was cytotoxic only at elevated concentrations. The daily supplementation of HMGF in the diet could be very effective for the treatment of hypercholesterolaemia.

© 2013 Elsevier Ltd. All rights reserved.

1. Introduction

Cholesterol is a molecule of primary importance in animals, including humans, but is not required in the diet because hepatocytes can synthesize it starting from acetyl-CoA. The HMGR is the rate-limiting enzyme in endogenous cholesterol biosynthesis and catalyzes the conversion of HMG-CoA into

mevalonate (Goldstein & Brown, 1990). Inhibition of HMGR has proven to be one of the most effective approaches for lowering plasma LDL and reducing cardiovascular event rates (Ross et al., 1999). As part of a compensatory mechanism due to cholesterol depletion in the liver, inhibition of HMGR leads to an increased synthesis of itself and low-density lipoprotein receptors (LDLR); this latter process allows a subse-

* Corresponding authors. Address: Dept. Pharmacy, Health and Nutritional Sciences, University of Calabria, Arcavacata di Rende, (CS) 87036, Italy. Tel.: +39 (0) 984 493119; fax: +39 (0) 984 493107 (V. Dolce). Dept. Chemistry and Chemistry Technologies, University of Calabria, Arcavacata di Rende, (CS) 87036, Italy. Tel.: +39 (0) 984 492083; fax: +39 (0) 984 492044 (G. Sindona).

E-mail addresses: vincenza.dolce@unical.it (V. Dolce), giovanni.sindona@unical.it (G. Sindona).

¹ These authors contributed equally to this work.

² Joint senior authors.

Abbreviations: HMGF, 3-hydroxy-3-methyl-glutaryl flavanones enriched fraction; FASN, fatty acid synthase; HMGR, 3-hydroxy-3-methylglutaryl-CoA reductase; H, hypercholesterolaemic; VLDL, very low-density lipoprotein; LDL, low-density lipoprotein; HDL, high-density lipoprotein; LDLR, low-density lipoprotein receptors; S, simvastatin; TC, total cholesterol; TG, triglycerides; MTT, (3-(4,5-dimethylthiazol-2-yl)-2,5-diphenyltetrazolium bromide)

1756-4646/\$ - see front matter © 2013 Elsevier Ltd. All rights reserved.

<http://dx.doi.org/10.1016/j.jff.2013.12.029>

quent clearance of LDL from systemic circulation (Brown & Goldstein, 1986), lowering the risk of atherosclerosis and coronary heart diseases (Balbisi, 2006; Miller, 1996).

The HMGCR inhibitors (statins) are the most effective, practical and largely prescribed class of drugs for reducing LDL concentrations, because they are pretty safe, well tolerated and highly efficient, nevertheless cardiovascular disease remains the main cause of mortality in westernized countries. The pursuit of novel therapies targeting the residual risk is focused on preventing the increase of LDL concentration and favouring the increase of HDL (deGoma & Rader, 2011). Some natural compounds found in the human diet have been shown to possess therapeutic and pharmacologic properties, in particular, the daily consumption of citrus fruit juice has been shown to positively influence plasma lipid levels and reduce the risk of coronary heart disease (Gorinstein et al., 2004; Srinivasan & Pani, 2013). Hypolipidaemic effects can be correlated to several components of citrus juice, such as flavonoids (naringin and hesperidin), pectins, and ascorbic acid, which have a high antioxidant potential and interfere with cholesterol metabolism (Chen, Ma, Liang, Peng, & Zuo, 2011; Chinapongtitiwat, Jongarontaprangsee, Chiewchan, & Devahastin, 2013; Gorinstein et al., 2005; Monforte et al., 1995).

Bergamot, the common name of the fruit *Citrus bergamia* Risso, belongs to the family Rutaceae, subfamily Esperidea, and is widespread in the Mediterranean area for centuries. The botanical and geographical origins are still uncertain; probably bergamot is native of Calabria, deriving by mutations of other citrus species, or even arrived in loco from Berga (hence the name of bergamot) otherwise from Antilles, Greece and Canary Islands. Under an ethno-botanical point of view, the history of calabrian bergamot cultivation is of interest because several cultures rule in the past (Greeks, Byzantines, Arabs) and the awareness of the “subsistence”, due to the poorly developed road network and the isolation of villages (Passalacqua, De Fine, & Guarrera, 2006). These events, together with the optimal habitat, promoted the intensification of bergamot cultivation that became a flagship product of calabrian agriculture, although the essential oil characteristics were not known and appreciated at the beginning (Rapisarda & Germanò, 2013). Afterwards, the terpene-rich essential oil, extracted from the peel of the pear-shaped fruit, and its volatile fraction have been largely employed in the cosmetic and perfumery products. In the early 18th century, Jean Paul Féminis created the “Aqua mirabilis”, a distillate exhibiting digestive and antiseptic properties which was subsequently used as cologne; after that, many famous perfumers (Guerlain, Roudnitska) widely exploited bergamot essential oil for their creations (Bijaoui, 2013).

Bergamot and its derivatives have also been used in calabrian folk medicine as fever palliative, antiseptic, anthelmintic, wound healing, anti-inflammatory and hypocholesterolaemic agent (Mollace et al., 2011; Trombetta et al., 2010; www.rc.camcom.gov.it). To date, bergamot essences are used in the food industry for the preparation of teas, jams, sherbet and other commodities, but also for the domestic preparation of liquors, ice creams and pastries by the calabrian confectionery industry (www.rc.camcom.gov.it). Bergamot juice has been considered, for a long time, a secondary and waste by-product of the essential oil extraction and, because

of its organoleptic properties and its bitter taste, did not reach the popularity of other citrus juices but was used to fortify fruit juice instead of synthetic additives (Di Donna et al., 2009). Later on, the discovery of the abundance and variety of bioactive compounds in the juice (e.g. naringin, neoeriocitrin, and neohesperidin), led to the development of several nutraceuticals (capsules, pills or soluble granular powders) in the global market (Lo Curto, 2013). Furthermore, other flavonoids, such as rhoifolin, neodiosmin, and some chrysoeriol derivatives, have been found in smaller amounts (Barreca, Bellocchio, Caristi, Leuzzi, & Gattuso, 2007; Dugo et al., 2005; Gattuso et al., 2006) and different tissues of the fruit produce the flavonoids diosmin and poncirin (Nogata et al., 2006).

We undertook a detailed analysis of dry extract from bergamot peel fruit. Some statin-like components such as brutieridin and melitidin (Di Donna et al., 2009, 2013), were found and isolated from the dry extract. The main aim was to investigate the effects of the extract (i.e. HMGF) on the total lipid profile of hypercholesterolaemic rats in comparison with simvastatin, examining the hepatic and serum lipid contents and the expression of the HMGCR, LDLR and FASN. Our study demonstrates the ability of HMGF to parallel the simvastatin effects on the lipid profile and, more importantly, to increase the HDL levels. Lastly, HMGF is cytotoxic only at very high doses and no genotoxic effects have been evidenced.

2. Materials and methods

2.1. Preparation of 3-hydroxy-3-methyl-glutaryl flavanones enriched fraction

A dry extract of bergamot fruit (*C. bergamia* Risso) provided from Gioiasucchi s.r.l. (Gioia Tauro, Italy) was submitted to flash chromatography using the VersaFlash™ system from Supelco (St. Louis, MO, USA); 35 g of C₁₈ 200–400 mesh (Aldrich, St. Louis, MO, USA) were used as stationary phase into a 40 × 37.5 mm column (Supelco, St. Louis, MO, USA). The column was activated eluting in sequence 200 mL of EtOH, 200 mL of H₂O/EtOH (50:50, v/v), 200 mL of H₂O/EtOH (75:25, v/v), 200 mL of H₂O/EtOH (87.5:12.5, v/v), and finally 500 mL of H₂O, maintaining the flow rate at 25 mL/min. The column was loaded pouring 2 g of dry extract dissolved in 10 mL of H₂O with a syringe; 100 mL of water were then eluted at 5 mL/min and the flow rate was gradually increased to 50 mL/min. The elution of the components of the dry extract was conducted using 4 L of H₂O collecting fraction of 0.5 L each, then 1 L of H₂O/EtOH (90:10, v/v) and 500 mL of H₂O/EtOH (70:30, v/v) were used, collecting fraction of 50 mL each. The first two fractions of the elution step with H₂O/EtOH (70:30, v/v) were combined and evaporated to dryness under vacuum. One hundred twenty-five milligrams of a mixture containing 62% of brutieridin, 14% of melitidin and 15% of another HMG-flavanone conjugated (i.e., HMG-neoeriocitrin, unpublished data) (Fig. 1) were obtained in a single run.

All fraction were monitored using a FractionLynx semi-preparative system from Waters (Milford, MA, USA) in analytical mode equipped with an UV detector and a Luna C₁₈ column 5 mm particle size, 25 cm × 4.6 mm (Supelco, St. Louis, MO, USA). The run time was 105 min, while the flow

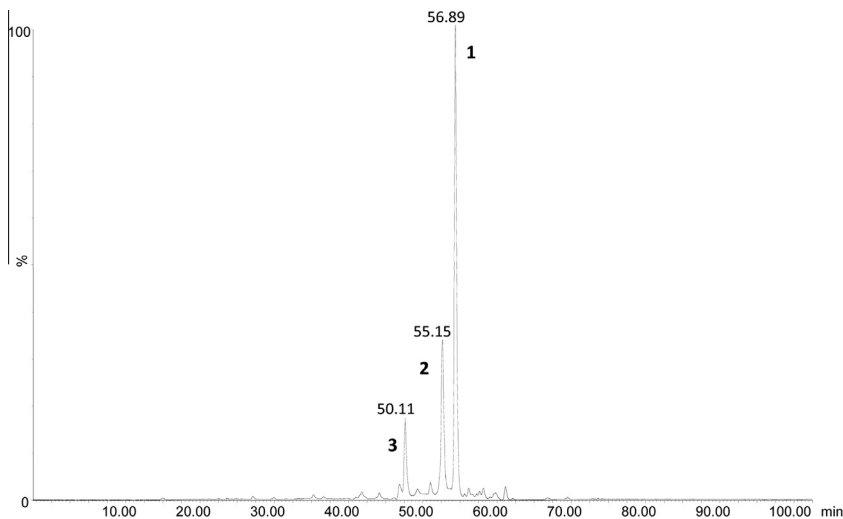


Fig. 1 – 280 nm HPLC/UV Chromatogram of the HMGF. The revealed molecules were: brutieridin (1, r.t. 56.89), melitidin (2, r.t. 55.15) and neoeriocitrin HMG conjugated (3, r.t. 50.11).

rate was set at 1 mL/min and the following eluents and gradient conditions were used: 0.1% HCOOH in H₂O (solvent A) and CH₃OH (solvent B); 10 min isocratic 80% A; 2 min linear gradient from 80 to 74% A; 65 min linear gradient from 74 to 31% A; 18 min linear gradient from 31 to 80%; 10 min isocratic 80% A. Twenty milliliters of each fraction were injected into the loop, while the absorption wavelength of the UV detector was set at 280 nm (Di Donna et al., 2009).

2.2. Animals and diets

Male Wistar strain rats, weighing about 150 g each, were purchased from Charles River (Lecco, Italy). All of the animal experiment protocols followed the institutional guidelines of the Italian Ministry of Health for Animal Care (D.M. 116/1992). Animals were housed 1 rat per cage, in an air conditioned room with a 12 h light–dark cycle and with *ad libitum* access to food and water. Before the experiment, all the animals were allowed to stabilize by being fed with regular rodent chow, then randomly divided into four groups of twelve animals each: group N (control) received the regular diet for 3 weeks; group H (hypercholesterolaemic) received the hypercholesterolaemic diet (regular diet +2% cholesterol +0.2% cholic acid) for 3 weeks; group H + S received the hypercholesterolaemic diet (regular diet +2% cholesterol +0.2% cholic acid) for 3 weeks; from the 2nd to the 3rd week each rat was administered by gavage with simvastatin (20 mg/kg bw/day) and group H + HMGF received the hypercholesterolaemic diet (regular diet +2% cholesterol +0.2% cholic acid) for 3 weeks; from the 2nd to the 3rd week each rat was administered by gavage with the HMGF (60 mg/kg bw/day).

Regular and hypercholesterolaemic diets were supplied by Charles River (Lecco, Italy), simvastatin was purchased from Sigma Aldrich (Milan, Italy).

During the experiment, rats were weighed daily and the 24 h food consumption was recorded. At the end of the study, the animals were killed by decapitation, under chloral hydrate anesthesia, and blood samples were collected in ethylenediaminetetraacetic acid (EDTA)-treated tubes, centri-

fuged at 2500g for 15 min and the serum was separated and stored at –20 °C until analyzed (Rai, Sharma, & Tiwari, 2009); liver was excised and immediately frozen in liquid nitrogen, then stored at –80 °C until used.

2.3. Biochemical estimations

The livers were cut into small pieces, washed several times in a cold buffer (0.25 M sucrose, 3 mM EDTA, 20 mM Tris–HCl, pH 7.0), next homogenized in the same buffer and treated as described in Muci et al. (1992) for TC extraction. Briefly, an aliquot of 10 mg protein sample was saponified with alcoholic KOH for 90 min at 85–90 °C. Unsaponifiable constituents were extracted three times (5 mL each) with light petroleum (b.p. 40–60 °C). The pooled extracts were then evaporated to dryness under N₂ and the residue, dissolved in 2-propanol (Muci et al., 1992). Total lipids were extracted from liver homogenate (10 mg protein) with chloroform/methanol (1:1, v/v) according to Bligh and Dyer (1959). The hepatic TC and TG levels were measured respectively by HPLC and direct enzymatic assays from (Chematil Srl, Salerno, Italy).

The TG, TC, HDL, LDL and VLDL levels were evaluated respectively by direct enzymatic assays using Trigliceridi Kit and Colesterolo kit (Chematil srl, Salerno, Italy), HDL Kit (Intermedical srl, Naples, Italy), LDL Kit (Biogemina srl, Catania, Italy) and VLDL ELISA Kit (antibodies-online GmbH, Aachen, Germany), according to manufacturer's instruction with some modifications.

2.4. RNA extraction, reverse transcription and quantitative real-time polymerase chain reaction

RNAs were extracted from liver as described by Zara et al. (2007) and aliquots of 1 µg were reverse-transcribed as reported in Iacopetta et al. (2011). Quantitative real-time polymerase chain reaction (RT-PCR) was performed with the obtained complementary DNAs (cDNAs) using the Applied Biosystems StepOne™. Real-Time PCR System (Applied Biosystems, Monza, Italy). Primers based on the cDNA sequences

of the genes of interest were designed using Primer Express (Applied Biosystems, Monza, Italy). In each sample of 20 μ L real-time PCR reaction 10 ng of cDNA, 10 μ L of the Power SYBR[®] PCR Master Mix (Applied Biosystems, Monza, Italy) and 0.3 μ L (150 nM) of the specific primers for each genes analyzed were used. Each experiment was repeated at least 3 times. The comparative threshold cycle method was used in relative gene quantification as previously described (Lunetti et al., 2013) using 18S gene as the endogenous control.

2.5. Microsomal fraction extraction and Western blot analysis

The liver homogenate, obtained as previously described, was centrifuged at 800g for 8 min, the pellet was discarded and supernatant centrifuged for 10 min at 12,000g. The pellet containing the mitochondrial fraction was discarded and the supernatant was first centrifuged at 20,000g for 20 min and then at 105,000g for 60 min to obtain the cytosolic fraction and pelleted microsomes. The latter were re-suspended in the homogenizing medium and centrifuged again under the same conditions. Contamination of microsomal preparation by other subcellular fractions, ranging from 5 to 9%, was determined by the assay of marker enzymes as described (Caputi Jambrenghi et al., 2007) and protein concentration was determined as in (Madeo et al., 2009). Western blot

analysis was conducted as described previously (Cappello et al., 2012; Iacopetta et al., 2010). Antibodies anti-HMGR (H-300), fatty acid synthase (FASN, H-300), LDL receptor (C-20), anti-calnexin (C-20), anti- β -tubulin (D-10), anti-GAPDH (FL-335) were supplied by Santa Cruz Biotechnology Inc. (Santa Cruz, CA, USA) and used following the manufacturer's instructions. Anti-calnexin, anti- β -tubulin or anti-GAPDH antibodies were used to confirm the equal loading of proteins.

2.6. HPLC analysis of total cholesterol in liver samples

The analyses of samples were performed following a method from literature (Duncan, Culbreth, & Burtis, 1979).

2.7. Cytotoxicity assays

The potential toxicity of the HMGF was investigated on HepG2 and 3T3-L1 cell lines, which were cultured in DMEM (Dulbecco's modified Eagle's medium) with phenol red, supplemented with 10% FBS and 100 μ g/mL penicillin/streptomycin. Cell proliferation using a Countess[™] automated cell counter (Invitrogen) and MTT viability assays were performed, as reported elsewhere (Knutson et al., 2012; Santolla et al., 2012), in order to determine the median cytotoxic concentration (CC₅₀). CC₅₀ is defined as the concentration of HMGF which reduces the viability/number of the cells such

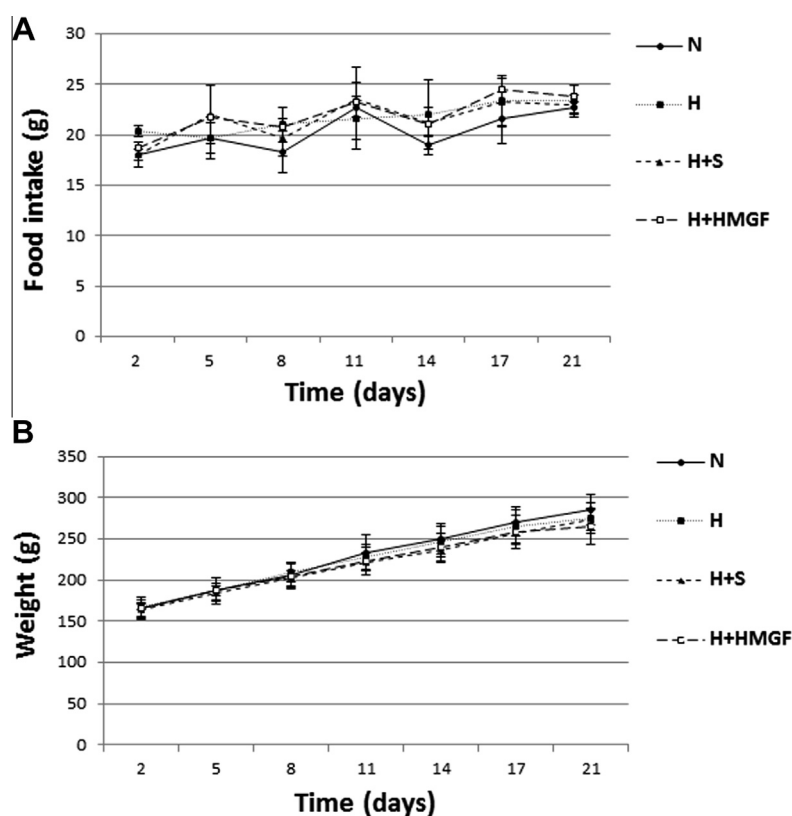


Fig. 2 – Summary of daily food intake and body weight changes over the study period for each group of rats. Hypercholesterolaemic rats group (filled squares, H) was fed and then treated with simvastatin (triangles, H + S) or HMGF (open squares, H + HMGF), as described in par 2.2. Regular diet fed rats group is indicated as N (dots). Values represent the mean \pm SD of the daily chow intake (panel A) and of the daily weight (panel B) for each rat respect to the group.

that only 50% of the cells survive, in comparison with the untreated group (only vehicle). Different concentrations, i.e. six to eight serial dilutions, of HMGF were tested in the experiments and the obtained data were used to construct a sigmoidal dose–response curve with variable slope. A non-linear regression curve fitting the sigmoidal model was performed employing GraphPad PRISM5 (GraphPad Software, La Jolla, CA, USA) to calculate CC_{50} . All cytotoxicity assays were performed in duplicate.

2.8. Genotoxicity experiments

Genotoxicity experiments were performed using the SOS-Chromotest™ kit (EBPI, Mississauga, Ontario, Canada) following the manufacturer's instructions, in presence or absence of rat liver S9 activation enzymes (EBPI, Mississauga, Ontario, Canada), used as exogenous metabolic activation system. The induction factor (IF) was calculated as the ratio of β -gal activity/Alkaline Peroxidase activity (determined in presence of increasing HMGF concentrations) and the β -gal activity/AP activity (in the absence of the HMGF). The enzyme activities were detected colorimetrically (Quillardet & Hofnung, 1993). In the SOS Chromotest assay, the compounds are classified as non-genotoxic, if the SOS IF remains <1.5, marginally genotoxic in the IF ranges between 1.5 and 2, and as genotoxic

if IF exceeds 2.0 (Kevekordes et al., 1999). The experiments were performed in triplicate.

2.9. Statistical analysis

All data are presented as means \pm SD ($n = 12$ rats/group). Data were analyzed by one-way ANOVA, followed by Dunnett's test using the GraphPAD Prism5 software (GraphPad Software, La Jolla, CA, USA). Differences were considered statistically significant at $P < 0.05$.

3. Results

3.1. Food intake and body weight gain

The data on food intake and body weight are shown in Fig. 2. In Fig. 2, panel A, it is summarized the daily food intake respect to the whole studies period for each group of rats. As positive treatment control in rats, we used one of the most prescribed statins in man, simvastatin. No significant differences in food intake were observed for each group (i.e. simvastatin or HMGF treated rats versus untreated). Fig. 2, panel B, shows the overview of changes in body weight over the study period for the different rat groups. For each rat the body weight normally increased during the studies period, without

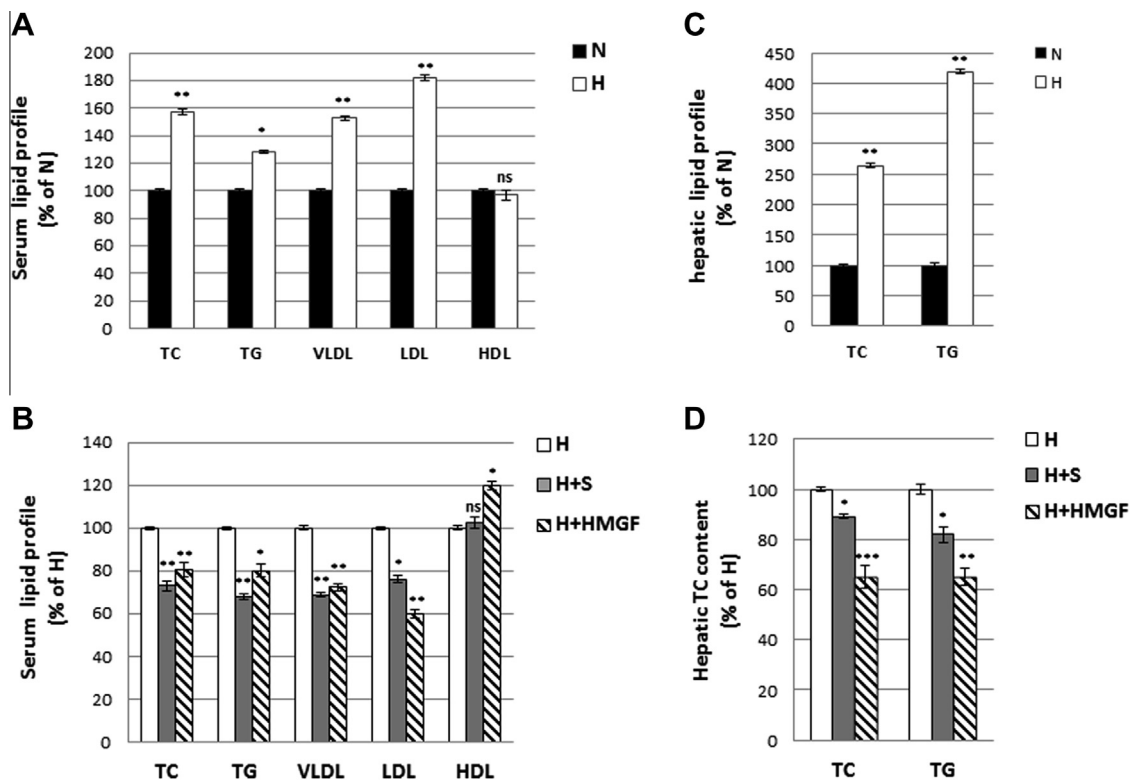


Fig. 3 – Serum and hepatic lipid profile variations between normal, hypercholesterolaemic and treated rats Normal (black bars, N), hypercholesterolaemic (white bars, H), simvastatin treated (grey bars, H + S) and HMGF treated (striped bars, H + HMGF) rats groups were fed as described in par 2.2. The total cholesterol (TC), triglycerides (TG), very low density lipoproteins (VLDL), low density lipoproteins (LDL) and high density lipoproteins (HDL) levels were measured in N and H serum (panel A, N as control) and in H + S and H + HMGF serum (panel B, H as control). TC and TG were also measured in N and H liver (panel C, N as control) and H + S and H + HMGF liver (panel D, H as control). The obtained results were plotted as percentage and columns are mean \pm SD of three independent experiments performed in duplicate. * $P = 0.01$ vs. control; ** $P < 0.01$ vs. control; *** $P < 0.005$ vs. control; ns, nonsignificant.

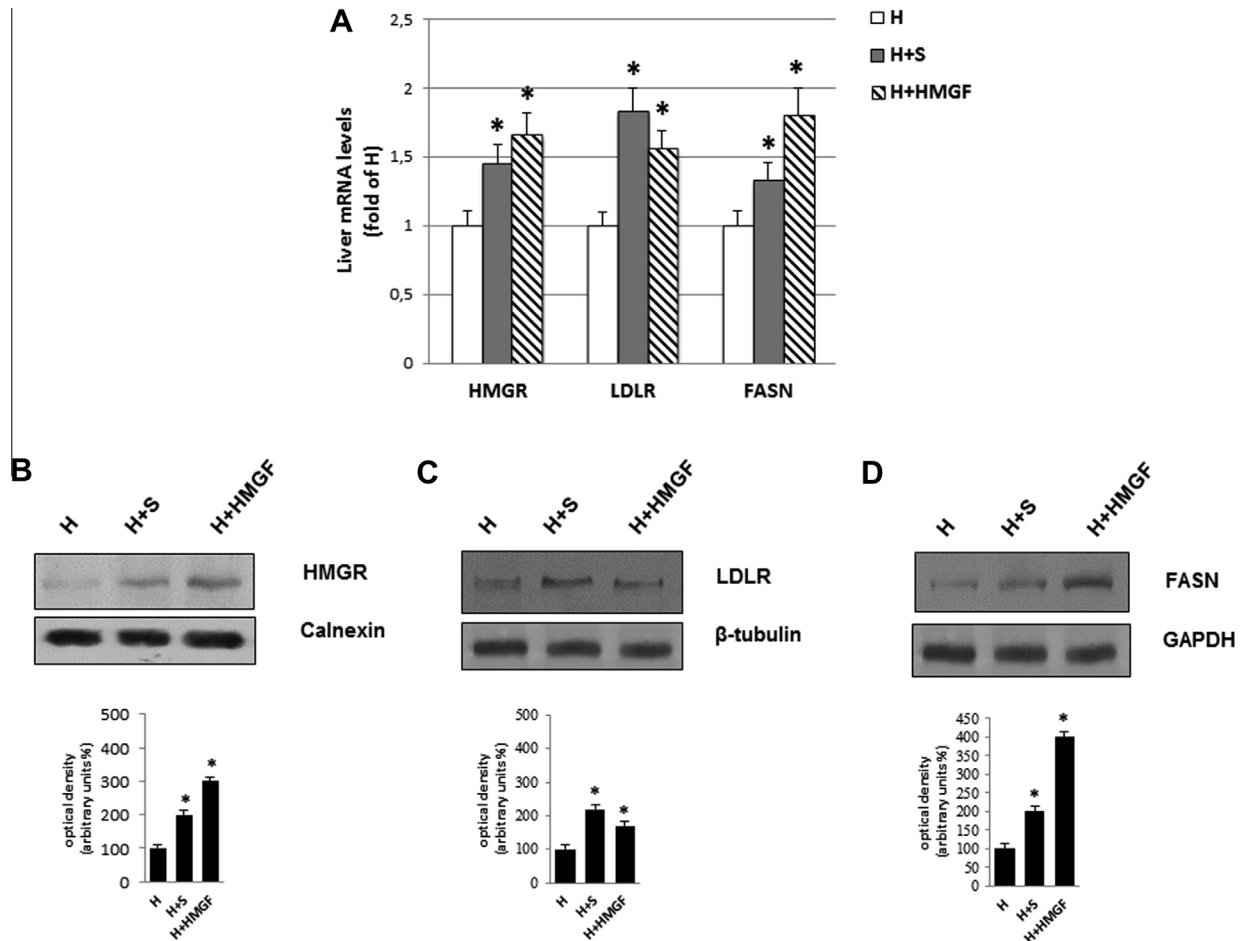


Fig. 4 – Effect of simvastatin and HMGF on HMGR, LDLR and FASN mRNAs and proteins expression in experimental rats. Panel A: livers were isolated from hypercholesterolaemic untreated rats (white bars, H), hypercholesterolaemic treated with simvastatin (grey bars, H + S) or with HMGF (striped bars, H + HMGF). The HMGR, LDLR and FASN mRNAs levels were analyzed by RT-PCR and normalized to that of 18S. The values are plotted as fold of H group and are representative of three independent experiments. * $P < 0.01$ vs. H. **Panel B–D:** protein levels of HMGR (97 kDa, panel B), LDLR (160 kDa, panel C) and FASN (270 kDa, panel D) are shown. A total of 100 μ g of microsomes or cellular liver extracts were used for Western blot analysis; Calnexin (90 kDa), β -tubulin (55 kDa) or GAPDH (37 kDa) were used as a control for equal loading and transfer. Densitometric analyses of the blots are also shown. The immunoblots are representative of three separate experiments. * $P < 0.01$ vs. H.

significant differences in weight within the same group or between the different groups. Moreover, the livers excised from each treated group rats were not significantly different in weight from those of the induced hypercholesterolaemic rats (data not shown). These observations indicate that the diet and treatments used in these studies were well tolerated in rats, given that no physical alteration, body weight loss or food intake reduction occurred over the period of the study. A group of regular diet fed rats was taken under evaluation as control to verify the induced hypercholesterolaemia.

3.2. Effect of simvastatin and HMGF on serum and hepatic lipid content

To examine the concentrations of TC, TG, VLDL, LDL and HDL in rat serum, we used a colorimetric assay, whereas the

hepatic TC and TG were measured by HPLC and colorimetric assay respectively. Firstly, we compared the serum and hepatic lipid profiles of the regular diet fed rats (group N) and the hypercholesterolaemic ones (group H, Fig. 3, panels A and C), in order to establish whether the hypercholesterolaemic rat model has been achieved. The results showed a clear increase of the lipid profile in serum (Fig. 3, panel A) and liver (Fig. 3, panel C) of H group rats. In particular TC, TG, VLDL and LDL serum levels were increased of 57, 28, 53 and 82% respectively, compared to the N group, which values were 79.85 ± 5.6 mg/dl for TC, 104.7 ± 9.3 mg/dl for TG, 19.02 ± 1.5 mg/dl for VLDL and 35.03 ± 3.1 mg/dl for LDL, whereas no significant variation has been found for HDL levels (for N group the HDL value was 43.52 ± 3.3 mg/dl). A marked raise of the hepatic TC and TG levels has been observed in H group (164 and 319% respectively) compared to N group, which values were 1.98 ± 0.9 mg/g liver for TC

Table 1 – Genotoxic effect of the HMGF in the absence of the exogenous metabolizing system S9 in the SOS Chromotest.

Sample	µg/mL	E. coli PQ37		
		β-galactosidase (units)	Alkaline phosphatase (units)	IF
4-NQO	20	4.37 ± 0.02	12.99 ± 0.09	7.350615858
HMGF	0	0.60 ± 0.03	13.11 ± 0.12	1
HMGF	10	0.62 ± 0.01	13.08 ± 0.11	1.035703364
HMGF	30	0.65 ± 0.05	13.05 ± 0.08	1.050797182
HMGF	60	0.67 ± 0.03	12.99 ± 0.09	1.03553029
HMGF	90	0.68 ± 0.02	13.01 ± 0.07	1.01336515

Data are expressed as the mean ± SD of three independent experiments. 4-NQO was used as a positive control. IF = inhibition factor.

and 4.87 ± 0.39 mg/g liver for TG. These results confirmed that H group can be used as a hypercholesterolaemic model in the following experiments.

After that, we investigated the effects elicited by the simvastatin and HMGF treatments on serum and hepatic lipid levels of hypercholesterolaemic rats and we observed a significant decrease of the serum TC (of about 30 and 20%, respectively) compared to H group (Fig. 3, panel B). We also observed a reduction in liver TC content of 11% in H + S group and a more significant reduction of 35% in H + HMGF group (Fig. 3, panel D). It is well known that an elevated concentration of LDL in blood is associated with a high risk of coronary heart disease and atherosclerosis plaque lesions (Berliner & Heinecke, 1996; Ross, 1993), thus we also evaluated serum levels of LDL and VLDL (Marzetta, Foster, & Brunzell, 1990). A significant reduction of VLDL and LDL was measured in H + S (33 and 24% lower, respectively) and H + HMGF (28 and 40% lower, respectively) groups (Fig. 3, panel B). Conversely, any significant difference in the HDL cholesterol was found in the H + S group, whereas, surprisingly, a significant increase was observed in the H + HMGF group (20% higher) respect to H group (Fig. 3, panel B).

Since HMGR inhibitors have been shown to contribute in decreasing plasmatic TG levels in experimental animals (Krause & Newton, 1995), we investigated this feature in our model. We measured serum and hepatic TG content observing that, in both cases, there was a decrease in H + S and H + HMGF groups respect to H group of about 32 and 20%, respectively, for serum TG (Fig. 3, panel B), and of about 18 and 35%, respectively, for hepatic TG (Fig. 3, panel D).

3.3. Effect of simvastatin and HMGF administration on hepatic HMGR, LDLR and FASN mRNAs and proteins levels

In order to further investigate the HMGF effects in H groups, we evaluated the transcriptional levels of two main proteins involved in cholesterol metabolism, i.e. HMGR and LDLR, and the expression of the main enzyme of fatty acid biosynthesis, i.e. FASN (Dolce, Cappello, Lappano, & Maggiolini, 2011). As shown in Fig. 4, panel A, simvastatin and HMGF treatments produced a similar modulation on the gene expression of the above mentioned proteins. Particularly, simvastatin administration, respect to H group, brought to an increased transcription of HMGR, LDLR and FASN genes in an extent of 1.45, 1.83 and 1.33-fold respectively. As well HMGF treatment increased the expression of HMGR, LDLR and FASN

genes of 1.66, 1.56 and 1.80-fold respectively. In all cases the mRNAs increase is appreciable respect to the untreated H group. These data were additionally verified by Western blot analyses conducted on the microsomal or cytoplasmic fractions or on liver homogenate extract, considering the different sub-localization of proteins analyzed. As shown in Fig. 4, panels B–D, according to RT-PCR results, both simvastatin and HMGF treatments led to a clear increase of HMGR, LDLR and FASN proteins respect to H group.

3.4. Bergamot and HMGF safety

Bergamot fruit is generally considered safe and no evidences exist about its toxicity and the juice has been granted for human nutrition (www.salute.gov.it). Furthermore, animal and human studies highlighted the protective effects of bergamot juice or extracts (Mollace et al., 2011; Trovato et al., 2010) and did not report any toxic effects. Conversely, since no literature data have been published about the HMGF toxicity, we carried out experiments to test the safety of our fraction. The potential cytotoxicity was tested on HepG2 and 3T3-L1 cell cultures as reported in Section 2 (par 2.7), and the results showed a low cytotoxic activity, as evidenced by CC₅₀ values of 54.04 ± 2.3 and 51.09 ± 1.8 mg/mL, respectively, for HepG2 and 3T3-L1 cells. Additionally, in order to establish if HMGF could exert some genotoxic and/or mutagenic effects by itself or even their metabolic derivatives, we performed the SOS Chromotest assay, in presence or absence of an exogenous metabolic activation system S9 from rat liver. The outcomes, shown in Tables 1 and 2, demonstrated that HMGF, used at doses up to 90 µg/mL, did not produce any DNA damage, also after being metabolized by hepatic enzymes.

4. Discussion

The cholesterol homeostasis is subtly regulated at several levels as intestinal absorption, hepatic uptake of LDL, *de novo* synthesis and excretion. When its blood concentration raise over certain levels, the incidence of atherosclerosis and cardiovascular/cerebrovascular diseases becomes higher (Steinberg, 1987), hence it followed the need to develop many statin classes, as advanced pharmacological treatment, during the twentieth century (Witztum, 1996). Besides, it became pretty clear that a more correct daily diet could prevent the hypercholesterolaemia, lowering the risk of the associated-diseases onset, as already reported from traditional cures

Table 2 – Genotoxic effect of the HMGF in the presence of the exogenous metabolizing system S9 in the SOS Chromotest.

Sample	µg/mL	E. coli PQ37 + (S9)		
		β-galactosidase (units)	Alkaline phosphatase (units)	IF
4-NQO	20	4.33 ± 0.03	13.01 ± 0.08	7.142009299
HMGF	0	0.61 ± 0.01	13.09 ± 0.11	1
HMGF	10	0.61 ± 0.03	13.07 ± 0.12	1.001530222
HMGF	30	0.63 ± 0.02	13.08 ± 0.10	1.050797182
HMGF	60	0.65 ± 0.04	12.96 ± 0.09	1.03553029
HMGF	90	0.66 ± 0.002	13.02 ± 0.10	1.01336515

Data are expressed as the mean ± SD of three independent experiments. 4-NQO was used as a positive control. IF = inhibition factor.

employed in folk medicine (Miceli et al., 2007). Concerning this, the right habit of eating foods containing many bioactive compounds, as flavonoids, pectins or ascorbic acid (Gorinstein et al., 2005; Monforte et al., 1995), has been shown to positively influence serum lipid levels and, most importantly, to reduce atherogenic lipoproteins. Recent studies have shown the presence of some statin-like compounds in the *C. bergamia* Risso (Di Donna et al., 2009; Mollace et al., 2011), to which can be ascribed the beneficial effects exerted on human health.

Starting from the latter data, in the present study we demonstrated that the three statin-like flavanones, extracted from bergamot peel and contained in HMGF, exert a similar behaviour respect to commercial simvastatin on a model of hypercholesterolaemic rats. The achievement of this model has been validated by the serum and liver lipid profile comparison of N vs. H group, which has been used in the subsequent experiments in order to test HMGF effects. The daily diet supplementation of H group with HMGF, over the period of the study, led to a decrease of serum TC and TG, as in H + S group, but exhibited a higher ability in decreasing LDL levels, accompanied by a significant increase in serum HDL content. The latter peculiarity represents a favourable event, given that HDL are able to picking up cholesterol from

peripheral tissues or cells and carries it back to liver (deGoma & Rader, 2011), where they are readily catabolized contributing to prevent atherosclerosis. It has been reported that elevated LDL levels and decreased HDL levels in serum represent independent risk factors for the onset of atherosclerosis associated diseases (Arsenault et al., 2009), whereas the data reporting the VLDL role in atherosclerotic plaque formation are still controversial (Stancu, Toma, & Sima, 2012). In our experiments, HMGF was found able to exert its beneficial actions on the LDL/HDL ratio but also to decrease VLDL serum levels, the latter event represents another very interesting feature. Then, we investigated the TC and TG hepatic levels, observing a drop of both in simvastatin treated rats hepatocytes and, in a higher extent, in HMGF treated group. The TG and TC diminished availability determines the observed fall in VLDL liver secretion, required for cholesteryl ester transport to extra-hepatic districts. The effects on serum and hepatic lipid contents are strictly related to the variation of hepatic key enzymes and proteins involved in TC and TG metabolism. Particularly, we evaluated the expression level of HMGR and LDLR transcripts and proteins, as main indicators of cholesterol metabolism, together with the transcript and protein levels of FASN gene, mainly involved in TG metabolism. We found an up-regulation in HMGR and LDLR

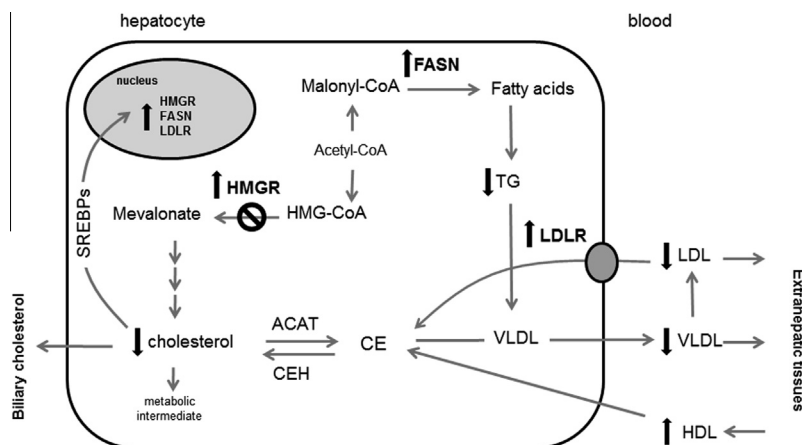


Fig. 5 – Model depicting HMGF effects on lipids metabolism elicited in rat hepatocytes. Black arrows indicate HMGF effects on genes, enzymes and metabolites levels. ⊘ indicates enzymatic inhibition. ACAT, Acyl-CoA:cholesterol acyltransferase; CE, cholesteryl ester; CEH, cholesteryl ester hydrolase; FASN, fatty acid synthase; HDL, high-density lipoprotein; HMG-CoA, 3-hydroxy-3-methylglutaryl-CoA; HMGR, 3-hydroxy-3-methylglutaryl-CoA reductase; LDL, low-density lipoprotein; LDLR, low-density lipoprotein receptor; SREBPs, sterol response element binding proteins; TG, triglycerides; VLDL, very low-density lipoprotein.

genes transcription under simvastatin treatment, according to previously published data (Kong et al., 2008) and also a significant induction of FASN gene transcription which should be included in the knowledge of simvastatin induced effects, not yet reported. Similar results have been obtained in H + HMGF group, but in a higher extent, confirming one more time the HMGR statin-like behaviour. This positive gene regulation consequently affects the proteins expression in liver indeed, in our experimental model, the increase in HMGR, LDLR and FASN gene transcription and protein translation under HMGF treatment is clearly evident and justify the hypolipidemic effects observed in rat serum. The blockade of HMGR activity and the induced expression of hepatic LDLR may be considered amongst the events responsible of TC and LDL decrease. As it is known, the HMGR expression and activity may change in response to the content of local cholesterol in cells and/or tissues (Goldstein & Brown, 1990). In our model, HMGR inhibition lead to a reduction of endogenous cholesterol which, in turn, is responsible of the up-regulation of HMGR and LDLR genes transcription, as well of the higher LDLR exposure within the hepatocytes membrane, through a compensating mechanism based on sterol regulatory element-binding proteins (SREBPs) pathway (Scharnagl et al., 2001). It should be recalled that cholesterol depletion below a certain threshold is also responsible of FASN gene transcription increase, via SREBPs activation (Sato, 2010; Scharnagl et al., 2001), which is one of the effects we observed under both simvastatin or HMGF treatments. These outcomes indicate that HMGF could be a high potential control agent in hypercholesterolaemia caused diseases, confirming one more time the ancient use of bergamot, as source of various nutraceuticals, for instance flavonoids. Indeed, in industrialized countries there has been a general trend towards the use of traditional medicines; for their pharmacological properties and, as well, for their low toxicity in animals, flavonoids have been considered as a *panacea* in several diseases treatment (Kurzawa-Zegota, Najafzadeh, Baumgartner, & Anderson, 2012; Nijveldt et al., 2001). Effectively, the three flavanones contained in HMGF did not show toxicity *in vitro*, if not at very elevated concentrations, neither a potential genotoxicity. Our results, summed up in Fig. 5, reinforce the traditional use of bergamot fruit by the calabrian population and may be useful to broaden the survey of the literature data about bergamot and its derivatives.

5. Conclusions

The results presented here support the large number of studies regarding the already known hypolipidaemic effects of diet integration with some citrus species, and bring an important contribution to the complexity of the effects exerted by bergamot fruit, focusing the attention on the presence of statin-like compounds which block the HMGR activity. In rats, the daily supplementation with HMGF in the diet was able to significantly reduce the TC, TG, VLDL and LDL and, more importantly, to increase contemporaneously the HDL serum levels. These data establish, in a model that is highly related to humans, that inhibition exerted by HMGF on HMGR is a promising nutraceutical strategy for the control of

hypercholesterolaemia, the main factor responsible of the increased cardiovascular diseases risk.

Acknowledgments

The work presented here was carried out in collaboration between all authors. V.D., G.S. and A.R.C. defined the research plan, discussed analyses, interpretations and edited the manuscript. D.I. and A.R.C. designed methods and experiments, carried out the biological assays, analyzed the data, interpreted the results and wrote the paper. L.D.D. designed the chemistry methods, provided the HMGF fraction and collaborated to manuscript writing. E.M., G.G. and M.F. cooperated in laboratory experiments.

This work is part of the Italian National Project, MIUR-PRIN 2009XZ7XAB_003.

REFERENCES

- Arsenault, B. J., Rana, J. S., Stroes, E. S., Despres, J. P., Shah, P. K., Kastelein, J. J., et al. (2009). Beyond low-density lipoprotein cholesterol: Respective contributions of non-high-density lipoprotein cholesterol levels, triglycerides, and the total cholesterol/high-density lipoprotein cholesterol ratio to coronary heart disease risk in apparently healthy men and women. *Journal of the American College of Cardiology*, 55(1), 35–41.
- Balbisi, E. A. (2006). Management of hyperlipidemia: New LDL-C targets for persons at high-risk for cardiovascular events. *Medical Science Monitor: International Medical Journal of Experimental and Clinical Research*, 12(2), RA34–RA39.
- Barreca, D., Bellocchio, E., Caristi, C., Leuzzi, U., & Gattuso, G. (2007). Flavonoid composition and antioxidant activity of juices from Chinotto (*Citrus × myrtifolia* Raf.) fruits at different ripening stages. *Journal of Agricultural and Food Chemistry*, 55(5), 3031–3036.
- Berliner, J. A., & Heinecke, J. W. (1996). The role of oxidized lipoproteins in atherogenesis. *Free Radical Biology & Medicine*, 20(5), 707–727.
- Bijaoui, N. (2013). Bergamot and its use in perfumery. In G. Dugo & I. Bonaccorsi (Eds.), *Citrus bergamia-bergamot and its derivatives* (Vol. 51, pp. 467–473). Boca Raton, FL: CCR Press.
- Bligh, E. G., & Dyer, W. J. (1959). A rapid method of total lipid extraction and purification. *Canadian Journal of Biochemistry and Physiology*, 37(8), 911–917.
- Brown, M. S., & Goldstein, J. L. (1986). A receptor-mediated pathway for cholesterol homeostasis. *Science*, 232(4746), 34–47.
- Cappello, A. R., Guido, C., Santoro, A., Santoro, M., Capobianco, L., Montanaro, D., et al. (2012). The mitochondrial citrate carrier (CIC) is present and regulates insulin secretion by human male gamete. *Endocrinology*, 153(4), 1743–1754.
- Caputi Jambrenghi, A., Paglialonga, G., Gnoni, A., Zanotti, F., Giannico, F., Vonghia, G., et al. (2007). Changes in lipid composition and lipogenic enzyme activities in liver of lambs fed omega-6 polyunsaturated fatty acids. *Comparative Biochemistry and Physiology Part B: Biochemistry and Molecular Biology*, 147(3), 498–503.
- Chen, Z. Y., Ma, K. Y., Liang, Y. T., Peng, C., & Zuo, Y. Y. (2011). Role and classification of cholesterol-lowering functional foods. *Journal of Functional Foods*, 3(2), 61–69.
- Chinapongtititwat, V., Jongaroontaprangsee, S., Chiewchan, N., & Devahastin, S. (2013). Important flavonoids and limonin in selected Thai citrus residues. *Journal of Functional Foods*, 5(3), 1151–1158.

- deGoma, E. M., & Rader, D. J. (2011). Novel HDL-directed pharmacotherapeutic strategies. *Nature Reviews of Cardiology*, 8(5), 266–277.
- Di Donna, L., De Luca, G., Mazzotti, F., Napoli, A., Salerno, R., Taverna, D., et al. (2009). Statin-like principles of bergamot fruit (*Citrus bergamia*): Isolation of 3-hydroxymethylglutaryl flavonoid glycosides. *Journal of Natural Products*, 72(7), 1352–1354.
- Di Donna, L., Taverna, D., Mazzotti, F., Benabdelkamel, H., Attya, M., Napoli, A., et al. (2013). Comprehensive assay of flavanones in citrus juices and beverages by UHPLC-ESI-MS/MS and derivatization chemistry. *Food Chemistry*, 141(3), 2328–2333.
- Dolce, V., Cappello, A. R., Lappano, R., & Maggiolini, M. (2011). Glycerophospholipid synthesis as a novel drug target against cancer. *Current Molecular Pharmacology*, 4(3), 167–175.
- Dugo, P., Presti, M. L., Ohman, M., Fazio, A., Dugo, G., & Mondello, L. (2005). Determination of flavonoids in citrus juices by micro-HPLC-ESI/MS. *Journal of Separation Science*, 28(11), 1149–1156.
- Duncan, I. W., Culbreth, P. H., & Burtis, C. A. (1979). Determination of free, total, and esterified cholesterol by high-performance liquid chromatography. *Journal of Chromatography*, 162(3), 281–292.
- Gattuso, G., Caristi, C., Gargiulli, C., Bellocco, E., Toscano, G., & Leuzzi, U. (2006). Flavonoid glycosides in bergamot juice (*Citrus bergamia* Risso). *Journal of Agricultural and Food Chemistry*, 54(11), 3929–3935.
- Goldstein, J. L., & Brown, M. S. (1990). Regulation of the mevalonate pathway. *Nature*, 343(6257), 425–430.
- Gorinstein, S., Leontowicz, H., Leontowicz, M., Krzeminski, R., Gralak, M., Delgado-Licon, E., et al. (2005). Changes in plasma lipid and antioxidant activity in rats as a result of naringin and red grapefruit supplementation. *Journal of Agriculture and Food Chemistry*, 53(8), 3223–3228.
- Gorinstein, S., Leontowicz, H., Leontowicz, M., Krzeminski, R., Gralak, M., Martin-Belloso, O., et al. (2004). Fresh Israeli Jaffa blond (Shamouti) orange and Israeli Jaffa red Star Ruby (Sunrise) grapefruit juices affect plasma lipid metabolism and antioxidant capacity in rats fed added cholesterol. *Journal of Agriculture and Food Chemistry*, 52(15), 4853–4859.
- Iacopetta, D., Lappano, R., Cappello, A. R., Madeo, M., De Francesco, E. M., Santoro, A., et al. (2010). SLC37A1 gene expression is up-regulated by epidermal growth factor in breast cancer cells. *Breast Cancer Research and Treatment*, 122(3), 755–764.
- Iacopetta, D., Madeo, M., Tasco, G., Carrisi, C., Curcio, R., Martello, E., et al. (2011). A novel subfamily of mitochondrial dicarboxylate carriers from *Drosophila melanogaster*: Biochemical and computational studies. *Biochimica et Biophysica Acta*, 1807(3), 251–261.
- Kevekordes, S., Mersch-Sundermann, V., Burghaus, C. M., Spielberger, J., Schmeiser, H. H., Arlt, V. M., et al. (1999). SOS induction of selected naturally occurring substances in *Escherichia coli* (SOS Chromotest). *Mutation Research*, 445(1), 81–91.
- Knutson, T. P., Daniel, A. R., Fan, D., Silverstein, K. A., Covington, K. R., Fuqua, S. A., et al. (2012). Phosphorylated and sumoylation-deficient progesterone receptors drive proliferative gene signatures during breast cancer progression. *Breast Cancer Research*, 14(3), R95.
- Kong, W. J., Wei, J., Zuo, Z. Y., Wang, Y. M., Song, D. Q., You, X. F., et al. (2008). Combination of simvastatin with berberine improves the lipid-lowering efficacy. *Metabolism*, 57(8), 1029–1037.
- Krause, B. R., & Newton, R. S. (1995). Lipid-lowering activity of atorvastatin and lovastatin in rodent species: Triglyceride-lowering in rats correlates with efficacy in LDL animal models. *Atherosclerosis*, 117(2), 237–244.
- Kurzawa-Zegota, M., Najafzadeh, M., Baumgartner, A., & Anderson, D. (2012). The protective effect of the flavonoids on food-mutagen-induced DNA damage in peripheral blood lymphocytes from colon cancer patients. *Food and Chemical Toxicology*, 50(2), 124–129.
- Lo Curto, R. (2013). Use of juice and by-products. In G. Dugo & I. Bonaccorsi (Eds.). *Citrus bergamia*-bergamot and its derivatives (Vol. 51). Roca Baton, FL: CCR Press.
- Lunetti, P., Cappello, A. R., Marsano, R. M., Pierri, C. L., Carrisi, C., Martello, E., et al. (2013). Mitochondrial glutamate carriers from *Drosophila melanogaster*: Biochemical, evolutionary and modeling studies. *Biochimica et Biophysica Acta*, 1827(10), 1245–1255.
- Madeo, M., Carrisi, C., Iacopetta, D., Capobianco, L., Cappello, A. R., Bucci, C., et al. (2009). Abundant expression and purification of biologically active mitochondrial citrate carrier in baculovirus-infected insect cells. *Journal of Bioenergetics and Biomembranes*, 41(3), 289–297.
- Marzetta, C. A., Foster, D. M., & Brunzell, J. D. (1990). Conversion of plasma VLDL and IDL precursors into various LDL subpopulations using density gradient ultracentrifugation. *Journal of Lipid Research*, 31(6), 975–984.
- Miceli, N., Mondello, M. R., Monforte, M. T., Sdrafkakis, V., Dugo, P., Crupi, M. L., et al. (2007). Hypolipidemic effects of *Citrus bergamia* Risso et Poiteau juice in rats fed a hypercholesterolemic diet. *Journal of Agriculture and Food Chemistry*, 55(26), 10671–10677.
- Miller, J. P. (1996). Hyperlipidaemia and cardiovascular disease. *Current Opinion in Lipidology*, 7(1), U18–U24.
- Mollace, V., Sacco, I., Janda, E., Malara, C., Ventrice, D., Colica, C., et al. (2011). Hypolipemic and hypoglycaemic activity of bergamot polyphenols: From animal models to human studies. *Fitoterapia*, 82(3), 309–316.
- Monforte, M. T., Trovato, A., Kirjavainen, S., Forestieri, A. M., Galati, E. M., & Lo Curto, R. B. (1995). Biological effects of hesperidin, a *Citrus* flavonoid. (note II): Hypolipidemic activity on experimental hypercholesterolemia in rat. *Farmaco*, 50(9), 595–599.
- Muci, M. R., Cappello, A. R., Vonghia, G., Bellitti, E., Zezza, L., & Gnoni, G. V. (1992). Change in cholesterol levels and in lipid fatty acid composition in safflower oil fed lambs. *International Journal for Vitamin and Nutrition Research*, 62(4), 330–333.
- Nijveldt, R. J., van Nood, E., van Hoorn, D. E., Boelens, P. G., van Norren, K., & van Leeuwen, P. A. (2001). Flavonoids: A review of probable mechanisms of action and potential applications. *American Journal of Clinical Nutrition*, 74(4), 418–425.
- Nogata, Y., Sakamoto, K., Shiratsuchi, H., Ishii, T., Yano, M., & Ohta, H. (2006). Flavonoid composition of fruit tissues of citrus species. *Bioscience, Biotechnology, and Biochemistry*, 70(1), 178–192.
- Passalacqua, N. G., De Fine, G., & Guarrera, P. M. (2006). Contribution to the knowledge of the veterinary science and of the ethnobotany in Calabria region (Southern Italy). *Journal of Ethnobiology and Ethnomedicine*, 2, 52.
- Quillardet, P., & Hofnung, M. (1993). The SOS Chromotest: A review. *Mutation Research*, 297(3), 235–279.
- Rai, S. K., Sharma, M., & Tiwari, M. (2009). Inhibitory effect of novel diallyldisulfide analogs on HMG-CoA reductase expression in hypercholesterolemic rats: CREB as a potential upstream target. *Life Sciences*, 85(5–6), 211–219.
- Rapisarda, A., & Germanò, M. P. (2013). *Citrus × bergamia* Risso & Poiteau botanical classification, morphology and anatomy. In G. Dugo & I. Bonaccorsi (Eds.). *Citrus bergamia*-bergamot and its derivatives (Vol. 51, pp. 9–11). Boca Raton, FL: CCR Press.
- Ross, R. (1993). The pathogenesis of atherosclerosis: A perspective for the 1990s. *Nature*, 362(6423), 801–809.
- Ross, S. D., Allen, I. E., Connelly, J. E., Korenblat, B. M., Smith, M. E., Bishop, D., et al. (1999). Clinical outcomes in statin treatment

- trials: A meta-analysis. *Archives of Internal Medicine*, 159(15), 1793–1802.
- Santolla, M. F., Lappano, R., De Marco, P., Pupo, M., Vivacqua, A., Sisci, D., et al. (2012). G protein-coupled estrogen receptor mediates the up-regulation of fatty acid synthase induced by 17beta-estradiol in cancer cells and cancer-associated fibroblasts. *Journal of Biological Chemistry*, 287(52), 43234–43245.
- Sato, R. (2010). Sterol metabolism and SREBP activation. *Archives of Biochemistry and Biophysics*, 501(2), 177–181.
- Scharnagl, H., Schinker, R., Gierens, H., Nauck, M., Wieland, H., & Marz, W. (2001). Effect of atorvastatin, simvastatin, and lovastatin on the metabolism of cholesterol and triacylglycerides in HepG2 cells. *Biochemical Pharmacology*, 62(11), 1545–1555.
- Srinivasan, S., & Pani, L. (2013). Antihyperlipidemic effect of diosmin: A citrus flavonoid on lipid metabolism in experimental diabetic rats. *Journal of Functional Foods*, 5(1), 484–492.
- Stancu, C. S., Toma, L., & Sima, A. V. (2012). Dual role of lipoproteins in endothelial cell dysfunction in atherosclerosis. *Cell and Tissue Research*, 349(2), 433–446.
- Steinberg, D. (1987). Lipoproteins and the pathogenesis of atherosclerosis. *Circulation*, 76(3), 508–514.
- Trombetta, D., Cimino, F., Cristani, M., Mandalari, G., Saija, A., Ginestra, G., et al. (2010). In vitro protective effects of two extracts from bergamot peels on human endothelial cells exposed to tumor necrosis factor-alpha (TNF-alpha). *Journal of Agriculture and Food Chemistry*, 58(14), 8430–8436.
- Trovato, A., Taviano, M. F., Pergolizzi, S., Campolo, L., De Pasquale, R., & Miceli, N. (2010). Citrus bergamia Risso & Poiteau juice protects against renal injury of diet-induced hypercholesterolemia in rats. *Phytotherapy Research*, 24(4), 514–519.
- Witztum, E. (1996). Drugs used in the treatment of hyperlipoproteinemias. In *The pharmacological basis of therapeutics* (9th ed., pp. 875–877). New York: McGraw-Hill.
- Zara, V., Dolce, V., Capobianco, L., Ferramosca, A., Papatheodorou, P., Rassow, J., et al. (2007). Biogenesis of eel liver citrate carrier (CIC): Negative charges can substitute for positive charges in the presequence. *Journal of Molecular Biology*, 365(4), 958–967.